

Student Poster Book of Abstracts

2013 IEEE Power and Energy Society General Meeting

Vancouver, BC, Canada

July 21-25 2013



Welcome Message from the Chair -

IEEE PES Student Activities Subcommittee

On behalf of the Student Activities Subcommittee, I welcome you to the Student Poster Contest at the 2013 IEEE Power & Energy Society General Meeting held at Vancouver, BC, Canada on July 23, 2013.

At the time of printing this book, we have 193 extended abstracts from students from different parts of the world confirmed to participate in the 2013 IEEE PES GM student poster contest. This book of extended abstracts is aimed at documenting the many outstanding research projects performed by undergraduate and graduate students at various educational institutions around the world. These extended abstracts are accompanied by student poster presentations at the conference venue on July 23, 2013 from 7 a.m. – 9 a.m. The research topics of these posters fall into 18 categories, namely:

- | | |
|--|--|
| 1. System-wide events and analysis methods | 9. Geomagnetic disturbance on electric power systems |
| 2. Advanced computational methods for power system planning, operation and control | 10. Integrating renewable energy into the grid |
| 3. Asset management | 11. Intelligent monitoring and outage management |
| 4. Cyber and physical security of the smart grid | 12. Market interactions in power systems |
| 5. Dynamic performance and control of power systems | 13. Power electronics |
| 6. Electric machine and drives | 14. Power system modeling and simulation |
| 7. Emerging software needs for the restructured grid | 15. Smart grid technology |
| 8. Flexible AC transmission systems | 16. Smart sensors, communication and control in energy systems |
| | 17. Substation and distribution automation |
| | 18. Power Engineering Education |

All students are invited to attend the Student/Faculty/Industry (SFI) luncheon to be held on July 24 from 12 p.m. to 1 p.m. where the student poster contest winners will be announced at the SFI luncheon.

Support from the Grainger Foundation, and the IEEE Power & Energy Society, especially the Power and Energy Education Committee (PEEC), for the student activities is gratefully acknowledged.

The subcommittee acknowledges the services of Prof. Chee-Wooi Ten, Assistant Professor, in the Dept. of Electrical and Computer Engineering at Michigan Tech University, Houghton, MI, in the compilation of this book of extended abstracts, and the Local Organizing Committee for planning and execution of the student poster session.

Siddharth (Sid) Suryanarayanan
Fort Collins, Colorado, USA.

IEEE PES Student Activities Subcommittee

Chair

Dr. Siddharth Suryanarayanan
Assistant Professor, Electrical and Computer Engineering
Colorado State University
Fort Collins, CO 80523-1373, USA
sid.suryanarayanan@ieee.org

Vice-Chair

Dr. Anurag K Srivastava
Assistant Professor
School of Electrical Engineering and Computer Science
Washington State University
PO Box 642752
EME 102
Spokane St Pullman
Washington 99164-2752, USA
asrivast@eecs.wsu.edu

Secretary

Dr. Jignesh M. Solanki
Assistant Research Professor
Lane Department of Computer Science and Electrical Engineering
West Virginia University
395 Evansdale Drive,
Morgantown, WV 26506-6109, USA
jmsolanki@csee.wvu.edu

Secretary Elect

Dr. Aaron St. Leger,
Assistant Professor,
Department of Electrical Engineering and Computer Science,
United States Military Academy,
646 Swift Rd,
West Point, NY 10996-1905, USA
aaron.stleger@usma.edu

LIST OF PARTICIPANTS AND POSTER TITLES

1. System-Wide Events and Analysis Methods

Page #	Poster Board #	Title of Poster	Student Name
16	101	Harmonic impact of LED lamps and PV panels	Yang Wang
17	102	Trajectory Sensitivities: Applications in Power Systems and Estimation Accuracy Refinement	Lei Tang
18	103	A Novel Approach for Ringdown Detection Using Extended Kalman Filter	Mehrdad Yazdani
19	104	Optimal PMU Placement for Two Level Linear State Estimation	Ming Meng
20	105	Voltage Instability Protection in Power Systems	Natalia Petryshyn

2. Advanced Computational Methods for Power Systems Planning, Operation, and Control

Page #	Poster Board #	Title of Poster	Student Name
21	201	Dynamic reserve zones for distinct scenarios	Joshua Lyon
22	202	Study of Artificial Neural Network Based Short Term Load Forecasting	Ashton Webberley
23	203	Hour-ahead Corrective Topology Control for Intermittent Renewables and N-1 Contingencies	Mojdeh Abdi Khorsand
24	204	Robust Corrective Topology Control	Kshay Korad
25	205	A Parallelizable Greedy Algorithm for Transmission Switching	Mostafa Sahraei-Ardakani
26	206	Multi Area State Estimation using Area Slack Bus Angle Adjustment with Minimal Data Exchange	Ankush Sharma
27	207	A Two-Level Parallel Decomposition Approach for Transient Stability Constrained Optimal Power Flow	Guangchao Geng
28	208	A Quadratic Robust Optimization Model for Automatic Voltage Control on Wind Farm Side	Tao Ding
29	209	Security constrained unit commitment with demand response	Guodong
30	210	Dynamic Programming Solution to Distributed Storage Operation and Design	Junjie Qin
31	211	A Software Performance Engineering Approach to Fast Transmission Probabilistic Load Flow Analysis	Tao Cui
32	212	Optimal blackstart capability for power system restoration	Yazhou Jiang
33	213	Transformation of Measurements for Using External Network Equivalents in State Estimation	Mahesh Vardikar
34	214	Synchrophasor State Estimation for Data Quality Improvement on the New York Transmission System	Scott Ghiocel
35	215	A Hybrid Maintenance Scheduling Model for Thermal Generators	Jasper Quach
36	216	Transmission Expansion Planning Considering Uncertainty in Demand	Luis Fernando Fuerte
37	217	Second-Order Cone Relaxations for the Alternating Current Optimal Power Flow problem	Chen Chen
38	218	Short-Term Wind Power Prediction Using a Wavelet Support Vector Machine	Jianwu Zeng

3. Asset Management

Page #	Poster Board #	Title of Poster	Student Name
39	301	Equivalent Indices for Shunt Power Capacitor Loading assessment	Yu Tian
40	302	Study of Transformer Winding Deformation by Frequency Response Analysis	Mohd Fairouz Mohd Yousof
41	303	Analysis of Grid Impacts of an Electric Vehicle DC Quick Charger	Nicole Zimmerman
42	304	Reconciling Consumer Behaviors with Demand Response in the Smart Home	Adam Zipperer
43	305	Security-Based Circuit Breaker Maintenance Management	Payman Dehghanian
44	306	Optimal Transformer Sizing with the Presence of Probabilistic Electric Vehicle Charging	Sachin Argade

4. Cyber and Physical Security of the Smart Grid

Page #	Poster Board #	Title of Poster	Student Name
45	401	Real-Time Price-Based Demand Response Management for Residential Appliances Considering Privacy Protection	Zhi Chen
46	402	Mitigation Measures against Cyber Intrusions at the Substations	Junho Hong
47	403	Power Grid Interdiction with Alternating Current Optimal Power Flow	Wei Yuan
48	404	A Real Time Cyber-Physical Test Bed	Ceeman Vellaithurai
49	405	Security Aspects in Computation of Smart Grid Systems	Ankur Majumdar
50	406	Attack-Resilient Measurement Design to Mitigate Topology Based Cyber Attacks in State Estimation	Aditya Ashok
51	407	Coordinated Attacks Detection using Cyber Physical Alert Correlation	Siddharth Sridhar

5. Dynamic Performance and Control of Power Systems

Page #	Poster Board #	Title of Poster	Student Name
52	501	Oscillation Modal Analysis from Ambient Synchrophasor Data using Distributed Frequency Domain Optimization	Jiawei Ning
53	502	Set Point Adjustment Strategy for Mitigating Transients in a Microgrid	Christopher Stone
54	503	Integration of Demand Response into Load Shedding in Distribution Network	Kaiumuzzaman Mollah
55	504	Adaptive PI Control of STATCOM for Voltage Regulation	Yao Xu
56	505	Control of UPFC Using Hamilton-Jacobi-Bellman Formulation Based Neural Network	Hamidreza Nazaripouya
57	506	Data Analysis and Visualization of Oscillation Monitoring System in Power Systems	Tianying Wu
58	507	Reactive Power Substitution Between Rapid and Slow Dynamic Var Compensators	Xuran Wang
59	508	Role of Electromechanical Wave Propagation in Power Systems	Tianya Li
60	509	Making On-line Transient Stability Decisions with Multi-level Decision Trees	Tuo Ji
61	510	Some issues with Quasi-Steady State Model in Long-term Stability	Xiaozhe Wang
62	511	Statistical Detection and Time-Localization of Forced Oscillations in Power Systems	Jim Follum
63	512	New Grid-tied Power Converter for Battery Energy Storage	Ahreyon Park
64	513	Power and Energy Capacity Requirements of Storages Providing Frequency Control Reserves	Theodor Borsche
65	514	Reduction of Harmonic Distortion in Off-Grid Energy Systems	Zach Ulibarri
66	515	Two-Level Control of Doubly Fed Induction Generator using Flatness-Based Approach	Variani Hassani
67	516	Load Factor Control Using Community Energy Storage and Neural Network Predictive Load Modeling	Ben Ollis

6. Electric Machines and Drives

Page #	Poster Board #	Title of Poster	Student Name
68	601	Evaluating FIDVR using an air conditioner stall model with real time digital simulator	Kumaraguru Prabakar
69	602	Current-Based Fault Detection for Wind Turbine Systems via Hilbert-Huang Transform	Dingguo Lu

7. Emerging software for restructured grid

Page #	Poster Board #	Title of Poster	Student Name
70	701	A Statistical Approach to End - User Energy Consumption	Jonas Traphner
71	702	Modeling and Analysis of Campus Microgrid Distribution System	Sayonsom Chanda
72	703	Multi-Agent-Based Information Collection Algorithm for Isolated Power Systems	Guanqun Wang

8. Flexible AC Transmission Systems

Page #	Poster Board #	Title of Poster	Student Name
73	801	Increased Security Rating of Overhead Transmission Circuits Using Compact Phase Design and High Phase Order	Brian Pierre
74	802	DC Impedance-Model-Based Resonance Analysis of a VSC-HVDC System	Ling Xu

9. Geomagnetic disturbance on electric power systems

Page #	Poster Board #	Title of Poster	Student Name
75	901	Review of Earth Conductivity Structure Modeling For Calculating Geo-electric Fields	Dong Boyd

10. Integrating Renewable Energy into the Grid

Page #	Poster Board #	Title of Poster	Student Name
76	1001	Output Power and Harmonic Currents Analysis of Photovoltaic Systems in Net-Zero-Energy Houses	Hesam Yazdanpanahi
77	1002	Optimized Design of Battery Storage with High Penetration Distributed PV Units to Solve the Overvoltage Issue	Ye Yang
78	1003	Increasing Wind Capacity Value in Tasmania Using Wind and Hydro Power Coordination	Mehdi Mosadeghy
79	1004	Dynamic Reserve Zones for Day-Ahead Unit Commitment with Renewable Resources	Fengyu Wang
80	1005	Economic Assessment of Bulk Energy Storage in Transmission Systems with High Penetration of Renewable Generation	Nan Li
81	1006	Inertial response capability of DFIG according to wind speed	Stefanie Kuenzel
82	1007	Reliability and Economic Study of Multi-terminal HVDC with LCC & VSC Converter for Connecting Remote Renewable Generators to the Grid	Kazi Nazmul Hasan
83	1008	Effects of HVDC Connection for Offshore Wind Turbines on AC Grid Protection	Lina He
84	1009	Optimal Storage Placement and Size Considering the Uncertainty of Wind Power Using PSO and Sensitivity Analysis	Shuli Wen
85	1010	Reactive Power Planning Considering High Penetration Wind Energy	Xin Fang
86	1011	Capacitor and Generator Output Adjustment by Using PSO Considering N-1 Contingency for Large Penetration of Photovoltaic Power	Sho Ando
87	1012	Load-Frequency Control (LFC) Model Including Renewable Power and Demand Response	Colin Young
88	1013	Impact of Available Electric Vehicle Battery Power Capacity on Power System Reliability	Bei Zhang
89	1014	A Generalized Data Preprocessing Method For Wind Power Prediction	Jiakun An
90	1015	Robustness Analysis on Electric Vehicle Energy Distribution Networks	Guangyu Lin
91	1016	of Distribution Feeder considering PV generation reactive power support	Yashodhan Agalgaonkar
92	1017	Dynamic Models of Wind Turbine Generators In Power System Toolbox	Felipe Wilches-Bernal
93	1018	A Decentralized Coordinated Controller for Load Sharing in a Microgrid with Renewable Generation	Md Abdul Barik
94	1019	Mitigating the Detrimental Impact of Solar PV Penetration on the Voltage Profile of Power Systems	Nitin Prakash
95	1020	Coordinated Control for Grid Integration of PV Array, Battery Storage and Supercapacitor	Huiying Zheng
96	1021	Modeling of an All-Vanadium Redox Flow Battery and Optimization of Flow Rates	Binyu Xiong

97	1022	Probabilistic Power Flow for Distribution Networks with Photovoltaic Generators	Ren Zhouyang
98	1023	Regulatory incentive for distribution system operators to integrate distributed generation: Portuguese case.	Angela Picciariello
99	1024	Ground Fault Location in Ungrounded Large Scale PV Generators	Shea Pederson
100	1025	Application of sequential decision theory on integrating distributed energy resources	Yalin Huang
101	1026	Analysis of the Impact of Distributed Generation Placement on Voltage Profile in Distribution Systems	Po-Chen Chen
102	1027	Short circuit Analysis for integration of 10MW Windfarm in Nigeria at the PCC	Sunday Adio Owolabi
103	1028	Wavelet-Adaptive ANN Forecaster for Renewable Energy Sources for Continuous Supply in Microgrid Applications	Ahmed Elsayed
104	1029	Financial Transmission Rights Perform Well in Power Markets with High Penetration of Wind Energy?	Yang Yu
105	1030	Evaluating Possibility of Reactive Power Counteraction among Voltage Regulators in a PV Solar Farm	Afshin Samadi
106	1031	An Affine Arithmetic Approach for Microgrid Dispatch with Variable Renewables	Mehrdad Pirnia
107	1032	The Effect of Plug-In Hybrid Electric Vehicle Penetration on an Electric Microgrid	Andrew Clarke
108	1033	Multi-objective Network Reconfiguration of Distributions Systems with Renewable Energy	Huihua Yu
109	1034	Real Time Modeling and Simulation of CERTS Microgrid	Fransiska Martina
110	1035	Trading Wind Power in a Competitive Electricity Market Using Stochastic Programing and Game Theory	Ting Dai
111	1036	Optimal Wind Power Penetration in the Real-Time Energy Market Operation	Jairo Cervantes
112	1037	Effectiveness of Traditional Mitigation Strategies for Neutral Current and Voltage Problems under High Penetration of Rooftop PV	Alam Jan E
113	1038	Optimal Operations of Energy Storage System for Renewable Energy Plant	Shu Zhen

11. Intelligent Monitoring and Outage Management

Page #	Poster Board #	Title of Poster	Student Name
114	1101	An Efficient Outage Planning Method for Electrical Power Facilities Using Two-layered Tabu Search	Aya Fujiwara
115	1102	Travelling Wave Based Fault Location Using Dominant Fault Induced Surges in Circuit	Guangbin Zhang
116	1103	Hedging against system protection malfunction	Jose Luis Calvo
117	1104	Transformer Condition Assessment	Kyle Wiedeman
118	1105	The effect of instrument transformer accuracy class on the WLS state estimator accuracy	Markos Asprou
119	1106	Identifying Protective Device Operations in Distribution and Transmission Systems	Min Lwin
120	1107	Outage Detection in Power Distribution Networks with Optimally-Deployed Power Flow Sensors	Raffi Sevlian

12. Market Interactions in Power Systems

Page #	Poster Board #	Title of Poster	Student Name
121	1201	Investment Strategies Assessment Under Uncertainty	Yanyi He
122	1202	Improving Convergence of Horizontally Decomposed Stochastic Day-Ahead Unit Commitment	Garret LaBove
123	1203	Horizontal Decomposition-based Stochastic Day-ahead Reliability Unit Commitment	Yingzhong Gu
124	1204	Real Time Reactive Power Spot Markets	David Ganger
125	1205	Bidding Strategy for Wind Generation Considering Conventional Generation and Transmission Constraints	Hao Huang
126	1206	Smart Location Targeting for Power Flow Control Devices via Shadow Price Weighting	Omar Urquidez
127	1207	Participation Model for Small Customers with Reliability Preference in Electricity Market	Zhongwei Zhang
128	1208	An Integrated Transmission and Distribution Systems Model with Distribution-based LMP (DLMP) Pricing	Nikita Singhal
129	1209	Hedging Decision of an Electricity Generating Firm with Market Power	Ekaterina Moiseeva
130	1210	Short-Term Electricity Price Forecasting	Erik Chalko
131	1211	Stability Analysis of an Energy Managed Smart Distribution System	Jesse Boyd
132	1212	Sensitivity Analysis of Real-Time Locational Marginal Price to SCADA Sensor Data Corruption	Dae-Hyun Choi

13. Power Electronics

Page #	Poster Board #	Title of Poster	Student Name
133	1301	Transformer less Intelligent Power Substation for 13.8 kV/480 V Grid Interface Applications	Sachin Madhusoodhanan
134	1302	Low Cross Regulation SIMO DC/DC Converter with Model Predictive Voltage Control	Wang Benfei
135	1303	On the Effects of Unbalances Harmonics and Interharmonics on PLL Systems	Luigi Feola
136	1304	Realizing Space Vector Modulation in MATLAB and PSCAD	Yan Ma
137	1305	Modeling soft-starter for wind generators in PSCAD	Jen-Pin Lin
138	1306	Adaptive SRF-PLL with Reconfigurable Controller for Microgrid in Grid-Connected and Stand-Alone Modes	Tarek Youssef
139	1307	Designing of a fuzzy controller based on Differential evolution tuning for VSC	Ivan Riano

14. Power System Modeling and Simulation

Page #	Poster Board #	Title of Poster	Student Name
140	1401	Parameter Identification of Doubly Fed Induction Generator (DFIG) Using Real-time Measurements	Shaotong GUO
141	1402	Managing Solar Uncertainty in Neighboring Systems with Stochastic Unit Commitment	Robin Broder Hytowitz
142	1403	Real Time Corrective Switching in Response to N-m Events	Pranavamoorthy Balasubramanian
143	1404	Modeling of Electrical Arc for Transient Simulation	Qingxin Shi
144	1405	Flexibility Assessment in Power Systems	Yury Dvorkin
145	1406	Factors Affecting Induced Voltage on Pipeline Located Close to High Voltage Transmission	Ahmed Alshahri
146	1407	Transient Stability Analysis Using Prony Analysis	Takuya Omi
147	1408	Supplementary Load Frequency Control with Storage Battery Operation Considering SOC under Large-scale Wind Power Penetration	Kurita Yu
148	1409	A Generator Output Adjustment Method considering Transient Stability ATC and Multi-swing Stability	Kaoru Nakamura
149	1410	A New Approximation Method for Generating Day-Ahead Load Scenarios	Yonghan Feng
150	1411	Semi-Definite Programming based Control for WECS over Full Operating Regions	Can Huang
151	1412	Voltage Quality Improvement in Distribution Networks Containing DERs using UPQC	Sumit Mazumder
152	1413	A Two-Level Online Parameter Identification Approach	Runze Chen
153	1414	Power System Online Security Operational Trend Analysis and Simulation Results	Feng Zhao
154	1415	Preliminary Modeling and Stability Analysis of Physically Distributed Power Systems with Constant Delay	Christian Schegan
155	1416	Stochastic Economic Dispatching for Wind-Penetrated Power Systems	Amir Hossein Shahrinia
156	1417	Order Recursive and Real-time Estimation of Power System Electromechanical Modes	Gurudatha Pai
157	1418	Multi-Band Sub-Synchronous Damping Controller (MBSSDC) for Type III DFIG Wind Power Farms	Jason Pannell
158	1419	Small Signal Stability Analysis of Two Area System with Magnetic Amplifier	Xiaohu Zhang
159	1420	Modeling Inverter PQ Control in PSCAD	Yin Li
160	1421	Simplified WECC Model with Wind Penetration	Yidan Lu
161	1422	Stability Analysis of Unbalanced Synchronous Machine Based Distributed Generators	Ehsan Nasr Azadani
162	1423	Switching Loss and Cell Capacitor Balancing of Modular Multilevel Converter under Various Modulation Frequencies	Hee Jin Kim
163	1424	A Real-Time Simulation Model of Community Microgrid	Ling Xu
164	1425	Improvement of Composite Load Modeling Accuracy Using	Jae-Kyeong Kim

		Parameter Shift Algorithm	
165	1426	Enhanced Frequency Regulation Service using Hybrid Energy Storage System against Increasing Power-Load Variability	Youngho Cho
166	1427	Investigation of Power Flow solution When Slack Generator Hits Reactive Power Limit	Hung-Ming Chou
167	1428	A Fast and Efficient Load Shedding Algorithm to Alleviate Transmission System Overloads and Under Voltages	Yaser Tohidi
168	1429	Implementing a Nuclear Power Plant Model for Evaluating Load-Following Capability on a Small Grid	Samet Egemen Arda
169	1430	Improved Cascading Outage Analysis model using Outage Checkers	Yezhou Wang
170	1431	Methodology to Determine Distribution Level Impact of Dynamic Transfers	David Kleinschmidt
171	1432	Effect of Price-Responsive Demand on Dispatch and Costs	Felipe Ramos Gaete
172	1433	Decision Support Concerning Demand Response Programs Design and Use_ A Simulation Tool	Pedro Faria
173	1434	PMU Testing and Hardware Interface Architecture for Synchrophasor Application Testing	Hyojong Lee
174	1435	A New Relaying Algorithm for Blocking Third Zone Distance Relays During Stable Power Swings In Power Systems	Dong Kang
175	1436	Simulation Study of PEM Fuel Cell and its Dynamic Characteristics	Yongli Zhu
176	1437	Sequence Network Models of Wind Turbine Generators for Short-Circuit Studies	Dustin Howard

15. Smart Grid Technology

Page #	Poster Board #	Title of Poster	Student Name
177	1501	Stability Analysis for Power Systems with Price-Based Demand Response	Zhechong Zhao
178	1502	Developing a Scenario-Based Demand Response for Short-Term Decisions of Electricity Retailers	Nadali Mahmoudi
179	1503	Ohmic Transmission Loss Minimization in the AC-DC Grids	Mohamadreza Baradar
180	1504	Multi-level state estimation utilizing synchronized phasor measurements	Lin Zhang
181	1505	New Non-Recursive Algorithms for Real Time Voltage Stability Monitoring using Synchrophasors	Saugata Biswas
182	1506	Active Network Management using Distributed Constraint Optimisation	Dimitrios Athanasiadis
183	1507	Vehicle-to-Grid Service Potential with Price Based PEV Charging/Discharging	Nima Tehrani
184	1508	Design of an Online Intelligent Alarming System for Cascading Failures of Group of Wind Farms	Jianan Mu
185	1509	Control of the Synchronization and Payback Related to the Provision of Frequency Services by Cold Appliances	Vincenzo Trovato
186	1510	On Using Synchrophasor Data to Assess Power System Steady-State Stability	Reinhard Karl
187	1511	A Hybrid Simulation Method for EVs' Operation considering Power Grid and Traffic Information	Shujun Xin
188	1512	Development of a Three Phase Unbalanced Continuation Power Flow Tool	Leslie Corson
189	1513	A Simultaneous Perturbation Approach for Solving Economic Dispatch Problems with Emission Storage and Network Constraints	Yu Xia
190	1514	Distributed Energy Management under Smart Grid Plug-and-Play Operations	Yuan Zhang
191	1515	Heuristic Approach to Resource Allocation in the Emerging Smart Grid	Timothy Hansen
192	1516	Voltage Assessment in Smart Grids Involving Distributed Generation	Ahmed Mohamed
193	1517	PHEV Home-Charging Model Based on Residential Activity Patterns	Pia Grahm
194	1518	Power Sharing Control with Frequency Droop in a Hybrid Microgrid	Megha Goyal
195	1519	Look-Ahead Energy Management of a Grid-Connected Residential PV System under Critical Peak Pricing Programs	Jaeyeong Yoo
196	1520	Demand Response as a Tool for Coordinated Charging of PHEV Parking Garages	Satish Kasani

16. Smart Sensors, Communication and Control in Energy Systems

Page #	Poster Board #	Title of Poster	Student Name
197	1601	Distributed Data Fusion for State Estimation in Cyber Physical Energy Systems	Abhinav Kumar Singh
198	1602	Control Strategies of Micro Sources in Microgrid	Xin Wang
199	1603	A Robust Multi-Objective Controller of VSC-Based DC-Voltage Power Port in Hybrid AC/DC Microgrids	Masoud Davari
200	1604	Hardware Design of Smart Home Energy Management System with Dynamic Price Response	Qinran Hu
201	1605	Smart Meter Deployment and Applications in the United States	Megan Milam

17. Substation and Distribution Automation

Page #	Poster Board #	Title of Poster	Student Name
202	1701	Distribution Locational Marginal Pricing for Optimal Electric Vehicle Charging Management	Ruoyang Li
203	1702	A Comparative Analysis of Volt-Var Control Algorithms for the Distribution System	Griet Devriese
204	1703	Maximizing the Penetration of Plug-In Electric Vehicles in Distribution Network	Junhui Zhao
205	1704	An Investigation of the Effectiveness of a Network Reconfiguration Experiment at Drexel University	Nicole Segal
206	1705	Standardization of Power System Protection Settings Using IEC 61850 for Improved Interoperability	Qiteng Hong
207	1706	PDC Testing and Characterization of Synchrophasor Based Applications	Jeong Hun Kim

18. Power Engineering Education

Page #	Poster Board #	Title of Poster	Student Name
208	1801	Action Research for Power System Engineering Education	Mostafa Farrokhbadi

Harmonic impact of LED lamps and PV panels

Yang Wang, *Student Member, IEEE*

Department of Electrical and Computer Engineering, University of Alberta, Edmonton, AB, Canada
Email: yang5@ualberta.ca

Abstract— Power electronic technology has been widely employed in renewable energy systems, like photovoltaic(PV) generation systems, wind generation systems; in home appliances, like compact fluorescent lamps (CFLs), LED lamps, microwaves. However, power electronic based devices are harmonic polluters, which could inject a relatively large amount of harmonics into the power grid relative to their power demand. This poster presents a study of the harmonic current characteristics of two kinds of LED lamps and a photovoltaic panel. Equivalent CFL index is used to compare the harmonic effects of different harmonic sources and to quantify their relative severity. On the other hand, the poster introduces the concern for high frequency components in LED lamps and PV panels.

I. KEY EQUATIONS

For each harmonic order h , the ratio of the harmonic source's current to that of the representative CFL current is determined by using the following equation:

$$Ratio_{h_HS} = \frac{I_{h_HS}}{I_{h_CFL}} \quad (1)$$

The ratios of different harmonic orders are aggregated into one value by using a weighted average as follows:

$$Equivalent - CFL_{HS} = \sqrt{\sum_{h=3}^H (w_h \times Ratio_{h_HS})^2} = \sqrt{\frac{\sum_{h=3}^H I_{h_HS}^2}{\sum_{h=3}^H I_{h_CFL}^2}} \quad (2)$$

II. KEY FIGURES

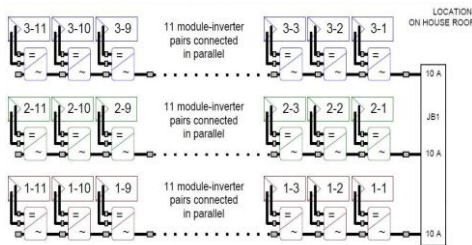


Fig.1 Single-line diagram of the measured PV system



Fig.2 Measurement for LED lamps

III. KEY RESULTS

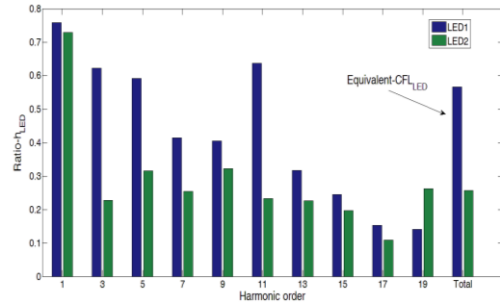


Fig.3 Harmonic current ratios of LED lamps

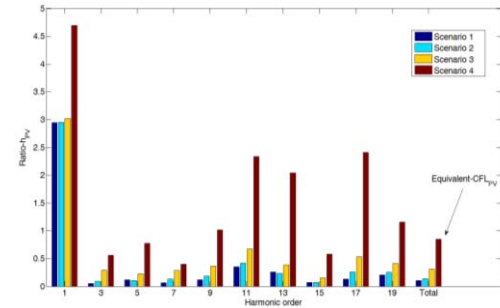


Fig.4 Harmonic current ratios of PV panels in different conditions(per 100W)

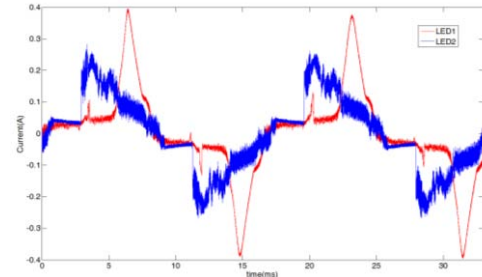


Fig.5 high frequency components in LED lamps

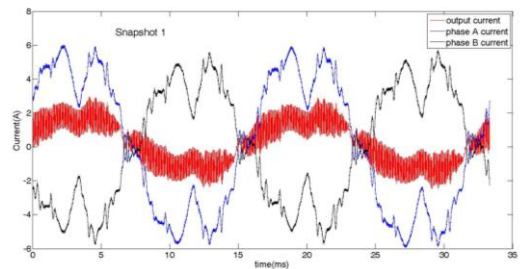


Fig.6 high frequency components in PV circuit current

Trajectory Sensitivities: Applications in Power Systems and Estimation Accuracy Refinement

Lei Tang and James McCalley
 Dept. of Electrical and Computer Engineering
 Iowa State University
 Ames, IA, USA
 ltang@iastate.edu and jdm@iastate.edu

Abstract—This poster first briefly summarizes the state-of-the-art work of trajectory sensitivity applications in various areas of power systems. Through linearizing the system along the nominal trajectories, trajectory sensitivities can estimate the trajectory deviations after small parameter change, but will inevitably cause estimation error due to system nonlinearity. Two strategies are proposed in this poster to refine the estimation accuracy in situations when the error is unacceptable. These two strategies are second order trajectory sensitivities and switching operating states method. The two strategies have been tested on New England 39-bus system. The results prove their validity.

Index Terms—Dynamic security assessment, trajectory sensitivity, accuracy refinement, second order trajectory sensitivities, switching operating states method

I. KEY EQUATIONS

$$\begin{aligned} \Delta z(t) &= \frac{\partial z}{\partial t_{cl}}(t)\Delta t_{cl} + \frac{1}{2!} \frac{\partial^2 z}{\partial t_{cl}^2}(t)\Delta^2 t_{cl} + \text{higher order terms} \\ &\approx \frac{\partial z}{\partial t_{cl}}(t)\Delta t_{cl} + \frac{1}{2} \frac{\partial^2 z}{\partial t_{cl}^2}(t)\Delta^2 t_{cl} \end{aligned} \quad (1)$$

$$\Rightarrow z_{t_{cl}}(t)\Delta t_{cl} + \frac{1}{2} z_{2t_{cl}}(t)\Delta^2 t_{cl} \quad (t \geq t_{cl}).$$

$$\begin{aligned} \dot{x}_{2\lambda} &= (f_{2x}x_\lambda + f_{xy}y_\lambda + f_{x\lambda})x_\lambda + (f_{yx}x_\lambda \\ &\quad + f_{2y}y_\lambda + f_{y\lambda})y_\lambda + f_{2\lambda} + f_x x_{2\lambda} + f_y y_{2\lambda} \end{aligned} \quad (2)$$

$$\begin{aligned} 0 &= (g_{2x}x_\lambda + g_{xy}y_\lambda + g_{x\lambda})x_\lambda + (g_{yx}x_\lambda \\ &\quad + g_{2y}y_\lambda + g_{y\lambda})y_\lambda + g_{2\lambda} + g_x x_{2\lambda} + g_y y_{2\lambda}. \end{aligned} \quad (3)$$

$$\begin{aligned} x_{2\lambda}^{k+1} &= x_{2\lambda}^k + \frac{\eta}{2} [(f_{2x}^k x_\lambda^k + f_{xy}^k y_\lambda^k + f_{x\lambda}^k) x_\lambda^k \\ &\quad + (f_{yx}^k x_\lambda^k + f_{2y}^k y_\lambda^k + f_{y\lambda}^k) y_\lambda^k \\ &\quad + f_{2\lambda}^k + f_x^k x_{2\lambda}^k + f_y^k y_{2\lambda}^k \\ &\quad + (f_{2x}^{k+1} x_\lambda^{k+1} + f_{xy}^{k+1} y_\lambda^{k+1} + f_{x\lambda}^{k+1}) x_\lambda^{k+1} \\ &\quad + (f_{yx}^{k+1} x_\lambda^{k+1} + f_{2y}^{k+1} y_\lambda^{k+1} + f_{y\lambda}^{k+1}) y_\lambda^{k+1} \\ &\quad + f_{2\lambda}^{k+1} + f_x^{k+1} x_{2\lambda}^{k+1} + f_y^{k+1} y_{2\lambda}^{k+1}] \end{aligned} \quad (4)$$

$$\begin{aligned} 0 &= (g_{2x}^{k+1} x_\lambda^{k+1} + g_{xy}^{k+1} y_\lambda^{k+1} + g_{x\lambda}^{k+1}) x_\lambda^{k+1} \\ &\quad + (g_{yx}^{k+1} x_\lambda^{k+1} + g_{2y}^{k+1} y_\lambda^{k+1} + g_{y\lambda}^{k+1}) y_\lambda^{k+1} \\ &\quad + g_{2\lambda}^{k+1} + g_x^{k+1} x_{2\lambda}^{k+1} + g_y^{k+1} y_{2\lambda}^{k+1}. \end{aligned} \quad (5)$$

$$\begin{bmatrix} \frac{\eta}{2} f_x - I & \frac{\eta}{2} f_y \\ g_x & g_y \end{bmatrix} \begin{bmatrix} x_{2\lambda}^{k+1} \\ y_{2\lambda}^{k+1} \end{bmatrix} = \begin{bmatrix} P_1(x^k, y^k, x^{k+1}, y^{k+1}) \\ P_2(x^k, y^k, x^{k+1}, y^{k+1}) \end{bmatrix}. \quad (6)$$

II. KEY RESULTS

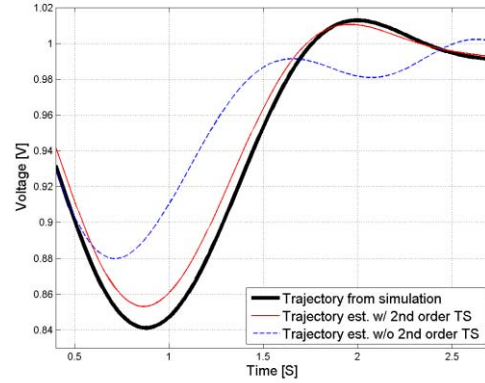


Figure 1 Worst case bus voltage comparison for SOTS

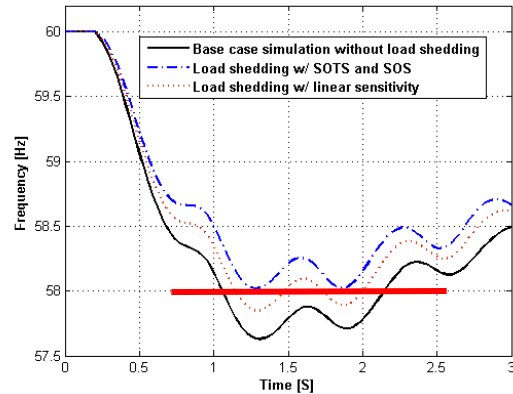


Figure 2 Frequency of generator 39

A Novel Approach for Ringdown Detection Using Extended Kalman Filter

Mehrdad Yazdaniyan, and Ali Mehrizi-Sani

School of Electrical Engineering and Computer Science, Washington State University, Pullman, WA, USA.
e-mails: m.yazdaniyan@email.wsu.edu, mehrizi@eeecs.wsu.edu.

Abstract—Estimation of electromechanical modes has attracted attention during past few decades because the estimation of these modes provides vital information about the stability of the power system. A new state-space model is developed for online detection of a ringdown signal using extended Kalman filter (EKF). The proposed model not only can estimate constant parameters, but it also can track time-varying parameters. Simulation results demonstrate the desirable performance of the proposed method for ringdown parameter estimation.

I. PROBLEM STATEMENT

ELECTROMECHANICAL oscillations are among the inherent characteristics of large interconnected power systems and the parameters of these oscillations have vital information about modes of the power systems. As a result, online identification of these parameters assists in determining power system stability in real-time and preventing system instabilities and blackouts.

This paper addresses ringdown detection in the presence of noise using an extended Kalman filter (EKF). The ringdown data can be expressed as the sum of exponentially damped sinusoids (EDS). These signals can be described as follows:

$$y(t) = \sum_{i=1}^N A_i e^{-\sigma_i t} \cos(\omega_i t + \phi_i) + n(t) \quad (1)$$

where A_i , σ_i , ω_i , and ϕ_i are real and unknown and $n(t)$ is a zero-mean white Gaussian noise. The aim of this paper is to develop a new approach to estimate σ_i and ω_i parameters using extended Kalman filter. In this case, both the damping factor and the frequency of the ringdown signal should be estimated simultaneously. These parameter help us to extract vital information about power system stability.

II. KEY EQUATIONS

The proposed state-space model for the ringdown signal is as follow:

$$\begin{aligned} x_{4i-3}(k+1) &= e^{-x_{4i}(k)} (\cos(x_{4i-1}(k))x_{4i-3}(k) \\ &\quad - \sin(x_{4i-1}(k))x_{4i-2}(k)) + w_{4i-3}(k) \\ x_{4i-2}(k+1) &= e^{-x_{4i}(k)} (\sin(x_{4i-1}(k))x_{4i-3}(k) \\ &\quad + \cos(x_{4i-1}(k))x_{4i-2}(k)) + w_{4i-2}(k) \\ x_{4i-1}(k+1) &= x_3(k) + w_{4i-1}(k) \\ x_{4i}(k+1) &= x_{4i}(k) + w_{4i}(k) \end{aligned} \quad (2)$$

and

$$y(k) = \sum_{i=1}^N k_{2i-1}x_{4i-3}(k) + k_{2i}x_{4i-2}(k) + n_k \quad (3)$$

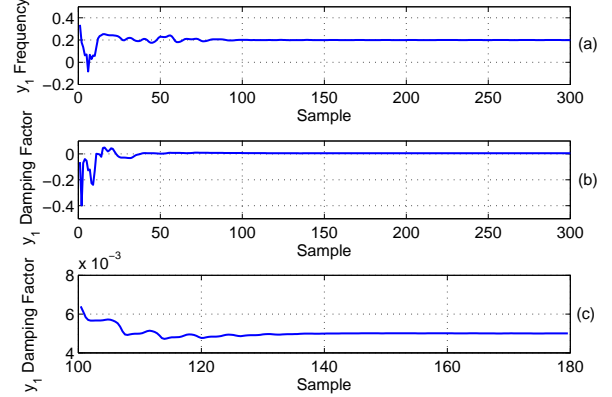


Fig. 1: Parameter estimation of the y_1 .

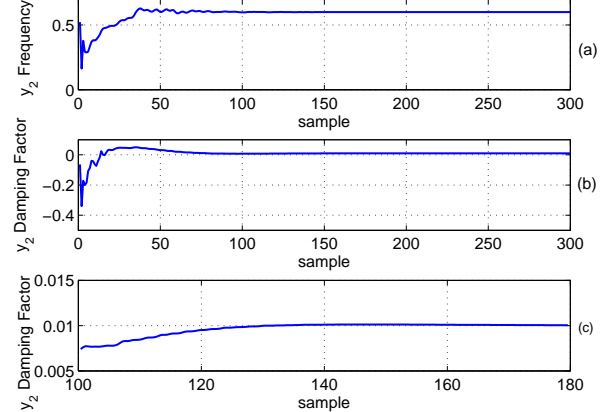


Fig. 2: Parameter estimation of the y_2 .

III. KEY SIMULATION RESULTS

The ability of EKF to estimate the parameters of a ringdown signal composed of two EDS signals is studied in this section. The input signal is

$$\begin{aligned} y(k) &= y_1(k) + y_2(k) \\ y_1(k) &= e^{-0.005k} \cos(0.2k) \\ y_2(k) &= e^{-0.010k} \cos(0.6k). \end{aligned} \quad (4)$$

Optimal PMU Placement for Two Level Linear State Estimation

Ming Meng and Dr. Anjan Bose(Advisor)

The School of Electrical Engineering and Computer Science, Washington State University, Pullman, Washington, USA
ming.meng@email.wsu.edu

Abstract—Phasor measurement unit is used for linear state estimation. Redundant PMU measurement is always desirable for better system observability. However, for large systems, it is impractical to install PMUs at all places, thus an approach for optimizing the PMU placement is presented in this poster. In the two-level state estimator, the PMU measurements are used by substation state estimator. In rare cases when substation cannot perform correctly, those measurements will be sent directly to the control center. The algorithm is based on calculating the rank of the incidence matrix for control center level topology, and finding the optimal PMU placement according to the substation level topology.

I. KEY EQUATIONS

Given a system of n buses and m branches, the linear voltage state function with voltage and current measurements on the branches is

$$\mathbf{z} = \mathbf{H}\mathbf{x} + \mathbf{r}$$

$$\mathbf{z} = \begin{bmatrix} \mathbf{V}_b \\ \mathbf{i}_b \end{bmatrix} \quad \mathbf{H} = \begin{bmatrix} \mathbf{I} \\ \mathbf{Y}_b \end{bmatrix}$$

Complex vector \mathbf{z} of which length is no larger than $n+2m$ contains voltage measurements on buses and current measurements on both ends of transmission lines or transformers. The length of \mathbf{x} is n . \mathbf{I} is identity matrix and \mathbf{Y}_b is the complex admittance matrix for the network.

Control center level PMU placement optimization

$$\min C(p) = c^T p = \sum_{i=1}^{2m} c_i p_i$$

$$\text{s. t. } \text{rank}(\mathbf{Z}) = n - 1$$

In which C represents the total cost of PMU, c is a vector which elements are costs for all PMUs. Since m branches has $2m$ ends, there are $2m$ locations for PMU, p is a binary vector of length $2m$.

$$p_i = \begin{cases} 1, & \text{If PMU is installed on location } i \\ 0, & \text{If PMU is not installed} \end{cases}$$

\mathbf{Z} is an $n \times 2m$ incidence matrix, for a PMU location j on a branch

$$z_{ij} = \begin{cases} 1, & \text{the branch is connected to bus } i \\ 0, & \text{otherwise} \end{cases}$$

The constraint means to find a single observable island that makes all buses observable.

II. KEY FIGURES

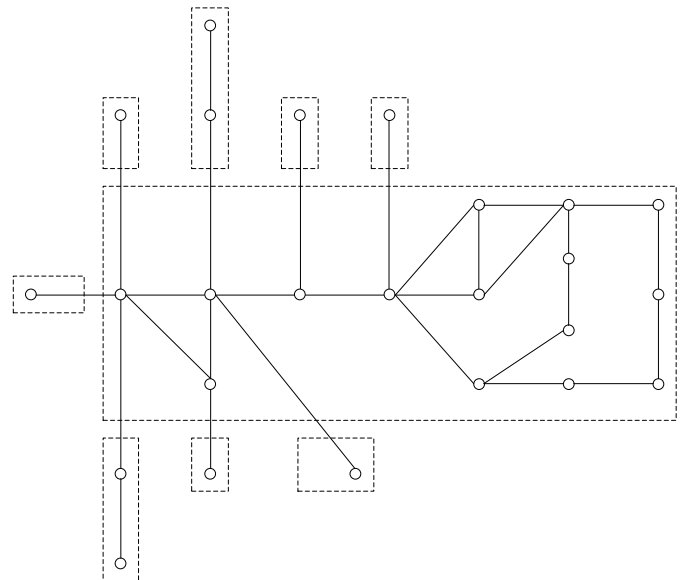


Figure.1 One-line diagram for above 250kv level buses in Idaho area of WECC

III. KEY RESULTS

TABLE I. BRANCHES FOR OPTIMAL PMU PLACEMENT

From Bus	To Bus	ID
BOISEBCH	CALDWELL	1
BROWNLEE	HELLSCYN	1
HUNT	MIDPOINT	1
MIDPOINT	MIDPOINT	1
ONTARIO	PADDOCK	1
BROWNLEE	OXBOW	1
DRAM	MPSN 1	1
QUARTZTP	QUARTZ&1	1
BROWNLEE	QUARTZTP	1
BOISEBCH	DRAM	1
BOISEBCH	PADDOCK	&1
BROWNLEE	PADDOCK	1
KINPORT	MIDPOINT	1
KINPORT	KINPT MP	1
BORAH	BORAH &1	1
BORAH	BRIDGER	&1
ADELAIDE	MIDPOINT	2
ADELAIDE	ADEL TAP	1
BORAH	ADEL TAP	1
BOISEBCH	MIDPOINT	&2
MIDPOINT	ADEL TAP	1
KINPORT	BRIDGE&2	1
BOISEBCH	BROWNLEE	&3
BRADY	KINPORT	1

Voltage Instability Protection in Power Systems

Nataliia Petryshyn, *Student Member, IEEE* and Ramakrishna (Rama) Gokaraju, *Member, IEEE*
 Department of Electrical and Computer Engineering, University of Saskatchewan, Saskatoon, SK, Canada
 Email: nataliia.petryshyn@usask.ca and rama.krishna@usask.ca

Abstract — The number of voltage instability incidents worldwide has increased. In most of the cases voltage collapse occurred after several minutes of initiation of the disturbance, so ability to predict this kind of event is extremely important. One of the existing mathematical methods, tested in this research, is based on calculation of the Improved Voltage Instability Monitoring Index (IVIMI) using Phasor Measurement Units (PMUs) data. It is able to detect the impending voltage instability at an early stage, which can facilitate the system operator to initiate some emergency control action for retaining the system stability. Application of the index has been carried out on the IEEE 39-bus New England System with the usage of Power System Analysis Toolbox (PSAT). Another method under study is defining Voltage Stability Margin (VSM) in the weak busses of the power system using the equivalent system representation at those busses. The system operator can be provided with useful information about how much load can be added to the bus before the system suffers voltage instability. Results from VSM, implemented on the IEEE 39-bus system, are verified by comparing it with continuous load flow data and graphical representation of the P-V curve method.

I. KEY EQUATIONS

IVIMI method, proposed in [3], is briefly summarized below:

$$IVIMI_i = w_1(i) \times \frac{VDR_i}{VDR_{max}} + w_2(i) \times \frac{CVD_i}{CVD_{max}} \quad (1)$$

$$w_1(i) + w_2(i) = 1 \quad (2)$$

$$VDR_i = V_{ref} - V_i \quad (3)$$

$$VDR_{max} = \min\{V_n\} - V_{min} \quad (4)$$

$$CVD_i = V_{i-1} - V_i \quad (5)$$

CVD_{max} of the system can be obtained by tracking the maximum of the CVD_i until any of the bus voltages falls below the V_{min} .

The VSM method [4] can define how close the system is to voltage collapse. With the use of equivalent system representation:

$$P_R = \frac{E_s E_R}{X} \sin \delta \quad (6)$$

$$Q_R = \frac{E_s E_R \cos \delta - E_R^2}{X} \quad (7)$$

At the maximum loading point (nose point) $dQ/dV = 0$.

$$V_L = \frac{Q}{\sqrt{(4Q^2 + P^2)}} \quad (8)$$

$$\text{Voltage Margin} = E_R - V_L \quad (9)$$

Where V_L is voltage at reference bus R at nose point, E_R is the present bus voltage.

II. KEY RESULTS

The IEEE 39-bus system model was modified by replacement of PQ loads with ZIP loads and the usage of IEEE Type 1 rotation excitation system. At $t=10$ s, the load was increased continuously at the rate of 0.005 p.u. MVA/sec. At $t=179$ s, the system experienced voltage collapse, shown in Figure 1.

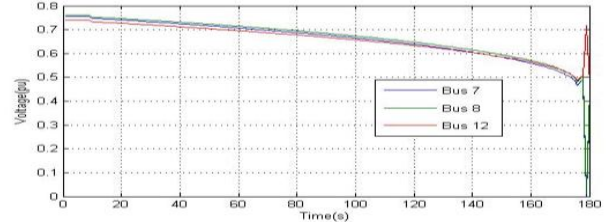


Figure 1 - Bus voltages for load increase

The IVIMI method for all the load busses in the system is depicted by Figure 2. The critical load busses, at the point where $IVIMI = 1$, have been found to be Bus 7, Bus 8 and Bus 12. $IVIMI$ at Bus 7 reaches the value of 1 at $t=86.7$ s, which gives us a voltage collapse prediction time of 92.3 s.

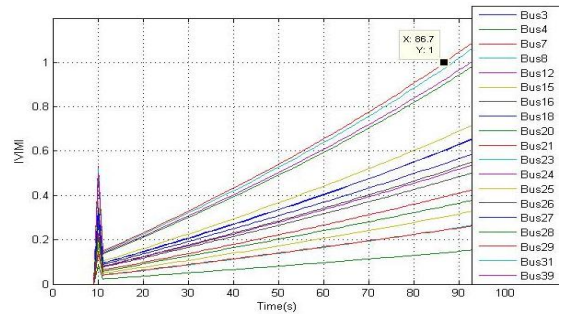


Figure 2 - IVIMI plot for load increase

Voltage Margin method has been applied to the system's weakest Bus 7. The results have been verified with the use of P-V curve by increasing the load factor to its maximum (nose) point ($K=2.3589$, $V=0.4276$) which is shown on Figure 3.

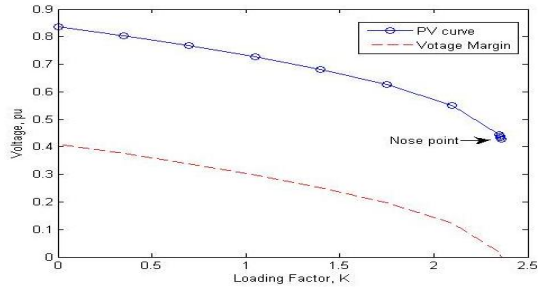


Figure 3 - P-V curve and voltage margin for the critical load bus 7

REFERENCES

- [1] Walter A. Elmore. Protective Relaying Theory and Applications. Marcel Dekker, Inc., New York, Basel, 2004.
- [2] Jan Machowski, Janusz W. Bialek and James R. Bumby. Power System Dynamics: Stability and Control. John Wiley & Sons, Ltd., UK, 2008.
- [3] Ranjana Sodhi, S C Srivastava and S N Singh, "A Simple Scheme for Wide Area Detection of Impending Voltage Instability", IEEE Transactions on Smart Grid, Vol.2, No. 3, pp 818-827, June 2012.
- [4] L. Neerugattu and G.S Raju, "New criteria for voltage stability evaluation in interconnected power system", National Power System Conference, Indian Institute of Technology (IIT-BHU), Varanasi, India, paper id: 12074, December 12-14, 2012 (In cd-rom).

Dynamic Reserve Zones for Distinct Scenarios

Joshua Lyon¹, *Student Member, IEEE*, Muhong Zhang¹, and Kory W. Hedman², *Member, IEEE*

¹Department of Industrial Engineering, Arizona State University, Tempe, AZ 85287, USA

²School of Electrical, Computer, and Energy Engineering, Arizona State University, Tempe, AZ 85287, USA

Email: joshua.lyon@asu.edu and kory.hedman@asu.edu

Abstract— The security constrained unit commitment problem schedules power generators to minimize cost subject to operating constraints. Reserve requirements ensure reserve is available to re-balance the system following a contingency but are generally not enough to guarantee reliability in congested systems when reserve activation is limited by congestion. Reserve zones are used to ensure local reserves but do not perfectly characterize reserve deliverability. To overcome the limitations of traditional reserve zones, operators end up procuring more reserve than is necessary at significant operational costs. We propose an alternative method designed to complement traditional reserve zones. We define a separate zone for individual scenarios that captures how congestion is likely to inhibit reserve deliverability for that scenario. The methodology identifies generators that are not allowed to contribute to the requirement for a *particular* scenario due to their location. This reserve zone methodology can be characterized as a generalized reserve down flag procedure. These reserve down flags are dynamic in that they change from period-to-period, i.e., they adjust when it is necessary for them to reflect changes in congestion patterns. We propose a two-stage decomposition algorithm for simultaneously updating the generalized reserve down flags while solving unit commitment. The proposed method is tested on a modified IEEE 73-bus test case and compared to stochastic programming and traditional reserve requirements. This work is based on [1].

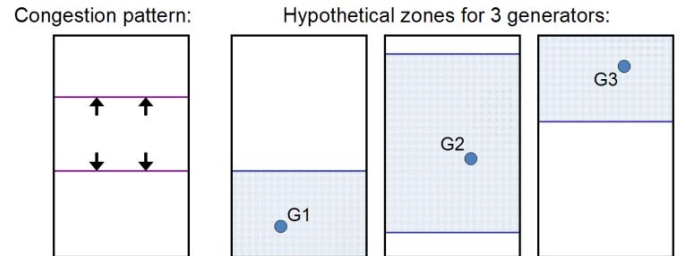


Fig. 2. Graphical interpretation of proposed zone format (one zone per contingency).

III. METHODOLOGY

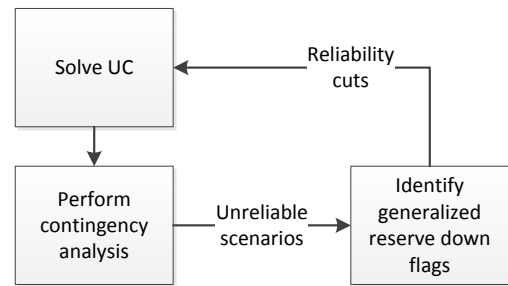


Fig. 3. Decomposition algorithm for day-ahead UC.

I. KEY EQUATIONS

Traditional reserve requirements, for each zone:

$$R \geq C - I + M \quad (1)$$

where R is the reserve quantity, C is the desired level of protection (e.g., the largest contingency for $N-1$), I is the import capability, and M is a reserve margin.

II. KEY FIGURES

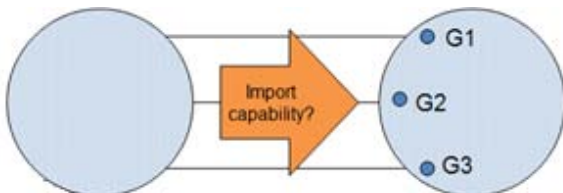


Fig. 1. Limitations of traditional reserve requirements.

IV. KEY RESULTS

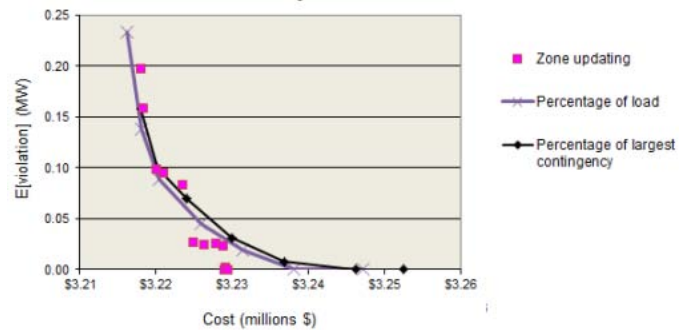


Fig. 4. Cost vs. reliability over iterations compared to baseline policies.

V. REFERENCES

- [1] J. D. Lyon, M. Zhang, and K. W. Hedman, "Dynamic reserve zones for distinct scenarios," *IEEE Trans. Power Syst.*, in preparation, Mar. 2013.

Study of Artificial Neural Network Based Short Term Load Forecasting

Ashton Webberley

Department of Electrical and Computer Engineering
University of Denver
Denver, USA
Ash.Webberley@du.edu

David Wenzhong Gao

Department of Electrical and Computer Engineering
University of Denver
Denver, USA
Wenzhong.Gao@du.edu

Abstract—With more and more renewable energy integrated into the power grid and demand response in smart grid environment, electric load forecasting becomes more important. Accurate load forecasting facilitates better renewable energy integration and electricity market operation. Over the years, different load forecasting methods have been developed and applied. Multiple linear regression and artificial neural network based methods are well accepted by industries. This paper focuses on ANN-based method and provides detailed steps of load forecasting including data processing and neural network design.

I. KEY EQUATIONS

To measure the accuracy of the Neural Network prediction, the following equations were used.

$$r = A_L - P_L \quad (1)$$

$$MAPE = \frac{1}{n} \sum_{L=1}^n \left| \frac{r}{100A_L} \right| \quad (2)$$

where A_L is the actual load, P_L is the predicted load value, and n is the number of forecast loads.

II. KEY FIGURES

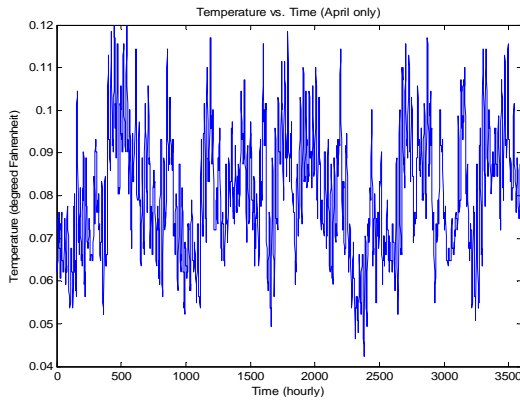


Figure 1: All the temperature points in four April months concatenated into one time frame

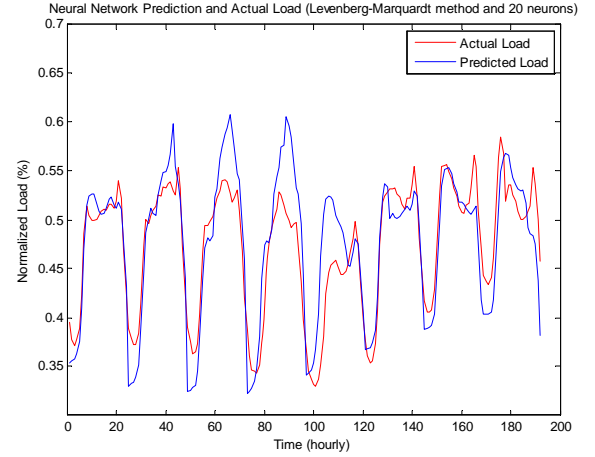


Figure 2: The actual load and the predicted load by the ANN model

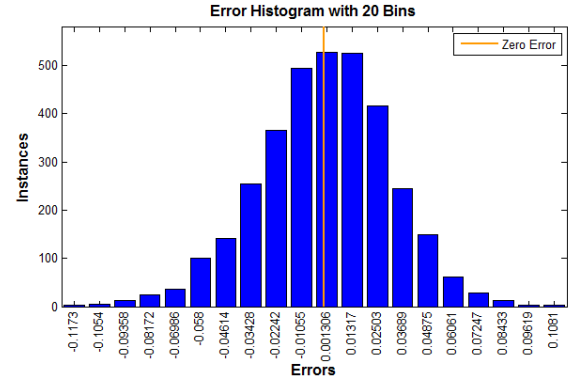


Figure 3: The Error Histogram of ANN model

III. KEY RESULTS

Number of Neurons	Levenberg-Marquardt Method	Bayesian Regularization Method
10	7.3985	5.7448
20	6.1636	9.2831
30	8.5008	7.6287

Hour-ahead Corrective Topology Control for Intermittent Renewables and N-1 Contingencies

Mojdeh Abdi Khorsand, *Student Member, IEEE*, and Kory W. Hedman, *Member, IEEE*
 School of Electrical, Computer, and Energy Engineering, Arizona State University, Tempe, AZ 85287, USA
 Email: mabdikho@asu.edu and kory.hedman@asu.edu

Abstract— The growth in variable renewable resources in the electric power grid has been significant worldwide recently and the fast growth is expected to continue. In order to overcome the uncertainties associated with renewables without sacrificing reliability, the operator should acquire additional reserve. However, simply procuring additional reserves does not guarantee reliability as the locations of the reserves are critical due to network congestion. The same problem exists today for N-1 contingencies, i.e., traditional reserve requirement modeling does not adequately emphasize the location of the reserves. With the growing dependence on variable and uncertain renewable resources, ensuring a continuous supply of electric power will become even more challenging as predicting the available transfer capabilities throughout the grid will be heavily dependent on the stochastic nature of such renewable resources. Frequently, there are conditions where the acquired reserves, in day-ahead and hour-ahead scheduling problems, are not fully deliverable due to network congestion. Instead of procuring additional *local* reserves, the operator can harness the flexibility in the transmission topology via topology control in order to enhance the transfer capability across the transmission grid. Topology control is a form of power flow control as it changes the flows on transmission lines, which allows the operator to choose a different topology in order to avoid line overloads. This added flexibility via topology control, thus, translates into providing more options in regards to dispatch solutions, which reduces the operational costs. Topology control also provides the ability to control post-contingency line flows and, thus, it can be and currently is used today as a corrective mechanism in order to respond to disturbances. An hour-ahead corrective topology control method is presented in this paper. Using this model, the operators would be able to identify potential corrective topology control actions at the hour-ahead time stage and then evaluate these potential corrective actions in real-time with a security assessment tool. First, a traditional (deterministic) hour-ahead unit commitment model is solved; in the next step, contingency analysis (select N-1 contingencies combined with wind scenarios) is conducted to verify if the hour-ahead unit commitment solution is reliable. The objective of this stage is to determine if it is possible to satisfy all (or select) N-1 contingencies and the wind scenarios without any constraint violations (e.g., load shedding). If there are constraint violations, then appropriate uneconomic adjustments must be made to the hour-ahead market solution in order to produce a reliable dispatch. The proposed contingency analysis framework has been extended to incorporate corrective topology control, (1)-(11), in order to reduce the constraint violations and,

hence, the need for costly uneconomic adjustments. All of the proposed corrective topology control solutions are stored in a look-up table to be used by a real-time security assessment tool. The proposed hour-ahead framework is tested on the IEEE 118-bus system.

I. KEY EQUATIONS

$$\text{Min } \sum_{n \in N} S_n \quad (1)$$

Subject to:

$$\sum_{g \in G(n)} P_g - \sum_{k \in KO(n)} P_k + \sum_{k \in KI(n)T_n} P_k + \sum_{w \in W(n)} P^w = d_n - s_n, \forall n \in N \quad (2)$$

$$P_k - b_k(\theta_{to} - \theta_{from}) + M_k(1 - Z_k Nl_k) \geq 0, \forall k \in K \quad (3)$$

$$P_k - b_k(\theta_{to} - \theta_{from}) - M_k(1 - Z_k Nl_k) \leq 0, \forall k \in K \quad (4)$$

$$P_g^{\min} U_g Nl_g \leq P_g \leq P_g^{\max} U_g Nl_g, \forall g \in G \quad (5)$$

$$-P_k^{\max} Z_k Nl_k \leq P_k \leq P_k^{\max} Z_k Nl_k, \forall k \in K \quad (6)$$

$$P_g - P_g^{\text{Scheduled}} Nl_g \leq R_g^+ U_g Nl_g, \forall g \in G \quad (7)$$

$$P_g^{\text{Scheduled}} Nl_g - P_g \leq R_g^- U_g Nl_g, \forall g \in G \quad (8)$$

$$0 \leq P^w \leq P_w^{\text{Forecasted}}, \forall w \in W \quad (9)$$

$$U_g = U_g^{\text{Scheduled}}, \forall g \in G^{\text{Slow}} \quad (10)$$

$$\sum_{k \in K} (1 - Z_k) \leq 1 \quad (11)$$

II. METHODOLOGY

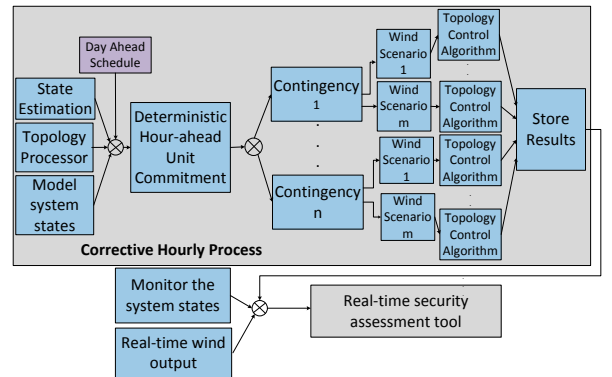


Figure 1. Hour-ahead corrective topology control

References

- [1] K. W. Hedman, R. P. O'Neill, E. B. Fisher, and S. S. Oren, "Optimal transmission switching with contingency analysis," *IEEE Trans. Power Syst.*, vol. 24, no. 3, pp. 1577 - 1586, Aug. 2009.

Robust Corrective Topology Control

Akshay S. Korad and Kory W. Hedman

School of Electrical, Computer, and Energy Engineering, Arizona State University, Tempe, AZ 85287, USA

Email: korad@asu.edu and Kory.Hedman@asu.edu

Abstract— Corrective topology control schemes are an essential part of grid operations and are used to improve the reliability of the grid as well as the operational efficiency. Today, the topology control schemes are established based on the operator's past knowledge of the system or based on rule-of-thumb methods. In this poster, the robust corrective topology control methodology is presented, which provides a systematic approach to respond to grid disturbances by utilizing the flexibility in the transmission network. The proposed methodology incorporates the uncertainty of wind through an uncertainty set and ensures N-1 feasibility by combining generation re-dispatch with topology control. The benefit of incorporating robust optimization into the corrective switching framework is that the switching solution is guaranteed to be feasible for a range of system operating states. The robust model can be solved offline to suggest switching actions that can be used in a dynamic security assessment tool in real-time. The proposed robust topology control algorithm can also generate multiple corrective switching actions for a particular contingency. The robust topology control formulation is tested on an IEEE-118 bus test case with different uncertainty sets. The robust topology control formulation is based on a DCOPF. Therefore, solutions obtained from the DCOPF based robust topology control algorithm are checked for AC feasibility.

I. KEY EQUATIONS

The generic form of robust topology control formulation is given in (1)-(6), which is a two part optimization problem.

$$\begin{aligned} \min_{x \in X} & (c^T x + \max_{w \in W} b^T y(w)) & (1) \\ \text{s.t.} & Fx \leq f, & (2) \\ & Hy(w) \leq h, & (3) \\ & Ax + By(w) \leq g, & (4) \\ & Ey(w) = d, & (5) \\ & x \in \{0,1\} & (6) \end{aligned}$$

II. KEY FIGURES

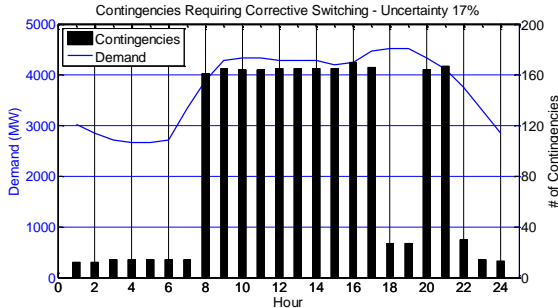


Figure 1. Number of contingencies requiring corrective switching in order to avoid load shedding.

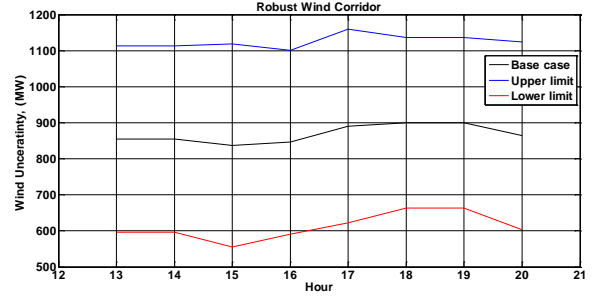


Figure 2. Robust wind corridor for wind integration.

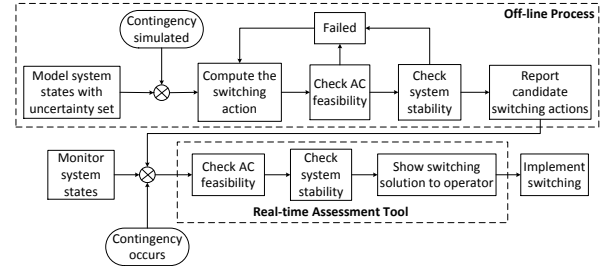


Figure 3. Robust corrective topology control methodology.

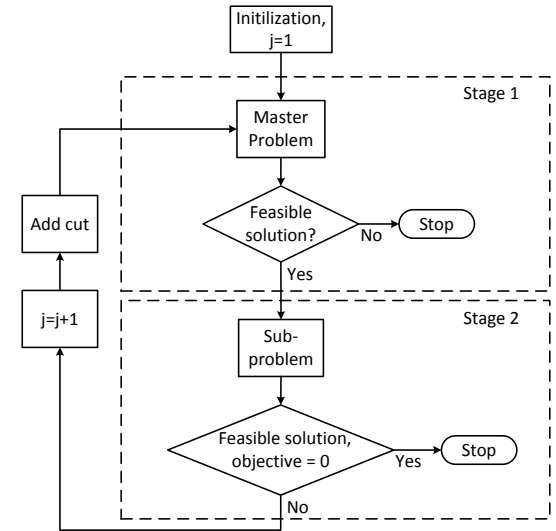


Figure 4. Solution method for robust corrective topology control.

A Parallelizable Greedy Algorithm for Transmission Switching

Mostafa Sahraei-Ardakani, *Graduate Student Member, IEEE*, and Kory W. Hedman, *Member, IEEE*
 School of Electrical, Computer, and Energy Engineering, Arizona State University, Tempe, AZ 85287, USA
 Email: mostafa@asu.edu and kory.hedman@asu.edu

Abstract— Optimal Transmission Switching (OTS) is a Mixed-Integer Program (MIP). With thousands of transmission assets in electric power systems, the number of potential switching solutions is extremely high, making the problem computationally expensive. It is currently not practical to solve the MIP in short-term applications due to the combinatorial nature of the problem. Previous research has proposed a rather fast heuristics to find near optimal solution for the OTS problem without solving the actual MIP, [1]. This prior heuristic is extended to include the ability to switch lines out of service as well as to identify lines to switch back into service. The proposed heuristic is then parallelized using high performance computing resources to significantly improve the computational time of the problem. Using the outputs of a simple DC optimal power flow, the values of both in service and out of service lines are calculated. Based on the calculated values, lines are ranked according to the expected savings they would provide if switched. P best candidates from the rank list are selected and sent to P parallel processors to be evaluated. The P potential switching actions are checked to see if they satisfy AC feasibility as well as whether the switching action causes instability. The potential switching actions that pass the AC and stability checks are then compared based on their actual cost savings. The best solution is picked and the topology is updated. This process is repeated until no further improvement is achieved. Using this sensitivity based heuristic and parallel programming techniques, the computational cost of the problem is significantly reduced. Such reduction in computational time is critical for very short-term applications such as real-time or hour-ahead markets. This poster will present efficiency results corresponding to the transmission switching cost savings and it will present computational results corresponding to the speed up factor of the parallelized greedy algorithm relative to the number of processors.

I. KEY EQUATIONS

The following equations determine the marginal value of switching actions for lines in and out of service. The ranking list in each stage of the algorithm is formed based on these values.

$$\gamma_k^{os} = B_k(s_k)(\theta_n - \theta_m) - P_k^{max}(f_k^- + f_k^+) \quad (1)$$

$$\gamma_k^{is} = P_k(LMP_m - LMP_n) \quad (2)$$

γ_k^{is} is the marginal value of switching an in-service line out of service, while γ_k^{os} is the marginal value of switching an out of service line back in. B_k is the susceptance of line k and s_k is the Lagrange multiplier

for the constraint forcing no flow on line k . θ_n is the voltage angle at node n while P is the active power. f_k^- and f_k^+ are the Lagrange multipliers for maximum and minimum flow limits on line k , which are zero for the case when the line is out of service. LMP is the locational marginal price.

II. ALGORITHM

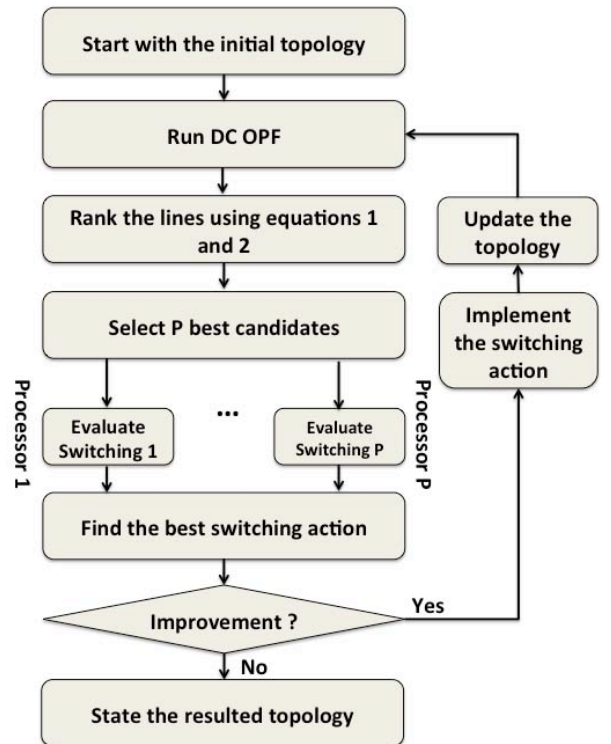


Figure 1. Parallelizable sensitivity-based heuristic for transmission switching

References

- [1] J. D. Fuller, R. Ramasra, and A. Cha, "Fast heuristics for transmission-line switching," *IEEE Trans. Power Syst.*, vol. 27, no. 3, pp. 1377 - 1386, August 2012.

Multi Area State Estimation using Area Slack Bus Angle Adjustment with Minimal Data Exchange

A. Sharma, *Student Member IEEE*, S. C. Srivastava, *Senior Member, IEEE*, and S. Chakrabarti, *Senior Member, IEEE*
 Department of Electrical Engineering, Indian Institute of Technology Kanpur, Kanpur-208016, India
 ankushar@iitk.ac.in, scs@iitk.ac.in, saikatc@iitk.ac.in

Abstract—This paper proposes a new Multi Area State Estimation (MASE) approach, which is suitable for the power system networks that can be divided into several sub-areas. In this approach, the Central Coordinator (CC) utilizes results of one extended sub-area state estimator to estimate the bus angles of the other sub-areas. It has been demonstrated that, with this approach, there is no requirement to share the topology information among the sub-areas and from sub-areas to the central coordinator. Also, with the lesser data exchange, communication bandwidth requirement will reduce. The effectiveness of the proposed method has been demonstrated on IEEE30 bus system and 246-Bus reduced Northern Regional Power Grid (NRPG) Indian system.

I. KEY EQUATIONS

The equations for sub-area level local State Estimator (SE):

$$\mathbf{x}^{k+1} = \mathbf{x}^k + (\mathbf{H}^T \mathbf{R}_z^{-1} \mathbf{H})^{-1} \mathbf{R}_z^{-1} (\mathbf{z} - \mathbf{h}(\mathbf{x}^k)) \quad (1)$$

$$[\mathbf{x}] = [\mathbf{x}^{int^T}, \mathbf{x}_b^{int^T}, \mathbf{x}_b^{ext^T}] \quad (2)$$

The equation for the calculation of area slack bus adjustment:

$$\Delta \theta_{(a-j)} = \theta_{(a-j)}^G - \theta_{(a-j)}^L \quad (3)$$

The equations used to run CC level linear SE:

$$\mathbf{x} = (\mathbf{A}^T \mathbf{R}_{cc}^{-1} \mathbf{A})^{-1} \mathbf{A}^T \mathbf{R}_{cc}^{-1} \mathbf{z} \quad (4)$$

$$\mathbf{R}_{cc} = \text{diag}[\mathbf{R}_{\text{sb}1}, \dots, \mathbf{R}_{\text{sb}i}, \dots, \mathbf{R}_{\text{sb}n}] \quad (5)$$

II. KEY FIGURES

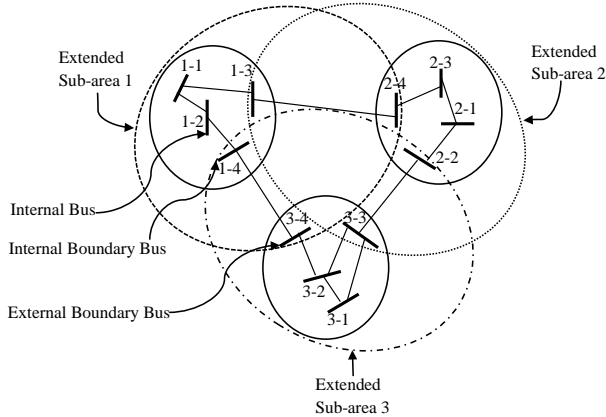


Figure 1. Sample network divided into 3 sub-areas

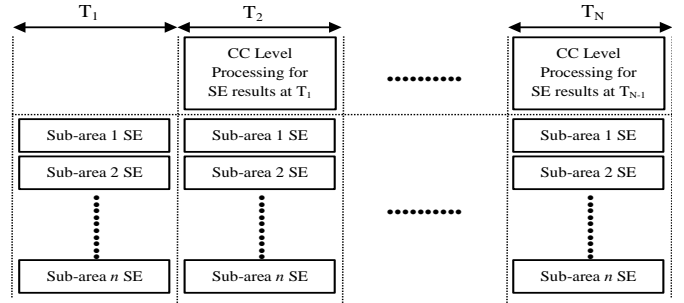


Figure 2. Block diagram showing the SE process at the sub-area level and at the CC level at various time instances

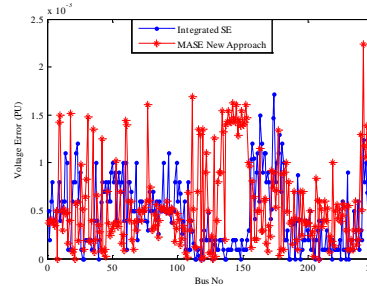


Figure 3. Voltage error in the state estimators for 246-Bus NRPG system

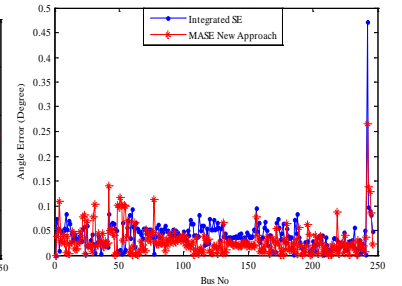


Figure 4. Angle error in the state estimators for 246-Bus NRPG system

III. KEY RESULTS

TABLE I. ERROR COMPARISON OF VARIOUS SE APPROACHES WITH RESPECT TO ACTUAL VALUES

SE Type	Maximum Error ^a		Average Sum of Square Error	
	Voltage	Angle	Voltage	Angle
Integrated SE	2.06×10^{-02}	0.3780	1.648×10^{-04}	0.0380669
Conventional MASE	3.69×10^{-02}	0.9306	1.574×10^{-04}	0.1419794
Proposed MASE	1.03×10^{-02}	0.4017	2.404×10^{-05}	0.0506752

TABLE II. ERROR COMPARISON OF INTEGRATED SE AND PROPOSED MASE WITH RESPECT TO ACTUAL VALUES

SE Type	Maximum Error ^a		Average Sum of Square Error	
	Voltage	Angle	Voltage	Angle
Integrated SE	1.72×10^{-03}	0.4723	3.2838×10^{-07}	2.804×10^{-03}
Proposed MASE	2.24×10^{-03}	0.26613	5.3512×10^{-07}	1.747×10^{-03}

a. Voltage in P.U. and Angle in Degree

A Two-Level Parallel Decomposition Approach for Transient Stability Constrained Optimal Power Flow

Guangchao Geng, Quanyuan Jiang
 College of Electrical Engineering
 Zhejiang University
 Hangzhou, China
 Email: ggc@zju.edu.cn, jqv@zju.edu.cn

Abstract — Transient stability constrained optimal power flow (TSCOPF) is able to reduce costs while keeping the operation point away from the stability boundary. Unacceptable computational time is one of the largest barriers in applying TSCOPF-based solutions. Based on reduced-space interior point method (RIPM), this paper introduces a parallel algorithm with high computing efficiency for multi-contingency TSCOPF problems. A two-level parallelism is developed to fully utilize the computing power of Beowulf clusters equipped with multi-core CPUs. Compute-intensive steps are decomposed according to different contingencies with mathematical equivalent transformations. Distributed computing tasks are accelerated using elemental decomposition on Jacobians, and multithreaded libraries are employed to exploit multi-core CPUs. The effectiveness of the proposed algorithm is benchmarked on a Beowulf cluster with 16 computing nodes with 128 CPU-cores using test cases including up to 2746 buses and 16 contingencies. Numerical results indicate that the proposed parallel approach has great capacity in accelerating TSCOPF solution.

I. KEY EQUATIONS

$$\min_x f(x)$$

$$s.t. \begin{cases} \mathbf{h}(x, \dot{x}) = 0 \\ \underline{\mathbf{g}} \leq \mathbf{g}(x) \leq \bar{\mathbf{g}} \end{cases} \quad \begin{cases} \dot{\delta}_i = \omega_0 \omega_i \\ \dot{\omega}_i = (P_{Gi} - P_{ei} - D_i \omega_i) / M_i \end{cases}$$

II. KEY FIGURES

$$\begin{matrix} \mathbf{h}_b \\ \mathbf{h}_f^1 \\ \vdots \\ \mathbf{h}_f^k \\ \vdots \\ \mathbf{h}_f^{N_f} \end{matrix} \begin{bmatrix} \mathbf{x}_{bc} & \mathbf{x}_{bs} & \mathbf{x}_f^1 & \cdots & \mathbf{x}_f^k & \cdots & \mathbf{x}_f^{N_f} \\ N_b & C_b & 0 & \cdots & 0 & \cdots & 0 \\ N_f^1 & C_b^1 & C_f^1 & \cdots & 0 & \cdots & 0 \\ \vdots & \vdots & \vdots & \ddots & \vdots & \vdots & \vdots \\ N_f^k & C_b^k & 0 & \cdots & C_f^k & \cdots & 0 \\ \vdots & \vdots & \vdots & \ddots & \vdots & \ddots & \vdots \\ N_f^{N_f} & C_b^{N_f} & 0 & \cdots & 0 & \cdots & C_f^{N_f} \end{bmatrix} \begin{matrix} \mathbf{v}_1^k & \mathbf{v}_2^k & \mathbf{v}_{N_T-1}^k & \mathbf{v}_{N_T}^k \\ \Delta \mathbf{f}_1^k & \mathbf{C}_{M,1}^k & & \\ \Delta \mathbf{f}_2^k & \mathbf{C}_{S,2}^k & \mathbf{C}_{M,2}^k & \\ \vdots & \vdots & \vdots & \ddots \\ \Delta \mathbf{f}_{N_T}^k & & & \mathbf{C}_{S,N_T}^k & \mathbf{C}_{M,N_T}^k \end{matrix}$$

Fig.1 Sparse block structures of the Jacobian matrix

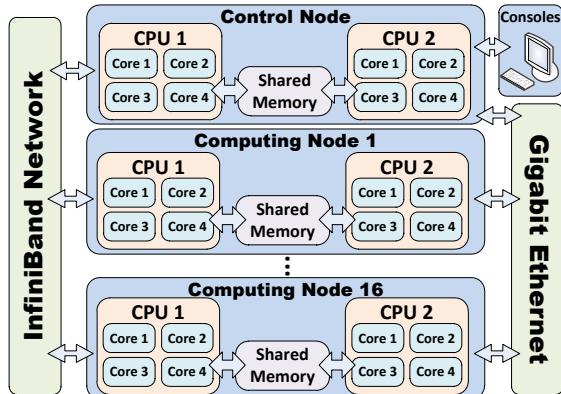


Fig.2 Hardware architecture of the Beowulf cluster used in this paper

III. KEY RESULTS

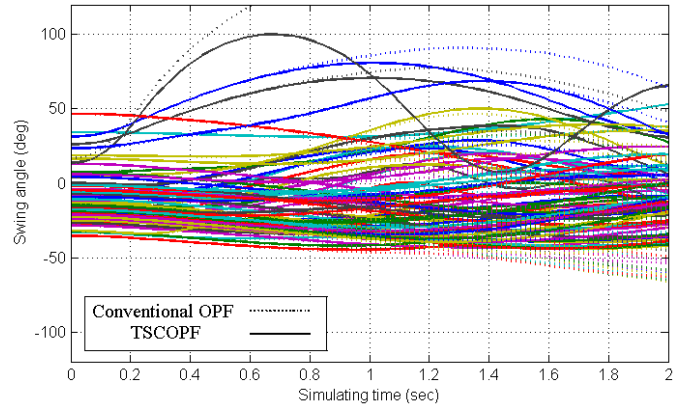


Fig.3 Swing curves for CASE300

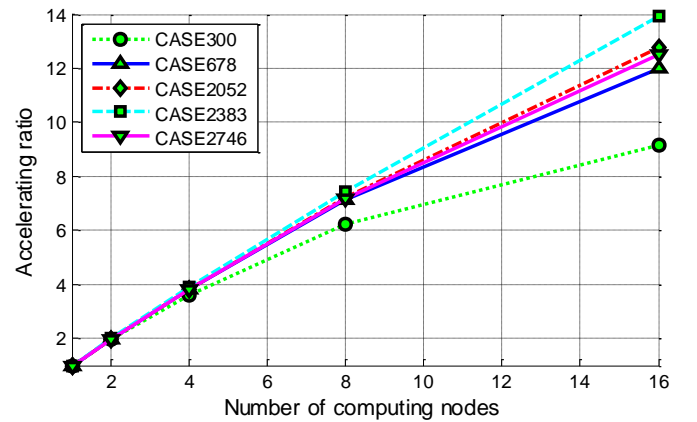


Fig.4 Accelerating ratio for different numbers of computing nodes

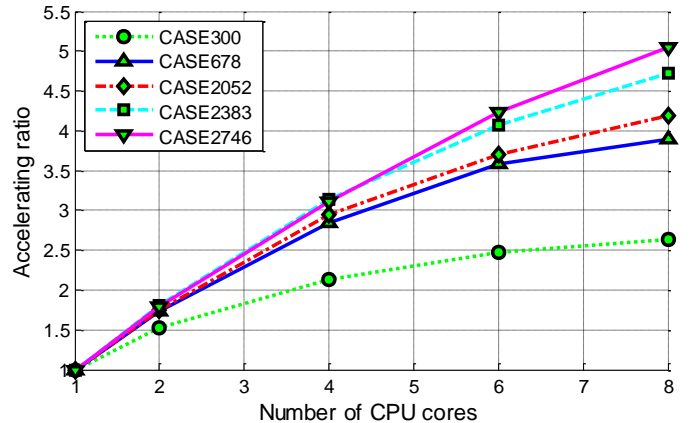


Fig.5 Accelerating ratios for different numbers of CPU cores in each node

A Quadratic Robust Optimization Model for Automatic Voltage Control on Wind Farm Side

Tao Ding, Qinglai Guo, Hongbin Sun, Bin Wang and Fengda Xu
 Department of Electrical Engineering, State Key Laboratory of Power Systems
 Tsinghua University, Beijing 100084, China

Email: dingt12@mails.tsinghua.edu.cn, guoqinglai@tsinghua.edu.cn and shb@tsinghua.edu.cn

Abstract—Connecting high penetration of wind power into power grid usually makes voltage fluctuate, due to the volatile nature of wind power injection. This paper therefore proposes a quadratic robust optimization model to guarantee the voltage of each wind unit within the security region, no matter how the wind power varies. Based on the wind power prediction, the prediction error is regarded as uncertainties, and the robust solution can be found by regulating the reactive power equipment and each wind unit using the duality filter method. In the proposed model, linearized derivation instead of original non-linear expressions in the objective function and constraints has been utilized. Furthermore, inner loop iterative method is introduced to reduce the linearized error, which divides the optimal voltage control into multiple steps with piecewise values and updates the sensitivity at each step, according to different wind farm size and condition. A test system with 36 wind units has been simulated, and the result using Monte Carlo simulation. Comparison with traditional method shows the effectiveness of proposed method.

I. KEY EQUATIONS

The quadratic robust optimization (QROM) model for Automatic Voltage Control on Wind Farm Side can be formulated as:

$$\min_{\Delta Q} \max_{\Delta P} \left\| \sum_{k=1}^n \frac{\partial U_{PCC}}{\partial Q_k} \Delta Q_k + \sum_{l=1}^m \frac{\partial U_{PCC}}{\partial Q_l} \Delta Q_l + \sum_{k=1}^n \frac{\partial U_{PCC}}{\partial P_k} \Delta P_k + U_{PCC}^i - U_{PCC}^{ref} + \eta_{PCC} \right\|_2 \quad (1)$$

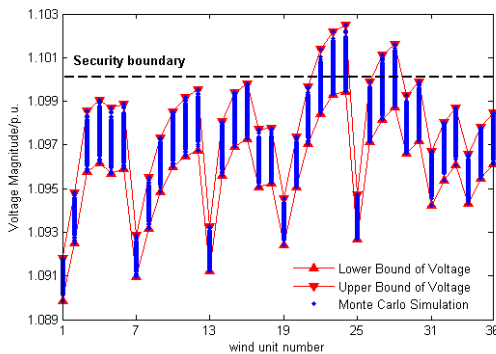
Subject to:

$$U_i \leq \sum_{k=1}^n \frac{\partial U_i}{\partial P_k} \Delta P_k + \sum_{k=1}^n \frac{\partial U_i}{\partial Q_k} \Delta Q_k + \sum_{l=1}^m \frac{\partial U_i}{\partial Q_l} \Delta Q_l + U_i^0 + \eta_i \leq \bar{U}_i \quad (2)$$

$$\underline{\Delta P}_k \leq \Delta P_k \leq \overline{\Delta P}_k \quad (3)$$

$$\underline{\Delta Q}_k \leq \Delta Q_k \leq \overline{\Delta Q}_k \quad (4)$$

$$\underline{\Delta Q}_l \leq \Delta Q_l \leq \overline{\Delta Q}_l \quad (5)$$



(3-a) Monte Carlo for voltage using Non-QROM method

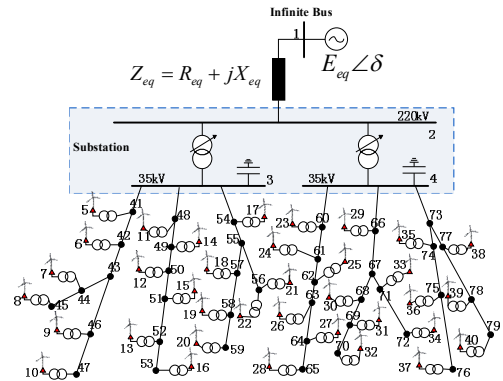
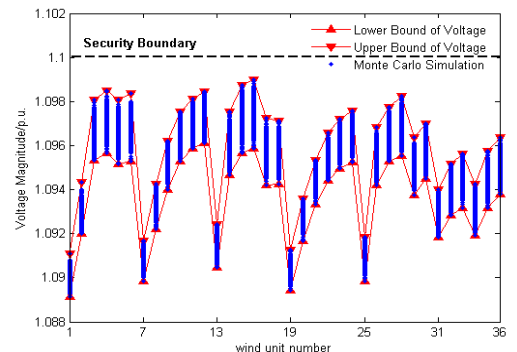


Fig.2 A tested wind farm with 36 wind units

II. KEY FIGURES



(3-b) Monte Carlo for voltage using QROM method

Fig.3 Comparison between QROM and Non-QROM for voltage with random disturbance using Monte Carlo simulation

Security Constrained Unit Commitment with Demand Response

Guodong Liu

Dept. of Electrical Engineering and Computer Science
The University of Tennessee
Knoxville, USA
Email: gliu5@utk.edu

Kevin Tomsovic

Dept. of Electrical Engineering and Computer Science
The University of Tennessee
Knoxville, USA
Email: tomsovic@utk.edu

Abstract—It has been widely accepted that demand response will play an important role in reliable and economic operation of future power systems and electricity markets. Demand response can not only influence the prices in the energy market by demand shifting, but also participate in the reserve market. In this paper, we propose a new model of demand response in which demand flexibility is fully utilized by a price responsive demand bid in energy market as well as spinning reserve market. A co-optimized day-ahead energy and spinning reserve market is proposed to minimize the expected net cost under all credible system states, i.e., expected total cost of operation minus total benefit of demand, and solved by mixed integer linear programming. Numerical simulation results on the IEEE Reliability Test System show that the proposed full demand response can shave the peak load, reduce both the system operating cost and energy price fluctuations. Compared to conventional demand shifting bids, the proposed model can further reduce the system operating costs.

Index Terms—Demand response, security-constrained unit commitment (SCUC), spinning reserve, reliability, electricity markets, mixed integer linear programming (MILP)

I. INTRODUCTION

The reliability and efficiency of power system operations has always been a high priority in competitive electricity markets. Reliable operation of power system necessitates a perfect balance between the generation and demand at all times. However, this is not easy given the fact that both generation and demand levels can change rapidly and unexpectedly due to many reasons, such as a sudden loss of generation units, transmission lines outages and sudden load changes. When renewable energy resources, such as wind and solar, are integrated, this problem becomes even more difficult. As flexibility of conventional generators is restricted by technical constraints, such as ramp rates, the maintaining power system reliability using only generation side flexibility becomes technically more difficult and potentially could compromise efficiency.

The main contribution of this paper is to propose a full demand response model in which the DRP can bid in the energy

This work was supported in part by the Engineering Research Center Program of the National Science Foundation and the Department of Energy under NSF Award Number EEC-1041877 and the CURENT Industry Partnership Program and in part through the Global Climate and Energy Project (GCEP) at Stanford University.

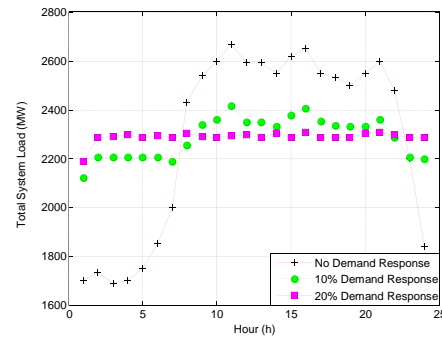


Fig. 1. Demand profiles under three cases

market as price responsive shiftable demand. Meanwhile, the same DRP could also bid in the spinning reserve. It should be noted that the principle of demand providing spinning reserve is different from that of generators. A generator has to operate at reduced output in order to have spinning reserve, whereas a consumer has to be scheduled in order to provide spinning reserve. In other words, a consumer has the potential to provide spinning reserve as long as it is scheduled in the energy market. For this reason, the proposed full demand response model can exploit flexibility from demand more than previous mentioned models. The proposed full demand response model is incorporated in a co-optimized day-ahead energy and spinning reserve market in which the expected net cost under any credible system state, i.e., expected total cost of operation minus total benefit of demand, is minimized. The market clearing problem is formulated as a two-stage stochastic SCUC and solved by mixed integer linear programming. The most economic solution with a probabilistic spinning reserve scheme is obtained by balancing the energy plus spinning reserve cost and cost of expected energy not served (EENS).

II. KEY RESULTS

The total demand profiles with different percentages of demand response are shown in Fig. 1.

Dynamic Programming Solution to Distributed Storage Operation and Design

Junjie Qin

Institute for Computational and Mathematical Engineering
Stanford University
Stanford, CA 94305

Ram Rajagopal

Department of Civil and Environmental Engineering
Stanford University
Stanford, CA 94305

Abstract—Energy storage provides an important way to average temporal variability of intermittent energy generation. Grid level distributed storage enables additional spatial averaging effect by sending stored energy through the network. However, the problem of optimal storage operation in the network, coupling storage and network constraints with randomness of renewable generation, is challenging. An efficient solution method to this problem based on dynamic programming (DP) is presented in this paper. This approach also leads to analytical expressions for the expected system cost and the optimal control parametrized by dual variables, which can be computed by solving a simple deterministic convex program. These analytical expressions simplify tasks such as network storage system design. The approach is illustrated with numerical examples.

I. DISTRIBUTED STORAGE OPERATION PROBLEM

The Distributed Storage Operation (**DSO**) problem has the form

$$\text{minimize } \mathbb{E} \left[\sum_{t=0}^{T-1} h_1^Q(\mathbf{u}(t), \tilde{\mathbf{v}}(t), \mathbf{d}(t)) \right] \quad (1a)$$

$$\text{subject to } \mathbf{x}(t+1) = \mathbf{x}(t) + \mathbf{u}(t), \quad (1b)$$

$$-\mathbf{x}(t) \leq \mathbf{u}(t) \leq \mathbf{B} - \mathbf{x}(t), \quad (1c)$$

$$-\mathbf{C} \leq \tilde{\mathbf{B}}_f \tilde{\mathbf{v}}(t) \leq \mathbf{C}, \quad (1d)$$

where h_1^Q is a quadratic cost function of the storage operation $\mathbf{u}(t)$, nodal phase angle $\tilde{\mathbf{v}}(t)$, and the stochastic net demand (load minus wind) $\mathbf{d}(t)$. The storage dynamics and capacity constraint, as well as network flow (using DC power flow approximation) and line capacity constraints are incorporated in the **DSO** formulation.

II. DP APPROACH TO DSO

The **DSO** problem is first re-casted as a problem of minimizing the Lagrangian function given the dual variable \mathbf{p} . This is solved analytically with DP.

Theorem II.1. (i). For each $\mathbf{x}(t)$ and $t = 0, \dots, T$, the cost-to-go function is

$$J(\mathbf{x}(t); t) = \mathbf{p}(t; t)^\top \mathbf{x}(t) + r(\mathbf{x}(t); t),$$

where

$$\mathbf{p}(t; t) = \mathbf{p}(t; t+1) + \mathbf{x}(t; t), \quad (2)$$

$$r(\mathbf{x}(t); t) = r(\mathbf{x}(t); t+1) + \hat{a}_1(\mathbf{x}(t); t) \quad (3)$$

$$- \frac{1}{2} (\hat{v}(\mathbf{x}(t); t) + \mathbf{F}^\top \mathbf{p}(t+1))^\top \mathbf{Q}^{-1} (\hat{v}(\mathbf{x}(t); t) + \mathbf{F}^\top \mathbf{p}(t+1)),$$

with $\mathbf{p}(t; T) = \mathbf{0}$, $r(\mathbf{x}(t); T) = 0$, $\hat{a}_1(\mathbf{x}(t); t) = \mathbb{E}[a_1(\mathbf{x}(t); t)]$, and $\hat{v}(\mathbf{x}(t); t) = \mathbb{E}[v(\mathbf{x}(t); t)]$.

(ii). For each $\mathbf{x}(t)$ and $t = 0, \dots, T-1$, the optimal control policy is

$$\nu^*(\mathbf{x}(t); t) = -\mathbf{Q}^{-1} (\hat{v}(\mathbf{x}(t); t) + \mathbf{F}^\top \mathbf{p}(t+1)).$$

Using the functional form of the optimal cost-to-go, we can in turn solve for the dual variable \mathbf{p} from a convex program.

Theorem II.2. Let \mathbf{p}^* be a solution of the dual problem

$$\text{maximize } \mathcal{L}(\mathbf{x}(\cdot), \mathbf{v}(\cdot), \mathbf{p}^*)$$

$$\text{subject to } \mathbf{p}^* \geq \mathbf{0}.$$

For $t = 0, \dots, T$, the optimal cost-to-go is

$$J(\mathbf{x}(t); t) = J(\mathbf{p}^*, \mathbf{x}(t); t).$$

For $t = 0, \dots, T-1$, the optimal control policy is

$$\nu^*(\mathbf{x}(t); t) = \nu^*(\mathbf{p}^*, \mathbf{x}(t); t).$$

The analytical form for the optimal expected cost obtained in Theorem II.1 simplifies other distributed storage related problems. The paper includes an example on the network storage design problem on how to choose the location and size for the storage facilities in a network for the purpose of averaging the intermittency of renewable generation.

III. NUMERICAL EXAMPLE

The result of a simple numerical study using IEEE 14 bus test case and 2011 BPA dataset is reported in Figure 1.

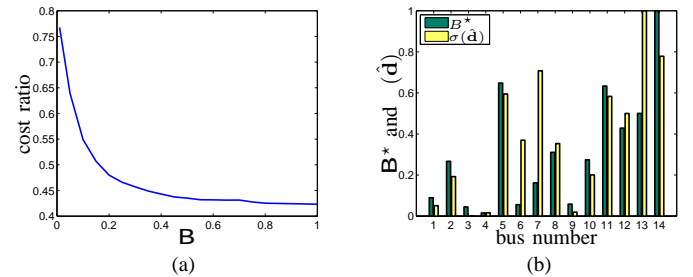


Fig. 1: (a) Ratio between costs of DP-based policy and $3\text{-}\sigma$ policy. (b) Optimal storage design (\mathbf{B}^*) and the data standard deviation of the predicted net demand process for each bus. Storage capacities and standard deviations are normalized by their maximum values, respectively.

R. Rajagopal is supported by the Powell Foundation Fellowship.

A Software Performance Engineering Approach to Fast Transmission Probabilistic Load Flow Analysis

Tao Cui, Franz Franchetti

Department of ECE, Carnegie Mellon University, Pittsburgh, PA, USA. Email: {tcui,franzf}@ece.cmu.edu

Abstract—The performance capability of modern computing platform has been growing rapidly at a roughly exponential rate in last several decades. This hints that certain conventional computational intensive problems might be solvable for online applications. However, fully utilizing the computing power of the hardware is very difficult, requiring the knowledge and efforts from both application domain and software performance engineering domain. In this paper, we present a highly optimized Monte Carlo simulation (MCS) based probabilistic load flow (PLF) solver for transmission grids on modern multicore CPUs. Despite the heavy computational requirement, an MCS based PLF solution provides flexibility, generality and ability to cope with large nonlinearity and large variances, etc. Given the advances of modern computer architecture, we show that by applying various performance optimization techniques and multiple levels of parallelization, the optimized MCS solver on a quadcore CPU is able to achieve more than 60x speedup comparing to a scalar baseline code and furthermore the performance is scalable with the trend of growing hardware parallel capability. We evaluated the MCS solver on the IEEE test systems and the Polish 2383-bus system. On a laptop computer with an Intel Sandy Bridge quadcore CPU, the optimized MCS solver is able to solve up to 1 million load flow cases within 5 seconds for the IEEE 118-bus system, which enables MCS as fast, high-accuracy, and generally applicable method for the PLF analysis.

I. KEY APPROACHES

A. Algorithm & Program Model

We use fast decoupled power flow (FDPF) algorithm as the base load flow algorithm and use general Monte Carlo simulation program model in Fig. 1.

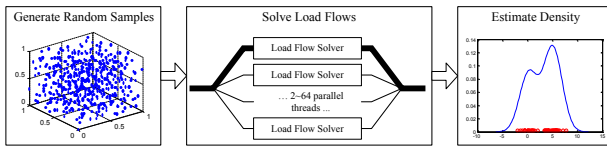


Fig. 1. Program model: Monte Carlo solver

Key code optimizations include: *sparse LU factorization*, *optimized data structure*, *unrolling sparse kernel* in Fig.2, *Single Instruction Multiple Data (SIMD)* in Fig.3, *Multicore for real time Monte Carlo* in Fig.4

II. KEY RESULTS

As key results, we show how many power flow cases can be solved every second using the fully optimized solver on a quadcore Intel Core i7 CPU in Table I. We show the accuracy of MCS results for PLF on IEEE 118 test system in Fig. 5.

```

for (col = 0; col < n; col++)
  for (row = col_ptr[col]; row < col_ptr[col+1]; row++)
    ...// access & compute on nonzero at (row, col)
}

↓ Unrolling

do {
  switch (case_pattern for 2 consecutive columns) {
  case pattern(2,2): {
    ...// access & compute on nonzero at (1, i)
    ...// access & compute on nonzero at (2, i)
    ...// access & compute on nonzero at (1, i+1)
    ...// access & compute on nonzero at (2, i+1)
    ...// access & compute on nonzero at (3, i+1)
    break;
  case ...
  }
} while (!all columns visited)

```

Fig. 2. Pseudo-code illustrating the loop unrolling in sparse matrix solver

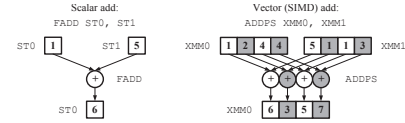


Fig. 3. Illustration of SIMD operation (SSE version)

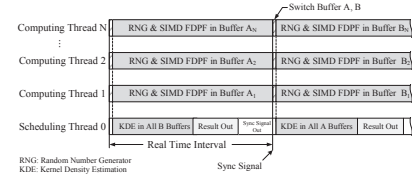
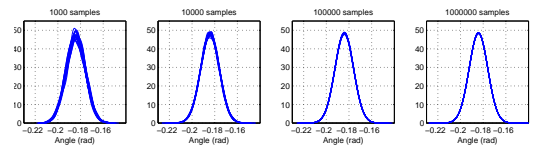


Fig. 4. Multi-thread MCS PLF solver for real time application.

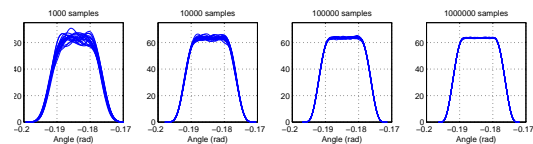
TABLE I
APPROX. LOAD FLOW CASES SOLVED PER SECOND ON CORE I7 2670QM

Sys Size.	Flops/Iteration	Approx. Speed [cases/s]	
		Baseline ¹	AVX 4-Core
14	1,034	39,000	1,920,000
24	1,788	23,000	1,066,000
30	2,242	19,000	860,000
39	2,715	23,000	697,000
57	4,467	15,000	414,000
118	9,130	7,000	202,000
300	23,370	3,000	76,000
2,383	175,365	340	8,100

1. **Baseline** is compiler optimized (Intel C Compiler & O3).



(a) Phase angle of Bus 59. Normal distributed $N(0, 10\text{MW})$ P injections on Bus 59,90,116



(b) Phase angle of Bus 59. Uniform distributed $(-10, 10)$ MW P injections on Bus 59,90,116

Fig. 5. Convergence of crude Monte Carlo simulation

Optimal Blackstart Capability for Power System Restoration

Yazhou Jiang and Chen-Ching Liu
 Washington State University, Pullman, WA, USA
 Email: yjiang1@eecs.wsu.edu and liu@eecs.wsu.edu

Wei Sun
 South Dakota State University, Brookings, SD, USA
 Email: wei.sun@sdstate.edu

Abstract—The paper proposes a new method to find optimal locations for installation of new blackstart units in a power system. Optimal blackstart capability is critical for an efficient restoration process. Additional blackstart units will help to increase the blackstart capability and reduce the system restoration time. However, there is a threshold beyond which the total restoration time will not improve further. A Mixed Integer Linear Programming (MILP) algorithm has been used for the optimization problem.

This research is sponsored by Electric Power Research Institute (EPRI). The objective is to develop a software tool to find the optimal blackstart capability that can serve as decision support for system operators or restoration planners during power system restoration.

I. KEY EQUATIONS

The Blackstart Capability =

$$\left\{ \sum_{i \in \Omega_{ALLU}} \left[(P_{i\max})^2 / (2Rr_i) + P_{i\max} (T - T_{icp} - P_{i\max} / Rr_i) \right] - \sum_{j \in \Omega_{NBSU}} P_{jstart} T \right\} - \left(\sum_{i \in \Omega_{ALLU}} P_{i\max} t_{istart} - \sum_{j \in \Omega_{NBSU}} P_{jstart} t_{jstart} \right) \quad (1)$$

When the critical load is to be picked up, the objective function is formulated as:

$$\text{Min} \sum_{j \in \Omega_{NBSU}} (P_{j\max} - P_{jstart}) t_{jstart} + \sum_{i \in \Omega_{Critical_Load}} P_{load} t_{istart} \quad (2)$$

$$\text{s.t.} \quad \left. \begin{array}{l} t_{istart} \leq T_{ic\max} \\ t_{istart} \geq T_{ic\min} \end{array} \right\} i \in \Omega_{NBSU} \quad (3)$$

$$\sum_{i \in \Omega_{ALLU}} Rr_i (t_{kstart} - t_{i1}^{t_{kstart}} - t_{i2}^{t_{kstart}}) - \sum_{j \in \Omega_{NBSU}} w_{j3} P_{jstart} \geq 0 \quad k \in \Omega_{NBSU} \quad (4)$$

II. METHODOLOGY

LP: linear programming
 MILP: mixed integer linear programming

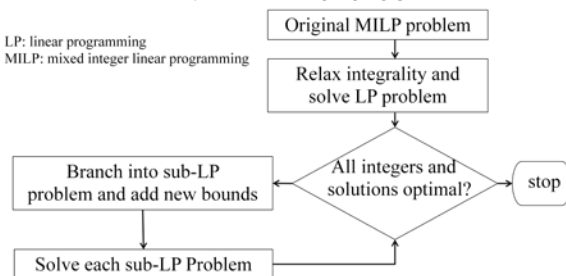


Fig 1. MILP Algorithm

III. KEY RESULTS

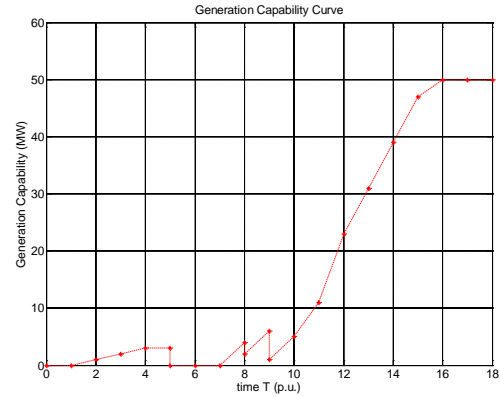


Fig. 2. Generation Capability Curve

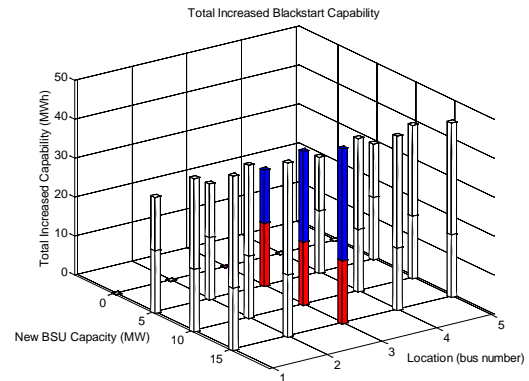


Fig. 3. Increased Blackstart Capability

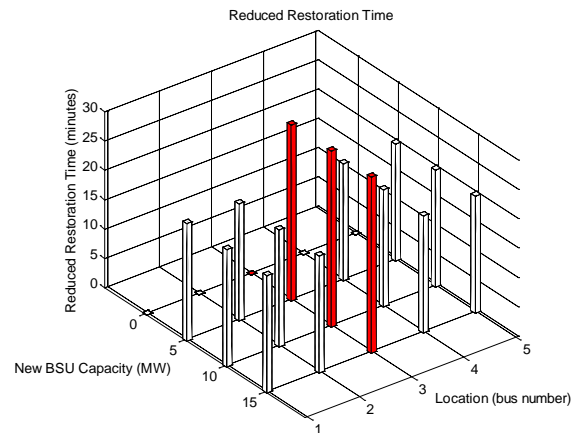


Fig. 4. Reduced Restoration Time

Synchrophasor State Estimation for Data Quality Improvement on the New York Transmission System

Scott G. Ghiocel, Joe H. Chow

Dept. of Electrical, Computer, and Systems Engineering
Rensselaer Polytechnic Institute
Troy, New York, USA

George Stefopoulos, Bruce Fardanesh, Deepak Maragal, Brent Blanchard
New York Power Authority
White Plains, New York, USA

Abstract—Validation and correction of phasor data through state estimation is the first step in ensuring that the synchrophasor data is useful for applications in monitoring, stability, and control. This paper presents a phasor state estimator (PSE) for improving data consistency by identifying angle biases and current scaling errors in the phasor data. These errors can arise from issues with the Global Positioning Signal (GPS), timing circuits, instrument channels, and/or data channel scaling. If left uncorrected, these errors can cause problems in the state estimation. The PSE is demonstrated using several sets of disturbance data from the Central New York Power System. The PSE can also provide estimates of line parameters and transformer tap ratios with sufficient measurement redundancy. Finally, the PSE allows the computation of interface power flows for disturbance and stability monitoring.

Keywords—synchrophasor, phasor measurement unit, state estimation, parameter estimation, redundancy, angle correction, transformer tap ratio

I. INTRODUCTION

This work is focused on the integration of high-sampling-rate distributed synchrophasor measurements to improve the quality of phasor measurement unit (PMU) data so that they can be used for power grid monitoring, visualization, and control [1]. The main idea is the development of a phasor state estimator (PSE) for high-voltage buses using redundant PMU data. The technique is applied to the Central New York (NY) State Power System using data from six multi-channel PMUs [2] deployed in six substations. The results clearly demonstrate the benefits of the PSE for improving data quality and monitoring of critical interface flows.

The main differences between a phasor PSE, that is, a state estimator using only synchrophasor data, and a conventional Supervisory Control and Data Acquisition (SCADA) state estimator (SE) [3] commonly used in control rooms are:

1. Phasor data contain both magnitude and phase information of voltages and currents, whereas conventional SE uses only voltage magnitude and power measurements of line flows and bus injections. In the PSE, bus voltage phasors at substations without PMUs can be directly computed using voltages and currents of neighboring buses with PMUs.
2. Phasor data are reported at 30 or more samples per second, whereas the SCADA systems typically receive new data every 4-5 seconds. Thus the PSE provides

dynamic visibility of the impact of disturbances propagating through critical parts of the system.

In Figure 1, we compare raw SCADA and PMU voltage data for the same loss-of-generation event. Note that the SCADA data does not capture the transient nature of the disturbance and exhibits a 6-second delay.

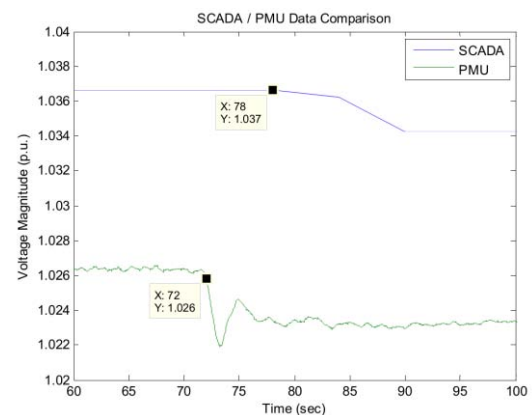


Figure 1: Comparison of SCADA and PMU data for the same loss-of-generation event.

In this work, we extend the PSE results in [4] to provide additional features, such as tap position estimation, current channel scaling, and line parameter estimation. The technique is illustrated using synchrophasor data from the high-voltage Central NY power system. In addition, the flows on five major transfer interfaces can be computed, showing the dynamic impact of various disturbances.

- [1] A. Phadke and J. Thorp, *Synchronized Phasor Measurements and Their Applications*. Springer, 2008.
- [2] B. Fardanesh, S. Zelingher, A. P. S. Meliopoulos, G. Cokkinides, and J. Ingleson, "Multifunctional Synchronized Measurement Network," *IEEE Computer Applications in Power*, vol. 11, no. 1, pp. 26–30, January 1998.
- [3] A. Abur and A. G. Expósito, *Power System State Estimation: Theory and Implementation*. Marcel Decker, 2004.
- [4] L. Vanfretti, J. H. Chow, A. Sarawgi, and B. Fardanesh, "A Phasor-Data-Based State Estimator Incorporating Phase Bias Correction," *IEEE Transactions on Power Systems*, vol. 26, pp. 111–119, February 2011.

A Hybrid Maintenance Scheduling Model for Thermal Generators

Jasper Quach¹, *Undergraduate Student Member* and Bo Zeng¹, *Member*, Brian Buckley²

1. Department of Industrial and Management System Engineering, University of South Florida, Tampa, FL 33620, USA, Email: jasper@mail.usf.edu and bzeng@usf.edu
2. Tampa Electric Company(TECO), Tampa, FL, USA

Abstract—Thermal generators are subject to performance degradation and random failures, which causes huge economic losses. In particular, coal-fired generators, which are expected to run constantly to generate electricity for base load, are typically old and suffer serious reliability issue, resulting in only 75 – 85% availability year round. Therefore it has become increasingly important in planning a preventative maintenance strategy to reduce the failure rate and increase the power generation. To address this challenge, we integrate statistical analysis and optimization modeling, especially robust optimization, to develop a scheduling framework for generator maintenance. First, we collect and clean real outage data of multiple generators over the last four years. Then, we perform a set of statistical analysis to predict generation capacity based on factors and patterns of degenerations and outages. Afterwards, we develop an optimization model to determine the optimal schedule for generating assets to minimize the gap between demand and generation capacity. In particular, we employ robust optimization strategy to capture random failures so that the resulting schedules are robust to unplanned outages. We expect that this research will ultimately increase power reliability, reduce cost and meet demand.

I. KEY EQUATIONS

Will be presented at the conference

II. KEY FIGURES

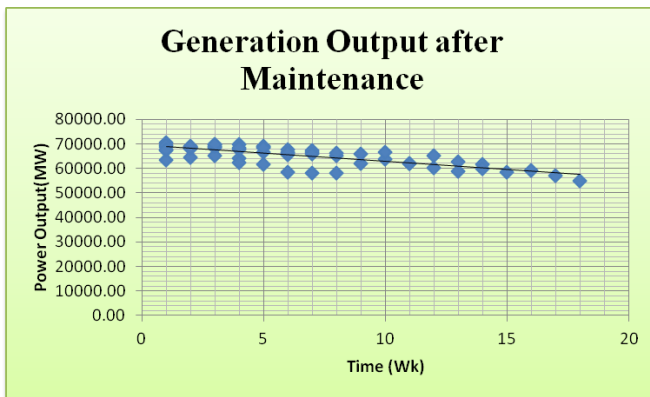


Figure 1: Power Output of Coal Generator

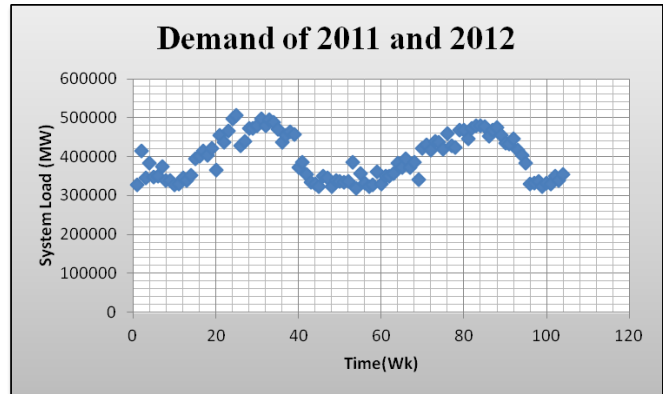


Figure 2: Demand of Electricity in Florida 2011 and 2012

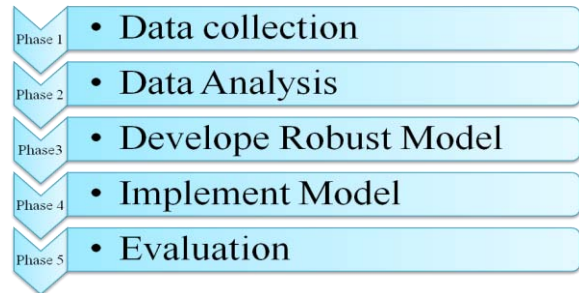


Figure 3: Key Framework

III. KEY RESULT

Will be presented in the conference

Transmission Expansion Planning Considering Uncertainty in Demand

Luis Fernando Fuerte Ledezma
 IEEE, student member
 Master Science of Electrical Engineering
 Morelia Institute Technologic
 Morelia, Mich. 58120, MEX
 Email: fernando.fuerte@ieee.org

Guillermo Gutierrez
 Graduate Program and Research in Electrical Engineering
 Master Science of Electrical Engineering
 Morelia Institute Technologic
 Morelia, Mich. 58120, MEX
 Email: ggutier@itmorelia.edu.mx

Abstract— This paper presents a static transmission expansion planning (TEP) minimizing operational and investment cost. The transmission expansion model is separate into investment and operation problems. The investment problem is solved using a binary particle swarm optimization algorithm (BPSO), whereas the operation problem is solved by a DC optimal power flow (DCOPF). Uncertainty, which is addressed in this paper, is modeled as stochastic demand at each node. To numerically evaluate the efficiency of the proposed method, simulation results on a case study are provided.

I. INTRODUCTION

From the system planning institution point of view, adding system necessary instruments must be proportional to the power system future and from the economic viewpoint, it should impose the least cost to the system and also assures the system desirable reliability. Uncertainty has always been an important issue for power system problems. The parameters such as load growth, fuel price fluctuation, generation level of renewable energy resources, costs of investment and regulations, some of them are not always certain, have a great effect on long-term expansion planning problem and operation.

II. PROBLEM FORMULATION

The power system's objective is to minimize the total cost including investment costs of new transmission lines and operational cost of existing thermal generation units. The mathematical problem can be formulated as follows:

$$\text{Min } z = \sum_{i=1}^{NL^+} CT_i * n_i + \sum_{i=1}^{NG} CG_i \quad (1)$$

$$\text{s.to } c * f + PG + PGV = D \quad (2)$$

$$f_{ij} = \frac{(n_{ij}^0 - n_{ij})(\theta_i - \theta_j)}{X_{ij}} \quad (3)$$

$$-f_{ij}^{max} \leq f_{ij} \leq f_{ij}^{max} \quad (4)$$

$$PG_j^{min} \leq PG_j \leq PG_j^{max} \quad (5)$$

$$0 \leq PGV_j \leq PGV_j^{max} \quad (6)$$

$$n_{ij}^0 \leq (n_{ij}^0 + n_{ij}) \leq n_{ij}^{max} \quad (7)$$

$$D_j^{min} \leq D_j \leq D_j^{max} \quad (8)$$

where CT_i is the investment costs for new transmission lines, $CG_i = b_i * PG_i$ is the operating costs of the generators,

b_i is the linear coefficient of unity, X_{ij} is the reactance of that circuit, n_{ij} is the number of circuits added in right-of-way $i - j$, n_{ij}^0 is the number of circuits in the base case, θ_i is voltage angles for node i , f_{ij} is the power flow, f_{ij}^{max} is the maximum power flow. C is the branch-node incidence matrix, f is a vector with elements f_{ij} , PG_i is the Power of Generator i , PG is a vector with elements PG_i , PG_j^{min} and PG_j^{max} over and upper generation limits, D_j is the load for each bus j , D is a vector with elements D_j , D_j^{min} and D_j^{max} are the limits of demand uncertainty, n_{ij}^{max} the maximum number of circuits that can be added in right-of-way $i - j$, PGV_j is virtual generation, PGV is the vector of artificial generations with elements PGV_j , PGV_j^{max} upper virtual generation limit, NG is the number of generators, NB is the number of nodes, NL^+ is the number of new lines.

III. CASE STUDY

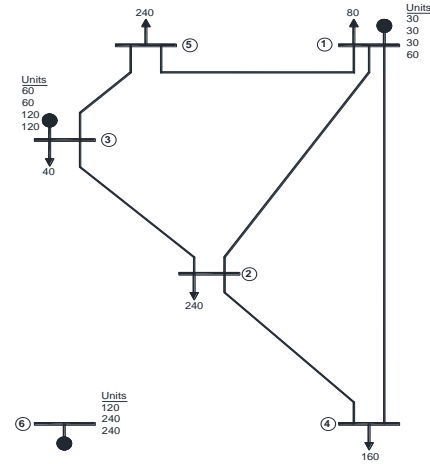


Figure 1. Garver's network.

REFERENCES

- [1]. I. J. Silva, M. J. Rider, R. Romero, C. A. Murari, "Influence of harmonics on power distribution system protection," *IEEE Trans. Power Delivery*, vol 21., pp. 1565 - 1572, Nov. 2006.
- [2]. V. H. Hinojosa, N. Galleguillos, B. Nuques, "A simulated rebounding algorithm applied to the multi-tage security-constrained transmission expansion planning in power systems," *Electrical Power and Energy Systems*, vol 47., pp. 168 - 180, Dec. 2012

Second-Order Cone Relaxations for the Alternating Current Optimal Power Flow Problem

Chen Chen, Alper Atamtürk, and Shmuel Oren
 Industrial Engineering & Operations Research
 University of California, Berkeley
 Berkeley, CA, USA
 E-mail: chenchen@berkeley.edu

Richard P. O'Neill
 Chief Economist
 FERC
 Washington DC, USA

Abstract—The AC Optimal Power Flow (ACOPF) problem is a nonlinear optimization problem for dispatching generators. Recent research shows that numerous instances of ACOPF can be solved exactly by its Lagrangian dual, which can be formulated using Semidefinite Programming (SDP). SDP is a type of conic programming and can thus be solved in polynomial time. We examine a relaxation that is formulated using Second-Order Cone Programming (SOCP). This SOCP relaxation can provide a faster but weaker lower-bound estimate of the optimal objective. We develop cuts to approximate the defining positive semidefinite matrix constraint in SDP. Applying these cuts to the SOCP relaxation enables iterative approximation of the ACOPF Lagrangian Dual using SOCP. A key to generating effective cuts is sparsification using a decomposition technique based on network topology. Computational experiments on IEEE test cases show the tractability of our method. By approximating ACOPF with SOCP, integer variables can also be incorporated via the Mixed-Integer Second-Order Cone Programming framework. This could enable the extension of power flow to problems such as Unit Commitment and Topology Control.

I. KEY EQUATIONS

Eigenvector linear cuts:

$$X \succeq 0 \equiv c^T X c \geq 0 \quad \forall c \in \mathbb{R}^n$$

$$\lambda_n(X) = d_n^T X d_n = \min_{c \in \mathbb{R}^n: \|c\|=1} c^T X c \quad (\text{lincut})$$

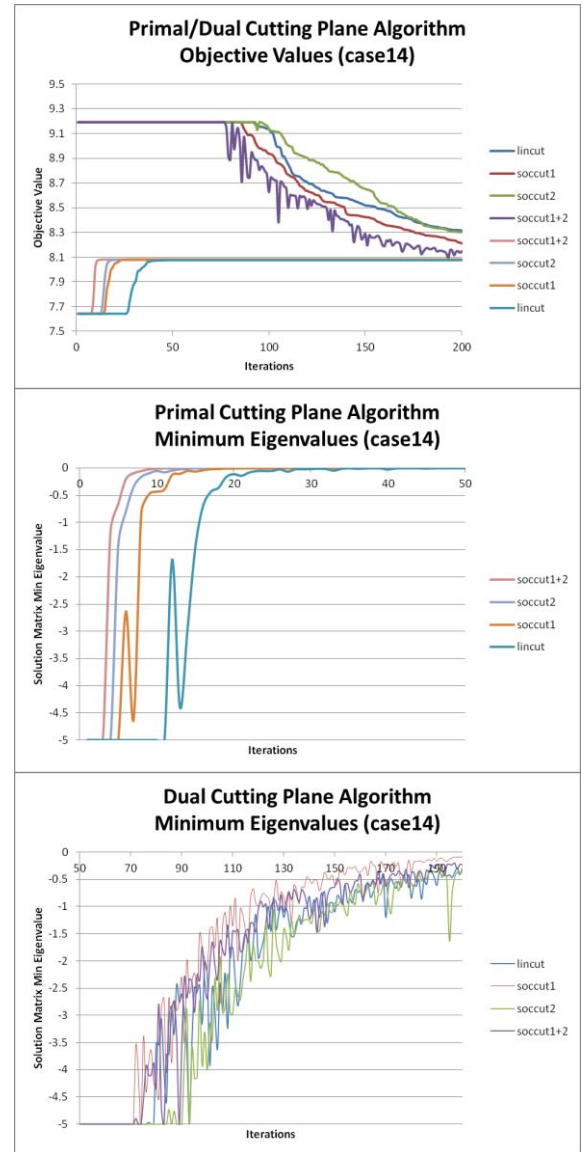
Second-order cone cuts:

$$X \succeq 0 \implies C^T X C \succeq 0 \quad \forall C \in \mathbb{R}^{n \times 2}$$

$$C^T X C \succeq 0 \equiv c_1^T X c_1 + c_2^T X c_2 \geq \|(2c_1^T X c_2, c_1^T X c_1 - c_2^T X c_2)^T\|$$

$$C_1^* = [d_1 \ d_2] \ (\text{soccut1}), C_2^* = [d_1 \ d_n] \ (\text{soccut2})$$

II. KEY RESULTS



Short-Term Wind Power Prediction Using a Wavelet Support Vector Machine

Jianwu Zeng, *Student Member, IEEE*, and Wei Qiao, *Member, IEEE*

Abstract—This paper proposes a wavelet support vector machine (WSVM)-based model for short-term wind power prediction (WPP). A new wavelet kernel is proposed to improve the generalization ability of the support vector machine (SVM). The proposed kernel has such a general characteristic that some commonly used kernels are its special cases. Simulation studies are carried to validate the proposed model with different prediction schemes by using the data obtained from the National Renewable Energy Laboratory (NREL). Results show that the proposed model with a fixed-step prediction scheme is preferable for short-term WPP in terms of prediction accuracy and computational cost. Moreover, the proposed model is compared with the persistence model and the SVM model with radial basis function (RBF) kernels. Results show that the proposed model not only significantly outperforms the persistence model but is also better than the RBF-SVM in terms of prediction accuracy.

I. KEY EQUATIONS

Least-square WSVM (LS-WSVM) and ε -WSVM:

$$\hat{y}(x_i) = \begin{cases} \sum_{i=1}^N \alpha_i \prod_{j=1}^D h\left(\frac{x_{i,j} - x_{i,j}}{a_i}\right) + b & (\text{LS-WSVM}) \\ \sum_{i=1}^N (\alpha_i - \alpha_i^*) \prod_{j=1}^D h\left(\frac{x_{i,j} - x_{i,j}}{a_i}\right) + b & (\varepsilon\text{-WSVM}) \end{cases} \quad (1)$$

a new wavelet mother function is proposed as follows.

$$h(x) = \cos\left(k \cdot \frac{x}{a}\right) \cdot \exp\left(-\frac{x^2}{a^2}\right) \quad (2)$$

II. KEY FIGURES

The proposed WPP model consists of three components:
Preprocessing

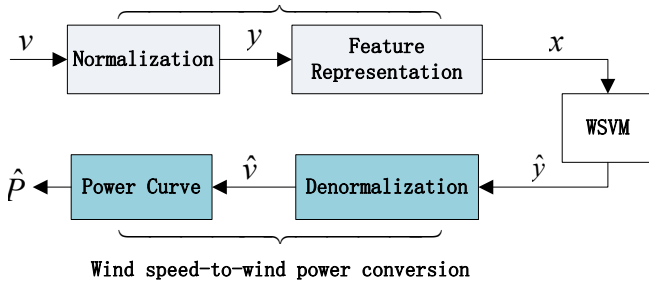


Fig. 1. The structure of the proposed WPP model.

preprocessing, WSVM-based wind speed prediction, and wind-speed-to-wind-power conversion, as shown in Fig. 1.

III. RESULTS

1-hour-ahead prediction result

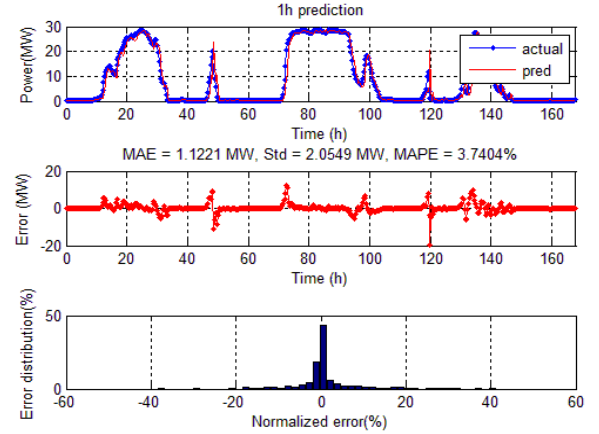


Fig. 2. 1h-ahead WPP using the WSVM model and fixed-step scheme.

Comparison among three models.

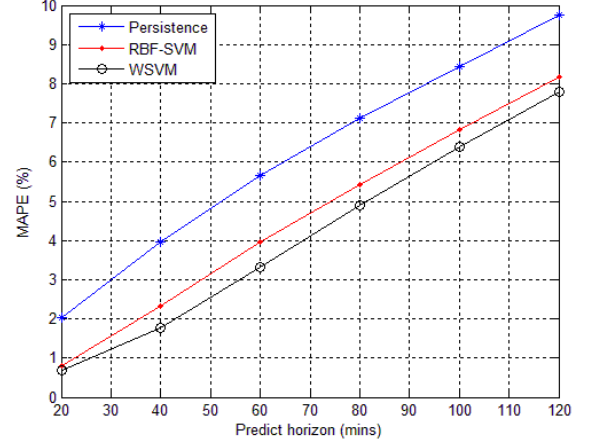


Fig.3. Comparison among the persistence, RBF-SVM and WSVM models.

Testing results with 30 months data.

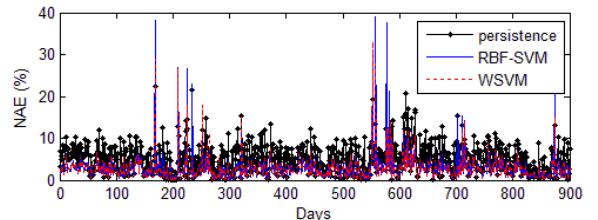


Fig. 4. The result of using 30 months testing data.

Equivalent Indices for Shunt Power Capacitor Loading assessment

Yu Tian

Department of Electrical and Computer Engineering, University of Alberta, Edmonton, Canada

Email: tian7@ualberta.ca

Abstract— Power capacitors are extensively used in power systems for voltage support and power factor correction. With the rapidly increased use of power electronic based devices and appliances, a large amount of harmonics is injected into power grid. The presence of harmonic voltages and currents can accelerate capacitor degradation to a significant extent, particularly when harmonic magnitudes are amplified by resonance conditions. This paper proposed a new method for loading assessment of shunt power capacitors based on capacitor insulation material lifetime model. Two new indices are defined. The first index is called 'equivalent voltage' applied to the capacitor. With this index, utility can determine capacitor loading level by using measured capacitor currents. The second index is called 'harmonic contribution factor'. With this contribution factor, the equivalent effect of harmonic voltage, compared to a pure sinusoidal voltage, on shunt capacitor loading can be quantified. General calculation procedures and application example is provided. Major factors which can affect capacitor loading condition are investigated through sensitivity studies. Finally, the proposed indices were employed to evaluate loading condition of a shunt capacitor installed in Edmonton, Alberta.

I. KEY EQUATIONS

Definition of the capacitor 'equivalent voltage':

$$V_{eq-pu} = (K_p)^{n_p} \cdot (K_{rms})^{n_{rms}} \cdot (K_s)^{n_s} \quad (1)$$

Where:

$$\begin{cases} K_p = V_p / V_{1p}^* \\ K_{rms} = V_{rms} / V_{1rms}^* \\ K_f = \frac{\omega_1}{\omega_0} \sqrt{\sum_{h=1}^N h^2 \alpha_h^2} \end{cases}$$

Capacitor 'equivalent voltage' higher than 1 indicates a case where the capacitor is overloaded. Higher 'equivalent voltage' implies severer overloading condition.

Definition of the 'harmonic contribution factor':

$$HCF = \frac{V_{eq-pu}}{V_{eq-pu, without harmonic}} \quad (2)$$

II. KEY FIGURES

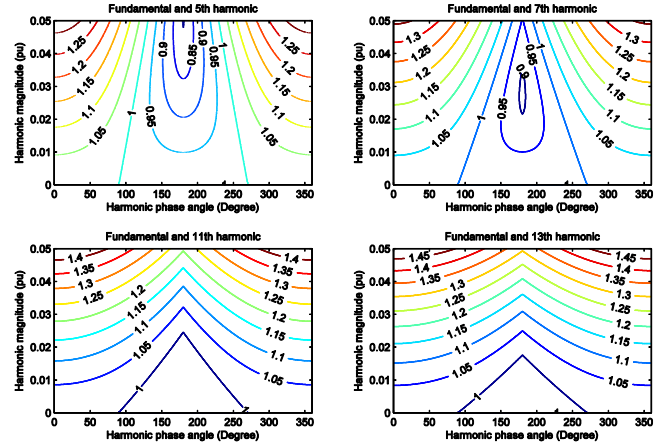


Fig. 1 Combination effect of harmonic magnitude and phase angle on the capacitor 'equivalent voltage'

III. KEY RESULTS

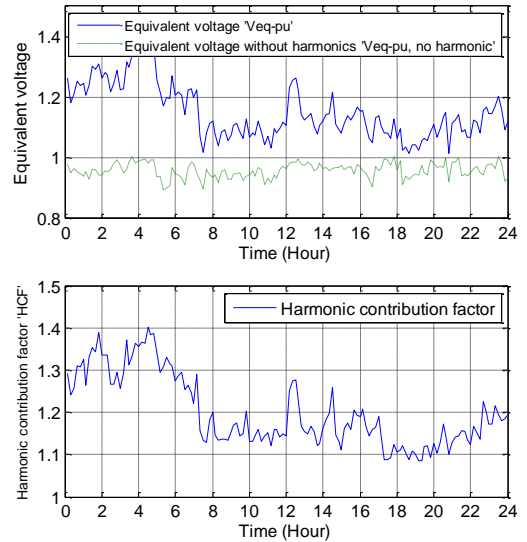


Fig. 2 Capacitor loading indices during 24 hours of a day

Study of Transformer Winding Deformation by Frequency Response Analysis

M. F. M. Yousof^{1,2,*}, C. Ekanayake¹ and T. K. Saha¹

¹The School of Information Technology and Electrical Engineering, The University of Queensland, Brisbane, Australia

²Faculty of Electrical and Electronic Engineering, Universiti Tun Hussein Onn Malaysia, Batu Pahat, Malaysia

*fairouz@ieee.org

Abstract—This paper proposes a methodology to interpret frequency response measurements of a deformed transformer winding due to conductors tilt. To achieve that, geometrical parameters of a three phase prototype transformer is used to simulate the frequency response of one of the windings using the multi-conductor transmission line model. To simulate the response, inter-turn, inter-disc and inter-winding capacitances of the winding based on normal and deformed conditions are computed using finite element method. Using the computed values, the frequency response for both normal and deformed conditions are simulated. The simulated responses are studied by subdividing into four frequency regions and compared using the correlation coefficient. For further analysis, the vector fitting algorithm was implemented to approximate the transfer function of each response. All transfer functions are then represented in the Nyquist diagram to analyse the shape of each plot. From the Nyquist diagram, it was observed that the real minimum of each plot increases as the winding deformation increases. This finding can be used to estimate the winding deformation severity based on the plotted attributes.

Index Terms—Frequency response analysis, multi-conductor transmission lines, transfer functions, transformer windings.

I. METHODOLOGY

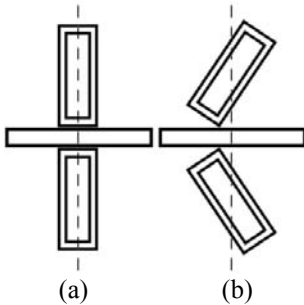


Fig. 1. (a) Normal and (b) tilted conductors.

TABLE I. CAPACITANCES FOR NORMAL AND DEFORMED WINDING

Condition		Capacitance (F)
Inter-turn capacitance, C_t	Normal	2.67×10^{-10}
	Tilted (20°)	2.41×10^{-10}
Inter-disc capacitance, C_d	Normal	9.85×10^{-12}
	1 disc tilted (20°)	8.03×10^{-12}
	2 discs tilted (20°)	7.72×10^{-12}
Inter-winding capacitance, C_g	Normal	2.30×10^{-11}
	Tilted (20°)	1.76×10^{-11}

II. KEY RESULTS

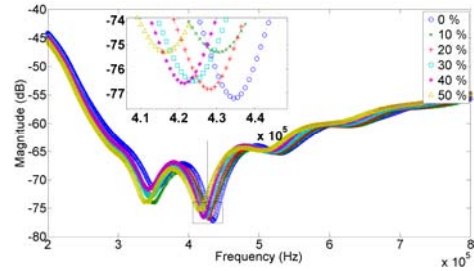


Fig. 2. The simulated frequency response of the transformer winding for normal and deformed conditions.

TABLE II. CORRELATION COEFFICIENT ACCORDING TO THE PERCENTAGE OF DAMAGE

Frequency sub-band (kHz)	Percentage of Winding Damage					
	0 %	10 %	20 %	30 %	40 %	50 %
< 2	1.0000	1.0000	1.0000	1.0000	1.0000	0.9999
2 to 20	1.0000	1.0000	1.0000	1.0000	1.0000	1.0000
20 to 400	1.0000	0.9999	0.9996	0.9995	0.9991	0.9986
400 to 1000	1.0000	0.9943	0.9890	0.9727	0.9609	0.9464

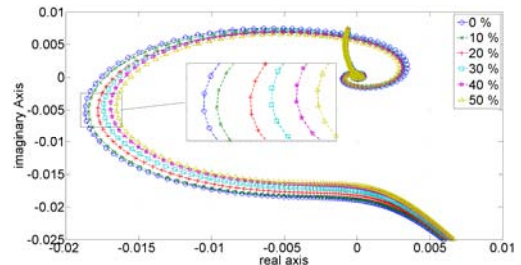


Fig. 3. The Nyquist plot for the simulated frequency response of the transformer winding.

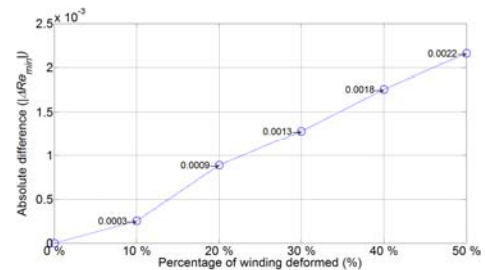


Fig. 4. The absolute difference versus the percentage of deformed winding.

The estimated linear equation for the plot in Fig. 4.

$$\text{Percentage of winding damage (\%)} = \frac{|\Delta Re_{min}| + 5.1 \times 10^{-4}}{4.5 \times 10^{-4}} \quad (1)$$

Analysis of Grid Impacts of an Electric Vehicle DC Quick Charger

Nicole P. Zimmerman, Emily L. McCallum, and Robert B. Bass

Department of Electrical and Computer Engineering
Portland State University
Portland, OR 97201, USA

Email: nicolepzimmerman@ieee.org, emcc2@pdx.edu, and robert.bass@pdx.edu

Abstract— Electric Avenue, on the Portland State University campus, offers the unique opportunity to analyze the effects that electric vehicle (EV) charging units have on power distribution infrastructure. At the site there are seven separate charging stations that have been donated by different manufacturers. This gives our research group the chance to monitor power flow on individual charging circuits while also performing an aggregate analysis on the feeder as whole.

In distribution system planning, it is essential to understand the impacts that EVs and the power electronics associated with their charging units may have on power distribution networks. Further, a deeper understanding of these matters will aid utilities in the design of electrical power systems, including asset planning, such as k-type rating for distribution transformers.

I. KEY EQUATIONS

Buchholz and Goodhue quantified power quality for unbalanced systems in their seminal works [1] and [2], which form the core of IEEE standard 1459-2010, “Power definitions for circuits with nonlinear and unbalanced loads.”[3] Our analysis of the Electric Avenue EV charge controllers relies on the metrics of apparent power defined in 1459-2010.

Equation 1 defines the effective apparent power (S_e) for an unbalanced three-phase system as:

$$S_e = 3 \cdot \sqrt{\frac{V_{ab}^2 + V_{cb}^2 + V_{ca}^2}{9}} \cdot \sqrt{\frac{I_a^2 + I_b^2 + I_c^2 + I_n^2}{3}} \quad (1)$$

From the fundamental effective apparent power component (S_{e1}), the amount of VA caused by the system unbalance can be found using Equation 2, where:

$$S_{U1} = \sqrt{S_e^2 - (S_1^+)^2} \quad (2)$$

where S_1^+ is the positive sequence apparent power. The nonfundamental effective apparent power, Equation 3, is composed of the power components due to current distortion,

(D_{e1}), voltage distortion (D_{eV}), and harmonic apparent power (S_{eH}).

$$S_{eN} = \sqrt{D_{e1}^2 + D_{eV}^2 + S_{eH}^2} \quad (3)$$

Where D_{e1} and D_{eV} are products of THD_I and THD_V , respectively, and S_{e1} . Further, S_{eH} is the product of THD_I , THD_V , and S_{e1} .

II. KEY FIGURES

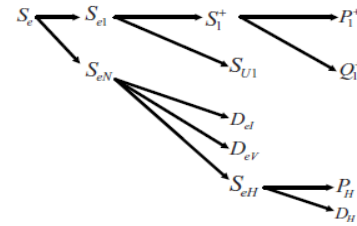


Figure 1. The powers' tree (IEEE Std. 1459-2012).

III. KEY RESULTS

Data analysis, using Equations 1-3, of the charging stations along Electric Avenue reveals issues of poor power factor, harmonic pollution, and load imbalance. This poster presents analysis and graphical examples of the severity of these power quality issues for two cases, a single DC fast charger and an aggregate of seven chargers as measured at their point of common connection.

REFERENCES

- [1] F. Buchholz, “Die drehstrom-scheinleistung bei ungleichmassiger belastung der drei zweige,” Licht und Kraft, no. 2, pp. 9-11, Jan. 1922
- [2] W. M. Goodhue, Discussion to “Reactive power concepts in need of clarification,” AIEE Transactions, vol. 52, p. 787, Sept. 1933.
- [3] A. E. Emanuel; R. Langella; A. Testa, “Power difinitions for circuits with nonlinear and unbalanced loads – The IEEE standard 1459-2010,” Power and Energy Society General Meeting, 2012 IEEE, pp. 1-6, 22-26 July 2012

Reconciling Consumer Behaviors with Demand Response in the Smart Home

Adam Zipperer, *IEEE Student Member*

Colorado State University, Fort Collins, Colorado, United States
adam.zipperer@colostate.edu

Abstract— Residences consume over a third of the net electricity generated in the United States, yet are often downplayed in demand response discussions. The Smart Grid Initiative and the ensuing proliferation of Advanced Metering Infrastructure rollouts will likely increase the adoption of dynamic electricity pricing structures in the residential sector. Consequently, residences will increasingly become demand response assets, capable of reducing or shifting peak demand in response to forcing signals. Smart meters, and the underlying communication infrastructure, are expected to enable the widespread emergence of the ‘smart home’. Despite this opportunity to seize significant environmental and economic benefits through peak load mitigation, challenging hurdles remain in the design of smart home controls.

Residential customers behave differently from commercial or industrial ones. For decades, engineers have focused on the technology necessary to implement a truly smart home. Now, relatively fewer technical barriers exist for the adoption of smart home technologies. Consensus is that the remaining barriers are economic in nature. However, perceived economic barriers are often psychological in nature, i.e., what initially may be thought of as prohibitively expensive may soon be thought of as a great convenience. Examples of this include telecommunication technologies such as cable TV, home broadband Internet connections, and wireless cellular service.

So, the challenge for the realization of the smart home is multi-disciplinary, involving both engineers and behavioral psychologists. How do we induce behavioral changes that may not appear personally beneficial, but are beneficial to society when aggregated? Utilities have nearly universally focused on price as the sole motivator for peak load shifting. While traditional economic theory would support this idea, research has shown that people rate environmental and societal motivations higher [1]. Additionally, even in home energy usage, people are even more influenced by the perceived actions of their peers (normative influence).

In this research, using the Analytic Hierarchy Process (AHP), an example of energy savings in a smart home is developed using time-of-use pricing with peak, mid-peak, and off-peak pricing. The example smart home features four programmable loads (electric vehicle, washing machine, dryer, and dishwasher), and accounts for user preferences in load scheduling. AHP structures a complex problem in terms of criteria and sub-criteria affecting a goal, and the alternative choices available that would satisfy that goal [2]. Comparing elements pair-wise is a natural methodology for any consumer, yet provides powerful information for the load-scheduling algorithm. The poster will present preliminary steps taken to

This work was supported in part by: the US National Science Foundation Award # 0931748 and the Program of Research and Scholarly Excellence (PRSE) grant from the Office of the Vice President for Research (VPR) at Colorado State University.

address these issues, as well as plans for continued research on the subject, including incorporating non-schedulable loads such as air conditioning and electric water heater.

I. KEY RESULTS

The author-generated preferences result in the cost and comfort priorities in Fig. 1. High peak prices result in non-critical loads shifting to off peak times as in Fig. 2, accounting for time-varying changes in user preferences specific to each load.

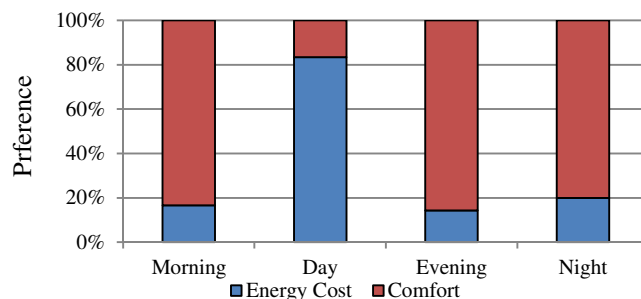


Fig. 1. User cost and comfort priorities.

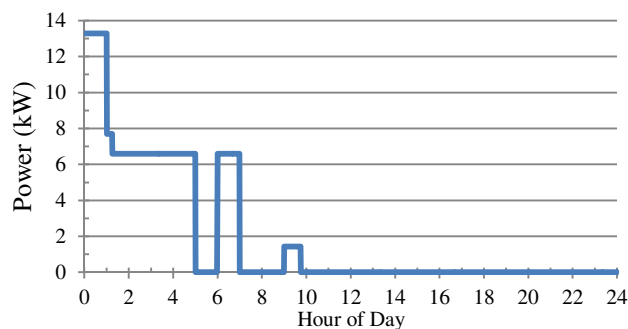


Fig. 2. Automatic load scheduling.

ACKNOWLEDGEMENTS

The author is grateful to Dr. Siddharth Suryanarayanan and Dr. Pat Aloise-Young of Colorado State University for their expertise in the operations of electric power systems and consumer energy behaviors, respectively.

REFERENCES

- [1] J. M. Nolan, P. W. Schultz, R. B. Cialdini, N. J. Goldstein, and V. Griskevicius, “Normative Social Influence is Underdetected,” *Personality and Social Psychology Bulletin*, vol. 34, no. 7, pp. 913–923, 2008.
- [2] T. L. Saaty, *Fundamentals of Decision Making and Priority Theory with the Analytic Hierarchy Process*. Pittsburgh, Pennsylvania: RWS Publications, 2004.

Security-Based Circuit Breaker Maintenance Management

Payman Dehghanian, Mladen Kezunovic, Gurunath Gurralla, Yufan Guan

Department of Electrical and Computer Engineering, Texas A&M University, College Station, Texas, USA
 payman.dehghanian@tamu.edu; kezunov@ee.tamu.edu; ggurralla@ece.tamu.edu; carling@tamu.edu

Abstract—Circuit breakers (CBs) play a vital role in maintaining system security since their malfunctioning could result in further component outages and may lead to the insecure operating conditions. This poster proposes a new approach for identifying the most risky CBs using the condition-based monitoring data and security-based impact evaluations. For a given substation configuration, those CBs which cause line outages due to mal-operation during contacts opening are identified and analyzed. The security oriented risk indices taking into account both voltage violations and overloading conditions as the consequence of CB mal-operations are proposed. A new breaker maintenance prioritization scheme based on the risk factors is elaborated. The proposed security-based risk framework is deemed to be an efficient approach in both CB maintenance planning and identification of those CBs which are unreliable for reconfiguration plans. The presented methodology is investigated and verified on the IEEE 14-bus test system.

I. KEY THEORY AND FORMULATION

Power system risk evaluation commonly incorporates general steps as depicted in Fig. 1. For each circuit breaker (CB) in a substation, if it is assumed to fail one at a time, one can evaluate the security-oriented risk factor via (1).

$$Risk_i = \sum_{i=1}^n Pr_i(E_i) \cdot Con_i(E_i) \quad (1)$$

System security is considered as the consequence of the CB malfunction as follows. It considers both the system overload (2) and over-voltage (4) index of security in the system post contingency state and finally the consequence term can be obtained through (6).

$$PI_{OL}(E_i) = \sum_{l=1}^{NL} \frac{w_l}{2n} \left(\frac{|P_l(E_i)|}{P_{l,max}(E_i)} \right)^{2n} \quad (2)$$

$$P_{l,max}(E_i) = \frac{V_i^{(E_i)} V_j^{(E_i)}}{x_{ij}} \quad (3)$$

$$PI_{OV}(E_i) = \sum_{l=1}^{NL} w_b \left(\frac{V_j^{(E_i)} - V_j^B}{V_j^{max} - V_j^{min}} \right)^{2n} \quad (4)$$

$$V_j^{max} - V_j^{min} = 1.05V_j^B - 0.95V_j^B = 0.1V_j^B \quad (5)$$

$$Con_i(E_i) = k_1 \cdot PI_{OL}(E_i) + k_2 \cdot PI_{OV}(E_i) \quad (6)$$

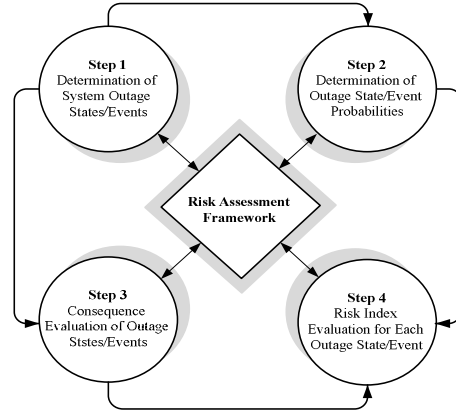


Figure 1. Risk assessment general framework in power system studies.

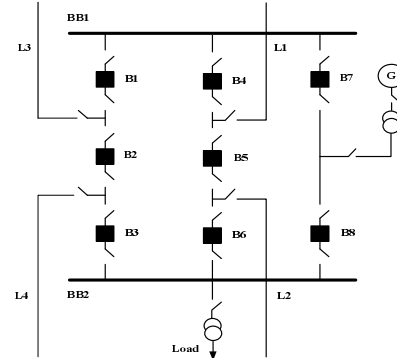


Figure 2. Substation configuration of bus 2 in IEEE 14-bus Test System.

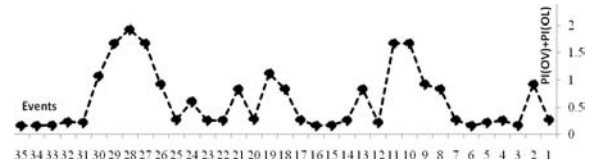


Figure 3. Security constrained consequence results.

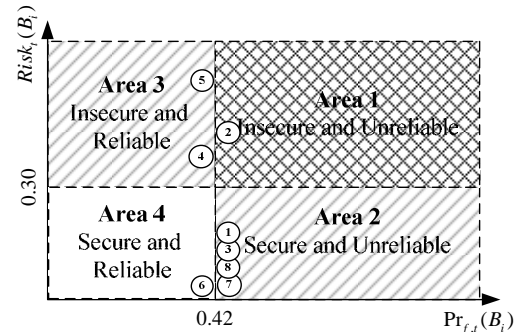


Figure 4. Risk-based decision framework to identify critical CB

The financial support for this research comes from ARPA-E through GENI project "Robust Adaptive Transmission Control".

Optimal Transformer Sizing with the Presence of Probabilistic Electric Vehicle Charging

Sachin Argade and Visvakumar Aravinthan

Department of Electrical Engineering and Computer Science
Wichita State University
{sgargade, visvakumar.aravinthan}@wichita.edu

Abstract—The loss of life of distribution transformers has become a significant concern with the prevalence of charging electric vehicles. In this work size of a distribution transformer with no-load losses is minimized while limiting the acceleration of the transformer loss of life and by taking in to consideration controlled and uncontrolled EV charging. Controlled and uncontrolled charging patterns are developed using a probabilistic model for vehicle arrival time and charge left at arrival. These charging patterns are used for transformer loading on top of the base loading of the transformer. An example is shown to illustrate the validity of this model.

Index Terms—Transformer sizing, probabilistic EV charging, transformer loss of life, reliability, distribution Transformer

I. OBJECTIVE FUNCTION TO MINIMIZE NO LOAD LOSSES

Impact of electric vehicle charging to the grid is of vital concern for distribution systems. Based on the stochastic nature of the EV charging load, controlled charging strategies are investigated by the authors [1]. These strategies are used in this work to model the optimal sizing of secondary distribution transformer. Objective is to find a balance between no load losses of transformer and performance requirements. Based on Fig.1 generalized relationship between a transformer no-load loss and a transformer rating (P_R) is

$$P_{Loss} = 1.4191P_R + 22.494 \quad (1)$$

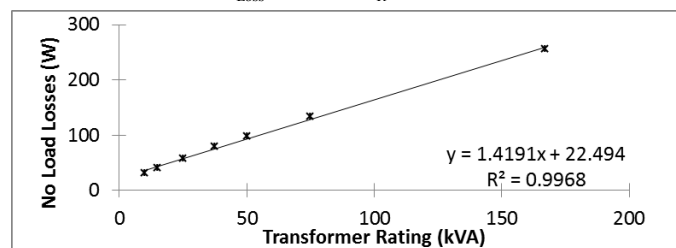


Fig. 1: Linearized Transformer Loss Curve for Single-Phase Transformer

II. CONSTRAINTS

Transformer aging: Based on IEEE std. C57.91–2011, transformer hot-spot temperature rise due to the electric vehicle charging for a day (annual average) is modified as,

$$\Theta P_R^2 - \sum \left[\frac{\Delta \theta_{TO,R}}{(R+1)^{0.8}} \left(P_R^2 + 0.8(L_t)^2 R \right) + \Delta \theta_{H,R}(L_{t-1})P_R \right] \geq 0 \quad (2)$$

Transformer loading: In addition to limiting transformer loss of life due to EV charging, it is important to limit the maximum loading. Relation is given as

$$P_R \geq \eta L_{max} \quad (3)$$

where $L_{max} = \max_{t=1 \dots N} \{L_t\}$, and η is maximum load limit factor.

III. OPTIMAL SOLUTION

Lagrangian for the above problem could be developed as

$$\mathcal{L}(P_R, \lambda_1, \lambda_2) = (bP_R + c) - \lambda_2 (P_R - \eta L_{max}) - \lambda_1 \left((\Theta - N\psi)P_R^2 - \left(\sum (\mathcal{G}_t) \right) P_R - \sum (\beta_t) \right) \quad (4)$$

Where, λ_1 and λ_2 are slack variables. Since this is a convex problem, the Karush-Kuhn-Tucker (KKT) condition is used.

The General Solution:

$$P_R^* = \begin{cases} \frac{(\sum (\mathcal{G}_t)) \pm \sqrt{(\sum (\mathcal{G}_t))^2 + 4(\Theta - N\psi)(\sum (\beta_t))}}{2(\Theta - N\psi)} & \text{if } f \geq 1 \\ \eta L_{max} & \text{if } f \leq 1 \end{cases} \quad (5)$$

$$f = \frac{(\sum (\mathcal{G}_t)) + \sqrt{((\sum (\mathcal{G}_t)))^2 + 4(\Theta - N\psi)(\sum (\beta_t))}}{2(\Theta - N\psi)\eta L_{max}} \quad (6)$$

IV. RESULTS

Optimal transformer rating determined for particular operating conditions, using proposed method is given in Fig 2.

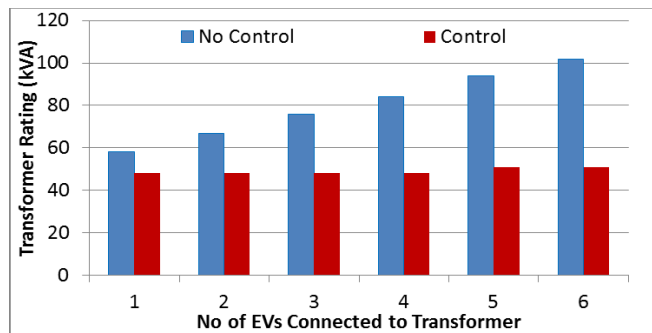


Fig. 2: Optimal Transformer Rating for Summer-Peaking Utility

V. REFERENCE

- [1] S. Argade, V. Aravinthan, and W. Jewell, "Probabilistic modeling of EV charging and Its Impact on Distribution Transformer Loss of Life," in *Proc. 1st IEEE Int. Electric Vehicle Conference*, March 2012

Real-Time Price-Based Demand Response Management for Residential Appliances Considering Privacy Protection

Zhi Chen, *Student Member, IEEE*, Lei Wu, *Member, IEEE*

Department of Electrical Engineering and Computer Science, Clarkson University, Potsdam, NY 13676, USA
lwu@clarkson.edu

Abstract— This paper explores electric privacy issues that may occur along with the proposed real-time price-based demand response (DR) energy management in smart meters via online stochastic optimization while considering uncertainties in real-time electricity prices. Three metrics are introduced to measure the spatial and/or temporal similarity of metered power profiles. The online stochastic optimization adopts the scenario-based approach via Monte Carlo (MC) simulation for minimizing the sum of the expected electricity payment and the weighted difference among metered power profiles for the entire day. In addition, batteries are employed to disguise the actual appliance power profile along with the scheduling horizon and enhance the privacy protection. The proposed approach is formulated as mixed-integer linear programming (MILP) problems and solved by state-of-the-art MILP solvers. Numerical case studies illustrate the effectiveness of the proposed approach for solving the real-time optimal DR management problem for residential appliances automatically and protecting electric privacy with residential appliances.

I. KEY EQUATIONS AND FIGURES

The proposed real-time DR management is formulated as a rolling procedure. In each stochastic optimization model execution, the first stage includes the first 5-minute time slot t_0 , in which the spot price is announced by the real-time market and the unique operation decisions will be obtained for all appliances. While in the second stage ranging from $t_0 + I$ to the end of the schedule horizon, multiple scenarios are generated via the MC simulation and scenario-dependent operation decisions are derived in response to electricity price uncertainties. The objective is to minimize the sum of the cost of the metered power, the weighted values of three similarity metrics, and the charging/discharging cost of the battery, in order to balance the tradeoff between the electricity payment and the privacy protection (1)-(5).

$$\min \left[\left(\sum_{a=1}^{NA} c_{t_0} \cdot p_{ca,t_0} + \sum_{b=1}^{NB} C_{b,t_0} \right) + \sum_{s=1}^{NS} \rho^s \cdot \sum_{\tau=t_0+1}^{NT} \left(\sum_{a=1}^{NA} c_{\tau}^s \cdot p_{ca,\tau}^s + \sum_{b=1}^{NB} C_{b,\tau}^s \right) \right] \\ \left[\gamma_1 \cdot \left(S1_{t_0} + \sum_{s=1}^{NS} \sum_{\tau=t_0+1}^{NT} \rho^s \cdot S1_{\tau}^s \right) + \gamma_2 \cdot \left(\sum_{s=1}^{NS} \sum_{a=1}^{NA} \rho^s \cdot S2_a^s \right) + \gamma_3 \cdot \left(\sum_{s=1}^{NS} \rho^s \cdot S3^s \right) \right] \quad (1)$$

$$S1_{t_0} = \sum_{a=1}^{NA-1} \sum_{i=a+1}^{NA} \left| p_{ca,t_0} - p_{ci,t_0} \right| \quad (2)$$

$$S1_{\tau}^s = \sum_{a=1}^{NA-1} \sum_{i=a+1}^{NA} \left| p_{ca,\tau}^s - p_{ci,\tau}^s \right| \quad (3)$$

$$S2_a^s = \sum_{t=1}^{t_0-1} \left| p_{ca,t_0} - \hat{p}_{a,t} \right| + \sum_{\tau=t_0+1}^{NT} \left| p_{ca,t_0} - p_{ca,\tau}^s \right| \quad (4)$$

$$S3^s = \sum_{\tau=t_0+2}^{NT} \left| \sum_{a=1}^{NA} p_{ca,\tau}^s - \sum_{a=1}^{NA} p_{ca,\tau-1}^s \right| + \left| \sum_{a=1}^{NA} p_{ca,t_0+1}^s - \sum_{a=1}^{NA} p_{ca,t_0}^s \right| \quad (5)$$

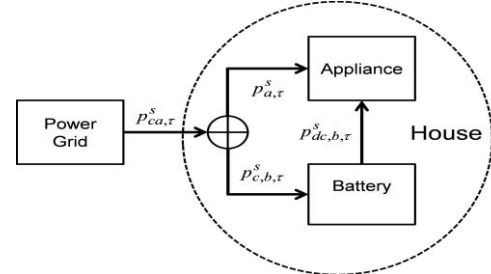


Fig. 1. Power flow between appliances and batteries

II. KEY RESULTS

Numerical results indicate that a better privacy protection performance can be achieved at the cost of a slightly higher bill payment cost and additional battery costs, as shown in Tables I-II and Fig. 2.

TABLE I RESULTS WITHOUT BATTERY

	Base Case	S1	S2	S3
Energy usage (kWh)	21.99	21.99	21.99	21.99
Electricity bill (\$)	0.777	0.855	0.816	0.871
SOD	11080	8119.5	6046.9	10321

TABLE II RESULTS WITH BATTERY

	S1	S2	S3
Energy usage (kWh)	22.17	22.15	24.27
Electricity bill (\$)	0.764	0.961	1.071
Battery cost (\$)	0.169	3.690	0.607
Total cost (\$)	0.933	4.651	1.678
COD	0.989	0.345	0.876

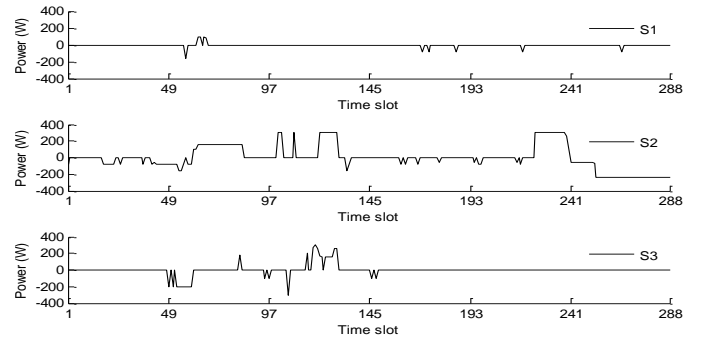


Fig. 2. Net power output of the battery

REFERENCE

- [1] Z. Chen, L. Wu, and Y. Fu, "Real-Time Price-Based Demand Response Management for Residential Appliances via Stochastic and Robust Optimization," *IEEE Trans. Smart Grid*, Vol. 3, No. 4, pp. 1822-1831, Dec. 2012.

Mitigation Measures against Cyber Intrusions at the Substations

Junho Hong, *Student Member, IEEE*,
Chen-Ching Liu, *Fellow, IEEE*,
Washington State University

Email: jhong@eecs.wsu.edu, liu@eecs.wsu.edu

Abstract—This paper proposed mitigation measures of the substations against cyber intrusions. Mitigation actions are conducted on the ICT side and the power grid side. On the ICT side, the anomaly detection system (ADS) and firewall have been used for mitigation. The temporal and rule-based anomaly detection have been used to detect host-based and network-based anomalies, respectively. Intruders are disconnected by collaboration between the ADS and the firewall. On the power grid side, emergency control actions are taken to mitigate the effects of cyber attacks as an attempt to restore a normal condition. The mitigation strategy here is to use the Optimal Power Flow (OPF) algorithm with an objective function that minimizes load shedding. The cyber intrusions have been simulated for the case study with three different ways: (1) substation communication network sniffing attack, (2) unauthorized control attack (circuit breaker binary status), and (3) packet altering attack (measured analog value).

I. KEY EQUATIONS

Temporal anomaly is determined by the two vectors that occur at two different time instants. The anomaly that occurred between the two time instants is determined by the normalized row vectors.

$$\Delta_{ta} = 1 - \frac{\sum_{i=1}^n (X_i - \bar{X})(Y_i - \bar{Y})}{\sqrt{\sum_{i=1}^n (X_i - \bar{X})^2} \sqrt{\sum_{i=1}^n (Y_i - \bar{Y})^2}} \quad (1)$$

II. KEY FRAMEWORK

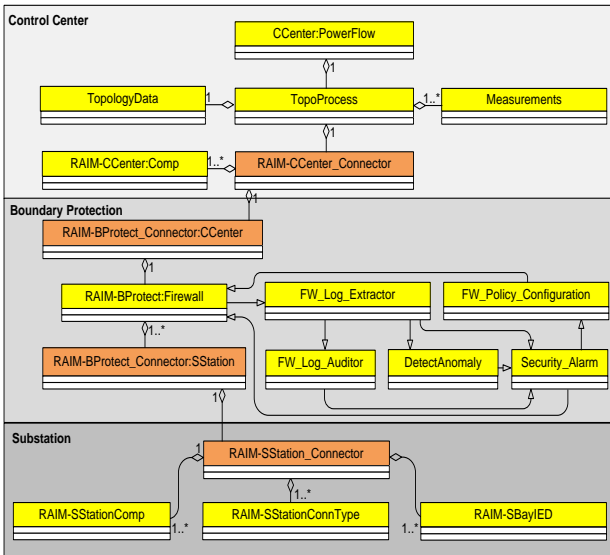


Fig. 1. The Data Object Models of Cyber-Physical Testbed.

III. KEY RESULTS

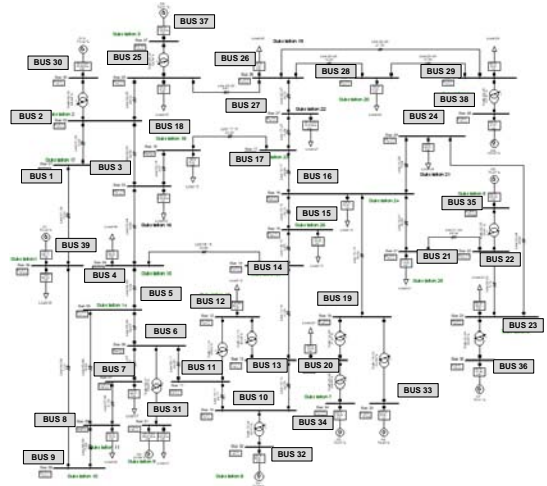


Fig. 2. IEEE 39 Bus System in a Power System Simulation Tool.

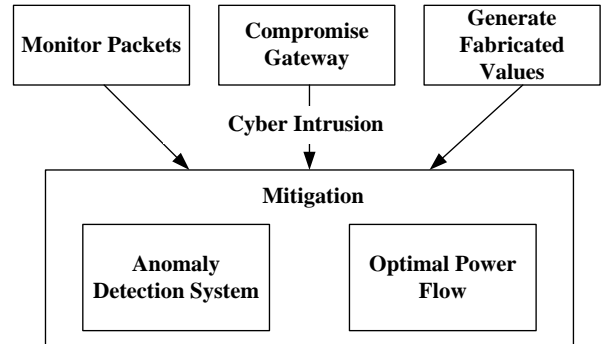


Fig. 3. Intrusion and Mitigation of Proposed Method.

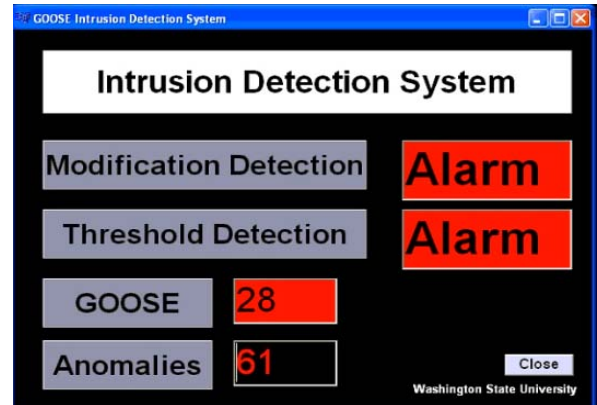


Fig. 4. Intrusion Detection System.

Power Grid Interdiction with Alternating Current Optimal Power Flow

Wei Yuan, *Student Member, IEEE* and Bo Zeng, *Member, IEEE*,

Abstract—Power grid interdiction problem is widely studied to evaluate the vulnerability of a power grid under contingencies or deliberate terrorists attacks. Due to the complexity of ac optimal power flow models, existing research in power grid interdiction are focused on using the relatively simple dc optimal power flow models to approximate the physics of a power grid. To exactly estimate power flows on a power grid, we propose to formulate the inner power flow model in power grid interdiction problem as an ac optimal power flow model. This ac power flow model is formulated as a semidefinite program to capture the reactive power flows and other nonlinearities in a real power grid. We develop and implement an algorithm to solve this power interdiction problem with semidefinite program ac optimal power flow model. Numerical studies on IEEE RTS 1996 test system are conducted to validate our algorithm.

I. INTRODUCTION

Power grid interdiction problem is formulated to evaluate the impacts of terrorists attacks on a power system. Such attacks is assumed as forcing a limited number of transmission assets out-of-service. In most literatures, power grid interdiction problem is characterized as a bilevel attacker-defender model. The outer level represents attacker’s decision on attack plans. The inner level problem is often formulated as a relatively simple dc optimal power flow model.

In our research, we propose to formulate the inner optimal power flow model as an ac power flow model to better represent a real physical power grid. To be specific, the ac power flow model is formulated as a semidefinite programming problem (SDP). The benefits of an ac power flow model over a dc power flow model is that an ac power flow model will help decision makers to exactly determine the outcomes of attacks. However, as far as we know, there is no existing exact algorithm that is capable of solving bilevel program with inner level problem as semidefinite program. Hence, we develop a new algorithm for this type of problem.

II. KEY EQUATION

An abstract formulation of the Attacker-Defender model with ac optimal power flow model is shown below,

$$\max_{\mathbf{w} \in \mathbb{W}} \min \sum_{n \in \mathcal{N}} d_n \quad (1)$$

$$\text{st. ACOF constraints with attack decisions} \quad (2)$$

$$\mathbb{W} = \{w_i \in \{0, 1\}, \sum_l w_l \leq R\} \quad (3)$$

W. Yuan and B. Zeng are with the Department of Industrial and Management Systems Engineering, University of South Florida, Tampa, FL, 33620 USA (e-mail: weiyuan@mail.usf.edu; bzeng@usf.edu)

d_n is the load shed at bus n , w_i is the binary attack decision variable. Detailed formulation will be provided in the poster.

III. KEY FIGURE

To validate our algorithm, we conduct case studies based on the IEEE RTS 96 reliability test system [1]. A random attack on 3 transmission lines is illustrated in Figure 1.

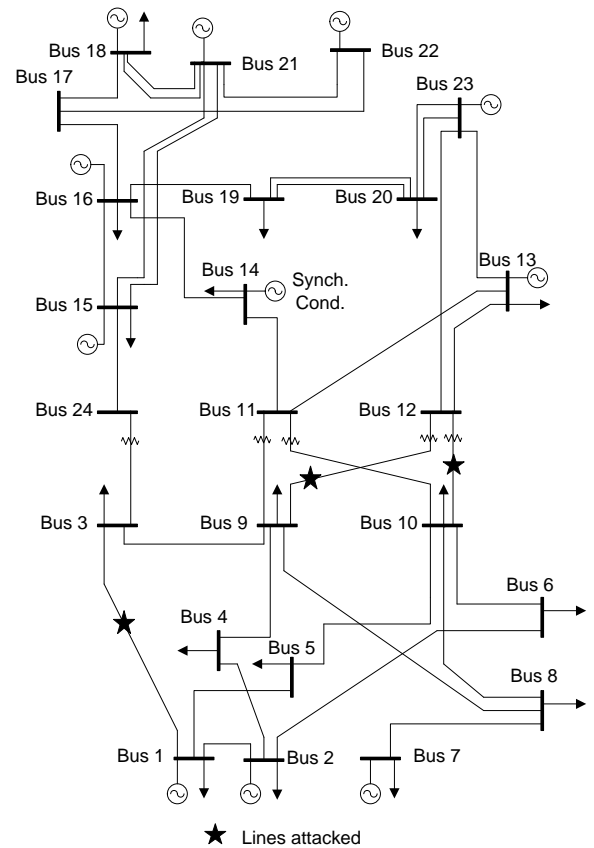


Fig. 1. IEEE RTS 96 reliability test system with 3 attacked transmission lines

REFERENCES

- [1] C. Grigg, P. Wong, P. Albrecht, R. Allan, M. Bhavaraju, R. Billinton, Q. Chen, C. Fong, S. Haddad, S. Kuruganty, W. Li, R. Mukerji, D. Patton, N. Rau, D. Reppen, A. Schneider, M. Shahidehpour, and C. Singh, “The IEEE reliability test system–1996,” *Power Systems, IEEE Transactions on*, vol. 14, no. 3, pp. 1010–1020, 1999.

A Real Time Cyber-Physical Test Bed

Ceeman Vellaithurai, *Student Member, IEEE*, and Anurag Srivastava, *Senior Member, IEEE*
 Smart Grid Demonstration and Research Investigation Lab (SGDRIL), Washington State University,
 Pullman, WA 99163, USA

email: ceeman.vellaithurai@email.wsu.edu and asrivast@eecs.wsu.edu

Abstract— The Electric Power System has been identified as one of the most critical infrastructure that is considered to be vulnerable to cyber-physical attacks. With the emphasis on making the grid “smarter”, there has been an increase in the deployment of several smart devices in the power grid, and automation of the power system has received a major boost. This makes the cyber-security of the power system even more relevant. Due to the unique nature of problems encountered in the power grid, it is necessary to consider the interdependencies of cyber and physical networks. Applications and algorithms developed for the smart grid need to be tested and evaluated using an integrated cyber-physical test bed for successful validation. In this work, we use the Real Time Digital Simulator (RTDS) and Network Simulator 3 (NS3) to develop a real time cyber-physical test bed.

I. DEVELOPED TEST BED

The RTDS is a virtual power system simulator designed for continuous real time operation. It can operate with a time step of 2 microseconds resulting in fast simulation. The RTDS can be connected to external hardware devices such as relays through various interfaces which allows for real time hardware in the loop simulation. NS3 is an exhaustive communication tool, which allows simulation and study of both wired and wireless network nodes. An interesting feature of NS3 utilized in this work is network emulation, meaning that it allows transfer of real network data packets over a simulated network. The RTDS simulates the power system, and measurement devices are used to measure various parameters as necessary. These data are then transferred through a NS3 emulated network, which has a model of the communication network to be used for the smart grid under consideration. By using these two tools, the cyber-physical test bed is setup.

There are several new applications being developed given availability of more sensor data within smart grid. With the advent of Phasor Measurement Units (PMUs) and their superior sampling rate, the scope and latency requirements of these applications generally vary. Using the developed cyber-physical test bed, applications such as ‘Voltage Stability Monitoring’ and ‘Distributed State Estimation’ based on PMU measurement as well SCADA data can be tested. In addition, other experiments such as the effect of change in delay due to change in the topology of the communication network on the working of the application can be studied.

II. KEY FIGURES

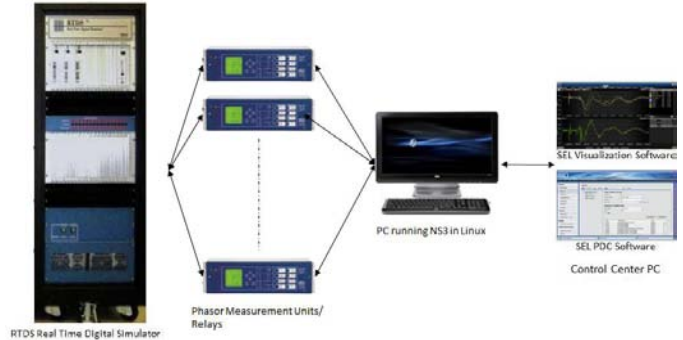


Fig. 1. Setup of the Cyber-Physical Test Bed

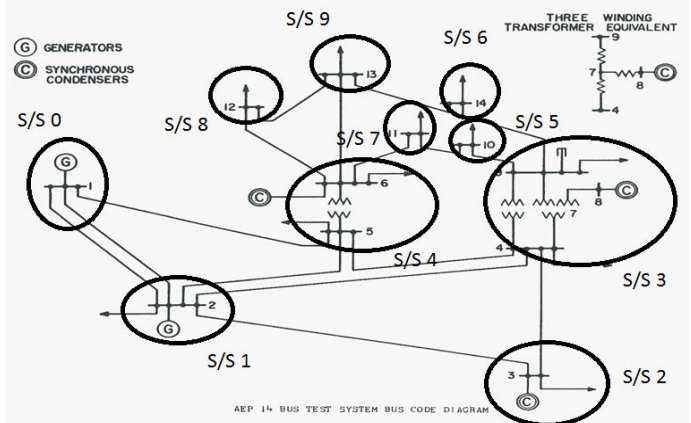


Fig. 2. Node Reduction of IEEE 14 bus system to form network nodes

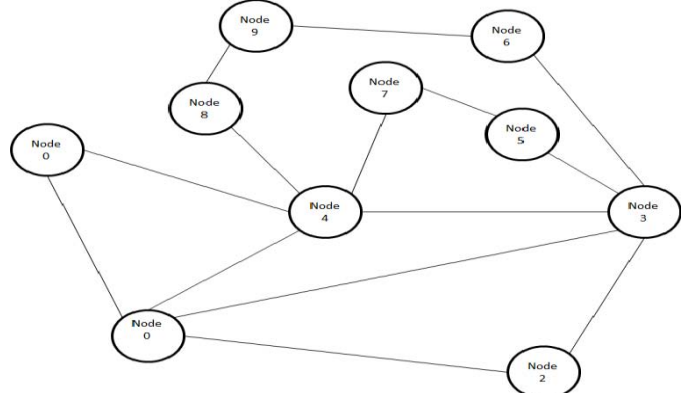


Fig. 3. Multi-hop communication network representation of IEEE 14 bus system

Security Aspects in Computation of Smart Grid Systems

Majumdar, Ankur

Department of Electrical and Electronic Engineering
Imperial College London
London, United Kingdom
ankur.majumdar@imperial.ac.uk

Pal, Dr. Bikash C.

Department of Electrical and Electronic Engineering
Imperial College London
London, United Kingdom
b.pal@imperial.ac.uk

Abstract—The electric distribution network is gradually making transition from a passive to an active and smart network, where it can improve the performance and flexibility of operation. It can improve and maintain the quality of service, reduce costs and increase the capacity of grid to host Distributed Generation. This smart distribution network will make efficient use of sensors and Automated Metering Infrastructure (AMI) in terms of measurement and communication architecture. To enable these smart functionalities of the network the states of the unbalanced distribution system need to be observed properly. Hence, the development of the Distribution System State Estimation (DSSE) has become an essential part of the distribution network operation. But this smartness of the system carries with it an inherent difficulty. With the proliferation of remote management and control of this smart system, security plays an important role, because the vastness of the system and the convenience of remote management can be exploited by adversaries or hackers for nefarious purposes. An adversary can influence the estimates by tampering with some of the meter data, the price information and control commands. The attacker can inject false data by targeting either some chosen or random state variables. Since most of the bad data detection algorithms depend on the residues of measurements, the attacker can take advantage of the fact that some of the measurements can pass the bad data detection test even if it is tampered. This poster aims to study the unbalanced Distribution System State Estimation (DSSE) which we aim to use it as a tool to inspect the stealthy attacks on the system and the countermeasures needed to protect the system against those attacks. The measurement data collected from remote terminal units (RTU) have inherent errors associated with them. To this end, we have used a modified version of IEEE-13 bus unbalanced system with a 4.16-kV feeder. The Weighted Least Squares (WLS) estimation has been used assuming that the errors are normally distributed. The zero injection measurements are considered as equality constraints to help avoid the ill-conditioning of the Gain matrix and thus the Gain matrix has been found to be numerically more stable than the conventional one. MATLAB is used for the modeling and simulation of the system. The feeders are modeled by modified Carson's equations, the measurements are modeled as real, virtual and pseudo measurements while the loads, considered as pseudo measurements, are modeled as ZIP loads. The study and results presented in this poster are intended to form a foundation for a further and more detailed analysis of the security aspects of the system.

Keywords—state estimation; Distribution System State Estimation (DSSE); Distribution Management Systems (DMS); smart meters

I. KEY FIGURES

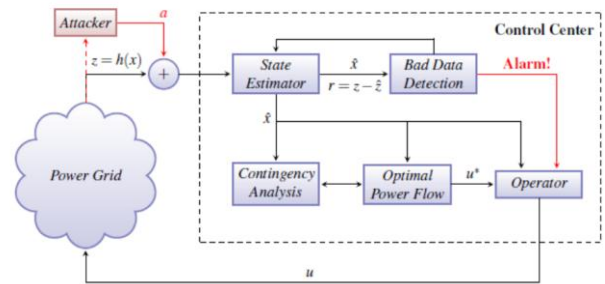


Figure 1: Schematic of DMS architecture

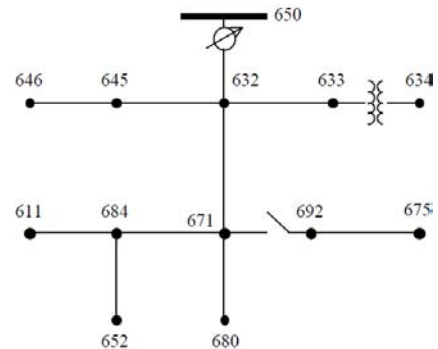


Figure 2: IEEE-13 bus distribution system

KEY REFERENCES

- [1] A. Abur and A. G. Exposito, "Power System State Estimation, Theory and Implementation," CRC Press
- [2] G. Hug and J. A. Giampapa, "Vulnerability Assessment of AC State Estimation With Respect to False Data Injection Cyber-Attacks," IEEE Transactions on Smart Grid, Vol. 3, No. 3, September 2012
- [3] Y. F. Huang, S. Werner, J. Huang, N. Kashyap and V. Gupta, "State Estimation in Electric Power Grids" IEEE Signal Processing Magazine, Page 33-43, September 2012

Attack-Resilient Measurement Design to Mitigate Topology Based Cyber Attacks in State Estimation

Aditya Ashok, Manimaran Govindarasu, Venkataramana Ajjrapu
 Department of Electrical and Computer Engineering
 Iowa State University
 Ames, Iowa.
 Email: aashok@iastate.edu

Abstract—Traditional measurement design problem in State Estimation provides a strategy for optimal placement of meters to ensure the overall system observability under possible single contingencies and loss of measurements. However, with the increased interconnectivity and exposure to public network infrastructures, the SCADA network is highly vulnerable to sophisticated cyber attacks that could potentially cause loss of meter data integrity or availability. It has been shown that the state estimates can be biased by malicious adversaries through carefully chosen topology manipulations. State Estimators use various pseudo measurements to handle cases where SCADA data does not provide total system observability, however, a loss of State Estimator accuracy when the system is operating under severe stress could cause the operator to take incorrect decisions. Therefore, it is extremely important to consider the system operating conditions, possibility of several types of contingencies and loss of measurements together in the measurement design problem to ensure system observability and acceptable State Estimator performance.

I. KEY QUESTIONS

The poster intends to address several key questions with respect to measurement design problem in state estimation:

- 1) Does the traditional measurement design capture all possible contingencies and loss of measurements?
- 2) How does the candidate measurement selection process work when more than one critical measurement is lost?
- 3) Does the measurement design problem capture State Estimate Accuracy requirements?

The measurement design problem can be formulated as follows:

$$\min \text{cost of new measurements}$$

subject to

1. satisfying total system observability for contingencies
2. satisfying accuracy requirements during contingencies

II. KEY FIGURES

The overall approach for identifying new measurements is presented in Figure 1.

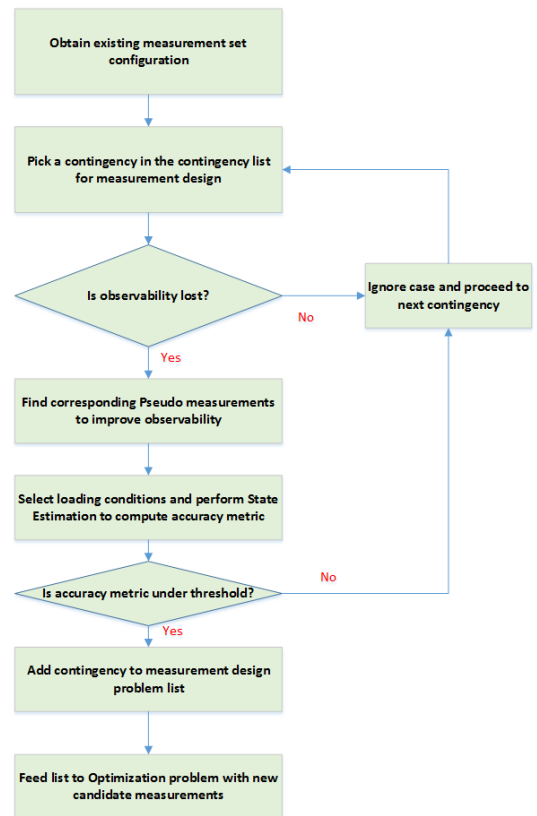


Fig. 1. Flowchart of attack-resilient measurement design

III. KEY RESULTS

We are working on a case study for this problem using the IEEE 14 bus test system. We will provide detailed results in the poster.

Coordinated Attacks Detection using Cyber-Physical Alert Correlation

Siddharth Sridhar, G. Manimaran
Department of Electrical and Computer Engineering
Iowa State University
Ames, IA 50010
Email: sridhar, gmani@iastate.edu

Chen-Ching Liu
School of Electrical Engineering and Computer Science
Washington State University
Pullman, WA 99164
Email: liu@eecs.wsu.edu

Abstract—The coupling between the cyber and physical elements of cyber-physical systems has strengthened with the arrival of advanced monitoring and control technologies. Omnipresent digital components such as smart meters have made the physical system vulnerable to the malicious actions effected through weaknesses in the computation and communication infrastructure. Traditional planning strategies in cyber-physical systems, such as the power system, accommodate the loss of single components (N-1 condition) due to inadvertent failures. However, the increased attack surface presented by cyber elements make the threat of forced multiple component failures (N-k condition) a possibility. An N-k condition could severely impact stability and economics of operation. In this poster, we present a general framework toward the detection of coordinated attacks through correlation of alerts from traditional intrusion detection systems and physical system monitoring system. We extend our framework to the detection of coordinated transmission line tripping attacks in power systems. Intrusion detection alerts from multiple substations are correlated with the state of the power system to detect coordinated tripping scenarios. We also address how the detection framework could be applied to the detection of other types of attacks on the power system.

REFERENCES

- [1] P. Ning, Y. Cui, and D. S. Reeves, “Constructing attack scenarios through correlation of intrusion alerts,” in *Proceedings of the 9th ACM conference on Computer and communications security*, ser. CCS '02. New York, NY, USA: ACM, 2002, pp. 245–254.

I. CYBER-PHYSICAL ALERT CORRELATION

Fig. 1 presents the methodology of our cyber-physical alert correlation system. Our detection framework is based on the hyper-alert correlation graph technique proposed in [1]. The three key components are - *i) knowledge base*, *ii) alert preprocessor* and *iii) correlation engine*. The objective of the alert correlation system is to identify cyber-physical attack signatures based on alerts from intrusion detection systems and critical power system measurements.

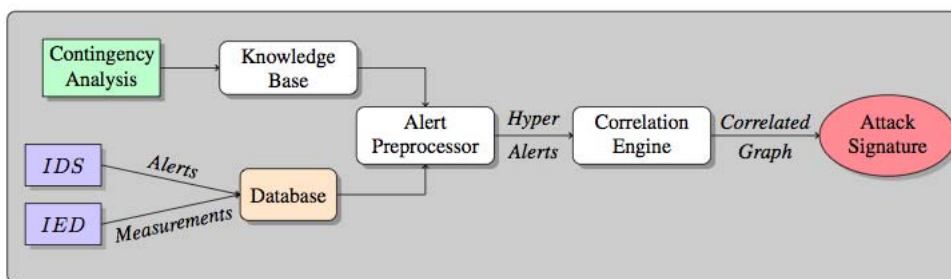


Fig. 1. Cyber-Physical Alert Correlator

Oscillation Modal Analysis from Ambient Synchrophasor Data using Distributed Frequency Domain Optimization

Jiawei “Alex” Ning, Vaithianathan “Mani” Venkatasubramanian

School of Electrical Engineering and Computer Science, Washington State University, Pullman, WA 99164, USA.

E-mails: jning@eecs.wsu.edu and mani@eecs.wsu.edu

Abstract-- A new distributed frequency domain algorithm for real-time modal estimation of large power systems using ambient synchrophasor data is provided. By dividing the computation between a supervisory central computer and local optimizations at the substation level, the algorithm efficiently estimates multiple dominant mode frequencies, damping ratios and mode shapes from wide-area power system measurements. The algorithm, called Distributed Frequency Domain Optimization, is tested on known test systems and archived real power system data from eastern and western power systems.

I. KEY EQUATIONS

The state equation of a linear system (power system operating around equilibrium point) can be given by

$$\begin{cases} \dot{\mathbf{x}}(t) = \mathbf{A}\mathbf{x}(t) + \mathbf{B}\mathbf{u}(t) \\ \mathbf{y}(t) = \mathbf{C}\mathbf{x}(t) + \mathbf{D}\mathbf{u}(t) \end{cases} \quad (1)$$

The transfer function of the i^{th} mode for any output y_j is given by

$$\mathbf{H}_{i,j}(s) = \frac{\mathbf{R}_{i,j}(s)}{s - \lambda_i} \quad (2)$$

Power Spectrum Density can be represented by the equation below

$$\mathbf{S}_{yy}(\omega) = \mathbf{H}(j\omega)\mathbf{S}_{uu}(\omega)\mathbf{H}(j\omega)^H \quad (3)$$

$$\mathbf{S}_{y_k y_k}(\omega) = \mathbf{H}_{all,k}(j\omega)\mathbf{M}\mathbf{H}_{all,k}(j\omega)^H \quad (4)$$

The transfer function for k^{th} output considering all modes

$$\mathbf{H}_{all,k}(j\omega) = \sum_{i=1}^n \frac{\mathbf{R}_{i,k}}{j\omega - \lambda_i} \quad (5)$$

For i^{th} mode, $\lambda_i = -\alpha_i + j\omega_i$, combine them and ignore cross terms

$$\begin{aligned} \mathbf{S}_{y_k y_k}(\omega) \Big|_{\omega \text{ close to } \omega_i} \\ \approx \frac{\mathbf{R}_{i,k}}{\alpha_i + j(\omega - \omega_i)} \mathbf{M} \frac{\mathbf{R}_{i,k}^H}{\alpha_i - j(\omega - \omega_i)} \end{aligned} \quad (6)$$

Furthermore, the magnitude of the frequency response (square root of PSD) can be presented by

$$\left| \mathbf{H}_{all,k}(j\omega) \right| \Big|_{\omega \text{ close to } \omega_i} \approx \frac{\sqrt{g}}{\sqrt{\alpha_i^2 + (\omega - \omega_i)^2}} \quad (7)$$

where g is a constant.

II. KEY FIGURE

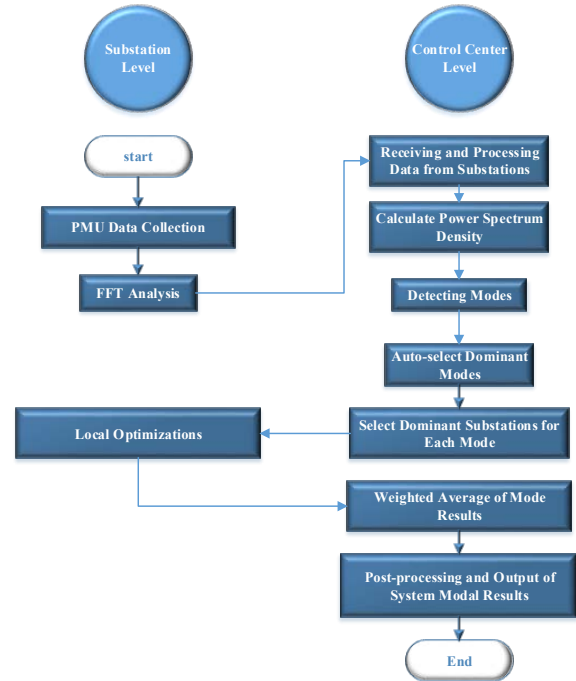


Fig. 1. Flowchart for DFDO

III. KEY RESULTS

TABLE I. RESULTS FOR WECC AUG. 10TH 1996 EVENT

Algorithm	Freq. (Hz)	Freq.Std. Dev.(Hz)	Damping Ratio(%)	Damping Ratio Std. Dev. (%)
Prony	0.2690	--	2.59	--
DFDO	0.2507	0.0011	1.70	0.54
FDD	0.2510	0.0002	1.60	0.18

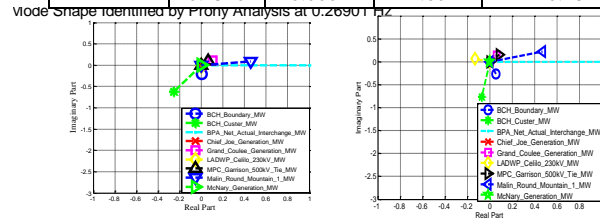


Fig. 2. Prony vs. DFDO mode shape results prior to Ross-Lexington tripping

Set Point Adjustment Strategy for Mitigating Transients in a Microgrid

Christopher Stone, *Graduate Student Member, IEEE*, and Ali Mehrizi-Sani, *Member, IEEE*
 School of Electrical Engineering and Computer Science, Washington State University, Pullman, WA, 99164 USA
 E-mail: christopher.stone@email.wsu.edu, mehrizi@eecs.wsu.edu

Abstract—In today’s power hungry society, the power system often operates close to the operational limits of distributed energy resource (DER) units to meet increased load demands and satisfy utilization purposes, e.g., utilizing waste heat to increase overall efficiency. Transients in such a system can push the system past these operational limits, which can cause instability, tripping of protective devices, and violations of the ratings of power electronically interfaced DER units. Typically the infinite bus assumption of the main grid means that load changes are negligible compared to the rest of the system and are easily compensated by the upstream plants and generators. However, this is not the case for small-scale power systems, such as microgrids in islanded mode, where there is significantly less generation capacity to accommodate large disturbances. Thus, there is a need for a strategy that can mitigate transients in these small-scale systems.

This poster presents a quadratic prediction strategy for set point automatic adjustment with correction enabled (SPAACE). SPAACE is an autonomous control strategy that operates between the primary, typically a PI, and secondary controllers of the DER. As the name implies, SPAACE works by adjusting the set point sent by the supervisory control system in order to mitigate transients that may violate operational limits in the system. This strategy improves on the existing ones by being able to work in conjunction with existing controllers in the system and by promoting plug-and-play functionality. It also is an adaptive control technique, i.e., it requires no *a priori* knowledge of the system and depends only on local variable. Thus, it does not require any extra communication channels or centralized controllers.

By sampling values of the DER unit’s output, SPAACE can be used to predict future values of the system. If a predicted value is in violation of the operational limits of the DER unit, SPAACE can adjust the set point of the variable in order to shape its output trajectory. Once the predicted output is within the limits, the set point is brought back to its original value. The proposed quadratic prediction strategy observes these sampled values and uses a Taylor Series approximation to predict future outputs.

I. KEY EQUATIONS

The equation for quadratic prediction is:

$$\hat{x}(t_0 + T_{\text{pred}}) = x(t_0) + r(t_0)T_{\text{pred}} + \frac{1}{2}q(t_0)T_{\text{pred}}^2 \quad (1)$$

where,

$$r(t_0) = \frac{dx(t_0 - \frac{T_{\text{pred}}}{2})}{dt}$$

$$q(t_0) = \frac{d^2x(t_0 - \frac{T_{\text{pred}}}{2})}{dt^2}$$

The prediction time T_{pred} is the distance of time into the future that the output is to be predicted. This value is determined heuristically through observation of the output response being

controlled. Using this predicted value, the set point is adjusted by the following rules for SPAACE:

$$x'_{sp} = \begin{cases} (1 + m)x_{sp}, & \text{if } \hat{x}(t_0 + T_{\text{pred}}) < x_{min} \\ (1 - m)x_{sp}, & \text{if } \hat{x}(t_0 + T_{\text{pred}}) > x_{max} \\ x_{sp}, & \text{otherwise} \end{cases} \quad (2)$$

where m is the factor by which the set point is adjusted.

II. KEY FIGURES AND RESULTS

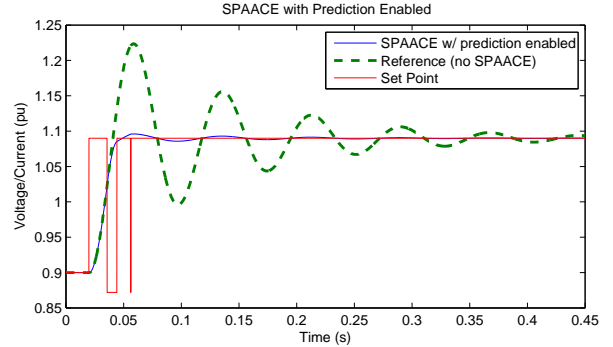


Fig. 1: SPAACE with quadratic prediction response to step input using a MATLAB simulation.

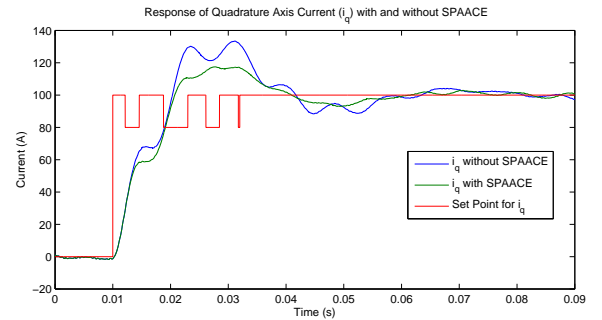


Fig. 2: SPAACE with quadratic prediction response to step input using a PSCAD simulation.

SPAACE with quadratic prediction is tested using MATLAB and PSCAD simulation environments. Fig. 1 was produced using MATLAB and compares the step change response of a signal from 0.9 to 1.09 pu with and without SPAACE intervention, where $x_{max} = 1.1$. The PSCAD case simulates a DER unit tied to a 14-bus feeder system. Fig. 2 shows the response of this system when a step change is applied to the quadrature axis current i_q from 0 to 100 A, where $i_{q,max} = 120$ A. Response is improved in both cases.

Integration of Demand Response into Load Shedding in Distribution Network

Kaium Uz Zaman Mollah , Momen Bahadornejad, Nirmal C-K Nair
 Department of Electrical and Computer Engineering
 University of Auckland, Auckland, New Zealand
 E-mail: kmol006@aucklanduni.ac.nz

Abstract—In this paper, a demand response (DR) based energy shedding scheme is proposed to comfort automatic under voltage load shedding (AUVLS) scheme for a radial distribution network. The proposed scheme is included DR to comfort the LS scheme, the energy index factor is used to identify the consumption pattern of the consumers to offer the incentive benefit, and an AUVLS scheme is used as a last resort to protect the system. A new concept of coordination of DR and automatic LS scheme is proposed. An example of the performance of proposed scheme on a 15 bus radial distribution test system is provided to illustrate effectiveness of the method and the shedding procedure. Different scenarios have been simulated with results showing that proposed method is effective in comfort the AUVLS scheme. PSS/E commercial software is used to simulate the results.

I. KEY EQUATIONS

The generalized form of voltage magnitude at each bus is obtained as following:

$$|V_{(i+1)}| = \left[\left\{ (P_{(i+1)} * R_{(i)} + Q_{(i+1)} * X_{(i)} - 0.5|V_{(i)}|^2)^2 - (R_{(i)}^2 + X_{(i)}^2)(P_{(i+1)}^2 + Q_{(i+1)}^2) \right\}^{0.5} - (P_{(i+1)} * R_{(i)} + Q_{(i+1)} * X_{(i)} - 0.5|V_{(i)}|^2) \right]^{0.5} \quad (1)$$

The injected active and reactive power at each bus is calculated as:

$$P_{(i+1)} = \sum_{j=i+1}^N P_{L(j)} + \sum_{j=i+1}^{N-1} L_{P(j)} \quad (2)$$

and:

$$Q_{(i+1)} = \sum_{j=i+1}^N Q_{L(j)} + \sum_{j=i+1}^{N-1} L_{Q(j)} \quad (3)$$

In (2) and (3), P_L and Q_L are the load active and reactive power at each bus, and L_P and L_Q are the line active and reactive loss, respectively.

The average energy consumption per customer can be obtained from energy index factor (EIF):

$$EIF = \frac{E_i}{\sum_{i=1}^n E_i} \quad (4)$$

II. KEY FIGURES

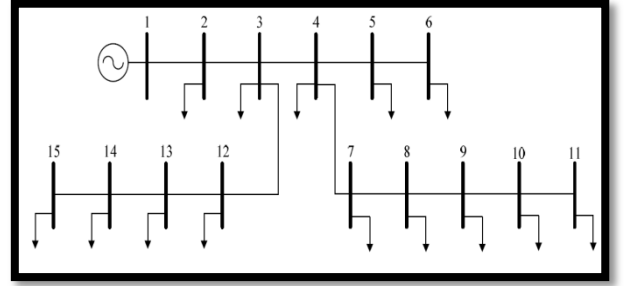


Fig. 1. Single line diagram of 15 bus radial system

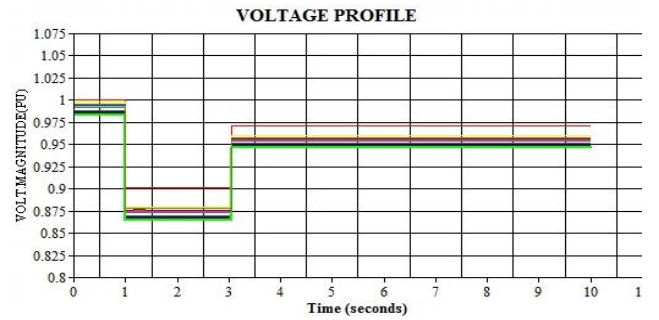


Fig.2. Voltage profile with energy shedding only

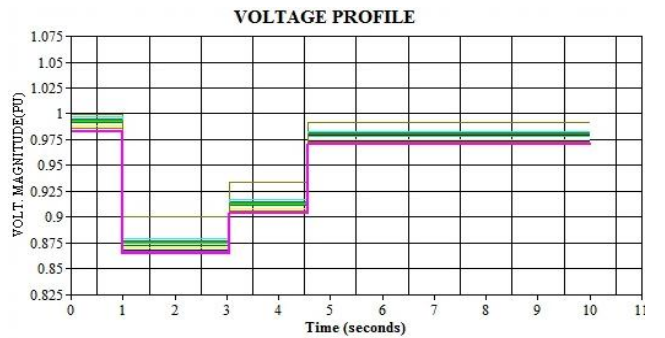


Fig.3. Voltage profile with coordinated energy shedding and under voltage load shedding

III. KEY RESULTS

TABLE 1. COMPARING TEST RESULTS

Bus	ES (MVA)	LS (MVA)	Incentive benefit is received?
Case-1	0.5409	-	Yes
Case-2	0.2404	0.4808	Yes

Adaptive PI Control of STATCOM for Voltage Regulation

Yao Xu and Fangxing Li

The Department of Electrical Engineering and Computer Science, the University of Tennessee (UT), Knoxville, TN 37996, USA,

Email: yxu25@utk.edu and fli6@utk.edu

Abstract—STATCOM can provide fast and efficient reactive power support to maintain power system voltage stability. In the literature, various STATCOM control methods have been discussed including many applications of proportional–integral (PI) controllers. However, these previous works obtain the PI gains via a trial and error approach or extensive studies with a tradeoff of performance and applicability. Hence, control parameters for the optimal performance at a given operating point may not be effective at a different operating point. This paper proposes a new control model based on adaptive PI control, which can self-adjust the control gains during disturbance such that the performance always matches a desired response, regardless of the change of operating condition. Since the adjustment is autonomous, this gives the plug-and-play capability for STATCOM operation. In the simulation test, the adaptive PI control shows consistent excellence under various operating conditions such as different initial control gains, different load levels, change of transmission network, and consecutive disturbances. As a comparison, the conventional STATCOM control with tuned, fixed PI gains usually perform fine in the original system, but may not perform as efficient as the proposed control method when there is a change of the system conditions.

I. KEY EQUATIONS

Voltage regulator PI gains can be computed by the following equations:

$$K_{p_v}(t) = \frac{k_v \times \Delta V(t)}{(\Delta V(t) + m_v \times \int_t^{\infty} \Delta V dt)} \quad (1)$$

$$K_{i_v}(t) = m_v \times K_{p_v}(t) \quad (2)$$

Current regulator PI gains can be obtained by:

$$K_{p_i}(t) = \frac{k_i \times \Delta I_q(t)}{(\Delta I_q(t) + m_i \times \int_t^{\infty} \Delta I_q dt)} \quad (3)$$

$$K_{i_i}(t) = m_i \times K_{p_i}(t) \quad (4)$$

II. KEY FIGURES

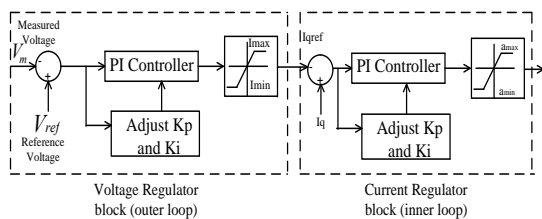


Fig. 1. Adaptive PI control block for STATCOM.

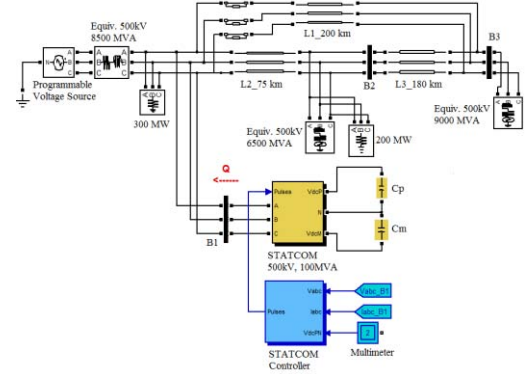


Fig. 2. The studied system.

III. KEY RESULTS

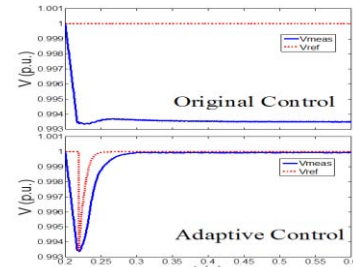


Fig. 3. Voltages with changed Kp and Ki in the original control.

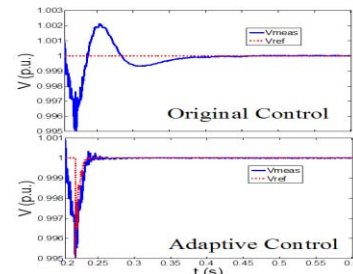


Fig. 4. Results of measured voltage with change of transmission network.

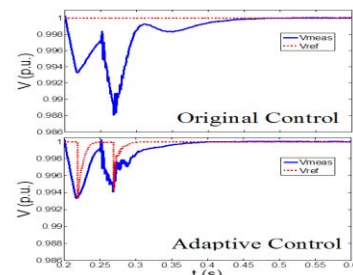


Fig. 5. Results of measured voltage in two consecutive disturbances.

Control of UPFC Using Hamilton–Jacobi–Bellman Formulation Based Neural Network

H. Nazaripouya , S. Mehraeen, *Member, IEEE*

School of Electrical Engineering and Computer Science, 3106C PFT Hall, Louisiana State University, Baton Rouge, LA 70803.
Contact author: hnazar1@lsu.edu, smehraeen@lsu.edu

Abstract—In this paper, the micro grid stability is investigated by utilizing a non-linear optimal controller and FACTS device. Using micro grid continuous-time model and control design impose a huge computational burden due to the required high sampling rate to achieve stability when utilizing a digital controller. Thus, developing of an advanced discrete-time (DT) stabilizing controller design is of paramount importance in the micro grids. In this paper a nonlinear discrete-time stabilizing controller using Unified Power Flow Controller (UPFC) is proposed for micro grids by employing the discrete-time Hamilton-Jacobi-Bellman (HJB) optimal control method. The designed optimal controller is applied to control the UPFC's series voltage and to optimally mitigate the power oscillations. The micro grid under consideration is comprised of a synchronous generator, renewable energy sources, and loads. The UPFC series voltage is considered as control input and the optimal strategy is applied. A discretized micro grid nonlinear dynamical model is derived and successive approximation method is utilized to approximate the cost function of the generator states and the UPFC control parameters. Finally, a neural network (NN) is utilized to approximate the cost function using the weighted residual method. By applying the developed optimal controller, it is shown that oscillations caused by faults are mitigated more effectively compared to the conventional generator controllers.

I. KEY EQUATIONS

The space state equations of the system composed of a synchronous generator and a UPFC in the form of $x_{k+1} = f_k + g_k u_k$:

$$\begin{bmatrix} \delta(k+1) \\ \omega(k+1) \end{bmatrix} = \begin{bmatrix} \omega T + \delta(k) \\ \frac{T}{M} (P_m - \frac{E'V_1}{X} \sin(\delta(k)) - D\omega(k)) + \omega(k) \end{bmatrix} \quad (1)$$

$$+ \begin{bmatrix} 0 \\ \frac{T}{M} \frac{E'V_1}{X} \cos(\delta) - \frac{T}{M} \frac{E'V_1}{X} \sin(\delta) \end{bmatrix} \begin{bmatrix} \gamma \\ \beta \end{bmatrix}$$

Infinite horizon cost function:

$$J_k = \sum_{j=k}^{\infty} r(x_j, u_j) = Q(x_k) + u_k^T R u_k + J_{k+1} \quad (2)$$

Value function :

$$V_k = \min_{u_k} \sum_{j=k}^{\infty} r(x_j, u_j) = Q(x_k) + u_k^{*T} R u_k^* + V(f_k + g_k u_k^*) \quad (3)$$

The discrete-time HJB equation

$$V(f_k + g_k u_k^*) - V(x_k) + Q(x_k) + u_k^{*T} R u_k^* = 0 \quad (4)$$

The optimal control input u_k^*

$$u_k^* = -[g_k^T \nabla^2 V_k g_k + 2R]^{-1} g_k^T [\nabla V_k^T + \nabla^2 V_k (f_k - x_k)] \quad (5)$$

Approximation of nonlinear value function with an NN as

$$V_L(x) = \sum_{l=1}^L \omega_l \sigma_l(x) = W_L^T \bar{\sigma}_L(x) \quad (6)$$

II. KEY RESULTS

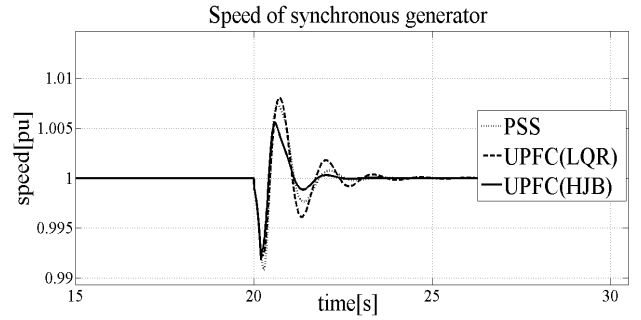


Fig. 1. Speed of synchronous generator before and after fault damped by two control method of UPFC (LQR, HJB) and PSS in Isolated micro grid

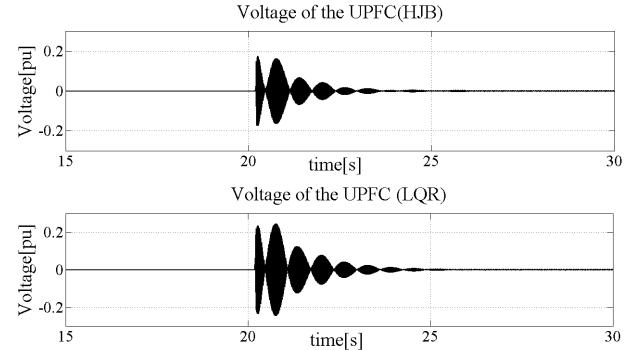


Fig. 2. UPFC series voltage before and after fault using two different in Gen-Infinite bus system controller (LQR, HJB) in Isolated micro grid

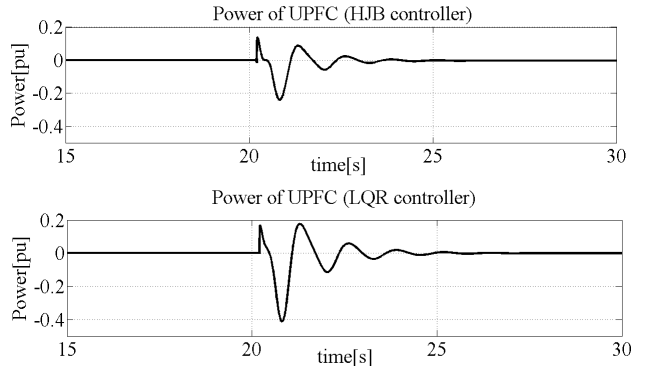


Fig. 3. Power of UPFC before and after fault using two different controllers (LQR, HJB) in Isolated micro grid

Data Analysis and Visualization of Oscillation Monitoring System in Power Systems

Tianying Wu and Vaithianathan “Mani” Venkatasubramanian

The School of Electrical Engineering and Computer Science, Washington State University
Pullman, WA 99163, USA

Email: tianying.wu@email.wsu.edu and mani@eecs.wsu.edu

Abstract—Based on the measurement data from synchrophasors or PMUs installed across the power grid, the Oscillation Monitoring System (OMS) is a real-time monitoring system that identifies the oscillatory modal properties in power systems. Generated by high volume of operational data from PMUs, the massive complex outputs of OMS, if not presented well, will bring in inefficiency in utilizing and analyzing these results. In this study, a data analysis and visualization engine has been developed which is aimed to monitor the electromechanical oscillations based on the output results from OMS, and therefore detect the poorly-damped oscillatory modes. The engine would first give an overview of all detected modes within user determined time range, and then, display the detail information of the specific mode, which includes frequency, damping ratio, mode energy, confidence level as well as the mode shape of different PMU channels. In order to improve the data quality, a moving average algorithm has been used to smooth out short-term fluctuations and highlight longer-term trends. Demos demonstrate the efficiency and versatility of the developed engine in extracting and analyzing the useful information from the large quantity of outputs.

II. KEY RESULTS

I. KEY FIGURES

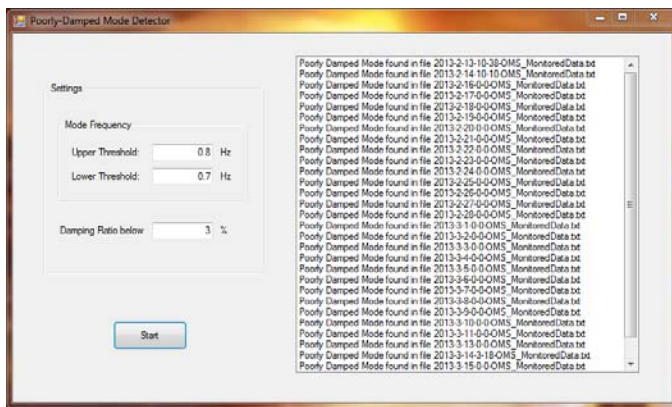


Fig. 1. Poorly-Damped Mode Detector

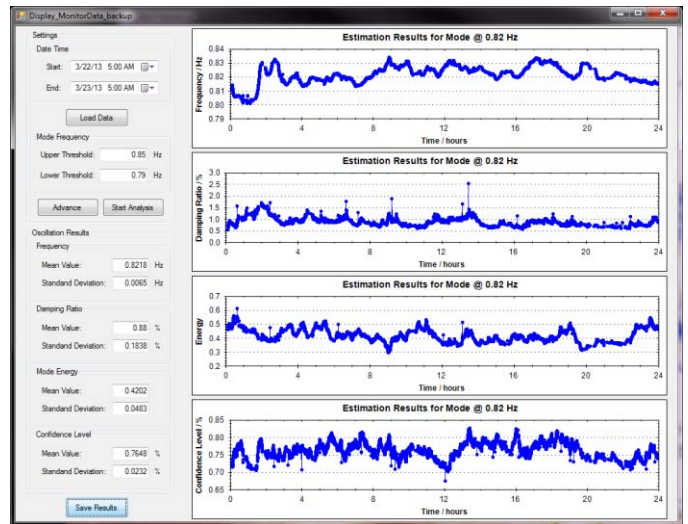


Fig. 2. An example of estimation results

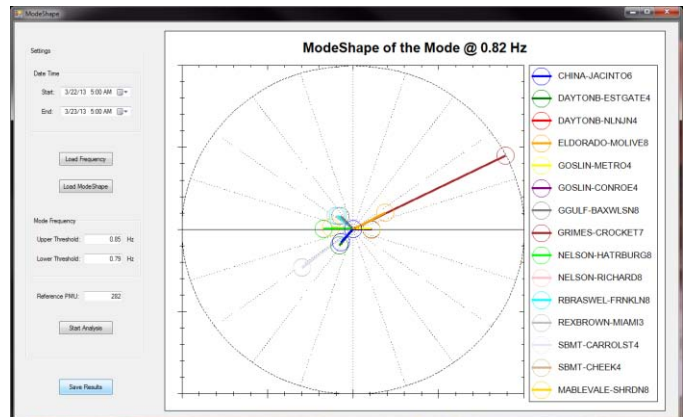


Fig. 3. An example of ModeShape results

Reactive Power Substitution Between Rapid and Slow Dynamic Var Compensators

Xuran Wang, Bin Wang, Qinglai Guo, *Member, IEEE*, Hongbin Sun*, *Senior Member, IEEE*,
Boming Zhang, *Fellow, IEEE*, Mingye Zhang

Dept. of Electrical Engineering, Tsinghua University, Beijing, China
Email: wxr08@mails.tsinghua.edu.cn

Abstract— By substituting the slow dynamic var compensator (such as synchronous generator) for rapid dynamic var compensator (such as SVC/SVG) in the static conditions, the rapid dynamic reactive power reservation can be significantly boosted. Therefore, the reactive power reservation can respond to the dynamic network disturbance more effectively. This paper proposes a quadratic programming based optimization model to implement the idea of substituting the slow dynamic reactive power for the rapid dynamic reactive power on the premise of ensuring the system security and keeping an approximate constant voltage of pilot buses. It can keep SVC/SVG a large upward and downward reactive power reservation and ensure the regional balanced reactive power of generators. Simulation results on the New England 39-bus system show that regional rapid dynamic reactive reservation is enhanced and the dynamic voltage stability is improved after the substitution.

I. KEY EQUATIONS

The objective function of the quadratic programming is as following:

$$\min_{\Delta Q_g} \left\{ \mathbf{w}_s \|\boldsymbol{\theta}_s\|^2 + \mathbf{w}_g \|\boldsymbol{\theta}_g\|^2 \right\}$$

The solution of the model must meet the security constraints as following:

$$\mathbf{V}_p^{\min} \leq \mathbf{V}_p + \mathbf{C}_{vpg} \Delta \mathbf{Q}_g \leq \mathbf{V}_p^{\max}$$

$$\mathbf{V}_g^{\min} \leq \mathbf{V}_g + \mathbf{C}_{vg} \Delta \mathbf{Q}_g \leq \mathbf{V}_g^{\max}$$

$$\mathbf{Q}_g^{\min} \leq \mathbf{Q}_g + \Delta \mathbf{Q}_g \leq \mathbf{Q}_g^{\max}$$

$$\mathbf{Q}_s^{\min} \leq \mathbf{Q}_s + \mathbf{C}_{qsg} \Delta \mathbf{Q}_g \leq \mathbf{Q}_s^{\max}$$

II. KEY RESULTS

TABLE I. COMPARISON FOR SVCs BEFORE AND AFTER THE SUBSTITUTION

SVC bus		11	18	23	29
Reactive power (MVar)	Before	13.9	31.0	35.2	8.2
	After	0.1	-0.1	-0.1	-0.4
Reactive power vector	Before	12.1%	31.6%	34.8%	7.8%
	After	0%	0%	0%	0%

TABLE II. COMPARISON FOR ALL THE GENERATOR BUSES BEFORE AND AFTER THE SUBSTITUTION

Generator bus		Total
Reactive power (MVar)	Before	1070.6
	After	1256.8

TABLE III. COMPARISON FOR ALL THE GENERATOR BUSES WITH AND WITHOUT CONSIDERATION OF GENERATOR BALANCE

Generator bus		Total
Reactive power (MVar)	With consideration of generator balance	1256.8
	Without generator balance consider	1312.4
Reactive power vector	With consideration of generator balance	0.755
	Without consideration of generator balance	0.901

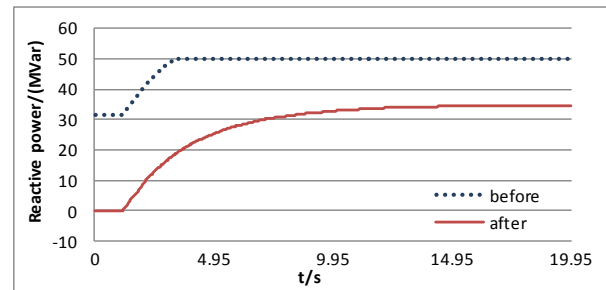


Figure 1. Reactive power of SVC 2 after the disturbance

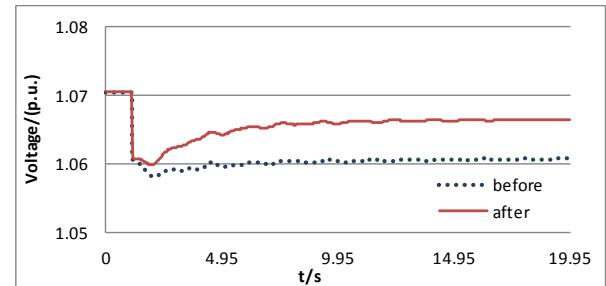


Figure 2. Voltage of SVC 2 after the disturbance

Role of Electromechanical Wave Propagation in Power Systems

Tianya Li, *Student Member, IEEE*, Gerard Ledwich, *Senior Member, IEEE*, and Yateendra Mishra, *Member, IEEE*
 School of Engineering and Computer Science, Queensland University of Technology, Brisbane, Australia

Email: t8.li@qut.edu.au, g.ledwich@qut.edu.au, yateendra.mishra@qut.edu.au

Abstract — In a large interconnected power system, disturbances initiated by a fault or other events cause acceleration in the generator rotors with respect to their synchronous reference frame. This acceleration of rotors can be described by two different dynamic phenomena, as shown in existing literature. One of the phenomena is simultaneous acceleration and the other is electromechanical wave propagation, which is characterized by travelling waves in terms of a wave equation. This paper demonstrates that depending on the structure of the system, the exhibited dynamic response will be dominated by one phenomenon or the other or a mixture of both. Two system structures of choice are examined, with each structure exemplifying each phenomenon present to different degrees in their dynamic responses. Prediction of dominance of either dynamic phenomenon in a particular system can be determined by taking into account the relative sizes of the values of its reduced admittance matrix.

I. KEY EQUATIONS

The classical swing equation, the corresponding continuum model in the form of a wave equation, and the wave phase speed equation are

$$\frac{2H}{\omega_0} \frac{d^2 \delta}{dt^2} + \omega_0 D \frac{d\delta}{dt} = P_a = P_m - P_e \quad (1)$$

$$\frac{\partial^2 \delta}{\partial t^2} + \gamma \frac{\partial \delta}{\partial t} - v^2 \nabla^2 \delta + u^2 (\nabla \delta)^2 = P \quad (2)$$

$$v = \sqrt{\frac{\omega V^2 \sin \theta}{2h|z|}} \quad (3)$$

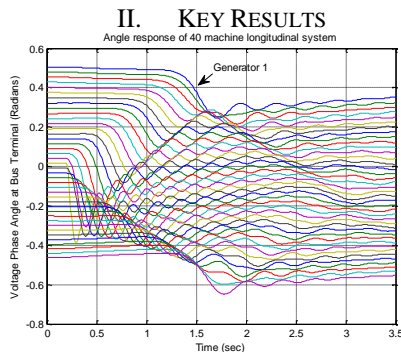


Figure 1 Angle Response of Strongly Connected Longitudinal System

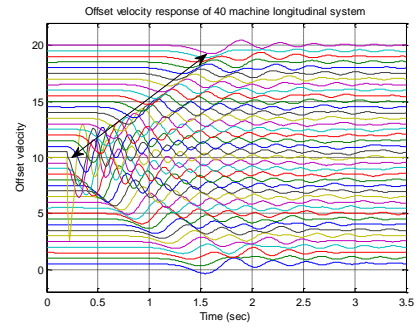


Figure 2 Offset Velocity Response of Strongly Connected Case

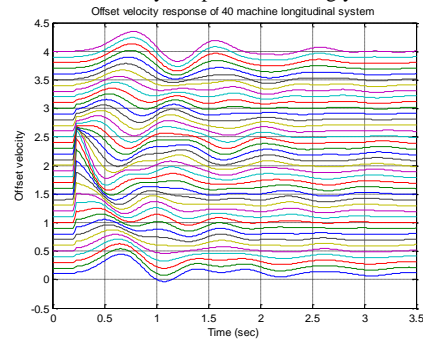


Figure 3 Offset Velocity Response of Weakly Connected Case

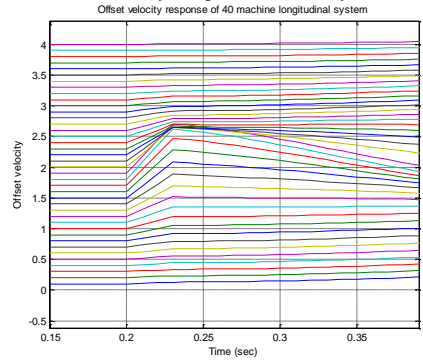


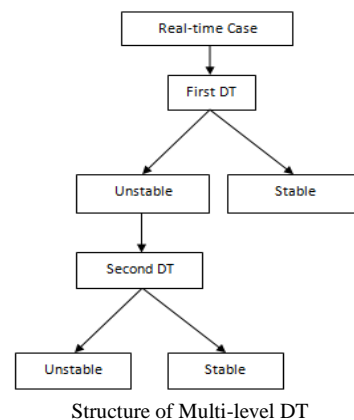
Figure 4 Enlarged Offset Velocity Response of Weakly Connected Case

Making On-line Transient Stability Decisions with Multi-level Decision Trees

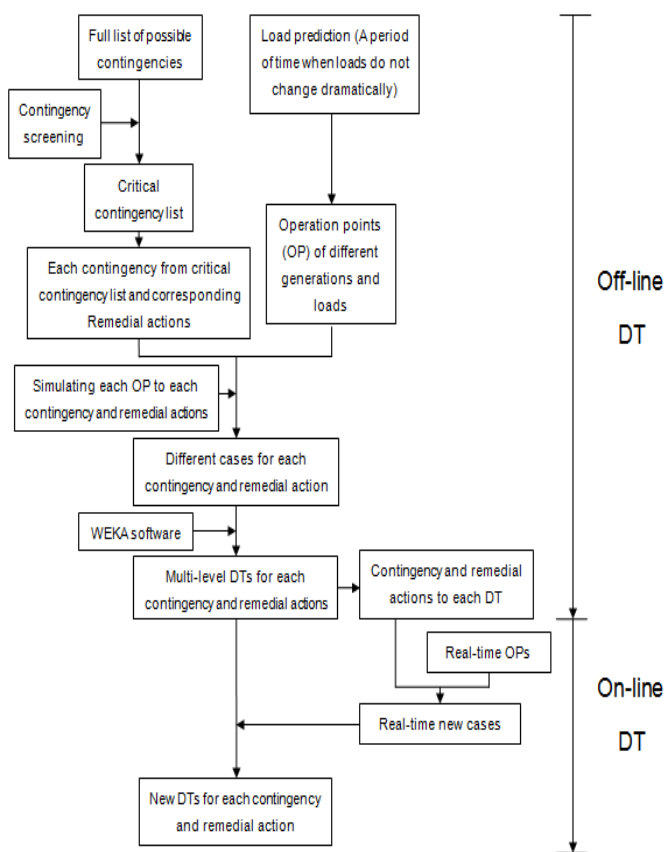
Tuo Ji, *Student Member, IEEE*, and Anjan Bose, *Fellow, IEEE*

Abstract—During recent years, power systems are becoming more and more stressed, and thus more vulnerable to various contingencies. For specific instability cases, engineers can conduct off-line studies to devise preventive and remedial actions. This paper however, proposes a multi-level decision tree scheme, which not only evaluates the dynamic security of power systems as what other companion papers have done using decision trees, but also suggests ways of making real-time remedial control actions based on the proposed scheme. To achieve these goals, we collect pre-fault and post-fault data with the help of PMU and build the multi-level decision trees to make on-line decisions.

Index Terms—Decision Trees, On-line, PMU, Transient Stability Prediction, Remedial Actions



I. KEY FIGURES



Flowchart of Building DTs

II. KEY RESULTS

TABLE I
CORRECT RATE FOR TRAINING DATA

DTs	Correct Rate
Ctg1_DT1	99.97%
Ctg1_DT2	99.86%
Ctg2_DT1	99.97%
Ctg2_DT2	99.97%

TABLE II
CORRECT RATE FOR TESTING DATA

DTs	Correct Rate
Ctg1_DT1	99.81%
Ctg1_DT2	99.48%
Ctg2_DT1	99.45%
Ctg2_DT2	99.61%

TABLE III
CORRECT RATE FOR MULTI-LEVEL DTs

DTs	Correct Rate
Ctg1	94.83%
Ctg2	97.88%

Some issues with Quasi-Steady State Model in Long-term Stability

Xiaozhe Wang, *Student Member, IEEE*, Hsiao-Dong Chiang, *Fellow, IEEE*
 Department of Electrical and Computer Engineering, Cornell University, Ithaca, NY, 14853 USA.
 E-mail: xw264@cornell.edu, hc63@cornell.edu.

Abstract—The Quasi Steady-State (QSS) model of long-term dynamics relies on the idea of time-scale decomposition. Assuming that the fast variables are infinitely fast and are stable in the long-term, the QSS model replaces the differential equations of transient dynamics by their equilibrium equations to reduce complexity and increase computation efficiency. Although the idea of QSS model is intuitive, its theoretical foundation has not yet been developed. In this paper, several counter examples in which the QSS model fails to provide a correct approximation of the complete dynamic model in power system are presented and the reasons of the failure are explained from the viewpoint of nonlinear analysis.

I. KEY EQUATIONS

TABLE I

THE MATHEMATICAL DESCRIPTION OF MODEL FOR POWER SYSTEM

complete model	$\begin{aligned} z'_c &= h_c(z_c, z_d, x, y) \\ z_d(k+1) &= h_d(z_c, z_d(k), x, y) \\ \epsilon x' &= f(z_c, z_d, x, y) \\ 0 &= g(z_c, z_d, x, y) \end{aligned}$
transient model (approximation for transient stability) short-term:0-30s	$\begin{aligned} \dot{x} &= f(z_c, z_d, x, y) \\ 0 &= g(z_c, z_d, x, y) \end{aligned}$
QSS model (approximation for long-term stability) long-term:30s-a few minutes	$\begin{aligned} z'_c &= h_c(z_c, z_d, x, y) \\ z_d(k+1) &= h_d(z_c, z_d(k), x, y) \\ 0 &= f(z_c, z_d, x, y) \\ 0 &= g(z_c, z_d, x, y) \end{aligned}$

II. KEY FIGURE

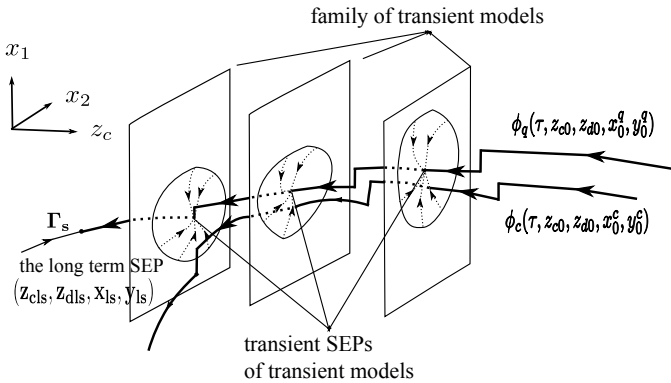


Fig. 1. When z_d firstly change to $z_d(k)$, the initial point of the complete model gets outside of the stability region of the transient model and the trajectory of the complete model moves far way from the QSS model from then on.

III. KEY RESULTS

A. Counter Example I

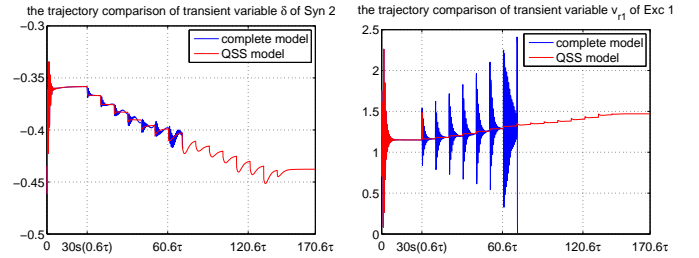


Fig. 2. The comparisons of trajectory between the complete model and the QSS model. The QSS model failed to provide correct approximations.

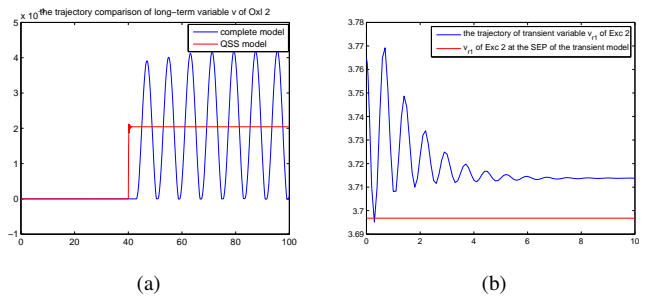


Fig. 3. (a). The comparison of trajectory between the complete model and the QSS model when load tap changers didn't change after 40s. (b). The trajectory of corresponding transient model when load tap changers changed at 40s which indicated that the point of the complete model was outside of the stability region of the corresponding transient model.

B. Counter Example II

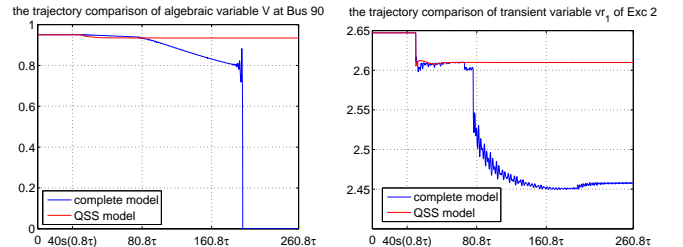


Fig. 4. The comparisons of trajectory between the complete model and the QSS model. The QSS model converged to a long-term SEP while the complete model suffered from voltage collapse.

Statistical Detection and Time-Localization of Forced Oscillations in Power Systems

Jim Follum and John Pierre

Department of Electrical and Computer Engineering,
University of Wyoming
Laramie, WY

Email: {jfollum, pierre}@uwyo.edu

Abstract—Forced oscillations (FOs) originate at generator sites and take the form of sinusoidal inputs to the system. Though they pose no threat to the system’s small-signal stability, the presence of an undamped oscillation in measurements causes current electromechanical mode estimation algorithms to mistake the FO for a dangerously low-damped mode. This effect can mask the true stability of the power system while causing false alarms for system operators. To mitigate the impacts of FOs, their frequencies, start times, and end times must be estimated. The first step in producing these estimates is detecting the FO’s presence. A detection algorithm based on the statistical distribution of the periodogram was developed for this purpose. The detection algorithm also provides the frequency estimate for the FO. Once detected, the FO is time-localized using the sample cross-covariance between the data and a sinusoid with frequency equal to that of the FO. The proposed method has been shown to successfully detect FOs of various amplitudes and accurately estimating the FO’s frequency, start time, and end time.

I. KEY EQUATIONS

The equations defining the power spectral density (PSD), periodogram, and their relation to the normalized periodogram are:

$$\phi(\omega) = \lim_{N \rightarrow \infty} E \left\{ \frac{1}{N} \left| \sum_{t=1}^N y(t) e^{-i\omega t} \right|^2 \right\} \quad (1)$$

$$\hat{\phi}(\omega) = \frac{1}{N} \left| \sum_{t=1}^N y(t) e^{-i\omega t} \right|^2 \quad (2)$$

$$\hat{\phi}_u(\omega) = \hat{\phi}(\omega) / \phi(\omega). \quad (3)$$

Use of the normalized periodogram (3) for forced oscillation detection is guided by the equations

$$\lim_{N \rightarrow \infty} \hat{\phi}_u(\omega) \sim \chi_2^2 \quad (4)$$

$$P_{FA} = 1 - (1 - e^{-\gamma})^B \quad (5)$$

$$P_D = Q_{\chi_2^2} \left(\frac{1}{2} D A^2 \right) \left(2 \ln \frac{B}{P_{FA}} \right). \quad (6)$$

A forced oscillation with estimated frequency $\hat{\omega}_p$ can be time-localized using

$$\hat{r}_p(g) = \frac{1}{L} \sum_{l=g+1}^L y(k_l) \cos(\hat{\omega}_p T(l-g)). \quad (7)$$

II. KEY FIGURES

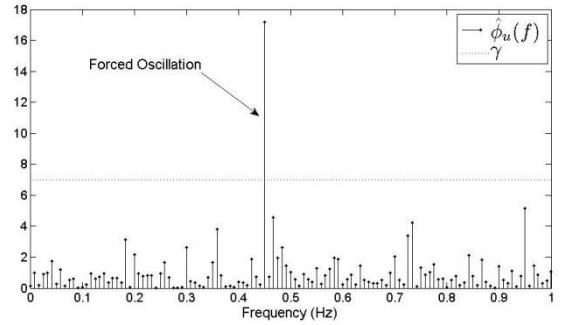


Fig.1 Example of a normalized periodogram with peak associated with a FO rising above the threshold, γ .

III. KEY RESULTS

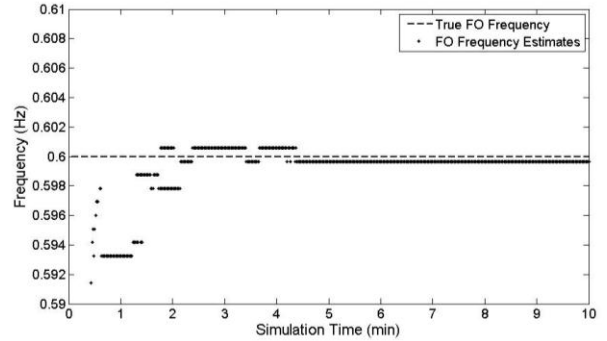


Fig.2 Frequency estimates for a 10 minute FO. Estimates improve as more data with the FO becomes available.

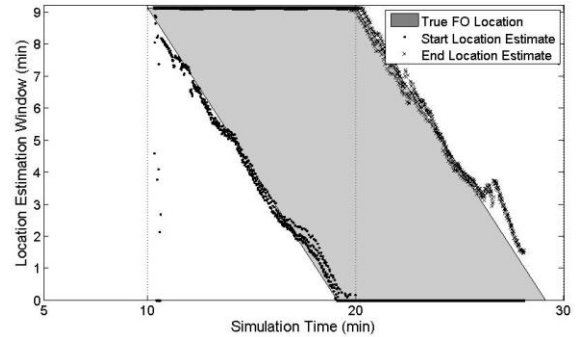


Fig. 3 Start and end time estimates for a 10 minute FO.

New Grid-tied Power Converter for Battery Energy Storage

Ah-Ryeon Park, Student Member, IEEE

I. INTRODUCTION

One simple topology for battery energy storage can be designed with a PWM inverter and 3-phase transformer, in which the modulation index of PWM inverter is controlled according to the voltage variation of battery. The insertion of DC-DC converter between the PWM inverter and battery can offer wider operation range and more control flexibility, but higher switching loss too. The insertion of an isolated soft-switching DC-DC converter can remove the line frequency transformer and reduce the system loss.

II. PROPOSED CONVERTER

This paper proposes a new structure of power converter for battery energy storage composed of a grid-tied inverter and an LLC resonant converter with 2-quadrant hybrid-switching chopper as shown in Fig. 1. The grid-tied inverter controls the active power and the DC link voltage, while the LLC resonant converter with 2-quadrant chopper controls the charging and discharging current through the battery. The LLC resonant converter offers electrical isolation between the AC source and the battery, and transfers power with lower switching loss because it operates in ZVS mode. Also, it has narrow variation in operation frequency regardless the load variation. The converter operation is divided into four modes according to the time interval.

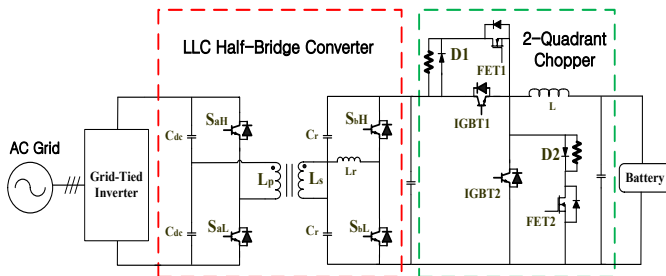


Fig. 1. Configuration of proposed power converter.

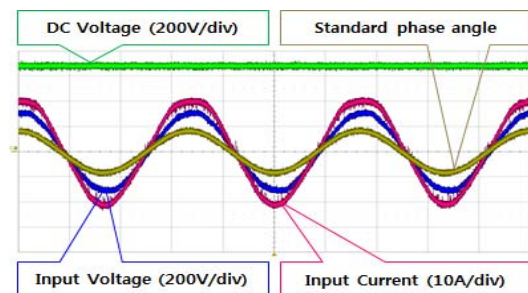


Fig. 2. input Voltage & Current in Forward Power Flow

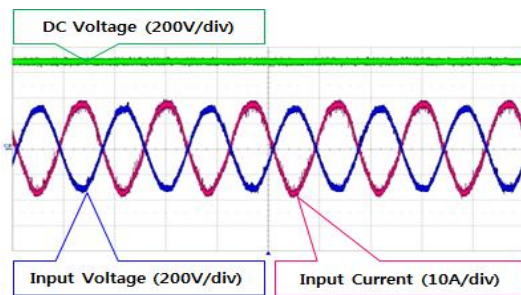


Fig. 3. Input Voltage & Current in Reverse Power Flow

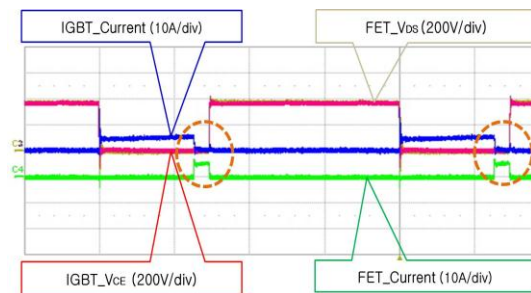


Fig. 4. Voltage & Current in Hybrid Switching Operation

III. HARDWARE EXPERIMENT

Fig.2 shows the phase-A voltage and current and the DC link voltage during charging mode. The input voltage is in phase with the input current, which means that the power factor correction is properly operated. And the DC link voltage is maintained as a constant value of 700V. Fig.3 shows the phase-A voltage and current, and the DC link voltage during discharging mode. The input current is 180° out phase with the input voltage, which means that the polarity of input current is negative during discharging. So, it is clear that the grid-tied converter can operate properly under accurate charging and discharging control. Fig.4 shows the voltage and current waveforms of IGBT and FET, which confirms the hybrid switching operation. The switching frequency can be raised up to 50kHz without any problem even though measured at 25kHz.

IV. CONCLUSION

This paper proposes a new grid-tied power converter for battery energy storage, which is composed of a PWM inverter and an LLC resonant converter in cascade with a 2-quadrant hybrid-switching chopper. The operation of proposed system was verified through computer simulations and experimental works with a hardware prototype. The proposed system can have relatively higher efficiency and smaller size than the existing system.

Power and Energy Capacity Requirements of Storages Providing Frequency Control Reserves

Theodor Borsche, Andreas Ulbig, Michael Koller, Göran Andersson
 Power Systems Laboratory, ETH Zürich
 {borsche, ulbig, andersson}@eeh.ee.ethz.ch, michael.koller_1@alumni.ethz.ch

Abstract—Due to their fast response time and high ramp rates, storage systems are capable of providing frequency control reserves. However, the limit in energy capacity poses difficulties as frequency control signals are, in general, not unbiased. We describe a scheme to recharge or discharge the storage without impeding the quality of the provided service, and formulate an analyzing method to investigate the resulting size of the storage. We show that even small storage sizes are sufficient to provide reliable primary and secondary frequency control reserves.

Provision of frequency control may be an economical feasible business case for storage systems. Batteries have also an added benefit of being able to react very fast to frequency deviations. A faster control response reduces overall frequency deviation and consequently reduces stress on the power system. It would therefore be in the interest of the TSO to include fast reacting storage systems in the primary frequency control scheme.

However, ancillary services are not guaranteed to be zero-mean, and losses are inherent to any storage system. This leads to violations of the storage capacity constraints and thus to an inability to provide the promised service to the grid. We propose to enable storage systems to participate in ancillary services by adjusting the operating point to allow for an appropriate charging or discharging that keeps the state of charge within acceptable levels. The adjustment of the working point has to be considerably slower than the associated service. In fact, our method guarantees that the rate of change is bounded for a bounded control signal. We evaluated our approach on real measurements of the primary and secondary frequency signal of the Swiss system operator swissgrid (full year 2009, 10 s sampling rate). A storage size of 30 min when providing primary control reserves and 2 h for secondary are shown to be sufficient.

I. KEY EQUATIONS AND RESULTS

The working point adjustment is performed according to

$$P_{WP}(k+d) = \frac{\sum_{j=k-a}^k (-P_{AS}(j) + P_{loss}(j))}{a} \quad (1)$$

$$P_{ext}(k) = P_{AS}(k) + P_{WP}(k), \quad (2)$$

where P_{AS} is the ancillary service signal, P_{WP} the working point and P_{ext} the total power consumption of the storage.

TABLE I: Required power capacity and energy capacity per offered unit of primary control reserve for a historic timeseries

η^2	a: 5 min, d: 5 min		a: 15 min, d: 15 min		a: 60 min, d: 60 min	
	P/P_{AS}	E/P_{AS} [h]	P/P_{AS}	E/P_{AS} [h]	P/P_{AS}	E/P_{AS} [h]
1	1.6733	0.1507	1.6161	0.3752	1.5272	0.9170
0.90	1.6685	0.1511	1.6114	0.3809	1.5043	0.9054
0.81	1.6631	0.1514	1.6063	0.3868	1.4808	0.8939
0.64	1.7466	0.1518	1.5942	0.3990	1.4311	0.8711

II. KEY FIGURES

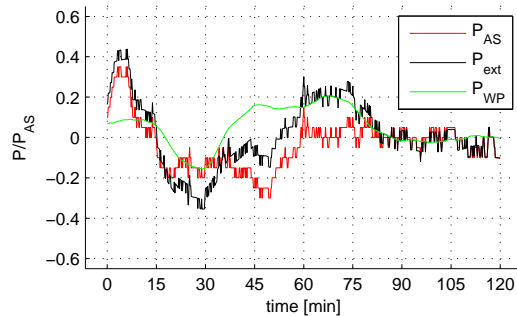


Fig. 1: Typical behaviour of storage system with setpoint adjustment. The response to the primary control signal is clearly visible, the working point changes comparably slow

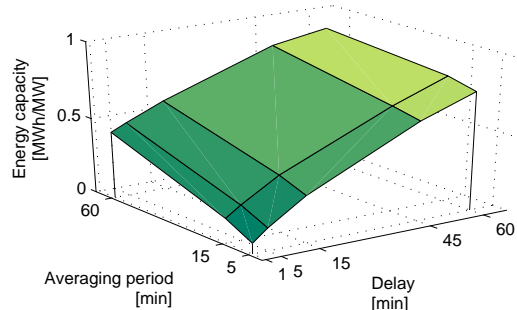


Fig. 2: Required energy capacity of a storage system for provision of primary control reserves with respect to a historic time series from the full year 2009

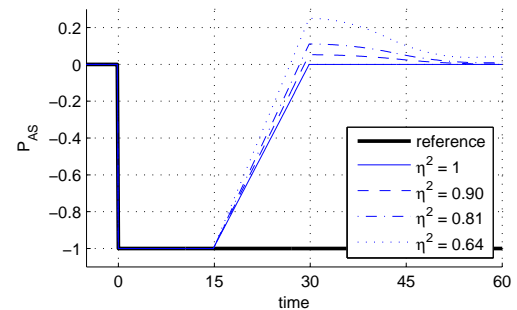


Fig. 3: Power production of storage system after negative step

Reduction of Harmonic Distortion in Off-Grid Energy Systems

Ahmed Habib, Jacob Lamb, and Zach Ulibarri
 Department of Electrical and Computer Engineering,
 Northern Arizona University
 Flagstaff, AZ 86001 USA

Email: ahh5@nau.edu, jml374@nau.edu, and zeu2@nau.edu

Abstract— Off grid energy sources are frequently utilized when connecting to a conventional power grid would be prohibitively expensive. However, many off-grid systems experience problems because non-linear electrical devices create harmonic distortion in the system’s power lines. A system with significant harmonics causes increased temperatures in electronics thereby shortening their lifespan while also damaging the power system itself. The purpose of this project was to create and test a shunt active power filter that reduced harmonic distortion in off-grid energy systems. The filter designed and created by the team reduces harmonics injected by a wide array of non-linear electrical devices commonly found in off-grid energy systems thus increasing their efficiency and longevity.

I. KEY FIGURES

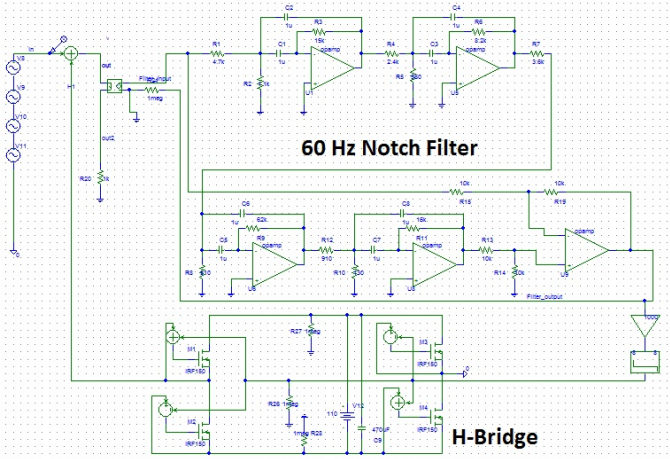


Figure 1: Filter Schematic.

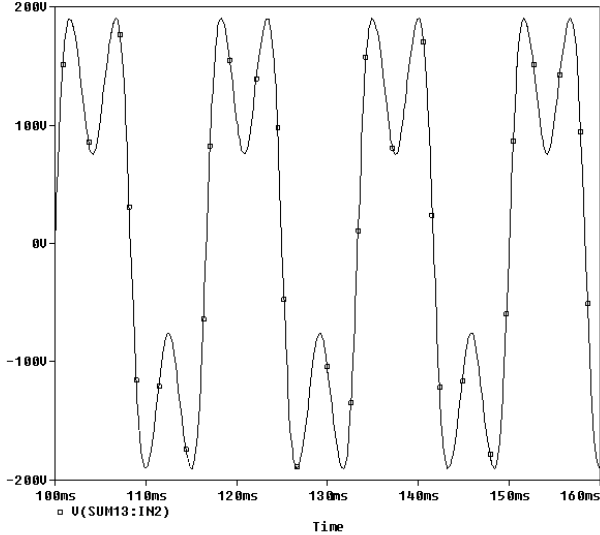


Figure 2: Simulated distorted waveform with third, fifth, and seventh harmonics.

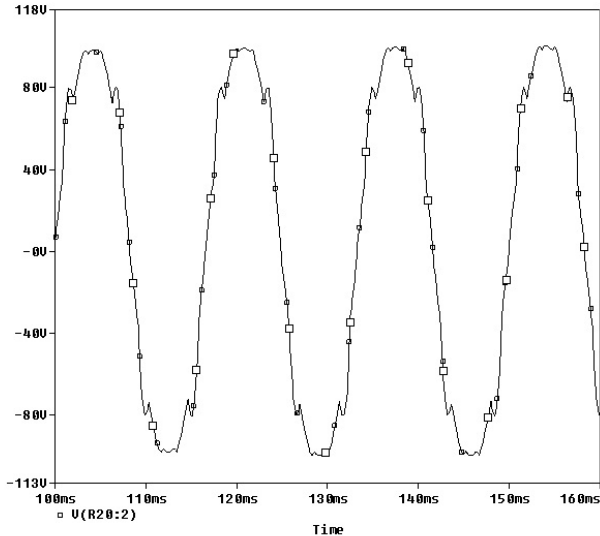


Figure 3: Simulated corrected waveform.

Two-Level Control of Doubly Fed Induction Generator using Flatness-Based Approach

Maryam H Variani and Kevin Tomsovic

Dept. of Electrical Engineering and Computer Science
University of Tennessee, Knoxville, TN 37996, USA,
Email: mhassani@utk.edu and tomsovic@utk.edu

Abstract— To allow for high penetration of distributed generation and alternative energy units, it is critical to minimize the complexity of generator controls and the need for close coordination. We propose that existing controls should be replaced by a two-tier structure of local control operating within a global context of situational awareness. In local control, individual components and individual loads operate in a manner to follow some desired trajectory based on local observations. The global control, on the other hand, refers to the desired trajectory which is determined by the context of the overall system needs for reliability, speed, and robustness. Flatness as an extension of controllability for non-linear systems is a key to enable planning and optimization at various levels of the grid in this structure. In this study, implementation of flatness-based control on Doubly Fed Induction Generator (DFIG) is investigated. Desired active and reactive powers are generated in the global level and are tracked by the local controllers.

I. KEY EQUATIONS

The guiding equations of an induction machine in arbitrary reference-frame variables are:

- voltage equations

$$\begin{aligned} v_{qs} &= r_s i_{qs} + \frac{\omega}{\omega_b} \psi_{ds} + \frac{\dot{\psi}_{qs}}{\omega_b} \\ v_{ds} &= r_s i_{ds} - \frac{\omega}{\omega_b} \psi_{qs} + \frac{\dot{\psi}_{ds}}{\omega_b} \\ v_{qr} &= r_r i_{qr} + \left(\frac{\omega - \omega_r}{\omega_b} \right) \psi_{dr} + \frac{\dot{\psi}'_{qr}}{\omega_b} \\ v_{dr} &= r_r i_{dr} - \left(\frac{\omega - \omega_r}{\omega_b} \right) \psi_{qr} + \frac{\dot{\psi}'_{dr}}{\omega_b} \end{aligned}$$

where

$$\begin{aligned} \psi_{qs} &= X_{ls} i_{qs} + X_M (i_{qs} + i'_{qr}) \\ \psi_{ds} &= X_{ls} i_{ds} + X_M (i_{ds} + i'_{dr}) \\ \psi'_{qr} &= X'_{lr} i'_{qr} + X_M (i_{qs} + i'_{qr}) \\ \psi'_{dr} &= X'_{lr} i'_{dr} + X_M (i_{ds} + i'_{dr}) \end{aligned}$$

- torque equation

$$\begin{aligned} T_e &= \frac{X_M}{D\omega_b} (\psi_{qs} \psi'_{dr} - \psi_{ds} \psi'_{qr}) \\ T_e &= 2H \frac{\dot{\omega}_r}{\omega_b} + T_L \end{aligned}$$

The dynamic equations can be written in terms of the rotor speed and argument of the stator flux linkage as flat outputs.

II. KEY FIGURES

The block diagram of the proposed approach is shown in Fig. 1, where y_i represents the flat outputs, u_i is the control input, a_i and z_i are state transformation functions and x is the state space variables.

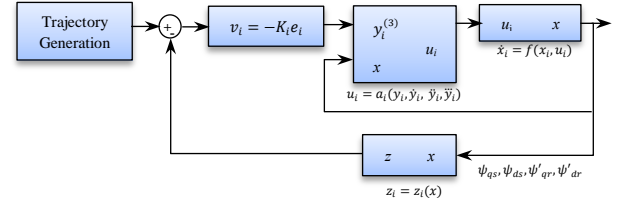


Figure 1. Flatness-Based control block diagram.

References:

- [1] P.C. Krause, *Analysis of Electric Machinery*, McGraw-Hill Book Company, 1987.
- [2] Ph. Martin, R. M. Murry, and P. Rouchon, "Flat systems, equivalence and trajectory generation," Ecole des Mines de Paris, Technical Report, April 2003.
- [3] Heberett Sira-Ramirez and Sunil K. Agrawal, *Differentially Flat Systems*, Marcel Dekker AG, New York, 2004.
- [4] A. Gensior, T. M. P. Nguyen, J. Rudolph, and H. Guldner, "Flatness-based loss optimization and control of a doubly-fed induction generator system," *IEEE Transactions on Control Systems Technology*, vol. 19, no.6, pp. 1457-1466.

Load Factor Control Using Community Energy Storage and Neural Network Predictive Load Modeling

Ben Ollis

Center for Ultra-Wide-Area Resilient Electric Energy Transmission Networks (CURENT), College of Electrical Engineering and Computer Science, University of Tennessee, Knoxville Knoxville, TN, USA

Michael Starke

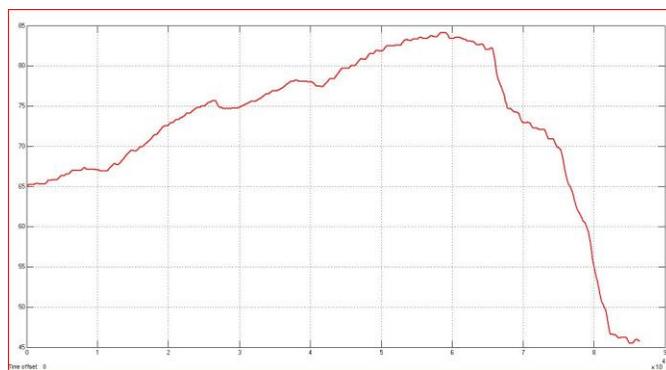
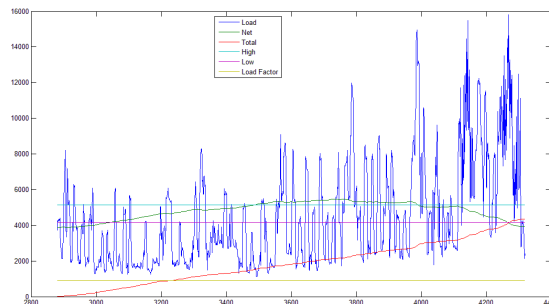
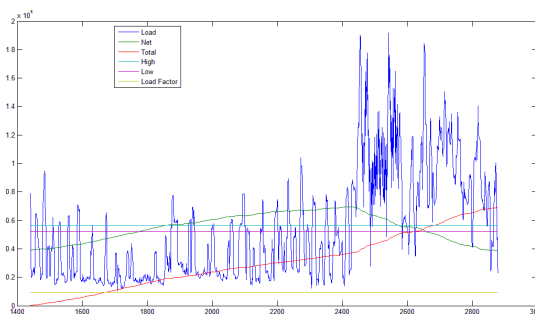
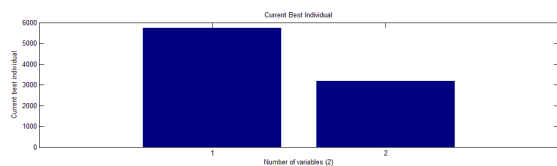
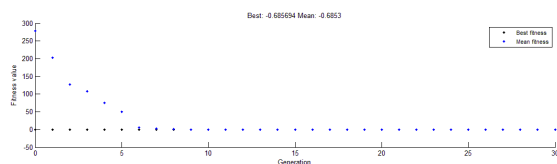
Oak Ridge National Lab
Oak Ridge, TN, USA

Abstract— This study will look at utilizing genetic algorithms to optimize the use of community energy storage systems for load factor control along with other grid benefits. Community energy storage systems are energy storage systems that are located between several residential homes and the transformer connecting the homes to the distribution feeder. These energy storage systems belong to the distributed energy system class and have drawn interest specifically in the area of secondary-use. Secondary-use is the application of used batteries from vehicles as the batteries are no longer considered viable for these vehicles and must either be recycled or repurposed for other applications. This paper will also discuss the initial testing of the algorithm on a community energy storage system with used vehicle batteries.

I. KEY EQUATIONS

The use of genetic algorithm optimization and neural networks prediction is critical to the results.

II. KEY FIGURES



Evaluating FIDVR using an air conditioner stall model with real time digital simulator

Kumaraguru Prabakar, *Student member, IEEE*, Tom D. Rizy, and Fangxing, Li, *Senior Member, IEEE*

Abstract—Single-phase air conditioner compressor motor units can stall and draw three or more times their rated current and reactive power during a 30 percent or more voltage sag such as from a sub transmission fault. The stalling of these motors can affect the entire power system and this system-wide phenomenon is known as fault induced delayed voltage recovery (FIDVR) or slow voltage recovery (SVR). This event is not only influenced by the air conditioner motors but also by the load composition in the power system. The single-phase induction machine available in the real time digital simulator (RTDS) is utilized to simulate the FIDVR event. This motor model along with different load compositions provides a method for extensively studying and evaluating the impacts of FIDVR impacts on the power system under different operating conditions.

Index Terms—Air conditioner stall model, Fault induced voltage recovery, Real time digital simulator, Single phase induction machine.

I. INTRODUCTION

AIR conditioner units used in household applications includes a condenser fan, air handler fan and a compressor. The single phase induction machine (SPIM) used in the compressor motor exhibits the stall nature and thus creates fault induced delayed voltage recovery (FIDVR) phenomenon. In this research, SPIM is modeled in real time digital simulator (RTDS) and installed in a test power system. The performance of the SPIM in the test system is presented.

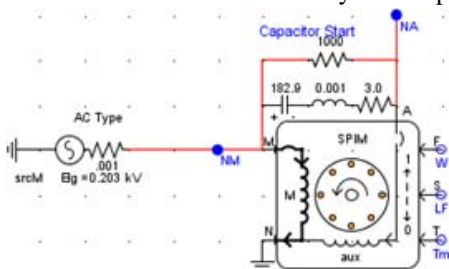


Fig. 1. RSCAD model of SPIM

II. MODELING FIDVR IN RSCAD

In the past, single phase motor models have been developed as a result of preventive measures taken by the NERC and other regulatory bodies[1]. Integration of motor modeling in RTDS will help in understanding the FIDVR phenomenon and take appropriate measures. The modeled SPIM operates in four stages. The four stages are indicated in Fig 2. The motor

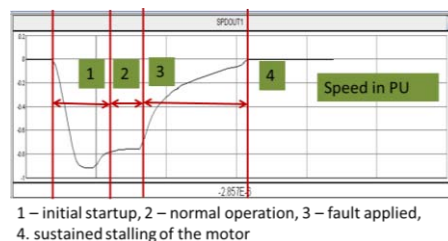


Fig. 2. Performance of the SPIM in RSCAD

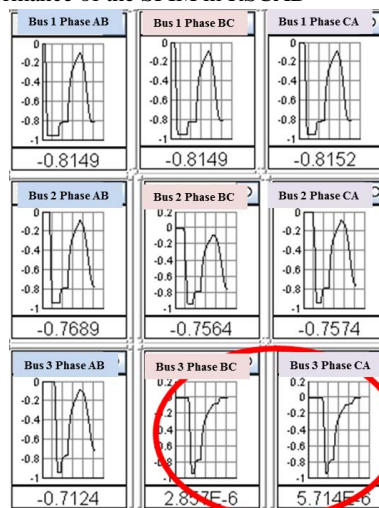


Fig. 3. Plots showing the performance of the system is installed in a test power system and the performance is shown in Fig 3. The performance of the SPIM in a typical system under fault condition suggests that not all the SPIM will enter stall mode under fault condition. In Fig. 3, phase BC and Phase CA of the bus 3 motors entered stall position while the rest of the motors in the system came back to normal mode.

III. CONCLUSION

The results from this research initiative provide a platform to understand the effect of such load composition. This model can help in building relay logic, control logic for SPIM, and also testing of such hardware.

REFERENCES

[1]Irminger, P., et al. Air conditioning stall phenomenon-Testing, model development, and simulation. in Transmission and Distribution Conference and Exposition (T&D), 2012 IEEE PES. 2012. IEEE.

Current-Based Fault Detection for Wind Turbine Systems via Hilbert-Huang Transform

Dingguo Lu, Wei Qiao, Xiang Gong and Liyan Qu

Power and Energy Systems Laboratory, Department of Electrical Engineering, University of Nebraska-Lincoln, Lincoln, NE 68588-0511, USA,

Email: stan1860@huskers.unl.edu, wqiao@engr.unl.edu, xiang.gong@huskers.unl.edu, and lqu2@unl.edu

Abstract—Mechanical failures of wind turbines represent a significant cost in both repairs and downtime. Detecting incipient faults of wind turbine components permits maintenance to be scheduled and failed parts to be repaired or replaced before causing failures of other components or catastrophic failure of the system. This paper proposes a Hilbert-Huang transform (HHT)-based algorithm to effectively extract fault signatures in generator current signals for wind turbine fault diagnosis by using the HHT’s capability of accurately representing the instantaneous amplitude and frequency of nonlinear and nonstationary signals. A phase-lock-loop (PLL) method is integrated to estimate wind turbine rotating speed, which is then used to facilitate the fault detection. The proposed method is validated by a real direct-drive wind turbine with different types of faults. The experimental results demonstrate that the proposed method is effective to detect various faults in wind turbine systems as well as to reveal the severities of the faults.

I. KEY EQUATIONS

The guiding equations of the Hilbert-Huang Transform are:

1): Empirical Model Decomposition (EMD)

$$h_1(t) = x(t) - m_1(t) \quad (1)$$

$$h_{11}(t) = h_1(t) - m_{11}(t) \quad (2)$$

$$h_{1k}(t) = h_{1(k-1)}(t) - m_{1k}(t) \quad (3)$$

$$r_1(t) = x(t) - c_1(t) \quad (4)$$

$$x(t) = \sum_{i=1}^n c_i(t) + r_n(t) \quad (5)$$

2): Hilbert transform

$$H[c_i(t)] = \frac{1}{\pi} PV \int_{-\infty}^{\infty} \frac{c_i(\tau)}{t - \tau} d\tau \quad (6)$$

$$Z_i(t) = c_i(t) + jH[c_i(t)] = a_i(t) \exp[j\theta_i(t)] \quad (7)$$

$$a_i(t) = \sqrt{c_i(t)^2 + \{H[c_i(t)]\}^2} \quad (8)$$

$$\theta_i(t) = \arctan \left\{ \frac{H[c_i(t)]}{c_i(t)} \right\} \quad (9)$$

$$\omega_i(t) = \frac{d\theta_i(t)}{dt} \quad (10)$$

$$x(t) = \text{Re} \left(\sum_{i=1}^n a_i(t) \exp \left[j \int \omega_i(t) dt \right] \right) \quad (11)$$

II. KEY FIGURE

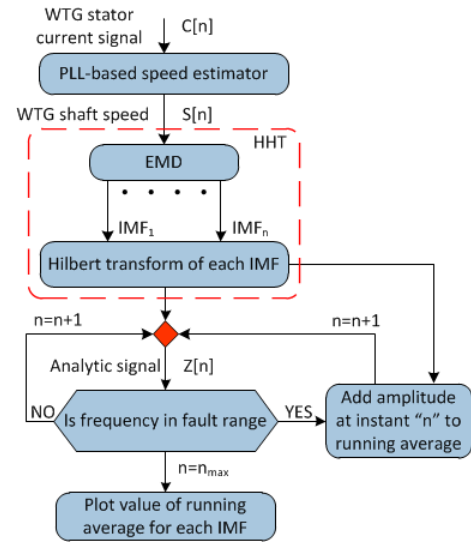


Figure 1. Flowchart of the HHT-based fault detection algorithm

III. KEY RESULTS

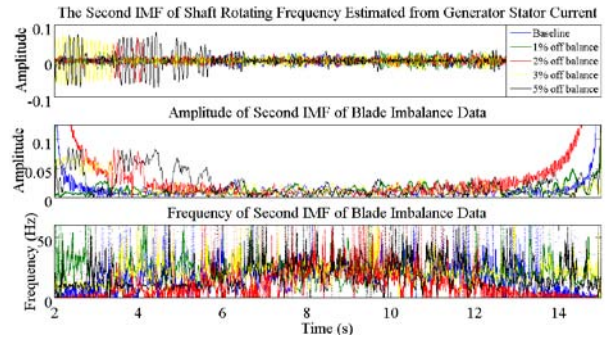


Figure 2. Hilbert transform of the second IMF for blade imbalance

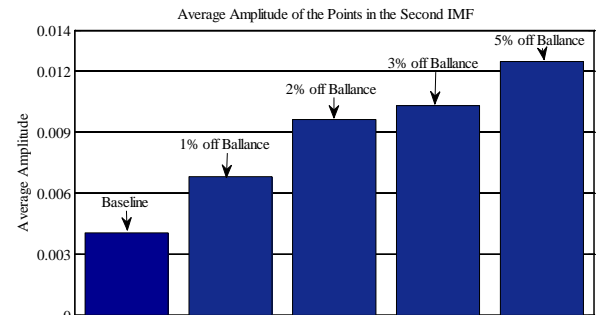


Figure 3. Average amplitude of the second IMF for blade imbalance

A Statistical Approach to End - User Energy Consumption

Jonas Traphöner and Surya Santoso

Department of Electrical and Computer Engineering, The University of Texas at Austin, Austin, TX 78712, USA
 Email: Jonas.traphoner@utexas.edu and ssantoso@mail.utexas.edu

Abstract— Local supply and demand concepts have an important contribution to make to the future scenarios of power supply systems. With a suitable load monitoring and management a better adaption to consumption patterns can be achieved.

Renewable energy sources, as well as local supply systems have the objective of enhancing the efficiency and reliability of energy supply with structures elevated close to the end consumer. An along going monitoring of the systems demand is entailed. Due to this movement, a specific local knowledge of the regional energy demand is a prerequisite for an ideal supply concept. The knowledge of consumption behaviors in a region is therefore a key variable, as it has a major impact on the ratings of local systems. The complex nature of local supply with its many varied influences demands a system approach that takes account of all the significant components. This refers not only to the generation systems but also to the system as a whole with its widespread networks, and in the end also the consumer himself, with his behaviors also contributing to overall optimization.

The poster project addresses the topic of using a statistical approach to give an outlook on a households energy consumption based on various factors such as weather, age, country, geography, climate, number of people in a household and multiple other factors. This theoretical approach will be compared with received consumer data from an ongoing project within the Austin, TX region.

The statistical data acquisition, once compared with the collected consumer data, will forecast the electric grid consumption on a regional level and give insight to electricity grid operators to control the energy grid more efficiently. In contrast to the operational techniques of a Virtual Power Plant, this technique does not only analyze the different supply systems available, but takes into account the different behaviors on the consumer side.

This approach could be part of the next generation SCADA systems; supporting the grid operator in decision making and being able to enhance durable timetable management. This has the potential to contribute to the highly discussed topic of Smart Grids.

I. KEY FIGURES

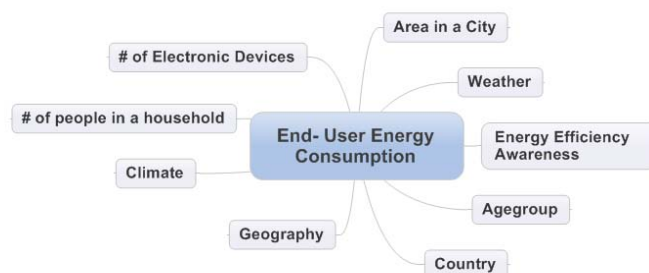


Figure 1 Factors impacting Energy Consumption

II. KEY EQUATIONS

This particular topic will be approached through the statistical method of regression. The least squares method is applied to derive estimators of various parameters.

$$E(Y|x_1, \dots, x_k) = \beta_1 + \beta_2 x_1 + \dots + \beta_{k+1} x_k \quad (1)$$

$$f_n(y|x, \beta_1, \beta_2, \sigma^2) = \frac{1}{(2\pi\sigma^2)^{\frac{n}{2}}} \exp \left[-\frac{1}{2\sigma^2} \sum_{i=1}^n (y_i - \beta_1 - \beta_2 x_i)^2 \right]$$

Modeling and Analysis of Campus Microgrid Distribution System

Sayonsom Chanda, *Student Member, IEEE* and Anurag K Srivastava, *Senior Member, IEEE*

Smart Grid Demonstration and Research Investigation Lab (SGDRIL)

Washington State University, Pullman, WA, USA

sayonsom.chanda@email.wsu.edu

Abstract--- Digital computer tools and software has enabled simulation of load flow and its analysis with unbalanced loads per phase and in each section of a feeder. However, there is a certain lack of depth and accuracy when it comes to modeling of end-use loads and low voltage distribution system. Presently, it is conventional for most utilities and researchers to model loads using aggregated constant impedance, constant current and constant power models, viz. ZIP models. There is a need to model the low voltage network and end-use loads specially with increasing penetration of distributed generation and demand response. In this poster, the benefits of better end-use load and network modeling using an example campus microgrid distribution system would be demonstrated, using software tools: SynerGEE and Gridlab-D.

Index Terms--- distribution system analysis, ZIP Model, microgrid, SynerGEE, Gridlab-D

I. INTRODUCTION & MOTIVATION

WECC Load modeling task force has concentrated on loading of large induction machines and studied its effect on the Transmission System [1]. End-use load is also an extremely stochastic phenomena, and hence a load model at one moment of time is never going to be accurate for another moment of time. However, if a better load model is available, it would enable the utilities to predict the network behavior for various preset load profiles[2]. Rapid penetration of renewable energy sources and stronger mandates favoring the same, has led to a new need to study impact of distributed generation (DG). A better load modeling and low voltage network model may assist in studying solution for DG intermittency.

II. METHOD OF WORK

A. Background

The simulation works will be based on the radial feeders for the city of Pullman, supplied by AVISTA Utilities. The computer models of these 13.2 kV feeders are available in SynerGEE. Some of these feeders are stepped down to 4.16 kV distribution system in the substations located inside Washington State University Pullman campus for its internal distribution.

B. Low Voltage Distribution System

In each of the 13.2 kV feeder models, the facilities of WSU has been modeled as a single lumped load, while in reality they can be fragmented to several individual buildings, connected to

The authors would like to sincerely acknowledge AVISTA Utilities and WSU Facilities and Operation for their cooperation with the development of this project.

the lower voltage circuit, i.e. 4.16kV radial feeders from the substations within the University. This has been incorporated into the model with existing connected loads and generators.

C. Adding probable future loads & generators

In [3], integration of detailed generator models into the radial feeders has been detailed. Using similar methods, it would also be possible to model the distributed generators, like wind farms or solar cells, can be incorporated into the feeder for local supply in the example campus microgrid.

D. Use of SynerGEE and Gridlab-D

The detailed load model would enable predictive research on "what-if" scenarios of the future. SynerGEE will be used to extend the load modeling from the 13.2kV MV circuit to a more descriptive 4.16kV LV circuit, to carry out simulations and analysis. Also, a similar model is to be developed in Gridlab-D, which has the capability for more accurate load modeling

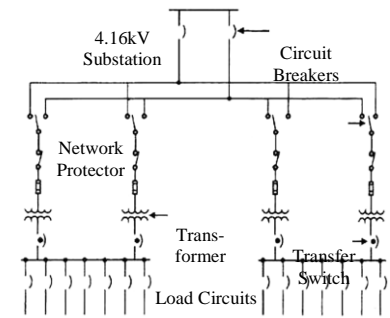


Fig: Typical Distribution System for simulations from the 4.16kV substations

III. RESULTS

The poster demonstrates the need of better load modeling, by showing that it leads to more accurate load-flow results, which facilitates better coordination of transactive signal from Utilities, helps studies on more efficient capacitor placement, effect of contingencies in the distribution system on the transmission system, and on probable impact of addition of more distributed generators to meet local needs in the campus.

REFERENCE

- [1] D. Kosterev, A. Meklin, J. Undrill, B. Lesieutre, W. Price, D. Chassin, P. Bravo, and S. Yang, "Load Modeling in Power System Studies: WECC Progress Update", *IEEE PES General Meeting*, July 2008.
- [2] I. Hisken, "Significance of Load Modelling in Power System Dynamics", Symposium Of Specialists In Electric Operational and Expansion Planning
- [3] N. Samaan, T. McDermott, B. Zavadil, and J. Li, "Induction Machine Test Case for the 34-Bus Test Feeder – Steady State and Dynamic Solutions", *IEEE PES General Meeting*, June, 2006.
- [4] K. P. Schneider, J. C. Fuller, "Detailed End Use Load Modeling for Distribution System Analysis", *IEEE PES General Meeting*, June 2010.

Multi-Agent-Based Information Collection Algorithm for Isolated Power Systems

Guanqun Wang¹, Chen-Ching Liu¹ and Feng Liu²

1. School of Electrical Engineering and Computer Science, Washington State University, Pullman, WA, 99163, USA
 2. Department of Electrical Engineering, Tsinghua University, Beijing 100084, China
- Email: gwang@eecs.wsu.edu, liu@eecs.wsu.edu and lfeng@mail.tsinghua.edu.cn

Abstract—The power system used on shipboards, airplanes or space stations, for example, are classified as isolated power systems (IPS). Compared with traditional centralized structure of IPS, the multi-agent-based decentralized structure can serve as a better structure for its avoiding single-point-of-failure and improving the survivability of IPS in extreme conditions. In multi-agent system, agent can only communicate with its neighboring agents, thus raises the problem that how can one agent get global information through information exchange between its immediate neighbors. Based on decentralizing of the Adjacent Matrix Algorithm, a distributed information collection algorithm is proposed in this work. Agents can get the global state information of all loads, generators and switches through coordination and iteration of local information, and then obtain global topology of the entire system. Compared with existing methods, this algorithm has a better calculating efficiency and can recognize complicated fault scenarios in system like the communicating fault or loss of agents. Based on this algorithm, further application can be made in multi-agent system such as load shedding and system reconfiguration.

I. KEY EQUATIONS

For a n -agent system, $A = (a_{ij})$ is the adjacent matrix. Assuming $x_i \in \mathbb{R}^n$ is the state vector of agent i , the iteration process is carried out as

$$x_i^{k+1} = \sum_{j=1}^n a_{ij} x_j^k$$

By iteration for at most n time, the global states of the system can be obtained by agent i .

II. KEY FIGURES

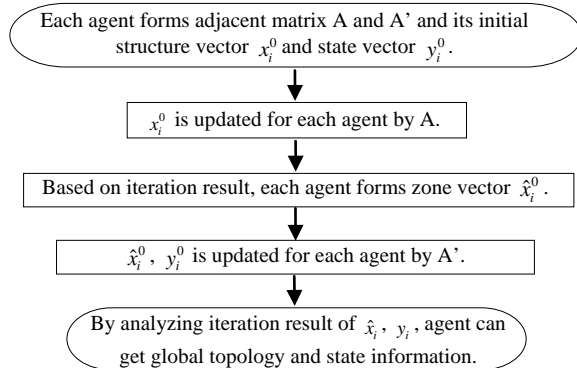


Figure 1. Flowchart of decentralized information collection algorithm

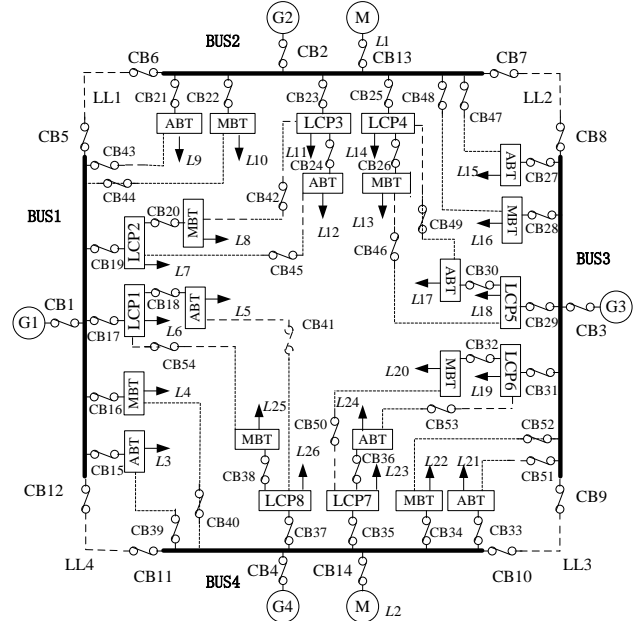


Figure 2. Simplified figure of a typical IPS

III. KEY RESULTS

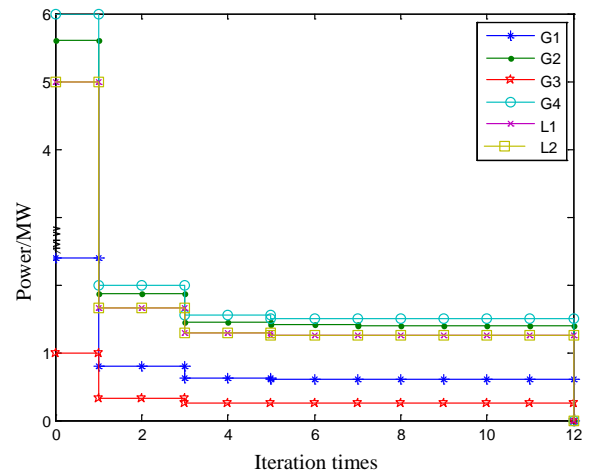


Figure 3. Iteration process of information collection algorithm

Increased Security Rating of Overhead Transmission Circuits Using Compact Phase Design and High Phase Order

Brian J. Pierre, Student Member, IEEE

G. T. Heydt, Life Fellow, IEEE

Abstract—The combination of compact phase design and high phase order (HPO), (e.g., \geq three phase) is used to enhance the security ratings of overhead transmission circuits. The advantages of both technologies are used with the objectives of raising the power transmission capability, reducing right of way requirements, reducing the phase angle difference between the sending and receiving end voltages, and reducing the cost of bulk power transmission. Disadvantages of the proposed technology are also discussed.

The phase to phase voltages of HPO circuits are less than three phase circuits. The lower phase to phase voltages allow closer phase to phase spacing. The closer phase spacing increases the mutual coupling between conductors decreasing the positive sequence reactance (X^+). The decrease in X^+ increases the security limit of the transmission line. To determine the exact increase in security limit for HPO lines vs. its three phase multicircuit counterpart, the sequence components of HPO lines are calculated in terms of self and mutual reactances from properties of circulant matrices. The sequence component equations for HPO lines are discussed.

The main objectives of the poster are to:

- Discuss the use of HPO to compact transmission lines
- Calculate HPO sequence reactances in terms of self and mutual reactances using properties of circulant matrices.
- Determine the increase in security rating for compact HPO vs. its three phase multicircuit counterpart.

I. KEY EQUATIONS

Six phase reactance matrix for the configuration seen in Fig. 1,

$$X_{6ph} = \begin{bmatrix} S & M_1 & M_2 & M_3 & M_2 & M_1 \\ M_1 & S & M_1 & M_2 & M_3 & M_2 \\ M_2 & M_1 & S & M_1 & M_2 & M_3 \\ M_3 & M_2 & M_1 & S & M_1 & M_2 \\ M_2 & M_3 & M_2 & M_1 & S & M_1 \\ M_1 & M_2 & M_3 & M_2 & M_1 & S \end{bmatrix} \quad (1)$$

Eigenvectors, which are arranged in columns to form $n \times n$ modal matrix T ,

$$v_m = \frac{1}{\sqrt{n}} \left[e^0, e^{-\frac{j2\pi m}{n}}, \dots, e^{-\frac{j2\pi m(n-1)}{n}} \right]^t \quad (2)$$

Sequence components,

$$X_{seq} = T^{-1} X_{ph} T. \quad (3)$$

Eigenvalues,

$$\lambda_m = \sum_{k=0}^{n-1} X_{ph,1,k} e^{-j2\pi mk/n}. \quad (4)$$

Six sequence components of a circularly configured six phase transmission line as seen in Fig. 1, in terms of self and mutual reactances.

$$X_{6seq} = \text{diag} \begin{bmatrix} 2M_1 + 2M_2 + M_3 + S \\ M_1 - M_2 - M_3 + S \\ -M_1 - M_2 + M_3 + S \\ -2M_1 + 2M_2 - M_3 + S \\ -M_1 - M_2 + M_3 + S \\ M_1 - M_2 - M_3 + S \end{bmatrix} = \text{diag} \begin{bmatrix} X_{0s} \\ X_{ps} = X^+ \\ X_{pt} \\ X_{ot} \\ X_{nt} \\ X_{ns} \end{bmatrix} \quad (5)$$

Similar analysis completed for twelve phase.

II. KEY FIGURES

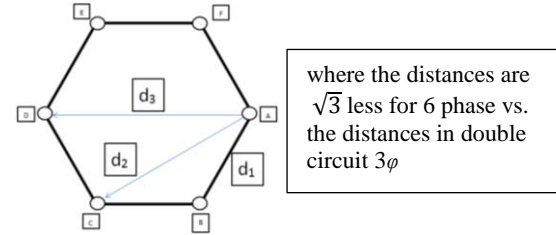


Fig. 1 Configurations for a double circuit 3 ϕ and 6 ϕ line.

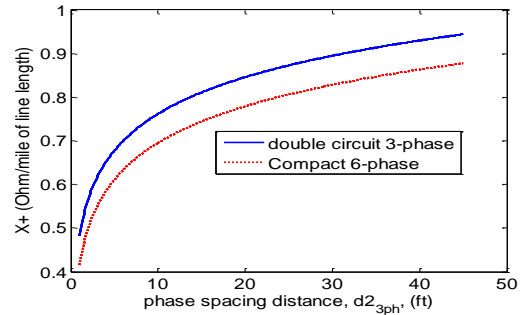


Fig. 2 Comparison of X^+ for double circuit 3 ϕ and compact 6 ϕ vs. phase spacing of the original double circuit 3 ϕ (for GMR of 0.0375 ft. Drake conductor).

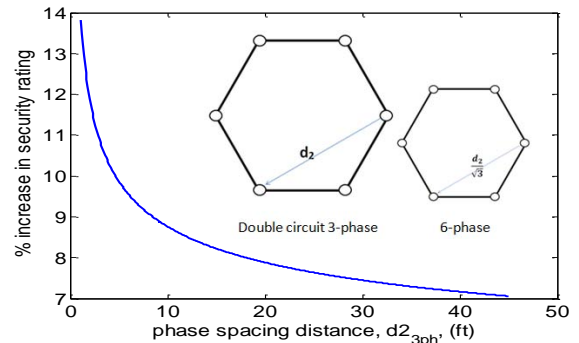


Fig. 3 The percent increase in security rating for compact 6 ϕ over double circuit 3 ϕ is plotted versus phase spacing (distance d_2) of the original double circuit 3 ϕ .

A Real-Time Simulation Model of Community Microgrid

Ling Xu, *Student Member, IEEE*, Zhixin Miao, *Senior Member, IEEE*, and Lingling Fan, *Senior Member, IEEE*

Department of Electrical Engineering, University of South Florida, Tampa, FL 33620, USA,
Email: lxu@mail.usf.edu, zmiao@usf.edu, linglingfan@usf.edu

Abstract—Distributed renewable energy resources are penetrating into community microgrid more and more nowadays. One solution to resolve the fluctuation of output power from those renewable energies is energy storage devices. Battery is a common candidate among various energy storage devices. However, how to coordinate the renewable energy source and battery, and how to improve the system performance during abnormal or fault condition are big concerns from the utility’s point of view. A comprehensive community microgrid consisting of PV panel, battery, induction motor, and synchronous generator is built in Real-Time Digital Simulator RT-Lab. The simulation can run in real-time, and the coordinated control of PV and battery and the system performance are evaluated.

I. KEY EQUATIONS

The PV model can be described as:

$$I_o = I_{o,n} \left(\frac{T}{T_n}\right)^3 \exp\left[\frac{qE}{\alpha K} \left(\frac{1}{T_n} - \frac{1}{T}\right)\right] \quad (1)$$

$$I_{o,n} = \frac{I_{sc}}{V} \frac{\exp\left(\frac{oc}{\alpha V_t}\right) - 1}{\exp\left(\frac{oc}{\alpha V_t}\right) - 1} \quad (2)$$

$$I_{pv} = [I_{sc} + K_t(T - T_n)] \frac{G}{G_n} \quad (3)$$

The battery model can be described as:

$$C_{capacity} \frac{dV_{soc}}{dt} + \frac{V_{soc}}{R_{self_discharge}} + I_{batt} = 0 \quad (5)$$

$$V_{oc} = -1.031 \cdot e^{-35 \cdot V_{soc}} + 3.685 + 0.2156 \cdot V_{soc} \quad (6)$$

$$-0.1178 \cdot V_{soc}^2 + 0.3201 \cdot V_{soc}^3$$

II. KEY FIGURES

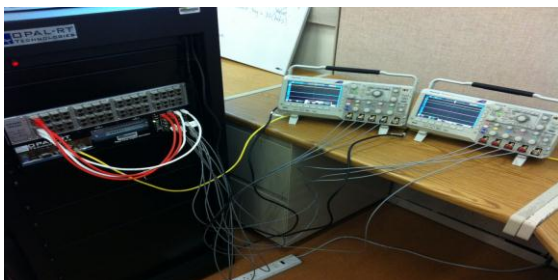


Figure 1. Real-time digital simulation setup using RT-Lab.

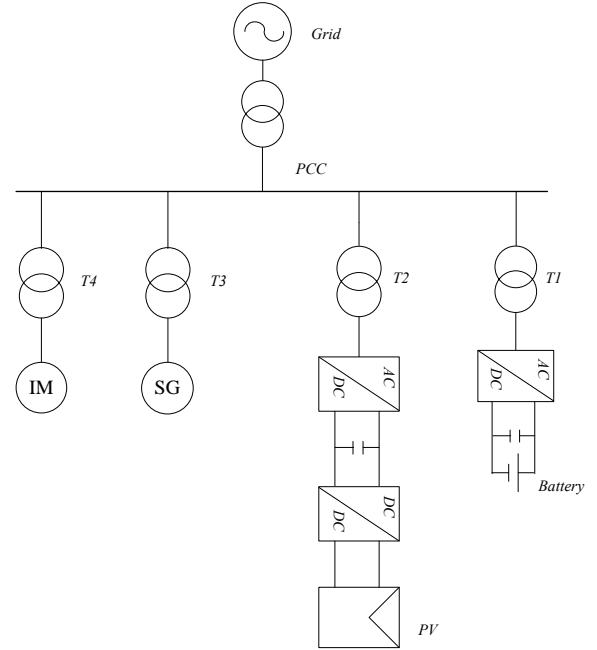


Figure 2. System topology of the microgrid.

III. KEY RESULTS

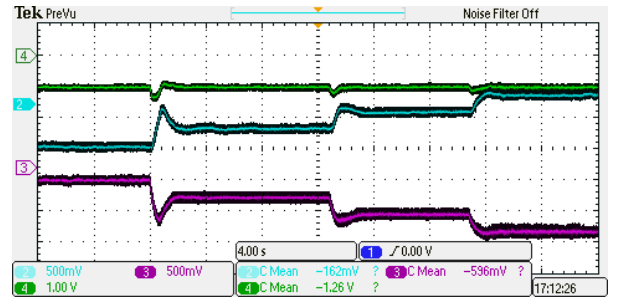


Figure 3. Power generated by PV and battery.

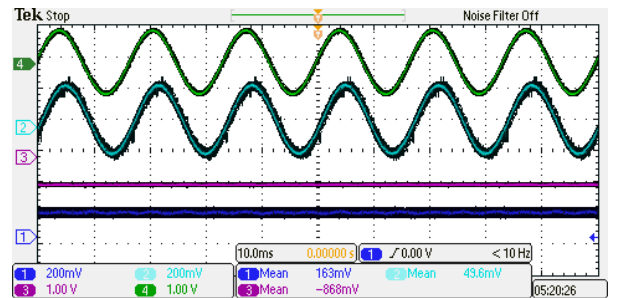


Figure 4. Current and power from SG and IM.

Review of Earth Conductivity Structure Modelling For Calculating Geo-electric Fields

Bo Dong^{1,2}, Zezhong Wang¹, David Boteler², Risto Pirjola²

1. Key Laboratory of High Voltage & EMC, North China Electric Power University, Beijing, China

2. Geomagnetic Laboratory, Natural Resources Canada, Ottawa, Canada

Email: dong.b@ncepu.edu.cn, David.Boteler@NRCan-RNCan.gc.ca

Abstract—During geomagnetic disturbances the electric field induced by geomagnetic variations drive geomagnetically induced currents (GIC) in conducting networks such as power systems and pipelines. The earth conductivity structure plays an important role in determining the size of the electric field that will be experienced by these systems. The earth conductivity is dependent on rock type and also varies with depth within the Earth. Methods and techniques for modelling different types of earth conductivity structures are reviewed and the advantages and limitations of different models and methods are discussed in this paper. Some methods are advantageous on computation speed while others on the accuracy. Appropriate modelling technique of conductivity structure is important for assessing geomagnetic hazard to power systems.

I. KEY EQUATIONS

$$Z = \sqrt{\frac{i\omega\mu_0}{\sigma}}, \quad (1)$$

$$\delta = \sqrt{\frac{2}{\omega\mu_0\sigma}}, \quad (2)$$

$$Z_n = Z_{0n} \frac{1 - L_{n+1} e^{-2k_n d_n}}{1 + L_{n+1} e^{-2k_n d_n}}, \quad (3)$$

II. KEY FIGURES

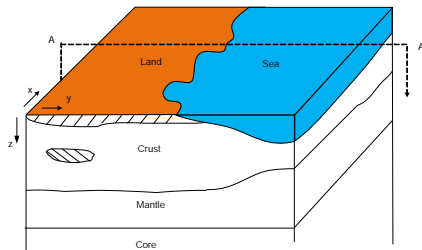


Figure 1. Example of the Earth Structure.

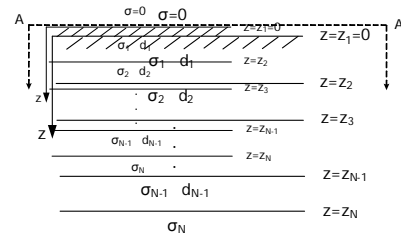


Figure 2. 1D N-Layered Earth Model for the section A-A' in Fig. 1.

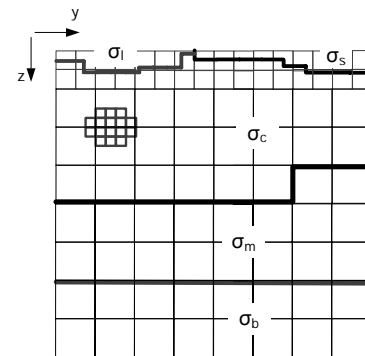


Figure 3. Grids of Finite Difference Method and Finite Element Method in Two-Dimensions. σ_l is the conductivity of land, σ_s is the conductivity of seawater, σ_c is the conductivity of crust, σ_m is the conductivity of mantle, and σ_b is the conductivity of bottom layer, which presents core.

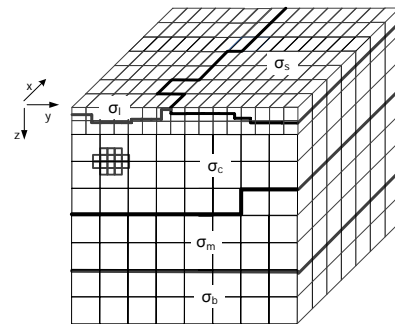


Figure 4. Three-Dimensional Model to Approximate the Earth Structure in Fig. 1

Output Power and Harmonic Currents Analysis of Photovoltaic Systems in Net-Zero-Energy Houses

Hesam Yazdanpanahi and Wilsun Xu

Department of Electrical and Computer Engineering, University of Alberta, Edmonton, AB, Canada, T6G2V4
 Email: yazdanpa@ualberta.ca

Abstract—Measurements have been conducted at two Net-Zero-Energy houses in Edmonton, Alberta and the output power and harmonic currents characteristics of Photovoltaic (PV) systems in these houses have been studied. The PV system in the first house consists of three PV circuits. In each circuit, 11 micro-inverters are connected in parallel and the total PV capacity of the house is 6.9 kW. In the second house, the PV system consists of two circuits. Each circuit has one full-scale inverter and the total PV capacity is 9 kW. In this study, the output power of the PV systems were monitored for a 10-day period, harmonic current components were extracted and power quality indexes such as TDD were calculated. These results will be used to generate probabilistic harmonic models for PV systems and assessing their harmonic impacts on the distribution network.

I. KEY FIGURES



Figure 1: Net-Zero-Energy House 1

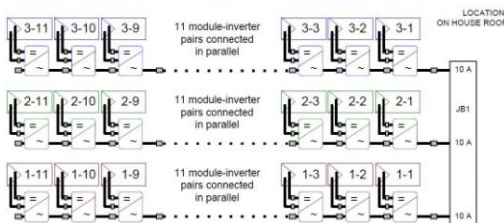


Figure 2: Single-line diagram of PV system in House 1



Figure 3: Net-Zero-Energy House 2

II. SAMPLE RESULTS

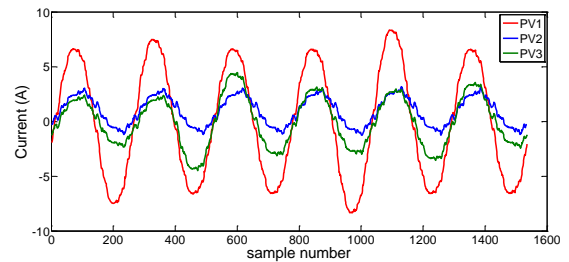


Figure 4: Current snapshot at House 1, 12:20:00, December 4th, 2012

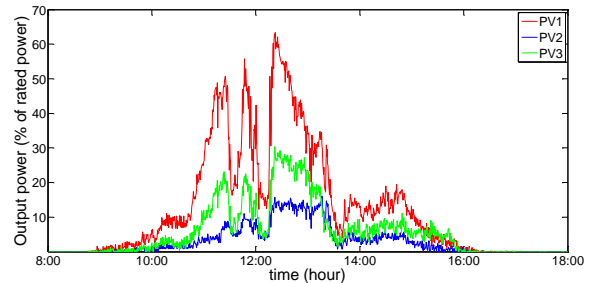


Figure 5: PV circuits output powers in House 1 at December 4th, 2012

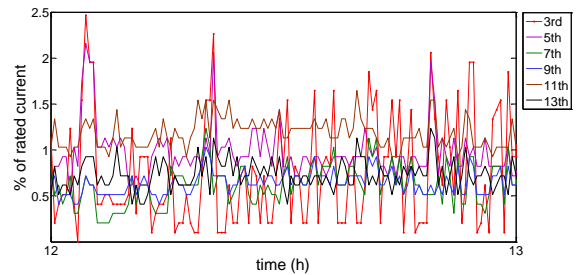


Figure 6: Harmonic current components of PV circuit 1 (house 1) for December 4th, from 12:00 to 13:00.

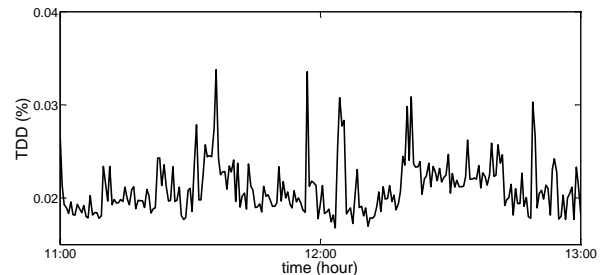


Figure 6: TDD of PV circuit 1 (house 1) 4th of December, 11:00 to 13:00.

Optimized Design of Battery Storage with High Penetration Distributed PV Units to Solve the Overvoltage Issue

Ye Yang, *Student Member, IEEE*, Hui Li, *Senior Member, IEEE*, Jianping Zheng, *Senior Member, IEEE* and Andreas Aichhorn, *Student Member, IEEE*

Center for Advanced Power Systems, Department of Electrical and Computer Engineering, Florida State University, Tallahassee, FL 32310, USA.

Email: yyang@caps.fsu.edu hli@caps.fsu.edu zheng@eng.fsu.edu andreasaihorn@gmail.com

Abstract— This paper proposes an effective method to evaluate the battery energy storage system (BESS) usage and cost when BESS is applied in the distributed network to solve the overvoltage issue under high photovoltaic (PV) penetration level. The main objective of the proposed method is to evaluate and derive the optimized design of BESS. The cost analysis presented in this paper considers factors of BESS influence on the work stress of voltage regulation devices, load shifting and shaved peaking power generation, as well as individual BESS usage and its lifetime estimation. Based on the cost analysis, the BESS optimization can be determined.

I. KEY EQUATIONS

The guiding equations of the economical analysis of BESS for distributed high penetration PV units are:

$$C_L = Q * \left(\frac{d * (1 + d)^n}{(1 + d)^n - 1} \right) \quad (1)$$

$$C_{BESS_i} = Q_{BESS_i} * LF_{ni} \quad (i = 201, 202, \dots, 207) \quad (2)$$

$$B_{OLTC/SVR} = Q_{OLTC+SVR} * LF_{no} * \frac{OT_{Saved}}{OT_{Average}} \quad (3)$$

$$B_{PPG} = Q_{PPG} * LF_{nc} \quad (4)$$

$$B_{PLS_i} = E_{PLS_i} * (EP_{On_peak} - EP_{Off_peak}) \quad (5)$$

$$B_{AC_i} = C_{BESS_i} - B_{PLS_i} - B_{PLG} * W_{1i} - B_{OLTC/SVR} * W_{2i} \quad (6)$$

II. KEY FIGURES

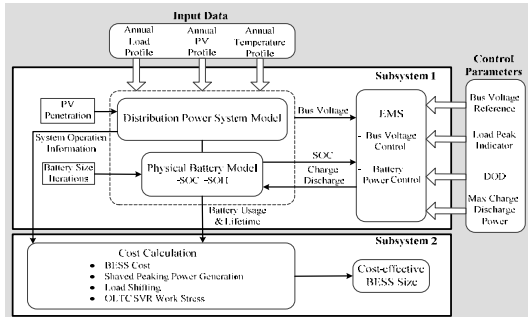


Figure 1. Proposed battery usage and cost analysis system diagram

III. KEY RESULTS

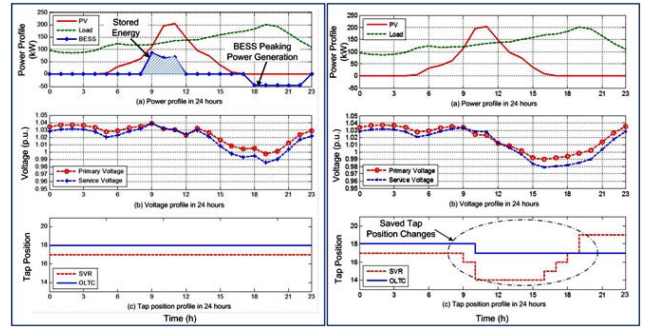


Figure 2. Battery usage and system performance in one day

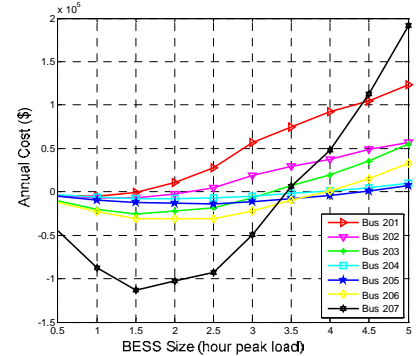


Figure 3. Annual cost analysis under PV penetration=70%

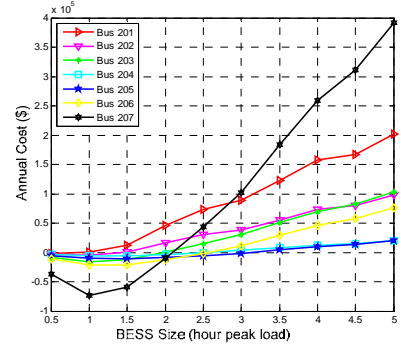


Figure 4. Annual cost analysis under PV penetration=50%

Increasing Wind Capacity Value in Tasmania Using Wind and Hydro Power Coordination

Mehdi Mosadeghy, Tapan Kumar Saha and Ruifeng Yan

School of Information Technology & Electrical Engineering

The University of Queensland, Brisbane, Australia

Email: m.mosadeghy@uq.edu.au, saha@itee.uq.edu.au and ruifeng@itee.uq.edu.au

Abstract— Wind power penetration is increasing in power system in many countries. To mitigate wind power fluctuations and maximize clean energy utilization, coordinating wind and hydro power is proposed in the literature. This paper investigates the benefits of coordinating hydro generators with wind farms, from reliability point of view in Tasmania, Australia. Reliability indices are computed in generation system adequacy assessment using the state sampling Monte Carlo technique. In accordance with these indices the capacity value of Tasmania’s wind power is calculated and the impact of hydro power coordination on this value is demonstrated. The results show that using hydro units to support wind power will improve the capacity value of the wind farms regarding their wind regime and the combined capacity.

I. KEY EQUATIONS

Demand not supplied due to the load level D exceeding the available generating capacity and the annualized loss of energy expectation are computed by (1,2):

$$DNS_k = \max \left\{ 0, D - \sum_{i=1}^m G_{ik} \right\} \quad (1)$$

$$LOEE = \frac{\sum_{k=1}^N DNS_k \times 8760}{N} \quad (2)$$

ARMA model of the Musselroe wind regime is shown in (3):

$$y_t = 1.0148y_{t-1} + 0.7822y_{t-2} - y_{t-3} + 0.1934y_{t-4} + \alpha_t - 0.2404\alpha_{t-1} - 0.8924\alpha_{t-2} + 0.3196\alpha_{t-3} \quad (3)$$

$$\alpha_t \in NID(0, 0.12633^2).$$

II. KEY FIGURES

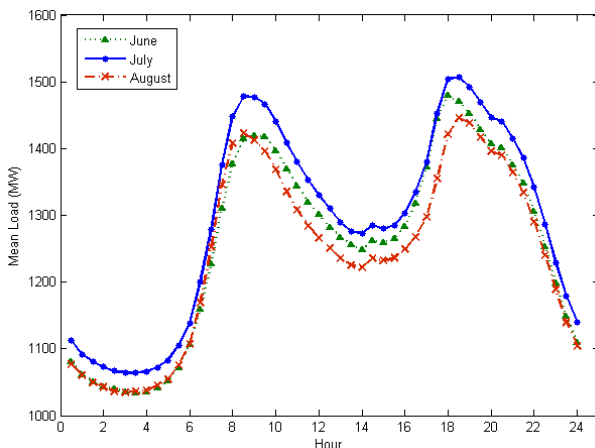


Figure 1. Mean value of Tasmania hourly winter load for 6 years (2007-12)

TABLE 1. WIND SPEED STATISTICAL DATA OF 6 YEARS FOR WOOLNORTH AND MUSSELROE SITES

Site	Mean (m/s)	Standard Deviation (m/s)
Woolnorth	9.73	4.94
Musselroe	6.80	3.65

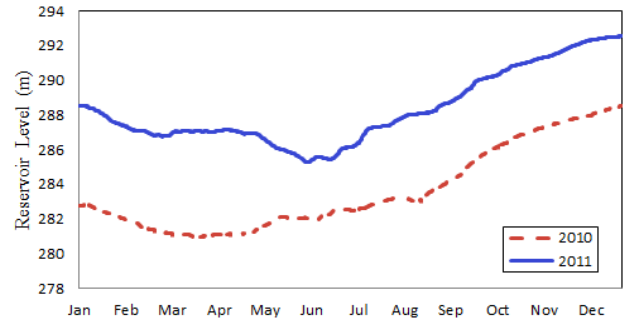


Figure 2. Gordon Reservoir levels in 2010 and 2011

III. KEY RESULTS

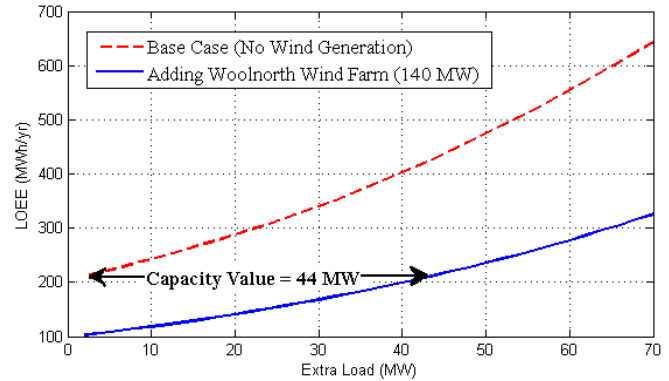


Figure 3. Capacity value of Woolnorth wind farm

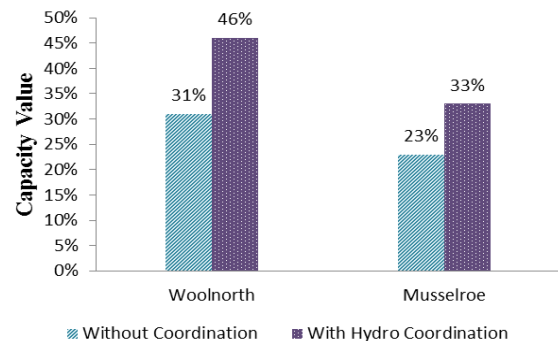


Figure 4. Capacity value of Tasmanian wind farms with and without hydro power coordination

Dynamic Reserve Zones for Day-Ahead Unit Commitment with Renewable Resources

Fengyu Wang, *Student Member, IEEE*, and Kory W. Hedman, *Member, IEEE*

School of Electrical, Computer, and Energy Engineering, Arizona State University, Tempe, AZ 85287, USA

Email: fengyu.wang@asu.edu and kory.hedman@asu.edu

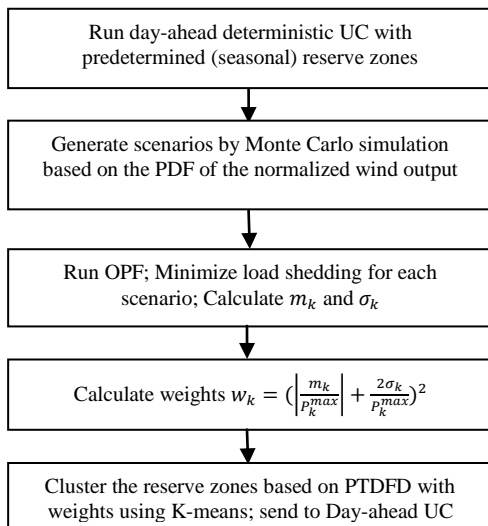
Abstract— With increasing levels of uncertain renewable resources, it will become more difficult to predict the available transfer capability and congestion. At the same time, renewable resources require operators to acquire additional operating reserves. With today’s reserve requirements unable to ensure the optimal location of the reserves, new reserve requirement procedures are necessary to ensure reserve deliverability while maintaining a reliable system at least cost. This paper proposes a daily reserve zone determination procedure, which is able to better reflect system operating conditions by utilizing probabilistic power flows. A statistical clustering algorithm, with the centrality measurement based on weighted PTDF differences, is used to cluster buses together to produce the zones. While the proposed reserve zone determination method is a heuristic, it is shown to be effective and it is computationally tractable. The proposed method can be used on its own and can be used along with stochastic programming techniques that implicitly determine reserves. The proposed method is validated by testing it on a modified IEEE 118-bus system for multiple days; the proposed method is compared against a stochastic programming technique and existing reserve zone partitioning procedures. This work is based on a working paper, [1].

I. KEY EQUATIONS

The mathematical expression for the weighted PTDFD:

$$WPTDFD_{ij} = \frac{\sum_{k=1}^{|K|} w_k |PTDF_{k,i}^R - PTDF_{k,j}^R|}{|K|} \quad (1)$$

II. METHODOLOGY



III. KEY RESULTS

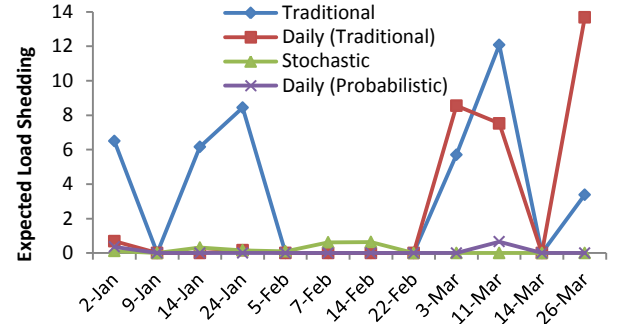


Fig. 1. Expected load shedding via scenario analysis (wind) (MWh).

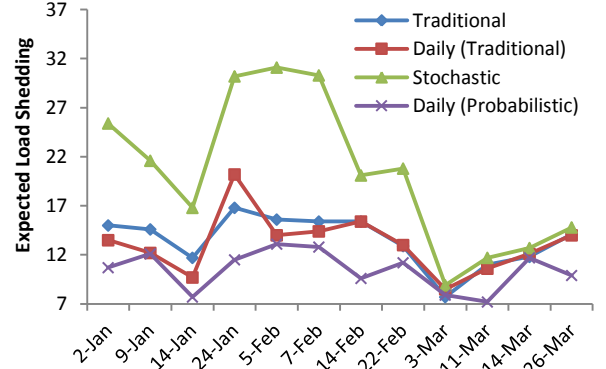


Fig. 2. Expected load shedding via scenario analysis (wind + N-1 contingencies) (MWh).

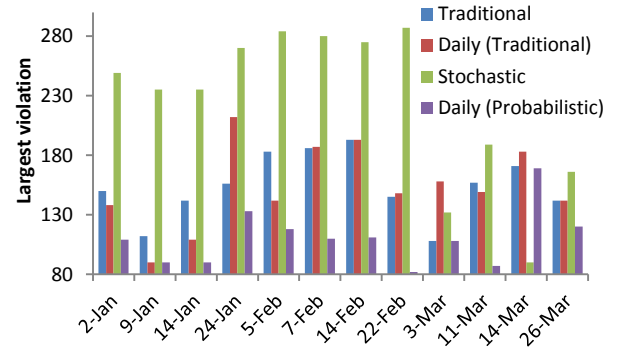


Fig. 3. Largest single violation via scenario analysis (MWh).

References

- [1] F. Wang and K. W. Hedman, “Dynamic reserve zones for day-ahead unit commitment with renewable resources,” *IEEE Trans. Power Syst.*, submitted for publication.

Economic Assessment of Bulk Energy Storage in Transmission Systems with High Penetration of Renewable Generation

Nan Li, *Student Member, IEEE*, and Kory W. Hedman, *Member, IEEE*

School of Electrical, Computer, and Energy Engineering, Arizona State University, Tempe, AZ 85287, USA

Email: nanli4@asu.edu and kory.hedman@asu.edu

Abstract— As renewable penetration increases, the intermittency and variability issues associated with many renewable resources should be addressed. Traditionally, the solution is to rely on conventional generators to provide backup generation and ancillary services. However, as the level of renewable penetration increases, the role of conventional generators will transition from primarily supplying energy to primarily providing reserves for intermittent renewable generation. Conventional generators may be required to operate at lower output levels and frequently change their outputs to compensate for the intermittency in renewable generation. As a result, conventional generators may suffer from higher operating costs while receiving lower profits. Furthermore, the generators' emissions per MWh are likely to increase due to the imposed ramping requirements. In contrast, as renewable penetration increases, bulk energy storage will become competitive since they can absorb excess clean energy when renewable resources are available and shift it to hours when scheduled generation is expensive or cannot meet demand. Energy storage also has fast ramping capability so that they can effectively balance the uncertainty in renewable generation. Yet the primary barrier with bulk energy storage is their high investment costs. This paper analyzes the effectiveness of bulk energy storage under high levels of renewable penetrations and identifies the break point (relative to the renewable penetration level) when bulk energy storage is competitive with conventional generators.

I. KEY EQUATIONS

Minimize:

$$\sum_{k=1}^K \pi_k \sum_{t=1}^T \left\{ \sum_{g \in \{\Omega_G, \Omega_P\}} [c_g P_{gkt} + c_g^{NL} u_{gkt} + c_g^{SU} v_{gkt}] + c_g^{SD} w_{gkt} + c_g^R (P_{gkt}) \right\} \quad (1)$$

$$c_g^R (P_{gkt}) = \sum_{l=1}^L c_{gl} \left[\frac{2l-1}{2} \cdot \frac{P_{gkt} - P_{g0,t}}{L} + P_{g0,t} \right], \quad (2)$$

$$\forall g \in \{\Omega_G, \Omega_P\}, k, t$$

$$\sum_{g \in \Omega_G} P_{gkt} + \sum_{g \in (\Omega_P, \Omega_C)} (P_{gkt}^{Out} - P_{gkt}^{In}) + \sum_{m(\cdot, \rightarrow n)} P_{mkt} \quad (3)$$

$$- \sum_{m(n \rightarrow \cdot)} P_{mkt} = d_{nkt} - \sum_{g \in \Omega_W} P_{wkt}^{Wind}, \quad \forall n, k, t$$

$$P_{mkt} = B_m (\theta_{n^+} - \theta_{n^-}), \quad \forall m, k, t \quad (4)$$

$$-P_m^{Max} \leq P_{mkt} \leq P_m^{Max}, \quad \forall m, k, t \quad (5)$$

$$P_g^{Min} u_{gkt} \leq P_{gkt} \leq P_g^{Max} u_{gkt}, \quad \forall g \in \Omega_G, k, t \quad (6)$$

$$s_{gk,t} = s_{gk,t-1} + \eta_g^1 P_{gkt}^{In} - P_{gkt}^{Out} / \eta_g^2, \quad \forall g \in \{\Omega_P, \Omega_C\}, k, t \quad (7)$$

$$L_g^{In} z_{gkt} \leq P_{gkt}^{In} \leq U_g^{In} z_{gkt}, \quad \forall g \in \{\Omega_P, \Omega_C\}, k, t \quad (8)$$

$$L_g^{Out} (1 - z_{gkt}) \leq P_{gkt}^{Out} \leq U_g^{Out} (1 - z_{gkt}), \quad \forall g \in \{\Omega_P, \Omega_C\}, k, t \quad (9)$$

$$s_g^{Min} \leq s_{gkt} \leq s_g^{Max}, \quad \forall g \in \{\Omega_P, \Omega_C\}, k, t \quad (10)$$

$$P_{g0,t} - P_{g0,t-1} \leq R_g^+ u_{g0,t-1} + R_g^{SU} v_{g0,t}, \quad \forall g \in \{\Omega_C, \Omega_G\}, t \quad (11)$$

$$v_{gkt} - w_{gkt} = u_{gk,t} - u_{gk,t-1}, \quad \forall g \in \{\Omega_C, \Omega_G\}, k, t \quad (12)$$

$$P_{g0,t-1} - P_{g0,t} \leq R_g^- u_{g0,t} + R_g^{SD} w_{g0,t}, \quad \forall g \in \{\Omega_C, \Omega_G\}, t \quad (13)$$

$$-R_g^{10-} \leq P_{gk,t} - P_{g0,t} \leq R_g^{10+}, \quad \forall g \in \{\Omega_C, \Omega_G\}, k, t \quad (14)$$

$$-R_g^- \leq P_{g0,t}^{Out} - P_{g0,t-1}^{Out} \leq R_g^+, \quad \forall g \in \Omega_P, t \quad (15)$$

$$-R_g^- \leq P_{gk,t}^{Out} - P_{g0,t}^{Out} \leq R_g^+, \quad \forall g \in \Omega_P, t \quad (16)$$

$$-R_g^- \leq P_{g0,t}^{In} - P_{g0,t-1}^{In} \leq R_g^+, \quad \forall g \in \Omega_P, t \quad (17)$$

$$-R_g^- \leq P_{gk,t}^{In} - P_{g0,t}^{In} \leq R_g^+, \quad \forall g \in \Omega_P, t \quad (18)$$

$$r_{gkt} \geq 0, \quad \forall g \in \{\Omega_G, \Omega_P, \Omega_C\}, k, t \quad (19)$$

$$r_{gkt} \leq P_g^{Max} u_{gkt} - P_{gkt}, \quad \forall g \in \Omega_G, k, t \quad (20)$$

$$r_{gkt} \leq R_g^{10+}, \quad \forall g \in \Omega_G, k, t \quad (21)$$

$$r_{gkt} \leq U_g^{Out} - P_{gkt}^{Out} + P_{gkt}^{In}, \quad \forall g \in \Omega_P, k, t \quad (22)$$

$$r_{gkt} \leq U_g^{Out} z_{gkt} - P_{gkt}^{Out} z_{gkt} + P_{gkt}^{In} (1 - z_{gkt}), \quad \forall g \in \Omega_C, k, t \quad (23)$$

$$r_{gkt} \leq R_g^+ z_{gkt} + P_{gkt}^{In} (1 - z_{gkt}), \quad \forall g \in \Omega_C, k, t \quad (24)$$

$$0 \leq r_{gkt}^{NS} \leq R_g^{NS} (1 - u_{gk,t}), \quad \forall g \in \{\Omega_G, \Omega_C\}, k, t \quad (25)$$

$$z_{gk,t} \in \{0, 1\}, \quad \forall g \in \{\Omega_P, \Omega_C\}, k, t \quad (26)$$

$$u_{gk,t} \in \{0, 1\}, \quad \forall g, k, t \quad (27)$$

$$0 \leq v_{gkt} \leq 1, 0 \leq w_{gkt} \leq 1, \quad \forall g, k, t \quad (28)$$

II. METHODOLOGY

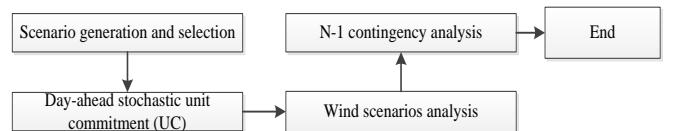


Figure 1. Day-ahead generation scheduling flowchart

Inertial response capability of DFIG according to wind speed

Stefanie Kuenzel, and Bikash C. Pal

Control and Power Research Group, Department of Electrical and Electronic Engineering
Imperial College London, UK

Email: stefanie.kuenzel06@imperial.ac.uk

Abstract—Conventional generators can keep a headroom to provide frequency response services, while reducing fuel costs. Wind generators do not pay for fuel and further loose renewable incentive payments when operating at reduced output. Hence wind turbines are set to produce maximum power output. Their inertial response is limited, since no headroom is left. This work analyzes the length of time a wind turbine can provide additional 10% output power, dependent on the wind speed.

I. INTRODUCTION

The inertial response requirement of generators has not been defined in grid codes, since conventional generators naturally exhibit this response. A requirement to increase power by 10% for 10 seconds is assumed here. The primary frequency response requirement in the Grid Code [1] by National Grid UK dictates that 10% additional output should be available within 10 seconds. Inertial response is needed up to the time primary response comes in, so it should last at least 10 seconds.

A. Key Equations

The power extracted by the turbine from the wind is:

$$P_t = 0.5\rho\pi R^2(C_p(\lambda, \beta))v_w^3 \quad (1)$$

The power coefficient C_p of a wind turbine is related to the tip speed ratio λ and pitch angle β [2]:

$$C_p(\lambda, \beta) = 0.5\left(\frac{116}{\lambda + 0.08\beta} - \frac{4.06}{\beta^3 + 1} - 0.4\beta - 5\right) \exp\left(-\frac{21}{\lambda + 0.08\beta} + \frac{0.735}{\beta^3 + 1}\right) \quad (2)$$

The tip speed ratio depends on the rotational speed, blade length and wind speed:

$$\lambda = \frac{\omega_t R}{v_w} \quad (3)$$

B. Key Results

The duration a turbine can supply additional 10% power output considering wind speed is shown in Fig.

1. For all wind speeds above 4.17 m/s the turbine can provide 10% additional power output for at least 10.4 seconds. In the low wind speed region the maximum time of additional output is 26.46 seconds at a wind speed of 4.7 m/s. For higher wind speeds the 10% additional power is higher, the kinetic energy in the turbine is higher due to faster rotation while wind power extraction reduces by a large amount during slow down. This leads to shorter response time. From about 12.3 m/s the response capability increases because the pitch angle can be reduced, increasing the output. However in the rated regime the response is further limited by the overrating capability of all turbine components. This has not been modelled, since it is manufacturer and material specific. It can be concluded that 10% inertial response can be provided until primary response is available, for all wind speeds above 4.17 m/s.

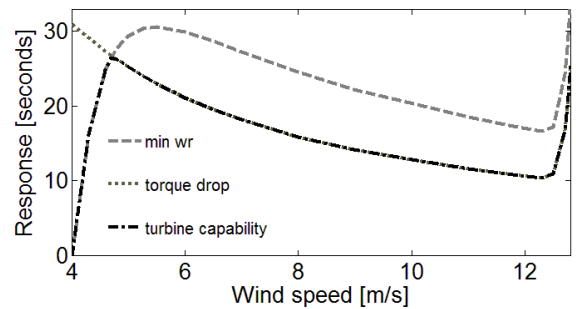


Fig. 1. Time of additional 10% power command capability of DFIG turbine according to wind speed, indicating limitation due to torque drop (solid line), limitation due to minimum rotational speed (dotted line), turbine overall capability (dashed and dotted line).

REFERENCES

- [1] NATIONAL GRID ELECTRICITY TRANSMISSION, "The grid code," http://www.nationalgrid.com/NR/rdonlyres/67374C36-1635-42E8-A2B8-B7B8B9AF2408/51019/Z_CompleteGridCode_I4R10.pdf, accessed 21/02/2012 10:42.
- [2] S. Heier, *Grid Integration of Wind energy conversion Systems*. Wiley, 1998.

Reliability and Economic Study of Multi-terminal HVDC with LCC & VSC Converter for Connecting Remote Renewable Generators to the Grid

Kazi Nazmul Hasan and Tapan Kumar Saha
University of Queensland, Brisbane, Queensland 4072, Australia

Abstract— This paper investigates reliability and economic challenges when large amounts of renewable generation are located long distances from load centers. Considering the distance, existing network, economics and controllability requirements, the optimum transmission system may be a multi-terminal HVDC with line commutated converter (LCC) and voltage source converter (VSC) stations. The LCC, VSC and multi-terminal HVDC system has been modeled and studied in PSS/E and MATPOWER software platform. The South East Australian test system has been simulated in OPF to investigate the integration of large scale geothermal power into the Australian National Electricity Market (NEM). The sensitivity of the simulated results to variations in generation capacity and system load have been assessed and provide the frontier of the reliability and cost-benefit analysis.

I. KEY EQUATIONS

A. Economic Evaluation

1) Cost Estimation

The annual required revenue (ARR) is calculated as,

$$ARR = \frac{r(I+r)^y}{(I+r)^y - I} \quad (1)$$

where, r is discount rate (10%), y is no. of years.

2) Net Market Benefit

The objective function of yearly net market benefit is formulated as below,

$$\left. \begin{aligned} & \sum_{i \in n_g} (p_g^i \cdot \lambda_g^i - p_g^i \cdot \phi_g^i) + \sum_{i \in n_d} (CS_d^i - CS_d^i) \\ & + \left(\sum_{i \in n_d} p_d^i \cdot \lambda_d^i - \sum_{i \in n_g} p_g^i \cdot \lambda_g^i \right) - \sum_{i \in n_g} (E_i \cdot \pi_{CO_2}) \\ & + \sum (\psi_i \cdot \sigma) \end{aligned} \right\} \quad (2)$$

where, t is time (hour), n_g is no. of generator set, n_d is no. of load set, p_g^i is generated power (MW), λ_g^i is locational marginal price (\$/MWh), ϕ_g^i is generation cost (\$/MWh), CS_d^i is consumer surplus (\$), CS_d^i is consumer surplus before augmentation (\$), p_d^i is consumed power (MW), λ_d^i is LMP at load bus i (\$/MWh), E_i is CO_2 emission (ton), π_{CO_2} is emission cost (\$/ton CO_2), ψ_i is renewable generation (MW), σ is LRET payment (\$/MWh).

B. Reliability Analysis

The E.U.E. is equal to the weighted sum of all energy curtailments at all load buses in the system [1, 2],

$$E.U.E. = \sum_{i \in S} P_i \cdot F_i \cdot D_i \quad MWh/Year \quad (3)$$

where, P_i , F_i , and D_i are the probability, frequency and duration of outage, respectively, in state i .

II. KEY RESULTS

ANNUAL REVENUE REQUIREMENT (ARR), NET MARKET BENEFIT (M\$/YEAR) AND BENEFIT TO COST RATIO (FOR 1000MW GEOTHERMAL POWER PENETRATION)

		SA	QLD	SA and QLD
HVAC	ARR (m\$/year)	173	288	461
	Benefit (m\$/year)	238	402	582
	Benefit to cost ratio	1.37	1.39	1.26
HVDC	ARR (m\$/year)	151	218	349
	Benefit (m\$/year)	237	444	587
	Benefit to cost ratio	1.56	2.03	1.68

RELIABILITY INDICES (EXPECTED UNSERVED ENERGY IN MWh/YEAR) (FOR 1000MW GEOTHERMAL POWER PENETRATION)

		SA	QLD	SA and QLD
AC	E.U.E.	2040	2030	1890
	Worst contingency	509-315	410-413	602-508, 602-413
HVDC	E.U.E.	2640	2400	2730
	Worst contingency	509-315	410-413	602-413, 602-413

SENSITIVITY OF GEOTHERMAL GENERATION – NET MARKET BENEFIT (M\$/YEAR)

Geothermal generation	SA (VSC)	QLD (LCC)	SA and QLD (VSC+LCC)
500MW	178	332	-
1000MW	237	444	587
1500MW	-	556	820

SENSITIVITY OF CARBON PRICE (FOR 1000MW GEOTHERMAL POWER PENETRATION) – NET MARKET BENEFIT (M\$/YEAR)

CO ₂ price	SA (VSC)	QLD (LCC)	SA and QLD (VSC+LCC)
20\$/ton	211	418	561
30\$/ton	299	506	649
40\$/ton	387	594	737
50\$/ton	475	682	825

Effects of HVDC Connection for Offshore Wind Turbines on AC Grid Distance Protection

Lina He (Advisor: Prof. Chen-Ching Liu)
 School of Mechanical and Materials engineering
 University College Dublin, Belfield
 Dublin, Ireland
 E-mail: lina.he@ucdconnect.ie

Abstract—The voltage source converter-high voltage direct current (VSC-HVDC) technology becomes an attractive option to integrate offshore wind power to onshore ac grids. Due to the use of pulse width modulation (PWM) control, the HVDC connection enables the independent adjustment of active and reactive power. In HVDC offshore wind networks, the grid side VSC (GSVSC) is usually assigned to control the dc voltage to balance the sending end and receiving end active power of HVDC. It also allows reactive power support for onshore ac grids to maintain the voltage of the point of common coupling (PCC) at a pre-determined level. When a transmission line close to a PCC encounters a short circuit, the resulting PCC voltage dip triggers fast reactive power control of the corresponding GSVSC to boost the PCC voltage. This tends to impact bus voltages and line currents close to the PCC. Since the capacity of VSC stations is expected to be large for bulk offshore wind power transmission, the resulting effect of reactive power on the performance of ac protection schemes can be significant. Distance protection is a good example. The basic principle of distance protection is based on the apparent impedance measurement that determines the approximate distance between the relay location and fault point during a SC fault. The fast reactive power control action can cause the fault distance to be overestimated by its backup relay located on the adjacent line. It is possible for a Zone 2 fault to be viewed as a Zone 3 event, resulting in mis-coordination between protective relays. Numerical simulations demonstrate the effect of HVDC offshore wind network on distance protection of an ac grid.

I. KEY EQUATIONS AND FIGURES

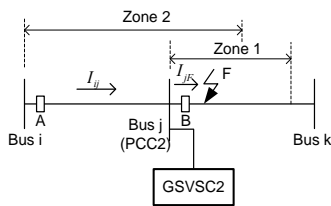


Fig. 1 Portion of ac grid with a converter

Assuming the fault impedance is 0, the impedance viewed by relay B is the line impedance from the fault point to the relay location.

$$Z_{m_B} = \frac{V_j}{I_{jF}} = Z_{BF} \quad (1)$$

In case of a failure of Zone 1 relay, say, relay B should operate but it does not, the apparent impedance viewed by the backup protection - relay A can be obtained as

$$Z_{m_A} = \frac{V_i}{I_{ij}} = \frac{V_j + Z_{ij} * I_{ij}}{I_{ij}} = \frac{V_j}{I_{ij}} + Z_{ij} \quad (2)$$

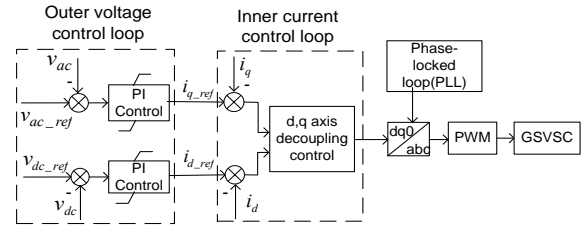


Fig. 2 Simplified control configuration of GSVSCs

II. KEY RESULTS

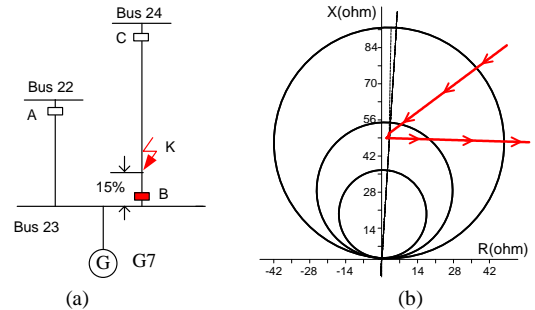


Fig. 3 (a) SC fault location on the IEEE 39 bus system; (b) Trajectory of relay A on IEEE 39 bus system

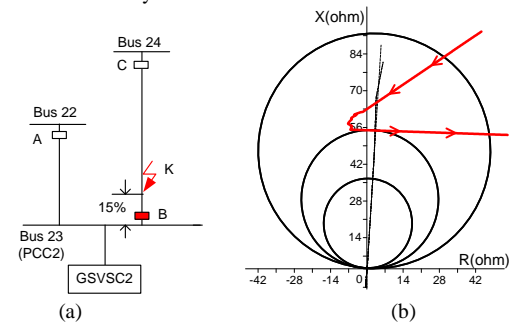


Fig. 4 (a) SC fault location on the integrated ac/dc system; (b) Trajectory of relay A on the integrated ac/dc system

ACKNOWLEDGEMENT

The authors would like to acknowledge the support from the EU project “Twenties,” Transmission system operation with large penetration of Wind and other renewable Electricity sources in Networks by means of innovative Tools and Integrated Energy Solutions.

Optimal Storage Placement and Size Considering the Uncertainty of Wind Power Using PSO and Sensitivity Analysis

Shuli Wen

Department of Electrical Engineering
University of Wisconsin, Milwaukee
Milwaukee, USA
shuliwen@uwm.edu

David C. Yu

Department of Electrical Engineering
University of Wisconsin, Milwaukee
Milwaukee, USA
yu@uwm.edu

Abstract— Energy storage system plays a significant role both in distributed power and utility power system. Among many of their benefits, loss and voltage profile improvement can be the salient specifications of storage system. Studies show that non-optimal size and placement of energy storage units leads to increase in loss and cost as well as the risk of voltage stability, especially in the case of high renewable energy penetration. To solve the problem, the heuristic optimization approach named Particle Swarm Optimization (PSO) is proposed in the paper to minimize the power loss and improve the system voltage profiles by changing locations and varying sizes of storage with considering the uncertainties in wind power production. By using Power-Voltage curve technique, voltage sensitivity is studied and evaluated to identify the potential locations for energy storage units, therefore, to minimize the PSO initialization. The efficiency of these approaches are tested on a modified IEEE 30-bus system. The results clearly demonstrate the necessity of optimal storage placement and sizing to avoid any possible problems associated with wind power uncertainty .

Index Terms— optimal placement and size, energy storage, renewable energy penetration, PSO, Power Voltage curve

KEY EQUATIONS

The main principle of PSO is related to the velocity and position. Each particle updates its velocity and position according to the following:

$$\left. \begin{aligned} v_i^{k+1} &= wv_i^k + c_1r_1(pb_{est}_i^k - x_i^k) + c_2r_2(gb_{est}^k - x_i^k) \\ x_i^{k+1} &= x_i^k + v_i^{k+1} \end{aligned} \right\} \quad (1)$$

I. KEY FIGURES

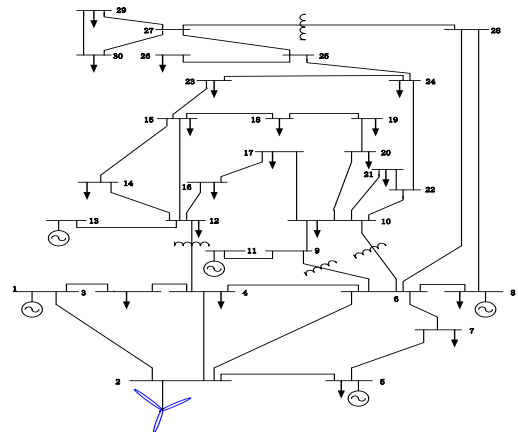


Fig.1 IEEE 30-Bus System

II. KEY RESULTS

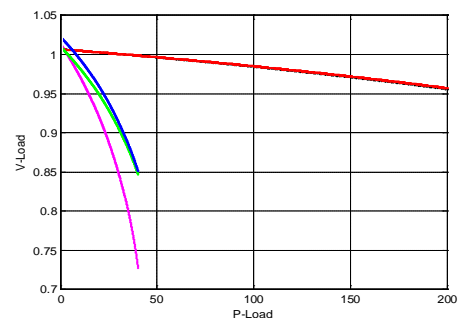


Fig.2 PV Curve of Sensitive buses

Reactive Power Planning Considering High Penetration Wind Energy

Xin Fang, *Student Member, IEEE*; Fangxing Li, *Senior Member, IEEE*; Yan Xu, *Senior Member, IEEE*; Yanli Wei, *Member, IEEE*; Haoyu Yuan, *Student Member, IEEE*

Department of Electrical Engineering and Computer Science, University of Tennessee, Knoxville, TN 37996, USA, Email: xfang2@utk.edu and fli6@utk.edu

Abstract— This paper addresses the optimal placement of reactive power (Var) sources under the paradigm of high penetration wind energy. The reactive power planning (RPP) investment in this particular condition involves a high level uncertainty due to the wind power characteristic. The correlation between wind speeds of different wind farms should also be considered when there are multiple wind farms. To properly model the wind generation uncertainty, a multi-scenario framework optimal power flow that considers the voltage stability constraints is developed. The objective of RPP is to minimize the total system cost (Var cost and the expected generation cost). So the RPP under this condition is to optimize the Var location and size, meanwhile minimizing the fuel cost and therefore find the global optimal RPP results. The approach is based on two sets of variables (TSV) combined with multi-scenario model. A case study is provided to verify the proposed method.

I. KEY EQUATIONS

Objective: Var cost

$$\text{Min} \sum_{k \in N^Q} (c_1 + c_2 Q_{ck}) \cdot u_k \quad (1)$$

Objective: Expected generation cost

$$\text{Min} \sum_{t \in W^N} p_t \sum_{i \in N^G} f(P_{Gi,t}) \quad (2)$$

-Two sets of Power flow constraints:

$$0 = P_{Gi,t}^* + P_{Wi,t}^* - (VSM_i^* + 1) \cdot P_{Li} - V_{i,t}^* \sum_{j=1}^n V_{j,t}^* (G_{ij} \cos(\theta_{i,t}^* - \theta_{j,t}^*) + B_{ij} \sin(\theta_{i,t}^* - \theta_{j,t}^*)) \quad (3)$$

$$0 = Q_{Gi,t}^* + Q_{Wi,t}^* + Q_{ci}^* - (VSM_i^* + 1) \cdot Q_{Li} - V_{i,t}^* \sum_{j=1}^n V_{j,t}^* (G_{ij} \sin(\theta_{i,t}^* - \theta_{j,t}^*) - B_{ij} \cos(\theta_{i,t}^* - \theta_{j,t}^*)) \quad (4)$$

$$0 = P_{Gi,t} + P_{Wi,t} - P_{Li} - V_{i,t} \sum_{j=1}^n V_{j,t} (G_{ij} \cos(\theta_i - \theta_j) + B_{ij} \sin(\theta_i - \theta_j)) \quad (5)$$

$$0 = Q_{Gi,t} + Q_{Wi,t} + Q_{ci,t} - Q_{Li} - V_{i,t} \sum_{j=1}^n V_{j,t} (G_{ij} \sin(\theta_i - \theta_j) - B_{ij} \cos(\theta_i - \theta_j)) \quad (6)$$

II. KEY FIGURE

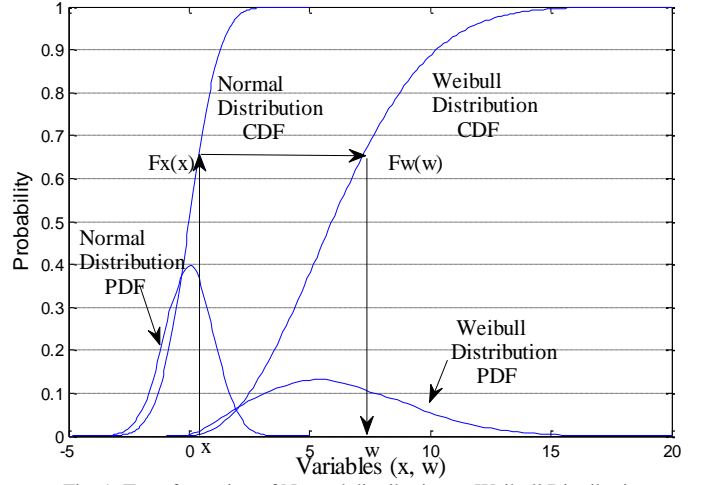


Fig. 1. Transformation of Normal distribution to Weibull Distribution

III. KEY RESULTS

TABLE I. Var compensation under different wind speed correlation

Correlation Coefficient	Var Compensation Bus			Objectives		
	9	10	14	Fuel cost (\$)	Var cost(\$)	Total cost(\$)
-1	3.44	5.18	15.44	7284.8	390.6	7675.37
-0.8	3.36	5.12	15.68	7296.1	391.6	7687.65
-0.4	3.61	5.23	14.76	7259.1	385.1	7644.12
0	3.47	4.74	15.89	7415.5	388.2	7803.45
0.4	3.37	5.34	14.85	7334.6	385.6	7720.24
0.8	3.25	4.83	15.29	7412.8	383.7	7796.47
1	3.62	5.13	14.85	7243.8	386	7629.84

TABLE II. Var compensation under different VSM

VSM	Var Compensation Bus				Objectives		
	9	10	12	14	Fuel cost(\$)	Var cost(\$)	Total cost(\$)
0	0	0	0	0	7239.2	0	7239.2
50%	0	0	0	0	7239.2	0	7239.2
80%	0	7.1	0	8.7	7239.2	257.9	7497.1
100%	16.98	11.93	1.25	12.7	7239.2	628.7	7867.9
120%	30	20.39	7.21	16.86	7239.2	944.6	8183.8

Capacitor and Generator Output Adjustment by Using PSO Considering N-1 Contingency for Large Penetration of Photovoltaic Power

Sho Ando, Aye Mya Mya Hlaing, Shinichi Iwamoto

Power Systems Laboratory, Department of Electrical Engineering and Bioscience, Waseda University, 169-8555, Tokyo, Japan
Email: ando.sho.pwrs@gmail.com

Abstract— In these recent years, the Southeast Asia countries are trying to promote the electricity utilization while decreasing the CO₂ emission and air pollution. For those reasons, the target of penetrating the amount of renewable energies has become larger and larger. That is, the target amount of renewable energies penetration to the power systems of Southeast Asia countries is set to be 274GW by 2030. Also, Japan has set its target amount for photovoltaic power penetration 53GW by the year 2030. If we penetrate such a large amount of photovoltaic power to the power system, several problems will take place by the growth of the PV usage. Therefore, we have to consider the suitable voltage profile within a proper voltage range. Therefore, in this research, we focus our attentions on the active power loss and the suitable voltage profile for penetration of a large amount of PVs by considering capacitors and generator output adjustments at the same time. For the generator output control, we proposed to use the power flow calculation in terms of minimizing active power losses and bus voltage deviations. The simulations are run by using IEEJ WEST 10 Machine O/V System Model to confirm the validity of the proposed method.

I . KEY EQUATIONS

$$v_i^{k+1} = \omega \cdot v_i^k + c_1 \cdot rand_1 \cdot (pbest_i - x_i^k) + c_2 \cdot rand_2 \cdot (gbest - x_i^k)$$

$$x_i^{k+1} = x_i + v_i^{k+1}$$

$$\omega = \omega_{max} - \frac{\omega_{max} - \omega_{min}}{iter_{max}} \times iter$$

$$min f = \omega_1 \cdot \sum (SC_i)^2 + \omega_2 \cdot P_{loss}(P_G) + \omega_3 \cdot \sum (V_{ref} - V_i)^2 + \omega_4 \cdot Penalty_1 + \omega_5 \cdot Penalty_2$$

II . KEY FIGURES

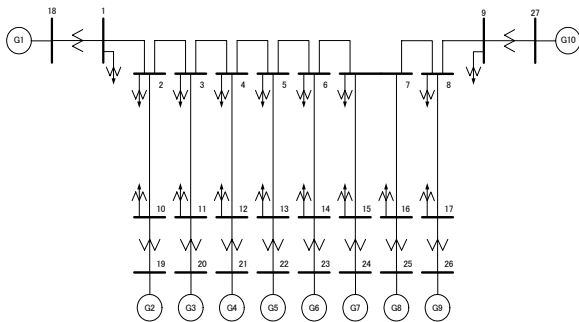


Figure 1 IEEJ WEST 10 Machine O/V System

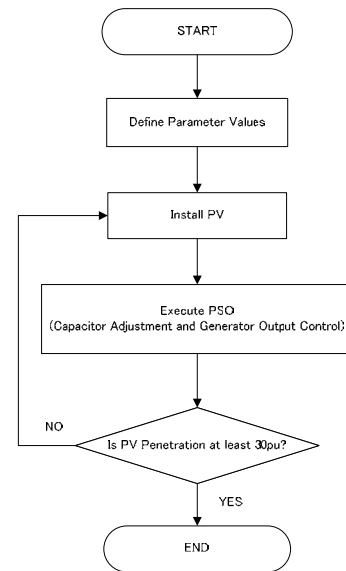


Figure 2 Flowchart of Proposed Method

III. KEY RESULTS

Capacitance in pu

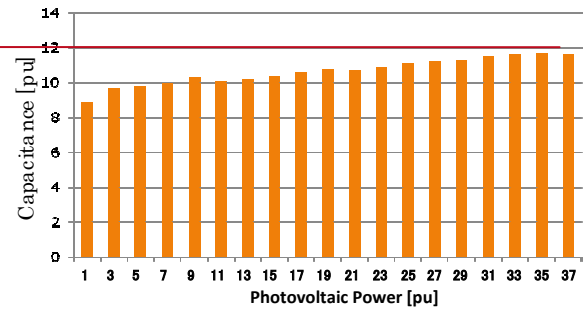


Figure 3 Capacitance after Adjustment

Active Power Loss Minimization

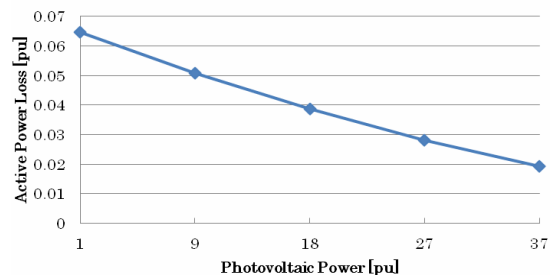


Figure 4 Active Power Loss Minimization

Load-Frequency Control (LFC) Model Including Renewable Power, and Demand Response

Colin Young and S. Ali Pourmousavi
Advisor: Hashem Nehrir

Department of Electrical and Computer Engineering
Montana State University
Bozeman, MT 59717
E-mail: Coliny157@gmail.com

Abstract— In future power systems, variable and uncertain renewable energy sources (RES) (e.g., wind and solar PV generation), storage devices (e.g., battery) and demand response (DR) will be included to achieve different goals. Government emission regulation, global warming, and the increased scarcity of fossil fuels will drive this change. At the moment, more research is needed to evaluate the impacts of this transition to the new era on the performance of the future power systems, specifically on frequency and voltage regulation. Also, the DR impacts and optimal operation of the system are other important topics which need more attention from power engineers and researchers.

There have been few studies that have tried to address a part of the above issues on the power system by including wind and solar PV systems to the single area load frequency control (LFC) model at the transmission level. These studies don't provide a comprehensive framework for optimal operation of the system with different RES and conventional power plants, large storage devices, and DR. In addition, the non-linear model of wind and solar are approximated. These approximations are incapable of providing a comprehensive assessment of the dynamics of the system. Also, the voltage dynamic performance of the power system has not been included and assessed in these research studies. Therefore, a new LFC model with the non-linear aspects of wind and solar PV models (i.e., non-linear frequency dependent model) will be introduced for single-area power system in this poster. Later, the proposed model will be extended to multi-area power system where both wind and solar power sources contribute to voltage and frequency changes within areas and between areas. In the multi-area power system model, automatic generation control (AGC) between areas and load disturbances in each area will be examined at the transmission level.

Since the proposed LFC model contains nonlinearities, conventional and optimal linear controllers will not be effective. Therefore, a non-linear controller, such as fuzzy logic, is required. Fuzzy logic control design is very useful for non-linear applications because it doesn't require a mathematical model of the system, and it can be used for a large range of operating conditions. General ideas of fuzzy logic controller application for the proposed LFC model will be presented in this poster. Figure 1 shows a schematic diagram of the proposed LFC model.

This research plan will be accomplished as follows: first, non-linear frequency-dependent model of wind and PV generation

sources will be added to the traditional single-area LFC model. Second, a large-scale energy storage model and DR will be added to the proposed single-area LFC model. In addition, a dynamic model of voltage at the transmission level will be included in the proposed LFC model. Third, a non-linear controller design (e.g., a fuzzy controller) will be developed to regulate frequency and voltage, which is necessary because of RES and load variations. It is also desired to apply another nonlinear control design for comparison purposes. The second controller might be an optimal management algorithm to dispatch generation and demand economically at each pre-defined interval. Finally, the proposed LFC model and controller design will be expanded to a general power system with multiple areas.

The proposed LFC model will give a comprehensive analyses and assessments of the impacts of variable RES generation and DR in a large-scale power system at the transmission level. It also provides researchers and system operators with a useful and accurate tool to quickly assess the dynamic behavior of the system.

The proposed nonlinear controller and optimal management algorithm introduce novel approaches for frequency and voltage regulation in the future power system.

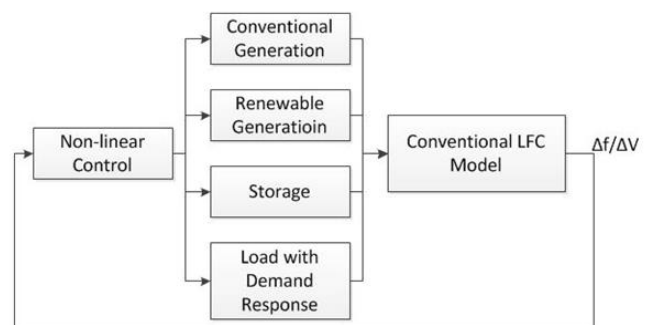


Figure 1: Overview of the non-linear control objective.

Impact of Available Electric Vehicle Battery Power Capacity on Power System Reliability

Bei Zhang, *Student Member, IEEE*, and Mladen Kezunovic, *Fellow, IEEE*

Department of Electrical and Computer Engineering, Texas A&M University, College Station, TX USA
Email: adele.zhang@neo.tamu.edu

Abstract—This poster focuses on estimating the available power capacity that electrical vehicles (EVs) can provide for the reserve market and evaluating its impact on power system reliability. The proposed approach estimates the available power capacity in a probabilistic manner based on traffic conditions through Markov process, which takes into account time durations when EVs are scheduled to provide the reserve services, the battery charge depletion limit and the energy needed for transportation purposes. A method to evaluate the reliability of the combined system (conventional system plus EVs) based on the probabilistic model is also presented. Meanwhile, numerical experiments are conducted to validate the effectiveness of the proposed approach and show significant impact of EVs on system's reliability through the ancillary service market.

I. KEY EQUATIONS

A. Mathematical Formulation

The cumulative distribution of the energy that EVs can provide to the grid at one moment is as follows:

$$F_Z(z) = \int_{-\infty}^z \sum_{j=1}^m \frac{\rho^{(N-j)}}{(N-j)!} e^{-\rho} \frac{1}{j\sqrt{2\pi}\sigma} e^{-\frac{(u-\omega)^2}{2\sigma^2}} du \quad (1)$$

Where m is the maximum capacity of the traffic system, N is the total of EVs in the large area, and j is the number of vehicles connected to the grid. We assume that the energy E in an EV is a variable in a normal distribution, which means $E \sim N(\omega, \sigma^2)$.

If we suppose the time duration is h , then the power from EVs can be obtained through equation (2).

$$power = \frac{F_Z^{-1}(0.05)}{h} \quad (2)$$

Where $F_Z^{-1}(0.05)$ is the exact amount of energy that can be provided by EVs.

Technically, batteries shouldn't be depleted below 20%. If we suppose that the total battery capacity of EVs in one large area is C_{to} , then the available power can be shown in equation (3).

$$power_{-20\%} = \frac{F_Z^{-1}(0.05) - 0.2 \times C_{to} \times \frac{N - \rho}{N}}{h} \quad (3)$$

Where ρ is λ / μ . λ is the incoming rate of the vehicles into the traffic system, and μ is the departure rate of the vehicles off the traffic system.

Moreover, if we take into account the vehicles are about to start their travel while ensuring that they can have enough energy to get to their destination without violating the 20% depletion rate, and suppose that every vehicle will need q energy on average to finish their travel, then the available power can be estimated by using equation (4).

$$power_{-20\%-leave} = \frac{F_Z^{-1}(0.05) - 0.2 \times C_{to} \times \frac{N - \rho}{N} - q \times \rho}{h} \quad (4)$$

We can get the Loss of Load Probability (LOLP) of the combined system including EVs and generators by equation (5).

$$LOLP = \sum_0^{L_p} F_Z(x) p(C_{gen} - x) \quad (5)$$

II. KEY FIGURES

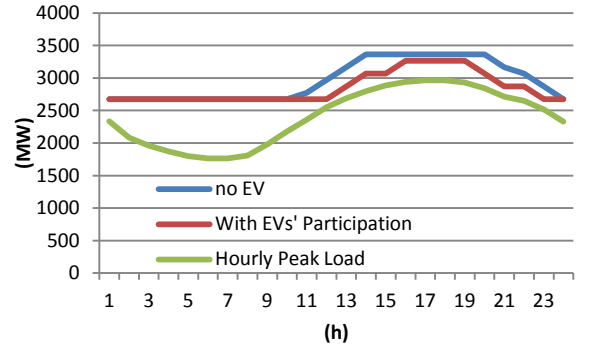


Fig. 1. Online Capacity with and without EVs and Hourly Peak Load

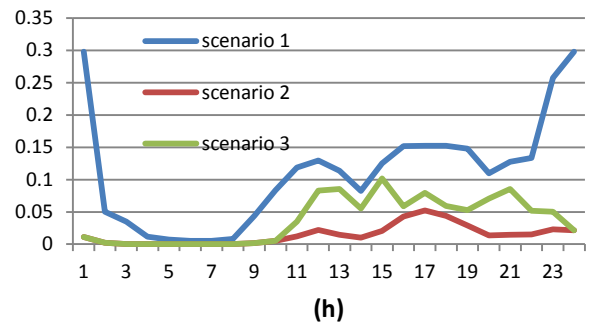


FIG. 2 ILLUSTRATION OF HOURLY LOLP IN THREE SCENARIOS

A Generalized Data Preprocessing Method For Wind Power Prediction

Jiakun An, Zhaohong Bie, Xiaozhong Chen, Bowen Hua, Shiyu Liu
 Department of Electrical Engineering, Xi'an Jiaotong University,
 Xi'an Shaanxi, 710049, P. R. China



1 Abstract

A generalized data preprocessing method is proposed in this paper to reduce the amount of outliers among historical data and further improve the power prediction accuracy. Historical data of wind farms are fit with an S-shape curve via Linear Regression Model. Based on this statistical curve, outliers can be identified considering different fitting error. Furthermore, the expansion of wind farm is identified through the number of outliers. Then a selection method for the allowed maximum fitting errors is recommended. The presented method has been integrated into the prediction system in Inner Mongolia of China with 36 farms. The actual application shows that the wind farm power prediction accuracy has been improved by at least 28% with this model. It is noteworthy that the proposed preprocessing method is just based on statistical analysis of historical data and thus compatible with various wind power prediction methods.

2 Introduction

- Wind power has attracted widespread attention and wind farm power prediction becomes more and more important. The basis for short-term prediction models is the consistency between historical data.
- There are many outliers in the historical data: wind power curtailment, NWP's missing, recording errors and wind turbines' statistical outage, wind-farm expansion.
- Accuracy of existing wind power prediction models is not satisfactory.
- This paper proposes a generalized data preprocessing method to reduce the amount of the outliers and further improve power prediction accuracy.

3 Wind Farm Data Characteristics and Data Preprocessing

Wind Farm Data Characteristics

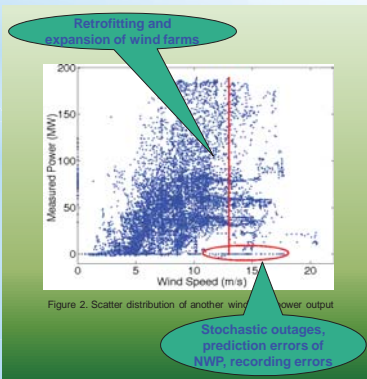
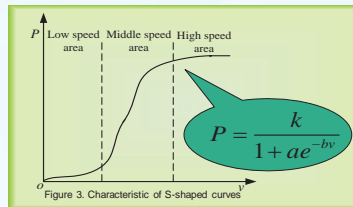


Figure 2. Scatter distribution of another wind farm power output

S-shaped Statistical Curve



Outliers and Wind-farm Expansion Identification

$$P_s = \frac{\hat{k}}{1 + \hat{a}_i e^{-\hat{b}_i v_i}} \quad (8)$$

$$P_i - P_s \geq PoErr \times P_{IN} \quad (9)$$

$$P_s - P_i \geq NgErr \times P_{IN} \quad (9)$$

- Outliers Identification**
Samples meet (8) or (9)
- Wind-farm Expansion Identification**
Count the number of samples that meet (8) for a short period (e.g., one week). If such samples constitute to a certain percentage of the whole sample space (e.g., 20%), the wind farm is identified as expanded.

Allowed Maximum Fitting Errors Selection

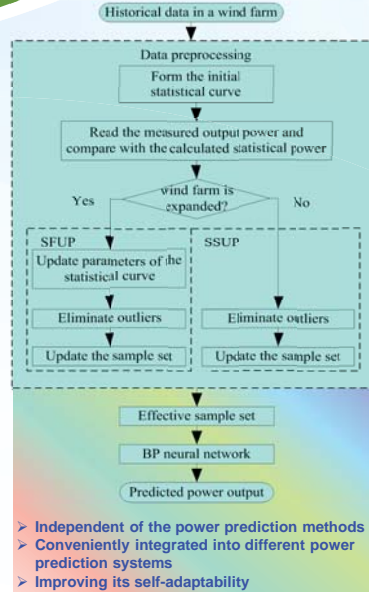
	High Speed Area	Middle Speed Area	Low Speed Area
PoErr	40%	25%	10%
NgErr	10%	25%	20%

It is found that the calculated statistical power is usually smaller than the measured power in high speed area while bigger in low speed area by analyzing the fitting errors.

Effective Samples Updating

- Wind farm is not expanded**
Sample Slow Updating Process (SSUP)
Updating the effective sample set with a long time interval
 - Wind farm is expanded**
Sample Fast Updating Process (SFUP)
Updating the effective sample set with a short time interval
- Initialize the counter flag Updated Sample Number (USN)
 - Reform the S-shaped statistical curve and update the parameters
 - Reduce the amount of the outliers
 - Update the effective sample set with short time interval
 - USN increasing, and judge whether it reaches to the specified number indicating that the statistical regularity of the expanded wind farm has been fitted
 - If yes, update the effective sample set with a long time interval; if not, go to (2)

4 Wind Power Prediction Incorporating Data Preprocessing



5 Case Study

Wind Farm Power Prediction

- Case 1: original samples;
- Case 2: preprocessed samples with equivalent allowed errors (PoErr=NgErr=20%);
- Case 3: preprocessed samples with different allowed errors shown in Table I.

	Case 1	Case 2	Case 3
Mean Absolute Error (MAE/MW)	77.69	47.79	28.99
RMSE	44.51%	27.09%	16.52%

Prediction error decreases almost 28%!!!

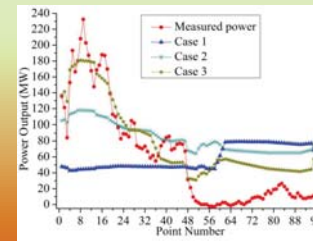


Figure 5. Power prediction results of one farm in December 30 of 2011

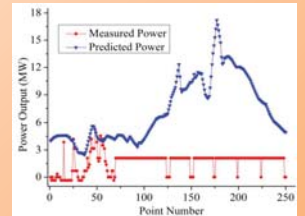
Power Prediction Errors Analysis

(1) The prediction accuracy of BP models is relevant to the power output.

Power Output (MW)	10	30	50	70	100
MAE (MW)	14.97	11.94	9.60	14.81	32.19
RMSE	13.98%	12.69%	9.73%	15.14%	29.16%

Most of the prediction errors are negative when the measured powers are bigger than 80 MW while positive when the measured powers are less than 20 MW.

(2) There are outliers in the prediction samples.



When the wind farm power curtailment or stochastic outage occurs, though the prediction error is high, the RMSE is meaningless.

(3) The data preprocessing method only considers the factor of wind speed and may weaken the influence of wind directions and temperatures on wind power output.

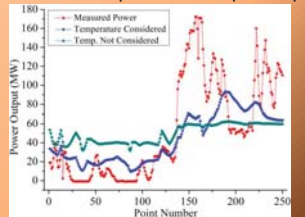


Figure 9. Influence of temperature on power output

6 Conclusions

- Many outliers exist in the historical data because of wind power curtailment and wind-farm expansion. This scenario is commonly seen in China.
- To reduce the amount of these outliers and further improve the power prediction accuracy, a generalized S-shaped-curve based data preprocessing method has been proposed in this paper.
- The practical application shows that the wind power prediction accuracy is improved by at least 28%.
- Prediction errors analysis shows that it is feasible to arrange less reserve when the predicted power is high.
- Especially, the proposed preprocessing method has a good versatility. As a result, it can be easily integrated into different power prediction systems, thus improving its self-adaptability and practicability.

$$RMSE = \sqrt{\frac{1}{N} \sum_{i=1}^N \left(\frac{P_{i,measure} - P_{i,forecast}}{P_N} \right)^2}$$

Robustness Analysis on Electric Vehicle Energy Distribution Networks

Guangyu Lin*, Ping Yi*, Liangqi Si†, Ting Zhu†, Xiuchen Jiang*, Guojie Li*, Miroslav M. Begovic‡

*School of Electronic, Information and Electrical Engineering, Shanghai Jiao Tong University, Shanghai, 200240, China

†Department of Computer Science, Binghamton University, Binghamton, NY, 13902, USA

‡School of Electrical and Computer Engineering, The Georgia Institute of Technology, 30332, Georgia, USA

Abstract—Electric Vehicles (EVs) can be used as a medium between the battery energy stored in EVs and the power grid through Vehicle-to-Grid (V2G). Combined with the characteristic that vehicles are mobile, EVs can provide a natural energy transmission system called EV energy network. This paper analyzes the features of energy routes in the EV energy distribution networks. Based on the characteristics of traffic congestion in the urban, sporadic congestion algorithm and recurring congestion algorithm are presented to simulate in a model of the EV energy network. Additionally, energy degree (ED) and energy source available rate (ESAR) are defined to reflect the current state of the EV energy network. The real-world transporting data in Manhattan and Pioneer Valley Transit Authority (PVTa) is utilized to analyze the robustness of the proposed EV energy network.

I. KEY FIGURES AND RESULTS

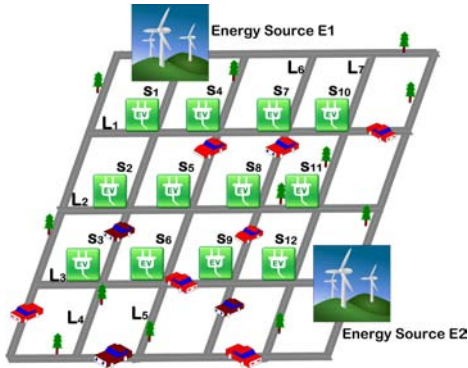


Fig. 1. Schematic diagram of bus lines

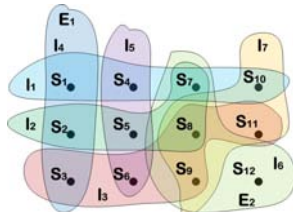


Fig. 2. hypergraph of bus lines

II. KEY EQUATIONS

$$ED = \langle \langle ed_{v_i} \rangle \rangle = \frac{1}{n} \sum_{v_i \in V} ed_{v_i} \quad (1)$$

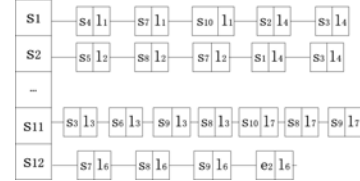


Fig. 3. edge lists of bus lines

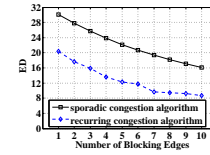


Fig. 4. ED under different numbers of clogged streets in Manhattan

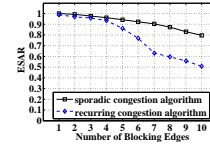


Fig. 5. ESAR under different numbers of clogged streets in Manhattan

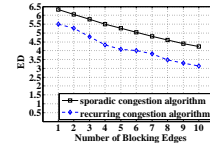


Fig. 6. ED under different numbers of clogged streets in PVTa

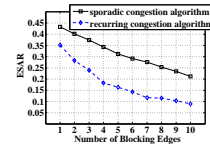


Fig. 7. ESAR under different numbers of clogged streets in PVTa

$$ed_{v_i} = |\Gamma_{v_i}|_{v_j \in V, v_i \neq v_j} \quad (2)$$

$$ESAR = \frac{1}{m(n-1)} \sum_{E_i \in E} \sum_{v_j \in V, v_j \neq E_i} \theta_{(v_j, E_i)} \quad (3)$$

$$ESAR = \frac{1}{m(n-1)} \sum_{E_i \in E} \sum_{v_j \in V, v_j \neq E_i} \theta_{(v_j, E_i)} \quad (4)$$

Optimal operation of Distribution Feeder considering PV generation reactive power support

Yashodhan Agalgaonkar, Student Member, IEEE, Bikash C Pal, Fellow, IEEE, Georgios Anagnostou, Student Member IEEE.
Control & Power Research Group, Department of Electrical & Electronics Engineering,
Imperial College London
London, United Kingdom
b.pal@imperial.ac.uk

Abstract— The uptake of variable MW from PV challenges distribution system operation. The primary problem is significant voltage rise on the feeder. Conventionally, overvoltage problem due to PV generation is solved with active power curtailment as PV generation operates at unity power factor. Upcoming medium voltage grid codes for PV generation are supportive of reactive power injection from PV inverter. This offers an opportunity for PV generation to participate in distribution voltage control. For PV generation different reactive power settings are proposed in grid codes namely, constant power factor, constant reactive power, variable power factor as active power varies (pf(P)), and variable reactive power as voltage varies (Q(U)). Most of PV inverter manufacturers in European market offer these settings for PV generators. Appropriate selection of one of the above settings can mitigate overvoltage caused by PV generation. Further, from Distribution network operators' point of view minimizing power loss on the distribution feeder is an important objective. This requires optimal dispatch of available reactive power sources in the distribution system including reactive power from PV generation. In this study optimal distribution reactive power dispatch is formulated in order to select reactive power setting for PV generator and other voltage control devices on the feeder. Strategy is based on the load and irradiance forecast. Distribution reactive power dispatch strategy uses unbalanced current injection technique and primal dual interior point method based optimization. Use of current injection technique enables utilisation of this strategy in case of radial or meshed distribution network. The objective is to minimize the power loss and maintain voltage. The proposed objective is achieved by coordinating various reactive power control options including that from PV inverter. The effectiveness of the approach is demonstrated by simulating realistic UK generic distribution system. PV generation output is adopted from practical five second time scale irradiance measurements made in year 2012 at test site at Loughborough, England.

Index Terms—PV, distribution networks, Loss minimization, reactive power optimization.

I. KEY EQUATIONS

Reactive power dispatch is formulated as power loss minimization problem subject to voltage constraints, On load tap changer limits, maximum power point tracking (MPPT) and the inverter capacity limits. Also reactive power limit of other sources in the system is considered.

Objective: Minimize
$$\sum_{h=1}^{h=24} P_{loss}$$

Subject to: $V_{min} \leq V \leq V_{max}$

$$Q_{min} \leq Q \leq Q_{max}$$

$$\sqrt{P_{solar}^2 + Q_{solar}^2} \leq S_{solar}$$

$$P_{solar} = P_{MPPT}$$

$$Tap_{min} \leq Tap \leq Tap_{max}$$

II. KEY FIGURES

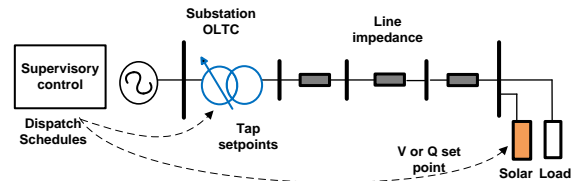


Figure 1: Distribution Reactive Power Dispatch

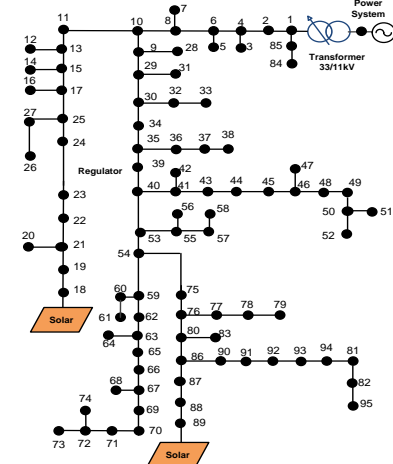


Figure 2: UK Generic Distribution test System

III. KEY RESULTS

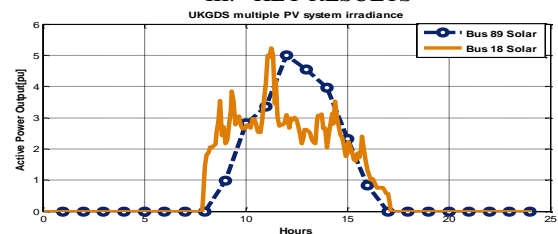


Figure 3: PV generation output adopted from practical measurements

Further Results and discussion about PV generation reactive power support modes will be added in the final draft of the poster.

Dynamic Models of Wind Turbine Generators In Power System Toolbox

Felipe Wilches-Bernal, *Student Member, IEEE*, and Joe H. Chow, *Fellow, IEEE*
 Department of Electrical and Computer and Systems Engineering
 Rensselaer Polytechnic Institute
 110 8th street, Troy, NY 12180, USA.

Abstract—Wind energy is rapidly becoming competitive with conventional power generation, leading to an increase in the levels of penetration of wind generation in power systems around the world. Wind generation is expected to continue and even increase as policies such as the Renewable Portfolio Standards are set in place in more countries and the existing targets for clean generation are expanded.

Because wind power plants are fundamentally different than the synchronous machines used in conventional generation (gas, nuclear, hydro), extensive research needs to be done in order to study the impacts that they pose to the power system. The first step to carry out this kind of research is to have realistic wind turbine models in an environment suited for power system studies and simulations. In this poster we present such models in a flexible environment for research. In particular, we use the Power System Toolbox (PST) [1] a MATLAB package in which dynamic power system behavior can be simulated as the platform for implementing wind turbine models of Type-3 (Doubly-Fed Asynchronous Generator) and Type-4 (Full Converter). Type-3 is the most common wind turbine technology in the USA and Type-4 is a promising technology for off-shore wind turbines. The models implemented are those presented in [2] and are the base of the generic WTG being advanced by the WECC [3], [4], [5]. It is important to highlight that the models interact with the grid as a controlled current source as depicted in Figure 1.

Here we present the model validation of the implemented models in an infinite bus system and their interaction with the power system. Also results on the integration of this models on a larger power system representing the US NPCC [6] interconnection, depicted in Figure 2, are exposed.

Index Terms—Wind Turbine Generator, dynamic modeling, wind power, power system stability.

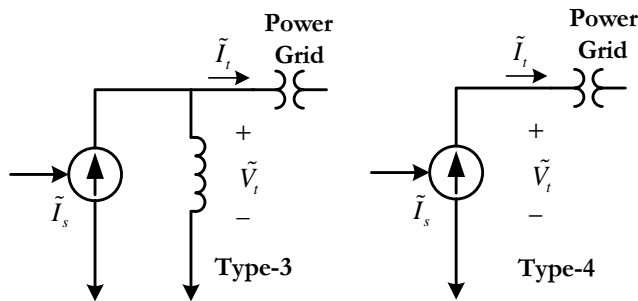


Fig. 1. WTGs models and their interaction with the grid.

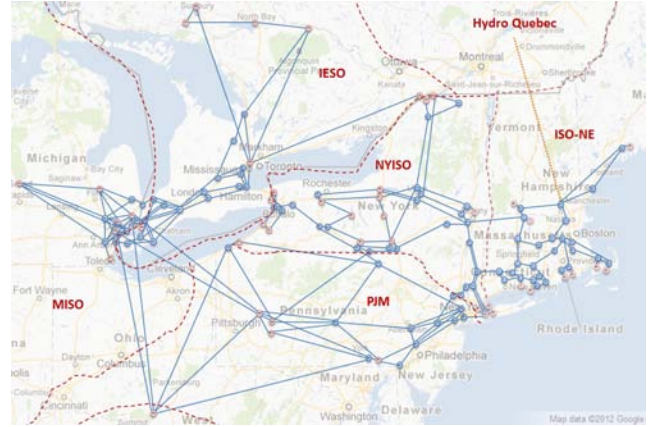


Fig. 2. Map of the 140-bus, 48-machine system reduced NPCC system first proposed in [6].

[2] K. Clark, N.W. Miller, J.J. Sanchez-Gasca, *Modeling of GE Wind Turbine-Generator for Grid Studies, Version 4.5*. General Electric International, Inc., April 2010.

[3] A. Ellis, Y. Kazachkov, E. Muljadi, P. Pourbeik, and J. Sanchez-Gasca, “Description and technical specifications for generic WTG models - A status report,” in *Power Systems Conference and Exposition (PSCE), 2011 IEEE/PES*. IEEE, 2011, pp. 1–8.

[4] A. Ellis, E. Muljadi, J. Sanchez-Gasca, and Y. Kazachkov, “Generic models for simulation of wind power plants in bulk system planning studies,” in *Power and Energy Society General Meeting, 2011 IEEE*. IEEE, 2011, pp. 1–8.

[5] M. Asmine, J. Brochu, J. Fortmann, R. Gagnon, Y. Kazachkov, C.-E. Langlois, C. Larose, E. Muljadi, J. MacDowell, P. Pourbeik *et al.*, “Model validation for wind turbine generator models,” *Power Systems, IEEE Transactions on*, vol. 26, no. 3, pp. 1769–1782, 2011.

[6] J. H. Chow, *Time-scale modeling of dynamic networks with applications to power systems*. Springer Verlag, 1982.

REFERENCES

[1] J. Chow and K. Cheung, “A toolbox for power system dynamics and control engineering education and research,” *Power Systems, IEEE Transactions on*, vol. 7, no. 4, pp. 1559–1564, 1992.

A Decentralized Coordinated Controller for Load Sharing in a Microgrid with Renewable Generation

Abstract

The aim of this paper is to introduce a control algorithm for load sharing in a microgrid with renewable generation mix. A decentralized coordinated power sharing control scheme is proposed considering both resistive and inductive line parameters, dynamics of the sources, weather condition, and multiple distributed energy resources (DERs). In this paper, a central power management unit is developed that specifies the reference real and reactive power generation for each distributed generator (DG) by considering the load demand and the generation availability. Local controllers are responsible for controlling the voltage and angle to inject the required amount of power into the grid. Simulation results show the viability of the proposed control scheme.

Mitigating the Detrimental Impact of Solar PV Penetration on the Voltage Profile of Power Systems

Nitin Prakash, *Student Member, IEEE*, Gerald T. Heydt, *Life Fellow, IEEE*, Vijay Vittal, *Fellow, IEEE*

School of Electrical, Computer and Energy Engineering, Arizona State University

Tempe, AZ 85287, USA

Abstract—Increasingly, conventional sources of energy are being displaced by renewable sources such as wind and solar with the view of making the electric power system more sustainable in the future. With the cost of solar photovoltaic (PV) panels reducing, it is plausible that amount of energy coming from these panels will increase over the years. A recent study had been conducted on the detrimental impacts of solar PV penetration on existing power systems in [1]. The problem of over-voltage is a detrimental impact of significant PV penetration on the system. The present work investigates mitigation measures which could be deployed to maintain the voltage profile of the system within acceptable limits when significant PV penetration occurs. A portion of WECC system has been selected for study with a significant amount of PV added both in the form of utility scale and rooftop PV sources. The impact of different mitigation measures such as reconfiguring shunt devices, changing the voltage set-point of generators and installing new shunt devices for improving the voltage profile of the system have been quantified. The mitigation methods have been prioritized and the solution which requires installing new shunt devices has been given the least priority. With the penetration of significant PV, the voltage magnitude of many buses violates acceptable limits and requires additional reactive power resources to keep those voltages within acceptable limits. A case for increasing the voltage limits on all the buses has been put forward by showing the extent of improvement that can be achieved by relaxing the acceptable voltage limits on buses by 1% and 2% beyond the existing limits.

I. KEY RESULTS

As shown in Figure 1, without taking any mitigation measure, 33% of the total buses in the test bed system face over-voltage with PV penetration in the existing system. If the acceptable voltage limits are relaxed by 1%, the number reduces to 16%. Mitigation measures like reconfiguring shunt devices, changing generator voltage set-point and installing new shunt devices have been taken one after the other with the goal of removing the voltage limit violations completely. At each stage, number of buses facing voltage violation after voltage limit relaxation has also been shown. It can be observed that after changing the generator voltage set-point, if the voltage limits are relaxed by 1% then system will not

need new shunt devices to be installed for removing voltage violations. In this way, different combinations of solution can be adopted by the concerned utility depending on the different resources available to them.

Improvement in voltage profile after implementation of different mitigation measures

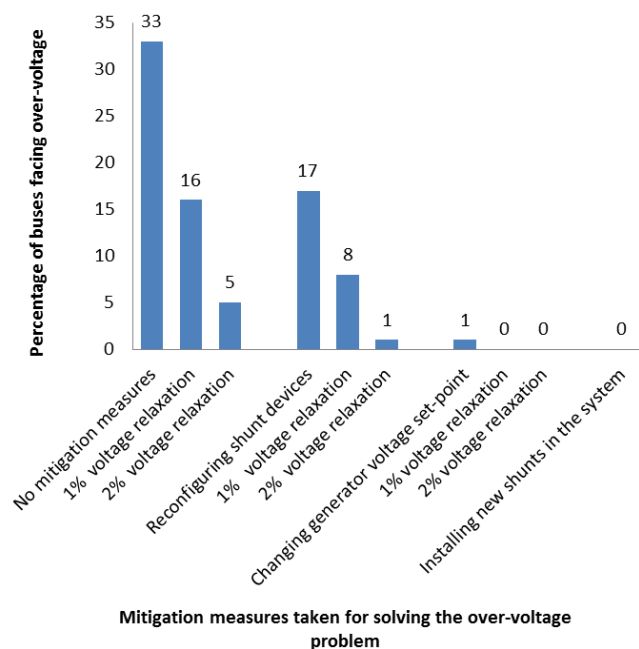


Figure 1. Chart showing the number of buses facing an over-voltage with PV penetration after the deployment of different mitigation measures

II. REFERENCE

- [1] S. Eftekharnajad, V. Vittal, G. T. Heydt, B. Keel, and J. Loehr, "Impact of Increased Penetration of Photovoltaic Generation on Power Systems," *IEEE Trans. Power Systems*, in press, issue: 99, 2012, Digital Object Identifier: 10.1109/TPWRS.2012.2216294.

Coordinated Control for Grid Integration of PV Array, Battery Storage, and Supercapacitor

Huiying Zheng, Shuhui Li

Department of Electrical & Computer Engineering
The University of Alabama
Tuscaloosa, USA
hzheng9@crimson.ua.edu, sli@eng.ua.edu

Chuanzhi Zang, Weijian Zheng

Shenyang Institute of Automation
Chinese Academy of Sciences
Xiamen Electric Power Supply Company
State Grid Corporation of China

Abstract— A substantial increase of solar photovoltaic (PV) power generators have taken place in recent years. The intermittent nature of PV energy and quick fluctuations of load demanding require energy storage units (ESU) which generally consists of storage battery and supercapacitor (SC). The development of coordinated control tools for next-generation PV installations, along with ESU, provides flexibility to distribution system operators. The objective of the control of this hybrid PV and energy storage system is to supply the desired active and reactive power to the grid and at the same time to maintain the stability of the dc-link voltage of the PV and energy storage system through coordinated control of power electronic converters. This paper investigates three different coordinated control structures and approaches for grid integration of PV array, battery storage, and SC. A computational experiment system is developed by using SimPowerSystems and Opal-RT real-time simulation technology. The performance of the coordinated control techniques is evaluated.

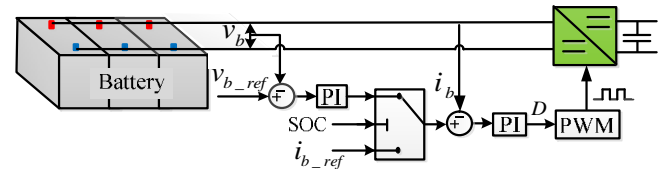


Fig. 3. Block diagram of nested-loop battery control strategy.

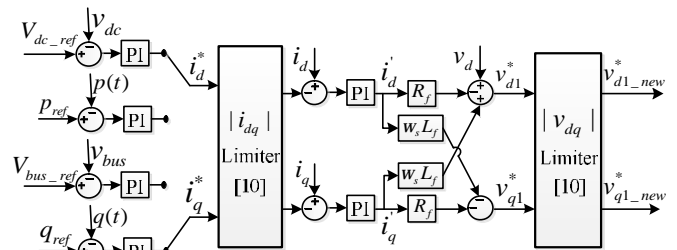


Fig. 4. GCC direct-current vector control structure.

I. KEY FIGURES

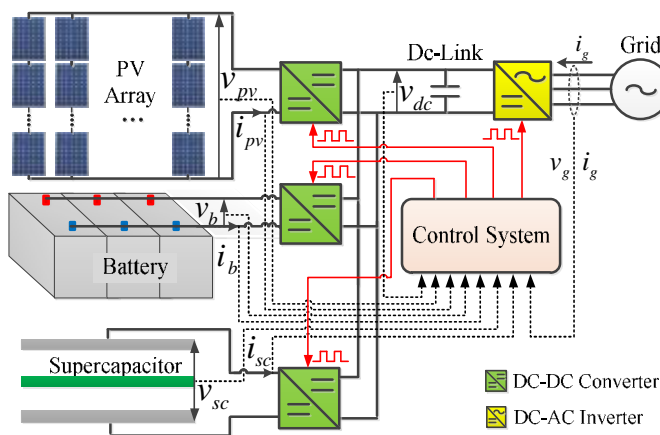


Fig. 1. Configuration of grid-connected PV system with energy storage units.

II. KEY RESULTS

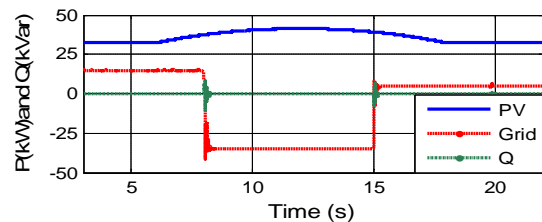


Fig. 6. PV system and grid active power with grid side reactive power.

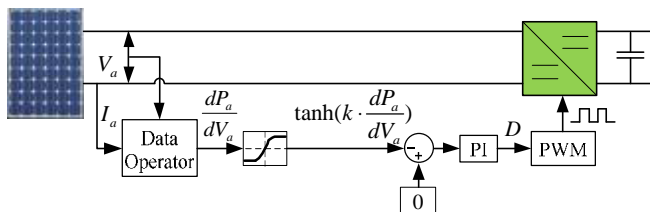


Fig. 2. Block diagram of S-PI MPPT method.

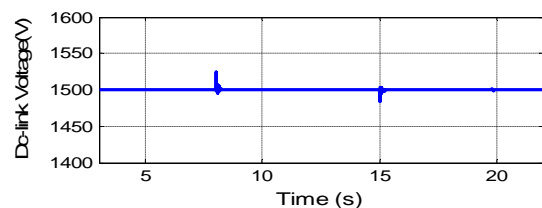


Fig. 7. Dc-link voltage is controlled at rated value of 1500V.

Modeling of an All-Vanadium Redox Flow Battery and Optimization of Flow Rates

Xiong Binyu, Zhao Jiyun and Li Jinbin

School of Electrical and Electronics Engineering, Nanyang Technological University

50 Nanyang Avenue, Singapore, 639798

Email: bxiong2@e.ntu.edu.sg

Abstract—Vanadium redox flow batteries (VRBs) are competitive for large energy storage systems due to low manufacture and maintenance costs and high design flexibility. Electrolyte flow rates have significant influence on the performance and efficiencies of the batteries. High electrolyte flow rates improve energy efficiency while degrade the battery efficiency due to high pump power losses. Thus, flow rates are necessary to be optimized for battery efficiency improvement. In this paper, an electrochemical model is firstly proposed to describe the charge-discharge characteristics based on the experimental data. Then, an empirical method is introduced to analyze the energy consumption of pumps under various flow rates. The optimal flow rates are obtained by applying new criteria. The results show that VRBs obtain peak battery efficiencies at the optimal flow rates around $90\text{cm}^3\text{s}^{-1}$ with respect to the proposed battery configuration. The optimal flow rates are provided as a reference for battery operations and control.

I. KEY EQUATIONS

The predicted stack voltage during discharge can be determined as,

$$U_{stack} = E_0 + N \frac{2mRT}{F} \ln \left(\frac{c_{v_{O_2^+},c}}{1 - c_{v_{O_2^+},c}} \right) \pm R_{c,d} i \quad (1)$$

The pump power has a relation with the pressure drop and the flow rate Q and is given by,

$$P_{pump} = P_{loss} = \Delta p \times Q \quad (2)$$

The pressure drop can be expressed by,

$$\Delta p = \Delta p_{friction} + \Delta p_{form} \quad (3)$$

The relationship between battery energy, stack energy and pump energy is stated in Eqn(5),

$$E_{battery} = \begin{cases} E_{stack} - E_{pump} = \int P_{stack} dt - \int P_{pump} dt & \text{during discharge} \\ E_{stack} + E_{pump} = \int P_{stack} dt + \int P_{pump} dt & \text{during charge} \end{cases} \quad (4)$$

II. KEY FIGURES

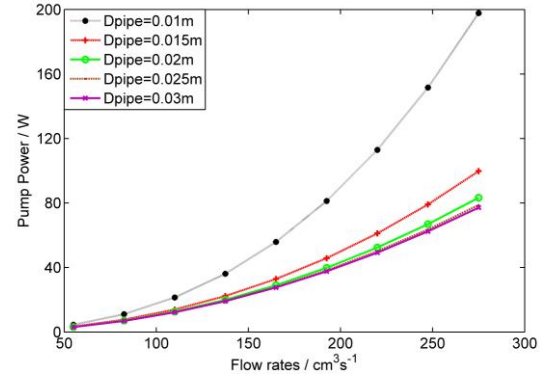


Figure 1 Pump power consumptions under various flow rates.

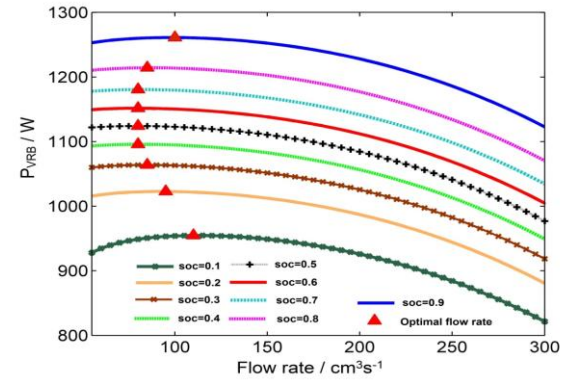


Figure 2 Optimal flow rates during discharge when $I=60A$.

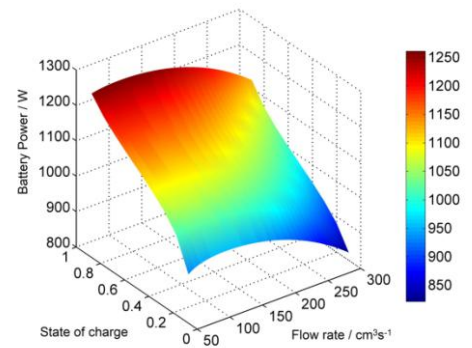


Figure 3 Battery power under flow rates and SOC at $I=60A$.

Probabilistic Power Flow for Distribution Networks with Photovoltaic Generators

Zhouyang Ren, Wei Yan, *Member, IEEE*, Xia Zhao, *Member, IEEE*, Yiming Li, Juan Yu, *Member, IEEE*
 State Key Laboratory of Power Transmission Equipment & System Security and New Technology, Chongqing University
 Email: rzhouyang@gmail.com, cquyanwei@cqu.edu.cn, zx@cqu.edu.cn, yi29281-q@126.com, dianlixi@cqu.edu.cn

Abstract--Based on Monte Carlo technique, this paper develops a probabilistic power flow (PPF) algorithm to evaluate the influence of photovoltaic (PV) generation uncertainty on distribution networks. In addition to randomness of PV power, the correlation of PV powers between adjacent time points and the uncertainty of start and end moments of PV output are taken into account with the presented method using the theory of conditional probability and nonparametric kernel density estimation. The measured power data of photovoltaic generator in Oregon State, USA and 34-bus distribution test network are used to demonstrate the application of the presented method.

I. KEY EQUATIONS

The moments of PV generation to start and stop producing power in one day (t_s and t_e) are completely random. The joint probability density function $f(t_s, t_e)$, which can be estimated by using the following multivariate kernel estimation:

$$f_H(t_s, t_e) = \frac{1}{n} \sum_{i=1}^n \frac{1}{h_1 h_2} k\left(\frac{t_s - T_{si}}{h_1}\right) k\left(\frac{t_e - T_{ei}}{h_2}\right) \quad (1)$$

The chronological probability model of PV powers at multiple hours is established by combining the multivariate kernel estimation with conditional probability concept. Take the pair of power outputs p_{i-1} at the $i-1$ o'clock and p_i at the i o'clock as an example. The conditional probability density function $f(p_i | p_{i-1})$ is built as follows, where $f(p_{i-1})$ and $f(p_{i-1}, p_i)$ can be estimated by using the kernel estimation theory.

$$f(p_i | p_{i-1}) = \begin{cases} \frac{f(p_{i-1}, p_i)}{f(p_{i-1})} & f(p_{i-1}) \neq 0 \\ 0 & f(p_{i-1}) = 0 \end{cases} \quad (2)$$

II. KEY FIGURES

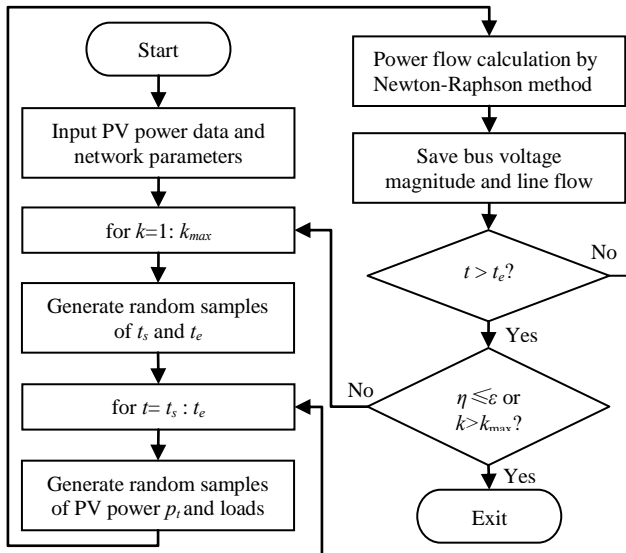


Figure.1 Flow chart of probabilistic power flow analysis

III. KEY RESULTS

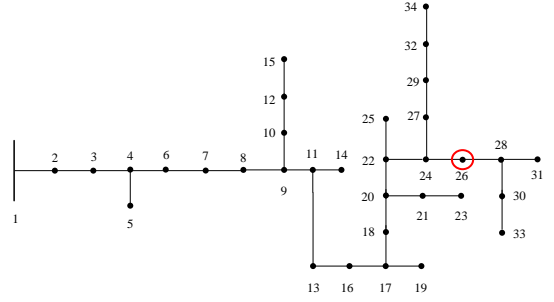


Figure.2 34-bus distribution network

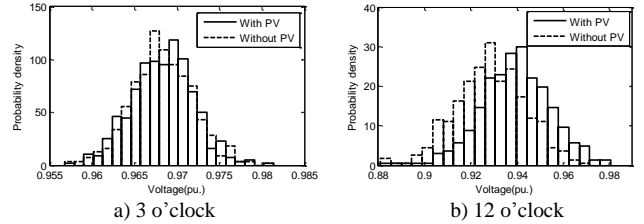


Figure.3 Histogram of the voltage magnitude at bus 26

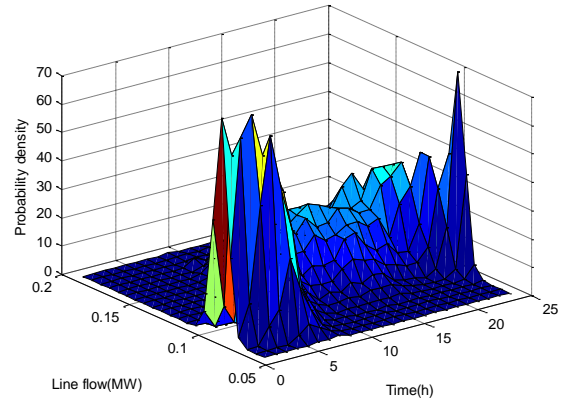


Figure.4 Histogram of line flow through line 24-26 without PV generator

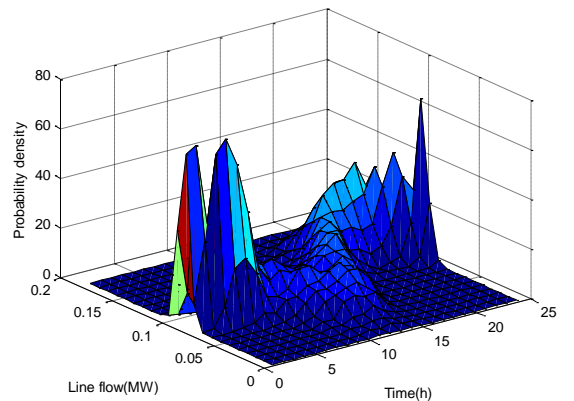


Figure.5 Histogram of line flow through line 24-26 with PV generator

Regulatory incentive for distribution system operators to integrate distributed generation: Portuguese case.

Angela Picciariello
 KTH Royal Institute of Technology
 School of Electrical Engineering
 Electric Power Systems
 Stockholm, Sweden
angela.picciariello@ee.kth.se

Abstract— Increasing amount of distributed generation (DG) connected to distribution grids is likely to affect the operation of the grids themselves, for example by changing the magnitude and, in some cases also the directions, of the power flows in the networks. This can have different economic consequences on the Distribution System Operators (DSOs) depending on the different enforced network regulations. This poster presents a method for how to calculate the incentive for DSOs to integrate DG into their grids. The calculation of this incentive is carried out for the Portuguese case. Only the operational aspects are considered to calculate costs and benefits for the DSO, including network tariffs, ancillary services costs, Operation and Maintenance (O&M) costs, and economic treatment of losses. The IEEE 34 Node Test Feeder is used to perform power flow analyses under different scenarios of DG penetration. The analysis shows that the Portuguese DSO would have an incentive to integrate a low level of DG penetration; in case of a higher level of DG penetration, however, this incentive would turn into a small disadvantage for the DSO. In both cases, the regulatory treatment of network losses turns out to be the relevant factor to determine such a result.

Keywords—distributed generation, network regulation, distribution losses, tariffs, Portuguese regulation.

I. METHOD DESCRIPTION

The method for the analysis of the impact of a certain regulation on the incentive for the DSO to integrate DG uses a *network model* and the *regulatory model*.

The *network model* can be represented by a distribution test system or a real network. Load flow analyses are performed, and network losses and the amount of energy exchanged with the transmission network, as well as consumption data at the load points, are obtained as results. Weighting factors are then used to extend the results from some representative hours to a whole year. As a further step, results from the network model are used as inputs for the regulatory model.

Input data for the *network model*:

- *Network data*: network structure and components.
- *Load data*: representative hourly profiles, used to approximate one-year loads profiles.

- *DG production data*: hourly production data corresponding to the same scenarios used for the loads over one year. Different scenarios of DG penetration are defined.

The *regulatory model* provides the network model with the methodology for calculating losses during load flow analyses; this methodology will be different based on definitions of losses in the different regulations.

$$\Delta I = \Delta I_{DUoS_charge} + \Delta I_{TUoS_charge} + \Delta I_{Ancillary} + \Delta I_{Losses} + \Delta I_{O\&M}$$

Definition of the *scenarios*:

Photovoltaic (PV) power plants represent the DG technology considered.

The three levels of PV penetration adopted, in this analysis, based on the definition in (2), are:

- Scenario 1 (base case): no PV in the grid.
- Scenario 2: low PV penetration, i.e. penetration level equal to 20%.
- Scenario 3: high PV penetration, i.e. penetration level equal to 40%.

I. RESULTS FROM THE CASE STUDY

Scenarios	Average losses	$I_{v,t}$ (Euro)
S1 (base case)	4.55	54482
S2 (low DG penetration)	4.00	63753
S3 (high DG penetration)	4.61	53578

TABLE 1. ANALYSIS RESULTS: LOSSES PERCENTAGE AND DSO'S INCOME FOR THE THREE SCENARIOS.

$$\Delta I^{S1} = I^{S1} - I^{S0} = 9271 * 3 = 27813 \text{ €}$$

$$\Delta I^{S2} = I^{S2} - I^{S0} = -904 * 3 = -2712 \text{ €}$$

Ground Fault Location in Ungrounded Large Scale PV Generators

Shea Pederson, *Graduate Student Member, IEEE*, Ramakrishna (Rama) Gokaraju, *Member, IEEE*
 Electrical & Computer Engineering, University of Saskatchewan, Saskatoon, Canada
shea.pederson@ieee.org, rama.krisha@usask.ca

Abstract—Locating ground faults in ungrounded systems is time consuming and tedious. In this work, we propose a fault location method for ungrounded photovoltaic systems utilizing the inherently present switching noise from the inverter and its interaction with system parasitic elements.

Keywords—photovoltaic systems, inverters, pattern recognition, parasitic capacitance, fault location, wavelet coefficients

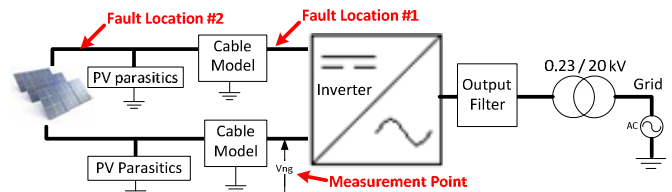


Figure 1 – Preliminary Model of PV System

I. INTRODUCTION

It has been shown in [1] that fault detection and location is possible for all ungrounded systems with parasitic elements that form a ringing circuit through ground and contain a mechanism to excite that ringing circuit, such as an inverter.

Reference [1] applied a MRA-based wavelet on voltage signals and classified these frequency domain representations by fault location. In order to detect and locate faults for large scale PV installations using pattern recognition techniques done in the frequency domain, the model needs to include significant parasitic elements for the whole system. For example, parasitic elements for the PV Array are modeled in [2].

Preliminary results from PSCAD/EMTDC [3] and MATLAB show that fault location for this PV System may be feasible by recognizing patterns in the processed voltage waveforms.

Figure 1 shows the preliminary PSCAD/EMTDC ungrounded model, the measuring point, and the two different ground fault locations analyzed in following figures. Further research will model a solar farm with distributed PV sources and parasitic modeling. Figures 2 and 3 compare the two different fault locations, showing strong potential for classifying the fault location. Figure 2 shows the energy in each frequency band after the voltage signals are passed through DB4 wavelet filters. Figure 3 shows the FFT magnitudes.

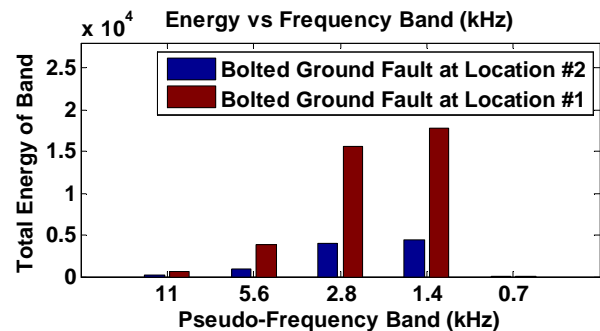


Figure 2 - Energy vs Frequency Band

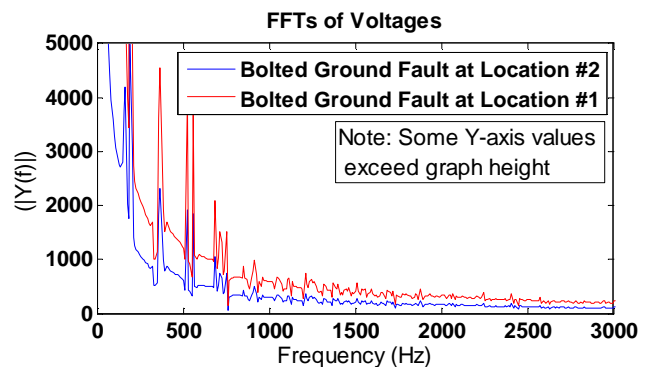


Figure 3 - FFT Magnitudes

REFERENCES

- [1] Yan Pan, Michael Steurer, and Thomas L. Baldwin, "Ground fault location testing of a noise-pattern-based approach on an ungrounded DC system", *IEEE Transactions on Industry Applications*, Vol. 47, No. 2, March/April 2011.
- [2] J.C. Hernandez, P.G. Vidal, A. Medina, "Characterization of the insulation and leakage currents of PV generators: Relevance for human safety", *Renewable Energy*, Vol. 35, pp. 593-601, 2010.
- [3] Manitoba HVDC Research Centre, PSCAD v4.5.1.0; 2012

Application of sequential decision theory on integrating distributed energy resources

Yalin Huang

School of Electric Power Systems
Royal Institute of Technology
Stockholm, Sweden
Email: yalin.huang@ee.kth.se

Abstract—Distribution system operators (DSOs) are facing new challenges when more distributed energy resources (DERs), which consist of distributed generation (DG), distributed storage and active demand load at the distribution level, are connected to the grid. Many researches focus on how to optimize the size or location of DERs, however, in most European countries such as Sweden and Germany electric power systems have been deregulated. Therefore the task of the DSO is to integrate the DERs in an optimal way. Furthermore, that the DERs are connected at the same time is a common assumption in integrating DERs literature. But the location and time of DER connections in deregulated countries mainly depend on DER owners. Thus a new connection decision depends on the state of the current grid considering the possible future connections. Most methods that have been reviewed before have serious limitations in their ability to model dynamic situations where the timings of the DER connections are uncertain information of DSOs. In contrast to previous work, this paper applies Markov decision process(MDPs), which is a kind of sequential decision model, to model integrating DERs into the existing distribution network. MDPs models can solve the problem step by step on time horizon considering the impact on the future. Thus when applying MDPs model in network planning with DERs, the results are optimal in the long-run considering the future uncertain connection of DERs.

components in a network planning problem are illustrated in Table 1.

TABLE I
COMPONENTS OF A MDP WITH AN EXAMPLE

MDP component	Description	Application to network planning for wind power connections
State space (S)	a set of all possible values of dynamic information relevant to the decision process	each bus and each possible DER connection can be represented as a state
Action space (A)	a set of decisions that can be made, A_s represents the decisions are available at state s	two actions: a1 connect to the closet bus in distance; a2 connect to the closet bus in voltage level
Transition probabilities (P)	a matrix describes the possibility for the transition from one state to another state by taking action a	the possibility of connecting to one bus by taking a action
Reward function (R)	a matrix of rewards received at state s by taking action a	the positive impact for the system of taking a connection action at that state
Decision epoch (T)	time at which decisions are made	time at a DER owner applies for connection

Fig. 1. Model a distribution system as an MDP

A case distribution system is shown in Fig 2. The squares represent the states of the system, where $s1$ to $s3$ represent the three existing buses connected with the grid, $s4$ to $s6$ are not connected so far but the DSO has received some application from those spots.

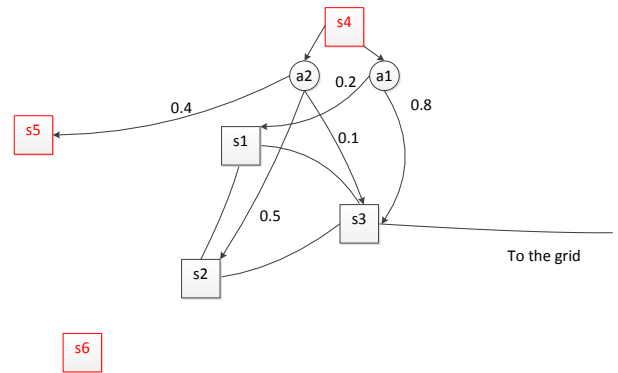


Fig. 2. Case study

I. KEY EQUATIONS

The objective of solving an MDP is to find the optimal policy that maximizes the long-run expected value. A value function is the expected sum of discounted future rewards since this moment at state s , and it can be expressed by Bellman's equation:

$$\forall s \in S, \quad v(s) = \max_{a \in A_s} \{r(s, a) + \gamma \sum_{j \in S} p(j | s, a) v(j)\} \quad (1)$$

The optimal policy is represented as:

$$\forall s \in S, \quad \pi(s) \in \arg v(s) \quad (2)$$

II. METHOD

Integrating DERs into the grid is modeled as a stationary randomized infinite-horizon discrete-time MDP in this paper. In this model, the DSO is the decision maker who has limited information on when and which DERs will be connected to the grid in the future. The DSO decides the connection action when the DER owner is applying for a connection since it is very hard to predict the future DER. The corresponding MDP

III. CONCLUSION

It is showed that MDPs can be used to model connecting DERs sequentially considering the timing uncertainty. However, the reward of one connection can be calculated in more detail. An improvement can be to obtain the optimal network configuration considering all possible DERs are connected at the same time first, then use the model to obtain a policy to reach the optimal network.

Analysis of the Impact of Distributed Generation Placement on Voltage Profile in Distribution Systems

Po-Chen Chen and Mladen Kezunovic

Power System Control and Protection Laboratory, Department of Electrical and Computer Engineering,
Texas A&M University, TX 77843

Email: pchen01@neo.tamu.edu, kezunov@ee.tamu.edu

Abstract— This paper analyzes the impact of distributed generation (DG) placement on voltage profile under certain penetration level in low-voltage (LV) distribution networks. DGs are allocated via different probabilistic approaches to account for uncertainties of DG installation in the future. The main contribution of this paper is in understanding how to apply proper probability distribution functions (PDFs) and constraints for DG placement location to prevent under- and over-voltage problems or unexpected load disconnections. The results prove that the developed approach can reduce the probability of having load voltage violations, which means the network may have more DGs accommodated. Such techniques can be considered as a tool for the network planning engineer to facilitate the installation of DGs in the future.

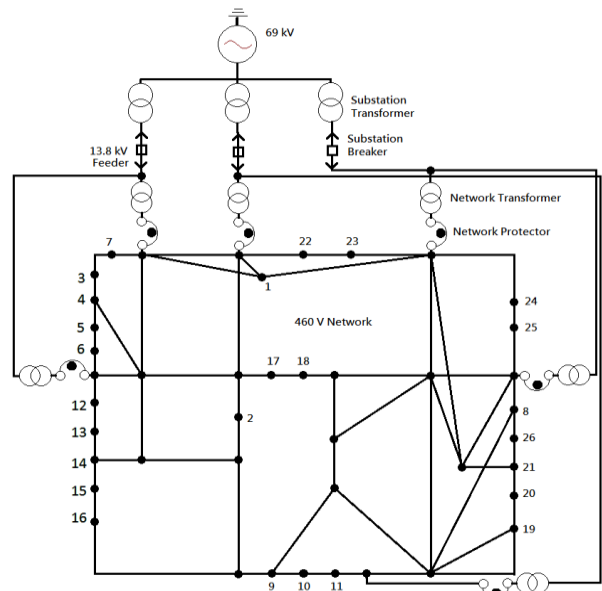


Figure 3. The test network.

I. KEY FIGURES

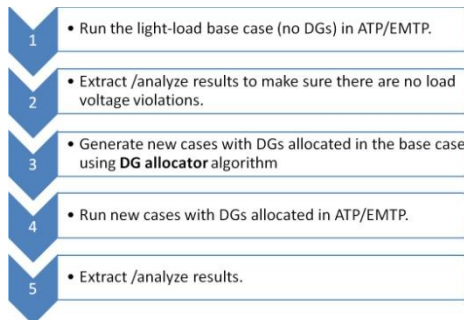


Figure 1. An overview of the study procedure.

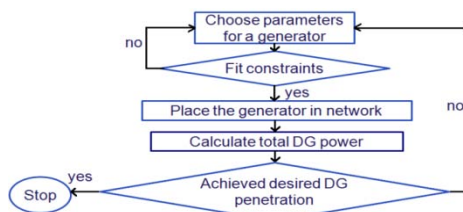


Figure 2. Allocation algorithm for non-deterministic DG units. .

II. KEY RESULTS

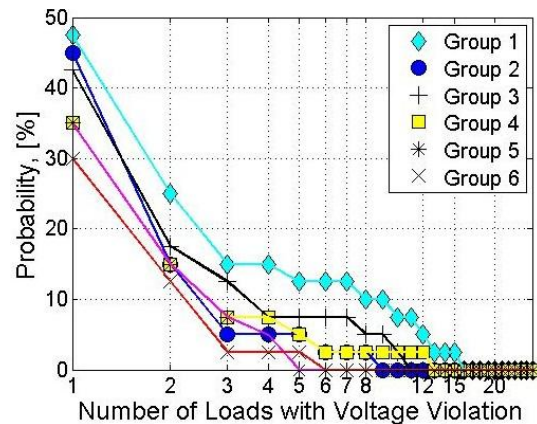


Figure 4. Probability of having voltage violations of more than $\pm 5\%$ versus the number of loads with violation.

Short circuit Analysis for integration of 10MW Windfarm in Nigeria at the PCC

Owolabi Sunday Adio, Xiangning Lin, *Senior member, IEEE*, Feng Zhao, Zhiqian Bo, *Senior member, IEEE*

Abstract—A short circuit in a power system can cause very high currents to flow to the fault location. The magnitude of the short circuit current depends on the impedance of system under short circuit conditions. However, to study the effect of windfarm integrated into Power Holding Company of Nigeria (PHCN) which is power bureau of the country, a short circuit calculation was performed. The analysis was carried out in two stages, one was using Thevenin equivalent to roughly check unbalance short current from PHCN external source from Kaduna substation at 132/33kV, although this was actually not part of the current studies. The second part was to performed short circuit analysis at network where the windfarm will be connected through 33/11kV level (PCC), which is for this current studies by using computer software tool (DigSILENT powerfactory). This was done to verify the withstands capacity for the main substation equipment and the new OHLs in comparison with the 3-phase and 1-phase to ground short circuit values of grid studies for the windfarm project. In the network calculation, consideration was made for both maximum and minimum short circuit conditions and it is performed according the IEC 60909 (2001) standards. However, the aim of the analysis was the assessment of the electrical parameters of the WindFarm during and after a three phase short circuit event at the 33 kV Katsina substation because this is the point where the windfarm have to be connected and also the location of the wind generators.

Index Terms--Windfarm, Thevenin equivalent, Short circuit, Simulation, clearing time, Over-head Line (OHL).

I. KEY EQUATIONS

Using standard network reduction techniques, the equivalent Thévenin circuit at the fault location main 132 kV buses can be derived for the external grid. The equivalent source is:

$$Z_k = [Z_{G1} + Z_{C1}] \parallel [Z_{M1} + Z_{C2}] \parallel [Z_{C3} + Z_{TX1} + (Z_{M2} \parallel Z_{M3})]$$

The initial symmetrical short circuit current is calculated from IEC 60909-0 in accordance to the follows equations:

$$I_k^* = \frac{cV_n}{\sqrt{3}Z_k} \quad (13)$$

Where I_k^* is the initial symmetrical short circuit current (A); c is the voltage factor that accounts for the maximum system voltage (1.05 for voltages <1kV, 1.1 for voltages >1kV); V_n is the nominal system voltage at the fault location (V); Z_k is the equivalent positive sequence short circuit impedance (Ω).

II. KEY FIGURES

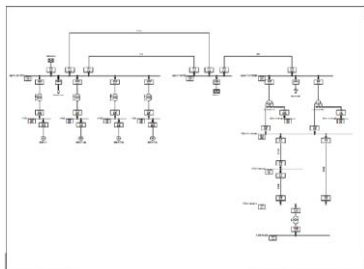


Figure.1. Line Diagram for 330/132/33kV PHCN networks to windfarm site.

III. KEY RESULTS

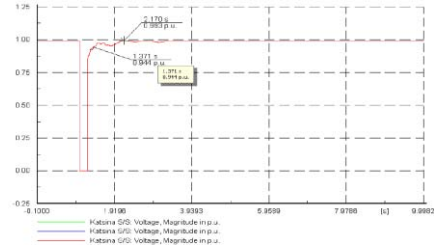


Figure.1. Voltage at 33 kV Katsina (Short circuit at Katsina Substation (S/S))

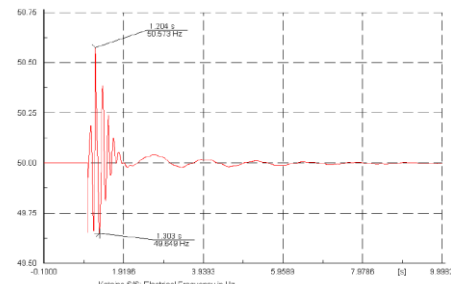


Figure.2. Frequency at 33 kV Katsina S/S (Short circuit at Katsina S/S)

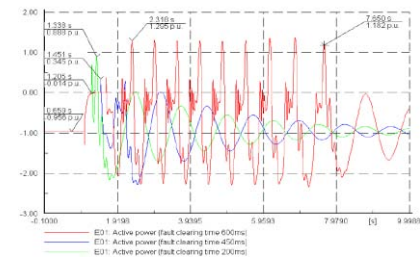


Figure.3. Wind turbine power (Short circuit at Katsina S/S) and (Comparison of different fault clearing times)

TABLE I SHOWS THE RESULTS SHORT CIRCUIT CALCULATION

TABLE I. THE MAXIMUM SHORT CIRCUIT CURRENT VALUES FOR THE MAIN MV AND LV SWGRS

Substation	Reference	I''_k [kA]	I_p [kA]	I_b [kA]
33 kV Katsina S/S	Calculated values	9.58	24.07	9.45
	Withstand limits ⁽¹⁾	20	n.a.	20
33 kV Layafa S/S	Calculated values	6.84	13.93	6.66
	Withstand limits ⁽¹⁾	n.a.	n.a.	n.a.
33 kV Wind Farm S/S BUS_PL	Calculated values	3.56	6.20	3.13
	Withstand limits ⁽¹⁾	16 (or 20)	n.a.	16 (or 20)
11 kV Layafa S/S	Calculated values	3.94	9.46	3.94
	Withstand limits ⁽¹⁾	25	n.a.	25
LV system of Wind Farm (maximum)	Calculated values	14.35	26.40	-
	Withstand limits ⁽¹⁾	25	n.a.	25

⁽¹⁾ The withstand limits are valid only for reference. The design of the Wind Farm has to be suitable for the calculated values.

Wavelet-Adaptive ANN Forecaster for Renewable Energy Sources for Continuous Supply in Microgrid Applications

Ahmed T. Elsayed, *Graduate Student Member, IEEE*, and Osama A. Mohammed, *Fellow, IEEE*
 Department of Electrical and Computer Engineering, Florida International University,
 Miami, FL 33174, USA

Email: Aghar002@fiu.edu , mohammed@fiu.edu

Abstract—In this paper, the performance of hybrid power system (HPS) with high penetration of renewable energy sources (RES) was investigated under dominant weather conditions. Hourly solar radiation and wind speed were forecasted for one week ahead (168h) using wavelet – adaptive feed forward artificial neural network. The load was forecasted for the same time horizon. Based on these forecasts, the supervisory control calculates available power from the installed PV modules and wind turbines then send the required reference signal to the voltage source inverter (VSI). The VSI will control the power flow at the point of coupling to guarantee continuous power supply to the loads. For better understanding of the interactions of the microgrid with the main AC grid under weather conditions and to validate the effectiveness of the system, an experiment was carried out in a laboratory based smart power system. The controller response and consequently, power flow were monitored, controlled and discussed.

I. KEY FIGURES

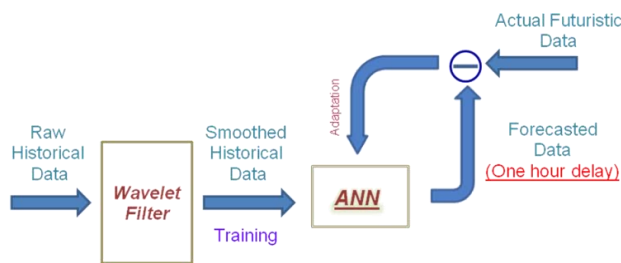


Fig. 1. Schematic diagram for the forecasting process.

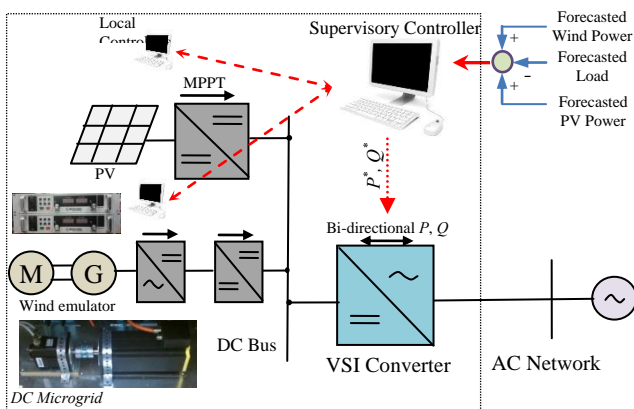


Fig. 2. Renewable energy sources implementation and control for the system under study in smart grid testbed.

II. KEY RESULTS

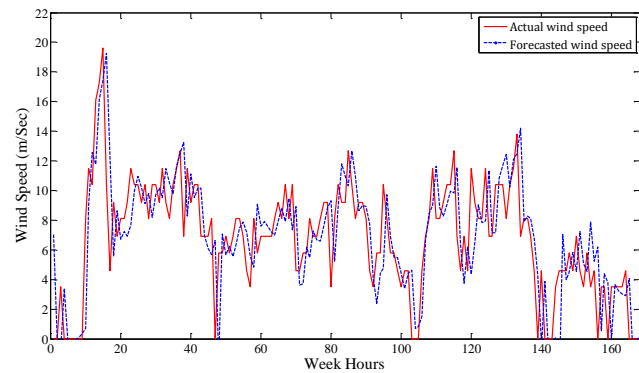


Fig. 3. Forecasted wind speed versus actual wind speed.

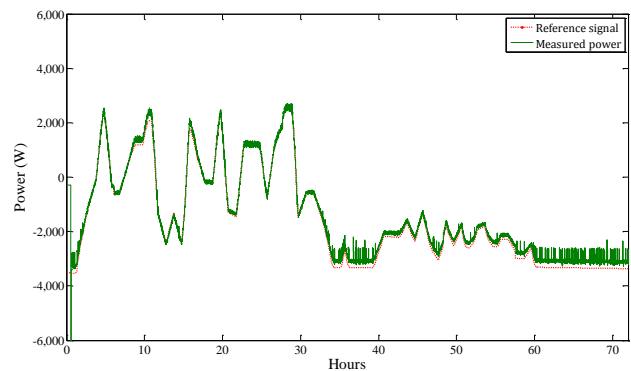


Fig. 4. Power flow at POC measured from the DC side.

III. CONCLUSION

In this work, solar radiation, wind speed and load were accurately forecasted using wavelet filtering and adaptive FFNN. The wavelet transform was used to smooth training data, the forecasted values are compared to actual ones and the error was used to adapt the network continuously. It was shown that this combination improved predictability. These forecasts were integrated to energy management system to achieve secure and continuous power supplying to the load from the renewable energy sources and the AC network (only if necessary). The carried out experiment has a setup consisting of PV and wind emulators connected to AC grid through a controlled VSI. Experimental results proved the suitability and effectiveness of the integrated system.

Financial Transmission Rights Perform Well in Power Markets with High Penetration of Wind Energy?

Yang Yu

Department of Civil and Environmental Engineering
Stanford University
Stanford, California 94305
Email: yangyu1@stanford.edu

Ram Rajagopal

Department of Civil and Environmental Engineering
Stanford University
Stanford, California 94305
Email: ramr@stanford.edu

Abstract—We investigate the impact of FTR in a grid with high penetration of renewables. In particular, we consider a two stage stochastic model with strategic market players and different forms of FTR and WPP integration policies. The proposed model captures startup and ramping constraints as well as information constraints faced by the SO and the market players. Based on this model we examine the impact of FTR and evaluate the extent to which FTRs hedge against price risk from transmission congestion under the current protocol that Wind Power Producers(WPPs) are allowed to participate in the real-time market. We also suggested a protocol to solve the revenue adequacy problem caused by the current protocol.

I. MODELS AND KEY EQUATIONS

In the day-ahead market, the optimal bidding strategy of G_1 must satisfy following properties:

$$c_1'(q_1^*) = p_1^{a*} + \alpha_1 \frac{p_{12} \partial E[(p_2^{r*} - p_1^{r*}) \mathbf{1}(p_{12} > K)]}{\partial q_1} \quad (1)$$

The day-ahead dispatch maximizes the expected total social net profit is:

$$\begin{aligned} \max E[u_s] &= E[u(q_2^a + q_2^r + \min\{W + q_1, K\}) \\ &\quad - c_1(q_1) - c_2(q_2^a + q_2^r)] \\ \text{s.t. } q_1 &\leq K \end{aligned} \quad (2)$$

The day-ahead dispatch schedule must satisfy following property:

$$c_1'(q_1^*) + \lambda = E[c_2(q_2^{a*} + q_2^{r*}) \mathbf{1}(q_1^* + W < K)] \quad (3)$$

II. KEY FIGURES

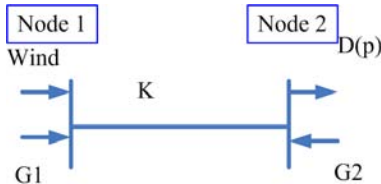


Fig. 1. Two Node Model

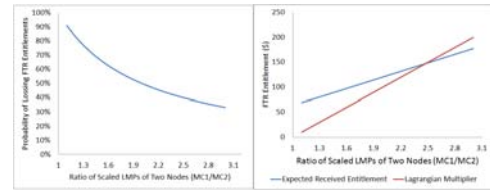


Fig. 2. Example of Risks and Entitlements in Two Nodes Model

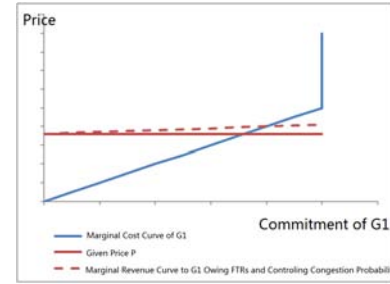


Fig. 3. Marginal Revenue to G_1 is Changed by Introducing FTRs into System

III. KEY RESULTS

In the real-time market, if the wind generation W is large enough to congest the transmission line, the FTRs' holders will lose their entitlement, which should be allocated to them

The WPPs being paid by the real-time LMP could be considered as a money transfer from FTR holders to WPPs.

In a market with higher penetration of wind power under current protocol, the FTR policy supplies the power producers opportunities to manipulate the power market by controlling the probabilities of transmission congestions. As a result, the utilization of wind power will be discouraged and the total consumption may increase. These two result can lead to high emissions in CO_2 and other pollutants.

Evaluating Possibility of Reactive Power Counteraction among Voltage Regulators in a PV Solar Farm

Afshin Samadi, Robert Eriksson and Lennart Söder

Electric Power System Department, KTH Royal Institute of Technology, Stockholm SE 100-44, Sweden

afshin.samadi@ee.kth.se, robert.eriksson@ee.kth.se, lennart.soder@ee.kth.se

Abstract— In recent years, the electric power systems across the world have undergone radical changes due to high penetration of the dispersed, intermittent renewable energy resources such as wind and photovoltaics (PV) into grids. The PV systems can be integrated either as small scales in residential areas or as large-scales in solar farms. In power system studies, the photovoltaic solar farms are modeled as one equivalent inverter connected through a step-up transformer to medium voltage or high voltage grids. However the solar farms are usually made of several central inverters that are connected through step-up transformers to the grid. By doing so, some inaccuracies regarding the performance of the aggregated model of PV plant, in contrast to individual PV models, might happen that are required deeming and addressing in aggregation studies. The PV plants are allowed to regulate the voltage at the connection point through reactive power contribution. The main objective of this study is making an equivalent model of several individual PV units of a solar farm and, along with it, investigating the probability of reactive power counteractions among PV systems in a solar farm that might not be seen and addressed in the equivalent model. PowerFactory is used as the simulation platform. The test solar farm consists of three individual 0.5 MVA PV systems connected through three transformers to a medium voltage grid. Simulation results demonstrate that though reactive power operating mode of individual PV systems in individual PV models might be different (capacitive or inductive), the performance of the voltage regulators in both equivalent and individual models would be similar.

I. KEY EQUATION, FIGURES AND RESULTS

The PV model is associated with a voltage control regulator as Fig. 1, where $F_{vac}(s)$ can, in general, be a PI controller. $F_{vac}(s)$ adjusts reactive power in such a way to regulate the voltage. The equivalent model should provide the equivalent reactive and active power with regard to individual PV units in order to study the dynamic aspects of irradiance variations on the voltage regulation. Since the equivalent model is connected to the same voltage level as individual PV units (Fig.2), the rated power of converter and PV array in one individual PV model should be scaled to make the equivalent model. Moreover, the DC link capacitor according to the following power equation must be scaled:

$$\frac{1}{2}C \frac{dv^2}{dt} = P_{dc} - P_{ac}$$

Different scenarios have been taken into account and one of them is shown in Fig. 3. In this scenario the individual transformers are assumed to be different while the voltage controller parameters are identical. Fig. 3(a) show that by changing the irradiance level from 1000 to 300 W/m², though reactive power mode differs between individual PV units, the total amount of reactive power in individual PV units is equal to the equivalent model. Moreover, the voltage regulation at the individual LV buses is almost similar to the equivalent LV bus. The similar results are derived for other scenarios as well.

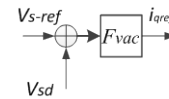


Figure 1. Block diagram of the voltage control in the PV model.

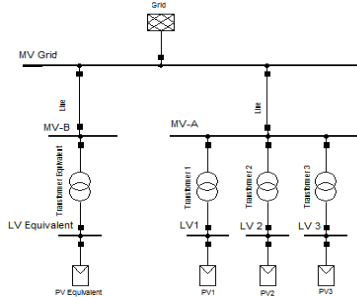


Figure 2. Test solar farm in PowerFactory

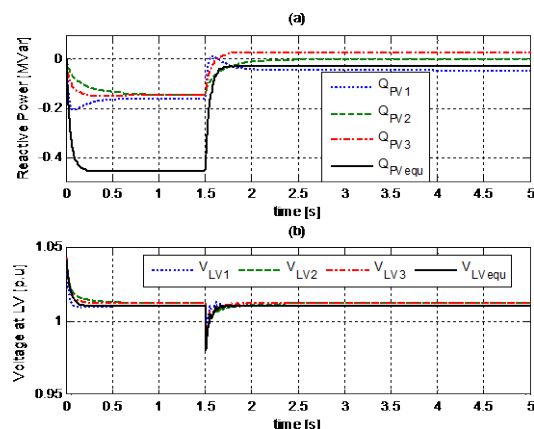


Figure 3. a) Reactive power in individual PV models and equivalent PV model, b) voltage at the low voltage connection point

An Affine Arithmetic Approach for Microgrid Dispatch with Variable Renewables

Mehrdad Pirnia, Claudio Canizares, Kankar Bhattacharya
 Department of Electrical and Computer Engineering
 University of Waterloo, Ontario, Canada, N2L 3G1

Alfredo Vaccaro
 University of Sannio, Italy

Email: mpirnia@uwaterloo.ca, ccanizares@uwaterloo.ca, kankar@uwaterloo.ca, vaccaro@unisannio.it

Abstract—An affine arithmetic (AA) method is proposed to solve a stochastic optimal power flow (OPF) problem in the context of microgrids. In the AA-based OPF problem, all the state and control variables are presented in affine form, comprising a center value and corresponding noise magnitudes, which can be due to weather forecast, models errors, and other unpredicted events. In order to find the center value, the deterministic OPF problem is solved, and then to obtain the noise magnitudes, a sensitivity analysis technique is used. The impact of intermittency in wind and solar generation will be considered in the above model with their associated AA representation to understand their impact on system operation. Knowing the affine forms of the control and state variables, the contraction method will be used to find the minimum noise variables associated with each noise partial deviation. Furthermore, the AA-based intervals will be calculated and compared with the MCS-based intervals. The obtained intervals can be used to find the operational margins of dispatchable generators (e.g., gas generators) in the short-term or to calculate the reserve requirements of the systems with renewables penetration.

I. KEY EQUATIONS

The state and control variables in the proposed AA-based OPF have the following affine forms, consisting of a center value and noise magnitudes, because of the presence of uncertainties in renewable generation:

$$\tilde{V}_i = V_{i,0} + \sum_{j \in nP} V_{i,j}^P \varepsilon_{P_j} + \sum_{k \in nQ} V_{i,k}^Q \varepsilon_{Q_k} \quad \forall i \in nQ$$

$$\tilde{\delta}_i = \delta_{i,0} + \sum_{j \in nP} \delta_{i,j}^P \varepsilon_{P_j} + \sum_{k \in nQ} \delta_{i,k}^Q \varepsilon_{Q_k} \quad \forall i \in nP$$

$$\tilde{P}_i = P_{i,0} + \sum_j P_{i,j}^P \varepsilon_{P_j} + \sum_j P_{i,j}^Q \varepsilon_{Q_j} + P_i^T \varepsilon_{T_i}$$

$$\tilde{Q}_i = Q_{i,0} + \sum_j Q_{i,j}^P \varepsilon_{P_j} + \sum_j Q_{i,j}^Q \varepsilon_{Q_j} + Q_i^T \varepsilon_{T_i}$$

II. KEY FIGURES

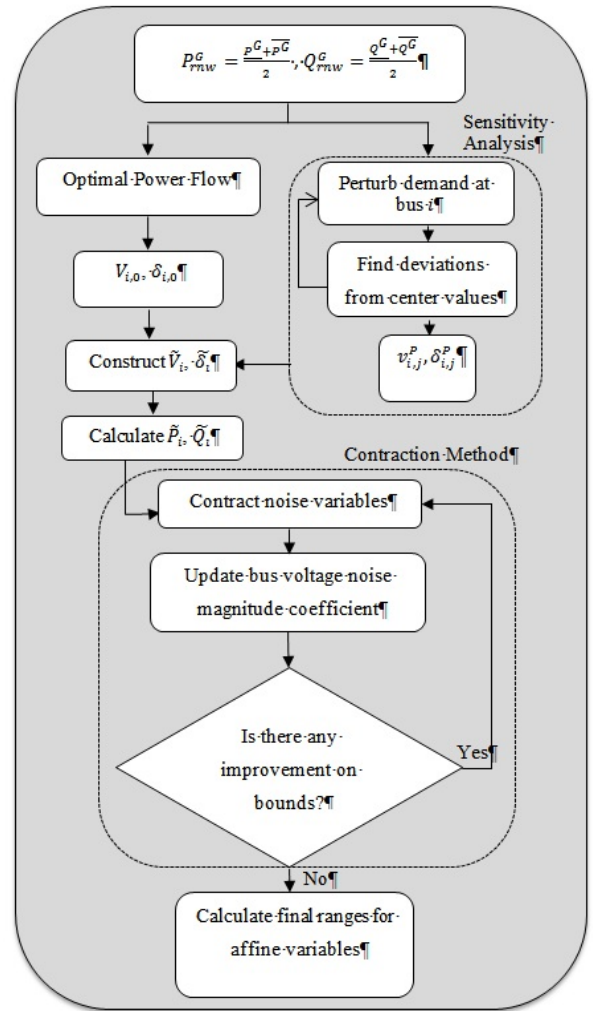


Fig. 1. AA-based OPF algorithm

The Effect of Plug-In Hybrid Electric Vehicle Penetration on an Electric Microgrid

Andrew Clarke, Student Member, IEEE, Himanshu Bihani, Student Member, IEEE,
 Elham Makram, Fellow, IEEE, and Keith Corzine, Senior Member, IEEE
 Holcombe Department of Electrical and Computer Engineering
 Clemson University
 Clemson, SC 29634, USA

Abstract— Plug in hybrid electric vehicle technology is becoming a promising alternative to traditional internal combustion engine vehicle technology due to its increased fuel efficiency and lower emissions. Before individual ownership penetration significantly increases, the consequences of connecting the vehicles to the grid must be examined. To investigate the effect that uncontrolled vehicle charging will have on the electric grid, an IEEE 13 node test feeder will be studied with added vehicle charging stations. Distributed generation units will be included in the system to simulate micro grid operation during grid connected mode. The distributed generation will include photovoltaic arrays and synchronous generators.

Index Terms—Electric vehicles, Electric Distribution System

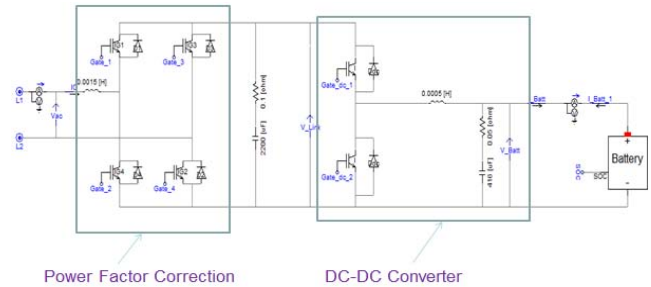


Figure 2. Topology of the AC-Level 2 Bidirectional Charger

I. KEY FIGURES

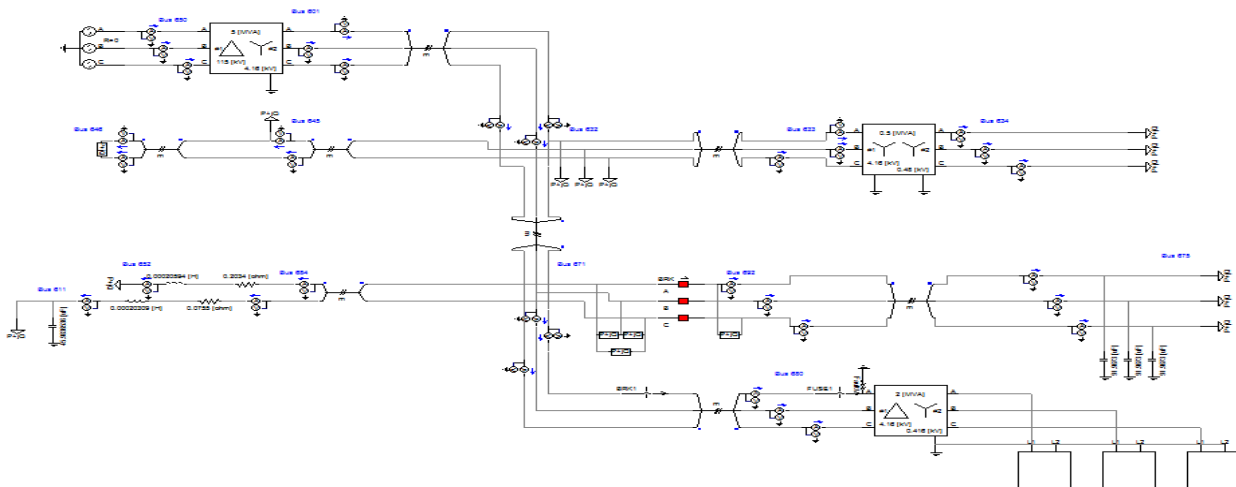


Figure 1. IEEE 13 Node Test Feeder [1-2]

II. REFERENCES

- [1] "IEEE 13 Node Test Feeder," *IEEE PES Distribution System Analysis Subcommittee*. [Online]. Available: <http://ewh.ieee.org/soc/pes/dsacom/testfeeders/feeder13.zip>
- [2] "Radial Distribution Test Feeders," *IEEE PES Distribution System Analysis Subcommittee*. [Online]. Available: <http://ewh.ieee.org/soc/pes/dsacom/testfeeders/testfeeders.pdf>

Multi-objective Network Reconfiguration of Distributions Systems with Renewable Energy

Huihua Yu

School of Electrical and Computer Engineering, Cornell University, Ithaca, NY 14850, USA,
Email: hy437@cornell.edu

Abstract— In this paper, a new problem formulation of network reconfiguration of distribution system to address the increasing challenge of system transfer capability brought by renewable energy is proposed. A novel integrated optimization method based on Multi-objective Particle Swarm Optimization (MOPSO) is developed to solve this problem, taking into account the preference of users. The two objectives of the formulation are to minimize the number of switching operations, and to minimize the active power losses. All the engineering and operational constraints, such as current limits, power consumptions and radially of the network are respected in the formulation. One distinguished feature of this formulation is to treat the load margin of the system as a very important constraint towards increasing system's transfer capability. The most challenging issue in solving the problem by MOPSO is to find a global best particle, which promote the diversity of search, in order to generate the complete Pareto front. An approach based on NSGA-II is used to find the global one. Two test systems will be used to illustrate the feasibility and effectiveness of the proposed approach.

I. KEY EQUATIONS

The problem statement considered is as following:

Given existed one-day ahead forecasted data of load demand $D(h)$, renewable energy $W(h)$, and generation $G(h)$ ($h=1, \dots, 24$) of each hour, as well as the initial topology $N(0)$ of the next day, we want to determine the topology $N(h)$ ($h=1, \dots, 24$) of the next day, for a three phase unbalanced radial distribution system, with requirement that the load margin should be bigger than 10% of the total load.

The model proposed is:

Minimizing switch actions:

$$\text{Min} \sum_{h=1}^{24} g[N(h) - N(h-1)] \quad (1)$$

Minimizing power losses:

$$\text{Min} \sum_{h=1}^{24} P_{LOSS}(N(h), D_p(h), G_p(h), W_p(h)) \quad (2)$$

$$\text{S.to } P_{N(h)}(D_p(h), G_p(h), \lambda W_p(h))=0 \quad (3)$$

$$Q_{N(h)}(D_q(h), G_q(h), W_q(\lambda W_p(h)))=0 \quad (4)$$

$$\lambda \geq 1.1 \quad (5)$$

$$V_i^{max} \leq V_i(h) \leq V_i^{min} \quad i, j = 1, \dots, k \quad (6)$$

$$|I_{ij}(h)| \leq I_{ij}^{max} \quad i, j = 1, \dots, k \quad (7)$$

where

h hour in a day, ranging from 1 to 24;
 λ load margin of the whole system.

II. KEY FIGURE

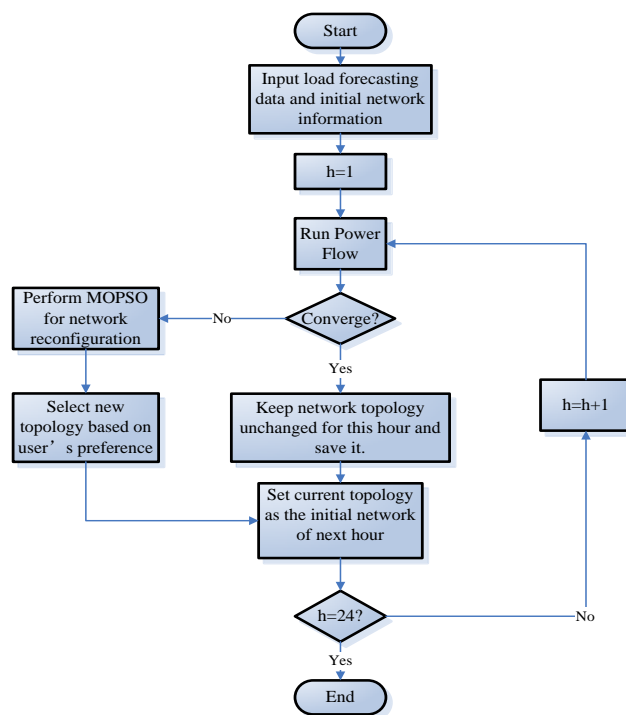


Fig. 1. The proposed method for one-day ahead network reconfiguration planning problem.

III. KEY ALGORITHM

The proposed MOPSO algorithm is as:

Step 1: Initialize particles' positions and velocities.

Step 2: Evaluate particles and select personal bests and global best particles based on Pareto ranking and elitism.

Step 3: Calculate velocity of each particle, and generate new positions.

Step 4: Check the termination condition. If not satisfied, go back to Step 2. If satisfied, go to Step 5.

Step 5: Process the results with user's preference, and output new topology information.

Real Time Modeling and Simulation of CERTS Microgrid

Fransiska Martina, Ramon Zamora, and Anurag Srivastava

Smart Grid Demonstration and Research Investigation Lab (SGDRIL),

School of Electrical Engineering and Computer Science, Washington State University, Pullman, WA 99163, USA

Email: fmartina@eecs.wsu.edu, rzamora@eecs.wsu.edu, and asrivast@eecs.wsu.edu

Abstract - Microgrid with distributed clusters of source and load can be connected with existing electrical grid in normal operation or disconnected from the grid when operational criteria is violated. The purpose of this work is to develop a microgrid model using real time digital simulator for system analysis. The developed microgrid model is based on CERTS microgrid. CERTS microgrid concepts incorporate three feeders, where two of them are connected to sensitive loads, while the third one is connected to traditional loads. The two feeders with sensitive loads are also connected to microsourses, where in this work all of the microsourses are modeled as photovoltaic array and each of them will supply 60kW electricity. The load banks are in the range of 0-90kW and 0-45kW. Minimum components required to develop one cluster of microsourses and loads are the model of

renewable energy source (RES), the small time-step bridge to accommodate power electronics components, measurement and control block, distribution line, transformer, and model of electric grid. The CERTS microgrid model developed is shown in Fig. 1. Real time digital simulator has a strong benefit in accommodating fast computation that is required for switching power electronics devices used to convert DC power produced by RES to AC power. This model allows us to perform different studies on microgrid performance, including but not limited to management and control during normal and islanding conditions, optimization of local microsourses operation, and protection schemes. However, this work is focus to study the performance of microgrid during transition period from grid-connected to islanding operation and vice versa.

I. KEY FIGURE

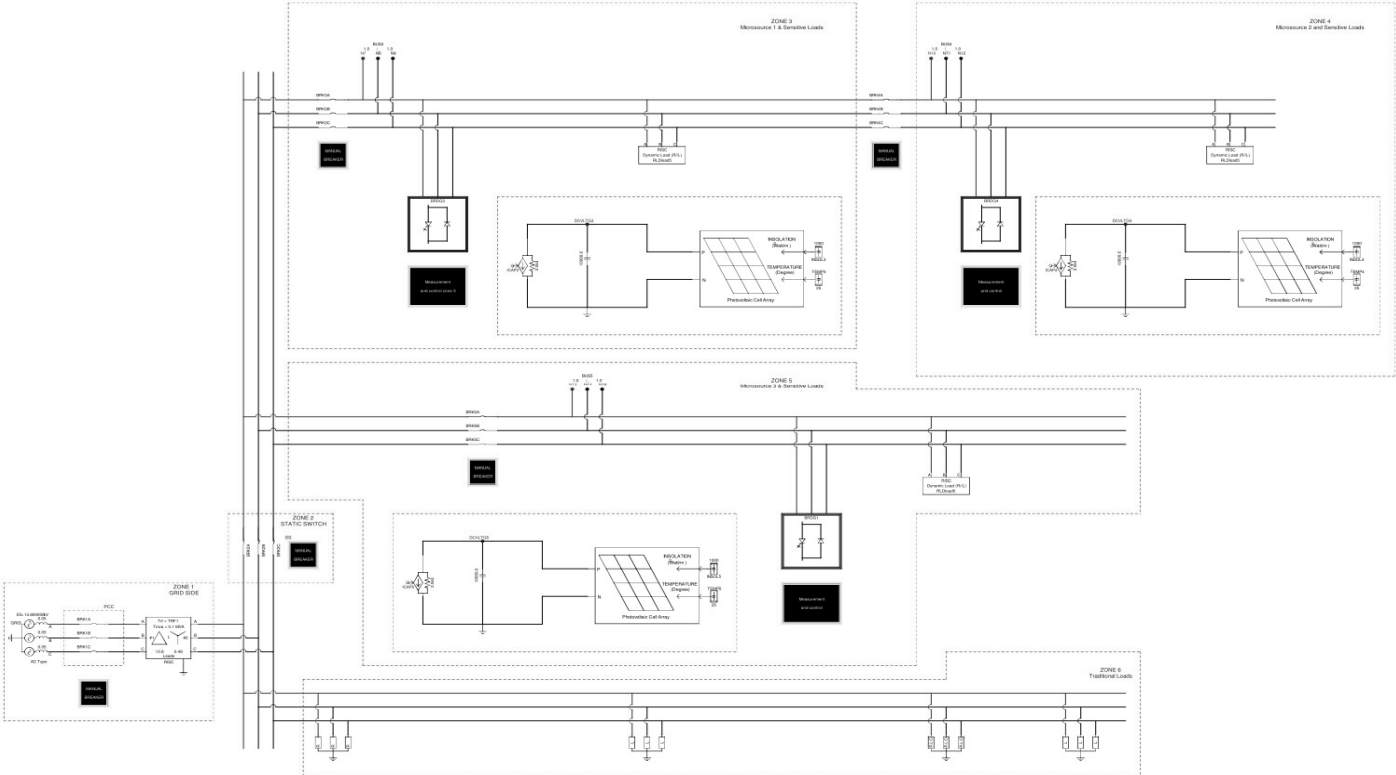


Fig. 2 CERTS Microgrid in Real Time Digital Simulator

Trading Wind Power in a Competitive Electricity Market Using Stochastic Programming and Game Theory

Ting Dai and Wei Qiao

Department of Electrical Engineering, University of Nebraska-Lincoln

Email: ting.dai@huskers.unl.edu

Abstract--Wind power is one of the most rapidly growing clean and renewable energy sources. However, due to the uncertainty and intermittency of wind power, the increasing penetration of wind power into electric power system will pose challenges to power system operators. Moreover, as a participant in a competitive electricity market, a wind power producer's behavior and profit will be influenced by other participants' behaviors. This paper proposes a model of using stochastic programming to generate optimal bidding strategies to maximize the total profits of wind and conventional power producers in both energy market and a bilateral reserve market, where the reserve price is settled between wind and conventional power producers by using game theory. Case studies using real-world data for games in an electricity market with different types of players are performed to show the effectiveness of the proposed model.

I. KEY EQUATIONS

Mathematical models to maximize the profit of wind power producers are shown below:

$$\begin{aligned} \text{Maximize } \pi_W = & \sum_{\omega=1}^{N_\Omega} pr_\omega \sum_{t=1}^{N_T} [\lambda_{t\omega}^D W_{t\omega}^D d_t + \lambda_{t\omega}^r \Delta_{t\omega}^+ - \lambda_{t\omega}^r \Delta_{t\omega}^- - \lambda_t^R W_t^R d_t] \\ & + \beta_W \left[\zeta - \frac{1}{1-\alpha} \sum_{\omega=1}^{N_\Omega} pr_\omega \eta_\omega \right] \end{aligned} \quad (1)$$

Subject to:

$$0 \leq W_{t\omega}^D \leq W^{\max}, \quad \forall t, \omega \quad (2)$$

$$\Delta_{t\omega}^+ - \Delta_{t\omega}^- = \Delta_{t\omega}, \quad \forall t, \omega \quad (3)$$

$$\Delta_{t\omega} = d_t (W_{t\omega}^{ac} + W_t^R - W_{t\omega}^D), \quad \forall t, \omega \quad (4)$$

$$0 \leq \Delta_{t\omega}^+ \leq (W_{t\omega}^{ac} + W_t^R) d_t, \quad \forall t, \omega \quad (5)$$

$$0 \leq \Delta_{t\omega}^- \leq W_{t\omega}^D d_t, \quad \forall t, \omega \quad (6)$$

$$W_{t\omega}^D = W_{t\omega}^D, \quad \forall t, \omega, \omega': \lambda_{t\omega}^D = \lambda_{t\omega'}^D \quad (7)$$

$$(\lambda_{t\omega}^D - \lambda_{t\omega'}^D)(W_{t\omega}^D - W_{t\omega'}^D) \geq 0, \quad \forall t, \omega, \omega' \quad (8)$$

$$\eta_\omega \geq 0, \quad \forall \omega \quad (9)$$

$$\zeta - \sum_{\omega=1}^{N_\Omega} pr_\omega \sum_{t=1}^{N_T} [\lambda_{t\omega}^D W_{t\omega}^D d_t + \lambda_{t\omega}^r \Delta_{t\omega}^+ - \lambda_{t\omega}^r \Delta_{t\omega}^- - \lambda_t^R W_t^R d_t] \leq \eta_\omega, \quad \forall \omega \quad (10)$$

II. KEY FIGURES

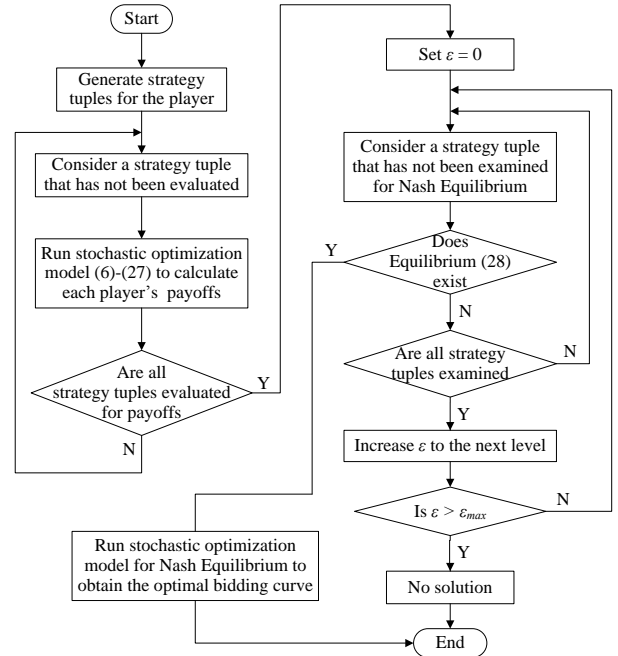


Fig. 1. Flow chart for trading wind power using the proposed model.

III. KEY RESULT

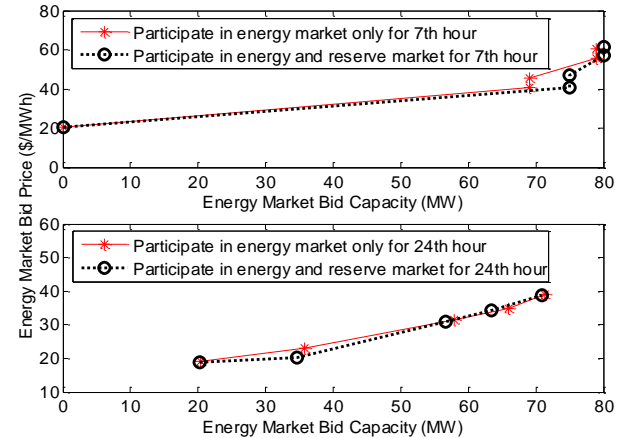


Fig. 7. Case 1: energy market bidding curves of the wind producer generated for the 7th and 24th hour.

Optimal Wind Power Penetration in the Real-Time Energy Market Operation

Jairo Cervantes, *Student Member, IEEE*, Ting Dai, *Student Member, IEEE*, and Wei Qiao, *Member, IEEE*
 Department of Electrical Engineering, University of Nebraska-Lincoln, Lincoln, NE 68588-0511, USA
 Email: jairo.cervantes@huskers.unl.edu, ting.dai@huskers.unl.edu and wqiao@engr.unl.edu

Abstract—This paper proposes a model to minimize the real-time operational cost of traditional generation in a power system with the optimal penetration of wind power. The model takes into account the security and operating constraints of the power system, such as the power flow and balance constraints, reserve requirements, system capacity limits, and wind power uncertainties. A probabilistic distribution function is used to characterize the wind speed and consequently the wind power distribution based on wind turbine power curves. The model is evaluated in IEEE New England 39-bus test system for several case studies. Results are provided to analyze the impact of wind power penetration on the operational costs of traditional generators in the system.

I. KEY EQUATIONS

The objective function of the proposed model is given by:

$$\begin{aligned} \text{Min } F_C = & \sum_i^N (C_i(P_{g,t}^i + P_{R,t}^i)) \\ & + StUP(P_{g,t}^i)(1 - U_{gStUp,t}^i) U_{g,t}^i \end{aligned} \quad (1)$$

The 10-min average wind power output of the wind farm:

$$P_{W,t}^i = N_W * \int_0^{\infty} p_w(v) * f(v, t) dv \quad (2)$$

Constraints system:

$$\begin{aligned} \sum_i^N P_{R,t}^i &= R_{10-min,t} \quad (3) \\ U_{g,t}^i &= \begin{cases} 0 & \begin{cases} T_{Up,t}^i \geq T_{UP,min}^i \\ T_{Down,t}^i > 0 \end{cases} \\ 1 & \begin{cases} T_{Down,t}^i \geq T_{Down,min}^i \\ T_{Up,t}^i > 0 \end{cases} \end{cases} \quad (4) \end{aligned}$$

$$(P_{D,t}^j + P_{d,t}^j(V, \theta)) - P_{g,t}^i = \alpha_{W,t}^i * P_{W,t}^i \quad (5)$$

$$(Q_{D,t}^j + Q_{d,t}^j(V, \theta)) - Q_{g,t}^i = 0 \quad (6)$$

$$P_{Load,t} + P_{Loss,t}(B'', P_g) = \left(\sum_i^N (P_{g,t}^i + \alpha_{W,t}^i * P_{W,t}^i) \right) \quad (7)$$

$$P_{g,min}^i \leq P_{g,t}^i + P_{R,t}^i \leq P_{g,max}^i \quad (8)$$

$$Q_{g,min}^i \leq Q_{g,t}^i \leq Q_{g,max}^i \quad (9)$$

$$V_{g,min}^i \leq V_{g,t}^i \leq V_{g,max}^i \quad (10)$$

$$0 \leq P_{W,t}^i(v) \leq p_{w,r} \quad (11)$$

$$0 \leq \alpha_{W,t}^i \leq 1 \quad (12)$$

II. KEY FIGURES

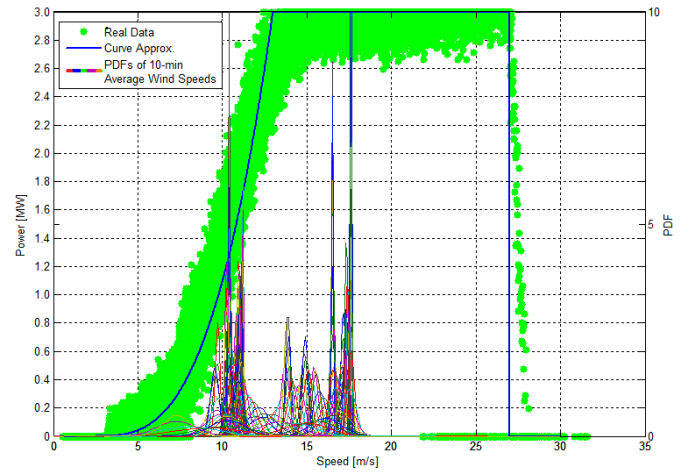


Fig. 1. 10-min average wind speeds curve and their PDF over the next hour.

III. KEY RESULTS

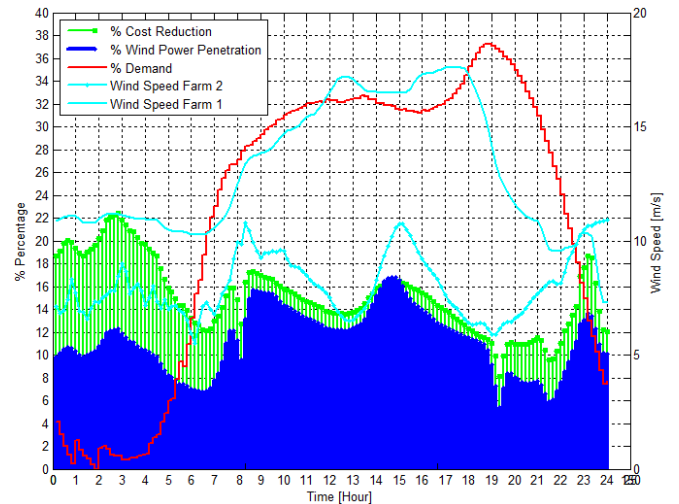


Fig. 2. Impact of adding two wind farms on the total cost of conventional generators in the system.

Effectiveness of Traditional Mitigation Strategies for Neutral Current and Voltage Problems under High Penetration of Rooftop PV

M. J. E. Alam, K. M. Muttaqi, and D. Sutanto

Endeavour Energy Power Quality and Reliability Centre, School of Electrical, Computer and Telecommunications Engineering, University of Wollongong, Wollongong, New South Wales, 2522, Australia,
Email: mjea982@uowmail.edu.au

Abstract— A high penetration of single phase rooftop photovoltaic (PV) units have the potential to exacerbate the existing neutral current and voltage problems in low voltage 4-wire distribution networks. This paper investigates the effectiveness of traditional strategies for mitigation of neutral current and voltage problems in the presence of a high penetration of rooftop PV. This paper analyses the limitations of traditional methods to mitigate neutral current and voltage problems caused by rooftop PV. The analysis shows that in the presence of unbalanced rooftop PV allocation, new mitigation strategies are required. The application of energy storage is explored in this paper as a potential mitigation strategy to reduce the neutral current and voltage problems. Results show that the reduction in neutral voltage by the application of energy storage can be achieved, within the acceptable limit, under daily variations of load demand and PV output.

I. KEY EQUATIONS

Equations used for analysis of neutral currents produced by load and PV unbalance:

$$I_N^n = (I_L^a + I_L^b + I_L^c) + (I_{PV}^a + I_{PV}^b + I_{PV}^c) = I_L^n + I_{PV}^n \quad (1)$$

Equations used for energy storage based neutral current/ voltage mitigation strategy:

$$P_{INJ}^R = P_{INJ}^a = P_{INJ}^b = P_{INJ}^c$$

$$\text{where, } P_{INJ}^a = (P_L^a + P_B^a) - P_{PV}^a, \quad P_{INJ}^b = (P_L^b + P_B^b) - P_{PV}^b, \quad (2)$$

$$\text{and, } P_{INJ}^c = (P_L^c + P_B^c) - P_{PV}^c$$

P_{INJ}^R is selected to be the minimum of the surplus power available at each of the phases

$$P_{INJ}^R = \min(|P_L^a - P_{PV}^a|, |P_L^b - P_{PV}^b|, |P_L^c - P_{PV}^c|) \quad (3)$$

$$P_{IMP}^R = P_{IMP}^a = P_{IMP}^b = P_{IMP}^c$$

$$\text{where, } P_{IMP}^a = P_L^a - P_{PV}^a, \quad P_{IMP}^b = P_L^b - P_{PV}^b, \quad (4)$$

$$\text{and } P_{IMP}^c = P_L^c - P_{PV}^c$$

$$P_{IMP}^R = \min(|P_L^a|, |P_L^b|, |P_L^c|) \quad (5)$$

II. KEY FIGURES

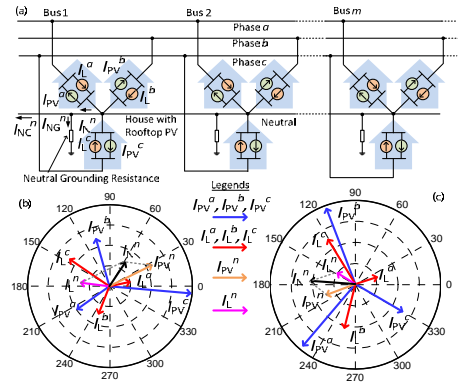


Fig. 1. The neutral current produced by unbalanced load and PV; (a) 4-wire feeder schematic diagram; (b) and (c) the phasor diagram of load and PV current.

III. KEY RESULTS

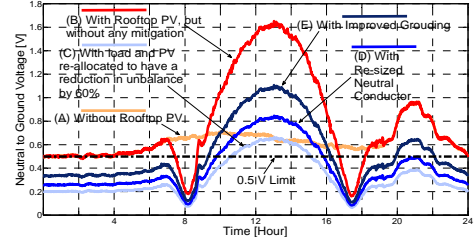


Fig. 1. NGV profiles with different traditional mitigation strategies.

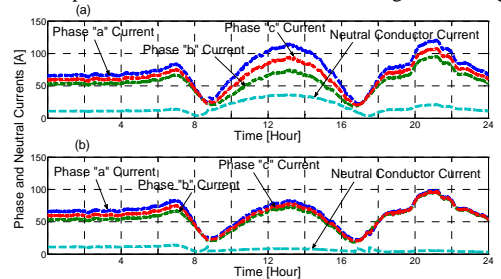


Fig. 2. Phase and neutral current flow through the test feeder; (a) without mitigation; (b) with mitigation by storage devices.

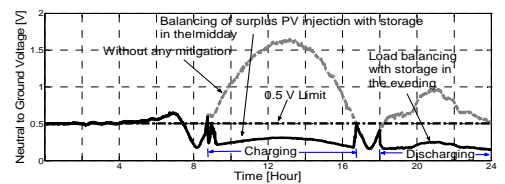


Fig. 3. NGV with the mitigation by storage devices.

Optimal Operations of Energy Storage System for Renewable Energy Plant

Zhen Shu and Panida Jirutitijaroen

Department of Electrical and Computer Engineering, National University of Singapore 119077, Singapore

Email: a0017032@nus.edu.sg and elejp@nus.edu.sg

Abstract— This poster presents an optimal policy for hourly operation of energy storage system (ESS) for grid-connected wind power plants, in order to maximize the expected daily profits following fluctuating wind generation and energy prices. The problem is formulated as a stochastic dynamic programming model, where uncertainties in time-dependent system parameters are incorporated based on hourly time interval. Case studies demonstrate that hourly optimal policy can allow plant operators to obtain considerably higher profits than those from deterministic policy.

I. KEY PROBLEM

For wind power plants, using ESS for energy time-shifting may result in higher profits thus making wind integration more attractive. Wind power output is usually high at night and low during daytime while electricity load and price are usually low at night and become higher during daytime. If wind energy is stored during low-price periods and discharged back to the grid during high-price periods, higher profit can be achieved and peak load can also be reduced to help alleviate transmission congestions. Operation strategy of ESS is very important in achieving optimal trade-off between operation cost and revenue growth. In this poster, the challenging arising from ESS operation problem due to stochastic behaviors of wind power and market prices is appropriately addressed.

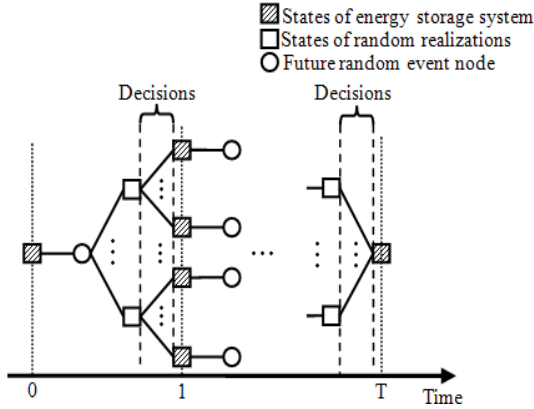


Fig. 1. Decision process of ESS operation

Objective function

$$\max_{(\Delta e_t, d_t) \in \mathcal{X}_t(e_t, \omega_t)} E \left\{ \sum_{t=0}^{t=T-1} (g_t - d_t - \Delta e_t) h_t + C_{op} \min(0, \Delta e_t) \right\} \quad (1)$$

Constraints:

$$0 \leq e_t \leq E_{Cap}, \forall t, t = T - 1, \dots, 1 \quad (2)$$

$$e_T = E_0 \quad (3)$$

$$e_0 = E_0 \quad (4)$$

$$-P_{Cap} \leq \Delta e_t / \Delta t \leq P_{Cap}, \forall t, t = T - 1, \dots, 0 \quad (5)$$

$$0 \leq g_t - \Delta e_t / \Delta t - d_t \leq L^{out}, \forall t, t = T - 1, \dots, 0 \quad (6)$$

$$d_t \geq 0, \forall t, t = T - 1, \dots, 0 \quad (7)$$

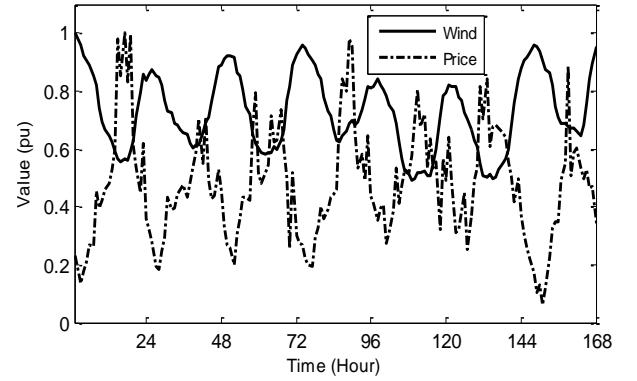


Fig. 2. Weekly curves of wind power and energy price

II. KEY RESULTS

TABLE I
RESULTS WITHOUT ESS AND RESULTS WITH ESS USING OPTIMAL OPERATION STRATEGY

	Winter	Spring	Summer	Fall
Profit without ESS ($\times 10^3$ \$/day)	15.764	13.657	23.822	10.901
Profit with ESS using Proposed Approach ($\times 10^3$ \$/day)	29.936	28.850	35.659	19.245
Increased Percentage	89.9%	111.25%	49.69%	76.54%

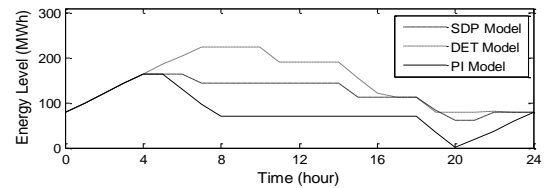
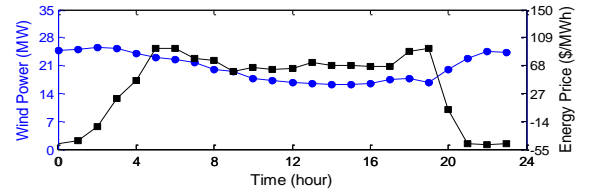


Fig. 3. Comparison of sample trajectories using SDP, deterministic (DET) and perfect information (PI) models

An Efficient Outage Planning Method for Electrical Power Facilities Using Two-layered Tabu Search

Aya Fujiwara, Chihaya Murakami and Shinichi Iwamoto

Power Systems Laboratory, Department of Electrical Engineering and Bioscience, Waseda University, Tokyo, 169-8555, Japan.

Email: fujiwara.aya.pwrs@gmail.com

Abstract—A new efficient outage planning method using two-layered Tabu Search is proposed in this paper. The proposed method can determine 1) Outage schedule, 2) Power system operation during outage works and 3) System switching of the power system in order to conduct outage works. In this paper, to shorten simulation time, circuit breakers near outage facilities are focused on, and an objective function is formulated with them. Also the circuit breakers are evaluated, and the creation of neighborhood solutions is restricted on the basis of their evaluated values. Finally, simulations are conducted using the IEEJ sub-transmission system model I to confirm the validity of the proposed method.

I. KEY EQUATIONS

In this paper, a term “two-layered TS” is used, which consists of first layer TS (TS1) and second layer TS (TS2), and TS2 is used to evaluate neighborhood solutions of TS1. The objective function of TS1 is formulated as (1) and the objective function of TS2 is formulated as (2).

$$\begin{aligned} \text{Minimize } f_1(x_1) &= \sum_{day=1}^D SW_{day} + \sum_{day=1}^D (SW_{day}^2) \times w_1 \quad \dots (1) \\ &+ \sum_{i=1}^3 (penalty_i \times w_{i+1}) \end{aligned}$$

where x_1 : outage start date, D : outage duration, SW : the number of switching during an outage plan calculated by TS2, $penalty_1$: existence of carry-over task constraint violation (0, 1), $penalty_2$: existence of an over-task constraint violation (0, 1), $penalty_3$: solution convergence of TS2 (0, 1), w_{\square} : weight function

$$\begin{aligned} \text{Minimize } f_2(x_2) &= OCB_{on} + ENS \times w_5 \quad \dots (2) \\ &+ OL \times w_6 + SOL \times w_7 \\ &+ penalty_4 \times w_8 + penalty_5 \times w_9 \end{aligned}$$

where x_2 : on/off condition of the circuit breakers, ENS : the amount of energy not supplied, OL : the rated capacity of over load flow of lines, SOL : the short time capacity of over load flow of lines, OCB_{on} : the number of circuit breakers evaluated 1 which are turned on, $penalty_4$: existence of the radial and interconnected power system constraint violation, $penalty_5$: existence of the power flow constraint violation.

II. KEY FIGURES

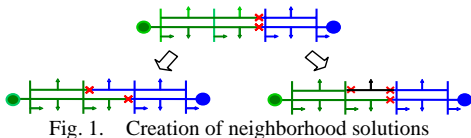


Fig. 1. Creation of neighborhood solutions

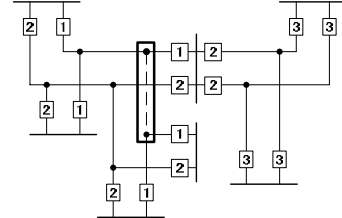


Fig. 2. Evaluation of circuit breakers

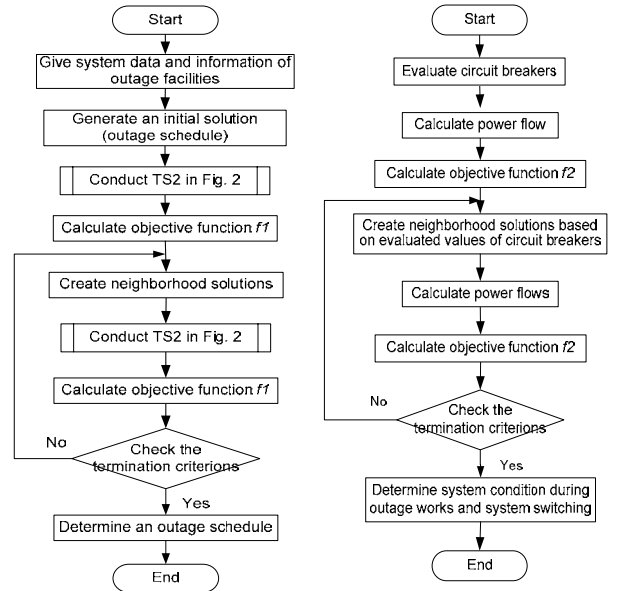


Fig. 3. Flowchart of TS1 (left) and TS2 (right).

III. KEY RESULTS

Table 1. Simulation Result

Outage facility	Outage date						
	1	2	3	4	5	6	7
11011							
12012							
20032							
24012							
31012							
37012							

Table 2. The number of the system switching

Day	1	2	3	4	5	6	7
Switching count	7	4	3	4	7	0	0

Table 3. Comparison of simulation results

Method	Simulation time ratio	Evaluated value ratio
Simple method (Backtracking and TS2)	100	100
The proposed method (TS1 and TS2)	3.29	100.92

Travelling Wave Based Fault Location Using Dominant Fault Induced Surges in Circuit

Zhang Guangbin Yu Jilai

School of Electrical Engineering and Automation
Harbin Institute of Technology
Harbin, China

Email: guangbin85@gmail.com and yupwrs@hit.edu.cn

Shu Hongchun

Faculty of Electric Power Engineering
Kunming University of Science and Technology
Kunming, China

Email: kmshc@sina.com

Abstract—Reliable and effective identification of surges as well as independent of remote data are essential for automatic travelling wave fault location. The inherent ring topology of transmission grid usually provides not only the shortest but also a sub shortest path for initial fault surge back to the monitored bus, which makes the corresponding lines connected with the bus separately detect the dominant fault induced surges. The dominant surges can be identified through comparing amplitude and phase of each line current, then their arrival time can be determined. Accordingly, a novel double-ended travelling wave fault location approach based on difference of dominant surges arrival using the data acquiring at the same substation is presented. The proposed method combines the advantages of independent of communications or timing synchronization with remote side, and without identification of reflected faulted wave. The method is confirmed feasible and effective by field tests.

I. KEY EQUATIONS

The expression of dominant fault induced surges of the faulted line and sound line:

$$i_{\text{dominant}}^{(f)} = (-1 + r_A) e^{-g^x} u_f / (Z_c + 2R_f) \quad (1a)$$

$$i_{\text{dominant}}^{(s)} = (-1 + r_A) e^{-g(l_0 - x + \sum_k L_k)} u_f \prod_k a_k / (Z_c + 2R_f) \quad (1b)$$

Expanding two-ended travelling wave location formula:

$$x = [l_f + l_s - (t_1 - t_0)v] / 2 = [l_\Sigma - (t_1 - t_0)v] / 2 \quad (2)$$

II. KEY FIGURES

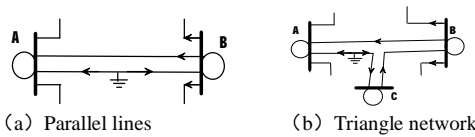


Figure 1. Propagation of fault initiated travelling wave in circuit

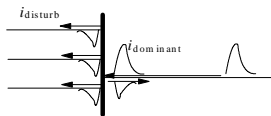


Figure 2. Amplitude and phase of dominant/disturbed transient current

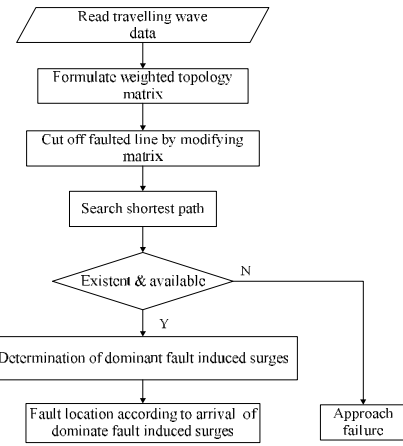


Figure 3. Flowchart of proposed method

III. KEY RESULTS

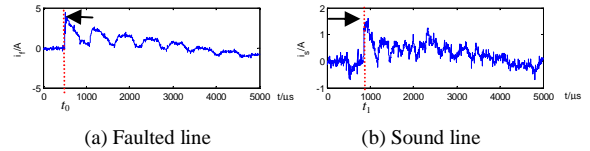


Figure 4. Dominant fault induced surges in circuit

TABLE I. LOCATING RESULTS FOR TYPICAL MEASURED FIELD DATA

Date	Time	Fault Type	Fault Position (km)	t_0 (μ s)	t_1 (μ s)	Locating Result (km)
2010/12/26	2:01	AG	34.8	506	525	34.5
2011/1/12	8:04	AG	27.4	503	576	26.5
2011/1/12	8:11	BG	27.4	510	586	26.0
2011/3/20	10:03	AG	17.6	508	1298	18.6
2012/2/27	2:05	CG	34	507	1177	36.1
2012/3/1	16:56	CG	5	506	1109	3.3

Hedging against system protection malfunction

Jose Luis Calvo, Simon H. Tindemans, Goran Strbac

Department of Electrical and Electronic Engineering, Imperial College
London, United Kingdom

Email: j.calvo10@imperial.ac.uk

Abstract— Corrective actions in the form of system protection schemes (SPS) can be used to enhance the utilisation of existing transmission assets. However, relying on these schemes is not risk-free: there are hazards that can result in incorrect operation. Quantifying and managing these risks is crucial before corrective security can be depended on in practice.

We consider a 3-bus representation of the Scotland-England corridor. After a line fault an intertripping scheme disconnects generation in Scotland and load in England, in order to reduce the load on remaining transmission lines. We quantify the costs associated with the operation of such a system and the risk of its failure to operate. In particular, the remote intertripping of a generator or load may fail altogether, or partial operation may lead to an imbalance in supply and demand.

For this system, we determine the optimal amount of intertripping capacity for a given pre-fault power flow. Our analysis reveals a surprising new strategy that relies on frequency services to alleviate thermal overloads in case of an SPS malfunction. This strategy reduces the risk associated with malfunction (mostly value of lost load) at the expense of increased utilization cost.

I. KEY CONCEPTS

An SPS in an intermediate bus increases power transfer limits beyond the N-2 security standard.

After a line fault (single or double) the SPS disconnects a predetermined amount of generation in the north node and load in the south one.

The SPS action is **not 100% reliable**, and can malfunction entirely or lead to an imbalance between load and generation.

Frequency regulation and defence plan actions are distributed proportionally in both nodes.

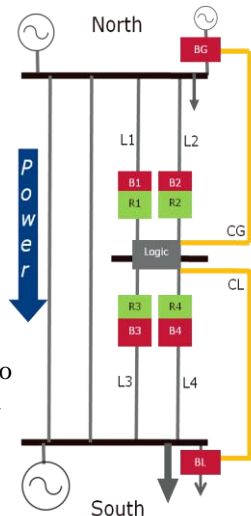


Fig. 1. Representation of GB power system

II. KEY FIGURES

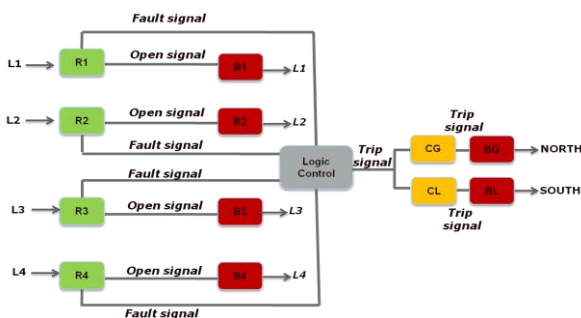


Fig. 2. SPS model. Relays are in green, breakers in red, control in grey and communication channels in yellow

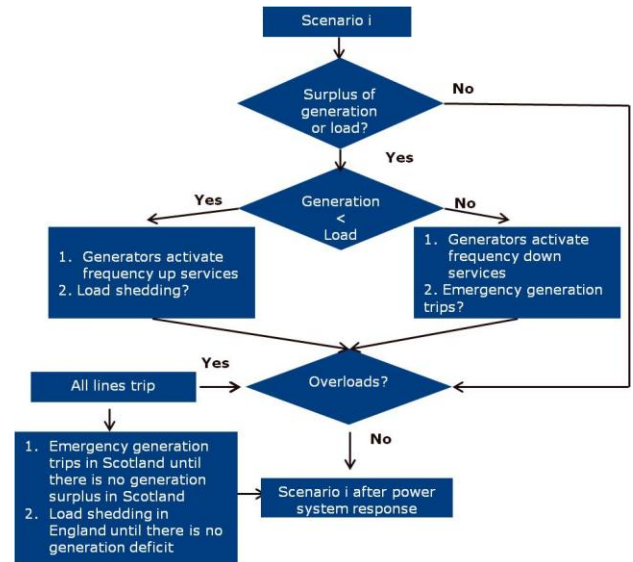


Fig. 3. Power system model to compute the impact from SPS outcomes

III. KEY RESULTS

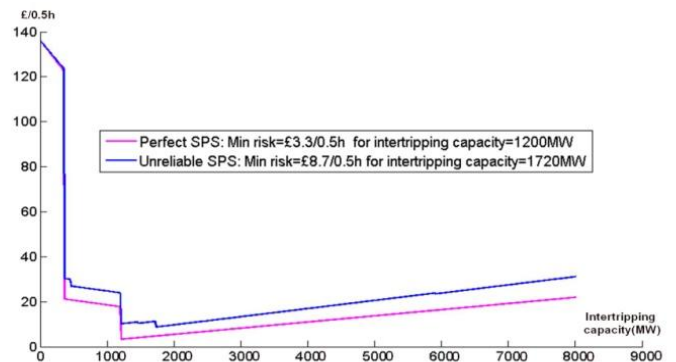


Fig. 4. Risk from SPS capacities for a particular operating point

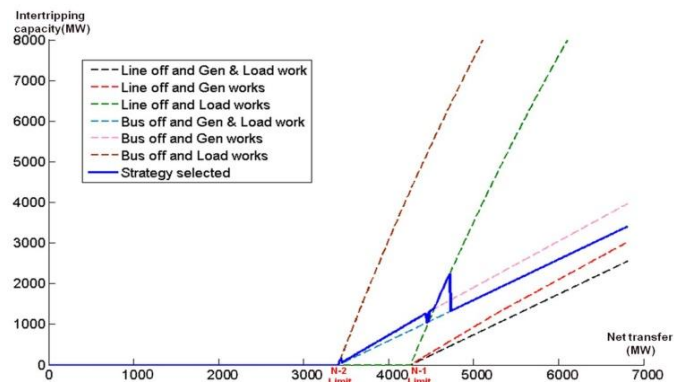


Fig. 5. Optimal amount of intertripping capacity for different transfer values vs optimal capacity for the different SPS scenarios

Transformer Condition Assessment

Richard Barnes, Kenneth Elgin, Scott Lederhos, Andrew Morin, and Kyle Wiedeman
Department of Electrical Engineering and Computer Science
Northern Arizona University
Flagstaff, Arizona, USA
Email: kylewiedeman@gmail.com and atm47@nau.edu

Abstract— Premature failure of large transformers is costly and threatens the transmission of safe and reliable power. Recent tests conducted as a part of Arizona Public Service (APS) routine transformer maintenance have shown the development of hot spots and abnormal levels of gasses within a transformer’s mineral oil at the Cholla Power Plant in Joseph City, Arizona. We examined possible sources of these problems. To accomplish this, we researched several transformer failure case studies, developed a program to rapidly analyze years of dissolved gas in oil data, and carefully examined other crucial data gathered during the life of this transformer. Our assessment of the transformer is a tool for APS to indicate if the transformer is near the end of its operation life. The results of this work will help APS continue to serve its customers with a reliable source of power.

I. BACKGROUND

It is important to predict the failure of a generation step up transformer well before that failure occurs, because it can take over nine months to replace a transformer of this size. Having a unit which is unable to generate power for several months results in large economic losses and can be detrimental to the integrity of the utility supply.

II. INTRODUCTION

Recent Dissolved Gas Analysis (DGA) tests of a generation step-up transformer at the Arizona Public Service (APS) Cholla Power Plant indicated that the transformer may be nearing the end of its useful lifetime. Along with the harmful gasses found in the oil, two of the transformer’s four oil cooling pumps were also taken out of service due to high vibration. APS scheduled a planned outage in March of 2013 to have these pumps replaced. During this time, an internal visual inspection of the transformer was performed. Our team was tasked to perform research and analyze data about the transformer as well, to identify the cause of the abnormal gas measurements and provide a condition assessment for the transformer.

Our team researched common reasons for transformer failures, predictive analysis techniques, and a variety of tests which would help APS better understand the condition of the transformer. Case studies of previous transformer failures included a correlation between the problems in other transformers before they failed and the problems with the transformer at Cholla. Several tests included in our research

assisted us with predictive analysis, and additional tests will allow our team to better understand the health and expected lifetime of the transformer. These tests will include oil testing that can be done with the unit online and electrical tests that can be performed when the unit is taken offline.

III. KEY FIGURES

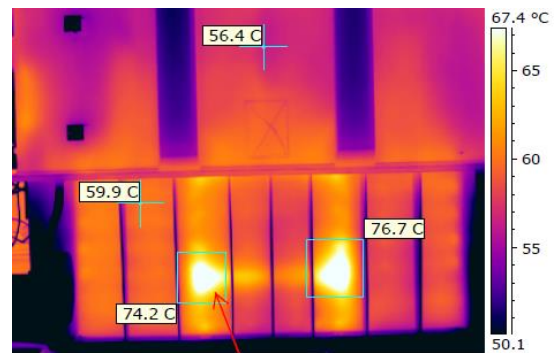


Fig 1 Thermal Images of the transformer

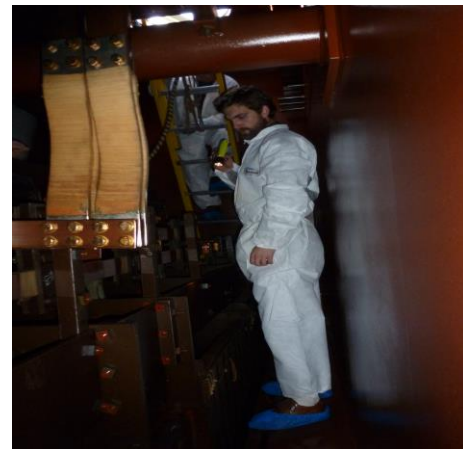


Fig. 2 Internal inspection of the transformer

ACKNOWLEDGMENT

We would like to thank Boyd Davis, Senior Electrical Engineer, and Tim Vachon, Consulting Engineer at the Cholla Power Plant for all of their help and support on this project.

The Effect of Variable Weights in a WLS State Estimator Considering Instrument Transformer Uncertainties

Markos Asprou and Elias Kyriakides

Electrical and Computer Engineering, KIOS Research
Center for Intelligent Systems and Networks
University of Cyprus
Nicosia, Cyprus
asprou.markos@ucy.ac.cy, elias@ucy.ac.cy

Mihaela Albu

Department of Electrical Engineering
Politehnica University of Bucharest
Bucharest, Romania
albu@ieee.org

Abstract—State estimator constitutes the cornerstone of the Supervisory Control and Data Acquisition (SCADA) system since it provides the power system operating situation in consecutive time intervals. Therefore, there is a need for the power system state estimator to be as much accurate as possible. The main source of uncertainty that may deteriorate the accuracy of a Weighted Least Squares (WLS) state estimator, provided that the network parameters are perfectly known, is the uncertainty that is encompassed in the measurements. In this poster, the effect of the measurement weights, which are calculated by taking into consideration both the standard uncertainties associated with the measurement devices and the instrument transformers, on the WLS state estimator is examined.

Keywords—Instrument transformer, measurement uncertainties, state estimation, synchronized measurements.

I. INTRODUCTION

In this poster the uncertainties of the instrument transformer, will be considered for updating the weights of the measurements coming from the measurement devices. Without loss of generality, the instrument transformers are considered calibrated and all sources of systematic errors are eliminated. Therefore, only the uncertainty derived from the accuracy class of the instrument transformer will be used. The methodology will be applied to a hybrid state estimator that uses both conventional and Phasor Measurement Units (PMUs) measurements; a comparison between the conventional methodology of measurement weighting and the proposed one with regards to the accuracy of the hybrid state estimator will be performed.

II. METHODOLOGY AND RESULTS

The simplified measurement chain for both the conventional and PMU measurements are depicted in Figs. 1 and 2 respectively. The combined uncertainties of the simplified measurement chains are used for weighting the measurements used in the hybrid state estimator. It should be noted that the measurement weights when the instrument

transformer uncertainties are taken into consideration are variable since the uncertainties of the instrument transformers vary with the power system operating condition.

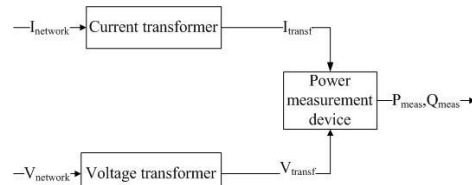


Fig. 1. Measurement chain diagram in a conventional power meter



Fig. 2. Measurement chain diagram in a PMU

The Sum of the Power Flow Mismatches (SPFM) between the real and the estimated power flows was used as a metric of comparison between the case where constant weights are used in the hybrid state estimator and in the case where variable weights are used and is calculated as,

$$SPFM = \frac{1}{T} \sum_{k=1}^T \left(\frac{1}{M} \sum_{i=1}^M \sum_{j=1}^B |P_{f_j}^{real} - \hat{P}_{f_j}^i| \right), \quad (1)$$

The proposed methodology was applied to the IEEE 118 bus system in the case where 10 PMUs were installed in the system. Based on the results in Table I, the variable weights improve the accuracy of the hybrid state estimator since the SPFM is smaller in the case of the variable weights than in the case of the constant weights. The theory behind the proposed methodology as well as more cases that show the effect of variable weights in the hybrid state estimator accuracy will be shown in the poster.

Variable weights	Constant weights
368.47	428.22

Identifying Protective Device Operations in Distribution and Transmission Systems

M. Lwin, Student Member, IEEE, S. Santoso, Senior Member, IEEE

Abstract—Improper coordination of protective devices in power systems can lead to unnecessary interruptions and outages. In distribution systems, automatic reclosers and fuses are the main form of overcurrent protection due to the radial nature of the network. In transmission systems, the network is typically a meshed circuit with multiple generators allowing current to flow across a line in both directions. In this case, distance relays are often used to protect the line from short-circuits. The goal of this poster is to build on an approach to determine which relay operated to clear a short-circuit condition based on voltage and current waveform data collected during a fault. This method will consider both distribution and transmission systems.

The approach developed in [1] allows for detection of recloser and fuse operations on distribution networks. This method involves using the wavelet transform to detect fault inception and estimate fault current duration. This information is then used to calculate the empirical operating point of the protective device. However, when applying this approach in simulations, [1] only considers waveforms associated with recloser fast operations.

This poster will include analysis of permanent faults between the recloser and fuse where the recloser operates on the delayed curve. Figure 1 provides an example of current waveforms seen by the recloser during a fault. Moreover, a similar method will be developed to identify distance relay operations on transmission systems using the mho characteristic. Cases which require operation of the backup relay due to primary relay misoperation will also be analyzed. Three-phase faults will be considered where voltage and current waveform data will be analyzed to detect and identify relay misoperation. Analysis will be conducted by simulation in PSCAD/EMTDC.

I. KEY EQUATIONS

Wavelet transform of signal $x(t)$:

$$W_x(a, b) = \int_{-\infty}^{\infty} x(t)\psi_{a,b}^*(t)dt \quad (1)$$

where

$$\psi_{a,b}(t) = |a|^{-\frac{1}{2}} \psi\left(\frac{t-b}{a}\right) \quad (2)$$

Analytic equation for pickup time of an inverse-time overcurrent curve:

$$t(I) = \frac{A}{M^P - 1} + B \quad (3)$$

Impedance locus of Mho characteristic:

$$Z_{reach} = \frac{Z_C - Z_C \angle \theta}{2} \quad (4)$$

II. KEY FIGURES

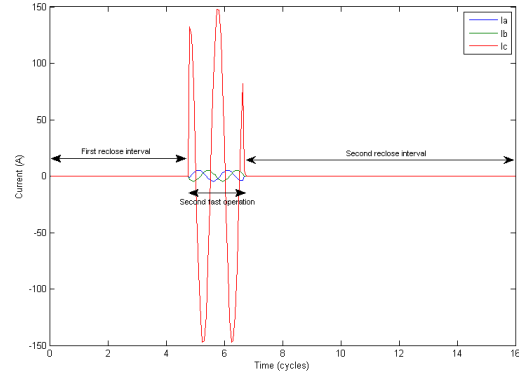


Figure 1. Three-phase current waveform data measured at recloser for first reclose attempt during a permanent fault.

REFERENCES

- [1] Santoso, S.; Short, T.A., "Identification of Fuse and Recloser Operations in a Radial Distribution System," *IEEE Transactions on Power Delivery*, vol.22, no.4, pp.2370-2377, Oct. 2007.
- [2] Santoso, S.; Powers, E.J.; Grady, W.M.; Hofmann, P., "Power Quality Assessment Via Wavelet Transform Analysis," *IEEE Transactions on Power Delivery*, vol.11, no.2, pp.924-930, Apr 1996.
- [3] "IEEE Standard Inverse-Time Characteristic Equations for Overcurrent Relays," *IEEE Std C37.112-1996*, 1997.

Outage Detection in Power Distribution Networks with Optimally-Deployed Power Flow Sensors

Yue Zhao^{*‡§}, Raffi Sevlain^{*§}, Ram Rajagopal[†], Andrea Goldsmith^{*} and H. Vincent Poor[‡]

^{*}Department of Electrical Engineering, Stanford University, Stanford, CA, 94305, USA

[†]Department of Civil and Environmental Engineering, Stanford University, Stanford, CA, 94305, USA

[‡]Department of Electrical Engineering, Princeton University, Princeton, NJ, 08540, USA

[§]These authors contributed equally to this work.

Abstract—An outage detection framework for power distribution networks is proposed. The framework combines the use of optimally deployed real-time power flow sensors and that of load estimates via Advanced Metering Infrastructure (AMI) or load forecasting mechanisms. The distribution network is modeled as a tree network. It is shown that the outage detection problem over the entire network can be decoupled into detection within subtrees, where within each subtree only the sensors at its root and on its boundary are used. Outage detection is then formulated as a hypothesis testing problem, for which a maximum a-posteriori probability (MAP) detector is applied. Employing the maximum misdetection probability P_e^{\max} as the detection performance metric, the problem of finding a set of a minimum number of sensors that keeps P_e^{\max} below any given probability target is formulated as a combinatorial optimization. Efficient algorithms are proposed that find the globally optimal solutions for this problem, first for line networks, and then for tree networks. Using these algorithms, optimal three-way trade-offs between the number of sensors, the load estimate accuracy, and the outage detection performance are characterized for line and tree networks using the IEEE 123 node test feeder system.

I. SYSTEM MODEL

- Load pseudo-measurements from intermittently collected AMI data, or load forecasts. These are considered noisy observations of the true load at any given time.
- Real-time measurements of the power flows on a fraction of the lines obtained using accurate sensors placed on the selected lines.

Each node V_n in the graph has a consumption load L_n . The pseudo-measurement of this load is \hat{L}_n . $L_i \sim N(\hat{L}_i, \sigma_i^2)$. We denote the vectors of true loads, load pseudo-measurements, and the error covariance matrix by \mathbf{L} , $\hat{\mathbf{L}}$ and $\mathbf{\Sigma}$, respectively. Thus, $\mathbf{L} \sim N(\hat{\mathbf{L}}, \mathbf{\Sigma})$, and $\mathbf{\Sigma}$ is a diagonal matrix due to the independence of errors.

$$S_n = \sum_{V_j \in \mathcal{T}(n) \setminus \mathcal{T}(i)} L_j, \quad \forall n \geq 1. \quad (1)$$

$$\begin{aligned} \min M \\ \text{s.t. } \exists \mathcal{M}, |\mathcal{M}| \leq M, \mathcal{M} \subseteq \{1, \dots, N\}, \\ P_e^{\max}(\hat{\mathbf{L}}, \mathbf{\Sigma}, \mathcal{M}) \leq P_e. \end{aligned} \quad (2)$$

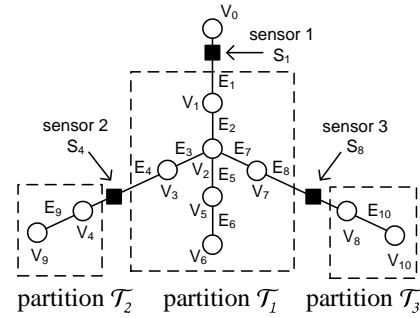
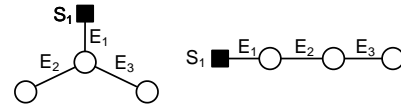
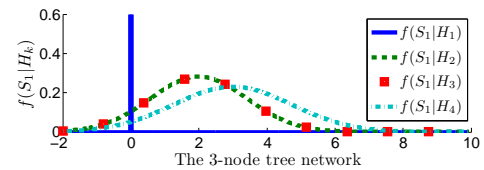
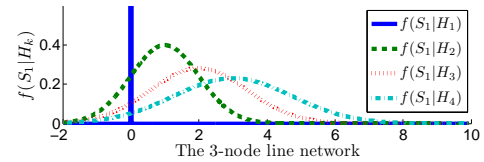


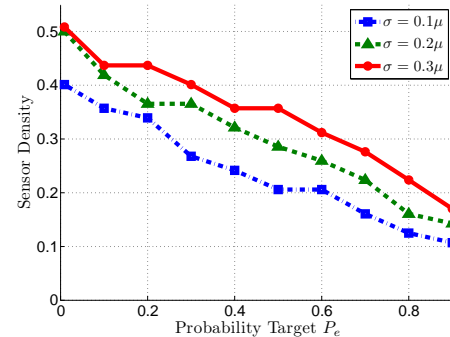
Fig. 1. Diagram for a distribution network with a tree structure.



(a) 3-node line and tree networks



(b) Conditional pdf $f(S_1|H_k)$



(c) Minimum number of sensors required for tree networks.

Investment Strategies Assessment Under Uncertainty

Yanyi He, Lizhi Wang

Industrial & Manufacturing Systems Engineering
Iowa State University
Ames, United States

heyanyi@iastate.edu, lzwang@iastate.edu

George Gross

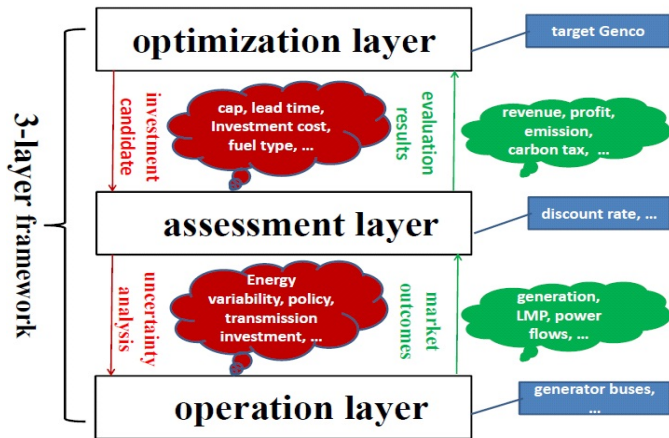
Electrical Engineering
University of Illinois
Urban-Champaign, United States

gross@illinois.edu

Abstract—This paper proposes a three-layered framework to assist the target generation company with long-term investment planning under uncertainties. The first layer is operations layer to clear the market under given scenarios; the second layer is assessment layer to comprehensively analyze the operations results and the third layer is optimization layer to rank the investment decisions. The uncertainties are grouped into statistical and systematic uncertainties. The case study is performed on WECC 240-bus network for twenty-year planning. Electricity load and renewable energy generation uncertainties are considered in the statistical uncertainty. For the systematic uncertainty, several environmental policies, transmission plans other generation companies' generation investments are considered. Two distinguished generation companies within CAISO are studied to observe impacts from both statistical and systematic uncertainties.

Keywords—generation expansion; environmental policies; statistical uncertainty; systematic uncertainty; CAISO; assessment;

I. FRAMEWORK

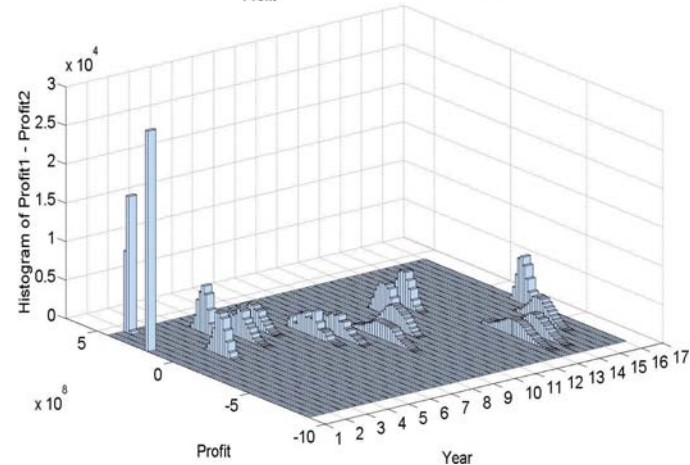
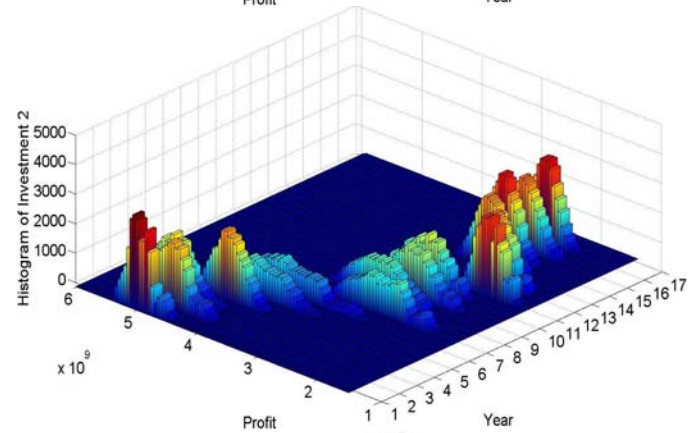
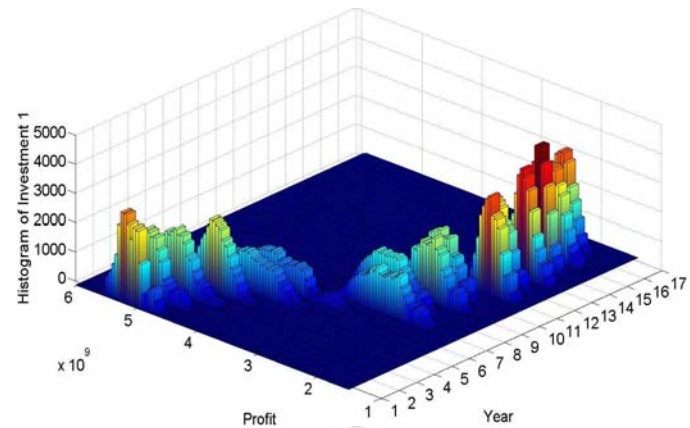


II. CASE STUDY

- Test system: Western Electricity Coordinating Council (WECC) 240-bus network with up to 940 generators and 547 transmission lines
- Environmental policy: Renewable Portfolio Standards, Carbon emission cap and carbon tax
- Statistical uncertainty: Renewable energy variability and demand uncertainty
- Systematic uncertainty: Transmission line investments, other companies' generation investments
- Candidate investment: Small hydro, nuclear, wind, geothermal, biomass, solar, gas or coal fired power plants

- Time frame: Hourly market outcomes, 16 year planning

III. RESULTS



Improving Convergence of Horizontally Decomposed Stochastic Day-Ahead Unit Commitment

Garret LaBove and Kory Hedman

School of Electrical, Computer and Energy Engineering
Arizona State University
Tempe, AZ, 85287, USA

Email: garret@asu.edu and kory.hedman@asu.edu

Abstract—As utilization of renewable and intermittent generation assets, including wind and solar power, continues to grow, new operations management challenges arise in ensuring reliability of power systems. Currently, reliability is managed by system operators using zone- and system-wide reserve policies, which may insufficiently address the supply-side uncertainty present in day-ahead forecasts for intermittent resources as well as the N-1 reliability requirements. Stochastic programming has previously been demonstrated to improve scheduling of conventional generation assets; however, the complexities associated with the extensive form of stochastic Mixed-Integer Linear Programming (MILP) models render practical application in large-scale systems intractable at worst, and prohibitive in computational time at best. Horizontal decomposition techniques, such as Progressive Hedging (PH), reduce the complexity associated with stochastic MILP optimization by separating the extensive form into several independent, deterministic problems, which are not significantly harder to solve than models in use today. In particular, PH has attractive properties in harnessing parallel and clustered processing units, thereby reducing barriers to high resolution analysis. However, PH may not converge to a solution within a reasonable timeframe when applied to stochastic unit commitment. This project seeks to examine the impact of methods to improve the utility and convergence properties of PH when applied to day-ahead unit commitment problems that have significant penetration of intermittent generation.

I. KEY EQUATIONS

The following describes the basic PH algorithm [1].

A. Initialization

$$\text{Minimize } c^T x + f_s^T y_s \quad \forall s \in S \quad (1)$$

$$\text{subject to } (x, y_s) \in \Omega_s \quad \forall s \in S \quad (2)$$

$$x_s^{(0)} = \begin{bmatrix} x \\ y_s \end{bmatrix} \quad \forall s \in S \quad (3)$$

$$\bar{x}^{(0)} = \sum_{s \in S} P(s) x_s^{(0)} \quad (4)$$

$$w_s^{(0)} = \rho(x_s^{(0)} - \bar{x}^{(0)}) \quad \forall s \in S \quad (5)$$

B. Iteration k

$$\text{Minimize } \forall s \in S \quad (c^T x + (w_s^{(k-1)})^T x + \frac{\rho}{2} \|x - \bar{x}^{(k-1)}\|^2 + f_s^T y_s) \quad (6)$$

$$\text{subject to } (x, y_s) \in \Omega_s \quad \forall s \in S \quad (7)$$

$$x_s^{(k)} = \begin{bmatrix} x \\ y_s \end{bmatrix} \quad \forall s \in S \quad (8)$$

$$\bar{x}^{(k)} = \sum_{s \in S} P(s) x_s^{(k)} \quad (9)$$

$$w_s^{(k)} = w_s^{(k-1)} + \rho(x_s^{(k)} - \bar{x}^{(k)}) \quad \forall s \in S \quad (10)$$

$$g^{(k)} = \sum_{s \in S} P(s) \|x_s^{(k)} - \bar{x}^{(k)}\| \quad (11)$$

C. Convergence

If $g^{(k)} < \varepsilon$, where ε is the supplied convergence criteria, the algorithm terminates. Otherwise, return to B ($k = k + 1$).

II. KEY FIGURES

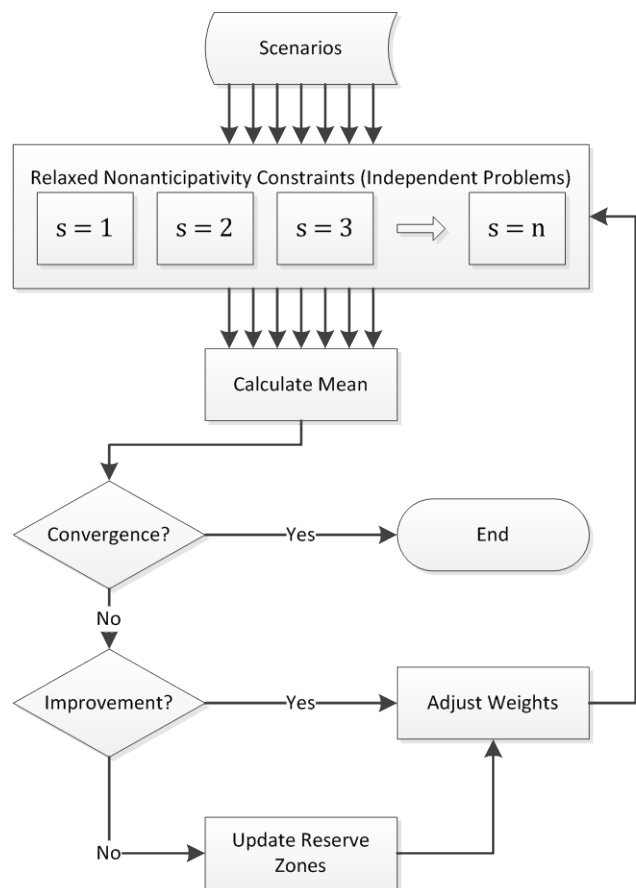


Fig. 1. Flow chart of presented technique.

REFERENCES

- [1] J.-P. Watson and D. L. Woodruff, "Progressive hedging innovations for a class of stochastic mixed-integer resource allocation problems," *Computational Management Science*, vol. 8, pp. 355–370, November 2011.

Horizontal Decomposition-based Stochastic Day-ahead Reliability Unit Commitment

Yingzhong Gu, *Student Member, IEEE*, Xing Wang, *Senior Member, IEEE* Le Xie, *Member, IEEE*
Email: lxie@ece.tamu.edu

Abstract— This poster presents a progressive hedging (PH) based decomposition algorithm to improve the computational efficiency of stochastic day-ahead reliability unit commitment (RUC). Stochastic programming is introduced into RUC to facilitate a better decision making for market operation efficiency and energy supply reliability. However, the computational burden of stochastic RUC using today's computing power is still significant. We propose to apply progressive hedging (PH) algorithm to decompose the stochastic RUC problem. It is shown that a PH-based algorithm allows parallel computation of stochastic RUC, which can be much faster than conventional stochastic programming methods. A practical power system is used to verify the effectiveness of the proposed computation framework.

I. KEY EQUATIONS

A. Mathematical Formulation

Based on the two-stage stochastic RUC model, the extensive form of a stochastic unit commitment problem can be written as follows:

$$\min : f = c^T x + \sum_{s \in S} P(s) q^T y_s \quad (1)$$

Subject to:

$$Ax = b, x \geq 0 \quad (2)$$

$$Tx + Wy_s = h, y_s \geq 0, \forall s \in S, \quad (3)$$

where S is the indicator of each scenario, $P(s)$ is the occurrence probability of scenario s , y_s is the vector of the second-stage decision variables of scenario s .

In order to solve the problem, the progressive hedging algorithm is applied. We formulate the initial sub-scenario problem in (4)-(6). By solving this problem for each scenario, a set of deterministic optimal solutions corresponding to each scenario is established.

$$\min : f = c^T x_s + q^T y_s \quad (4)$$

Subject to:

$$Ax_s = b, x_s \geq 0 \quad (5)$$

$$Tx_s + Wy_s = h, y_s \geq 0, \forall s \in S. \quad (6)$$

The main activity of the progressive hedging algorithm is to converge to the stochastic optimal solution (by iterations) that ensures both optimality and implementability. For each iteration, an auxiliary sub-scenario problem is solved.

$$\min : f = c^T x_s + q^T y_s + w_s^{k-1} x_s + 0.5\rho \|x_s - \bar{x}^{k-1}\|^2$$

Subject to:

$$Ax = b, x \geq 0, \quad (7)$$

$$Tx + Wy_s = h, y_s \geq 0, \forall s \in S. \quad (8)$$

In the auxiliary sub-scenario problem, the multiplier term $w_s^{k-1} x_s$ forces the scenario decision variables to change in the direction toward the mean solution while the penalty term $0.5\rho \|x_s - \bar{x}^{k-1}\|^2$ keeps the optimal solution within a certain neighborhood of the mean solution for the sake of convergence stability.

II. KEY FIGURES

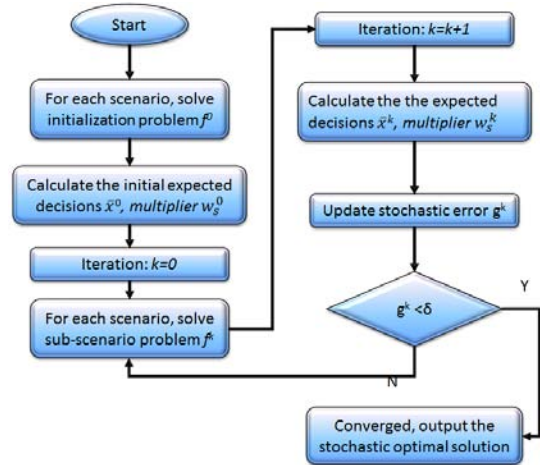


Fig. 1. FLOWCHART OF PROGRESSIVE HEDGING ALGORITHM

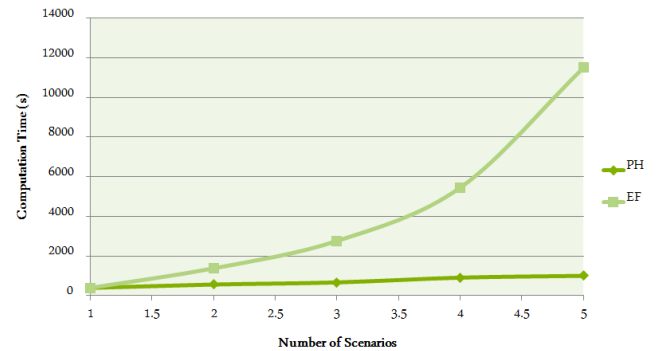


FIG. 2 COMPUTATIONAL PERFORMANCE: PROGRESSIVE HEDGING VERSUS CONVENTIONAL STOCHASTIC PROGRAMMING

Real Time Reactive Power Spot Markets

David Ganger, Ji Zhao, Mojgan Hedayati, Akhil Mandadi

Department of Electrical, Energy and Computer Engineering
Arizona State University, Tempe, USA

E-mail: {dganger, jzhao36, mhedayat, amandadi}@asu.edu

Abstract—Reactive power spot markets have been proposed by many in the power engineering community as a means of reactive power compensation within the U.S. deregulated energy markets. Cited benefits include incentive for proper reactive power investment for power system stability, the minimization of costs to meet load, and proper reactive power price signals. However, the market power that can be exercised by utilities may render the market useless for consumer participants. In addition, the zero price of reactive power as well as the volatility in demand may not inspire the investment that spot markets are thought to encourage, and current methods of pricing reactive power involve time-consuming optimizations. An ACOF simulation was run utilizing a representative urban transmission and distribution system, confirming many of the weaknesses theorized to exist in real time reactive power spot markets including exercise of market power and price volatility. A 10-bus 230 kV looped transmission system was chosen to represent a typical system that serves a large city, based off of the Phoenix, Arizona subsystem.

I. KEY FIGURES

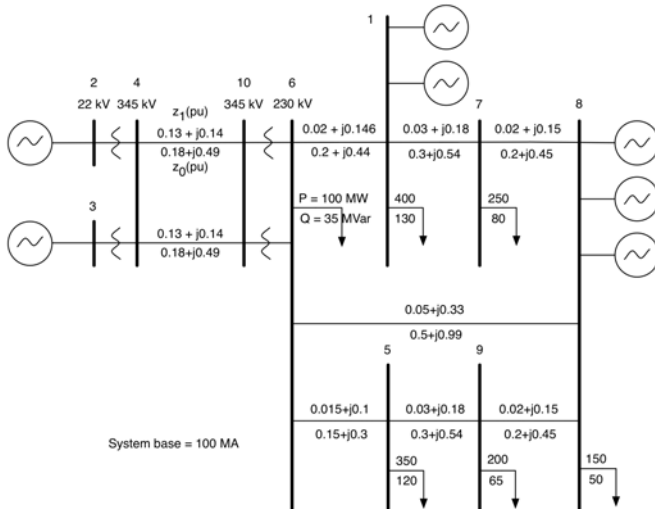


Figure 1. 10-bus 230 kV looped transmission network, representative of an large urban power system, based off the the Phoenix system [14]

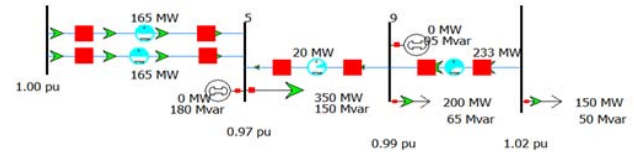


Figure 2. Increased reactive power demand at Bus 5 causing voltage drop when local condenser is unable to provide the VAR support

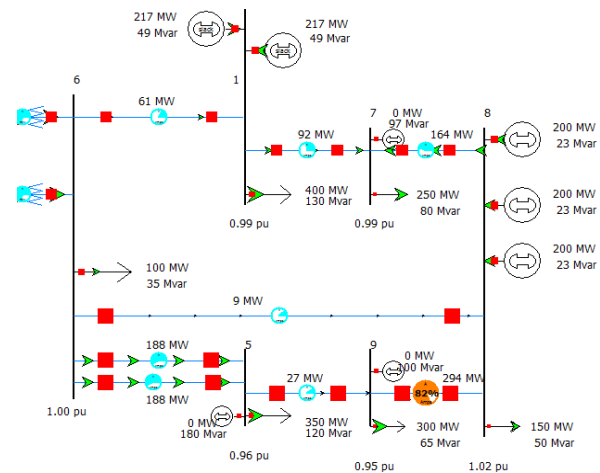


Figure 3. Increasing the real power demand at bus 9 shows redispatch of all generation units, also substantially lowering the pu voltage at buses 5 and 9

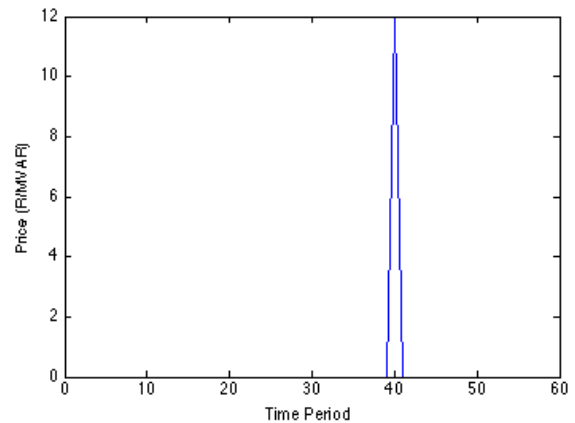


Figure 4. Reactive power nodal prices for bus 5 under a contingency at period 40

Bidding Strategy for Wind Generation Considering Conventional Generation and Transmission Constraints

Hao Huang and Fangxing Li

EECS Department of The University of Tennessee, Knoxville, TN 37909

Email: hhuang11@utk.edu and fli6@utk.edu

Abstract- This paper develops bidding models under two schemes for variable wind generation to analyze the competition among generation companies (GENCOs) with transmission constraints considered. The proposed method employs the supply function equilibrium (SFE) for modeling a GENCO's bidding strategy. The bidding process is solved as a bi-level optimization problem. In the upper level, individual GENCO's profit is maximized; while in the lower level, the market clearing process at the independent system operator (ISO) is modeled to minimize the production cost. An intelligent search based on Genetic Algorithm (GA) and Monte Carlo simulation (MCS) is applied to obtain the solution. The PJM five-bus system and the IEEE 118-bus system are used for numerical studies. The results show when wind GENCOs play as strategic bidders to set the price, they can make significant profit uplifts as opposed to playing as a price taker, because the profit gain will outweigh the cost to cover wind uncertainty and reliability issues. However, this may lead to increased total production cost and other units' profit, which means consumers need to pay more. Thus, an update of the existing market architecture and structure considering these pros and cons is necessary to maintain a healthy competitive market.

I. KEY EQUATIONS

Wind generation as a bidder

if it is a conventional GENCO

$$\max_i \text{profit}_i = \max_{i,s} (LMP_{i,s} \cdot G_{i,s} - c_i \cdot G_{i,s}) \quad (1)$$

or if it is a wind GENCO with $G_j > G_{j,s}$

$$\max_j \text{profit}_j = \max_{j,s} \left(\begin{array}{l} LMP_{j,s} \cdot G_{j,s} - c_j \cdot G_{j,s} \\ + LMP_{j,s} (G_{j,s} - G_j) \end{array} \right) \quad (2.a)$$

or if it is a wind GENCO with $G_j < G_{j,s}$

$$\max_j \text{profit}_j = \max_{j,s} (LMP_{j,s} \cdot G_{j,s} - c_j \cdot G_{j,s}) \quad (2.b)$$

$$s.t. \quad b_{i,\min} \leq b_{i,s} \leq b_{i,\max}, \quad b_{j,\min} \leq b_{j,s} \leq b_{j,\max} \quad (3)$$

$$\min \sum_{i=1}^M b_{i,s} \cdot c_i \cdot G_{i,s} + \sum_{j=M+1}^T b_{j,s} \cdot c_j \cdot G_{j,s} \quad (4)$$

$$s.t. \quad \sum_{l=1}^n G_l = \sum_{l=1}^n D_l \quad (5)$$

$$G_{i,\min} \leq G_{i,s} \leq G_{i,\max}, \quad G_{j,\min} \leq G_{j,s} \leq G_{j,\max} \quad (6)$$

$$\sum_{l=1}^n GSF_{k-l} \cdot (G_l - D_l) \leq \text{Limit}_k \quad (7)$$

for $k=1,2,\dots,m$ and all s .

II. KEY ALGORITHM

a. For wind GENCO Scheme I:

- 1) System initialization:

- 2) Suppose bidding strategies of opponents' generator are fixed. Update conventional GENCO i 's bidding strategies until no unit will change its bidding strategy, while the current biological generation number is less than the maximum generation number.
- 3) $i=i+1$ and repeat 2) to find each conventional GENCO's optimal bidding strategies in response to the opponents' bidding strategies.
- 4) Go to 2) and repeat the procedure until no generator would change its bidding strategy, i.e., no one can gain more by unilaterally changing its bidding strategy.

b. For wind GENCO Scheme II:

- 1) Similar to *a.1*), add initialization for all $b_{j,s}$ for all wind GENCOs and set $j=M+1$ and the biological generation counter to zero.
- 2) The same as *a.2*) and *a.3*)
- 3) Similar to *a.2*), change the index from conventional GENCO i to wind GENCO j .
- 4) $j=j+1$ and repeat 4) to find each wind GENCO's optimal bidding strategies in response to the opponents' bidding strategies.
- 5) Go to 2) and repeat the procedure until no generator would change its bidding strategy, i.e., no one can gain more by unilaterally changing its bidding strategy.

III. KEY RESULTS

A. PJM five bus system

1) Scheme I - Wind generation as a constraint

TABLE III PROFIT GENERATION AND PRICE EXPECTATION FOR EACH GENERATOR

Generator	Alta	Park City	Solitude	Sundance	Brighton
Expected profit(\$)	1129	0	0	0	1664
Expected Output(MW)	100	0	212.82	0	587.19
Expected Price(\$/MW)	18.78	18.78	30	38.56	12.77

2) Scheme II - Wind generation as a bidder

TABLE IV PROFIT GENERATION AND PRICE EXPECTATION FOR EACH GENERATOR

Generator	Alta	Park City	Solitude	Sundance	Brighton
Expected profit(\$)	1893.80	0	0	0	9593.3
Expected Output(MW)	69.84	0	238.38	0	591.77
Expected Price(\$/MW)	27.39	27.39	30	31.99	25.99

Smart Location Targeting for Power Flow Control Devices via Shadow Price Weighting

Omar A. Urquidez*, Le Xie*

*Department of Electrical and Computer Engineering, Texas A&M University, College Station, TX
USA

Email:dantes92@tamu.edu, Lxie@ece.tamu.edu

Abstract— Grid systems across the nation are reaching an epidemic of congestion related issues. The US Department of Energy completed the National Electric Transmission Study in 2006, 2009 & 2012 concerning the impacts of electrical congestion. Conclusions suggest that relief of congestion will aid in more even pricing in the wholesale markets and significant relief of curtailment on renewable resources such as wind power generated behind barriers of transmission congestion. Our previous work investigated conversion of AC lines to DC lines in congestion corridors to decrease system dispatch costs. The results showed significant savings when applied to a 24 bus ERCOT equivalent system.

In this paper a method of Smart Location Targeting is developed to select the prime location for power flow control in a meshed network that best reduces dispatch cost using existing historical data without heuristic searching. This method combines a well-developed concept of linear power flow approximation with a new way of looking at power flow control as an injection-extraction pair. This produces what has been termed as flexible line system capacity (FLSC). The FLSC is then weighted by historical shadow price data for each line in the system to approximate reduction in cost via the flexibility. The use of a distribution of historical data as a means of weighting also allows for incorporation of diurnal & seasonal influences on congestion patterns.

Flow control that utilizes existing transmission infrastructure is especially beneficial in systems with high renewable penetration. The better utilization of existing infrastructure will serve as a low cost way to transition convention power systems to green energy systems. Numerical tests using Smart Location Targeting and Exhaustive Search are performed on a 24 bus system ERCOT equivalent model. The comparison shows promising results.

I. KEY EQUATIONS

$$B = \text{imag}(Y_{Bus}) \quad (1)$$

$$B \xrightarrow{\text{slack_reduced}} B_R \quad (2)$$

$$B_{Branch} = \text{diag}(s) \quad (3)$$

$$H = B_{branch} \cdot A^T \cdot B_R^{-1} \quad (4)$$

$$F = H \cdot P \quad (5)$$

$$P_{INJ} = \begin{bmatrix} 0 \\ P_I \\ 0 \\ 0 \\ 0 \end{bmatrix}, P_{EXT} = \begin{bmatrix} 0 \\ 0 \\ P_E \\ 0 \\ 0 \end{bmatrix}, \text{ where } P_I = -P_E \quad (6)$$

$$\Delta F_f = H \cdot (P_{INJ} + P_{EXT}) \quad (7)$$

$$\Delta C_{tot} = \mu \cdot \Delta F_f \quad (8)$$

$$\Delta F_F = H \cdot P_{L_P} \text{ where, } P_{L_P} = A \quad (9)$$

$$\Delta C_{TOT} = \mu \cdot \Delta F_F \quad (10)$$

II. KEY FIGURES

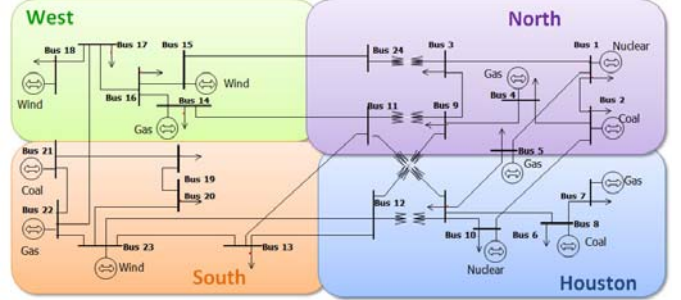


Figure 1. ERCOT Model System modified from IEEE RTS 24.

III. KEY RESULTS

TOP TEN FLOW CONTROL CANDIDATES

Smart Location Targeting		Exhaustive Search		
Rank	Line	Dispatch Savings (\$/day)	Line	Dispatch Savings (\$/day)
1	17	5,351	17	5,045
2	15	3,566	14	3,432
3	14	3,432	15	3,337
4	27	3,000	27	3,000
5	5	2,324	5	2,324
6	9	2,272	9	2,272
7	18	1,796	18	1,568
8	19	1,329	19	1,329
9	21	908	21	908
10	13	620	13	597

Participation Model for Small Customers with Reliability Preference in Electricity Market

Zhongwei Jake Zhang, *Graduate Student Member, IEEE*, and Nirmal-Kumar C Nair, *Senior Member, IEEE*
 Electrical & Computer Engineering, University of Auckland, New Zealand
 Email: zzha115@aucklanduni.ac.nz and ncnaair@ieee.org

Abstract—Demand-side Participation by small customers is more complicated than large electricity customers because of current supporting infrastructure, regulatory concern and conventional business model. A pricing and load dispatch model is proposed to utilize the savings from Demand Dispatch to compensate for the reliability cost of load control. A concept of Reliability Premium is proposed, through which customers can express their different levels of reliability preference and adjust the network tariff payments accordingly. It also gives indication of their willingness to reduce consumption through Demand Dispatch. The pricing and load dispatch in the participation model help small customers easily participate in Demand Dispatch based on their unique levels of reliability preference. The participation model integrates both wholesale and retail markets, which serves as a complementary tool for system operator, retailers, aggregators, distributors and planners to engage small customers.

I. KEY EQUATIONS

To differentiate customer reliability preference, it is proposed that a Reliability Premium (RP) can be charged in addition to the minimum network charge.

$$RP_{m,n} = (IP_{m,n} + DP_{m,n} \times r) \times \lambda \quad (1)$$

$$RDC_{m,n} = IC + RP_{m,n} \quad (2)$$

The RP based load dispatch in the participation model has the objective function to maximize the net benefit, NB , for the combined entity of energy retailers and distribution network companies.

$$NB = WS1 + WS2 - TPC \quad (3)$$

$$WS1 = \sum L_{m,n} \times K_{m,n} \times (P_{prs} - P_{ret}) \quad (4)$$

$$WS2 = \sum L_{m,n} \times (1 - K_{m,n}) \times (P_{nrs} - P_{prs}) \quad (5)$$

$$TPC = \sum (DP_{m,n} + L_{m,n} \times VoLL) \times K_{m,n} \quad (6)$$

The first constraint considers the strict compliance requirement that is similar as the dispatch instruction of the generators.

$$L_{dd} = \sum L_{m,n} \times K_{m,n} \quad (7)$$

The second constraint imposes the limit on the allowed hours of load interruption every year for each customer load or device.

$$T_{m,n} + \frac{K_{m,n}}{2} + \lambda_m \times r_m < T \quad (8)$$

II. KEY FIGURES

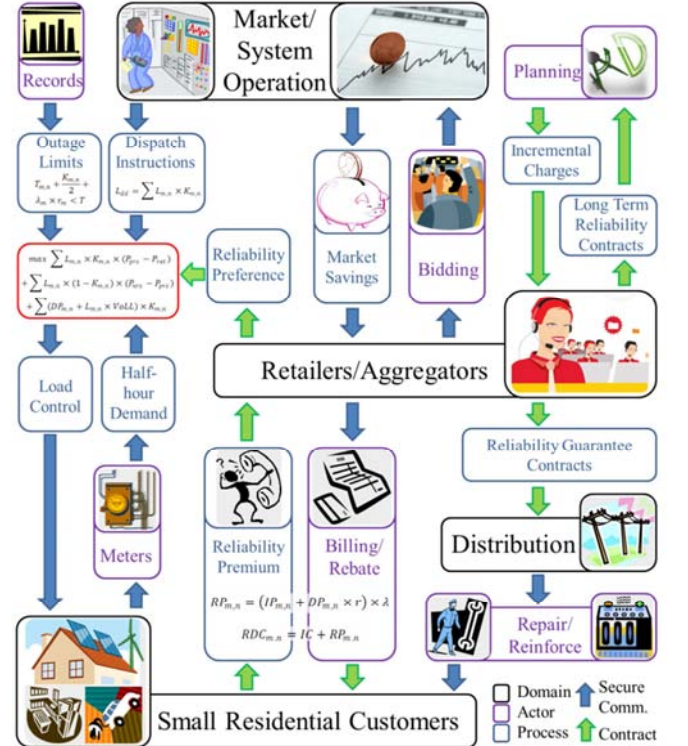


Figure 1. The pricing and load dispatch processes in the participation model

An Integrated Transmission and Distribution Systems Model with Distribution-based LMP (DLMP) Pricing

Nikita G. Singhal, *Student Member, IEEE*, Oluwaseyi Akinbode, *Student Member, IEEE*, and Kory W. Hedman, *Member, IEEE*

School of Electrical, Computer, and Energy Engineering, Arizona State University, Tempe, AZ 85287, USA
 Email: nsinghal@asu.edu, oakinbod@asu.edu, and kory.hedman@asu.edu

Abstract— The distribution grid is expected to change in the near future as a result of recent advancements in the field of smart grids. The future grid will accommodate all generation and storage options, active consumer participation through demand response schemes, and the widespread installation of smart energy management systems. With more demand side participation, distributed generators, and (potentially) meshed distribution systems, there is a push to integrate transmission and distribution systems models together. Ideally, the transmission and distribution systems should be modeled by an integrated optimal power flow (OPF) framework and solved simultaneously to schedule the generation and demand in the entire system. In comparison, existing practices do not include the distribution system when solving the OPF for the transmission system; instead, the load is estimated and placed at the connection point at the sub-transmission level. However, integrating transmission and distribution system models together is a challenge for OPF due to the size of the system, which makes these problems computationally intractable with existing technologies.

Prior work has examined applying the concept of locational marginal pricing to the distribution system, which is referred to as a Distribution based LMP, or DLMP. The goal of developing and applying a DLMP is to incentivize the loads and distributed resources in the distribution system to schedule their assets efficiently. However, prior work has primarily focused on a one-shot approach: first, the traditional transmission system OPF framework is solved (where each distribution system is modeled as a single, equivalent bus with one load) and then a distribution system model is solved (without the transmission system being modeled) to produce the DLMPs. However, this prior work does not examine the integration of transmission and distribution systems.

This project proposes an iterative approach to integrate the transmission and distribution systems together. The integrated OPF problem is decomposed into two subsequent OPF problems: the transmission OPF and the distribution OPF. The distribution system model incorporates characteristics of the distribution system resources (distributed generation, demand curves, etc.) and determines the appropriate DLMP in order to incentivize efficient scheduling of the resources. Instead of using a one-shot approach where the transmission system modeled is solved only once, we resolve the transmission system with an updated residual demand curve. The distribution system is modeled by its aggregate demand curve in the transmission system OPF while the

transmission system is modeled by a transmission constrained residual supply curve in the distribution system OPF. This process is repeated until the cleared demands are the same between the transmission system and distribution system models.

This iterative technique achieves optimal coupling between the two sub-systems by ensuring that the flexible demand and distributed resources are appropriately represented in the transmission OPF through residual demand curves, which are updated based on the utilization of a DLMP pricing structure. By doing so, we can improve the economic efficiency and the system reliability as the distribution resources can be controlled to behave in a way that benefits the power system as a whole. Ongoing work is focused on developing a technique to obtain transmission constrained residual supply curves at the individual distribution connection points.

I. METHODOLOGY

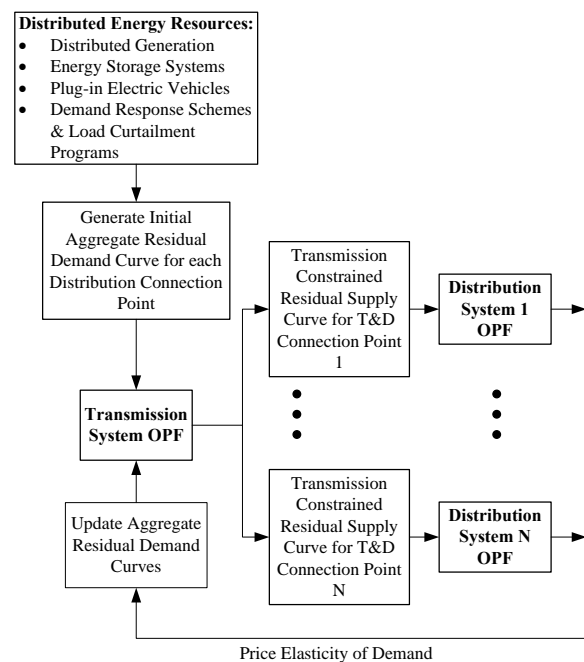


Fig. 1. An integrated transmission and distribution systems model with DLMP pricing.

Hedging Decision of an Electricity Generating Firm with Market Power

Ekaterina Moiseeva and Mohammad R. Hesamzadeh

Electricity Market Research Group, KTH - Royal Institute of Technology, Stockholm, Sweden

Email: moiseeva@kth.se

Abstract—The electricity market structure aims to provide the effective competition among producers and consumer-beneficial pricing for the electricity. However, the exercise of market power affects considerably the prices and induces the wealth transfer from consumers to generators. It is widely recognized that the incentive of generator to exercise market power depends on its hedging decision. The hedged generator, i.e., with high volume of capacity pre-sold to the forward markets, has very little or no tendency to exercise market power. Existing approaches for forecasting market power typically take the hedge cover level as an external input to the model, providing an open-loop analysis. In practice, the level of hedge is chosen by a generating firm and treated confidentially. We model a two-stage game, where in the first stage the generator decides on the profit-maximizing level of hedging and in the second stage is taking part in Cournot game, deciding on the amount of output sold in the spot market. We show that in the oligopoly case with no constraints on installed capacity and transmission limits there is no equilibrium in pure strategies, which corresponds to the "all or nothing" decision. In the case, when transmission and capacity constraints are binding, we use backward induction approach and close-loop analysis to find subgame perfect Nash equilibrium (SPNE) on the level of hedging and corresponding SPNE in spot market.

I. KEY EQUATIONS

We begin with the case of n generators and not binding capacity and transmission limits. The generator i will choose the maximum level of hedging x_i^{max} , if the expected profit $E\pi_i(x_i^{max}, X_{-i})$ is greater than the expected profit $E\pi_i(x_i^{min}, X_{-i})$ in the case of minimal hedging level x_i^{min} . This happens if the markup of forward price f over the costs of generator c is greater than the markup of average spot market prices, which arise in case of maximum and minimum hedging level p_i^{max} , p_i^{min} :

$$E\pi_i(x_i^{max}, X_{-i}) > E\pi_i(x_i^{min}, X_{-i}) \Leftrightarrow \\ \Leftrightarrow f - c > \frac{(p_i^{max} - c) + (p_i^{min} - c)}{n + 1}$$

There is no equilibrium in which traders expect the firm to choose the minimum level of hedging and, similarly, there is no equilibrium in which traders assume the contrary. In other words, there is no rational expectations equilibrium in pure strategies.

In the second case we consider transmission and capacity limits. The common approach for constrained bi-level games is to take the hedge cover level as an input parameter. This is also called open-loop analysis. Instead, we use close-loop analysis to solve the equilibrium problem with equilibrium

constraints (EPEC):

$$\begin{aligned} & \underset{q_i}{\text{maximize}} && \pi_i(q_i) \\ & \underset{x_i}{\text{maximize}} && \pi_i(x_i) \\ & \text{subject to} && \text{capacity and transmission limits} \\ & && \text{energy balance equation} \end{aligned}$$

We derive the SPNE in spot market and iteratively obtain the equilibrium for the forward market by applying backward induction analysis.

II. KEY FIGURE

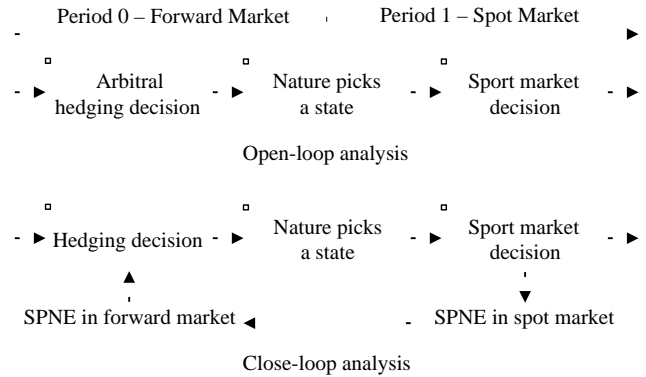


Fig. 1: Comparison of open and close loop types of bi-level game analysis

III. KEY RESULTS

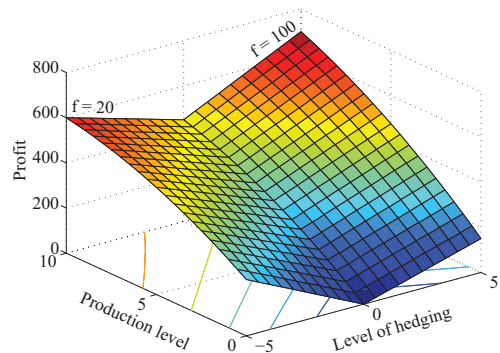


Fig. 2: All or nothing decision. Profit function dependent on the level of hedging and production in the case of $f = 20$ and $f = 100$

Short-Term Electricity Price Forecasting

A. Arabali, E. Chalko, *Student Members IEEE*, M. Etezadi-Amoli, *LSM, IEEE*, M. S. Fadali, *SM IEEE*

Abstract— Price forecasting has become an important tool in the planning and operation of restructured power systems. This paper develops a new short-term electricity price forecasting scheme based on a state space model of the power market. A Gauss-Markov process is used to represent the stochastic dynamics of the electricity market. Kalman and H_∞ filters, two methods based on the state space model, are applied in order to estimate the electricity price and compare the quality of their state estimates. Our results show that performance measures for the H_∞ filter are generally superior to those for the standard Kalman filter.

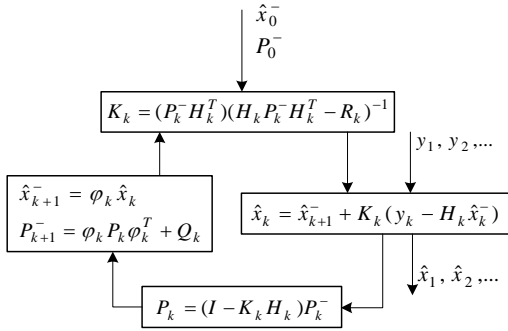


Fig.2. Flowchart of the Kalman filter.

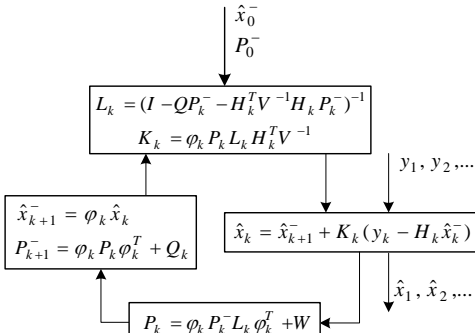


Fig.3. Flowchart of the H_∞ filter.

Table I: Performance measure for the Kalman and H_∞ filter.

Method	MAE (%)	RMSE
Kalman filter (for a day)	0.1021	5.7787
H_∞ filter (for a day)	0.0592	3.3505
Kalman filter (for a week)	0.1353	12.9476
H_∞ filter (for a week)	0.0754	7.4677

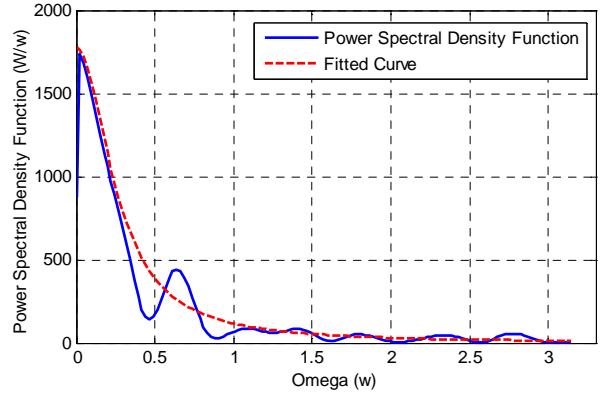


Fig.4. Power Spectral density function and fitted curve.

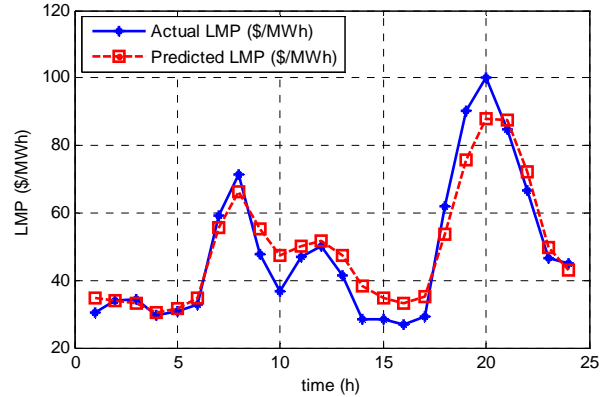


Fig.5. Actual vs. predicted LMP using Kalman filter for a specific day.

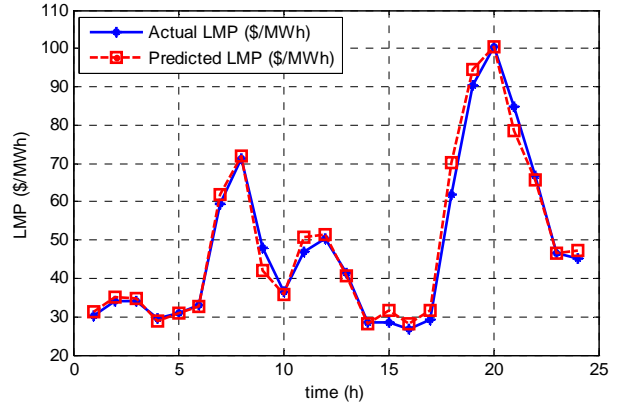


Fig.7. Actual vs. predicted LMP using H_∞ filter for a specific day.

Stability Analysis of an Energy Managed Smart Distribution System

Jesse M. Boyd, *Student Member, IEEE*, Gerald T Heydt, *Life Fellow, IEEE*

Department of Electrical, Computer and Energy Engineering
Arizona State University
Tempe, AZ, U.S.A

Email: {jesse.m.boyd}, {heydt} @asu.edu

Abstract— The Future Renewable Electric Energy Distribution Management (FREEDM) center focuses on a semiconductor switched, smart distribution energy management system. In this paper, a proposed energy management system is modeled and analyzed. Discrete modeling in the z -domain is used in view of the communication and computation that is envisioned. A basic pricing signal, denominated the distribution locational marginal price, is used as a control signal. The study includes stability analysis, typical system response, and communication bandwidth requirements.

Index Terms—FREEDM system, distribution engineering, energy management, smart grid, z -transform, stability, demand response, elasticity.

I. KEY FIGURES

The model of Fig. 1 shows the basic idea of using *price* as a control signal in demand response. A key parameter in this diagram is the feedback gain B .

II. KEY EQUATIONS

The price elasticity of electric demand is formulated

$$E = \left(\frac{\Delta L}{L_0}\right) \left(\frac{LMP_0}{\Delta LMP}\right) \quad (1)$$

In the z domain the elasticity is made up of two components, self- and cross-elasticity

$$E(z) = SE + \sum_{n=1}^{N-1} CE_n z^{-n}. \quad (2)$$

The demand response of the load to the price can be modeled using the elasticity values

$$\Delta L_i = L_{0,i} SE_{i,i} \frac{\Delta LMP_i}{LMP_i} + \sum_{j=1}^{j < i} L_i CE_{i,j} \frac{\Delta LMP_j}{LMP_j}. \quad (3)$$

The load response can also be put into the z domain

$$\Delta L(z) = L_0 \frac{DLMP(z) - TLMP(z)}{TLMP} E(z). \quad (4)$$

A system composed of a price control signal and load response can thus be analyzed with a z domain transfer function

$$H(z) = Z\{h(nT)\} = \frac{\Delta L(z)}{d(z)} \quad (5)$$

III. KEY RESULTS

The stability of the system was determined by evaluating the z domain pole locations while ‘sweeping’ the feedback gain, as shown in Fig. 2. A pole location $|z| < 1$ indicates bounded input, bounded output stability.

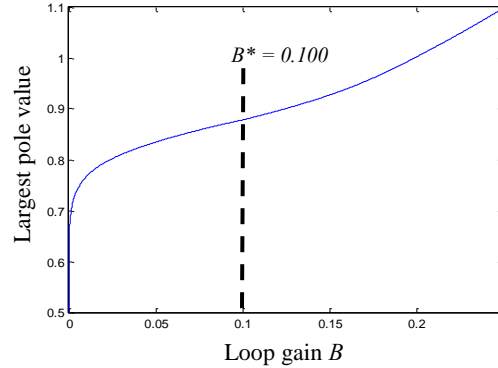


Fig. 2 The values of $\max_i |p_i|$ versus loop gain B

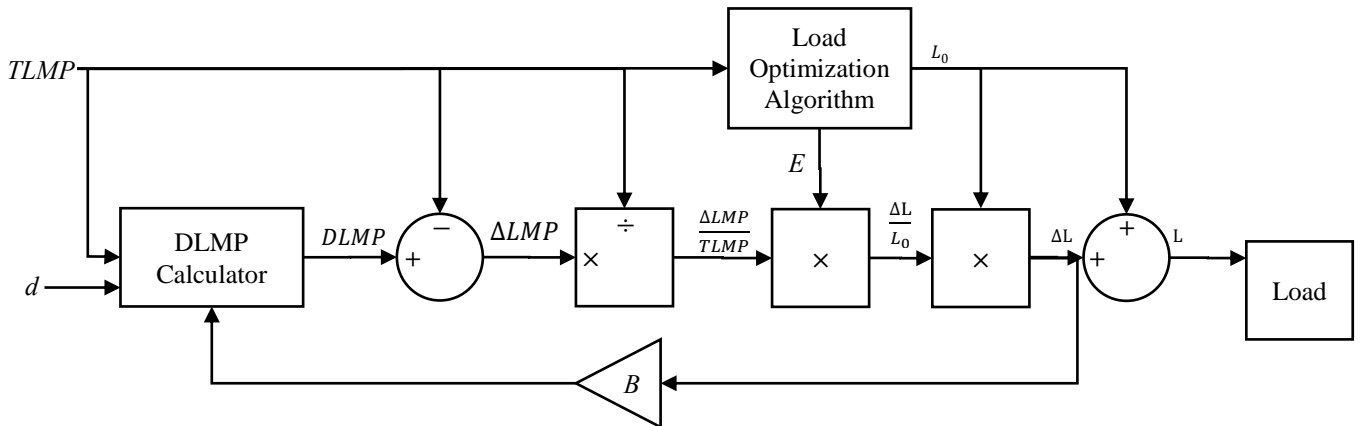


Fig. 1 Distribution energy management system functional block diagram

Sensitivity Analysis of Real-Time Locational Marginal Price to SCADA Sensor Data Corruption

Dae-Hyun Choi, *Student Member, IEEE*, and Le Xie, *Member, IEEE*

Abstract—This paper examines the impact of SCADA data corruption on real-time locational marginal price (LMP) in electricity markets. We present an analytical framework to quantify LMP sensitivity with respect to changes in sensor data. This framework consists of a unified LMP sensitivity matrix subject to sensor data corruption. This sensitivity matrix reflects a coupling among the sensor data, an estimation of the power system states, and the real-time LMP. The proposed framework offers system operators an *online* tool to: 1) quantify the impact of corrupted data at any sensor on LMP variations at any bus; 2) identify buses with LMPs highly sensitive to data corruption; and 3) find sensors that impact LMP changes significantly and influentially. It also allows system operators to evaluate the impact of SCADA data accuracy on real-time LMP. The results of the proposed sensitivity based analysis are illustrated and verified with IEEE 14-bus and 118-bus systems with both Ex-ante and Ex-post real-time pricing models.

Index Terms—State estimation, SCADA, power market, economic dispatch, locational marginal price, sensitivity analysis.

I. INTRODUCTION

STATE estimation is one of the key applications for power system energy management systems (EMSs). The impact of bad data on power systems has been intensively investigated in recent decades in power system state estimation literature. Measurement noise and/or manipulated sensor errors in a supervisory control and data acquisition (SCADA) system may mislead system operators about real-time conditions in a power system, which in turn may impact the price signals in real-time power markets. This paper attempts to provide a novel analytical framework with which to investigate the impact of bad sensor data on electric *power market* operations. In future power system operations, which will probably involve many more sensors, the impact of sensor data quality on grid operations will become increasingly important.

Locational marginal price (LMP) is the core variable in market operations. In real-time power markets, LMP is obtained as the by-product of security constrained economic dispatch (SCED) in either of the two main pricing models: Ex-ante (e.g. in ERCOT, NY ISO) and Ex-post (e.g. in ISO New England, PJM, and Midwest ISO). Both pricing models are built on the power flow and network topology results given by the state estimator, which uses two types of sensor data: 1) analog (e.g., the power injection/flow and voltage magnitude); and 2) digital (e.g., the on/off status of a circuit breaker). In this paper, we focus on a sensitivity analysis of real-time LMP subject to corrupted *analog* data fed into the state estimator. Fig. 1 illustrates that via state estimation, SCADA measurement z may impact the results of a pair of Ex-ante nodal price and

optimal generation dispatch $\{(\hat{x}_A(z)), P_g^*(\hat{x}_A(z))\}$ and the Ex-post price $(\hat{x}_P(z))$.

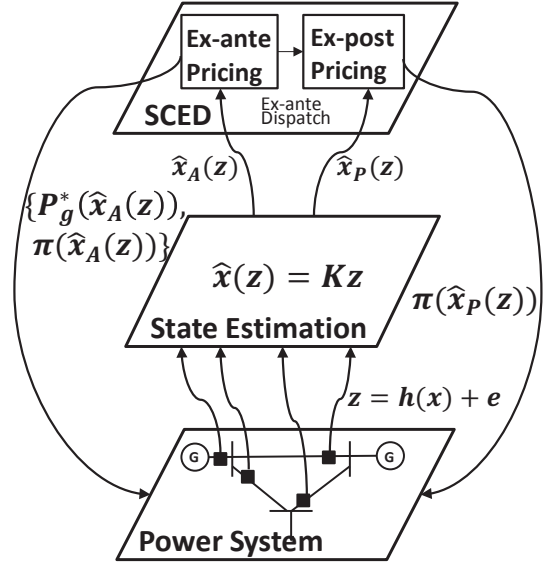


Fig. 1. A three-layered framework illustrating the coupling of the physical power system, state estimation, and SCED.

Our paper is motivated by a desire to study the effect of data corruption on LMP via *state estimation*. In particular, this paper provides an analytical framework for answering the following questions:

- 1) How much does LMP change at every bus given a set of SCADA measurements with corrupted data?
- 2) What is the impact of data accuracy on LMP sensitivity at each bus?

Here, data corruption refers to both natural noise and man-made attacks.

The novelty aspect of this paper is that it provides system operators with an analytical tool for assessing the financial risks of bad/malicious data in light of secure market operations. To this end, a unified LMP sensitivity matrix subject to data corruption is developed, describing the coupling between LMP, the estimation of power system states, and the sensor data. This matrix offers system operators an *online* tool to: 1) quantify the impact of corrupted data at any sensor on LMP variation at any bus; 2) identify buses with LMP highly sensitive to data corruption; 3) find significant and influential sensors with regards to LMP change; and 4) study the effect of data accuracy on LMP sensitivity.

Transformer less Intelligent Power Substation for 13.8 kV/480 V Grid Interface Applications

Sachin Madhusoodhanan, Subhashish Bhattacharya

FREEDM Systems Center, Department of Electrical and Computer Engineering, North Carolina State University, Raleigh, NC 27606, USA

Email: sachin@ncsu.edu

Abstract – There is a need for a 3-phase interface at the substations between the 13.8 kV distribution grid and the 480 V utility grid for controlling the power flow. Traditionally the line frequency transformers have been used for this purpose which has certain limitations. They are bulky in size and weight. They don't have a provision for improving the quality of power drawn from the grid. They only allow unidirectional power flow. They have improper voltage regulation and offer lesser flexibility in control. So an alternative is needed to replace these conventional transformers. What is being proposed in this study is to replace these transformers with SiC semiconductor devices based 3-phase Solid State Transformer called Transformer less Intelligent Power Substation (TIPS). Concept of solid state transformers has been developed sometime back. But because of unavailability of Silicon based semiconductor devices which can block such a high level of voltage, it never got materialized. Recently, with the development of Silicon Carbide (SiC) based devices with higher voltage blocking capability of up to 15kV, this is feasible. TIPS, rated at 1 MVA acts as an interface between the 13.8 kV and 480 V grids and is based on newly developed 15kV SiC-IGBT and 1200 V SiC-MOSFET. It has 3 power transfer stages: The input stage or the Front End Rectifier (FEC) stage composed of a 3-Level Neutral Point Clamped converter (3L-NPC), the isolation stage composed of a Dual Active Bridge (DAB) and the output stage composed of 2-Level converters. FEC, DAB and 2-level converter operates at 3 kHz, 10 kHz and 17 kHz switching frequencies respectively. The high frequency Pulse Width Modulation based switching of these devices offers a considerable reduction in size and weight. These switching devices offer a greater flexibility in control. This results in a topology with bidirectional power flow capability. Through control of these devices it is possible to maintain unity power factor at the grid, thus improving the power quality. Also it will be possible to improve the grid voltage profile under necessary conditions such as fault, voltage sag etc. through reactive power compensation. All these features are achievable at efficiency very close to that of the conventional transformers.

I. KEY FIGURES

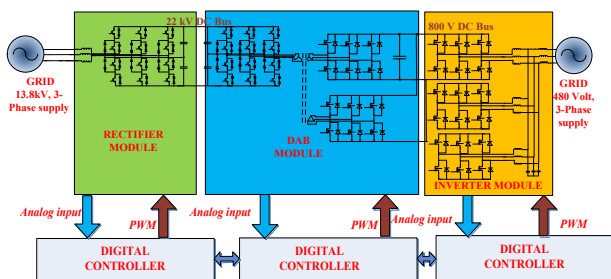


Figure 1: Block diagram of TIPS

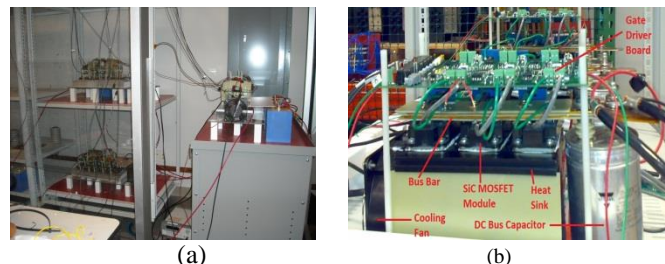


Figure 2: (a) 15 kV/ 20A SiC IGBT based FEC and (b) 1200V/ 100A SiC MOSFET based 2-level converter of TIPS developed at FREEDM Systems Center

II. KEY RESULTS

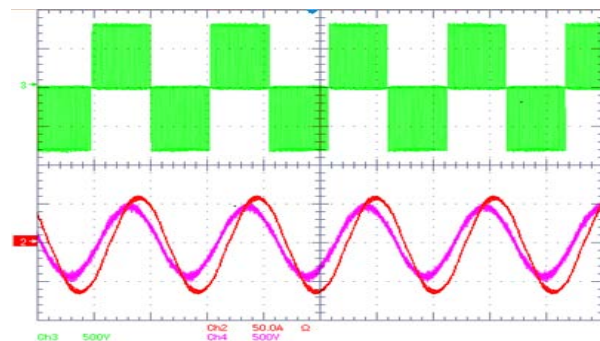


Figure 3: SiC MOSFET 2L-VSC test results at 35 kVA, 800 V dc bus, 20 kHz switching frequency; Ch2 – Line current, Ch3 – Line voltage before filter, Ch4- Line voltage after filter (Current: 50A/div, Voltage: 500V/div, Time:8ms/div)

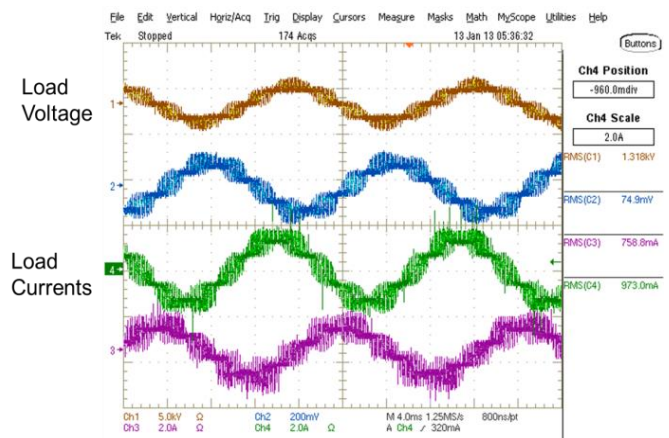


Figure 4: Experimental results for the 3-level converter at 3 kV dc bus and 10 kHz switching frequency in inverter mode and open loop (Ch1: line voltage; Ch2 (0.1 V/A), Ch3 and Ch4: phase currents)

Low Cross Regulation SIMO DC/DC Converter with Model Predictive Voltage Control

B. F. Wang, *Student Member, IEEE*, K. T. Tan, *Student Member, IEEE*, P. L. So, *Senior Member, IEEE*

School of Electrical and Electronic Engineering
Nanyang Technological University
Singapore 639798
Email: eplso@ntu.edu.sg

Abstract—This paper presents a model predictive voltage control method for single-inductor multiple-output (SIMO) DC/DC converters operating in the continuous conduction mode (CCM). The state-space model for a SIMO DC/DC converter system is formulated and a Model Predictive Control (MPC) strategy, which has the capability to track the reference voltage automatically and reduce the impact of cross regulation problem, is proposed to regulate the system. Considering that the switches in the converter only have ON/OFF modes, the quadratic programming algorithm is employed to obtain the MPC's solution. Simulation studies are conducted in MATLAB/Simulink to verify the performance of the proposed method.

I. KEY EQUATIONS

$$\begin{aligned} \mathbf{x}(k+1) &= \bar{\mathbf{A}}\mathbf{x}(k) + \bar{\mathbf{B}}S(k) \\ \mathbf{y}(k) &= \mathbf{C}\mathbf{x}(k) \end{aligned} \quad (1)$$

where

$$\begin{aligned} \mathbf{x}(k) &= [I_L(k) \quad V_C(k) \quad I_R(k)]^T \\ \bar{\mathbf{A}} &= \begin{bmatrix} 1 & -T_S/L & 0 \\ T_S/C & 1 & -T_S/C \\ 0 & 0 & 1 \end{bmatrix} \\ \bar{\mathbf{B}} &= [T_S V_{in}/L \quad 0 \quad 0]^T \\ \mathbf{C} &= [0 \quad 1 \quad 0]^T \\ J &= \sum_{i=N}^{N+N_p} [y(k+i) - r(k+i)]^2 + \lambda \sum_{i=1}^{N_c} [\Delta S(k+i-1)]^2 \end{aligned} \quad (2)$$

II. KEY FIGURES

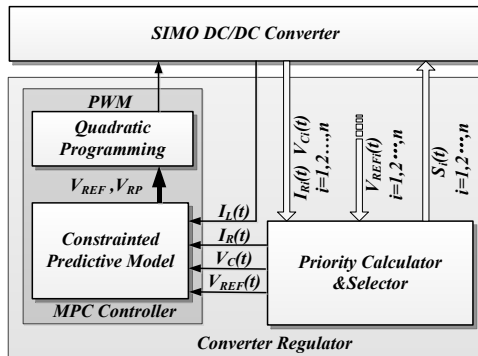


Figure 1. System architecture of MPC for SIMO converter

III. KEY RESULTS

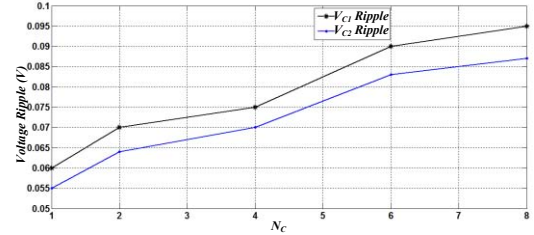


Figure 2. Voltage ripple vs. control horizon N_c

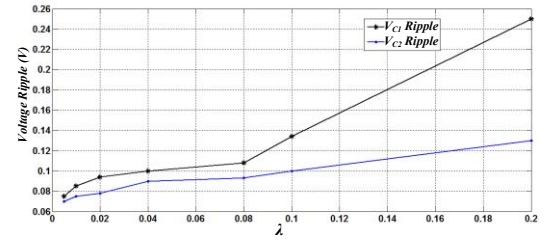


Figure 3. Voltage ripple vs. Lagrange multiplier λ

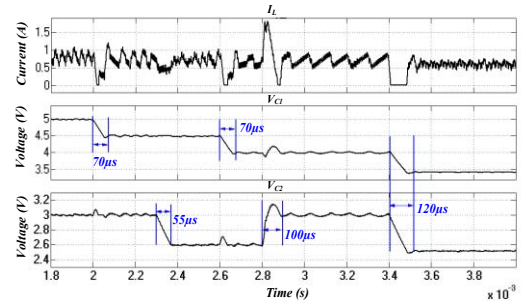


Figure 4. Transient responses to reference variations of MPC

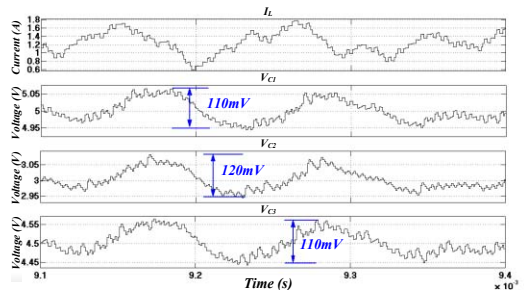


Figure 5. MPC for a SIMO DC/DC buck converter results with load conditions: $I_{R1}=500\text{mA}$, $I_{R2}=300\text{mA}$ and $I_{R3}=450\text{mA}$.

On the Effects of Unbalances, Harmonics and Interharmonics on PLL Systems

L. Feola, *Student Member, IEEE*, R. Langella, *Senior Member, IEEE* and A. Testa, *Fellow, IEEE*

Department of Industrial and Information Engineering – Second University of Naples, DIII-SUN, Aversa (CE) - Italy
E-mail: luigi.feola@unina2.it; roberto.langella@unina2.it; alfredo.testa@unina2.it

Abstract— The presence of voltage unbalances, harmonics, and interharmonics superimposed on the fundamental produces a lack of accuracy in phase-locked loop (PLL) systems, which are used on static converters and Power Quality (PQ) measurement instruments. The set points of the control systems of static converters, such as those used by distributed generation systems (DG), active filters (AF), static VAR compensator (SVC), uninterruptible power supply (UPS), etc, may start oscillating. PQ instruments may be affected in terms of lack of accuracy of measured quantities such as RMS value, active and reactive power, etc. In the poster, the cumulative effects of unbalances, harmonics, and interharmonics on PLL systems, based on a synchronous reference frame, are analyzed. An analytical assessment of the phase-angle and frequency errors for three- and mono-phase PLLs in the presence of disturbances is performed to obtain simple analytical formulas.

I. KEY EQUATIONS

The frequency error with a non-ideal input of the three-phase PLL is:

$$\hat{f}(t) - f(t) = E_{\hat{f}}^-(t) + \tilde{E}_{\hat{f}}^+(t) + \tilde{E}_{\hat{f}}^-(t), \quad (1)$$

$$E_{\hat{f}}^- = K_d \cdot \left[V_{\omega_f}^- \cdot \left| G_{\hat{f}}(\Delta\omega_{\omega_f}^-) \right| \sin(\theta^- + \theta + \angle G_{\hat{f}}(\Delta\omega_{\omega_f}^-)) \right], \quad (2)$$

$$\begin{aligned} \tilde{E}_{\hat{f}}^+ = K_d \cdot & \left[\sum_{\substack{h \in H \\ h \neq \omega_f}} V_h^+ \cdot \left| G_{\hat{f}}(\Delta\omega_h^+) \right| \sin(\theta_h^+ - \theta + \angle G_{\hat{f}}(\Delta\omega_h^+)) + \right. \\ & \left. + \sum_{h \in IH} V_{ih}^+ \cdot \left| G_{\hat{f}}(\Delta\omega_{ih}^+) \right| \sin(\theta_{ih}^+ - \theta + \angle G_{\hat{f}}(\Delta\omega_{ih}^+)) \right], \quad (3) \end{aligned}$$

$$\begin{aligned} \tilde{E}_{\hat{f}}^- = K_d \cdot & \left[\sum_{\substack{h \in H \\ h \neq \omega_f}} V_h^- \cdot \left| G_{\hat{f}}(\Delta\omega_h^-) \right| \sin(\theta_h^- + \theta + \angle G_{\hat{f}}(\Delta\omega_h^-)) + \right. \\ & \left. + \sum_{h \in IH} V_{ih}^- \cdot \left| G_{\hat{f}}(\Delta\omega_{ih}^-) \right| \sin(\theta_{ih}^- + \theta + \angle G_{\hat{f}}(\Delta\omega_{ih}^-)) \right], \quad (4) \end{aligned}$$

$$\Delta\omega_h^+ = h\omega_F - \omega, \quad \Delta\omega_h^- = h\omega_F + \omega, \quad (5) \quad (6)$$

$$\Delta\omega_{ih}^+ = ih\omega_F - \omega, \quad \Delta\omega_{ih}^- = ih\omega_F + \omega. \quad (7) \quad (8)$$

where θ and ω are, respectively, phase-angle and angular frequency of the fundamental of the PLL input signal, ω_F is the Fourier fundamental angular frequency, K_d is the gain of the PLL phase detector, $G_{\hat{f}}(s)$ is the transfer function of PLL in non ideal condition, $\theta^{(\cdot)}_h$ ($\theta^{(\cdot)}_{ih}$) and $V^{(\cdot)}_h$ ($V^{(\cdot)}_{ih}$) are, respectively, phase-angle and the amplitude in pu of the fundamental of sequence (\cdot) of general harmonic h (interharmonic ih) component $(\cdot)=+, -$.

II. RESULTS

Same results are reported in Fig. 1 and Fig. 2.

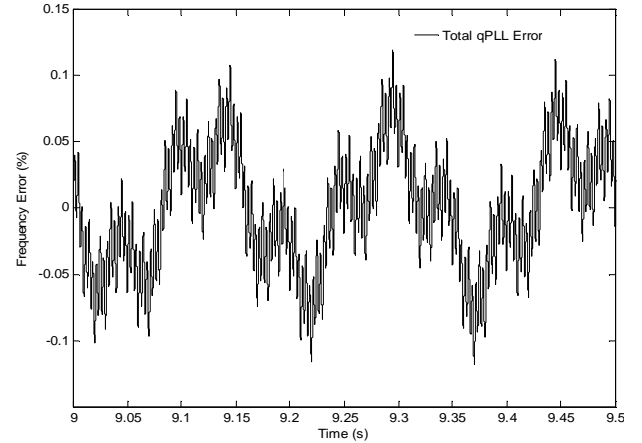


Fig. 1. Three-phase qPLL: frequency error versus the time produced by: an unbalance with amplitude of 2%, a 3rd harmonic of zero sequence with amplitude of 5%, a 5th harmonic of negative sequence with amplitude of 6%, a 7th harmonic of positive sequence with amplitude of 5%, a single three-phase interharmonic tone of positive sequence with amplitude of 1% and frequency of 44Hz and a pairs of symmetric three-phase interharmonic tone of positive sequence producing prevailing phase modulation (PPM) with amplitude of 0.5% and modulation frequency of 20Hz.

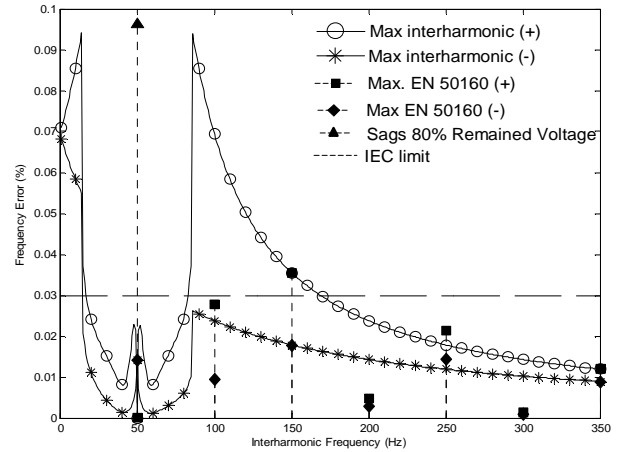


Fig. 2. Three-phase qPLL: max of frequency error versus interharmonic frequency for: interharmonics of positive sequence (circle) and negative sequence (star) with amplitudes equal to maximum limits for LV systems suggested by IEEE 519; 2nd, 3rd, 4th, 5th, 6th, and 7th harmonics of positive sequence (square) and negative sequence (diamond) with amplitudes equal to 2%, 5%, 1%, 6%, 0.5%, and 5%, respectively; single-phase sag with 80% of retained voltage without voltage phase-angle jump (triangle).

Realizing Space Vector Modulation in MATLAB and PSCAD

Yan Ma, Lingling Fan

Department of Electrical Engineering, University of south Florida
Tampa, U.S.

Email: linglingfan@usf.edu

Abstract— Space vector modulation (SVM) is a frequently used method to implement PWM in three-phase switching converters. It allows us not only to simplify the control organization, but also to maximize the exploitation of the converter hardware. This project realizes SVM in MATLAB and PSCAD.

Keywords—Space Vector; MATLAB; PSCAD

I. KEY EQUATIONS

For a typical 3-phase sinusoidal wave, we can represent the 3-phase vectors by one vector as following.

$$V_s = V_a e^{j0} + V_b s^{j\frac{2\pi}{3}} + V_c s^{j\frac{4\pi}{3}}$$

For a 3-phase 2-level inverter, the per phase output voltage can be represented as

$$V_a = q_a \times \frac{V_d}{2}, V_b = q_b \times \frac{V_d}{2}, V_c = q_c \times \frac{V_d}{2}$$

Where q_a , q_b and q_c can be 1 or 0 depends on the active switch is on or off. We can get 8 vectors by function 1 and function 2.

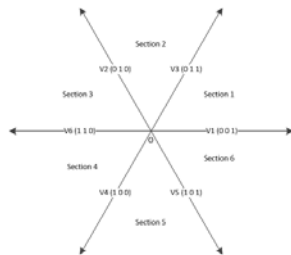


Fig.1 space vector sector

Where V_0 and V_7 are zero vector. In a short time T_s , we can consider space vector as constant. Therefore, every space vector can be determined by

$$V_s = t_a \times V_a + t_b \times V_b + \frac{t_0}{2} \times V_0 + \frac{t_0}{2} \times V_7$$

Where $t_a + t_b + t_0 = T_s$, and V_a, V_b are the two nearest vectors of the sample vector.

II. KEY ALGORITHM

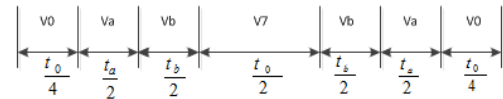
The key algorithm is as:

Step 1: Compute the space vector of the setting 3-phase output voltage. Choose the nearest two vectors as V_a and V_b . For instant, if the space vector is in sector 1, V_1 and V_3 will be choose as V_a and V_b

Step 2: Compute t_a , t_b and t_0 by the space vector of step 1. And set the time sequence as

$$\left[\frac{t_0}{4} \quad \frac{t_a}{2} \quad \frac{t_b}{2} \quad \frac{t_0}{2} \quad \frac{t_b}{2} \quad \frac{t_a}{2} \quad \frac{t_0}{4} \right]$$

Step 3: The output control signal will be



V_0 means 3 switches are all off, while V_7 means they are all on. When space vector is in sector 1, V_a is V_1 means only the active switch of phase a is on, V_b is V_3 means phase a and phase c is on and phase b is off.

III. KEY RESULTS

The result of the system on MATLAB is like following.

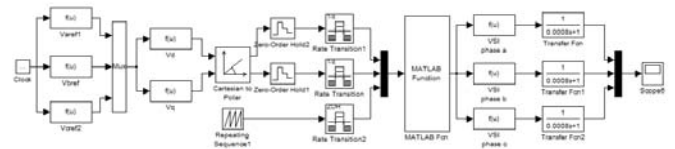


Fig.2 Simulation block in MATLAB

The output voltage after the filter is like the following:

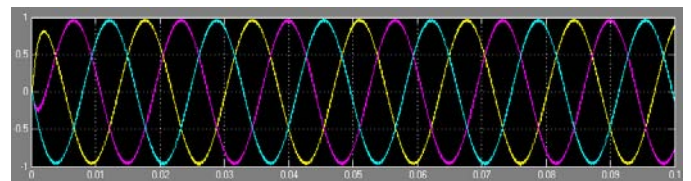


Fig.3 3-phase output voltage after filter in MATLAB

Modeling soft-starter for wind generators in PSCAD

Jen-Pin Lin, Lingling Fan

Department of Electrical Engineering, University of South Florida
Tampa, Florida, United States

Jenpin@mail.usf.edu, linglingfan@usf.edu

Abstract—Soft starter is one effective component in wind generator that can control the inrush current to protect the machine. The experiment is deal with the problem caused by induction machine connected to wind turbines can generate inrush current, which is so big that can hurt equipment, and voltage dropout, which can deteriorate quality of power. This work, design and simulate by using PSCAD/EMTDC, evidences impact of switching operations, especially focus on start-up or the change the generator windings. By controlling the angle of control signal, current gradually reaches to maximum instead of reaching its maximum immediately to destroy components. Application in wind system can adjust current and voltage when wind just rotates the blade or change speed. Since the mechanical parameters defining the performance of the rotor are rarely given by manufactures, a series of simplified wind speeds are put in the experiment to analysis. The performance and the logic control of soft starter gradually connecting to induction generator of the wind turbine to the rotor are also studied.

Keywords—soft starter; wind; generator; induction machine

I. KEY FIGURES

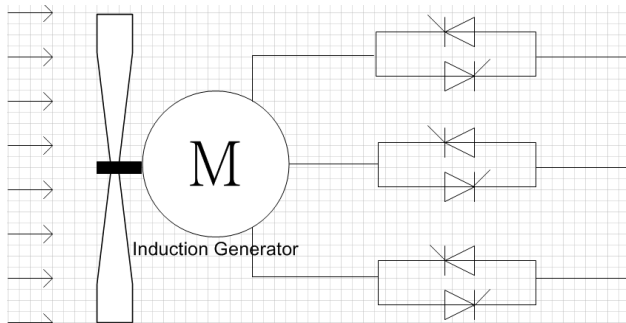


Figure 1. Simplified performance of the soft-starter

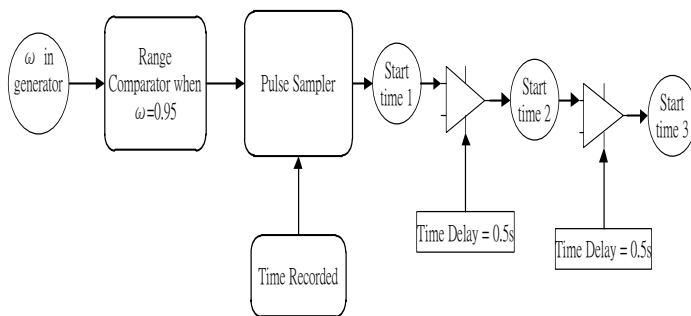


Figure 2. Soft-starter operating point control logic

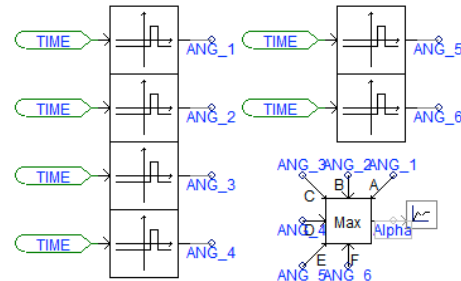


Figure 3. Thyristor firing pulse control circuit

Mixing all firing pulse from time to time to form a complete firing angles.

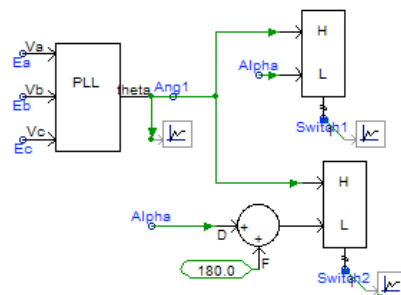


Figure 4. Soft-starter control circuit diagram

PI control first generates ramp signals from 0° to 360° to the input voltages, comparing ramp signals to firing angle order, Alpha, to control switches.

II. KEY RESULTS

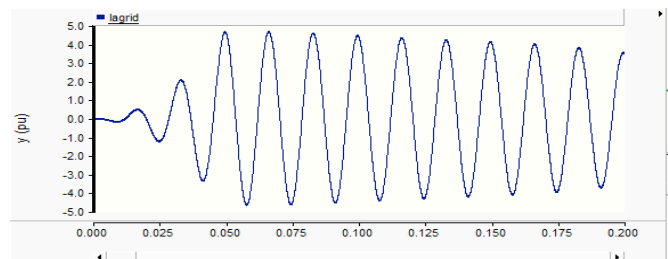


Figure 5. Inrush current before installing soft-starter

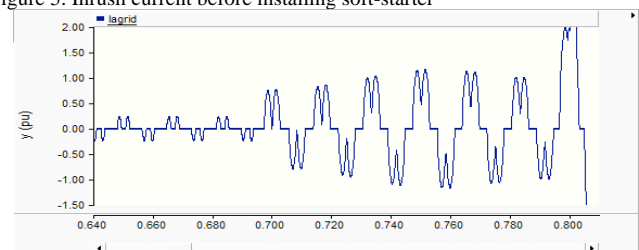


Figure 6. Inrush current improvement after installing soft-starter

Adaptive SRF-PLL with Reconfigurable Controller for Microgrid in Grid-Connected and Stand-Alone Modes

Tarek Youssef, *Graduate Student Member, IEEE*, and Osama A. Mohammed, *Fellow, IEEE*
 Department of Electrical and Computer Engineering, Florida International University,
 Miami, FL 33174, USA

Email: tyous001@fiu.edu , mohammed@fiu.edu

Abstract—Accurate detection of grid voltage phase angle under fault and distorted voltage conditions is essential for distributed generation (DG). Failure to detect supply voltage phase angle accurately will lead to frequency fluctuation, power oscillation and harmonic currents. For Microgrid applications, the synchronization mechanism should be able to detect the frequency drift during islanding mode and provide stable frequency reference for standalone operation. To realize this goal, an adaptive synchronous reference frame phase locked loop (ASRF-PLL) with islanding detection capability is proposed. A reconfigurable inverter controller that supports both grid connected and stand-alone operation modes is also proposed. This provides stable operation under various grid conditions and maintains stable frequency reference during islanding mode. Simulation results were carried out to validate the proposed PLL to synchronise the power converter link between the Microgrid with hybrid generation and the AC Grid. The proposed PLL was implemented using the dSPACE 1103. The experimental results confirm excellent performance of the proposed technique and agree with the simulation results moreover. The proposed PLL performance was compared with the conventional SRF-PLL. The results verify the validity of the proposed PLL showing its ability to maintain stable operation under various conditions.

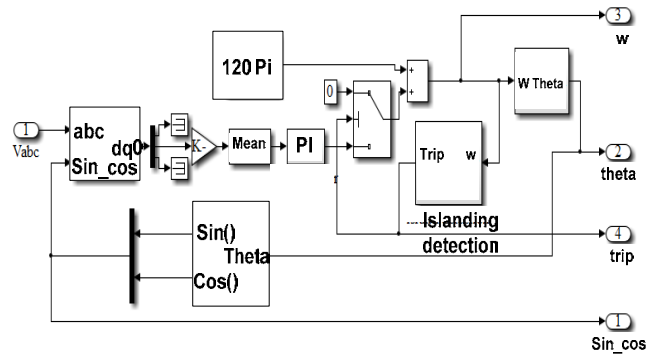


Fig. 2. SIMULINK model for proposed ASRF-PLL with islanding detection algorithm and internal frequency reference.

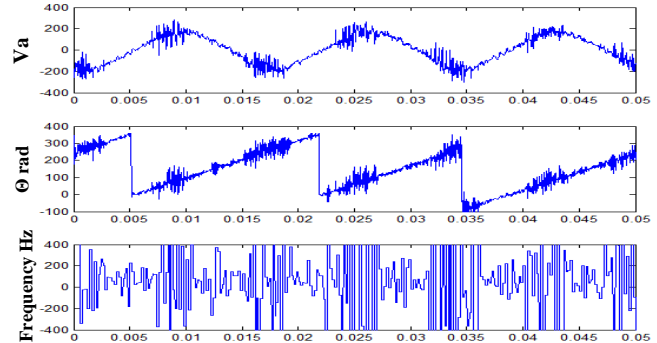


Fig. 3. Conventional SRF-PLL experimental results

I. KEY FIGURES

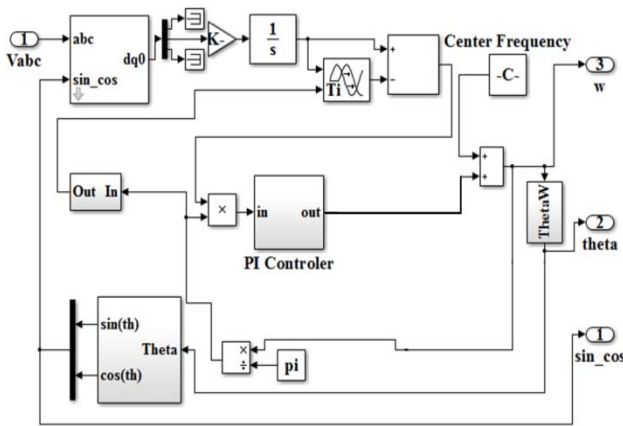


Fig. 1. Proposed ASRF-PLL with adaptive moving average filter.

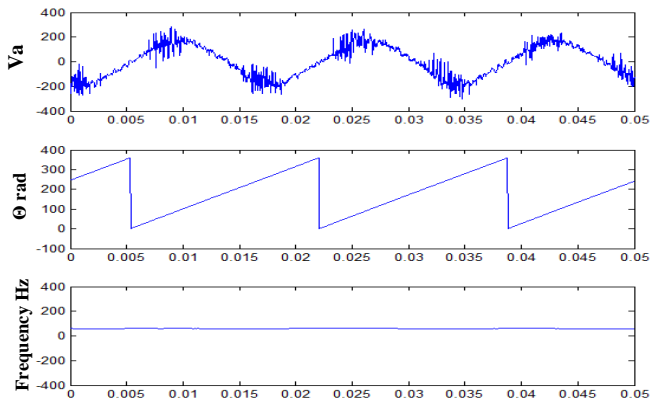


Fig. 4 Proposed ASRF-PLL experimental results

Desing of a fuzzy controller based on Differential evolution tuning for VSC

Ivan Riaño¹
 Carlos Hidalgo¹
 Nelson Diaz¹

¹Laboratorio de Investigación en Fuentes Alternativas de Energía, Facultad de Ingeniería, Universidad Distrital Francisco José de Caldas, Carrera 7 N° 40-53 Piso 5, Bogotá, Colombia.

Abstract—This paper present the develop of a differential evolution algorithm for tuning a fuzzy basis function expansions (FBFE) for the control of reactive power and the DC Voltage at the rectifier station of a VSC-HVDC system.

Index Terms— Differential evolution, FBFE, AC/DC Converter, VSC.

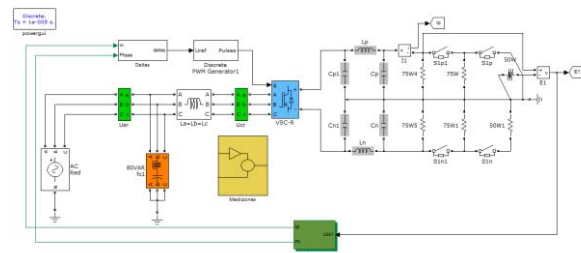


Fig.1 VSC Model

I. INTRODUCTION

Looking for an efficient interconnection between different characteristics generation systems is necessary to implement a reliable and low cost solution that allows a nearly optimal control of a Voltage Source Converter (VSC). Due to the complex mathematical modelling required to identify and design linear controllers for a grid-connected VSC, and the difficulty of tuning knowledge base fuzzy controllers proved in previous researches, this work presents a differential evolution

algorithm for tuning a FBFE to control a VSC.

Fist the control variables operation ranges are found through a switch based model of VSC System Fig. 1. Then, it is shown the development of a fuzzy control system and its tuning process by using Differential evolution algorithms, finally, the results are presented and are compared with linear controllers designed in precedent works, all that using the MatlabToolbox SimpowerSystem on stepped load changes.

II. DIFERENTIAL EVOLUTION ALGORITHM

The fuzzy control model of the VSC was developed as an FBFE which means and deviations were tuning using a Differential Evolution algorithm Fig. 2. Finally the best fuzzy control system was validated in the VSC model against some steps changes in load, and compared with a strategy of classic control linearization.

III. RESULTS

In the DC Voltage control Fig. 3 it can be seen that the fuzzy tuned system present an steady state time of 120ms that represent a 40% better behaviour that the almost 200ms of linear control strategies proposed in precedent works. Additionally, the distortion in stable state is reduced in 60%.

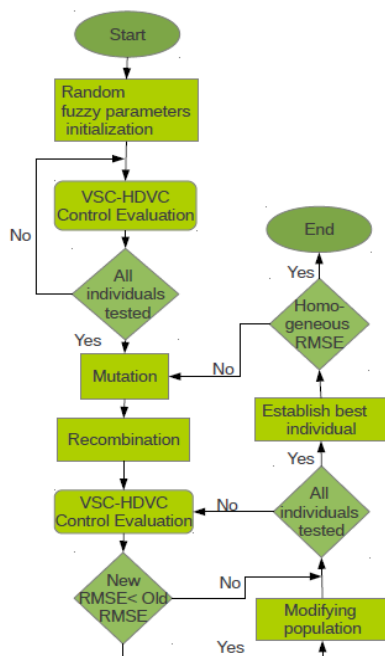


Fig. 2 Diagram flow of the differential evolution algorithm implemented.

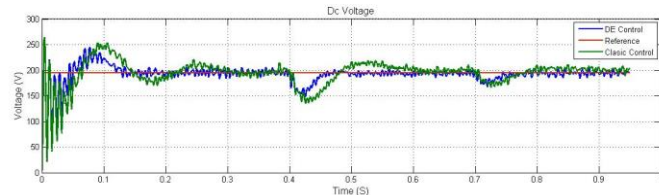


Fig.3 Dc Voltage control

Managing Solar Uncertainty in Neighboring Systems with Stochastic Unit Commitment

Robin Broder Hytowitz, *Student Member, IEEE*, and Kory Hedman, *Member, IEEE*
 School of Electrical, Computer and Energy Engineering, Arizona State University, Tempe, AZ 85281, USA
 Email: robin.hytowitz@asu.edu and kory.hedman@asu.edu

Abstract—With the increasing number of renewable energy resources coming online, reliability and uncertainty have become essential issues facing system operators and planners. To reliably manage uncertainty in a small grid system with a high penetration solar photovoltaic power, a stochastic mixed integer linear program for day-ahead unit commitment is modeled. In order to describe the issues that arise in this system, a complex mathematical formulation and intricate main-grid microgrid interactions are developed. The framework developed to account for uncertainty is based on a stochastic programming model used to compare multiple solar scenarios. In order to handle the computational complexities, Benders’ decomposition is used. With this approach, the problem is divided into three stages; the first is a non-iterative system-wide unit commitment problem to establish the operating costs of the main grid without the influence of trading. The second and third stages are the master and sub-problem of Benders’ decomposition, respectively. The master is an hourly unit commitment of the microgrid involving trading and line switching, and the sub-problem is a five-minute optimal power flow with differing solar scenarios. This multi-stage structure is used to appropriately model the important interactions between the two neighboring systems. The second-stage structure ensures pareto-improvements are achieved for both systems in order for the microgrid to improve its ability to predict operational conditions of the main-grid and, hence, trading opportunities for both energy and ancillary services. Additional modeling was used to ensure that uncommitted non-spinning generators would be available for use in the third stage OPF. Future studies will also consider the impacts of energy storage and electric vehicles on the system.

I. KEY EQUATIONS

$$\min \sum_{\forall T \in \text{HOURLY}} \sum_{\forall g \in \text{GEN}} (c_g P_{g,T} + c_g^{SU} S U_{g,T} + c_g^{NL} u_{g,T}) \quad (1)$$

$$\min \eta \quad (2)$$

$$\eta \geq \sum_{\forall T \in \text{HOURLY}} (\sum_{\forall u \in \text{MICRO}} c_u P_{u,T} + c_u^{SU} S U_{u,T} + c_u^{NL} u_{u,T}) + (c_T^{-F} P I_T^{-F} + c_T^{-NF} P I_T^{-NF}) - (c_T^{+F} P I_T^{+F} + c_T^{+NF} P I_T^{+NF}) + \sum_{\forall g \in \text{GEN}_{fast}} \rho_c (c_g^{SU} + c_g^{NL}) (1 - u_{g,t,c}^{NSP}) \quad (3)$$

$$\eta \geq \sum_{\forall z \in Z} \lambda_z^k b_z + \sum_{\forall u \in \text{MICRO}} c_u P_{u,T} + c_u^{SU} S U_{u,T} + c_u^{NL} u_{u,T} + \sum_{\forall g \in \text{GEN}_{fast}} (\rho_c * (c_g^{SU} + c_g^{NL}) (1 - u_{g,t,c}^{NSP})) \quad (4)$$

$$\min \sum_{\forall t \in \text{MIN}} \sum_{\forall c \in \text{SCEN}} \rho_c (\sum_{\forall g \in \text{GEN}} c_g (P_{g,t,c} + P_{g,t,c}^{NSP}) + c^{PV} P V_{i,t}^{curtail} + (\Delta_t^{+F} \kappa_t^{+F} + \Delta_t^{+NF} \kappa_t^{+NF} + \Delta_t^{-F} \kappa_t^{-F} + \Delta_t^{-NF} \kappa_t^{-NF})) \quad (5)$$

II. KEY FIGURE

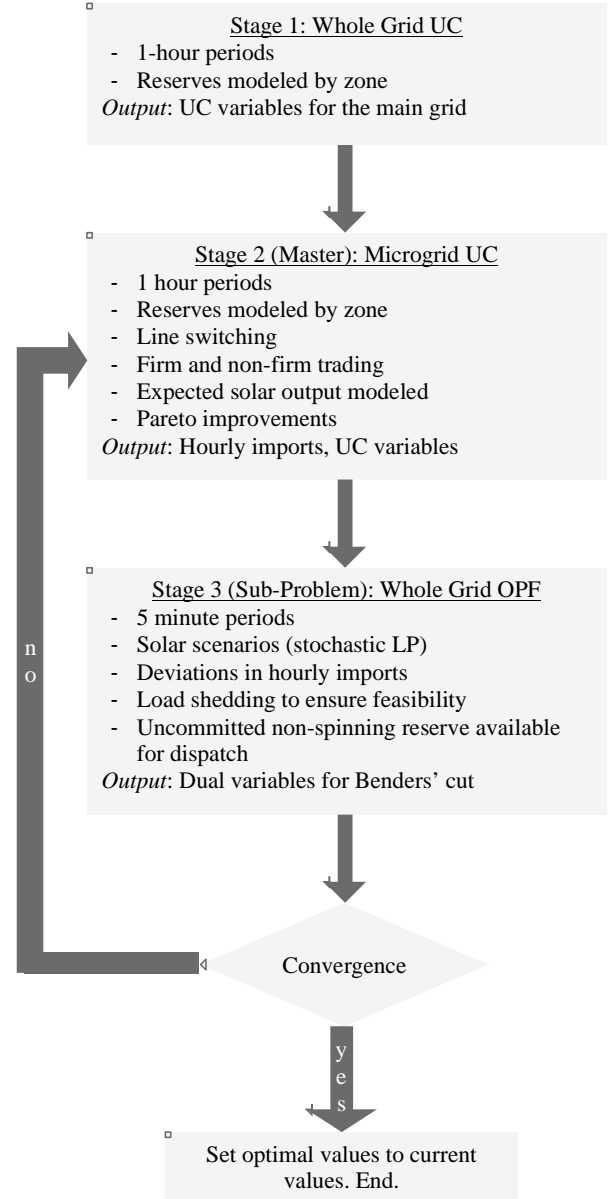


Figure 1. Flowchart of the three stages used in the microgrid model. Stages two and three are the master and sub-problem of Benders’ decomposition respectively.

Real Time Corrective Switching in Response to N-m Events

Pranavamoorthy Balasubramanian, *Student Member, IEEE*, and Kory W. Hedman, *Member, IEEE*
 School of Electrical, Computer, and Energy Engineering, Arizona State University, Tempe, AZ 85287, USA
 Email: pbalasu3@asu.edu and kory.hedman@asu.edu

Abstract— The standard optimal power flow (OPF) problem is an economic dispatch (ED) problem combined with transmission constraints, which are based on a static topology. Prior research has demonstrated that co-optimization of generation dispatch and transmission topology results in improved cost savings. However, the computational complexity associated with topology control (TC) has been a major deterrent to its implementation. The proposed work investigates the application of a heuristic, a greedy algorithm (GA), to improve the computational time for the TC problem while still maintaining the ability to find quality solutions. An expression is derived indicating the impact on the objective for a small change in the transmission line’s impedance. This expression is used to generate a priority list with potential candidate lines for switching, which may provide huge improvements to the system. The advantage of this method is that it eliminates the need to solve a mixed integer program (MIP) to find a switching solution. Corrective topology control strategies for real time applications is presented, which includes N-1 events, N-m events, and an application for arresting cascading events. The proposed algorithm specifically targets cases that lead to load shedding in the system and provides a quick and efficient method to restore the loads by improving the deliverability of reserves via topology control. Simulation results on the IEEE 73 bus and IEEE 118 bus test systems suggest a significant improvement in the amount of load served to the system with TC as opposed to without TC with minimal time and computational efforts.

I. KEY EQUATIONS

$$\gamma_k^{os} = B_k(s_k)(\theta_n - \theta_m) - P_k^{\max}(f_k^- + f_k^+) \quad (1)$$

$$\gamma_k^{is} = P_k(LMP_m - LMP_n) \quad (2)$$

II. KEY FIGURES

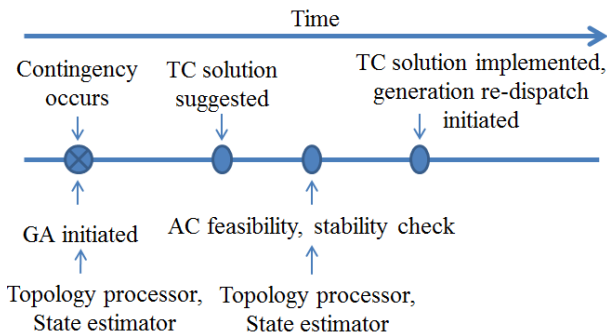


Figure 1. Real-time Corrective Switching Timeline.

III. METHODOLOGY

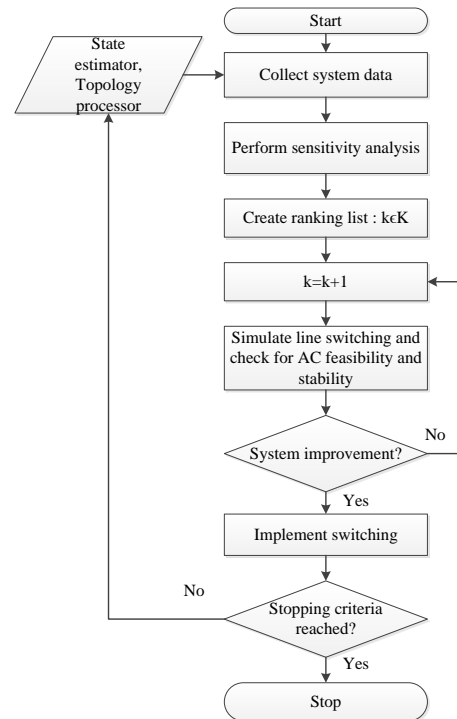


Figure 2. Flow chart for the greedy algorithm.

IV. KEY RESULTS

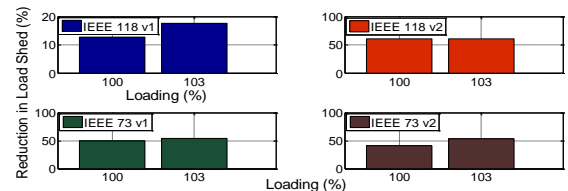


Figure 3. Comparison of reduction in load shed with greedy algorithm for all N-2 contingencies.

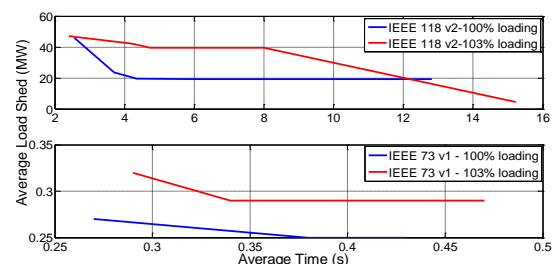


Figure 4. Comparison of accuracy of solution versus time for greedy algorithm.

Modeling of Electrical Arc for Transient Simulation

Qingxin Shi

Power Disturbance & Signaling Research Laboratory, Department of Electrical and Computer Engineering,
University of Alberta, Edmonton, AB, Canada, T6G 2V4
Email: qingxin1@ualberta.ca

Abstract— Electrical arc is common in the power system. A short circuit fault always occurs with transient electrical arc, while arc furnace can keep a continuous arc. The modeling of dynamic arc is a tough work due to its non-linear characteristic. According to the large number of measured data, the arc can be regarded as a resistive element of the circuit because its current is in phase with the voltage. This poster focuses on the dynamic model of AC arc, which can be represented by multi-variable equations. According to the measured data of arc voltage and current, three kinds of empirical formula have been proposed to describe the time-varying arc resistance and arc (V-I) characteristic. The simulation result shows that electrical arc have a significant influence on the power system dynamic and power quality.

I. KEY EQUATIONS

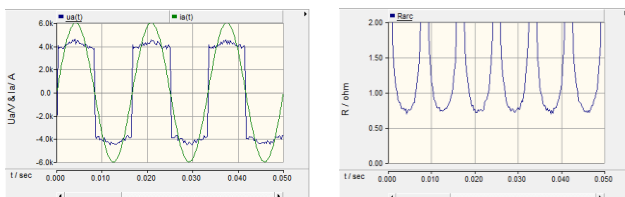
Dynamic model of AC arc can be represented by multi-variable equations. According to the measured data of arc voltage and current, three major dynamic arcing models are presented in the following. Equation (1) ~ (3) shows the distorted rectangular model, piecewise-linear model and distorted sinusoidal model respectively.

$$u_{a0}(t) = (U_a + U_b \frac{I_0}{i_b(t)} + R_\delta |i_b(t)|) \text{sgn}(i_a) + \xi \quad (1)$$

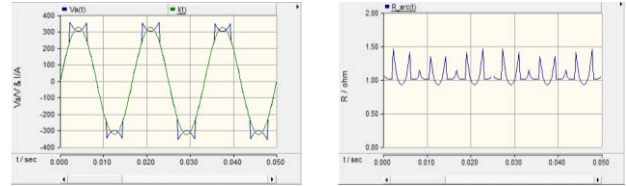
$$v_a(t) = \begin{cases} iR_1, & 0 \leq |i(t)| \leq i_1 \\ iR_2 + V_{ig} \left(1 - \frac{R_2}{R_1}\right), & i_1 < |i(t)| \leq i_2 \end{cases} \quad (2)$$

$$v_a = \frac{2V_0 \sin \omega t}{1 - \frac{\sin(2\omega t + \psi_a)}{\sqrt{1 + (2\omega\tau_a)^2}}} \quad (3)$$

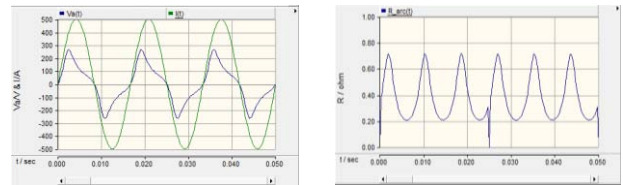
II. KEY FIGURES



a. Arc voltage and arc current
b. Arc resistance
Fig. 1 Time response of arc parameters (distorted rectangular model)



a. Arc voltage and arc current
b. Arc resistance
Fig. 2 Time response of arc parameters (piecewise-linear model)



a. Arc voltage and arc current
b. Arc resistance
Fig. 3 Time response of arc parameters (distorted sinusoidal model)

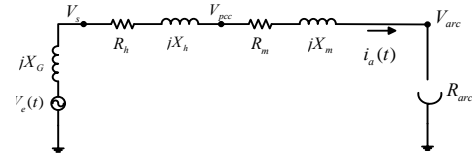
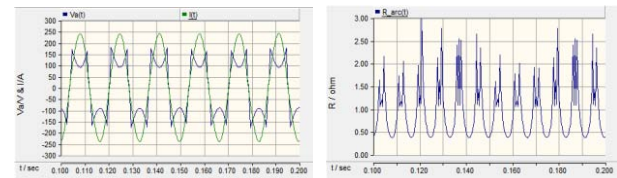


Fig. 4 A typical AC arc furnace system.

III. KEY RESULTS

To evaluate the influence the arc furnace has on the power quality of power system, the voltage spectrum at the point of common coupling (PCC) is presented.



a. Arc voltage and arc current
b. Arc resistance
Fig. 5 Simulated arc parameters of electric arc furnace

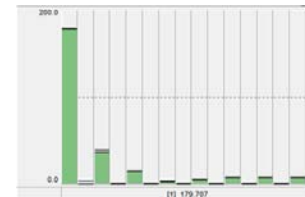


Fig. 6 Voltage frequency spectrum at PCC

Flexibility Assessment in Power Systems

Yury Dvorkin, Miguel A. Ortega-Vazquez, Daniel S. Kirschen

Department of Electrical Engineering
University of Washington
Seattle, USA.

E-mail: dvorkin@uw.edu

Abstract—This poster describes an approach to assess day-ahead flexibility requirements. The poster discusses the newly developed probabilistic characteristics of the intra-hour net load variability. Then, the results of the Kolmogorov-Smirnov test applied these characteristics are presented to demonstrate that parametric PDFs poorly fit net load variability. To overcome this inaccuracy, the non-parametric MIP-based approach is proposed and tested to optimally determine hourly flexibility requirements at a given probability level for each regulation interval.

Keywords—Power system operation, flexibility, wind integration

I. KEY EQUATIONS

Each historical deviation, ζ_k , from the net load forecast can be characterized by its magnitude (ΔP_k), ramp rate (ΔR_k), and ramp duration (ΔT_k):

$$\zeta_k \triangleq \{\Delta P_k, \Delta R_k, \Delta T_k\}. \quad (1)$$

Fig. 1 illustrates the process of obtaining a complete set of these deviations for each operating hour for $1 \leq \Delta T_k \leq 60$ minutes. When the complete set of deviations for each operating hour and each regulation interval is obtained, this information can be graphically interpreted as shown in Fig. 2. Therefore, if a box captures a given percentage, ω , of the most probably deviations within a particular regulation interval, its dimensions represent the required flexibility requirements (p^{req} , r^{req} , t^{req}) in up and down directions. To position these boxes optimally, the following optimization problem with the objective function (2), minimizing the normalized dimensions of each box, is proposed for each regulation interval:

$$\min \left[\frac{p_{\text{up}}^{\text{req}} - p_{\text{dn}}^{\text{req}}}{\Delta P_{\text{up}}^{\text{max}} - \Delta P_{\text{up}}^{\text{min}}} + \frac{r_{\text{up}}^{\text{req}} - r_{\text{dn}}^{\text{req}}}{\Delta R_{\text{up}}^{\text{max}} - \Delta R_{\text{up}}^{\text{min}}} + \frac{t_{\text{up}}^{\text{req}} - t_{\text{dn}}^{\text{req}}}{\Delta T_{\text{up}}^{\text{max}} + \Delta T_{\text{up}}^{\text{min}}} \right] \quad (2)$$

$$p_{\text{up}}^{\text{req}} \geq u_i^{\text{up}} \cdot \Delta P_i^{\text{up}}, \quad p_{\text{dn}}^{\text{req}} \leq u_j^{\text{dn}} \cdot \Delta P_j^{\text{dn}}, \quad (3)$$

$$r_{\text{up}}^{\text{req}} \geq u_i^{\text{up}} \cdot \Delta R_i^{\text{up}}, \quad r_{\text{dn}}^{\text{req}} \leq u_j^{\text{dn}} \cdot \Delta R_j^{\text{dn}}, \quad (4)$$

$$t_{\text{up}}^{\text{req}} \geq u_i^{\text{up}} \cdot \Delta T_i^{\text{up}}, \quad t_{\text{dn}}^{\text{req}} \leq u_j^{\text{dn}} \cdot \Delta T_j^{\text{dn}}, \quad (5)$$

$$\sum_{i=1}^{N^{\text{up}}} u_i^{\text{up}} = 1, \quad \sum_{j=1}^{N^{\text{dn}}} u_j^{\text{dn}} = 1 \quad (6)$$

$$\sum_{i=1}^{N^{\text{up}}} u_i^{\text{up}} \cdot d_i^{\text{up}} + \sum_{j=1}^{N^{\text{dn}}} u_j^{\text{dn}} \cdot d_j^{\text{dn}} \geq \frac{\omega}{100} \cdot (N^{\text{up}} + N^{\text{dn}}) \quad (7)$$

In (3)-(6) the hourly flexibility requirements are selected and a given percentage, ω , of captured data points is enforced in (7).

II. KEY FIGURES

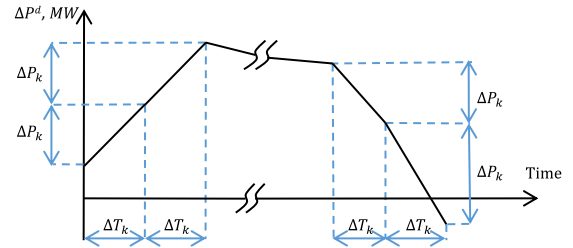


Fig. 1. Obtaining all net load deviations for a given time scale, ΔT .

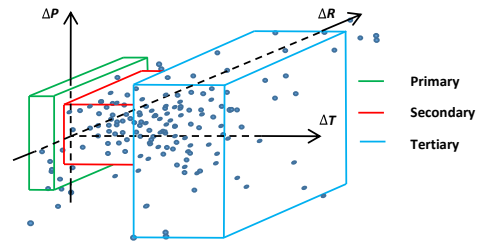


Fig. 2. Optimizing flexibility requirements over a set of net load deviations.

III. KEY RESULTS

The findings of this study includes optimal hourly flexibility requirements obtained for primary, secondary, and tertiary regulation (Fig. 3) intervals as well as the results of the Kolmogorov-Smirnov tests proving that non-parametric statistics fits net load variability better than parametric.

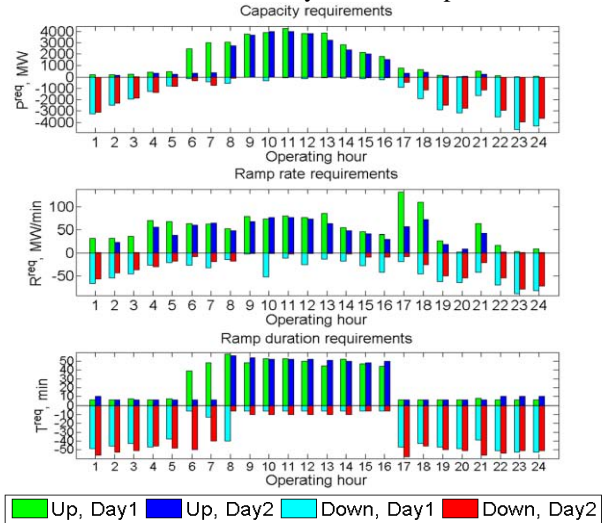


Fig. 3. Flexibility requirements for the tertiary regulation interval.

Factors Affecting Induced Voltage on Pipeline Located Close to High Voltage Transmission

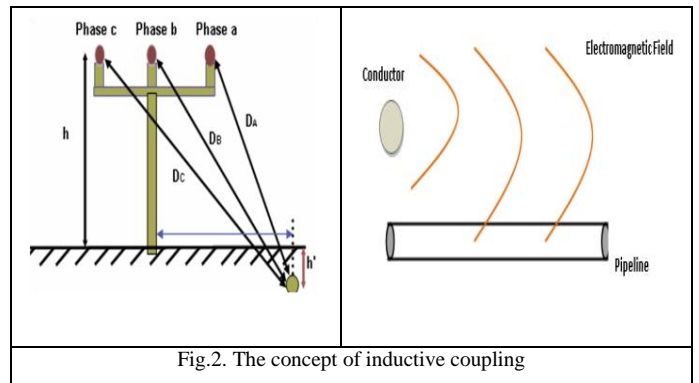
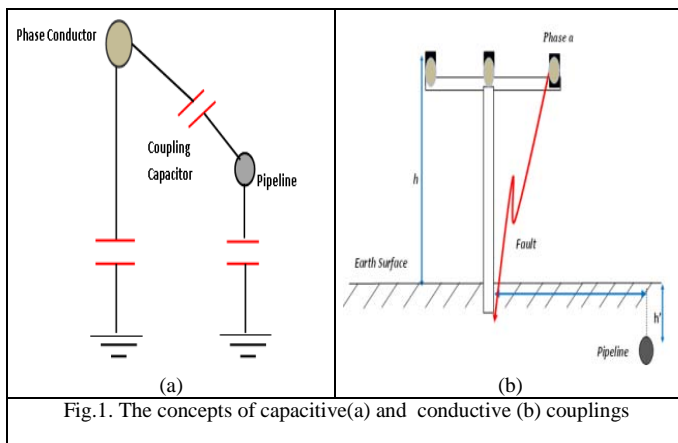
Ahmed. S. AlShahri, *Graduate Student Member, IEEE* and Nirmal. K. Nair, *Senior Member, IEEE*
 Department of Electrical and Computer Engineering
 University of Auckland, Auckland, New Zealand

Email: aaou604@aucklanduni.ac.nz, n.nair@auckland.ac.nz

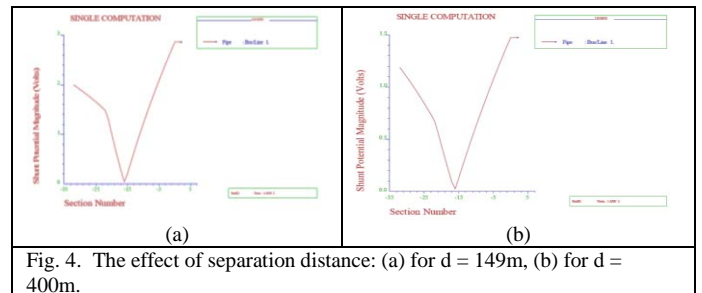
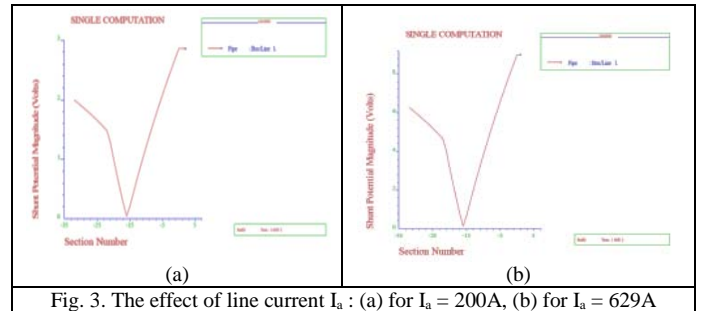
Abstract— The effect of AC interferences on pipelines has become a common issue in recent years due to improvements in pipeline technology, general increase in fault levels and an increased tendency to locate pipelines in power utility corridors. This kind of induced voltage can place both human safety and pipeline integrity at risk. A pipeline which shares a common corridor with AC transmission lines (OHTL) can become energized by the magnetic and electric field surrounding the charged line via the air and soil. This AC interference can result in an electrical shock hazard for people in contact with the pipeline or any metallic structure connected to the pipelines or by standing in close proximity. The objective of this paper is to apply Current Distribution Electromagnetic interference Grounding and Soil structure analysis software (CDEGS) to model, simulate and analyze a typical case in order to investigate and identify the prominent coupling effect due to overhead high voltage transmission line (OHTL) running parallel to adjacent pipelines. Also, it proposes the effect of some factors such as the line fault current and separation distance on pipeline induced voltage.

Index Terms— CDEGS, Induced voltage, OHTL, Pipeline.

I. KEY FIGURES



II. KEY RESULTS



Transient Stability Analysis Using Prony Analysis

Takuya Omi, Takato Hiraiwa, Shinichi Iwamoto

Power Systems Laboratory, Department of Electrical Engineering and Bioscience, Waseda University, Tokyo, 169-8555, Japan
Email: omi.takuya.pwrs@gmail.com

Abstract-- Electric power systems are becoming larger and more complex, making their control increasingly difficult. For this reason, transient stability has recently attracted increased attention. A concern about longitudinal power systems such as those used in Japan is the possibility of multi-swings, and predicting them has become an important issue. Analytical solutions to this issue are difficult, however, due to multi-modes in the swings. In this paper, we use Prony analysis to reduce the problem to simple swings, easing analysis of swing dynamics. We propose a new method of fault screening by applying Prony analysis and the single machine equivalent method. We verify the validity of the proposed method by simulation on a 10-machine, 47-bus system.

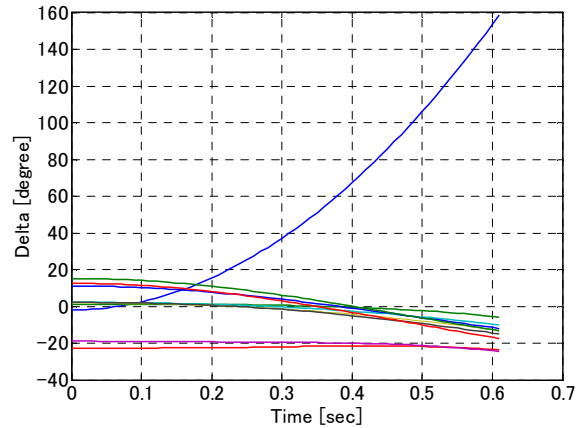


Figure 2 Local Step-out

I. KEY EQUATIONS

$$y(k) = \sum_{i=1}^n B_i Z_i^k \quad (k = 1, 2, \dots, N) \dots\dots\dots (1)$$

$$Z_i = e^{\lambda_i \Delta t} \dots\dots\dots (2)$$

$$\begin{bmatrix} y(n-1) & y(n-2) & \dots & y(0) \\ y(n) & y(n-1) & \dots & y(1) \\ \vdots & \vdots & \ddots & \vdots \\ y(N-2) & y(N-3) & \dots & y(N-n-1) \end{bmatrix} \begin{bmatrix} a_1 \\ a_2 \\ \vdots \\ a_n \end{bmatrix} = \begin{bmatrix} y(n) \\ y(n+1) \\ \vdots \\ y(N-1) \end{bmatrix} \dots\dots\dots (3)$$

$$M \frac{d^2 \delta}{dt^2} = P_m - P_e \dots\dots\dots (4)$$

$$M = \frac{M_C M_N}{M_T}, M_T = \sum_{i \in ALL} M_i \dots\dots\dots (5)$$

$$\delta = \delta_C - \delta_N \dots\dots\dots (6)$$

II. KEY FIGURES

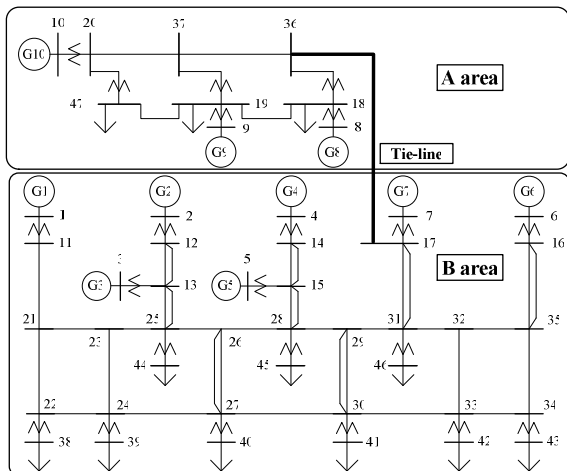


Figure 1 EAST 10 machine 47 bus system

III. KEY RESULTS

TABLE I. ESTIMATED VALUES BY PRONY ANALYSIS METHOD

(a) Output Rate : 60%				
Mode	Damping ratio (%)	Frequency (Hz)	Magnitude (degree)	Initial phase (degree)
1		0	14.0	0
2		0	0.74	0
3		0	0.59	0
4	2.35	0.77	8.50	49.6
5	8.89	1.66	0.20	161
(b) Output Rate : 70%				
Mode	Damping ratio (%)	Frequency (Hz)	Magnitude (degree)	Initial phase (degree)
1		0	15.5	0
2	-0.58	0.73	11.5	57.0
3	-14.5	0.65	0.37	-36.1
4	23.9	2.71	4.10	-143
5	98.0	0.28	46.6	-87.8

Table 2 Ranking of fault cases for poor damping

Ranking	Fault Point	Damping Ratio [%]
1	19-37	1.40
2	19-47	1.44
3	19-18	1.53
4	9-19	1.54
5	37-19	1.82
.	.	.
.	.	.
8	19-9	1.91

Supplementary Load Frequency Control with Storage Battery Operation Considering SOC under Large-scale Wind Power Penetration

Yu Kurita, Masato Toge, Shinichi Iwamoto

Power Systems Laboratory, Department of Electrical Engineering and Bioscience, Waseda University, 169-8555, Tokyo Japan

Email: kurita.yu.pwrs@gmail.com

Abstract—Wind power is a major source of renewable energy, and is in great demand around the world. However, wind power is difficult to manage due to large fluctuations in power output. To alleviate such fluctuations, this paper proposes a method for suppressing frequency deviation in wind power generation using storage battery systems that considers state of charge (SOC) and response speed differences between generators and storage battery systems. The method adjusts storage battery output according to present SOC, and applies H_∞ control theory to the generator controller to achieve robust control considering parameter fluctuations generated by state variations in the power system. Using this approach, we design a load frequency control system that controls both internal variation caused by power system dynamics and external variation caused by wind power generators. To verify the validity of the proposed method, we perform LFC simulations and compare frequency deviations between the proposed and conventional methods.

I. KEY EQUATIONS

$$\begin{cases} P_{SB}' = P_{SB} \times \frac{SOC[\%]}{\alpha} & (SOC < \alpha \text{ and } P_{SB} > 0), \\ P_{SB}' = P_{SB} \times \left(1 - \frac{SOC[\%] - \beta}{100 - \beta}\right) & (SOC > \beta \text{ and } P_{SB} < 0). \end{cases}$$

$$\Delta P_D = \Delta P_{load} - \Delta P_{wind}$$

$$\left\| W_S \frac{P_i}{1 - P_i K_i} \right\|_\infty < 1, \quad \left\| W_T \frac{P_i K_i}{1 - P_i K_i} \right\|_\infty < 1$$

$$|\Delta_m(j\omega)| \leq |W_T(j\omega)|, \quad \forall \omega$$

$$\begin{cases} W_S = \frac{0.0001s + 0.1}{s + 0.002}, \\ W_{T1} = \frac{2.5s}{s + 0.5}, \quad W_{T2} = \frac{1.25s}{s + 0.5}. \end{cases}$$

II. KEY FIGURES

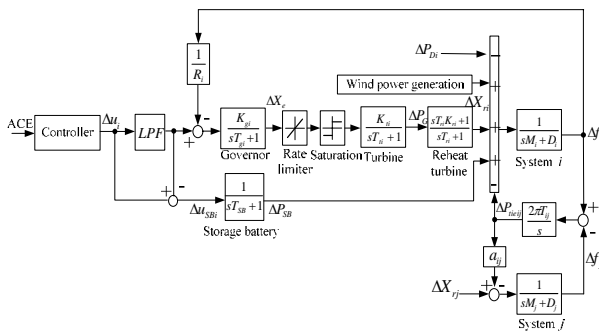


Figure 1 Linear model of LFC (Area i)

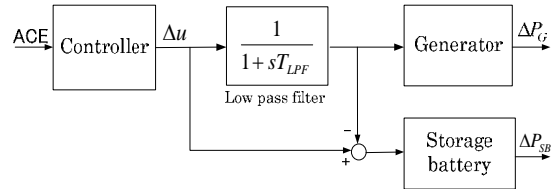


Figure 2 LPF block diagram

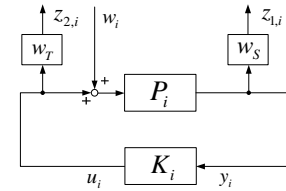


Figure 3 Generalized plant

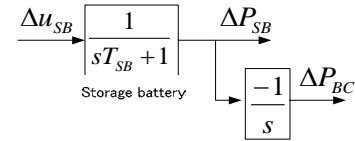


Figure 4 Storage battery model

III. KEY RESULTS

Table 1 Evaluation values

	Δf_{max} [Hz]
Simple method (integral controller)	0.419
Proposed method (integral controller)	0.241
Simple method (H_∞ controller)	0.275
Proposed method (H_∞ controller)	0.155

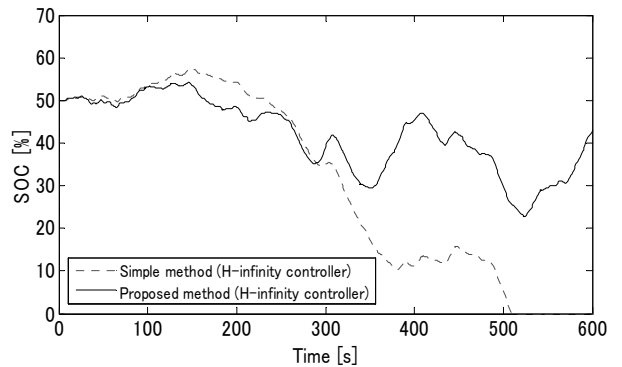


Figure 5 State of charge (H_∞ control applied)

A Generator Output Adjustment Method considering Transient Stability ATC and Multi-swing Stability

Kaoru Nakamura, Takahiro Chiku, Shinichi Iwamoto

Power Systems Laboratory, Department of Electrical Engineering and Bioscience, Waseda University, Tokyo, 169-8555, Japan

Hideo Hosogoe, Mitsuhiro Matsumoto

Tohoku Electric Power Company, Sendai, 980-8550, Miyagi, Japan

Email: nakamura.kaoru.pwrs@gmail.com

Abstract— Recently, in the process of deregulation, the transactions of the electricity among areas have been increased. Especially the tie-line ATC(Available Transfer Capability) is one of the important indices in the transactions from the viewpoint of the effective use of networks. In Japan, a large scale introduction of renewable energies is expected because of the global warming and the Great East Japan Earthquake. In addition, multi-swing is caused by the increase of the tie-line power flows in longitudinal power systems such as the Japanese system. In this paper, first we define transient stability ATC as ATC with transient stability constraints. Second, we focus our attention on characteristics of ATC and reduce the calculation time drastically by it, and we propose an effective generator output adjustment method considering transient stability ATC and multi-swing stability. Finally, we verify the validity of the proposed method by simulations on an IEEJ EAST 10 machines 47 bus-system.

I. KEY EQUATIONS

$$\begin{cases} \frac{d\theta_i}{dt} = \omega_i \\ M_i \frac{d\omega_i}{dt} = P_{mi} - P_{ei} - R_i P_{COA} \end{cases} \quad (1)$$

$$\Delta P_{tie,max} = \frac{\Delta P_{tie,i} \times (0.1 - CCT_i)}{CCT_{i+1} - CCT_i} \quad (2)$$

II. KEY FIGURES

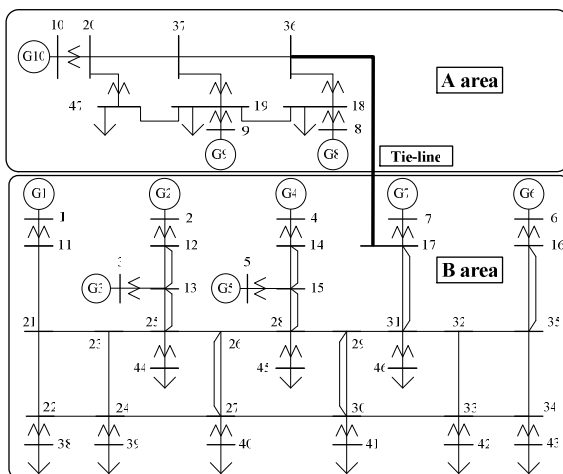


Figure 1 EAST 10 machine 47 bus system

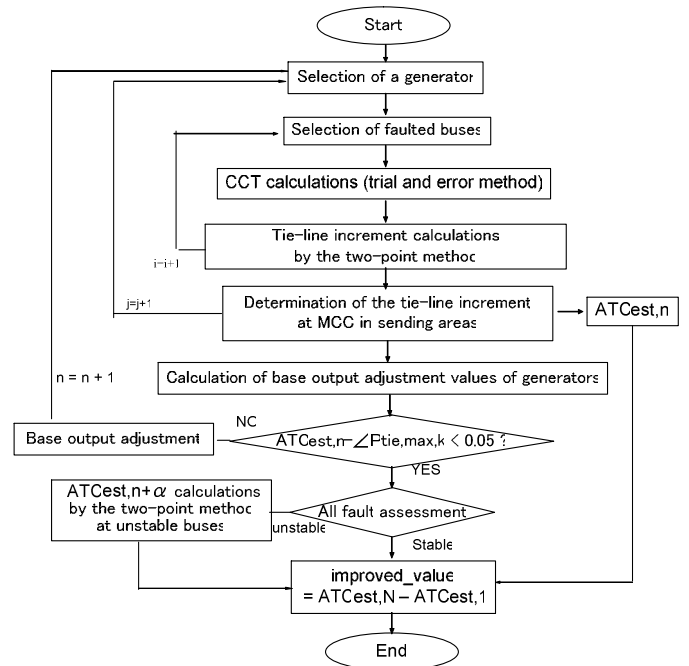


Figure 2 The flowchart of the proposed method

III. KEY RESULTS

Table 1 Base output changes of generators (80%)

	G8	G9	G10
Conventional method	0.0355 [pu]	0.0313 [pu]	-0.0669 [pu]
Proposed method	0.2248 [pu]	0.2450 [pu]	-0.4698 [pu]

Table 2 Transient stability ATC

	G8up	G9up	G10up	ATC
Original condition	1.31 [pu]	1.30 [pu]	1.20 [pu]	1.20 [pu]
Conventional method	1.31 [pu]	1.30 [pu]	1.32 [pu]	1.30 [pu]
Proposed method	1.31 [pu]	1.29 [pu]	1.29 [pu]	1.29 [pu]

A New Approximation Method for Generating Day-Ahead Load Scenarios

Yonghan Feng, Dinakar Gade, and Sarah M. Ryan
 Iowa State University
 Ames, IA, USA
 {yhfeng,dgade,smryan}@iastate.edu

Jean-Paul Watson
 Sandia National Laboratories
 Albuquerque, NM, USA
 jwatson@sandia.gov

Roger J-B Wets and David L. Woodruff
 University of California Davis
 Davis, CA, USA
 {rjbwets,dlwoodruff}@ucdavis.edu

Abstract— Unit commitment decisions made in the day-ahead market and resource adequacy assessment processes are based on forecasts of load, which depends strongly on weather. Two major sources of uncertainty in the load forecast are the errors in the day-ahead weather forecast and the variability in temporal patterns of electricity demand that is not explained by weather. We develop a stochastic model for hourly load on a given day, within a segment of similar days, based on a weather forecast available on the previous day. Identification of similar days in the past is based on weather forecasts and temporal load patterns. Trends and error distributions for the load forecasts are approximated by optimizing within new class of functions specified by a finite number of parameters. Preliminary numerical results are presented based on data corresponding to a U.S. independent system operator.

Index Terms— Demand forecasting, Load modeling, Power system planning, Stochastic processes.

I. KEY FIGURES

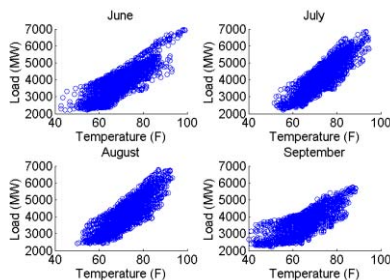


Figure 1. Load vs. day-ahead temperature forecast in the four summer months, 2010-12.

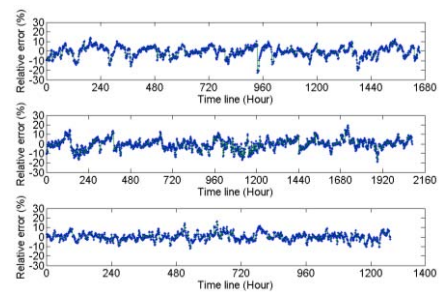


Figure 2. Time series plots of errors in hot, moderate, and cool summer days (from top to bottom) of the training set.

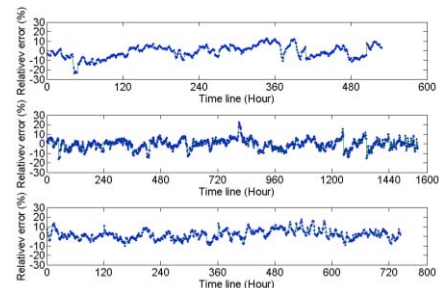


Figure 3. Time series plots of errors in hot, moderate, and cool summer days (from top to bottom) of the test set.

Semi-Definite Programming based Control for WECS over Full Operating Regions

Can Huang, Zhiqiang Jin and Fangxing Li

EECS Department, University of Tennessee, Knoxville, TN 37996

Email: chuang16@utk.edu

- Abstract**— In this paper, a new control strategy based on semi-definite programming (SDP) method is proposed to control variable speed variable pitch wind energy conversion system (WECS) over its full operating regions (both the partial load and the full load regions). The SDP-based controller is designed to provide the required trade-off between energy maximization or power regulation while reducing the drive train torsional torque fluctuations and pitch actuator activity. It can improve the power quality of the electrical power generated by the WECS and increase the life time of the mechanical parts of the system.

I. MODELING OF WECS

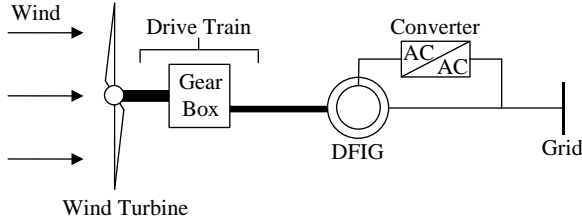


Fig. 1. Wind energy conversion system.

II. CONTROL PROBLEM FORMULATION

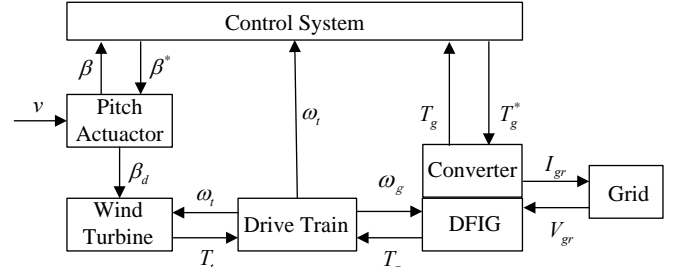


Fig. 2. Block diagram of control system in WECS.

$$\min V_N(x_0, \mathbf{u}, \mathbf{d}) = \frac{1}{2} \left[\sum_{k=1}^N \left(q_1 (\omega_{g, \text{rat}} - \omega_g)_k^2 + q_2 (P_{g, \text{rat}} - P_g)_k^2 \right) + \sum_{k=0}^{N-1} \left(r_1 (\Delta T_g^*)_k^2 + r_2 (\Delta \beta_d)_k^2 \right) \right]$$

Subject to

$$\Delta \beta_{\min} \leq \Delta \beta_d(k) \leq \Delta \beta_{\max}, \quad \beta_{\min} \leq \beta_d(k) \leq \beta_{\max}$$

$$0 \leq T_g^* \leq T_{g, \max}, \quad P_{g, \min} \leq P_g(k) \leq P_{g, \max}, \quad \omega_{g, \min} \leq \omega_g(k) \leq \omega_{g, \max}$$

III. SIMULATION RESULTS

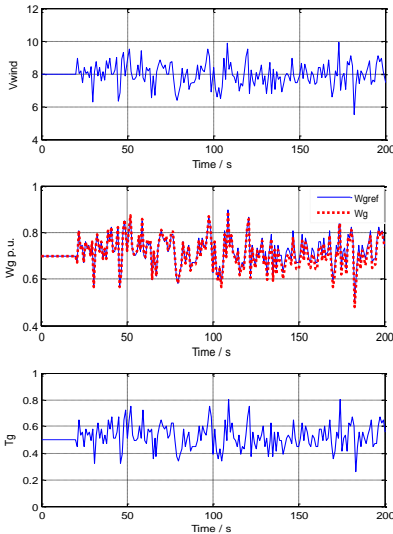


Fig. 3. Results in the partial load region

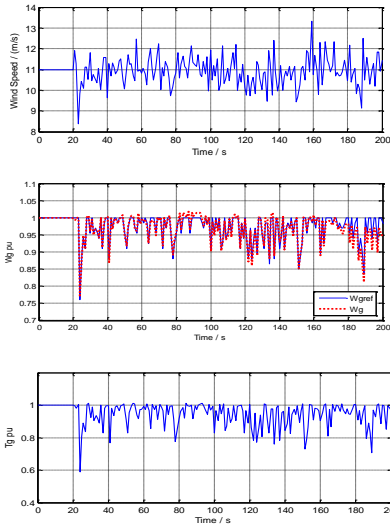


Fig. 4. Results in the transition region

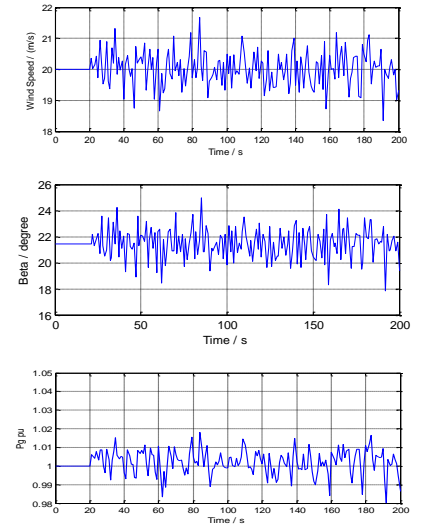


Fig. 5. Results in the full load region

Voltage Quality Improvement in Distribution Networks Containing DERs using UPQC

Sumit Mazumder, Arindam Ghosh and Firuz Zare

School of Electrical Engineering and Computer Science, Queensland University of Technology, Brisbane, Australia

Email: s.ami@qut.edu.au, a.ghosh@qut.edu.au

ABSTRACT – Single phase distributed energy resources (DERs) can cause voltage rise along distribution feeder and power imbalance among the phases. Usually transformer tap setting are used to mitigate voltage drop along feeders. However this can aggravate the voltage rise problem when DERs are connected. Moreover if the power generation in a phase is more than its load demand, the excess power in that phase will be fed back to the transmission network. In this paper, a unified power quality compensator (UPQC) has been utilized to alleviate the voltage quality excess power circulation problems. Through analysis and simulation results, the mode of operation of UPQC is highlighted. The proposals are validated through extensive digital computer simulation studies using PSCAD and MATLAB

I. KEY FIGURE

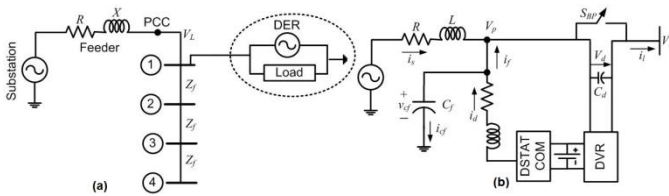


Fig. 1. (a) Distribution system structure (b) The PCC of the system with UPQC

II. KEY RESULTS

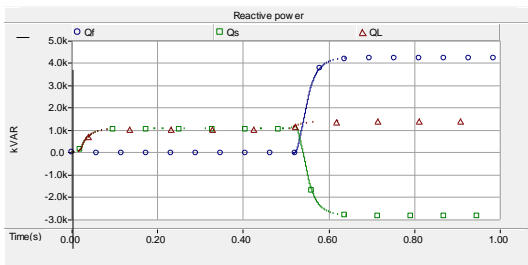


Fig. 2. System reactive power in PF operation without UPQC

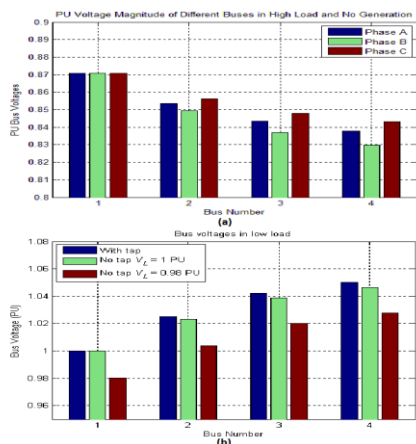


Fig. 3. Bus voltages in pf operation (a) with no reactive power backflow. (b) of Phase a in high DER generation

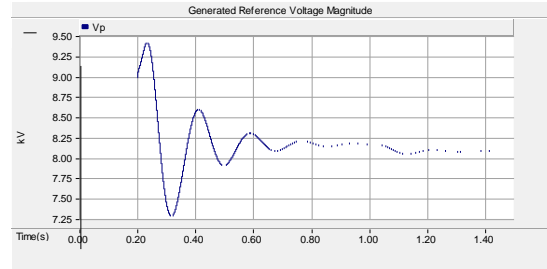


Fig. 4. PCC voltage magnitude with UPQC operation.

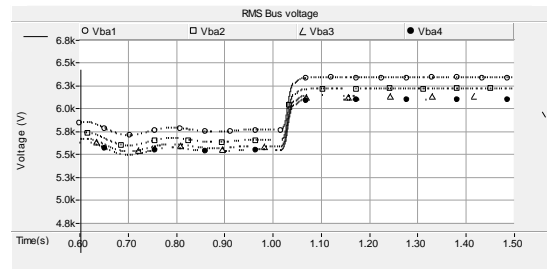


Fig. 5. RMS load bus voltages in phase-a after UPQC operation in high load.

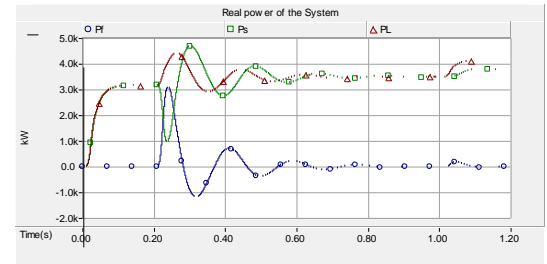


Fig. 6. Real power of the system after UPQC operation in high load.

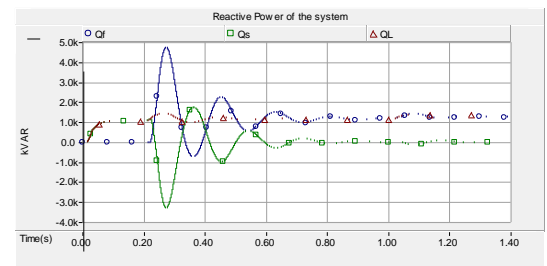


Fig. 7. Reactive power of the system after UPQC operation in high load.

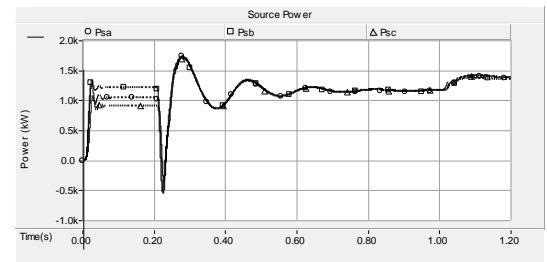


Fig. 8. 3 phase source power circulation after UPQC operation in high load.

A Two-Level Online Parameter Identification Approach

Runze Chen, Wenchuan Wu, Hongbin Sun, Boming Zhang

Department of Electrical Engineering, Tsinghua University, Haidian, Beijing, China

Email: chenrz_francis@vip.126.com and wuwench@mail.tsinghua.edu.cn

Abstract—In this paper, a novel online parameter identification approach with two-level architecture is proposed. In this approach, identifiability analysis, parameter identification and parameter validation is developed and integrated in a two-level manner. Firstly, an identifiability index based on trajectory sensitivity is defined to select measurements scans that satisfy the condition of identifiability. Parameter identification is then done with the selected measurements scans, which has the ability to compress measurements error. These two functions are deployed at substations or plants to guarantee efficiency. A hybrid simulation based parameter validation method is also developed which is deployed in control center. With this two-level online parameter identification approach, parameters of models can be identified and verified automatically. Numerical tests from real application show that the proposed approach has good performance.

I. KEY EQUATIONS

The trajectory sensitivity can be calculated by

$$J(\theta_i, k) = \frac{[y(\theta_{i0} + \Delta\theta_i, k) - y(\theta_{i0} - \Delta\theta_i, k)] / y(\theta_{i0}, k)}{2\Delta\theta_i / \theta_{i0}} \quad (2)$$

$i=1, 2, \dots, m$

With sensitivities of all the parameters, we get sensitivity matrix $\mathbf{J}_{m \times n}$. Then parameter identification can be described as solving the algebraic equation,

$$\mathbf{J}(\boldsymbol{\theta}) \cdot \Delta\boldsymbol{\theta} = -\Delta\mathbf{y} \quad (3)$$

Define pseudo-Hessian matrix as

$$\mathbf{H} = \mathbf{J}^T \mathbf{J} \quad (4)$$

Least square solution of the parameter deviation vector:

$$\Delta\boldsymbol{\theta} = -\mathbf{H}^{-1} \mathbf{J}^T \Delta\mathbf{y} \quad (5)$$

Solution sationarity is affected by the condition number :

$$k(\mathbf{H}) = \frac{\sigma_{\max}}{\sigma_{\min}} \quad (6)$$

We can choose a threshold as:

$$\text{threshold}_k = \frac{1}{\sqrt{n \times \tau}} \quad (7)$$

II. KEY FIGURES

The architecture of the proposed approach is shown in Fig.1.

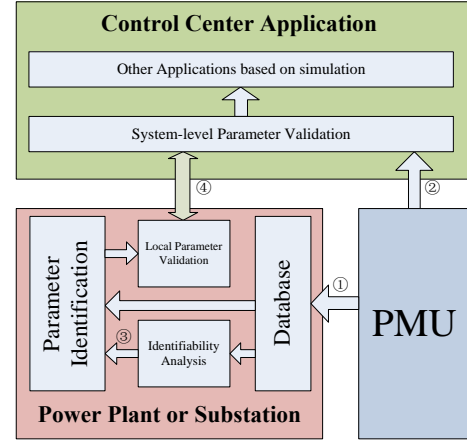


Fig. 1 Framework of the two-level OPI system

III. KEY RESULTS.

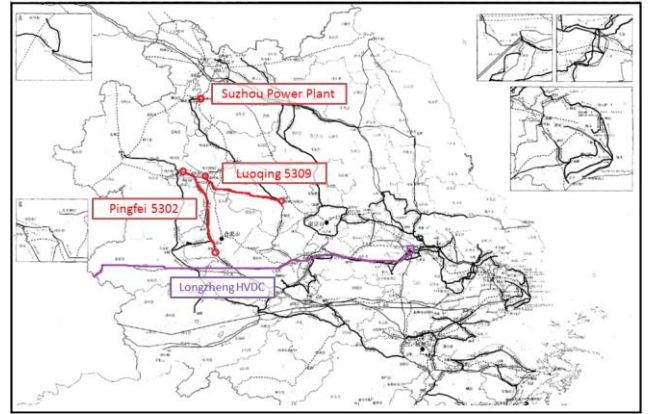


Fig. 2 Part of the CEG containing Suzhou Power Plant

TABLE I
PARAMETER IDENTIFIABILITY RESULT

	Default	Scenario 1	Scenario 2	Scenario 3
$X'd/p.u.$	2.155	2.040	2.046	2.037
$X'q/p.u.$	2.100	1.535	1.518	1.530
K	2327	1959	1954	1976
$X''d/p.u.$	0.301	0.292	0.247	0.321
$X''q/p.u.$	0.223	0.143	0.221	0.143
$T'd0/p.u.$	8.610	7.580	7.070	7.710
$T'd0/p.u.$	0.045	0.030	0.031	0.029
$X'q/p.u.$	0.448	0.324	0.292	0.307
$X''q/p.u.$	0.218	0.116	0.260	0.112
$T'q0/p.u.$	0.950	0.500	0.920	0.480
$T'q0/p.u.$	0.069	0.071	0.095	0.056

Power System Online Security Operational Trend Analysis and Simulation Results

Feng Zhao, Qinglai Guo, *Member, IEEE*, Hongbin Sun*, *Senior Member, IEEE*, Mengxia Wang, Bin Wang
 Dept. of Electrical Engineering, Tsinghua University, Beijing, China
 Email: f-zhao09@mails.tsinghua.edu.cn

Abstract—A novel power system online security operational trend analysis method is proposed in this paper. Based on the online operational mode and ultra-short term forecast operational mode (15mins later), the worst contingency set is determined as the union of the worst contingency in online and ultra-short term forecast operational mode, and the power system security evaluation indices are given out online for different security subject, such as voltage stability, critical interface stability, and transient stability. Simulation results on IEEE 39-bus system show that the proposed method can determine the worst contingency set and security evaluation index online accurately, reduce the number of contingencies, and improve security analysis efficiency.

I. KEY FIGURES

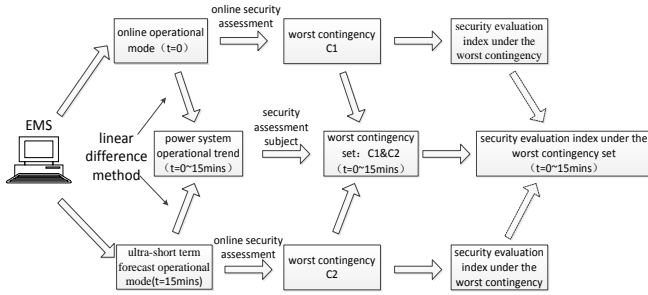


Figure 1. Framework of power system online security operational trend analysis method

II. KEY EQUATIONS

Power system operational trend ($t=0\sim 15\text{mins}$) is obtained through liner difference method. And the power system state variables X_i at time t_i ($t_a < t_i < t_b$) is shown as equation (1).

$$X_i = X_a + \frac{t_i}{t_b - t_a} (X_b - X_a) \quad (1)$$

where X_a is the power system state variables at time t_a , and X_b is the power system state variables at time t_b .

The security evaluation index k_i at time t_i is shown as equation (2).

$$k_i = k_a + \frac{t_i}{t_b - t_a} (k_b - k_a) \quad (2)$$

where k_a is the security evaluation index at time t_a , and k_b is the security evaluation index at time t_b .

III. KEY RESULTS

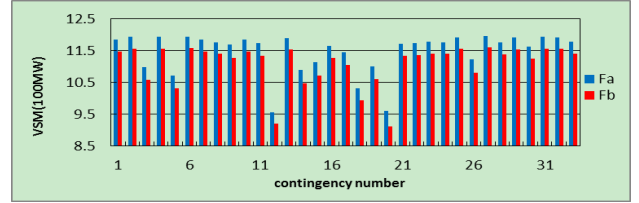


Figure 2. VSMs under the contingency set in operational mode F_a and F_b

TABLE I. THE WORST CONTINGENCY AND VSMs UNDER THE WORST CONTINGENCY IN OPERATIONAL MODE F_a AND F_b

Operational mode	F_a	F_b
Worst contingency line	6-11	15-16
VSM under the worst contingency line (MW)	956	913

TABLE II. THE ASSESSED WORST CONTINGENCY AND VSMs UNDER THE WORST CONTINGENCY IN OPERATIONAL MODE F_1, F_2, F_3 AND F_4 THROUGH THE PROPOSED TREND ANALYSIS METHOD

Operational mode	F_1	F_2	F_3	F_4
Worst contingency line set	6-11,15-16	6-11,15-16	6-11,15-16	6-11,15-16
VSM under the worst contingency line set (MW)	947	939	930	922

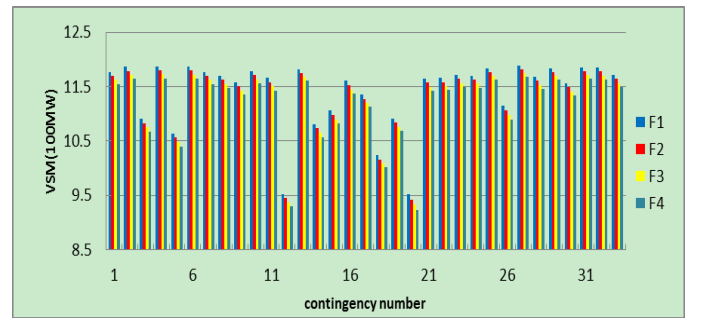


Figure 3. VSMs under the contingency set in operational mode F_1, F_2, F_3, F_4

TABLE III. THE WORST CONTINGENCY AND VSMs UNDER THE WORST CONTINGENCY IN OPERATIONAL MODE F_1, F_2, F_3, F_4

Operational mode	F_1	F_2	F_3	F_4
Worst contingency line	6-11	15-16	15-16	15-16
VSM under the worst contingency line set (MW)	952	942	933	923
Deviation between calculated VSM and assessed VSM (%)	0.5	0.3	0.3	0.1

Preliminary Modeling and Stability Analysis of Physically Distributed Power Systems with Constant Time Delay

Christian M. Schegan, Karen Miu

Center for Electric Power Engineering, Electrical and Computer Engineering Department, Drexel University, Philadelphia, PA 19104, USA,

Email: cms68@drexel.edu, karen@coe.drexel.edu

Abstract—This poster presents key concepts in the design and analysis of remote, non-destructive testing of physically distributed power systems. Preliminary modeling of a linearized, two-bus, physically distributed power system and its communication and control interface is given. The main objective is to determine regions of stable operation for a given range of network parameters, subject to communication delay introduced by the interface. The delay is assumed to be constant in order to establish general bounds on total roundtrip delay that ensures stable operation. The resulting regions of stable operation provide design constraints for the physical implementation of the communication and control interface hardware.

This poster describes how the system shown in Fig. 1. is linearized and modeled as the system in Fig. 2. Equations (1) - (4) are then used to represent the system for a given value of delay. The region of stable operation for the time delayed system is then determined (Fig. 3.).

I. KEY EQUATIONS

The state space equation for the physically distributed power system is shown in (1). The remaining equations are the characteristic equation [1] of the system and the limiting value of delay for stable operation of the system [2].

$$\dot{x} = Ax(t) + A_{\tau_1}x(t - \tau_1) + A_{\tau_2}x(t - \tau_2) + Bu(t) \quad (1)$$

$$\Delta(s, \tau) = \det[sI_n - A_0 - A_d e^{-s\tau}] = M(s) + N(s)e^{-s\tau} = 0 \quad (2)$$

$$A_d e^{-s\tau} = (A_{\tau_1} + A_{\tau_2})e^{-s(\tau_1 + \tau_2)} \quad (3)$$

$$\tau_{\text{limit}}^* = \min_{\forall k} \tau_k^* (\Phi_i) = \min_{\forall k} \left\{ \frac{1}{\omega_k} \tan^{-1} \left\{ \frac{\text{Im} \left\{ \frac{M(j\omega_k)}{N(j\omega_k)} \right\}}{\text{Re} \left\{ \frac{-M(j\omega_k)}{N(j\omega_k)} \right\}} \right\} \right\} \quad (4)$$

II. KEY FIGURES

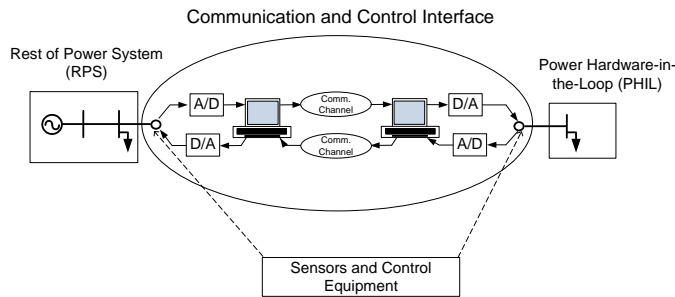


Fig. 1. Example of a physically distributed powersystem that highlights the communication and control interface.

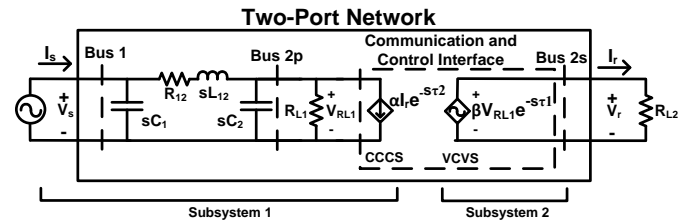


Fig. 2. Example of a linearized, two-port representation of a 2-bus, physically distributed power system.

III. KEY RESULTS

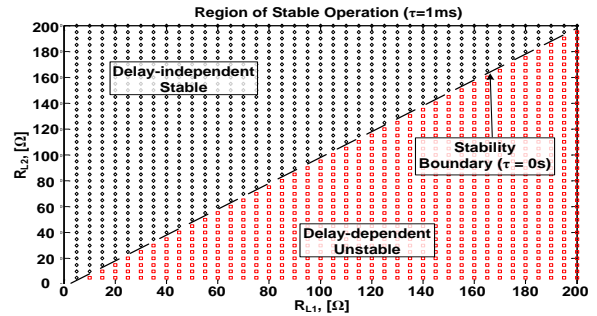


Fig. 3. Region of stable operation for the time-delayed system in with $\tau=1\text{ms}$.

Fig. 3 shows the R_{L1} and R_{L2} parameter space for a total roundtrip delay of $\tau=1\text{ms}$. Note that when $\tau=0\text{s}$, the region of stable operation is the entire quadrant.

REFERENCES

- [1] K. Walton and J. E. Marshall, "Direct method for TDS stability analysis," *IEE Proceedings*, vol. 134, pt. D, no. 2, Mar. 1987.
- [2] R. Fischl, et al, "Sim-Stim Interface for Research and Development," final report submitted to the Office of Naval Research for N00014-01-C-0045, Jan. 6, 2003.

Stochastic Economic Dispatching for Wind Penetrated Power System

A.H.Shahirinia¹, D.C.Yu¹, E.Soofi²

1- Department of Electrical and Computer Engineering,

2- Sheldon B Lubar School of Business

University of Wisconsin–Milwaukee, Kenwood Blvd. Milwaukee, WI 53201-0413

Email: shahiri2@uwm.edu, yu@uwm.edu and esoofi@uwm.edu

Abstract— This poster introduces a new algorithm for economic dispatching problems of wind-penetrated power systems. This algorithm, called Stochastic Economic Dispatcher (SEconD), takes the uncertainty about the wind speed into account and optimizes the economic dispatch of the corresponding fossil fuel power plants. SEconD is an integrated algorithm consisting of a statistical software package and a dynamic programming based optimizer. Since the proposed algorithm utilizes the entire wind speed spectrum as input, it will maximize the wind energy participation in the economic dispatch. The SEconD algorithm produces summary statistics of the variables such as wind power, outputs of fossil fuel generators, transmission loss, and total cost of power generation. The survival function is introduced to compare the probability distributions of the outputs of the algorithm and to provide the

planners with a more qualitative description of the statistical results. The SEconD algorithm will allow the planner to estimate associated univariate statistical measures and confidence intervals as well as bivariate relationships between pairs of variables and the associated correlation measures.

Key Equations:

$$\min_P OC = \sum_{i=1}^N a_i P_i^2 + b_i P_i + c_i \quad (1)$$

where $\mathbf{P} = (P_1, \dots, P_N)$ subject to

$$P_D + P_L - \sum_{i=1}^N P_i = 0 \quad (2)$$

$$P_i^{min} \leq P_i \leq P_i^{max}, \quad (3)$$

$$P_L = \sum_{i=1}^N \sum_{j=1}^N P_i B_{ij} P_j + \sum_{i=1}^N B_{i0} P_i + B_{00}. \quad (4)$$

Key Results:

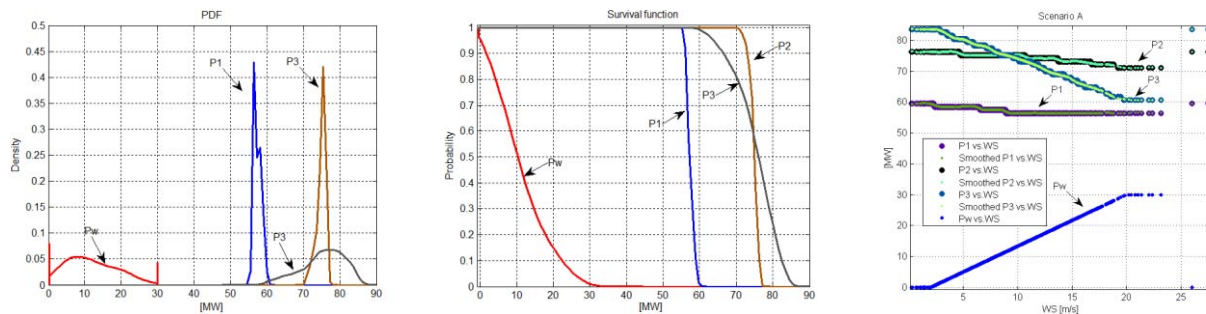


Fig. 1. Distributions of the wind power, optimal output power generation and the scatter plots of the optimal outputs of three fossil generators and wind power

Order Recursive and Real-time Estimation of Power System Electromechanical Modes

Gurudatha K. Pai (gpai@uwyo.edu)
Dept. of Electrical and Computer Engineering,
University of Wyoming, Laramie, WY 82070

John W. Pierre (Pierre@uwyo.edu)
Dept. of Electrical and Computer Engineering,
University of Wyoming, Laramie, WY 82070

Abstract—Power system electromechanical modes can be estimated using ambient synchro-phasor measurements. This particular work relates to modeling the ambient time series measurements as an auto-regressive (AR) model with varying model orders simultaneously.

A modular structure called lattice filter is used for the modeling purpose and is related to the classical AR model (of different model orders) via the Levinson-Durbin algorithm. The modes of the power system are obtained as roots of the AR polynomials. To estimate the parameters of the lattice filter a weighted least squares approach, called the “QR decomposition based least squares lattice (QRD-LSL) is used. This approach provides modeling flexibility to the user without needing to re-initialize the algorithm with a different model order choice.

The new approach is validated using linearized models of the power system in a Monte Carlo simulation set-up. The simulation results suggest that the new algorithm provides consistent estimates of the modes and is capable of tracking slowly time varying modes. The convergence properties of QRD-LSL algorithm is similar to those of the popular recursive least squares algorithm. A demonstration of the estimation of the modes using measured power system data is also presented.

I. KEY EQUATIONS

The forward /backward prediction errors (time series model)

$$f_M(t) = y(t) - \hat{y}_{f,M}(t) = f_{M-1}(t) + \kappa_{f,M} b_{M-1}(t-1),$$

$$b_M(t) = y(t-M) - \hat{y}_{b,M}(t) = b_{M-1}(t-1) + \kappa_{b,M} f_{M-1}(t).$$

Lattice filter estimation problem -

$$\hat{\kappa}_{f,M}(t) = \underset{\kappa_{f,M}}{\operatorname{argmin}} \left\{ \sum_{i=0}^t \lambda^{t-i} f_M^2(t) \right\}, \quad (1)$$

$$\hat{\kappa}_{b,M}(t) = \underset{\kappa_{b,M}}{\operatorname{argmin}} \left\{ \sum_{i=0}^t \lambda^{t-i} b_M^2(t) \right\}. \quad (2)$$

Levinson-Durbin Algorithm -

$$\underline{a}_{f,m} = \begin{bmatrix} \underline{a}_{f,m-1} \\ 0 \end{bmatrix} + \kappa_{f,m} \begin{bmatrix} \underline{a}_{b,m-1} \\ 1 \end{bmatrix}, \quad (3)$$

$$\underline{a}_{b,m} = \begin{bmatrix} 0 \\ \underline{a}_{b,m-1} \end{bmatrix} + \kappa_{b,m} \begin{bmatrix} 1 \\ \underline{a}_{f,m-1} \end{bmatrix}.$$

Calculation of frequency \underline{f} (Hz) and damping ratio (DR) $\underline{\zeta}$ -

$$\underline{z} = \operatorname{roots}(A_{f,M}(z)) \quad \left| \quad \underline{s} = F_s \log(\underline{z}), \quad (4)$$

$$\underline{f} = \Im(\underline{s})/(2\pi) \text{ (Hz)} \quad \left| \quad \underline{\zeta} = -\Re(\underline{s})/|\underline{s}| \text{ (%)}$$

II. KEY FIGURES

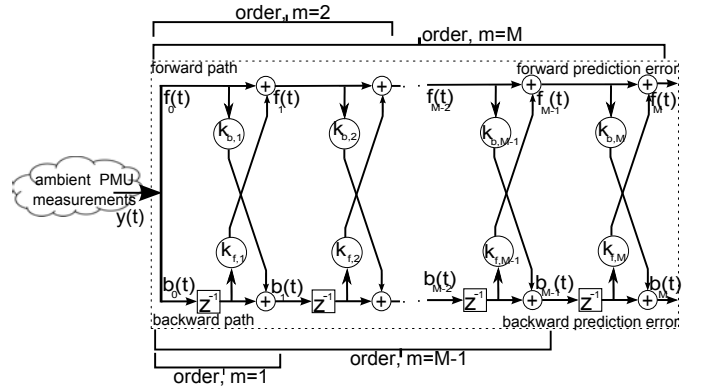


Fig. 1. Lattice filter based linear prediction model for ambient PMU data.

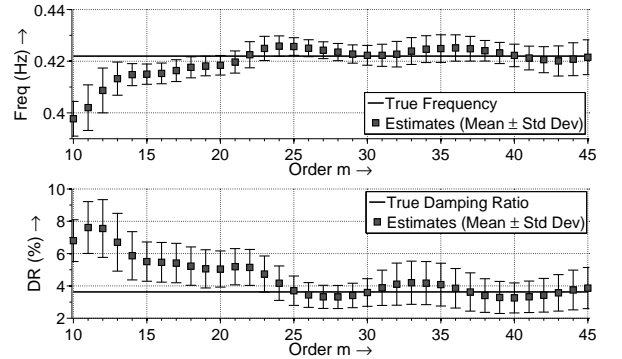


Fig. 2. Frequency and damping ratio estimation accuracy of QRD-LSL algorithm for varying model orders.

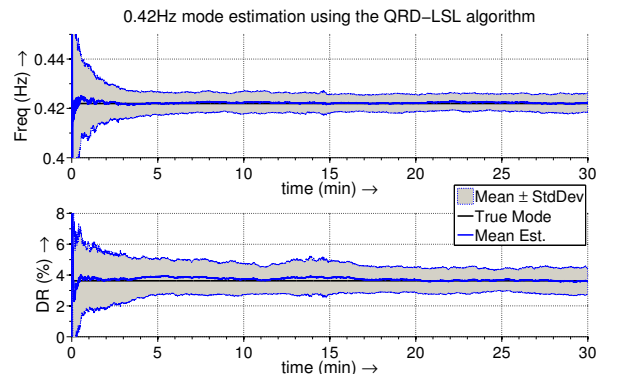


Fig. 3. Frequency and damping ratio estimates of the 0.42Hz mode of the seventeen machine model with stationary modes. Mean and standard deviation of the estimates over 100 Monte Carlo trials are shown. $m = 30$, $\rho = 0.999$.

Multi-Band Sub-Synchronous Damping Controller (MBSSDC) for Type III DFIG Wind Power Farms

Jason Pannell, *Student Member, IEEE*, Ramakrishna Gokaraju, *Member, IEEE*, Olivier Larocque, *Member, IEEE*
 Electrical & Computer Engineering, University of Saskatchewan, Saskatoon, Canada
jason.pannell@usask.ca rama.krisha@usask.ca

Abstract-- This paper presents a method to damp the low frequency power oscillations that can develop between Type III DFIG wind turbine generator systems and series compensated AC transmission lines. This problem is most prevalent when a Type III DFIG is connected radially to a load through a long series compensated transmission line. The method proposed involves placing a multi-band controller in parallel with the existing generator controls allowing the system to function as designed during normal operation while allowing the multi-band controls to operate to maintain system stability in the case of an Sub-Synchronous Oscillation (SSO) event. The frequency bands of the controller are dictated by the specific configuration of the system under study and are determined through frequency analysis of the generator output. The method demonstrated shows improved stability in regards to fault response and system response to the insertion of series compensation along transmission lines on the model system.

Index Terms-- Control systems, Power system stability, Power transmission, Wind power generation

I. KEY EQUATIONS

Lead-Lag Compensator
$$\frac{Y}{X} = A \frac{(s-z_1)(s-z_2)}{(s-p_1)(s-p_2)}$$

II. INTRODUCTION

THE system shown below is a high level view of the model studied in this paper. The system consists of 150 3 MW Type III induction generators connected to a ‘long’ transmission line of approximately 240 km (150 miles), which is in turn connected to the infinite bus modeled by a stiff voltage source.

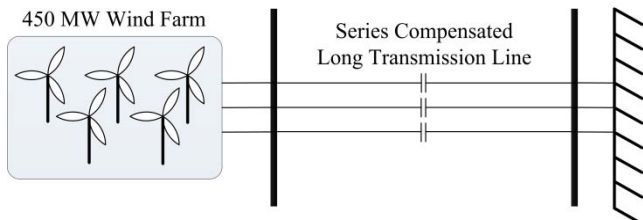


Figure 1 - High Level View of Wind Farm System

Connection of a series capacitor to the transmission line to bring the compensation level to 50% will cause the system to start oscillating and quickly stability. The model system which is stable without series compensation would lose stability with compensation values of less than 10%. A block diagram of the MBSSDC implemented on the wind farm system is shown

below in figure 3. This design involves an auxiliary control system with multiple frequency bands placed in parallel with the existing excitation control. The MBSSDC is a cost effective solution that works by altering the excitation of the doubly fed induction generator, to damp out the oscillations encountered when an SSO event is occurring.

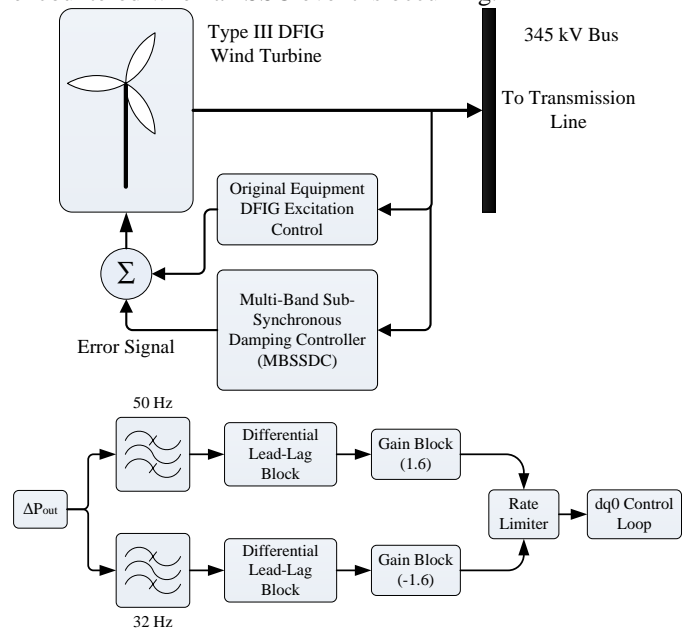


Figure 2. – MBSSDC Implementation & Block Diagram

Shown below is the wind farm output when 50% series compensation is connected to the system at five seconds with and without the MBSSDC.

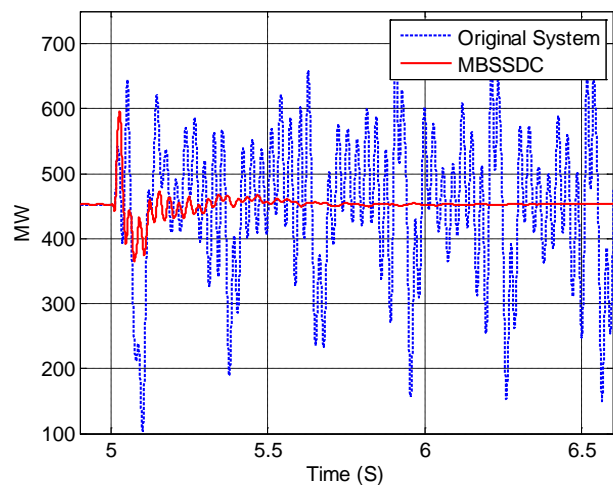


Figure 3. – System Outputs with 50% Compensation

Small Signal Stability Analysis of Two Area System with Magnetic Amplifier

Xiaohu Zhang¹, Keman Lin¹, Kevin Tomsovic¹ and Aleks Dimitrovski²

¹Dept. of Electrical Engineering and Computer Science, University of Tennessee, Knoxville, Tennessee, USA

²Oak Ridge National Laboratory, Oak Ridge, Tennessee, USA

Email: xzhang46@utk.edu

Abstract—The small signal (or Linear) stability of power system is an important concern for power engineers. It provides valuable information about the inherent dynamic characteristics of the power system. After linearizing the power system equations, the oscillation modes can be divided into two categories: local and inter-area modes. Damping inter-area modes are more difficult because they are influenced by global states. Since the system oscillations are closely related to the line impedance, controlling the line impedance can help the system to damp the inter-area oscillations. Magnetic Amplifier (MA) is a series reactor with continuous reactance regulation which is controlled by a simple power electronics circuit. The cost is far less than a comparative FACTS device. In this study, linear analysis of Kundur’s two area system incorporated with a MA is presented. The residue method is adopted to design the damping controller for MA. Simulation results show that the MA with proper control design is highly effective at damping inter-area oscillations.

I. KEY EQUATIONS

Linearizing the power system around its equilibrium point, the following can be obtained:

$$\begin{aligned}\Delta\dot{x} &= A\Delta x + B\Delta u \\ \Delta y &= C\Delta x + D\Delta u\end{aligned}\quad (1)$$

The eigenvalues λ_i are determined by state matrix A :

$$\det(\lambda I - A) = 0 \quad (2)$$

The key equations for damping controller design based on residue method are [1]:

$$\varphi_{comp} = 180^\circ - \arg(R_i) \quad (3)$$

$$\alpha = \frac{T_1}{T_2} = \frac{1 + \sin(\frac{\varphi_{comp}}{m_c})}{1 - \sin(\frac{\varphi_{comp}}{m_c})} \quad (4)$$

$$T_2 = \frac{1}{\omega_{pi}\sqrt{\alpha}}; T_1 = \alpha T_2 \quad (5)$$

$$K = \left| \frac{\lambda_{i,des} - \lambda_i}{R_i H(\lambda_i)} \right| \quad (6)$$

II. KEY FIGURES

The two area system is used as the test system [2].

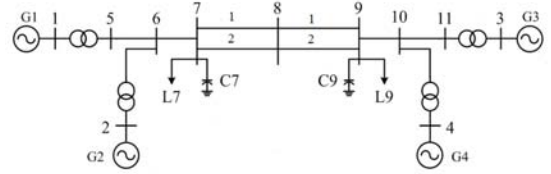


Fig. 1. Test System.

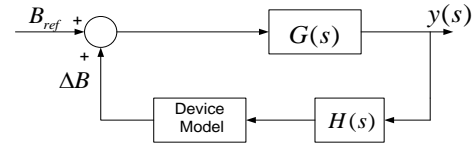


Fig. 2. Closed-loop system with MA damping controller.

III. KEY RESULTS

The desired damping ratio for the inter-area mode is 8%. The disturbance for the simulation is that the mechanical power of G1 decreased by 10% during 100 ms.

TABLE I
INTER-AREA MODES FOR DIFFERENT CASES

	No controller	ω_{SIME} as input	ΔP_{tie} as input
$\xi\%$	-1.3019	7.1172	7.8792
f (Hz)	0.6173	0.6337	0.6200

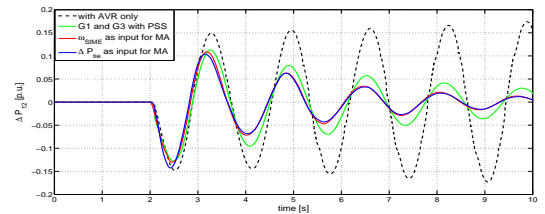


Fig. 3. Deviation of the tie line power flow.

REFERENCES

- [1] N. Yang, Q. Liu, and J. McCalley, “TCSC controller design for interarea oscillations,” *IEEE Trans. Power Syst.*, vol. 13, pp. 1304-1309, Nov. 1988.
- [2] P. Kundur, *Power System Stability and Control*. New York: McGraw-Hill, 1994.

Modeling Inverter PQ Control in PSCAD

Yin Li, Student Member, Lingling Fan, Senior Member, IEEE
 Department of Electrical Engineering
 University of South Florida, Tampa, United States

Abstract— In this project, a grid-connected inverter is controlled to have decoupled PQ regulating capability. The controller output is three-phase voltage (magnitude and angle) from the inverter while the measurements include grid voltage and current to the grid. Vector control is employed to have decoupled PQ regulation. To realize the vector control, dq components of voltage and currents are computed and the angle of the converter will be “locked” to the grid through phase locked loop (PLL). PSCAD modeling is conducted in this project.

i. System Configuration

For designing a feedback control system, we just need to add two blocks, the PLL and the DQ2ABC, in the normal one like Figure 1. The system has two DC power supplies and they are converted into three-phase power via a gate block named Averaged ideal three-phase VSC. The gate block is controlled by the input reference, and the input reference is produced by the process of the PLL and the DQ2ABC.

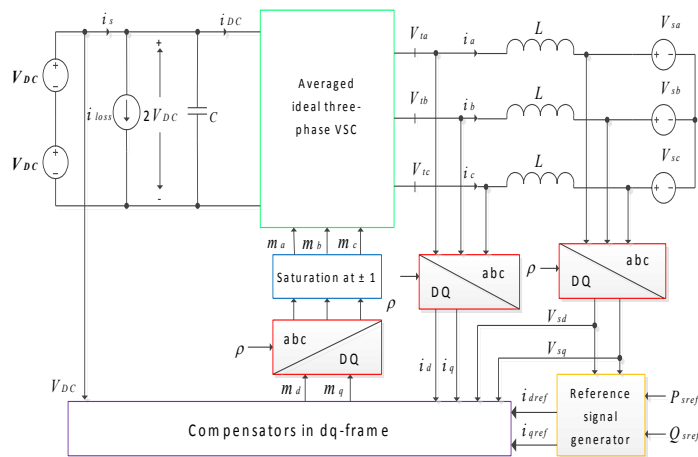


Figure 1: the configuration of the generator system

The key element of the feedback control is the PLL block. It can process the three-phase voltages and give frequency and the phase angle, ρ . The phase angle is the key parameter to produce the input reference.

Converter voltage can be decomposed into dq components. Changing d-axis voltage will only impact real power P while changing q-axis voltage will only impact reactive power Q. Thus, decoupled control is realized.

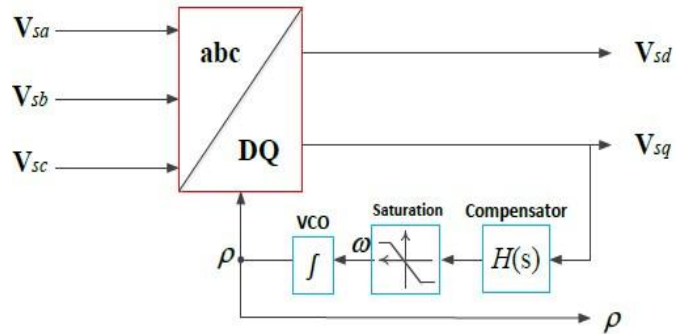


Figure 2: the configuration of the PLL block

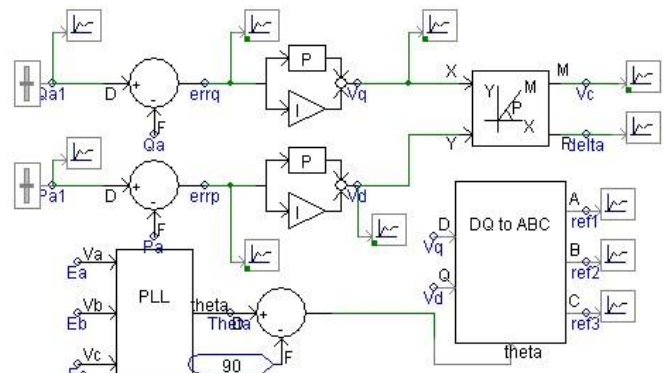


Figure 3: converter control block

ii. Key Results

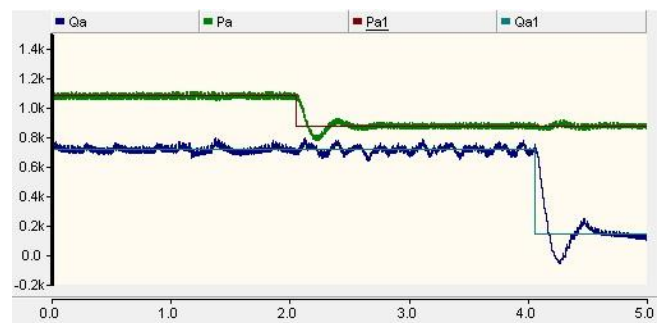


Figure 1: the plots of the expected power which can be controlled and the actually power which the system generates.

Simplified WECC Model with Wind Penetration

Yidan Lu and Kevin Tomsovic

Dept. of Electrical Engineering and Computer Science
The University of Tennessee
Knoxville, TN, USA
Ylu16@utk.edu

Yilu Liu

Dept. of Electrical Engineering and Computer Science
The University of Tennessee
Knoxville, TN, USA
Liu@utk.edu

Abstract— This work aims at building equivalent reduced models of WECC network with different levels of wind penetration as base case and test system for RAS development for future power system. The dynamic equivalence is verified by similar frequency response of the reduced model compared with FNET data. California-Oregon Interface (COI) transfer limit of the reduced WECC system at different wind penetration is calculated and compared with CAISO standard value. Critical generator rejection and load shedding is applied as a protection scheme to improve transfer limit at high wind penetration.

Keywords— transfer limits; wind penetration; protection scheme; load shedding introduction

I. INTRODUCTION

The modern power grid is undergoing a dramatic change in its generation mix. Conventional energy sources are being replaced by renewable energy sources. The rapid change in generation as well as transmission indicates a potential revolution in power system which intrigues the study of large scale test-bed to represent large grids of the future.

II. DYNAMIC EQUIVALENCE VERIFICATION BY FREQUENCY RESPONSE

On the occurrence of 1400MW generation drop in Montana, frequency data are recorded. Table I shows the structures of reduced WECC systems with three different level of renewable penetration. Table II shows the comparison of frequency responses to the specified contingency among proposed systems and FNET data.

TABLE I. SYSTEM STRUCTURES

Element\Bus	Bus	Total Generation	Wind Capacity
Detailed Case	15600	154.4GW	0GW
Case I	179	61.441GW	0GW
Case II	190	61.441GW	7.37GW
Case III	190	61.441GW	13.45GW

TABLE II. FREQUENCY RESPONSE COMPARISON

Element	FNET	Case III	Case II	Case I
Wind Percentage	-----	22%	12%	0%
Max Freq. Drop	145mhz	120mhz	148mhz	124mhz
Recovery Time	15S	Negative Damping	15S	12S
Final Deviation	85mhz	48mhz	50mhz	49mhz

III. WECC N-1 COI TRANSFER LIMIT ANALYSIS WITH WIND PENETRATION

As three reduced WECC networks with different wind penetration are constructed. A stability assessment based on COI transfer capacity on the wind penetrated cases is carried out and system equivalence is verified by similar transfer limit compared with CAISO 2012 OSS report [1] on 179 bus base case. The transfer limit on base case is calculated based on WECC-NERC standards with only single element outage. Criteria involved in the OSS report are also included in the base case transfer limit calculation. The COI transfer limit of different reduced systems compared to CAISO standard value is shown in Table III. Then, load shedding according to generator rejection of critical machine is applied as a protection scheme on case III, which has the heaviest wind penetration. The effect of protection scheme on transfer limit is shown in Table IV.

TABLE III. TRANSFER LIMIT COMPARISON

System\Event	Transfer Limit	Limiting Factor	Contingency
Detailed Case	4800MW	VAR Limit	DC outage
Case I	4690MW	Freq. drop in Canada	DC outage
Case II	4673MW	Volt. drop in CA	DC outage
Case III	4414MW	Angle instability in Idaho Wind Units	DC outage

TABLE IV. LOAD SHEDDING EFFECT ON CASE III TRANSFER LIMIT

System	No Protection	Standards	With Protection
Case III	4414MW	Event based Generator rejection and load shedding	4505MW

IV. CONCLUSION AND FUTURE WORK

The frequency response and N-1 COI transfer limit on base case demonstrates that the proposed reduced 179 bus WECC model is fairly equivalent to the original system. The increase of wind penetration will decrease the system stability by reducing the interface transfer capacity, which can be partially restored by applying load shedding. More sufficient RAS still need to be developed for stability fully recovery.

REFERENCES

- [1] R. Chakkapalli and P. Poonpun, " SYSTEM OPERATING LIMIT STUDY REPORT," CAISO, folsom, CA January 31, 2012 2012.

Stability Analysis of Unbalanced Synchronous Machine Based Distributed Generators

Ehsan Nasr Azadani, *Student Member, IEEE*, Claudio Canizares, *Fellow, IEEE*, Kankar Bhattacharya, *Senior Member, IEEE*

Power and Energy System Group, Department of Electrical and Computer Engineering,
University of Waterloo, CANADA

Abstract— There are many technical aspects and challenges in distributed generation (DG) that have not been properly understood and addressed so far. Distribution systems cannot be considered as balanced three-phase systems, because these are inherently unbalanced in steady-state operation. A full characterization of the unbalanced system with respect to system stability allows a better understanding of the dynamic behaviour of such systems. A comprehensive investigation of the effects of system unbalance on the stability of the distribution systems with synchronous machine based DG units at different loading levels is presented. Detailed steady-state and dynamic analyses of the system are performed. Based on voltage, small-perturbation, and transient stability studies, it is demonstrated that system unbalance can significantly affect the distribution system dynamic performance.

Keywords- *Distributed generation, unbalanced power systems, voltage stability, angle stability.*

I. KEY RESULTS

A real-life distribution system from Japan is used for the studies. Both dynamic and static analyses are carried out using the PV curves and maximum loadability computations [1]. Static voltage stability studies are based on three phase power flows [2]. In this case, the static maximum loadability is associated with a loading level at which there is no power flow solution. Dynamic voltage stability studies are carried out using time domain simulations in PSCAD/EMPTC, based on the detailed dynamics of DGs and their AVRs.

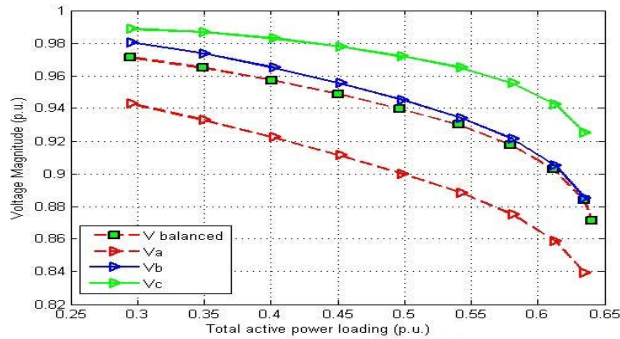


Fig 1. PV curves for $k=10\%$.

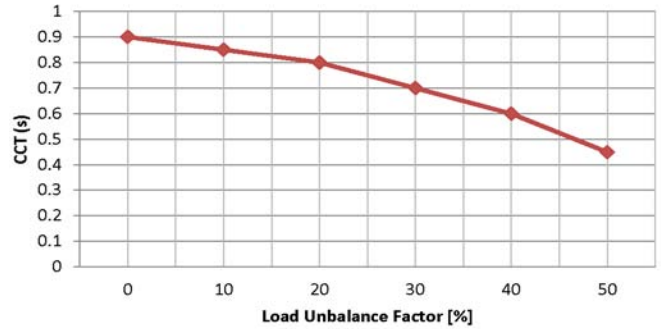


Fig. 2. CCT of the test system for base loading and a three phase-to-ground fault.

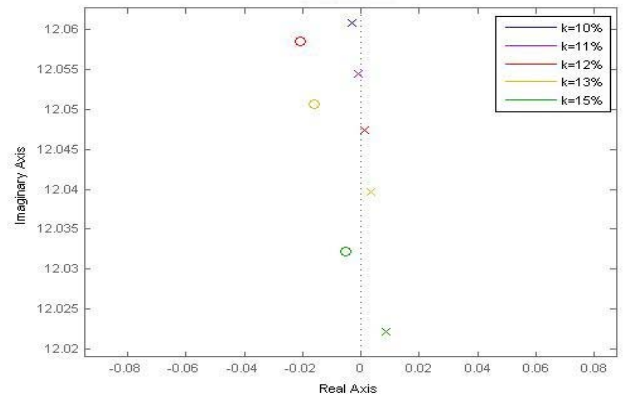


Fig. 3. Zero-pole map of the generator speed around critical unbalanced conditions.

When the system is more heavily loaded, the critical poles cross the imaginary axes and the system becomes unstable as unbalancing increased.

II. REFERENCES

- [1] E. Nasr Azadani, C. Canizares, and K. Bhattacharya, "Modeling and stability analysis of distributed generation", in *Proc. IEEE Power and Energy Society General Meeting*, Jul 2012.
- [2] M. Z. Kamh and R. Iravani, "Unbalanced model and power-flow analysis of microgrids and active distribution systems," *IEEE Trans. Power Del.*, vol. 25, no. 4, pp. 2851–2858, Oct. 2010.

Switching Loss and Cell Capacitor Balancing of Modular Multilevel Converter under Various Modulation Frequencies

Hee Jin Kim and Sukki Jung

School of Electronic and Electrical Engineering, Yonsei University
Seoul, South Korea

E-mail: jimmykim07@gmail.com and sk_cloud@hotmail.com

Abstract—The poster presents the characteristics of switching loss, cell capacitor balancing, and total harmonic distortion (THD) of modular multilevel converter (MMC) system under various modulation frequencies. To generate the desired waveform, MMC uses a large number of power-electronic switching which produces losses. Under various switching frequencies, the MMC system shows different performance of loss, capacitor balancing, and THD. To evaluate the MMC system, we modeled the MMC system as a detailed equivalent circuit. Using method, each MMC arm is represented by a Th’evenin equivalent branch. The nearest level control strategy, including a voltage balancing method, for the operation of an MMC is presented. As modulation frequencies increases, loss increases, but cell capacitor balancing is improved and THD is also reduced.

Index Terms—MMC, Cell capacitor balancing, Switching loss, THD, a detailed equivalent model.

I. KEY FIGURE

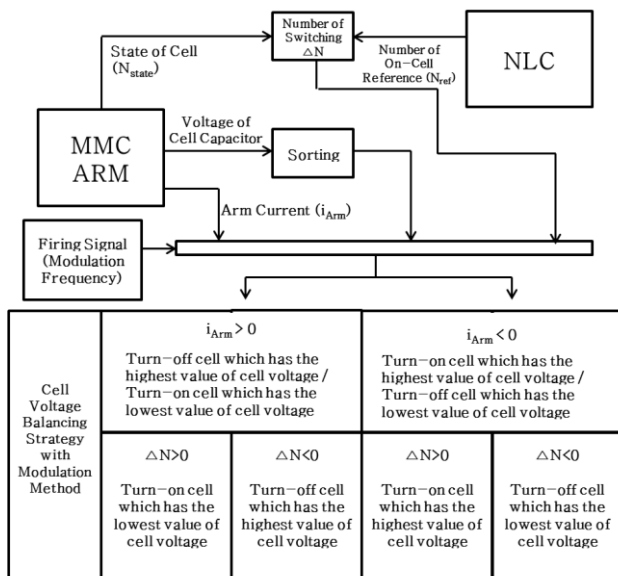


Fig. 1. Cell voltage balancing strategy with modulation method.

II. KEY TABLE

TABLE I. SPECIFICATION OF TEST SYSTEM

AC Grid 1	230 kV _{L-L}	AC Grid 2	115 kV _{L-L}
AC Converter Voltage	180.5 kV _{L-L}	Nominal Power	400 MW
DC Voltage	±200 kV	Number of Cell per Arm	200
SCR of AC Grid	3.5	Cell Capacitor Value	4.5 mF

TABLE II. LOSS AND THD UNDER VARIOUS FREQUENCIES

Modulation Frequency (kHz)	Switching Frequency for One Cell (Hz)	Switching Loss (%)	Conducting Loss (%)	Total Loss (%)	THD (%)
35	217	0.164	0.36	0.524	6
40	246	0.188	0.36	0.548	0.87
60	344	0.262	0.36	0.622	0.57

III. KEY RESULT

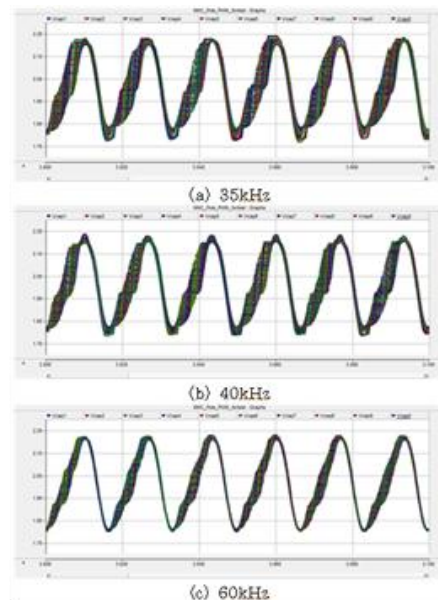


Fig. 2. Performance of cell voltage balancing strategy with various modulation frequencies (Phase A, Upper Arm in MMC connected to AC grid 1).

DC Impedance-Model-Based Resonance Analysis of a VSC-HVDC System

Ling Xu, *Student Member, IEEE*, and Lingling Fan, *Senior Member, IEEE*
 Department of Electrical Engineering, University of South Florida, Tampa, FL 33620, USA,
 Email: lxu@mail.usf.edu

Abstract—Resonances can have negative impact on a Voltage Source Converter-High Voltage DC (VSC-HVDC) system. This paper develops dc impedance models for the rectifier and inverter stations for a VSC-HVDC system when they are viewed from a dc terminal. The impedance models take converter controllers into account. The derived impedance models are validated by comparing frequency responses of the analytical model and the impedance measured at the dc terminal from a detailed VSC-HVDC model simulated in a real-time digital simulator. Resonances are examined in frequency domain (e.g., Bode plots and Nyquist plots) using the derived analytical impedance models. The analysis is verified by time-domain simulations. Real-time digital simulation in RT-Lab demonstrates that the dc capacitor has significant impact on resonances while power transfer level has insignificant impact on resonances.

I. KEY EQUATIONS

The DC impedance model of VSC-HVDC is:

$$M_{i_{dc}} = \left\{ I - [I + Y_i(s)Z(s)]^{-1} (G_c(s)G_{p1} + Y_i(s)G_{v1}) \right\}^{-1} [I + Y_i(s)Z(s)]^{-1} (G_c(s)G_{p2} + Y_i(s)G_{v2}) \quad (1)$$

$$M_{v_{dc}} = \begin{bmatrix} sL - \frac{E_{d0}}{i_{d0}} & 2sL \frac{i_{q0}}{i_{d0}} + \omega L \\ -\omega L & -sL \end{bmatrix} M_{i_{dc}} \quad (2)$$

$$M = \begin{bmatrix} i_{dc0} & v_{dc0} \\ i_{d0} & i_{d0} \\ 0 & 0 \end{bmatrix} + \begin{bmatrix} i_{d0} & i_{q0} \end{bmatrix} M_{v_{dc}} + \begin{bmatrix} v_{d0} & v_{q0} \end{bmatrix} M_{i_{dc}} \quad (3)$$

$$Z_{dc} = \frac{\Delta v_{dc}}{\Delta i_{dc}} = \frac{M(1,2) - v_{dc0}}{i_{dc0} - M(1,1)} \quad (4)$$

II. KEY FIGURES

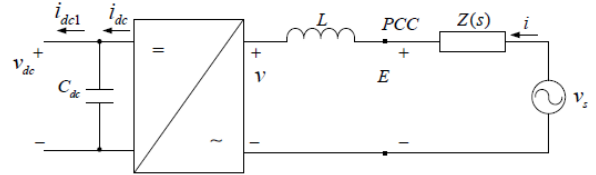


Figure 1. A model of VSC and grid.

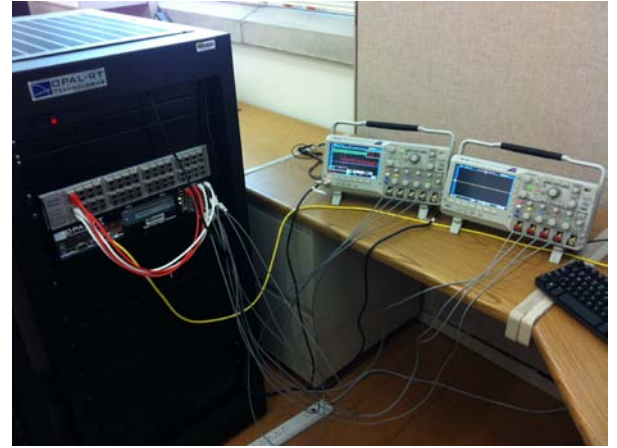


Figure 2. Real-time digital simulation setup using RT-Lab.

III. KEY RESULTS

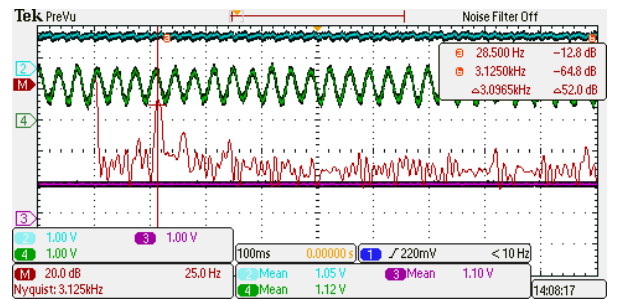


Figure 3. Simulation results of 900uF capacitor.

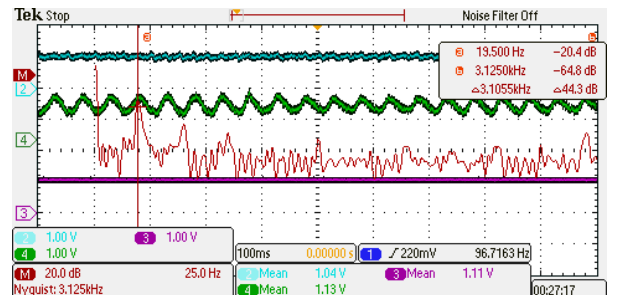


Figure 4. Simulation results of 1800uF capacitor.

Improvement of Composite Load Modeling Accuracy Using Parameter Shift Algorithm

Jae-Kyeong Kim

School of Electrical and Electronic Engineering, Yonsei University, Seoul, South Korea,
Email: Jk.Kim@yonsei.ac.kr

Abstract— This poster presents parameter shifting algorithm in measurement-based load modeling. Owing to the nonlinear characteristics and complexity of model structure, some solutions of load modeling usually stall at local minimum points on boundary. In proposed algorithm, the parameters on upper or lower boundary could be shifted to opposite side depending on boundary and initial values. This process is able to decrease possibility of boundary stall problem happening and then improves accuracy of the load model. The simulations are carried out for evaluating the performance of the proposed method using various data. Testing results indicate that the proposed algorithm presents the competitively high accuracy of the load model with traditional model.

Index Terms— Composite Load Modeling, Nonlinear Optimization, Levenberg-marquardt method, Measurement approach

I. KEY EQUATIONS

The levenberg-marquardt equation for nonlinear least square is:

$$\mathbf{x}_{i+1} = \mathbf{x}_i - (\mathbf{J}^T \mathbf{J} + \lambda \mathbf{I})^{-1} (\mathbf{y} - \mathbf{f}(\mathbf{x}_i)) \quad (1)$$

The equations of parameter shifting algorithm are :

$$x(i) = \frac{(n-1)x_{lower\ bound} + x_{upper\ bound}}{n} \quad (2)$$

$$x(i) = \frac{(n-1)x_{upper\ bound} + x_{lower\ bound}}{n}$$

II. KEY FIGURES

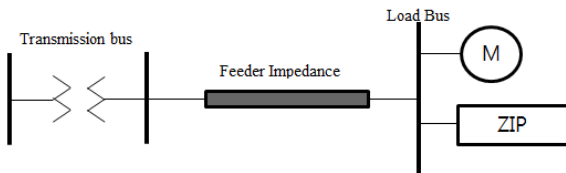


Figure 1. Structure of composite Load model

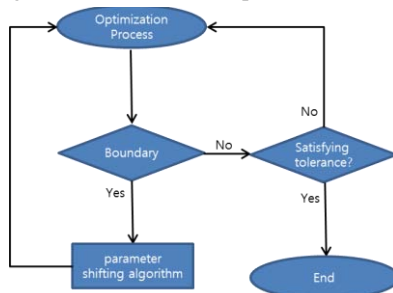


Figure 2. Flow chart of Parameter Shifting Algorithm

III. KEY RESULTS

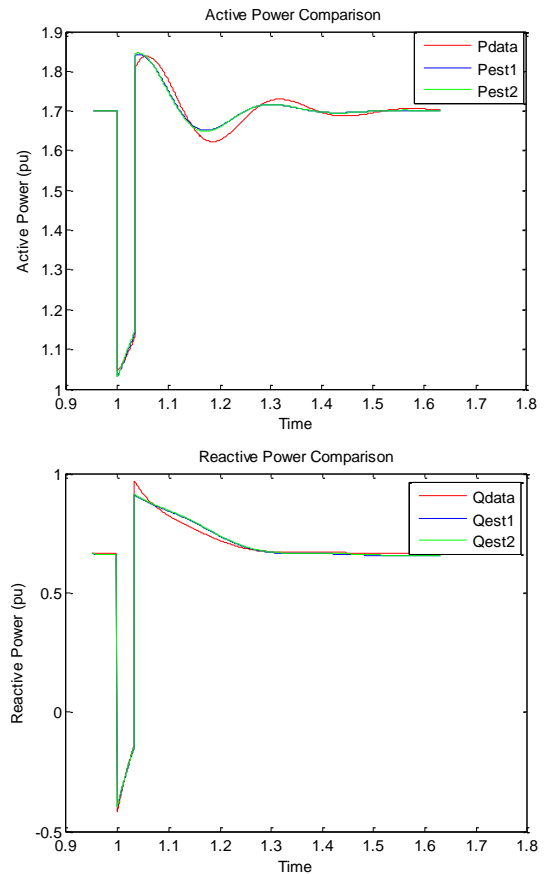


Figure 3. Optimization results of classical and proposed method

	H	motor ratio	Pi	Qz
low boundary	0.1	0.1	0	0
Standard Method	1.501	0.39	0.8	0
Using Algorithm	1.536	0.365	0.39	0.002
upper boundary	3	0.6	0.8	0.8

Table 1. Parameter table of composite load model

Enhanced Frequency Regulation Service using Hybrid Energy Storage System against Increasing Power-Load Variability

¹Youngho Cho, ¹Jae Woong Shim, ²Seog-Joo Kim, *Member, IEEE*, ²Sang Won Min, *Member, IEEE* and ¹Kyeon Hur, *Senior Member, IEEE*

¹School of Electrical and Electronic Engineering, Yonsei University, Seoul, Korea

²Korea Electrotechnology Research Institute, Uiwang, Korea

Email: sglab@yonsei.ac.kr, jeuhnshim@yonsei.ac.kr, sjkim@keri.re.kr, swmin@keri.re.kr, khur@yonsei.ac.kr

Abstract—Increasing penetration of wind energy resource raises concerns about system frequency regulation because wind turbines lack in control capability necessary to provide regulation in compensating generation-load imbalance. Inherent variability on every time scale, in fact contributes to a need for more sophisticated regulation; existing load-following spinning reserves may be too slow or limited in responding to the imbalance. One feasible solution for enhancing regulation capability is the use of Hybrid Energy Storage System (HESS) as proposed in this paper. In this research, the HESS is designed to be composed of a Li-ion battery and supercapacitor (SC), exploiting their respective high energy and power capabilities to fully handle long-term and short-term changes. This paper demonstrates the effectiveness of HESS for frequency regulation in meeting the grid code while smoothing the net variability (load-wind) for an isolated power system modeled using an electromagnetic transient program.

Index Terms—HESS, battery, SC, moving average, frequency control.

I. KEY FIGURES

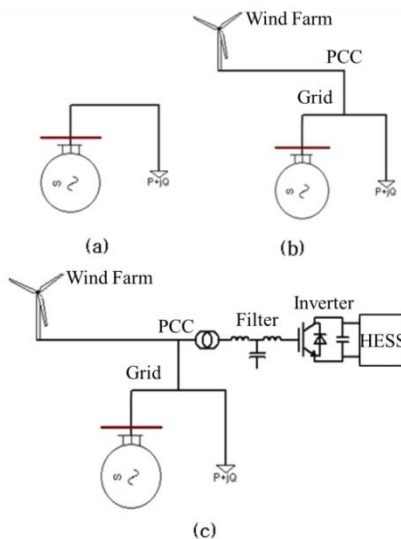


Fig. 1. Three system configurations. (a) The grid with the only load. (b) The wind farm is added to (a). (c) It consists of wind and HESS.

II. KEY RESULTS

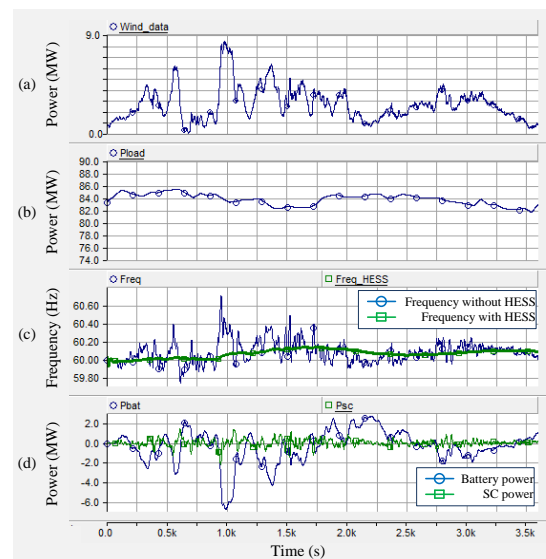


Fig. 2. The comparison of simulation results of fig 1. (b) and (c). (a) Wind power generation. (b) Load demand. (c) Grid frequency at PCC point with/without HESS. (d) Power compensation of battery and SC.

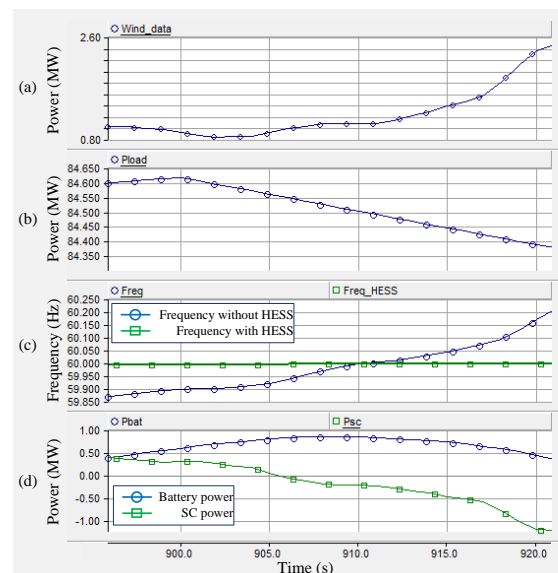


Fig. 3. The enlarged graph of Fig. 2 for analyzing the operation of each storage.

Investigation of Power Flow solution When Slack Generator Hits Reactive Power Limit

Hung-Ming Chou and Karen L. Butler-Purry

Department of Electrical and Computer Engineering, Texas A&M University, College Station, TX 77843 USA

Email:hmchou@tamu.edu and klbutler@tamu.edu

Abstract—In the conventional power flow formulation, the slack bus is assumed to provide enough reactive power to serve as the voltage reference in the power flow program. However, in the autonomous operation of microgrid, there may be no generators that can serve as the slack bus that can have enough reactive power capability. Unlike the conventional power system, normally the reactive power capacity of generator connected in the microgrid is limited. When the reactive power of the generator hits the limit, the terminal voltage will deviate from the nominal value and there is no voltage reference point in the power flow formulation. In this poster, the impact of the reactive power limit of the slack bus is investigated by using a simple two-bus example. The mathematical equations are derived and the physical interpretation will be made.

I. KEY EQUATIONS

When the reactive power is within the limit, the voltage equations of the two bus can be solved in closed form as:

$$|V_1| = 1 \quad (1)$$

$$|V_2| = \sqrt{\frac{[|V_1|^2 - 2\beta P_D x] \pm \sqrt{|V_1|^4 - 4P_D x(\beta|V_1|^2 + P_D x)}}{2}} \quad (2)$$

Assume the load is constant power load: $Q_D = \beta P_D$. The critical real power that will cause the reactive power of the generator at bus 1 will be

$$P_{D-crt} = \frac{-\frac{\beta}{x} \pm \sqrt{(\frac{\beta}{x})^2 - 4(Q_{G-max}^2 - \frac{1}{x}G_{G-max})}}{2} \quad (3)$$

When the real power load is greater than P_{D-crt} , the generator will hit the reactive power limit. The voltage equations of the two bus can be solved in closed form as:

$$|V_1| = \frac{\sqrt{P_D^2 + Q_{G-max}^2}}{\sqrt{\frac{Q_{G-max} - Q_D}{x}}} \quad (4)$$

$$|V_2| = \frac{\sqrt{P_D^2 + Q_D^2}}{\sqrt{\frac{Q_{G-max} - Q_D}{x}}} \quad (5)$$

II. KEY FIGURES AND RESULTS

P_G (MW)	Q_G (MVar)	$ V_1 $	θ_1	P_D	Q_D	$ V_2 $	θ_2
100	45	1	0	100	33	0.9604	-5.977
100	41	1.2	0	100	33	1.1688	-4.008
100	39	1.4	0	100	33	1.3742	-2.479

TABLE I. RESULT FROM POWER WORLD

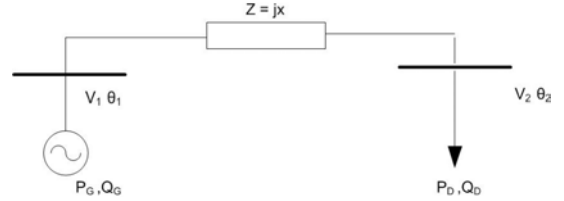


Fig. 1. One line diagram of the two-bus system

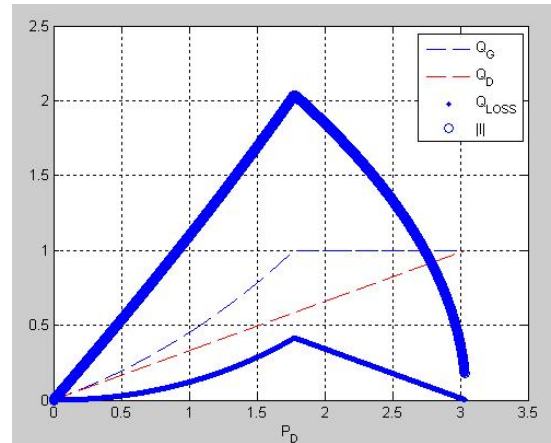


Fig. 2. Q_G , Q_D and $|I|^2$ versus P_D

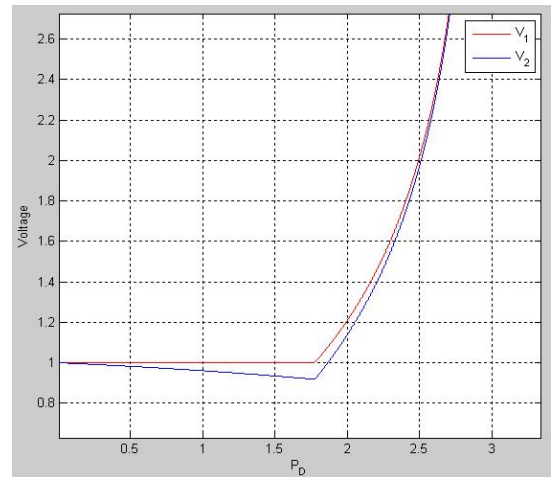


Fig. 3. $|V_1|$ and $|V_2|$ versus P_D

A Fast and Efficient Load Shedding Algorithm to Alleviate Transmission System Overloads and Under Voltages

Yaser Tohidi⁺, Amir Safdarian⁺⁺, and M. Hesamzadeh⁺

⁺Electricity Market Research Group, KTH Royal Institute of Technology, Stockholm, Sweden

⁺⁺Electrical Engineering Department, Sharif University of Technology, Tehran, Iran

Email: tohi@kth.se

Abstract— Power systems are becoming older and more intense. Thus, disturbances are inevitable and it is important to develop a powerful methodology to lessen the damages afterward. This paper proposes a new linear formulation based on an approximated version of AC power flow model to compromise between speed and accuracy of decision making process. In the proposed, voltage and reactive power violations as well as transmission system overloads are alleviated by either or both of generation rescheduling and load shedding. The developed method adopts the line flows and square of voltage magnitudes as the problem state variables. Simulation results on the IEEE-RTS96 system reveal that the proposed method outperforms the conventional one from the execution time and the computational effort viewpoints while keeping the accuracy of the results.

Keywords-power flow model; linear model; steady state power system analysis.

I. KEY EQUATIONS

The model developed in order to determine a secure post contingency operating point with lower computational complexity is presented below:

$$\min \sum_i \left(\text{voll}_i \cdot p_i^c + \sum_{k \in G_i} C_i^k(p_i^k) \right) \quad (1)$$

Subject to

$$\sum_{k \in G_i} p_i^k - \sum_l A_{il} \cdot p_l - \sum_l A'_{il} \cdot p_l^{\text{loss}} = p_i^d - p_i^c \quad (2)$$

$$\sum_{k \in G_i} q_i^k - \sum_l A_{il} \cdot q_l - \sum_l A'_{il} \cdot q_l^{\text{loss}} - B_{ii} \cdot V_i^2 = q_i^d - q_i^c \quad (3)$$

$$2(r_l \cdot p_l + x_l \cdot q_l) + V_j^2 - V_i^2 = -(r_l \cdot p_l^{\text{loss}} + x_l \cdot q_l^{\text{loss}}) \quad (4)$$

$$\sum_{l \in c} x_l \cdot p_l - r_l \cdot q_l = 0 \quad (5)$$

$$p_l^{\text{loss}} = p_l^{\text{loss}} \Big|_{\text{Operating point}} + \left[\frac{2 \cdot p_l \cdot r_l}{V_j^2} \quad \frac{2 \cdot q_l \cdot r_l}{V_j^2} \quad - \frac{p_l^2 \cdot r_l + q_l^2 \cdot r_l}{V_j^4} \right]_{\text{Operating point}} \times \begin{bmatrix} p_l \\ q_l \\ V_j^2 \end{bmatrix} \quad (6)$$

$$q_l^{\text{loss}} = q_l^{\text{loss}} \Big|_{\text{Operating point}} + \left[\frac{2 \cdot p_l \cdot x_l}{V_j^2} \quad \frac{2 \cdot q_l \cdot x_l}{V_j^2} \quad - \frac{p_l^2 \cdot x_l + q_l^2 \cdot x_l}{V_j^4} \right]_{\text{Operating point}} \times \begin{bmatrix} p_l \\ q_l \\ V_j^2 \end{bmatrix} \quad (7)$$

II. KEY RESULTS

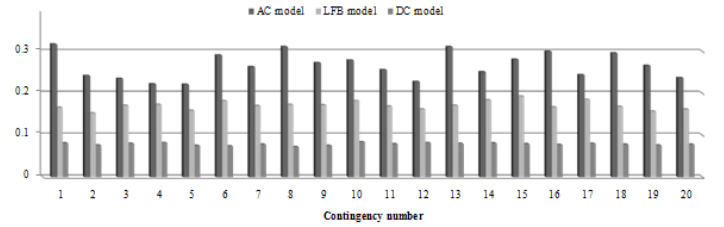


Figure 1. Comparison of the run time (sec.) associated with different models for the IEEE-RTS96.

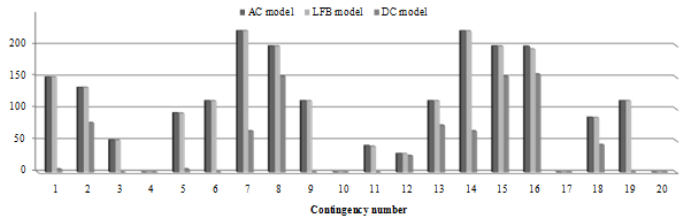


Figure 2. The amount of load curtailment associated with simulated contingencies obtained by different models for the IEEE-RTS96.

Implementing a Nuclear Power Plant Model for Evaluating Load-Following Capability on a Small Grid

Samet Arda, *Student Member, IEEE*, Keith E. Holbert, John Undrill

School of Electrical, Computer and Energy Engineering, Arizona State University, Tempe, AZ 85287-5706 USA

E-mail: sarda1@asu.edu, holbert@asu.edu, and john.undrill@asu.edu

Abstract— A pressurized water reactor (PWR) nuclear power plant (NPP) model is introduced into Positive Sequence Load Flow (PSLF) software by General Electric in order to evaluate the load-following capability of NPPs. The nuclear steam supply system (NSSS) consists of a reactor core, hot and cold legs, plenums, and a U-tube steam generator. The physical systems listed above are represented by mathematical models utilizing a state variable lumped parameter approach. A steady-state control program for the reactor, and simple turbine and governor models are also developed. Adequacy of the isolated reactor core, the isolated steam generator, and the complete PWR models are tested in Matlab/Simulink and dynamic responses are compared with the test results obtained from the H. B. Robinson NPP. Test results illustrate that the developed models represent the dynamic features of real-physical systems and are capable of predicting responses due to small perturbations of external reactivity and steam valve opening. Subsequently, the NSSS representation is incorporated into PSLF and coupled with built-in excitation system and generator models. Different simulation cases are run when sudden loss of generation occurs in a small power system which includes hydroelectric and natural gas power plants besides the developed PWR NPP. The conclusion is that the NPP can respond to a disturbance in the power system without exceeding any design and safety limits if appropriate operational conditions, such as achieving the NPP turbine control by adjusting the speed of the steam valve, are met. In other words, the NPP can participate in the control of system frequency and improve the overall power system performance.

I. KEY EQUATIONS

Point kinetics and Mann's model for heat transfer in the core are represented by following equations.

$$\frac{d\delta P}{dt} = \frac{-\beta}{\Lambda} \delta P + \lambda \delta C + \frac{P_0}{\Lambda} (\alpha_F \delta T_F + \alpha_M \delta T_M + \delta \rho_{ca}) \quad (1)$$

$$\frac{d\delta C}{dt} = \frac{\beta}{\Lambda} \delta P - \lambda \delta C$$

$$\frac{dT_F}{dt} = \frac{f}{(mc)_F} P - \frac{1}{\tau_F} (T_F - \theta_1) \quad (2)$$

$$\frac{d\theta_1}{dt} = \frac{(1-f)}{(mc)_C} P + \frac{1}{\tau_C} (T_F - \theta_1) - \frac{2}{\tau_R} (\theta_1 - \theta_m) \quad (3)$$

$$\frac{d\theta_2}{dt} = \frac{(1-f)}{(mc)_C} P + \frac{1}{\tau_C} (T_F - \theta_1) - \frac{2}{\tau_R} (\theta_2 - \theta_1) \quad (4)$$

II. KEY FIGURES

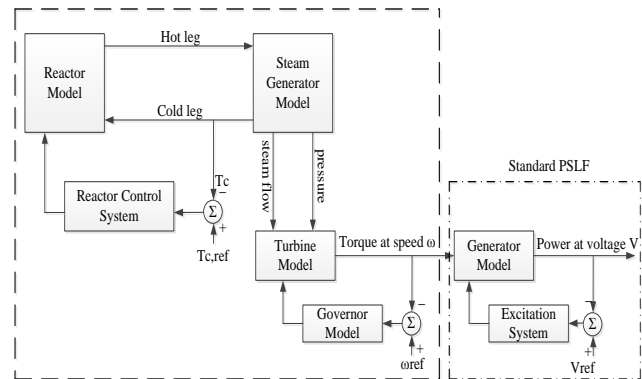


Figure 1. Block diagram of a PWR NPP

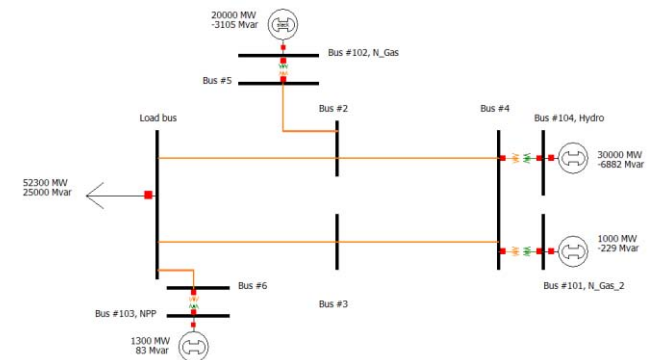


Figure 2. Small network model used in simulations

III. KEY RESULTS

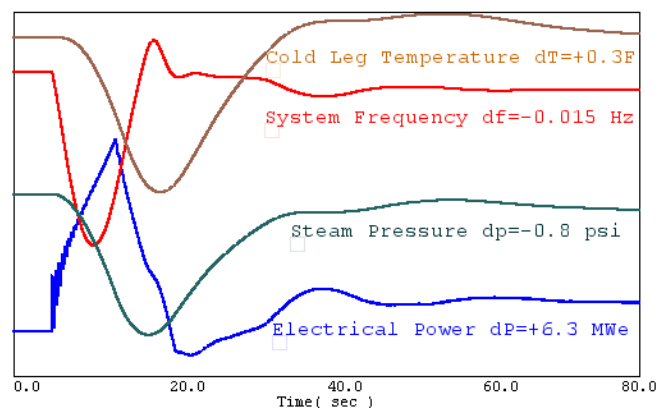


Figure 3. Response of NPP to loss of generation on the power system

Improved Cascading Outage Analysis model using Outage Checkers

Yezhou Wang
 School of Electrical and Computer Engineering
 University of Texas at Austin
 Austin, Texas, 78712
 Email: nickncwang@utexas.edu

Ross Baldick
 School of Electrical and Computer Engineering
 University of Texas at Austin
 Austin, Texas, 78712
 Email: baldick@ece.utexas.edu

Abstract—Large blackouts are generally caused by a consecutive series of various outages following an initial disturbance. Once a critical component of power systems is failed, the outages including generator and load trips can sequentially spread and frequently lead to large blackouts. Most blackouts involve a sequence of cascading outages. In this paper, outage checkers to identify potential cascading process that might lead to large blackouts are proposed. Four outage checkers, namely the transient stability checker, the frequency outage checker, the line outage checker and the voltage outage checker are implemented. The outage checkers are operated according to a newly proposed algorithm to determine the status of the resulting operating state or equilibrium. Detailed modeling of the protection schemes, including but not limited to rotor angle deviation relays, under frequency load shedding schemes, under/over voltage relays and over current relays are implemented.

The proposed sequential outage checkers for analyzing cascading outages and preventing large blackouts are verified using the IEEE 118-bus system, and the IEEE RTS-96 system.

I. KEY FIGURES AND RESULTS

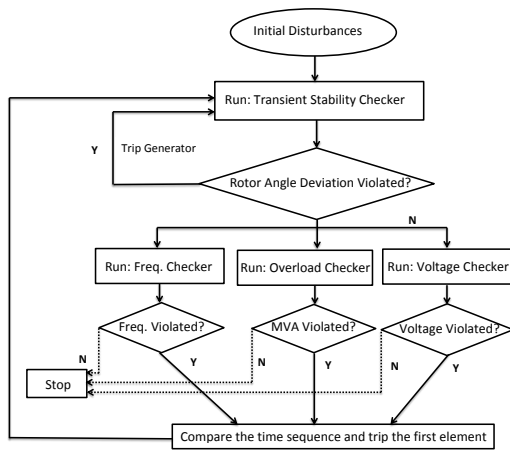


Fig. 1. Improved workflow of the COA

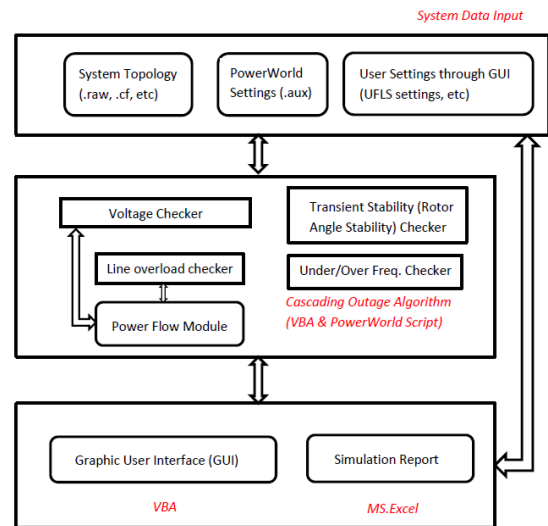


Fig. 2. Implementation framework of the COA

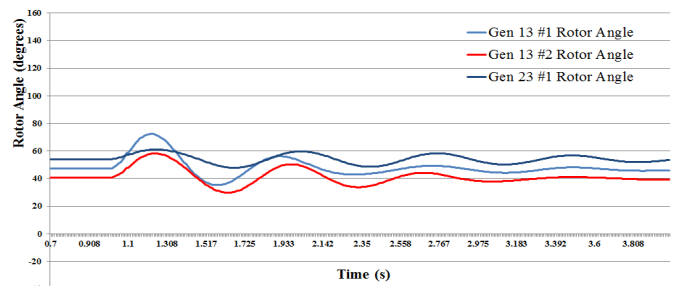


Fig. 3. Generator angle for scenario one, stable swing

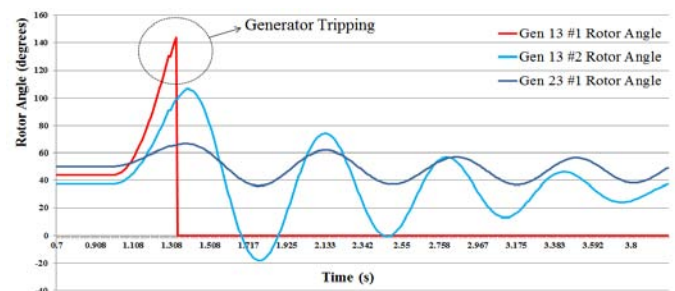


Fig. 4. Generator angle for scenario two, unstable swing

Methodology to Determine Distribution Level Impact of Dynamic Transfers

David Kleinschmidt, *Student Member, IEEE*, and Anjan Bose, *Fellow, IEEE*
 School of Electrical Engineering and Computer Science, Washington State University,
 Pullman, WA 99164, USA
 Email: dkleinsc@eecs.wsu.edu and bose@wsu.edu

Abstract— As a consequence of the increasing penetration of renewables and demand responsive loads, utilities are seeing a higher degree of variability in the operation of the power system. In particular, large, unexpected wind or PV generation ramps can cause a balancing authority (BA) to seek balancing reserves in or through an adjacent BA. These variable flows, known as dynamic transfers, have the potential to force a power system into an insecure state. Furthermore, dynamic transfers can result in increased switching operation of major equipment, voltage fluctuations outside of specified tolerances, and dynamic instability issues even if the overall flows do not exceed the standard operating limit (SOL) of the path.

To address these issues, the Wind Integration Study Team’s (WIST) Dynamic Transfer Capability (DTC) task force devised a methodology to calculate a transfer variability limit (TVL). This methodology relies on the determination of the impact of dynamic transfers on distribution level utilities (transmission “customers”), with a particular focus on voltage regulation. Specifically, the magnitude of voltage variation that the distribution utility can tolerate while still meeting ANSI standards must be known. The potential for reduced equipment life due to increased switching operation is also a component of the variability limit.

This work develops a methodology to determine the impact of greater voltage variation (magnitude and frequency) on distribution utilities in order to calculate TVLs. The methodology involves integrating a more detailed distribution system model into the transmission system base case, ensuring to include voltage regulating equipment such as LTC transformers and switched capacitor banks. A time series power flow is utilized to simulate potential dynamic transfers and the resulting voltage impact on the distribution utility. Increased switching operation of voltage regulating equipment is also quantified using this method to determine the potential for shortened equipment life. Both IEEE standard test cases and actual WECC member models are employed to test the methodology.

I. KEY EQUATIONS

Sum of static transfers (ST) and variable transfers (VT) is less than the standard operating limit (SOL):

$$ST + VT \leq SOL \tag{1}$$

$$SOL = \text{Max SL}, \text{ when } VT = 0 \tag{2}$$

II. KEY FIGURES

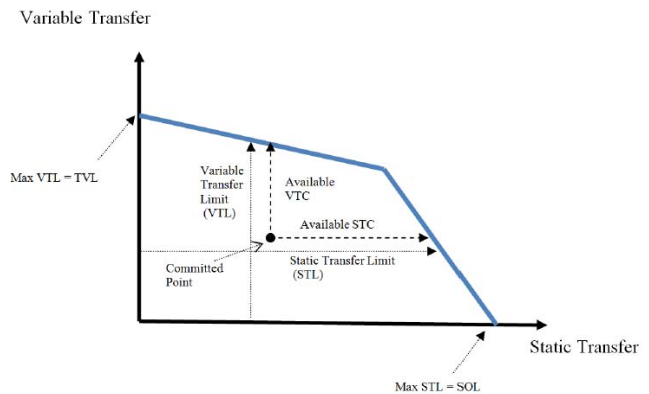


Fig. 1. Relationship between static and dynamic transfers [1]

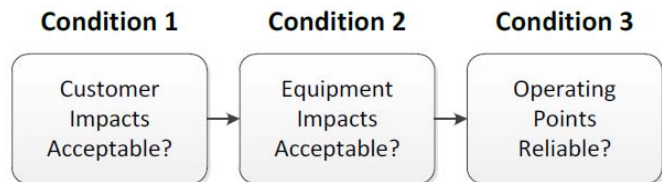


Fig. 2. Factors for determining transfer variability limit [1]

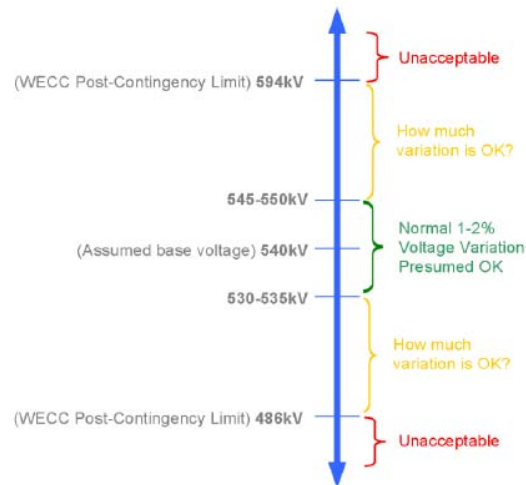


Fig. 3. Voltage variation range for high voltage system [1]

III. REFERENCES

[1] G. Dobson-Mack et al. (2011, Dec.). WIST DTC Task Force Phase 3 Report. ColumbiaGrid, Portland, OR. [Online]. Available: <http://www.columbiagrid.org/DTCTF-documents.cfm>

Effect of Price-Responsive Demand on Dispatch and Costs

Felipe Ramos-Gaete, Claudio Canizares, Kankar Bhattacharya,

Power and Energy Systems Group, Department of Electrical and Computer Engineering, University of Waterloo,
Ontario, Canada, N2L 3G1,

Email: framosga@uwaterloo.ca, ccanizares@uwaterloo.ca, kankar@uwaterloo.ca

Abstract—A demand elasticity model has been developed and tested for the dispatch of microgrids. The price obtained from dispatching the network in a base-case scenario is used as input to a demand elasticity model, which is then used to determine the price-responsive demand for the next iteration, assuming that the load schedule is defined a day-ahead.

Under this scheme, trends for demand, hourly prices and total operation costs for the microgrid can be obtained. This approach allows to study the effects on line congestion of demand response. Specifically in a microgrid, the effect on the scheduling of diesel generators and energy storage systems (ESS) as well as renewable energy sources (RES) can be analyzed with respect to demand elastic loads.

Some of the most interesting results of the presented studies are that the more the elastic demand in the system, the longer it takes for the dispatch to converge to a final condition. Another interesting find is that even though for single-hour cases, price and demand may oscillate, the interrelated 24-hour model converges to a fixed point, with the prices and costs at their lowest values for different scenarios.

I. KEY EQUATIONS

The mathematical modeling for dispatch in microgrids considers a cost function minimization with variable demand taking into account the following linear formulation:

$$Cost = \sum_{g,t} (a_g \cdot W_{g,t} + b_g \cdot P_{g,t} + SUC_g \cdot U_{g,t} + SDC_g \cdot V_{g,t}) + \sum_{s,t} C_s \cdot (W_{scs,t} + W_{sds,t})$$

$$P_{D_{i,t}} + P_{RES_{i,t}} = \sum_g P_{G_{g,t}} + \sum_j b_{i,j} (\delta_{i,t} - \delta_{j,t}) + \sum_s P_{ESS_{s,t}}$$

$$P_{D_{i,t}} = P_{0_{i,t}} \cdot \left(1 + \alpha \cdot \sum_k \varepsilon_{t,k} \left(\frac{\rho_k}{\rho_0} - 1 \right) \right)$$

II. KEY FIGURES

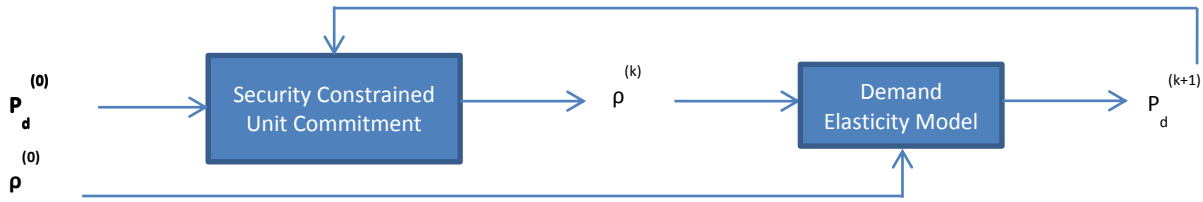


Fig. 1. Iterative procedure for dispatch and demand correction.

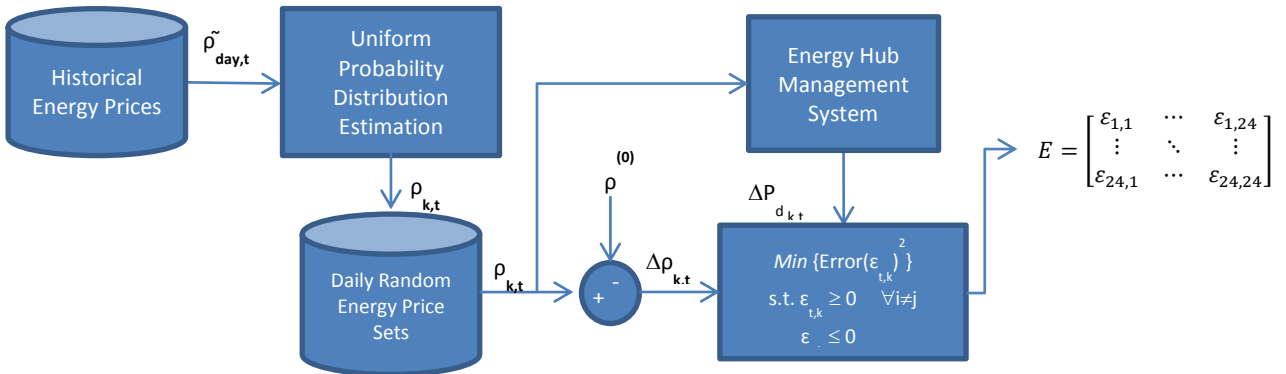


Fig. 2. Demand elasticity model estimation.

Decision Support Concerning Demand Response Programs Design and Use – A Simulation Tool

Pedro Faria, Zita Vale

GECAD - Knowledge Engineering and Decision Support Research Center
 IPP - Polytechnic Institute of Porto
 Porto, Portugal
pnfar@isep.ipp.pt, zav@isep.ipp.pt

Abstract— Demand response (DR) can play a very relevant role in the context of power systems with an intensive use of distributed generation (DG). More active consumers' participation can help improving the system reliability and decrease or defer the required investments. However, new business models and DR programs are needed to take full advantage of DR. The work here presented uses DemSi (see Fig. 1), a DR simulator that has been developed by the authors to simulate DR actions and programs, which includes realistic power system simulation performed in PSCAD®, to support the decisions of DR players. The simulator also includes the use of deterministic and metaheuristic approaches for optimization, and machine learning methods. The present work demonstrates the simulation of a fault in a line that originates the islanding operation of a network with DG and DR. The optimal schedule of resources is performed based on the minimization of operation costs using GAMS™, including the objective function (1) and the constraints in (2)-(4). The DR capacity available in each consumer is determined using DR Performance Evaluation (PE) methods (4). Fig. 2 presents the VOLL (Value Of Lost Load) results with DR, without DR, and with PE, regarding a fault in each period of the day. The full work includes the results from PSCAD® simulation.

I. KEY EQUATIONS

Minimize

$$OC = \sum_{c=1}^{Nc} \left(P_{Red(c)} \times C_{Red(c)} + P_{Cut(c)} \times C_{Cut(c)} \right) \quad (1)$$

$$P_{DG} = \sum_{c=1}^{Nc} \left(P_{Load(c)} - P_{Red(c)} - P_{Cut(c)} \right) \quad (2)$$

$$P_{Cut(c)} = P_{MaxCut(c)} * X_{Cut(c)}, \quad \forall c \in \{1, \dots, Nc\}, X_{Cut(c)} \in \{0,1\} \quad (3)$$

$$P_{Red(c)} = P_{MaxRed(c)}, \quad \forall c \in \{1, \dots, Nc\} \quad (4)$$

$$PBL(t) = \frac{\sum_{xb=1}^{nb} C(t-xb)}{nb} \quad (5)$$

II. KEY FIGURES

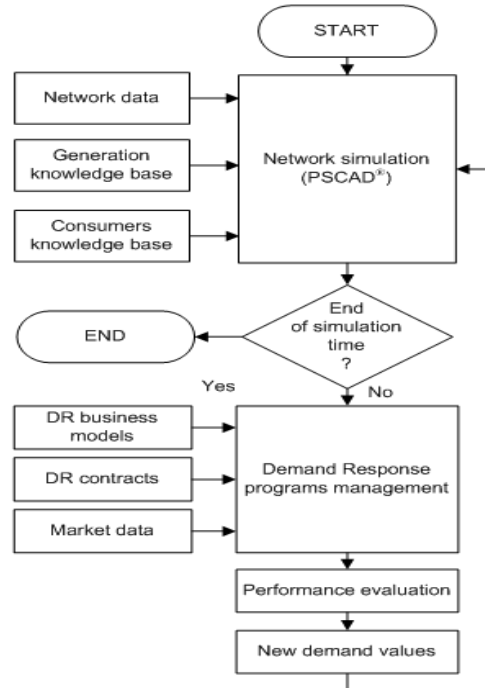


Fig. 1. DemSi functional diagram.

I. KEY RESULTS

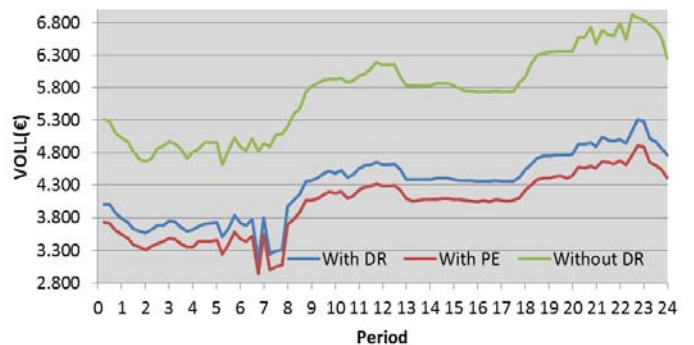


Fig. 2. VOLL with DR, without DR, and with PE.

This work is also supported by FEDER Funds through the “Programa Operacional Factores de Competitividade – COMPETE” program and by National Funds through FCT “Fundação para a Ciência e a Tecnologia” under the projects FCOMP-01-0124-FEDER: PEst-OE/EEI/UI0760/2011, PTDC/EEA-EEL/099832/2008, PTDC/SEN-ENR/099844/2008, and PTDC/SEN-ENR/122174/2010.

PMU Testing and Hardware Interface Architecture for Synchrophsor Application Testing

HyoJong Lee, *Student Member, IEEE*, and Anurag K. Srivastava, *Senior Member, IEEE*
 Smart Grid Demonstration and Research Investigation Lab, Washington State University

Email: hyojong.lee@wsu.edu, asrivast@eecs.wsu.edu

Abstract—Real time monitoring and control of emerging power system is becoming increasingly important with changing operational paradigm. Synchrophsor devices help in realizing this vision for transmission grid. The accuracy and reliability of a Phasor Measurement Unit (PMU) is an important issue. This poster will address development of real time simulation test bed for testing of devices and applications. According to IEEE Std C37.118.1, performance criterion including Total Vector Error (TVE), Frequency Error (FE), and Rate of Change of Frequency Error (RFE) have been tested in balanced/unbalanced/off-nominal steady state operating conditions. Poster also addresses dynamic condition testing for PMU. Test bed development with different PMU interfacing architecture for application testing has been also discussed.

I. KEY EQUATIONS

Total Vector Error (TVE).

$$TVE(n) = \sqrt{\frac{(\hat{X}_r(n) - X_r(n))^2 + (\hat{X}_i(n) - X_i(n))^2}{(X_r(n))^2 + (X_i(n))^2}} \quad (1)$$

Frequency Measurement Error (FE).

$$FE = |f_{ture} - f_{measured}| = |\Delta f_{ture} - \Delta f_{measured}| \quad (2)$$

ROCOF Measurement Error (RFE).

$$RFE = |(df/dt)_{ture} - (df/dt)_{measured}| \quad (3)$$

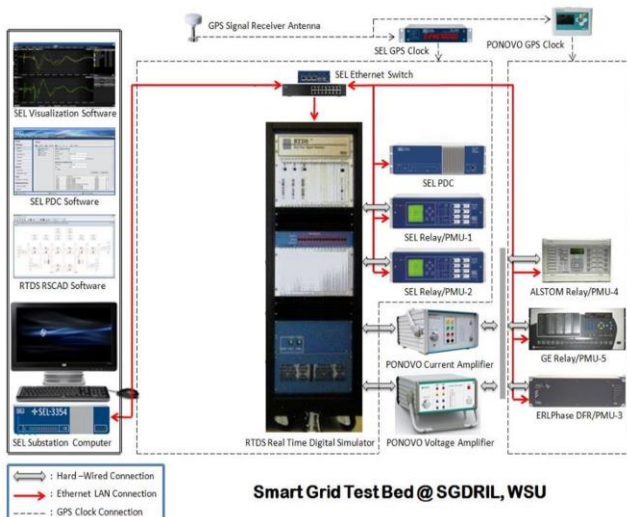


Fig. 1. The design of Smart-grid Testbed.

II. KEY RESULTS

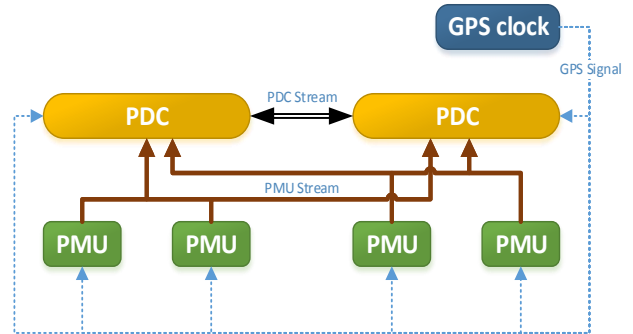


Fig 3. PDC – PMU interface architecture 1

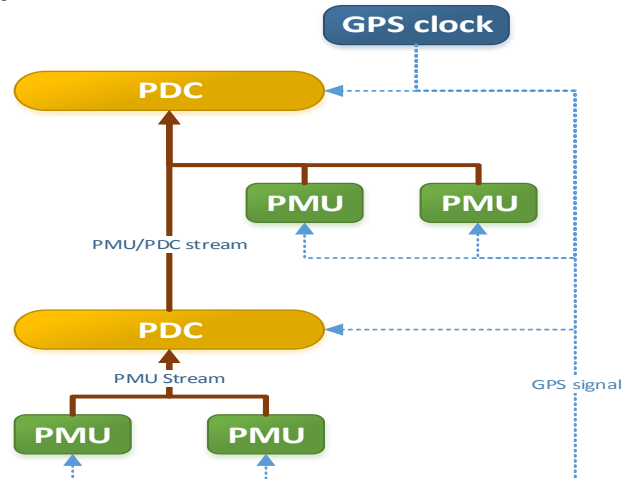


Fig 3. PDC – PMU interface architecture 2

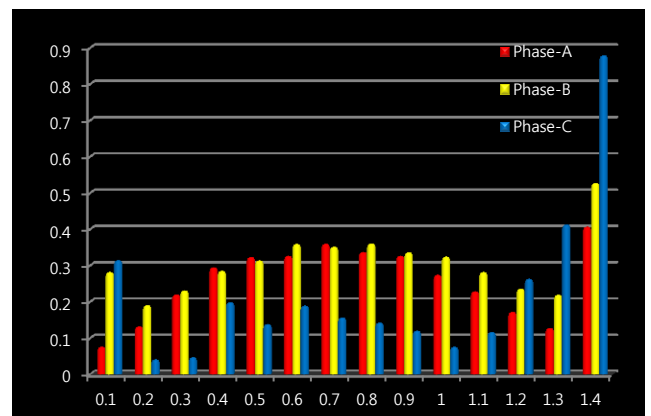


Fig 4. % TVE of PMU 1 Voltage

A New Relaying Algorithm for Blocking Third Zone Distance Relays During Stable Power Swings In Power Systems

Don Kang, Ramakrishna(Rama) Gokaraju, *Member, IEEE*

Department of Electrical & Computer Engineering, University of Saskatchewan,
Saskatoon, SK, Canada

Email: dok524@mail.usask.ca and rama.krishna@usask.ca

Abstract—This research proposes a fast and elegant methodology for blocking the third zone protection during stable power swings, which can prevent unnecessary tripping of distance relays during stable power swings. The proposed algorithm also overcomes the shortcomings of the conventional power swing identification methods when applied for the third zone blocking. The research also introduces an innovative first zero-crossing concept. The proposed algorithm can be applied at every discrete time interval or time step that the power system relay uses to detect power swing points. It can be also applied to every transmission line in the power system by developing an equivalent single machine infinite bus configuration individually for each line on a real-time basis. The research involves detailed electromagnetic transient simulations (PSCAD) of the power system during various faulted conditions. The proposed algorithm will also be verified using hardware-in-the-loop simulations (experimentally tested) on Real Time Digital Simulator (RTDS), to verify the speed and effectiveness of the proposed scheme. The relay algorithm would be implemented on a digital signal processing board (DSK 6713 from ADSP). Finally, a prototype of the relay module will be developed in this research.

I. KEY EQUATIONS

From the power flow equations for the SIMB system the synchronous machine speed equation during a stable power swing can be obtained.

$$\cos\delta = \frac{E^2 - QX}{EV} \quad (1)$$

$$\frac{dP}{dt} = \left(\frac{EV}{X}\right) \left(\frac{E^2 - QX}{EV}\right) \left(\frac{d\delta}{dt}\right) \quad (2)$$

$$\frac{dP}{dt} = \left(\frac{E^2 - QX}{X}\right) \omega \quad (3)$$

II. KEY FIGURES

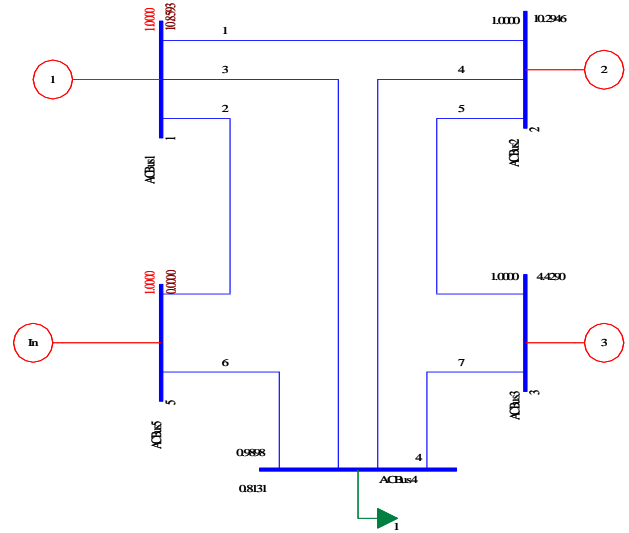


Figure 1. PSAT™ TMIB system for stable power swing identification

III. KEY RESULTS

The proposed scheme is testified in PSCAD on Single Machine Infinite Bus(SMIB) system, Three Machine Infinite Bus(TMIB) system and will be testified on IEEE 39 bus system.

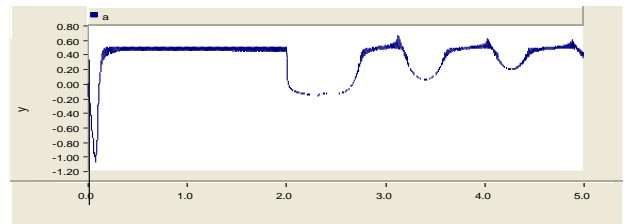


Figure 2. Calculated system equivalent impedance during a stable power swing on SMIB system.

Simulation Study of PEM Fuel Cell and its Dynamic Characteristics

ZHU Yongli

Iowa State University, IA 50011, USA

zhuyongli@ieee.org

Abstract—This paper presents a complete modeling and simulation work of proton exchange membrane fuel cell (PEMFC) in PSCAD/EMTDC. The PEMFC model is established according to some concise electrochemical equations. To verify this model, the static and dynamic characteristics are investigated respectively and simulation results are discussed in detail. As a base for future work, the developed model also shows a potential to study the control system of PEMFC stack as well. Some definite conclusions referred to the operation characteristic of PEMFC are summed up in the end of this paper.

Keywords—PEMFC; fuel cell; renewable energy; distributed generation; simulation

I. KEY EQUATIONS

$$U_{cell} = E_{Nernst} - V_{act} - V_{ohmic} - V_{con} \quad (1)$$

$$E_{Nernst} = 1.229 - 8.5 \times 10^{-4} \times (T - 298.15) + 4.3085 \times 10^{-5} \times T \times (\ln p_{H_2} + 0.5 \ln p_{O_2}) \quad (2)$$

$$V_{act} = -[x_1 + x_2 T + x_3 T \ln(c_{O_2}) + x_4 T \ln(I)] \quad (3)$$

$$c_{O_2} = p_{O_2} / 5.08 \times 10^6 \times \exp(-498/T) \quad (4)$$

II. KEY FIGURES

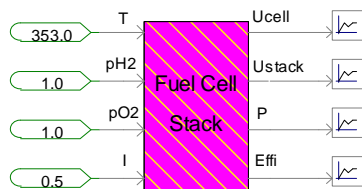


Figure 1. Model of PEMFC stack in PSCAD.

III. KEY RESULTS

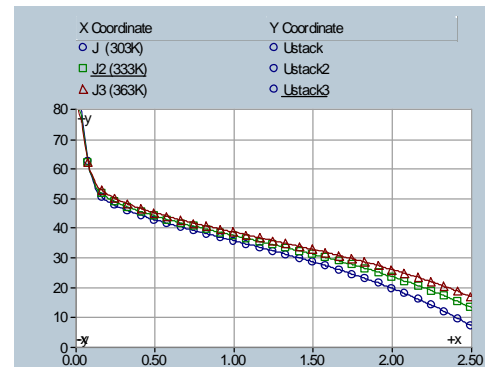


Figure 2. Temperature effect on the PEMFC polarization curve.

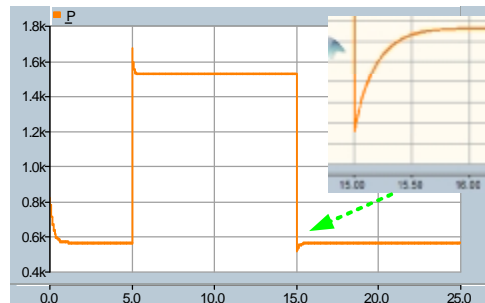


Figure 3. PEMFC output power



Figure 4. PEMFC output efficiency.

Stability Analysis for Power Systems with Price-Based Demand Response

Zhechong Zhao, *Student Member, IEEE*, Lei Wu, *Member, IEEE*

Department of Electrical Engineering and Computer Science, Clarkson University, Potsdam, NY 13676, USA

Abstract—This paper adopts a closed loop model between the economic dispatch (ED) and the price-sensitive DR load adjustment for exploring the stability of power systems with price-based DR. The stability refers to the ability that the system will finally converge to a fixed point after finite iterations between the ED problem and the price-sensitive DR load adjustment procedure. Ellipse curves and exponential curves are used to represent the non-linear price elasticity characteristics of DR, and the cobweb plot is applied to analyze the stability of power systems with price-based DR loads. Numerical case studies illustrate how the system stability is affected by parameters of non-linear price elasticity DR curves.

I. KEY EQUATIONS AND FIGURES

The objective of this paper is to quantitatively analyze the stability of power systems with price-sensitive DR. A closed loop model as shown in Fig. 1 is used to describe the dynamic system and study the stability.

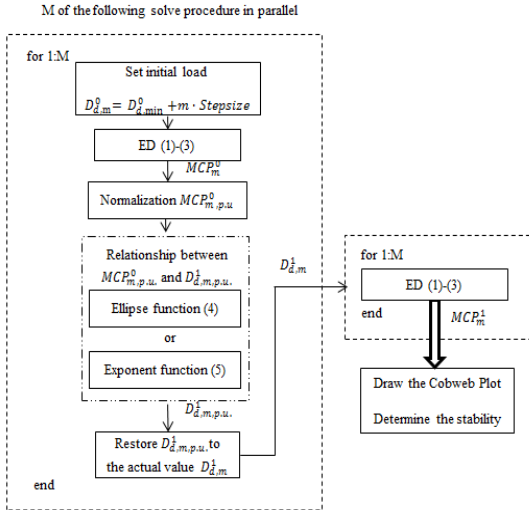


Fig. 1. Flowchart of the proposed closed loop procedure

The ED problem (1) is to minimize the total operation cost subjected to prevailing system and unit constraints. (2) describes the system load balance, and (3) includes maximum and minimum capacity limitations. MCP^n is calculated by the optimal dual variable solution of the system load balance constraint (2). Ellipse curves (4) and exponential curves (5) are used to represent non-linear price elasticity of DR loads.

$$\text{Min} \left\{ \sum_{i=1}^{NG} a_i \cdot p_i^2 + b_i \cdot p_i + c_i \right\} \quad (1)$$

$$\sum_{i=1}^{NG} p_i = \sum_{d=1}^{ND} D_d \quad (2)$$

$$p_{i,min} \leq p_i \leq p_{i,max} \quad (3)$$

$$\frac{(D_{d,p.u.}^{n+1} - g)^2}{j^2} + \frac{(MCP_{p.u.}^n - h)^2}{k^2} = 1 \quad (4)$$

$$MCP_{p.u.}^n = z + r \cdot e^{w \cdot D_{d,p.u.}^{n+1}} \quad (5)$$

II. KEY RESULTS

Numerical case studies quantitatively analyze the system stability with DR, which illustrate that the stability of the system with DR will be affected by parameters of the non-linear price elasticity curves of DR, as shown in Tables I-II and Figs.2-3.

TABLE I RESULTS OF CASE 1 (ELLIPSE CURVE)

Line	j	k	(g,h)	Curvature	Stability
Blue/Solid	0.45	2.12	(0.8,0.8)	0.1	Unstable
Red/Solid	0.50	1.33	(0.8,0.8)	0.28	Unstable
Green/Solid	0.55	1.11	(0.8,0.8)	0.45	Unstable
Purple/Solid	0.60	1	(0.8,0.8)	0.6	Stable
Blue/Dash	0.95	1.06	(1,1)	0.95	Stable
Red/Dash	1	1	(1,1)	1	Stable
Green/Dash	1.81	1.25	(2.2/√2, 2.2/√2)	1.16	Stable
Purple/Dash	9.64	2.66	(10/√2, 10/√2)	1.36	Stable

TABLE II RESULTS OF CASE 2 (EXPONENTIAL CURVE)

Line	z	r	w	Stability
Blue/Solid	-0.58	1.58	-1	Unstable
Red/Solid	-0.019	1.02	-4	Stable
Green/Solid	-0.0025	1.0025	-6	Stable
Purple/Solid	0	1	-12	Stable

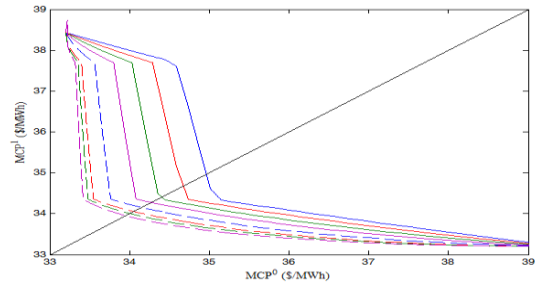


Fig. 2. The Cobweb Plot—Case 1

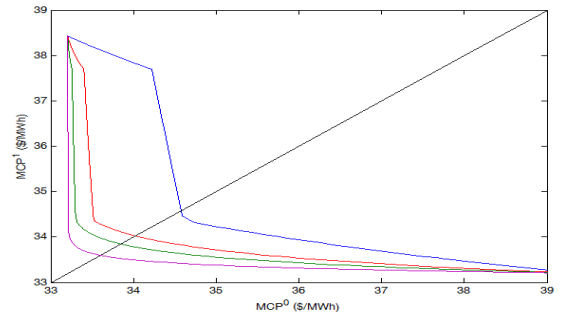


Fig. 3. The Cobweb Plot—Case 2

REFERENCE

- [1] Z. Zhao and L. Wu, "Stability Analysis for Power Systems with Price-Based Demand Response via Cobweb Plot," *IEEE PES. General Meeting*, 2013.

Developing a Scenario-Based Demand Response for Short-Term Decisions of Electricity Retailers

Nadali Mahmoudi, Tapan Kumar Saha, Mehdi Eghbal
 School of Information Technology and Electrical Engineering
 The University of Queensland, Brisbane, Australia
 n.mahmoudi@uq.edu.au, saha@itee.uq.edu.au, m.eghbal@uq.edu.au

Abstract— This paper deals with short-term decisions of retailers. It is assumed that a retailer aims to minimize the cost of procuring energy from two sources: one is the commonly-used pool market, and the other is the demand response (DR) program proposed in this paper. A reward-based DR is mathematically formulated where the volume of load reduction is modeled as a stepwise function of offered incentives by the retailer. Furthermore, a novel scenario-based participation factor is developed here to take into account the unpredictable behavior of customers. The presented problem is formulated in stochastic programming where its feasibility is evaluated on a realistic case of the Queensland region within the Australian National Electricity Market. Additionally, we define four distinct cases to study the impact of uncertainties associated with both resources, particularly DR, on short-term decisions of the retailer.

I. KEY EQUATIONS

Reward-based DR program:

$$P^{DR}(t) = \sum_{w'} \pi(w') \cdot \sum_{j=1}^{N_j} PF(w', t) \cdot \bar{P}_j^{DR}(t) \cdot v_{DR,j}(t) \quad (1)$$

$$R^{DR}(t) = \sum_{j=1}^{N_j} R_j^{DR}(t) \quad (2)$$

$$\bar{R}_{j-1}^{DR}(t) \cdot v_{DR,j}(t) \leq R_j^{DR}(t) \leq \bar{R}_j^{DR}(t) \cdot v_{DR,j}(t) \quad (3)$$

$$\sum_{j=1}^{N_j} v_{DR,j}(t) = 1 \quad (4)$$

The overall cost function:

$$\begin{aligned} \text{Min } CF = & \sum_w \pi(w) \cdot \sum_{t \in T} [\sum_{j=1}^{N_j} PF(w, t) \cdot \bar{P}_j^{DR}(t) \cdot R^{DR}(t) \cdot d(t) + \\ & \sum_{t \in T} P^p(t, w) \cdot \lambda^p(t, w) \cdot d(t)] + \rho \cdot (\xi + \frac{1}{1-\beta} \sum_w \eta_w \cdot \pi_w) \end{aligned} \quad (5)$$

Subject to:

- Equations (1)-(4) as DR cost constraints;

- CVaR constraints:

$$\text{Cost}(w) - \xi - \eta(w) \leq 0; \forall w \quad (6)$$

$$\eta(w) \geq 0; \forall w \quad (7)$$

- The energy balance equation as below:

$$P^{REQ}(t) = P^p(t, w) + P^{DR}(t) \quad (8)$$

II. KEY FIGURES

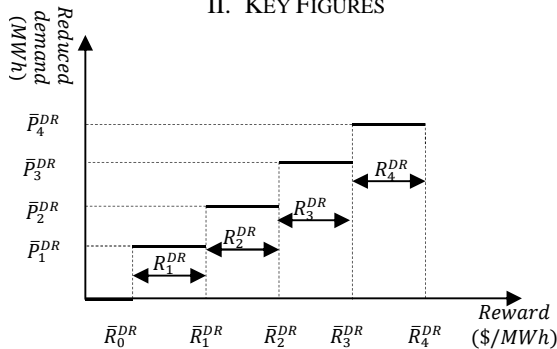


Figure 1. Reward-based DR curve

III. KEY RESULTS

C1) both the pool and DR are uncertain; C2) only the pool is uncertain; C3) only DR is uncertain; C4) both the pool and DR are deterministic.

TABLE I. OFFERED REWARDS AND ENERGY PROCURED FROM DR (PERIOD 1 AS AN EXAMPLE)

ρ	DR Energy (MWh)				Reward (\$/MWh)			
	C1	C2	C3	C4	C1	C2	C3	C4
0	102	180	106	180	98	98	98	98
0.5	170	300	0	180	106	106	-	98
1	203	360	0	180	110	110	-	98
2	238	420	0	180	114	114	-	98
3	272	420	0	180	118	114	-	98
4	272	480	0	180	118	118	-	98
9	306	480	0	180	122	118	-	98

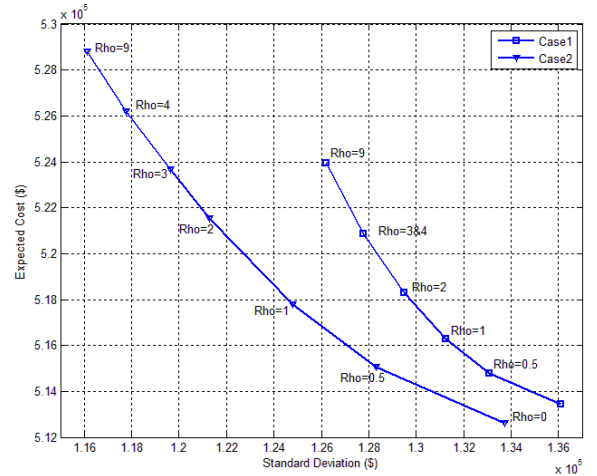


Figure 2. The expected cost versus its standard deviation

TABLE II. THE PERCENTAGE OF CHANGES OF THE EXPECTED COST AND STANDARD DEVIATION IN CASE 1 THAN CASE 2

ρ	Expected Cost Changes in C1 than C2	Standard Deviation Changes in C1 than C2
0	0.16%	1.77%
0.5	-0.05%	3.74%
1	-0.29%	5.18%
2	-0.61%	6.76%
3	-0.53%	6.80%
4	-1.01%	8.52%
9	-0.92%	8.67%

Ohmic Loss Minimization in the AC Grids with Smart Grid Technologies: VSC-DC Grids

Mohamadreza Baradar, *Student Member, IEEE*, Mohammad R. Hesamzadeh, *Member, IEEE*
and Mehrdad Ghandhari, *Member, IEEE*,

KTH Royal Institute of Technology, School of Electrical Engineering, Department of Electric Power Systems
mohamadreza.baradar@ee.kth.se, mrhesamzadeh@ee.kth.se and mehrdad.ghandhari@ee.kth.se

Abstract—The HVDC systems built based on the voltage source converters (VSC) can bring several benefits to the AC power systems. Better voltage profile, increasing power flow controllability, lower ohmic loss, and higher transfer capability are some major benefits of smart grid technologies. This paper investigate the impact of VSC-type DC grids installed in the AC power systems on the ohmic transmission losses. This is done by formulating a convex optimization problem which minimises the ohmic losses (both in AC and DC grids) subject to the technical constraints of both AC and DC system. The formulated optimisation problem is a conic optimisation problem which can be solved using the commercially available optimisation softwares. The conic AC-DC optimal power flow, CAD-OPF, is coded in GAMS platform and solved using the MOSEK solver. The IEEE 30-bus example system is modeled and studied.

Index Terms—Voltage Source Converter (VSC)-High Voltage DC Grids (HVDC)-Ohmic loss.

I. PROPOSED OPTIMIZATION FORMULATION

The proposed optimization formulation is derived as follows:

$$\begin{aligned} & \text{Minimize} \quad \sum_{n_{AC}} P_{loss_{AC}} + \sum_{n_{DC}} P_{loss_{DC}} \\ & \text{Subject to} \quad \mathbf{AX} = \mathbf{b} \\ & \quad \quad \quad \mathbf{X} \leq \mathbf{X} \leq \bar{\mathbf{X}} \\ & \quad \quad \quad \mathbf{X} \in \kappa \end{aligned} \quad (1)$$

where \mathbf{X} is the optimization variable vector which is defined as follows:

$$\mathbf{X} = [W_{AC}^T, W_{DC}^T, P_{r,AC}^T, P_{r,DC}^T, Q_r^T, P_{loss,AC}^T, P_{loss,DC}^T, Q_{loss,AC}^T, P_{CONV}^T, Q_{CONV}^T]^T \quad (2)$$

where W_{AC} and W_{DC} are the square of DC and AC voltages, $P_{r,AC}$ and Q_r are vectors of AC line flow active and reactive powers, $P_{r,DC}$ is vector of DC line flows, $P_{loss,AC}$ and $Q_{loss,AC}$ are vectors of AC line flow active and reactive power losses and $P_{loss,DC}$ is vector of DC line power losses. κ is a set of convex cones with the following formulations:

$$\kappa_{SOC} = \left\{ \mathbf{X} \in R^{n_{set_i}} : x_1 \geq \sqrt{\sum_{j=2}^{n_{set_i}} x_j^2} \right\} \quad (3)$$

$$\kappa_{RQC} = \left\{ \mathbf{X} \in R^{n_{set_i}} : 2x_1x_2 \geq \sum_{j=3}^{n_{set_i}} x_j^2, x_1, x_2 \geq 0 \right\} \quad (4)$$

TABLE I
THE RESULTS OF CAD-OPF FOR IEEE 30-BUS TEST SYSTEM WITHOUT (WO) AND WITH (W) TWO INSTALLED VSC DC GRIDS

	P_{G_i} (MW)		Q_{G_i} (MVAR)	
	WO	W	WO	W
G1	215.86	208.65	0	4.57
G2	82.78	82.78	14.23	-2.06
G5	0	0	33.60	-2.47
G8	0	0	39.91	27.59
G11	0	0	17.58	8.54
G13	0	0	24.00	10.53
			WO	W
Total Cost (\$)			5972.95	5828.71
Total P-losses (MW)			15.24	5.24
Total Q-losses (MVAR)			61.58	17.79
Total P-Generation (MW)			298.64	291.43
Total Q-Generation (MVAR)			129.34	46.71
Total Q_{CONV} (MVAR)			-	36.48
Total P-losses-DC grid (MW)			-	2.19

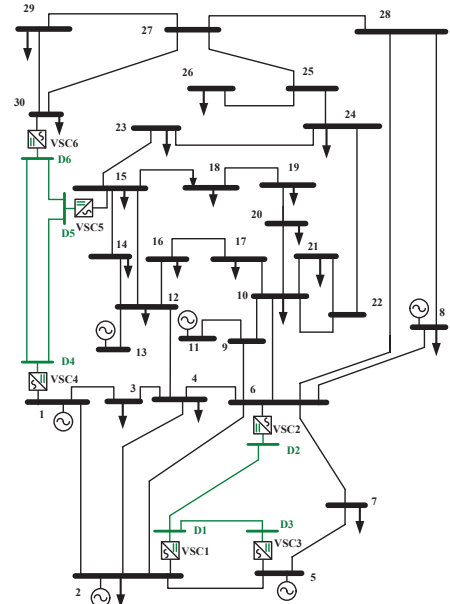


Fig. 1. IEEE 30 bus test system with two installed VSC HVDC systems.

Multi-level state estimation utilizing synchronized phasor measurements

Lin Zhang and Anjan Bose

School of Electrical Engineering and Computer Science
Washington State University
Pullman, WA, USA
lin.zhang@wsu.edu

Abstract—with the advent of synchronized phasor measurement, state estimation becomes non-iterative and more efficient. However, so much PMU streaming data flush into one control center; it will be a challenge for communication. In this poster, we propose a multi-level state estimation to mitigate the impact of too much streaming PMU data. This is a continuation of our two-level state estimation. In two-level state estimation, only local state estimation (LSE) and control center state estimation (CCSE) may not be adequate to track down the states of a very large-scale power system. We can divide the whole grid into a couple of sub-sites, which runs the intermediate level regional state estimation (RSE) between LSE and CCSE. RSE use the measurements from outputs of LSE and run its own state estimator (linear or nonlinear). The advantage of doing this is that the measurements have been filtered out first in LSE, so results of RSE should be more accurate. So does CCSE.

I. KEY IDEAS

It's known that the communication is expensive rather than PMUs. Therefore, from the perspective of communication, if in future with so many PMU data streaming into one control center, it could be a huge challenge for the requirement of QoS e.g. latency, deadline, rate, criticality, geography and quantity. Hence if RSE is already accurate due to the filtering effect of substation level SE, CCSE can be run relatively slower than TSE. And it can also save much communication resources.

So far, in practical there are not enough PMU completely installed at the very large-scale power grid for linear SE. It's known that the PMU are being installed mostly at the highest level voltage buses. So we could run a RSE among those buses with PMUs. The benefit of doing this is that normally more attention is paid on the highest voltage buses. The highest voltage level substations are the most important infrastructures in power grid. The second benefit is that the sampling rate of PMU can let our linear SE running 6 times/second or even faster 30 times/second. And also we can get more accurate outputs of the SE and let us get better real time model of the core of power grid. The third benefit is that with the help of

Gridstat, the output of the linear SE at one site could be sent to other RSE as pseudo measurements so as to increase the accuracy of their SE.

II. KEY FIGURES

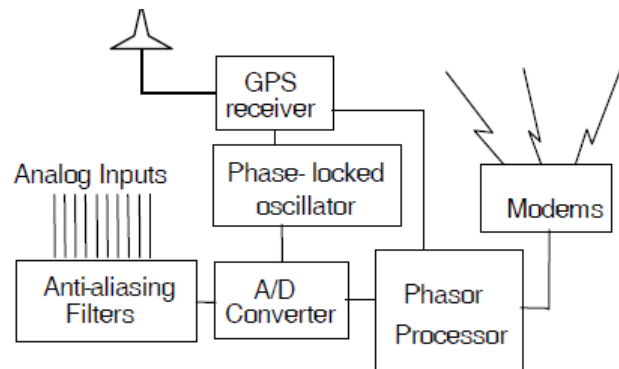


Figure 1. Synchronized phasor measurement

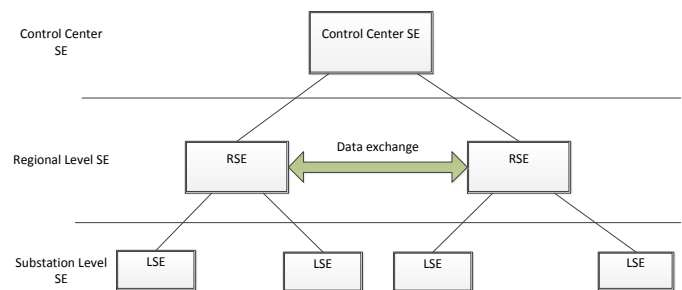


Figure 2. Multi-level state estimation

III. KEY RESULTS

Not yet established, will be completed before July 21, 2013

New ‘Non-Recursive’ Algorithms for Real Time Voltage Stability Monitoring using Synchrophasors

Saugata S. Biswas, *Student Member, IEEE* and Anurag K. Srivastava, *Senior Member, IEEE*,
Smart Grid Demonstration & Research Investigation Lab (SGDRIL),
Washington State University, Pullman, WA, USA

Abstract — With the advent of synchrophasor technology, real time voltage stability analysis has been the focus of many researchers resulting in the development of several new algorithms. However, these algorithms have several advantages as well as limitations. In this work, two new ‘non-recursive’ real time voltage stability algorithms have been developed, one of which is measurement based, whereas the other is measurement and model based. The poster describes the theory of these two new algorithms and then discusses the advantages of these algorithms over the existing ones that are presently being used in the power system industry. The poster further presents the results of simulation of both these new algorithms using standard IEEE test cases, thus validating their accuracy under different power system conditions like contingencies and load increase.

I. KEY EQUATIONS

Two different ‘non-recursive’ or ‘iteration-free’ fast methods have been devised for the estimation of Thevenin’s equivalent network parameters using synchrophasors in real time as seen by a load bus in the monitored power system. One of these methods is completely measurement based, while the other is a hybrid approach that makes use of measurements as well as network topology model. Once, the Thevenin’s equivalent network parameters have been calculated in a non-iterative manner, following are the equations that have been used to calculate the Voltage Stability Assessment Index (VSAI) for all the load buses in the power system –

$$Eeq = \left| \frac{(Eth - \bar{I} * Zth)}{(1 + \frac{Zth}{Z})} \right| \quad (1)$$

$$\delta eq = \angle \left(\frac{(Eth - \bar{I} * Zth)}{(1 + \frac{Zth}{Z})} \right) \quad (2)$$

$$VSAI = \left| \frac{Eeq - VL}{VL} \right| \quad (3)$$

Where –

Eeq: Thevenin’s Equivalent Voltage Magnitude considering ZIP Load Model

δeq: Thevenin’s Equivalent Voltage Angle considering ZIP Load Model

VL: Load Bus Voltage Phasor

Eth & Zth: Thevenin’s Equivalent parameters without considering ZIP Load model

Z: Impedance of Constant Impedance type Load

I: Current drawn by Constant Current type Load

II. KEY FIGURE

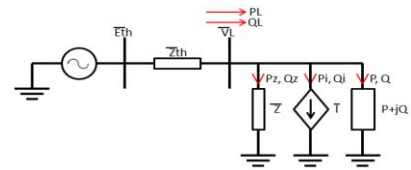


Fig. 1. Thevenin’s Equivalent Network as seen by the load bus

III. KEY RESULTS

For the algorithm which estimates Thevenin’s parameters using measurements only, following are the results –

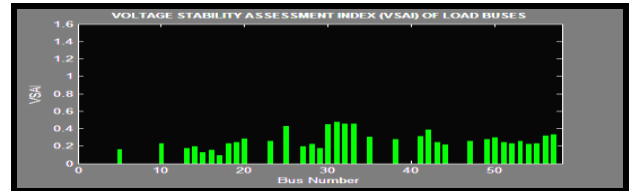


Fig. 2. VSAs at base loading before contingency for IEEE-57 bus system

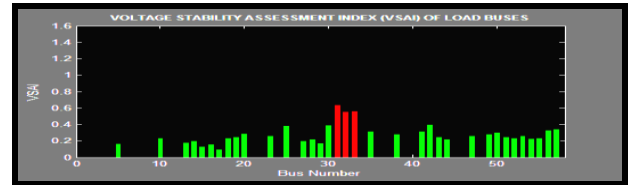


Fig. 3. VSAs at base loading after contingency for IEEE-57 bus system

For the algorithm which estimates Thevenin’s parameters using measurements and model, following are the results –

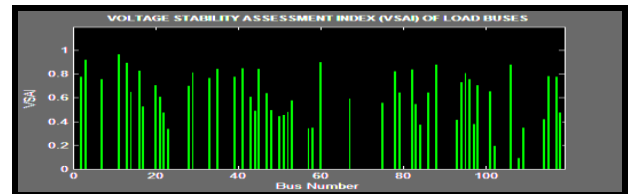


Fig. 4. VSAs at base loading for IEEE-118 bus system

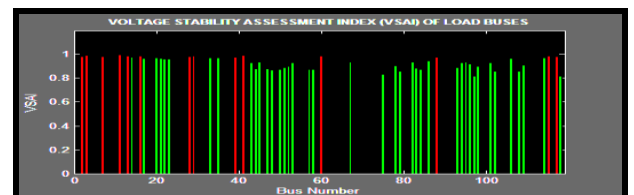


Fig. 5. VSAs at increased loading (near PoC) for IEEE-118 bus system

From the results, it can be seen that with contingencies and load increase, the VSAI of load buses increase indicating higher system stress during such events.

Active Network Management using Distributed Constraint Optimisation

Dimitrios Athanasiadis, *Student Member, IEEE* and Stephen McArthur, *Senior Member, IEEE*
 Department of Electronic & Electrical Engineering, University of Strathclyde, Glasgow, G1 1XW, UK
 Email: dimitrios.athanasiadis@strath.ac.uk and s.mcarthur@eee.strath.ac.uk

Abstract— A fully distributed intelligence and control philosophy is needed for future flexible grids to facilitate the low carbon transition and the adoption of emerging network technologies. Future grids need scalable network management solutions in order to cope with the increase in uncertainty and complexity. Fundamental research in intelligent systems and network control will deliver the next generation of intelligent electricity network. This research presents a network management function formalised as a Distributed Constraint Optimization (DCOP) problem, in particular power flow management. DCOP is an approach to negotiation and arbitration within decentralised control systems where conflicting control decisions arise. Furthermore, the problem will be visualized and decomposed as a factor graph which is a graphical presentation of factorization of a global function into a product of local functions. Additionally, a message passing algorithm, the max-sum algorithm, will be applied which can provide almost optimal results for decentralised coordination problems and limits the computation and communication problems.

I. KEY EQUATIONS

The aim of max-sum algorithm is to maximize the sum of the functions $\sum_{i=1}^{|F|} F_i$ where each function is a factor of the factor graph that determines utility values of its variable assignments. Any edge of the factor graph contains two different messages. The messages are from variable node x_i to function node f_j noted as $q_{i \rightarrow j}$ and also from function node f_j to variable node x_i noted as $r_{j \rightarrow i}$. The messages can be defined as:

- From variable to function

$$q_{i \rightarrow j}(x_i) = a_{ij} + \sum_{j' \in M(i) \setminus j} r_{j' \rightarrow i}(x_i) \quad (1)$$

where $M(i)$ is the set of factor nodes that this variable is connected to in the graph and a_{ij} is a scalar such that

$$\sum_{x_i} q_{i \rightarrow j}(x_i) = 0 \quad (2)$$

- From function to variable

$$r_{j \rightarrow i}(x_i) = \max_{x_{j \setminus i}} \left(f_j(x_j) + \sum_{i' \in N(j) \setminus i} r_{i' \rightarrow j}(x_{i'}) \right) \quad (3)$$

where $N(j)$ is the set of variables nodes that this factor node is connected to in the graph, $f_j(x_j)$ is the utility function and $x_{j \setminus i} \equiv \{x_{i'}: i' \in N(j) \setminus i\}$. The local utility of each agent can be evaluated by the sum of all messages that flowing into a variable and it can be defined as:

$$Z_i(x_i) = \sum_{j \in M(i)} r_{j \rightarrow i}(x_i) \quad (4)$$

The PFM can be expressed as a DCOP such that:

$$\langle V, D, F \rangle \quad (5)$$

$$V = \{Gen_1, Gen_2, \dots, Gen_n\} \quad (6)$$

$$D_{Gen_1} = \{1, 0.6, 0.4, 0\} \quad (7)$$

$$D_{Gen_2} = \{1, 0.6, 0.4, 0\} \quad (8)$$

$$D_{Gen_n} = \{v_1, \dots, v_n\} \quad (9)$$

$$F_{Power\ Flow} = \{-S_{ij}^{min} \leq S_{ij} \leq S_{ij}^{max}\} \quad (10)$$

$$F_{Contractual} = \{4, 3, 2, 1\} \quad (11)$$

$$F_{maxDG} = \{max \sum_{n=1}^N P_{G_i}\} \quad (12)$$

II. KEY FIGURES

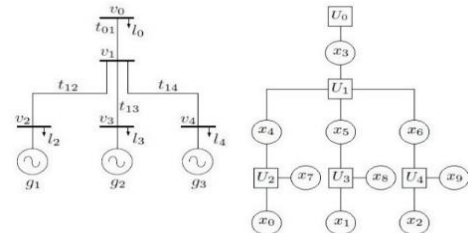


Figure 1. Part of the electricity network case study where g is for the generators, l is for loads, t is for line thermal capacity and decomposition of electricity network to factor graph.

Vehicle-to-Grid Service Potential with Price Based PEV Charging/Discharging

Nima H. Tehrani

Division of Power Engineering
School of EEE, NTU
Singapore
nimal@e.ntu.edu.sg

G. B. Shrestha

Department of EEE
IIT Guwahati
Guwahati, India
gbshrestha@iitg.ernet.in

Peng Wang

Division of Power Engineering
School of EEE, NTU
Singapore
epwang@ntu.edu.sg

Abstract—Penetration of plug-in electric vehicles (PEVs) and renewable power sources will increase tremendously in future power systems. In this paper the operation of distributed charging infrastructure of plug-in electric vehicles (PEVs) is characterized. Charging and discharging pattern is optimized according to price variations to maximize the social benefit of PEV participation as energy storage in the electricity market. 2009 US National Household Travel Survey (NHTS) data set has been used in several ways to probabilistically quantify the PEVs' status in order to characterize the real time mobility behavior. Proposed parameters like aggregated energy consumption, share of parked cars and plug accessibility have been utilized to incorporate vehicles commuting behavior to solve the optimization problem. Finding of the simulation studies such as impact on energy consumption and regulating power potential have been presented. Grid regulation ancillary service potential of the vehicle fleet is calculated based on the results of optimization problem.

I. KEY EQUATIONS

$$\text{Min } F = \sum_{t=1}^{168} c_{el}(t) \times (P_c(t) - P_d(t)) \quad (4)$$

for $t > 1$:

$$E_{bat}(t) = E_{bat}(t-1) + \left[P_c(t) \cdot \eta_{cnv} - \frac{P_d(t)}{\eta_{cnv}} \right] \cdot \Delta t - E_{cns}(t) \quad (5)$$

if $t = 1$:

$$E_{bat}(t) = E_{min} + \left[P_c(t) \cdot \eta_{cnv} - \frac{P_d(t)}{\eta_{cnv}} \right] \cdot \Delta t - E_{cns}(t) \quad (6)$$

$$E_{min} \leq E_{bat}(t) \leq E_{max} \quad (7)$$

$$P_c(t) \cdot \eta_{cnv} \leq r_{cmax} \cdot acc(t) \quad (8)$$

$$\frac{P_d(t)}{\eta_{cnv}} \leq r_{cmax} \cdot acc(t) \quad (9)$$

$$P_c(t) \cdot \eta_{cnv} \leq acc(t) \cdot (E_{max} - E_{bat}(t)) \quad (10)$$

$$\frac{P_d(t)}{\eta_{cnv}} \leq acc(t) \cdot (E_{bat}(t) - E_{min}) \quad (11)$$

II. KEY RESULTS

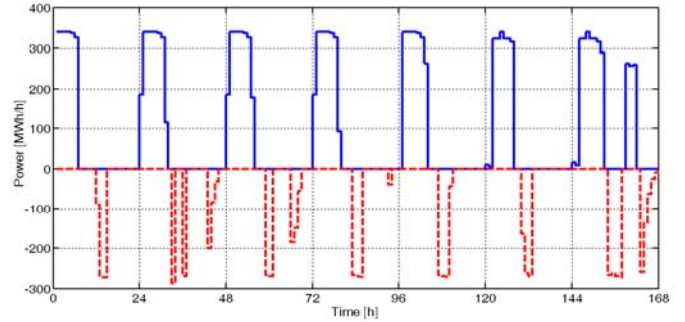


Figure 4. PEV charging and discharging pattern with 3.5 kW average connections

$$R_{up}(t) = \min \left\{ \begin{array}{l} [(E_{bat}(t) - E_{min}) \cdot acc(t)] \\ r_{cmax} \cdot acc(t) - \frac{P_d(t)}{\eta_{cnv}} \end{array} \right\} \cdot \eta_{cnv} + P_c(t) \quad (13)$$

$$R_{down}(t) = \min \left\{ \begin{array}{l} \frac{(E_{bat}(t) - E_{min}) \cdot acc(t)}{\eta_{cnv}} \\ r_{cmax} \cdot acc(t) - P_c(t) \cdot \eta_{cnv} + P_d(t) \end{array} \right\} \cdot \eta_{cnv} \quad (14)$$

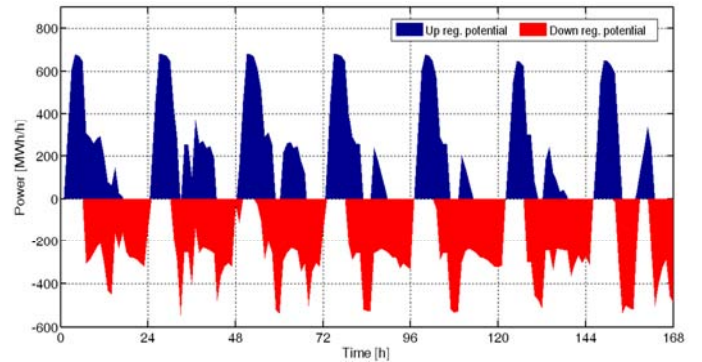


Figure 6. Potential regulating power with 3.5 kW PEVs average connections

Design of an Online Intelligent Alarming System for Cascading Failures of Group of Wind Farms

Jianan Mu, Hongbin Sun, Qinglai Guo, Wenchuan Wu, Fengda Xu, Boming Zhang
 Department of Electrical Engineering, State Key Laboratory of Power Systems
 Tsinghua University, Beijing, 100084, China
 Email: mjn06@mails.tsinghua.edu.cn and shb@tsinghua.edu.cn

Abstract—In China, large-scale wind power is integrated to the power grid in a concentrating way by connecting a group of wind farms together. Each wind farm is consisted of hundreds of wind turbines and covers a large geographical area. However, such a system is vulnerable to occasional faults which can easily develop into cascading failures of adjacent wind farms, making the wind farms lose most of their power in a very short time. Cascading failures have occurred several times in reality. It is urgently necessary to construct an online assistant system to detect, analyze and explain the cascading events timely and effectively. Given that Phasor Measurement Units (PMUs) are widely installed in Chinese wind farms, the dynamic process can be recorded effectively, supplemented with Supervisory Control and Data Acquisition system (SCADA) signals. In this paper, a conceptual design of an online intelligent alarming system for cascading failures of wind farms based on PMUs and SCADA is introduced. The system is justified using real data collected in wind farms.

I. KEY FIGURES

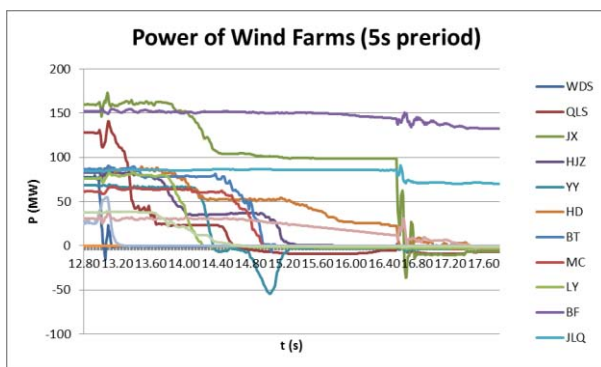


Figure 1. Power of wind farms during cascading failures

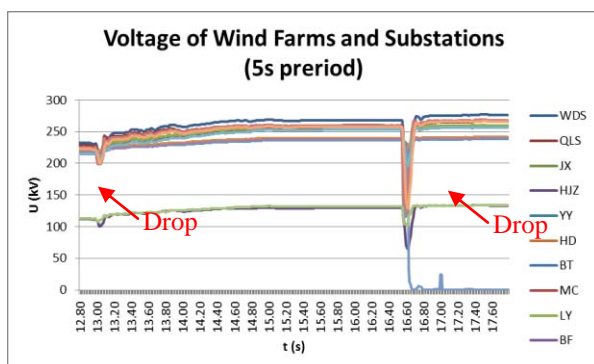


Figure 2. Voltage of wind farms during cascading failures

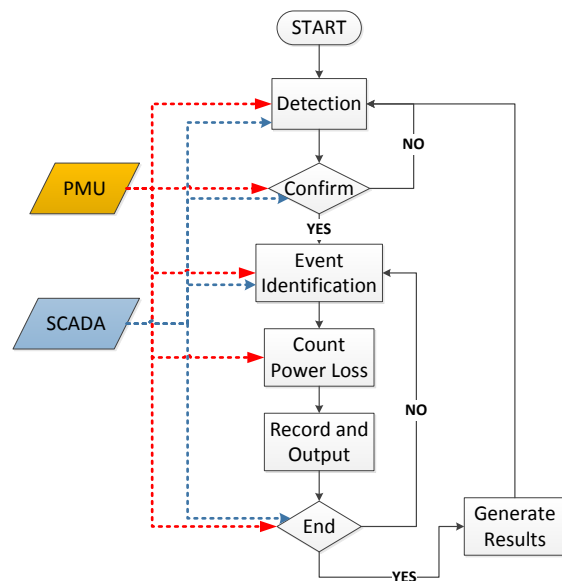


Figure 3. Flow chart of the proposed system

II. KEY RESULTS

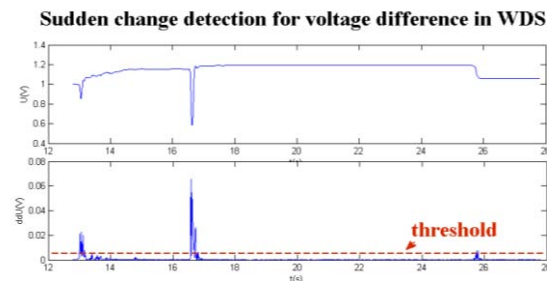


Figure 4. Sudden change detection for WDS's voltage difference

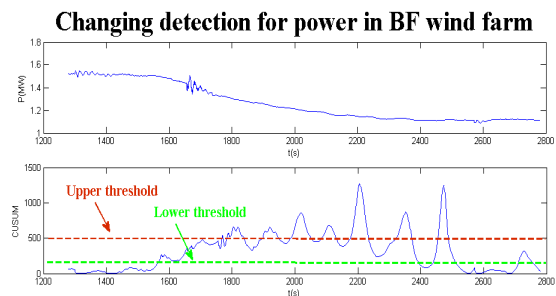


Figure 5. Changing detection for power in BF using CUSUM

Control of the Synchronization and Payback Related to the Provision of Frequency Services by Cold Appliances

Vincenzo Trovato, Simon H. Tindemans, Goran Strbac

Department of Electrical and Electronic Engineering, Imperial College
London, United Kingdom

Abstract— Traditionally, the frequency balancing mechanism has been implemented by flexing generation. This requires synchronous conventional generators to be run part loaded decreasing the efficiency of the power plant with increased fuel costs and CO₂ emissions. Our work concerns the use of dynamic demand support in the provision of frequency services. Thus, “smart” demand facilitates the grid recovering the nominal frequency by dynamically adjusting domestic appliances’ power consumption. In particular, we focus on thermal loads, such as refrigerators. The control strategies proposed in literature thus far exhibit troublesome side-effects. In order to classify these shortcomings, we identify key performance dimensions of desired controllers: 1) The ability to provide a sufficient reduction in power consumption at short notice; 2) The capability to delay and control the payback of energy that the power system ‘borrows’ from the responsive demand; 3) Avoiding synchronization of the duty cycles, which causes large-scale cyclic load patterns. We first present an analysis of physical constraints of using such thermal loads for frequency response services. We determine the total amount of energy ‘borrowed’ from the appliances by the power system. Conversely, the power system must subsequently “pay back” additional energy to allow the devices to come back to a steady state condition defined by a nominal total power consumption and a nominal average temperature. We demonstrate that not all the borrowed energy needs to be paid back. We also analyze two previously proposed control strategies for refrigerators in detail: a deterministic control and a stochastic control. Both methods are revealed to have drawbacks. For our simulation studies, we use fourth and second order models of cold appliances. For system studies, these are integrated within a simplified GB power system model. The key contribution of this paper is the design of a hybrid controller based on the set-point temperatures updates that are proportional to the frequency deviation and its rate of change. This makes the collective contribution of the devices both larger and faster. Furthermore, the presence of a randomized disengagement strategy drastically reduces the synchronization, delaying the onset of the payback. Finally, we also quantify the ability of dynamic demand to replace fast frequency services provided by expensive and pollutant generation by slower units.

I. KEY CONCEPTS

Fig.1 shows the general framework of the algorithm.

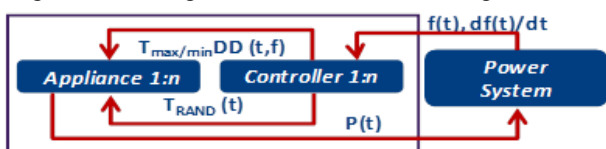


Fig. 1 Framework of the hybrid control strategy.

The controller of each device identifies the frequency deviation Δf (Hz), evaluates its rate of change, $d(\Delta f)/dt$ and updates the temperature limits according to:

$$T_{\max DD}(t, f) = T_{\max} - K_{DD}[\Delta f(t) + K_{ROC} d(\Delta f(t))/dt]$$

$$T_{\min DD}(t, f) = T_{\min} - K_{DD}[\Delta f(t) + K_{ROC} d(\Delta f(t))/dt]$$

Moreover, a drastic reduction of the synchronization and a delayed payback is obtained due to the inclusion of a randomized disengagement strategy, which is triggered when ($t \geq t_r$) and $\Delta f(t) \leq 0.05\text{Hz}$. Then, each appliance selects a random temperature T_{rand} within the uniform distribution $[T_{\min}, T_{\max}]$.

II. KEY FIGURES

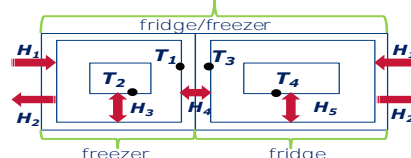


Fig. 2 Schematic thermal model for a cold appliance with the heat flows involved.

III. KEY RESULTS

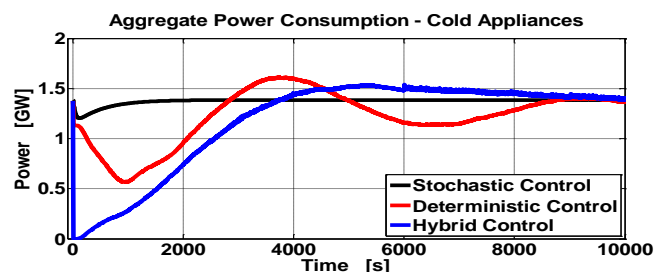


Fig. 3 Time evolution of the aggregate power consumption of dynamic demand cold appliances after a 1800 MW loss with 60 GW of system demand: comparison between hybrid control, stochastic control and deterministic control.

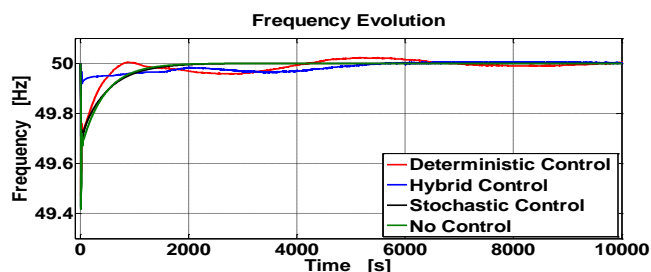


Fig. 4 Frequency evolution after 1800MW loss and 60GW of system demand: comparison between the strategies and the reference case.

On Using Synchrophasor Data to Assess Power System Steady-State Stability

Karl Reinhard

Department of Electrical and Computer Engineering, University of Illinois at Urbana-Champaign (UIUC) Urbana, IL 61802
reinhrd2@illinois.edu

Abstract—Abstract--- In electric power systems, a key challenge is quickly estimating the system’s proximity to its stability limits. This poster describes efforts using synchrophasor measurements at two buses connected by a transmission line to calculate parameters for a pair of Thevenin equivalent sources, which when connected by the transmission line model provide an equivalent power system representation that may be useful as an indicator of steady-state system stability.

I. INTRODUCTION

Focusing upon the phase angle power system stability constraint, this poster describes using synchrophasor measurements from two buses to compute model parameters for a pair of Thevenin sources, which with the connecting transmission line parameters enable a two-bus equivalent power system representation. The difference between the resulting Thevenin equivalent source angles (AnglxSys) is proposed as an indicator of how close the system is to its stability limits.

II. ESTIMATING THEVENIN EQUIVALENTS FROM SYNCHROPHASOR DATA

The objective is to develop a Thevenin equivalent circuit representation composed of an equivalent voltage source and impedance, which i) characterizes the power system’s behavior as seen from the end of a particular transmission line and ii) is easily calculable from field measurements. The left boxed portion of the circuit in Fig. 1 represents such a Thevenin equivalent of the power system looking into bus 1. A second Thevenin equivalent representing the power system behind the terminals at bus 2 completes the proposed circuit. The proposed Thevenin equivalent stability indicator is $\delta_1 - \delta_2$, AnglxSys.

There are multiple approaches to solving the Thevenin equivalent problem: i) to use a set of 2 sequential PMU measurements to enable an exact solution, ii) to use 3 or more sequential measurements to find a least squares error (LSE), and iii) to reduce the number of unknowns by fixing one or more of the four unknown values.

A. Test Data Description

The study used synchrophasor data set from a 765KV transmission line that includes line-to-line voltage magnitude and phase angle. Typically, the data values over short time periods showed only small changes.

B. Exact and Least Squares Estimate Solution Results

The exact and least squares solutions were found to be unsuitable. Condition numbers calculated from the test data were consistent with this estimate. The effects of poor matrix conditioning were observed in wildly fluctuating parameter estimates – both for exact and least squares estimate approaches.

C. Simplified Thevenin Equivalent Model

In this model, the source magnitudes $|E_1| = |E_2|$ are set to 1_{pu} and the Thevenin equivalent impedances are assumed to be purely reactive, i.e. $R_1 = R_2 = 0$. The difference is the desired AnglxSys. The application of this model using the synchrophasor test data provides promising results consistent with expected power system behaviors.

III. CONCLUSION

The obvious approach using exact and least squares estimate solutions proved to be unsatisfactory with our sample synchrophasor test data, which is attributed to very large matrix condition numbers arising from the test data. Using simplifying assumptions about the Thevenin equivalent model, our alternate approach produced a Thevenin model consistent with expected system behavior. Future efforts will investigate the efficacy of using the simplified Thevenin equivalent model using data from multiple synchrophasor data streams to assess system stability with respect to stability limits.

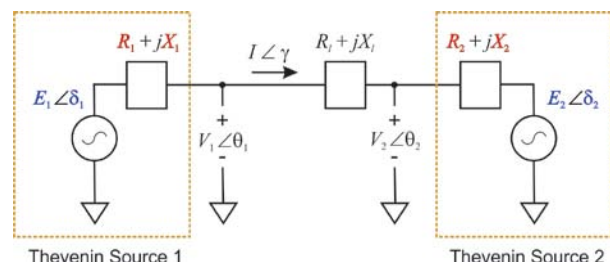


Figure 1. Thevenin Equivalent Circuit Model

Collaborators:

Professor Peter Sauer, University of Illinois at Urbana-Champaign,
psauer@illinois.edu;

Professor Alejandro Dominguez-Garcia, University of Illinois at Urbana-Champaign, aledan@illinois.edu

A Hybrid Simulation Method for EVs' Operation considering Power Grid and Traffic Information

Shujun Xin, Qinglai Guo, *Member, IEEE*, Hongbin Sun*, *Senior Member, IEEE*,
Zhengshuo Li, Boming Zhang, *Fellow*, Shaobo Zhang
Department of Electrical Engineering
Tsinghua University
Beijing, P.R.China
shb@mail.tsinghua.edu.cn

Abstract—As the penetration of electric vehicles (EVs) increases, it is required to consider both power grid and traffic information when analyzing EVs distribution and charging loads. This paper presents a hybrid simulation method for real-time operation of EVs, charging stations, traffic and the grid. It first describes the traffic model and electric model, then builds a hybrid model for EVs to combine these two models. The paper presents a detailed timing simulation method afterwards. After generating EV inflows and traffic flows in different places and setting EV's charging behavior, EVs' State of Charge (SOC) and spatial moving and charging stations' working states can be viewed through simulation. An example is presented to illustrate the impact of EV inflows on the charging power of charging stations. This method can be applied in other researches, and it will be utilized for future research work on the interaction between power grid and traffic network.

I. KEY EQUATIONS

The spatial and SOC state of EV at time point $\beta+1$ can be calculated through the formulas below:

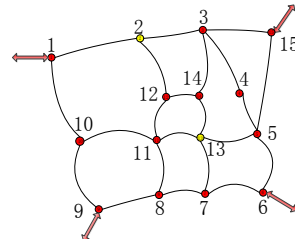
$$[G_1^\beta, G_2^\beta, l^\beta] = \begin{cases} [G_1^{\beta-1}, G_2^{\beta-1}, l^{\beta-1} + V_{G_1^{\beta-1}G_2^{\beta-1}} \times \Delta t] \\ \text{when } l^{\beta-1} + V_{G_1^{\beta-1}G_2^{\beta-1}} \times \Delta t \leq S_{G_1^{\beta-1}G_2^{\beta-1}} \\ [G_2^{\beta-1}, G_3^{\beta-1}, V_{G_1^{\beta-1}G_2^{\beta-1}} \times (\Delta t - \frac{S_{G_1^{\beta-1}G_2^{\beta-1}} - l^{\beta-1}}{V_{G_1^{\beta-1}G_2^{\beta-1}}})] \\ \text{when } l^{\beta-1} + V_{G_1^{\beta-1}G_2^{\beta-1}} \times \Delta t \geq S_{G_1^{\beta-1}G_2^{\beta-1}} \end{cases}$$

$$SOC^\beta = \begin{cases} SOC^{\beta-1} - \frac{E_{ave}}{E_{full}} \times V_{G_1^{\beta-1}G_2^{\beta-1}} \times \Delta t \\ \text{when } l^{\beta-1} + V_{G_1^{\beta-1}G_2^{\beta-1}} \times \Delta t \leq S_{G_1^{\beta-1}G_2^{\beta-1}} \\ SOC^{\beta-1} - \frac{E_{ave}}{E_{full}} \times (V_{G_1^{\beta-1}G_2^{\beta-1}} \times (\Delta t - \frac{S_{G_1^{\beta-1}G_2^{\beta-1}} - l^{\beta-1}}{V_{G_1^{\beta-1}G_2^{\beta-1}}}) + l^{\beta-1}) \\ \text{when } l^{\beta-1} + V_{G_1^{\beta-1}G_2^{\beta-1}} \times \Delta t \geq S_{G_1^{\beta-1}G_2^{\beta-1}} \end{cases}$$

II. KEY FIGURES



Transportation Network



Topological Graph

Fig. 1. The Transportation Network and its Topological Graph

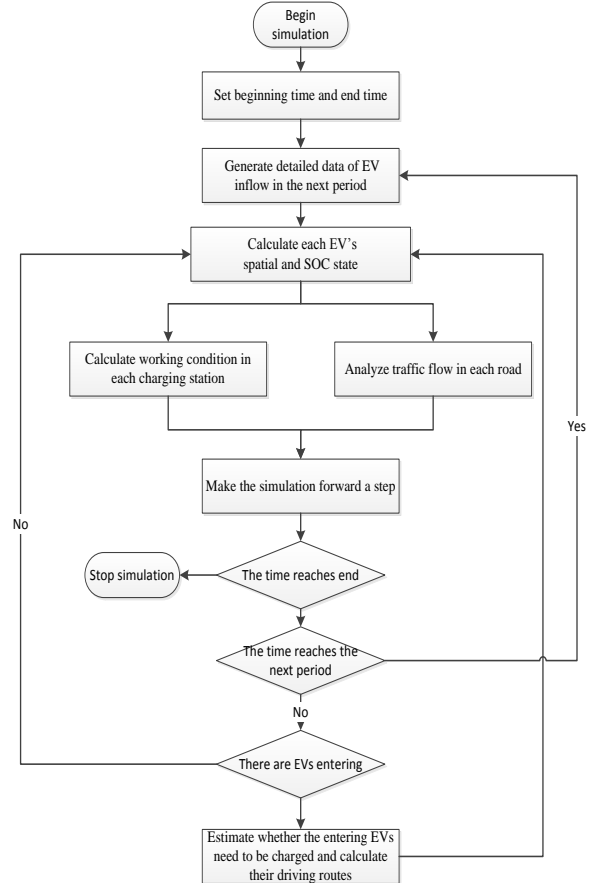


Fig. 2. Detailed simulation method

III. KEY RESULTS

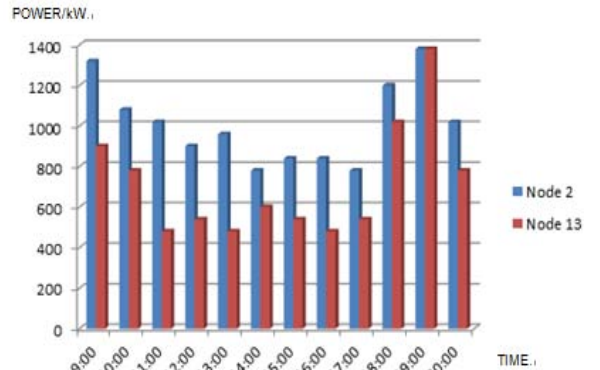


Fig. 3. Fluctuation of charging power in each charging station

Development of a Three Phase Unbalanced Continuation Power Flow Tool

Leslie Corson, *Student Member, IEEE*, and Anurag K. Srivastava, *Senior member, IEEE*

Smart Grid Demonstration and Research Investigation Lab (SGDRIL), School of Electrical Engineering and Computer Science, Washington State University, Pullman, WA 99163, USA
Email: leslie.corson@email.wsu.edu and asrivast@eecs.wsu.edu

Abstract—The electric distribution power systems in the United States have typically been designed to operate radially. This has primarily been a centralized model of the energy infrastructure of generation and distribution characterized by large-scale power plants, with all decisions for this model based on the central authorities owning the infrastructure. With the increasing demand for applications for renewable energies (small-scale energy) and smart electric grids there is a need to apply a decentralized energy model. The decentralized model allows for individuals to make decisions for their power energy choices, unlike the centralized model. With distributed generation being incorporated into the meshed distribution networks, voltage stability is a critical issue. The voltage stability studies are imperative in maintaining a systems stable operating conditions and to prevent power blackouts. Three phase unbalanced continuation power flow (CPF) has been developed utilizing the current injection method. Voltage stability of distribution systems can be analyzed using this three-phase continuation power flow tool. The results from this CPF program will create a benchmark, validating the CPF and allowing voltage stability analysis. Utilizing the CPF tool, the maximum loading point for the system can be found. This CPF program will be tested and validated using commercial software. Future work will integrate this CPF tool with Mathematical Programs of Equilibrium Constraints (MPEC) utilizing Feed-In-Tariff (FIT) policy for distribution systems to form stable design solutions (steps for this framework are seen in Fig. 1).

I. KEY EQUATIONS

The CPF uses a corrector and predictor with the constraints

$$f(x, \lambda) = 0 \quad (1)$$

$$(\lambda+1)P^{sp} - P(x) = 0 \quad (2)$$

$$(\lambda+1)Q^{sp} - Q(x) = 0 \quad (3)$$

where P^{sp} and Q^{sp} are the specified values for real and reactive power.

ACKNOWLEDGMENT

The authors would like to thank NSF for providing financial support for this project.

REFERENCES

- [1] Mariosa Crow, "Computational Methods for Electric Power Systems", 2003, CRC Press.
- [2] Shilpa Toppo, "Development of Current Injection Three Phase Unbalanced Continuation Power Flow for Distribution System," Master Thesis 2010, Mississippi State University.

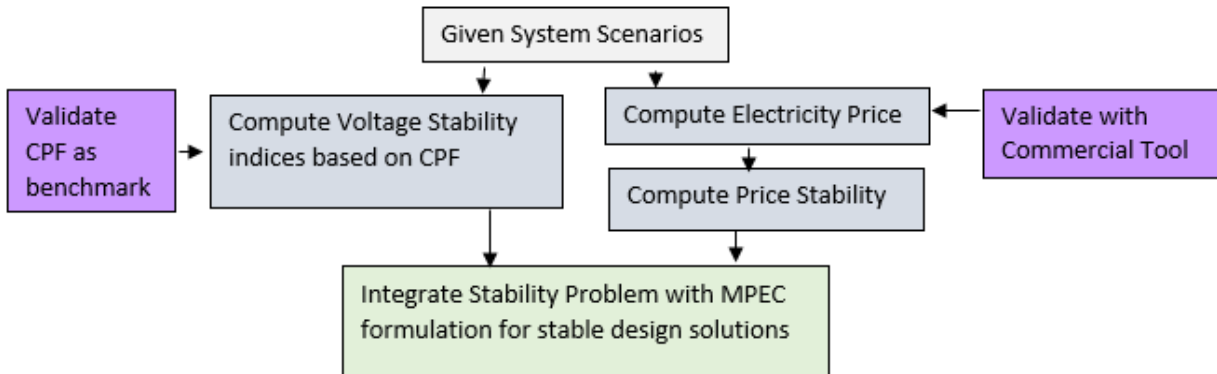


Fig. 1. Framework to achieve Stable Design Solutions

A Simultaneous Perturbation Approach for Solving Economic Dispatch Problems with Emission, Storage, and Network Constraints

Yu Xia and Joe H. Chow
Rensselaer Polytechnic Institute
Troy, NY, USA
xiay4@rpi.edu, chowj@rpi.edu

Abstract— Power system operators are faced with an increasingly complex economic dispatch problem as distributed energy sources, energy storage, and environmental constraints are introduced to the grid. Optimizing these resources over time to provide energy reliably and economically often involves dealing with constraints across multiple time periods. These inter-temporal constraints add considerable difficulty to the economic dispatch problem because they couple the time periods of the optimization.

Power system optimization problems are commonly posed as constrained optimization problems and formulated as linear or nonlinear programming problems that incorporate a Lagrange multiplier for each equality constraint. Lagrangian relaxation solution algorithms attempt to iteratively find a solution by temporarily relaxing the Lagrange multipliers and hence temporarily decoupling optimization across time periods. For constraints spanning multiple periods, we further relax the Lagrange multiplier for those inter-temporal constraints to decouple the optimization across time periods. A simultaneous perturbation technique for economic dispatch problems with inter-temporal constraints has been previously proposed and shown to have good convergence properties while solving for all time periods simultaneously. However, this technique was previously illustrated only by coordinating a hydro unit and a single composite steam unit without a network model.

In this poster, we extend the simultaneous perturbation technique to new inter-temporal constraints, including emissions cap policy and energy storage. We also introduce additional steam and hydro units and include a network model with line flow constraints. We demonstrate the effectiveness of the method for these added complexities with illustrative examples.

Key Words—Lagrange Relaxation, optimization, Hydro-thermal coordination, emission constraints, optimal power flow, energy storage

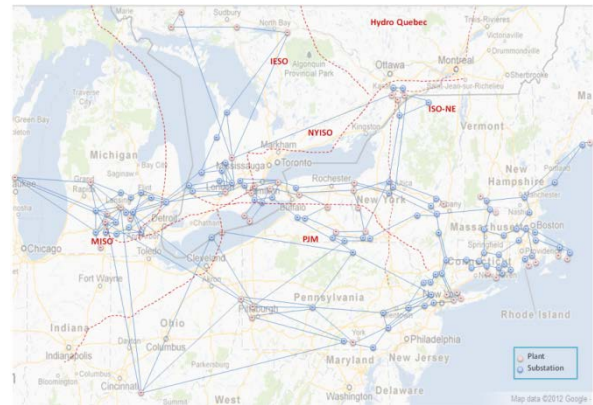


Figure 1. NPCC 140-bus system map

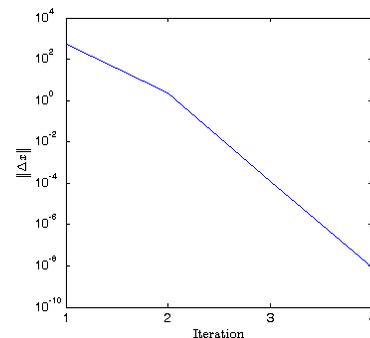


Figure 2. Convergence plot for NPCC 140-bus system

Distributed Energy Management under Smart Grid Plug-and-Play Operations

Ziang Zhang, Yuan Zhang, and Mo-Yuen Chow

Department of Electrical and Computer Engineering, North Carolina State University, Raleigh, NC 27695, USA
Email: z Zhang15, y Zhang50, c Chow@ncsu.edu

Abstract—With the increasing penetration of distributed generation, the plug-and-play energy resources or energy storage devices will become a required functionality of future power systems. Effective distributed control algorithms could be embedded in distributed controllers to allocate energy among the generating systems economically when a plug-and-play operation is performed. The Incremental Cost Consensus (ICC) algorithm can solve this kind of Economic Dispatch Problem (EDP) in a distributed fashion. Several case studies are presented to demonstrate the performance of the ICC algorithm under smart grid plug-and-play operations.

I. INCREMENTAL COST CONSENSUS ALGORITHM

$$C_i(P_{g,i}) = a_i + b_i P_{g,i} + c_i P_{g,i}^2 \quad (1)$$

$$\Delta \tilde{P}_i[k+1] = W \Delta \tilde{P}_i[k] + \Delta P_i[k] - \Delta P_i[k-1] \quad (2)$$

$$\Delta \tilde{P}_i[k+1] = W \Delta \tilde{P}_i[k] + P_{d,i}[k] - \left(\frac{1}{2c_i} \lambda_i[k] - \frac{b_i}{2c_i} \right) - \Delta P_i[k] \quad (3)$$

$$\lambda_i[k+1] = W \lambda_i[k] + \alpha \Delta \tilde{P}_i[k] \quad (4)$$

II. KEY RESULTS

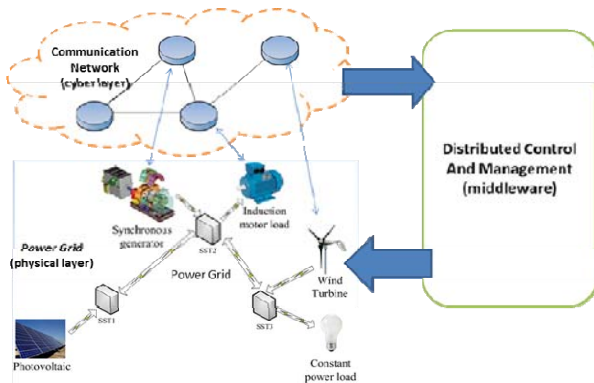


Figure 1. The three layer structure of Smart Grids

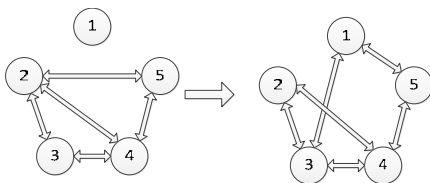


Figure 4. Communications layer topology reconfiguration

TABLE I. PARAMETERS OF THE FIVE-UNIT-SYSTEM

Unit	a_i	b_i	c_i	Local Demand (MW)
1	561	7.92	0.001562	200
2	310	7.85	0.00194	200
3	78	7.97	0.00482	200
4	561	7.92	0.001562	200
5	78	7.97	0.00482	200

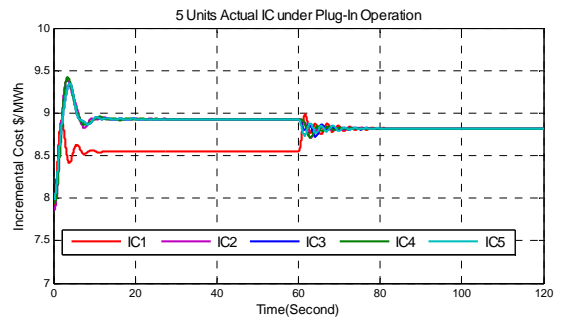


Figure 2. Case Study ICs

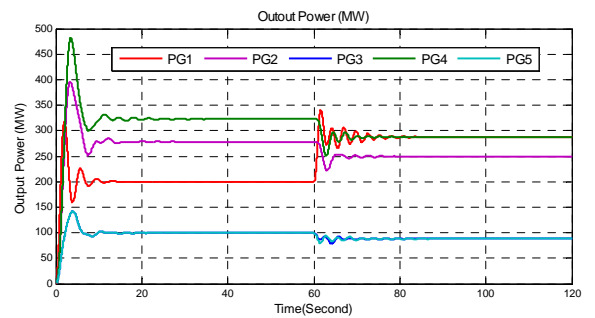


Figure 3. Case Study Output Power

III. CONCLUSION

The performance of the ICC algorithm under smart grid plug-and-play operation has been explored. The simulation results demonstrates that the ICC algorithm is effective and robust even in the absence of a centralized control center.

Heuristic Approach to Resource Allocation in the Emerging Smart Grid

Timothy Hansen

Colorado State University
 Department of Electrical and Computer Engineering
 Fort Collins, CO 80523, USA
 Email: timothy.hansen@colostate.edu

Abstract—As the Smart Grid introduces profound changes in the operation of the electric power industry, the need for efficient and robust resource allocation (RA) algorithms arise. This is especially difficult due to the increasingly stochastic nature of the availability of highly distributed resources. Similar challenges exist in resource allocation in the realm of computing. This work draws upon these links to solve the Smart Grid RA (SGRA) problem using a heuristic approach, such as a genetic algorithm.

The SGRA in question is utilizing end-user customer loads to perform load shifting. The *aggregator* is a proposed for-profit market player, in a deregulated market, that will act as a means for the end-user to engage in the bulk market. This will occur by the end-users making available their loads for reassignment by the aggregator, modeled as a multi-agent based distribution management system. In a Demand Response (DR) situation initiated by the independent system operator (ISO), the aggregator will reassign the end-user reassignable loads to: (a) perform load shifting, and (b) maximize its profit. The aggregator will choose which loads to reassign using proposed heuristic techniques while meeting the system and customer constraints.

I. KEY FIGURES

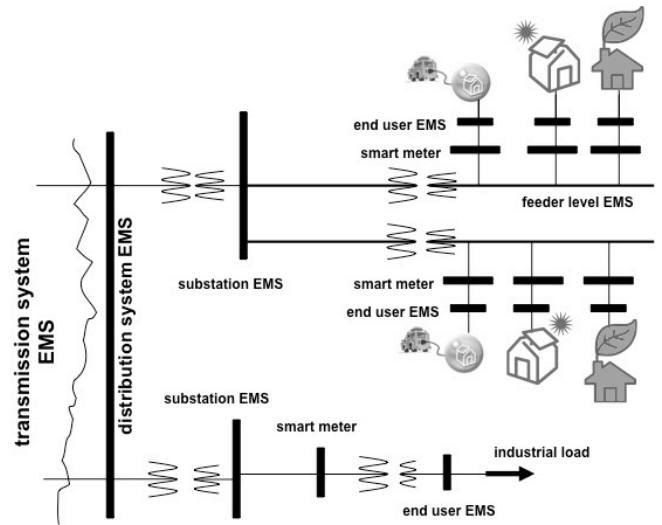


Figure 1: An illustration of an example smart distribution system with distributed assets.

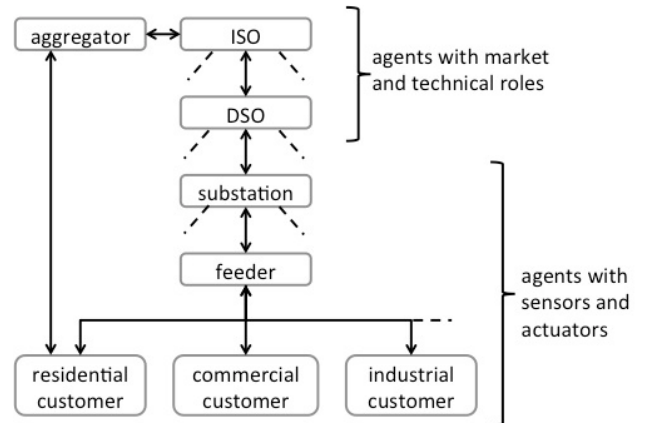


Figure 2: Architecture of the agent-based distribution system model. Dashed lines indicate connections with multiple agents.

This work was supported by the National Science Foundation under grant number CNS-0905399 and the Colorado State University George T. Abell Endowment.

Voltage Assessment in Smart Grids Involving Distributed Generation

Ahmed Mohamed, *Student Member, IEEE*, Ahmed Elsayed, *Student Member, IEEE*, Tarek Youssef, *Student Member, IEEE* and Osama A. Mohammed, *Fellow, IEEE*

Abstract—In this paper, the application of wide area measurement and control for voltage assessment of hybrid AC/DC smart grid is investigated. The power available from renewable energy assets and storage elements on the microgrids is utilized to maintain system voltage stability. The system under study consists of two DC microgrids coupled to a multi-bus AC system. In case of voltage violation at any of the buses, the minimum reactive power needed from each of the microgrids in order to restore the voltage magnitude to a value that is between the permissible limits is determined in real time by solving an optimization problem. Simulation, as well as experimental, results are included to verify the validity of the proposed wide area control technique.

I. KEY FIGURES

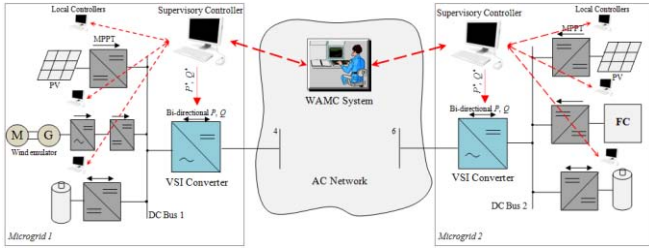


Fig. 1. Distributed generation implementation and control in the system under study.

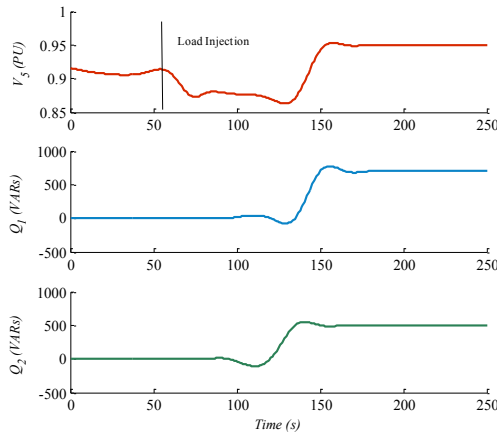


Fig. 2. Experimental results of the case study.

I. KEY EQUATIONS

The genetic algorithm is used to yield the amount of reactive power required from the two different microgrids such that their summation is minimum. Therefore, each individual of the population represents a trial solution to the problem of minimizing the value of the fitness function, which is given by:

$$F(Q_1, Q_2) = (Q_1 + Q_2)^2 \quad (1)$$

s.t.

$$\begin{cases} 0.9 < V_i \leq 1.1 \\ Q_1 < Q_{U1} \\ Q_2 < Q_{U2} \end{cases} \quad (2)$$

Where V_i is the voltage at the bus number i , Q_{U1} and Q_{U2} are the upper limits of the reactive power that can be drawn from *Microgrid 1* and *Microgrid 2*, respectively.

I. KEY RESULTS

The test system is shown in Fig. 1. The experiment that was performed is as follows; the system was initially operating in a steady-state mode. All the voltages were within acceptable limits. After a while, a relatively high resistive-inductive load of 2.5 kW and 4.2 kVAR was applied to the circuit as shown in Fig. 2, and hence the voltage at bus 5 dropped to 0.86 PU. The voltage at bus 5 expresses a high difference in phase angle from the reference value and will be a-synchronized from the other phasors. Based on the information sent from PMU 5, the wide area monitoring and control system will act to solve the load flow problem to determine the amount of Q required from each of the microgrids to mitigate this voltage drop. The load flow problem is solved, the obtained solution is optimized using the Genetic Algorithms (GA). Optimum solution is characterized by using minimum reactive power from each grid to recover the bus voltage without causing any issues to the microgrids. After setting the required reactive power from *microgrids 1* and *2*, each local control in microgrid will send the required amount of reactive power through the bi-directional converter. This injected extra amount of reactive power will react to increase the voltage at bus 5. In this case study, the solution of the optimization problem yielded an amount of 700 VAR from *Microgrid 1* and 500 VAR from *Microgrid 2*. After injecting these values, the voltage at bus 5 goes up to 0.96 PU.

II. CONCLUSION

In this paper, the utilization of wide area monitoring and control in voltage assessment of hybrid AC/DC power system was presented. The WAMC solves an optimization problem to determine how much power the main AC grid requires from each of the two DC microgrid, containing renewable energy assets and storage, in order to restore the voltage to an acceptable value. An experimental test was performed in order to verify the proposed system.

PHEV Home-Charging Model Based on Residential Activity Patterns

Pia Grahn, Joakim Munkhammar, Joakim Widén, Karin Alvehag, Lennart Söder, KTH Royal Institute of Technology, School of Electrical Engineering, Division of Electric Power Systems, Teknikringen 33, SE-100 44 Stockholm, Sweden, Email: pia.grahn@ee.kth.se

Abstract—Electric vehicles (EVs) provide an opportunity to reduce greenhouse gas emissions in the transport sector. With increased numbers of EVs the electric vehicle charging (EVC) behavior in an area will induce changes in load profiles, and it becomes important to investigate what impact EVC has on load profiles due to expected EVC behavior of residents. This poster presents a model for generating plug-in hybrid electric vehicle (PHEV) home-charging patterns by combining PHEV usage with synthetic activity generation of residents' electricity-dependent activities. Synthetic activities are simulated based on time-of-use data, and forms the basis for estimations of EVC behavior and residential electricity consumption. The model is general and can be used where similar residential time-of-use data are available. The results are estimates of total residential load profiles and deviations which can be used in load shaving studies to investigate moveable activities.

I. KEY FIGURES AND RESULTS

Input data are used to generate synthetic activities $A_{m,i,j}$, which in parallel are input to the PHEV home-charging model. The model output is the total household load profile P_i^{tot} at time i which is the sum of the PHEV charging load, P_i^V and the load due to other electricity-dependent activities $P_{i,j}^h$.

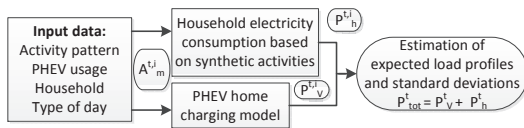


Fig. 1: Modeling approach

TABLE I: Electricity consumption and load peaks

PHEV	Apartment	Total	PHEV share
2.4 kWh/day	9.6 kWh/day	12.0 kWh/day	20%
0.3 kW	0.6 kW	0.8 kW	30%

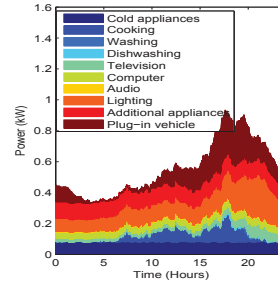


Fig. 2: Estimate of mean load $\bar{P}_i^V, \bar{P}_{A_{m,i}}$.

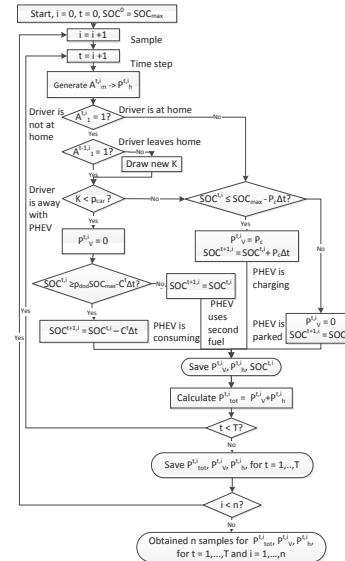


Fig. 3: Simulation algorithm for a household with a PHEV and one driver

Power Sharing Control with Frequency Droop in a Hybrid Microgrid

Megha Goyal, *Student Member, IEEE*, Arindam Ghosh, *Fellow, IEEE* and Firuz Zare, *Senior Member, IEEE*
 School of Engineering and Computer Science, Queensland University of Technology, Brisbane, Australia
 Email: m1.goyal@qut.edu.au, a.ghosh@qut.edu.au

ABSTRACT – A microgrid may contain a large number of distributed generators (DGs). These DGs can be either inertial or non-inertial, either dispatchable or non-dispatchable. Moreover, the DGs may operate in plug and play fashion. The combination of these various types of operation makes the microgrid control a challenging task, especially when the microgrid operates in an autonomous mode. In this paper, a new control algorithm for converter interfaced (dispatchable) DG is proposed which facilitates smooth operation in a hybrid microgrid containing inertial and non-inertial DGs. The control algorithm works satisfactorily even when some of the DGs operate in plug and play mode. The proposed strategy is validated through PSCAD simulation studies.

I. KEY FIGURE

The microgrid structure under consideration is comprised of three DGs, one of them is inertial DG (Diesel Generator) and others are converter interfaced DGs (UPS and PV), as shown in Fig. 1.

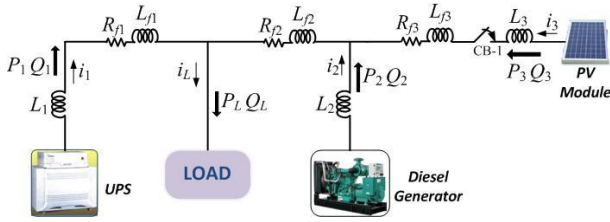


Fig. 1. Microgrid structure.

III. KEY EQUATIONS

A. Governor and Swing Equations

The mechanical power of the governor is

$$P_m = \frac{G}{1+sT} P^* - D\Delta\omega \quad (1)$$

where ω is obtained from droop (1) and

$$D = \frac{1}{m}, \quad \Delta\omega = \omega - \omega_r$$

The swing equations are

$$\frac{d\delta}{dt} = \omega_r \Delta\omega_{sw} \quad (2)$$

$$\frac{d\Delta\omega_{sw}}{dt} = \frac{1}{2H} (-K_D)\Delta\omega_{sw} + \frac{1}{2H} (P_m - P_e) \quad (3)$$

$$\omega_{UPS} = \omega + \Delta\omega_{sw} \quad (4)$$

III. KEY RESULTS

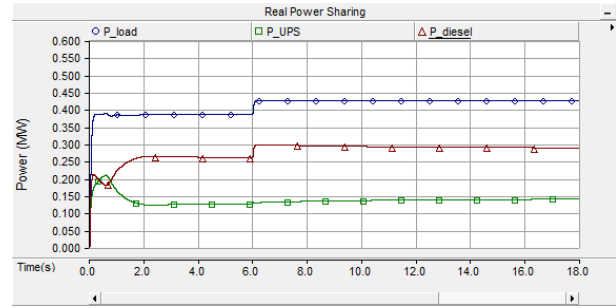


Fig. 9. Real power sharing in Case-1.

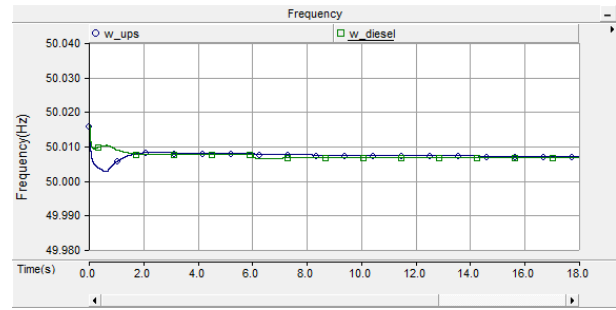


Fig. 10. Frequencies of the two DGs in Case-1.

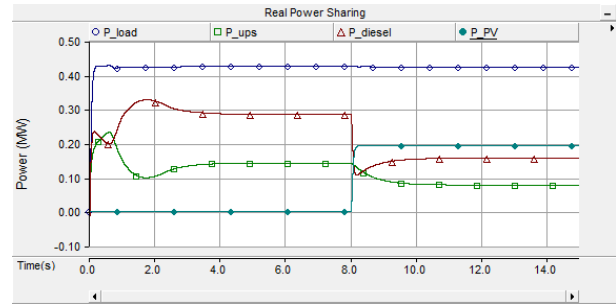


Fig. 11. Power sharing in Case-2 when the PV is switched on.

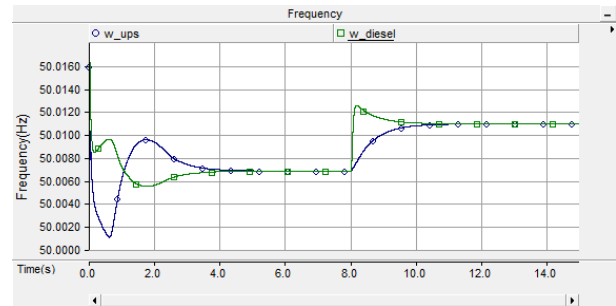


Fig. 12. Frequencies in Case-2 when PV is switched on.

Look-Ahead Energy Management of a Grid-Connected Residential PV System under Critical Peak Pricing Programs

Jaeyoung Yoo

School of Electrical and Electronic Engineering, Yonsei University, Seoul, South Korea,
Email: jy-yoo@yonsei.ac.kr

Abstract—This poster presents look-ahead energy management system for a grid-connected residential photovoltaic (PV) system with battery under critical peak pricing for electricity. In the proposed system, the PV system is the primary energy source with the battery for storing (or retrieving) excessive (or stored) energy to pursue the lowest possible electricity bill but it is grid-tied to secure electric power delivery. Premise energy management scheme with an accurate yet practical load forecasting capability based on a Kalman filter is designed to increase the predictability in controlling the power flows among these power system components in the premise. The case study with particular operating condition demonstrates the validity of the proposed system and significant cost savings through operating the energy management scheme.

I. KEY EQUATION

$$x(k) = F(k)x(k-1) + v(k-1) \quad (1)$$

$$z(k) = H(k)x(k) + n(k) \quad (2)$$

$$E[v(k)] = E[n(k)] = 0 \quad (3)$$

$$E[v(i)v^T(j)] = E[n(i)n^T(j)] = 0 \quad \text{for } i \neq j \quad (4)$$

$$E[v(k)v^T(k)] = Q_1, E[n(k)n^T(k)] = Q_2 \quad (5)$$

$$K(k) = [F(k)P(k)H^T(k)][H(k)P(k)H^T(k) + Q_2]^{-1} \quad (6)$$

$$\hat{x}(k+1) = F(k)\hat{x}(k) + K(k)[z(k) - H(k)\hat{x}(k)] \quad (7)$$

$$P(k+1) = [F(k) - K(k)H(k)]P(k)[F(k) - K(k)H(k)]^T + K(k)Q_2K^T(k) \quad (8)$$

II. KEY TABLE

TABLE I
ESTIMATED COEFFICIENTS OF THE PROPOSED FORECASTING MODEL.

α_1	α_2	α_3	α_4	α_5
0.5962	0.2373	0.2182	0.0559	0.2963
α_6	α_7	α_8	α_9	α_{10}
0.3962	0.1912	0.1962	0.1989	0.2991

III. KEY RESULT

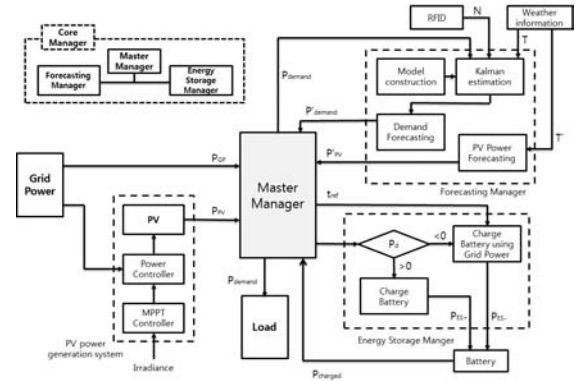


Fig. 1. Configuration of the proposed premise energy management system.

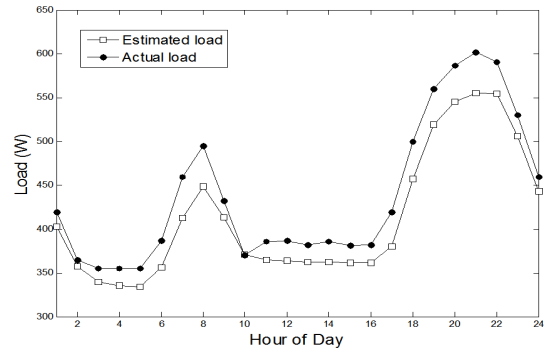


Fig. 2. Actual and estimated load demands for Scenario

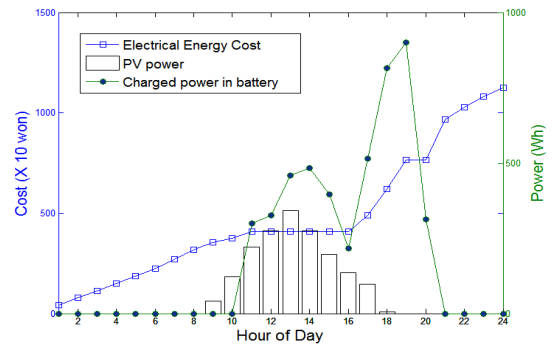


Fig. 3. Use of PV power, SOC of the battery and electricity price under Scenario

Demand Response as a Tool for Coordinated Charging of PHEV Parking Garages

Venkata Satish Kasani, Sarika Khushalani Solanki and Jignesh Solanki

Lane Department of Computer Science and Electrical Engineering, West Virginia University

Morgantown, WV 26505, USA

Email: vkasani@mix.wvu.edu and Sarika.Khushalani-Solanki@mail.wvu.edu

Abstract - Increase in the penetration of Plug-in Electric Vehicle (PHEVs) and optimal utilization of existing infrastructure to satisfy the charging needs require smart charging techniques. As the charging stations or parking garages are best suitable locations to charge the vehicles either at office or homes when looking in the V2G prospective, this poster presents a two stage coordinated charging process aiming at maximizing their profit as well as satisfying the customer needs. Maximizing profits of PGs indirectly maximizes the power delivered to the vehicles without exceeding the network limits. The network sensitivities are considered in the constraints in the first stage of optimization. The new peaks that resulted from the optimization are flattened by implementing demand response at the charging stations. The network sensitivities are obtained from OpenDSS and MATLAB linear programming is employed to obtain the charging rates of PHEVs.

I. KEY EQUATIONS

Stage – 1: Optimization

$$\max \sum_{l=1}^L \sum_{m=1}^M B_{ml} \times S_{ml} \times P_{max} \times (g_l - c_l)$$

$$s. t. \sum_{m=1}^M B_{ml} \times S_{ml} \times P_{max} \leq A_l T_l \phi, \forall l \in \{1,2,3, \dots, L\}$$

$$SOC_m^D \times C_m \leq (\sum_{m=1}^L B_{ml} \times S_{ml} \times P_{max} + SOC_m^A \times C_m) \leq C_m$$

$$V_{min\ i} \leq V_{init\ i} + \mu_i B_{ml\ i} + \sum_{n=1}^N \mu_{ji} B_{ml\ j} \leq V_{max\ i}$$

Stage – 2: DR Model

Self Elasticity Coefficient

$$E(l, l) = \frac{\Delta d(t_l)/d_0}{\Delta p(t_l)/p_0}$$

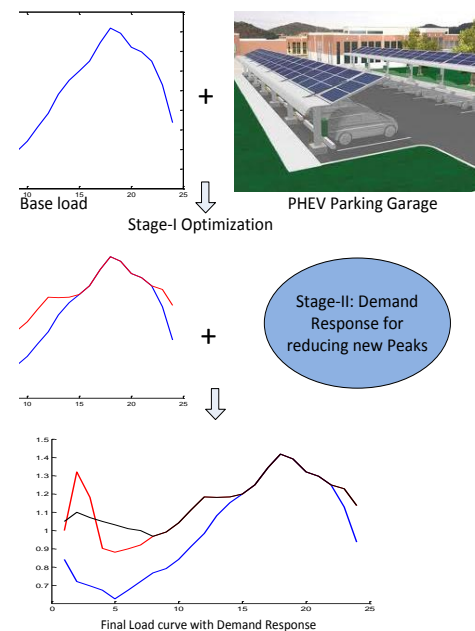
Cross Elasticity Coefficient

$$E(l, j) = \frac{\Delta d(t_l)/d_0}{\Delta p(t_j)/p_0}$$

Demand Reduction for each hour:

$$\Delta d(t_l) = \sum_{j=1}^{24} E(l, j) * \left(\frac{\Delta p_j}{p_0} \right) * d_0$$

II. KEY FIGURES



Distributed Data Fusion for State Estimation in Cyber Physical Energy Systems

Abhinav Kumar Singh, *Student Member, IEEE*, and Bikash C. Pal, *Fellow, IEEE*

Abstract—This poster proposes an adaptive algorithm for dynamic state estimation in cyber physical energy systems. The algorithm involves distributed estimation based on unscented Kalman filtering, and subsequent multi-path data fusion of the local estimates. The distributed estimation takes into account the inherent shortcomings of networked systems, viz., packet dropout, packet disordering and variable time delays. The multi-path data fusion strategy endeavours to convert the highly stochastic and uncertain packet delivery model of present day networks into a deterministic model with very high packet delivery probabilities and fixed time delays. The combined strategy of distributed estimation and multi-path data fusion has been demonstrated on a representative 68-bus power system model.

Index Terms—data-fusion, distributed, cyber physical energy systems, phasor measurement units, unscented Kalman filtering.

I. INTRODUCTION

IT is envisioned that future power systems are going to be highly interconnected [1]. Each sensing or actuating component of the power system, such as phasor measurement units (PMUs), smart meters, relays, FACTS devices etc., will be allotted an IP address, so that it can easily communicate in real-time with the rest of the power network. This will generate huge amounts of data and information which can be used to better assess and control the system. The Networked Controlled System (NCS) approach is very appropriate in such a context. In NCS the control loops are closed through a real-time network, and the control and feedback signals are exchanged among the system's components in the form of packets of data and information [2]. NCSs suffer from some problems which have not been taken into account in traditional control systems such as packet-dropout, time-delays and packet-disordering [2]. In this paper, a strategy to counteract these problems has been proposed which is based on multi-path data-fusion and distributed state-estimation.

II. METHODOLOGY

It is assumed that each generation unit is connected to its neighboring unit and a centralised control unit through networked connections. PMUs are installed on each unit for local state estimation. An algorithm based on decentralized Kalman filtering using unscented transformation [3] runs on each unit and estimates the local states of the unit using the

Abhinav Kumar Singh (a.singh11@imperial.ac.uk) and Bikash C. Pal (b.pal@imperial.ac.uk) are with the Control and Power Group, Department of Electrical and Electronic Engineering, Imperial College London, SW7 2BT, London. This work was supported by EPSRC, U.K., under Grant EP/G066477/1.

PMU measurements. The estimation at one unit is completely independent from the estimation at other units.

A time cycle is divided into two time periods. In the first, shorter period, every unit calculates its local state estimates and sends those estimates to its immediate neighbours. In the remaining longer period, every node sends its cumulative data (i.e. its own data combined with its neighbours data) to the central controller. The controller waits for the data from all the sending nodes in the combined time period, after which it discards all the late data arrivals. This scheme is shown to operate with high delivery probability and fixed time delay. A block diagram of such a system is shown in Fig. 1.

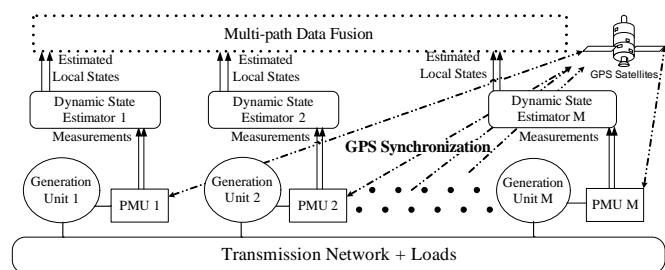


Fig. 1. System block-diagram and an overview of the methodology

III. MODELING AND SIMULATION

A 16-machine, 68 bus model test system has been used for the case study. The packet drop process is modeled as a Bernoulli process, and a random delay is introduced in their transmission. The strategy of distributed estimation and multi-path data fusion is then implemented on the test system.

IV. CONCLUSIONS

A strategy for distributed estimation has been devised and combined with multi-sensor data fusion to accurately estimate the dynamic states of a power system. It is the belief of the authors that the proposed distributed data fusion has good potential for dynamic security assessment in cyber physical energy systems.

REFERENCES

- [1] C. Hauser, D. Bakken, and A. Bose, "A failure to communicate: next generation communication requirements, technologies, and architecture for the electric power grid," *IEEE Power and Energy Mag.*, vol. 3, pp. 47–55, Mar.-Apr. 2005.
- [2] G. Walsh, H. Ye, and L. Bushnell, "Stability analysis of networked control systems," *IEEE Trans. Control Syst. Tech.*, vol. 10, pp. 438–446, May 2002.
- [3] S. Julier, J. Uhlmann, H.F. Durrant-Whyte, "A new method for the non-linear transformation of means and covariances in filters and estimators," *IEEE Trans. Autom. Control*, vol. 45, no. 3, pp. 477–482, Mar. 2000.

CONTROL STRATEGIES OF MICRO SOURCES IN MICROGRID

Xin Wang, *Student Member, IEEE* and Wei-Jen Lee, *Fellow, IEEE*

Energy Systems Research Center, Department of Electrical and Computer Engineering,
University of Texas at Arlington, Arlington, TX 76013, USA

Email: xin.wang70@mavs.uta.edu and wlee@uta.edu

Abstract-- Due to potential wide spread impact on the power system caused by short circuit and other incidents in an interconnected grid, many countries devote significant efforts in developing robust, fault isolation, and self healing power system to meet the need of future digital society. Among them, Micro grid is one of the most effective ways to reduce the damage brought by the instabilities in grid. Through the advanced control and coordination, Micro grid has the potential to deliver electrical energy as well as thermal energy to customers in a most efficient and reliable manner. This poster discusses the control strategies of distributed generations within the Micro grid during autonomous operations.

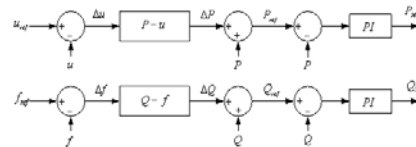


Fig. 3. The schematic diagram for Droop control

II. SIMULATION FOR DROOP CONTROL

The schematic diagram for the application of droop control in Microgrid is shown in Figure. 4

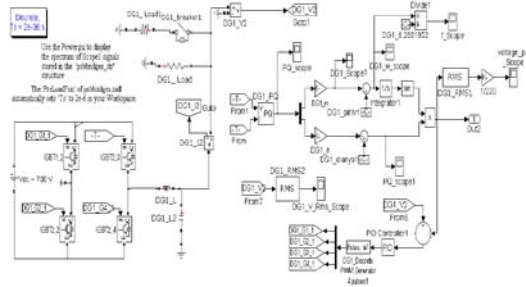


Fig. 4. Droop control in Microgrid

I. KEY CONTROL METHODS

There are three main control methods: P/Q control, Droop control and U/f control.

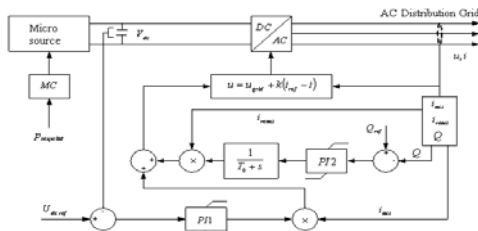


Fig. 1. The schematic diagram for P/Q control

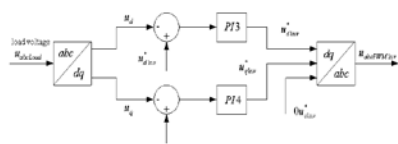


Fig. 2. The schematic diagram for U/f control

III. KEY RESULTS

The simulation is implemented on MATLAB. The reactive/active power consumption and system frequency responses are shown in Fig. 5:

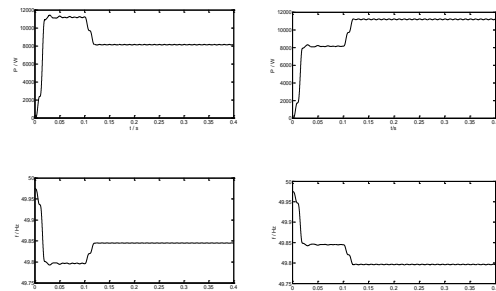


Fig. 5. Simulation results

A Robust Multi-Objective Controller of VSC-Based DC-Voltage Power Port in Hybrid AC/DC Microgrids

Masoud Davari and Yasser Abdel-Rady I. Mohamed

Department of Electrical and Computer Engineering,
University of Alberta
Edmonton, Canada

davari@ualberta.ca and yasser2@ualberta.ca

Abstract— Hybrid ac/dc multi-terminal microgrids are gaining high momentum under the smart grid paradigm to integrate renewable and clean energy resources either in the transmission or distribution systems. This poster presents a robust multi-objective controller for the voltage-source-converter (VSC)-based dc-voltage power-port in hybrid ac/dc networks. The proposed controller ensures excellent tracking performance, robust disturbance rejection, and robust stability against operating point and parameter variation with a simple fixed-parameter low-order controller. A two-degree-of-freedom control structure is proposed, where feed-forward tracking and base-line robust disturbance rejection controllers are employed to decouple disturbance rejection and tracking objectives. A disturbance rejection controller is designed, based on the singular-values (Mu) synthesis approach, to achieve robustness against variation in converter operation point. Further, the effect of parametric uncertainty in the effective dc-link capacitance is mitigated by modifying the robust disturbance rejection controller, via the polynomial method, to ensure that the closed-loop poles are allocated in the pre-defined region in the complex plane even under parameter variation. A comparative simulation and experimental results are presented to show the effectiveness of the proposed control structure rather than previous controller, PI-lead controller.

Keywords— Hybrid dc/ac networks, micro-grids, dc-energy pool, dc-link voltage control, voltage-source converters, robust control.

I. KEY EQUATIONS, KEY FIGURES, AND KEY RESULTS

The power balance equation is as follows:

$$\frac{d}{dt}(0.5C_{eq}V_{DC}^2) = P_{ext} - P_{DC} - P_{loss} \quad (1)$$

If the energy stored in the interface reactors is not ignored, then after linearizing around one specific operating point, the power balance equation can be given by (2). The most important feature of equation (2) is that it is non-minimum system when converter operates in the rectification mode.

$$\begin{aligned} \tilde{V}_{DC}^2(s) = & \frac{R_p}{R_p C_{eq} s + 1} \tilde{P}_{ext}(s) - \frac{3}{2} R_p (V_{sd0} + 2RI_{d0}) \frac{LI_{d0} s + 1}{0.5R_p C_{eq} s + 1} \tilde{I}_d(s) \\ & - \frac{3}{2} \frac{R_p I_{d0}}{0.5R_p C_{eq} s + 1} V_{sd0} - 3RR_p I_{q0} \frac{Ls/2R + 1}{0.5R_p C_{eq} s + 1} \tilde{I}_q(s) \end{aligned} \quad (2)$$

The proposed controller of the voltage power port is shown in Fig. 1 where $P_f(s)$, $G_{N-i}(s)$, and $G_i^{-1}(s)$ are pre-filter, non-invertible part of equation (2), and invertible part of equation (2), respectively. Since equation (2) is non-minimum phase in rectification mode, the following method has been adopted to design $K(s)$; first, controller $K(s)$ is synthesized based on the structured singular values (μ) analysis to reject P_{ext} in different operating points. Then, the designed μ -analysis-based controller is employed in polynomial method to benefit from polytopic structures in order to have robustness against equivalent capacitance variation, which exists due to connection/disconnection of dc-sources and/or loads to/from dc link.

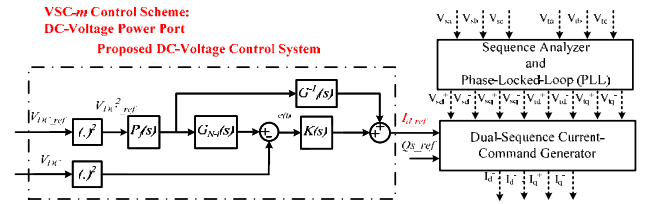


Fig. 1. Proposed control scheme for the dc-voltage power-port in hybrid ac/dc micro-grid.

Fig. 2 and Fig. 3 show the key simulation and experimental results of the proposed controller.

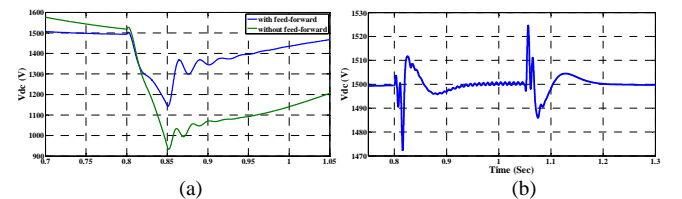


Fig 2. a) PI-lead controller b) proposed controller when there is an asymmetric line-to-ground (LG) fault in one of the grids when the converter works as rectifier

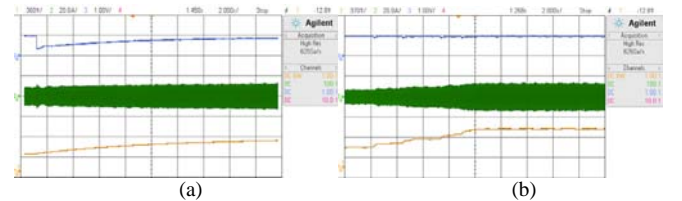


Fig 3. experimental results of a) PI-lead controller with moderate changes of the dc micro-grid load (dc motor load) b) the proposed controller with uncertainty in the dc-link capacitance and operating point variation. Channel 3 (top): V_{dc} in per-unit, Channel 2 (middle): one phase ac-line current; Channel 1 (bottom): I_d in per-unit.

Hardware Design of Smart Home Energy Management System with Dynamic Price Response

Qinran Hu, Fangxing(Fran) Li

Department of Electrical Engineering and Computer Science, the University of Tennessee,
Knoxville, TN 37996, USA,
Email: ghu2@utk.edu, fli6@utk.edu

Abstract— The smart grid initiative and the electricity market operation drive the model known as demand-side management or controllable load. The home energy management has received increasing interest due to the significant amount of loads in the residential sector. This paper presents a hardware design of a smart home energy management system (SHEMS) with the application of communication, sensing technologies, and machine learning algorithms. With the proposed design, consumers are able to have a real-time price-responsive control strategy over loads including electrical water heater (EWH), heating, ventilation, and air conditioning (HVAC), electrical vehicle (EV), dishwasher, washing machine, and dryer. Also, they may interact with suppliers or load serving entities (LSEs) to facilitate the management at the supplier side. Further, SHEMS is designed with sensors to detect human activities and then apply a machine learning algorithm to intelligently help consumers reduce total payment on electricity without little involvement of consumers. This paper also presents simulation and experiment results based on the SHEMS prototype to verify the hardware system.

I. HARDWARE DESIGN OF SHEMS

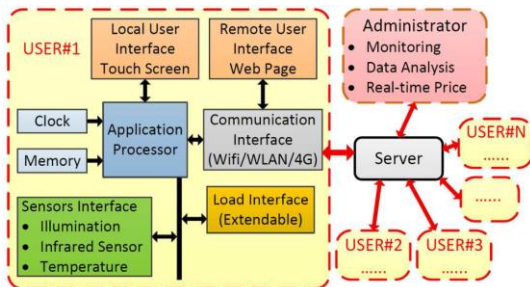


Fig. 1. Brief Hardware Design of SHEMS

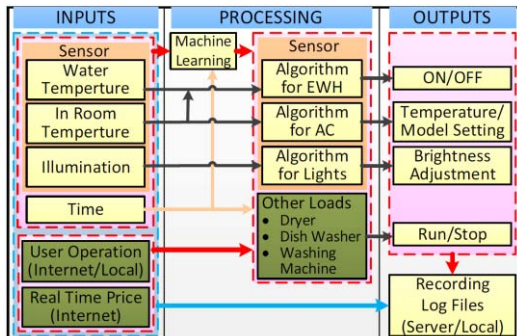


Fig. 2 Schematic Design of SHEMS (User End)



Fig. 3 Prototype platform of SHEMS

II. KEY RESULTS

TABLE I. SIMULATION RESULTS OF MACHINE LEARNING ALGORITHM

Activity Name	Right	Wrong	Accuracy(%)
Going out to work	11	1	91.67
Toileting	70	14	83.33
Bathing	13	5	72.22
Grooming	33	4	89.19
Preparing breakfast	9	5	64.29
Preparing lunch	13	4	76.47
Preparing dinner	6	2	75.00
Washing dishes	6	2	75.00
Doing laundry	19	0	100.00
Total	180	37	82.95

Table II. HVAC Results with SHEMS

	Different Comfort Level		
	+/- 0°C	+/- 3°C	+/- 5°C
Energy Consumption (% w.r.t w/o SHEMS)	91%	79%	72%
Payment (% w.r.t the case w/o SHEMS)	86%	73%	64%

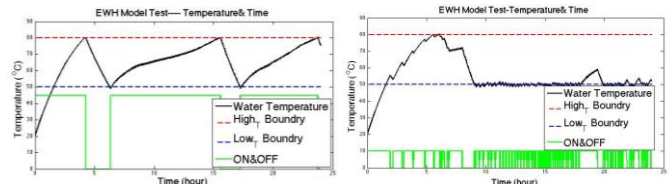


Fig. 4 Typical Versus Optimized EWH Strategy (40% Saved)

Effects of SHEMS in Load Shifting

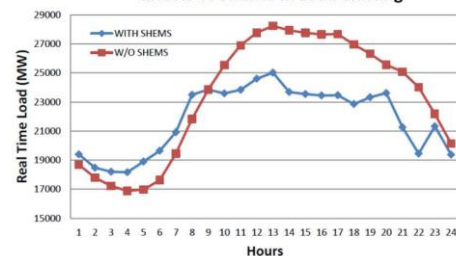


Fig. 5 Load Curve Comparison with and without SHEMS

Smart Meter Deployment and Applications in the United States

Megan Milam, *Student Member IEEE* and G. Kumar Venayagamoorthy, Ph.D, *Senior Member IEEE*
Holcombe Department of Electrical and Computer Engineering
Clemson University, SC 29631, USA
Email: mrmilam@g.clemson.edu and gkumar@ieee.org

Abstract— The purpose of this study is to present the current status of smart meter technology and its applications today. First of all, the most common smart meter models (from companies such as Itron [3] and Elster [1]) were compared and evaluated based on cost, features, accuracy, customer involvement, installation ease, and impact on the electricity usage and demand response.

Additionally, surveys were generated to track current smart meter deployment initiatives in the United States. A survey was sent to utility companies that owned projects listed on the US Department of Energy’s Smart Grid website [5] under the Recovery Act Smart Grid Program. The survey provides information such as duration of the project, region covered, budget, number of meters deployed (for residential, commercial and industrial use), benefits (financial- and performance-based for customer and power companies), and obstacles. Emphasis is given to the gains and setbacks the companies faced during implementation. Furthermore, the recipients of smart meter technology (homeowners, business owners) were polled on their satisfaction with the performance of the smart meter.

This study is aimed at bringing awareness to the electricity community of the overall progress across the U.S. towards development and deployment of Automated Metering Infrastructure (AMI) systems and the resulting impacts.

I. KEY FIGURES



Fig. 1. Itron’s OpenWay Centron, a residential smart meter [3].



Fig. 2. Elster’s EnergyAxis monitoring software used to track and control energy use [1].

REFERENCES

- [1] *elster.com*. Elster. 2013. Web. 10 Mar. 2013.
- [2] “Energy Efficiency Trends in Residential and Commercial Buildings.” *Energy Efficiency and Renewable Energy*. U.S. DOE, Oct. 2008. PDF file. 20 Feb. 2013.
- [3] *itron.com* Itron. 2013. Web. 10 Mar. 2013.
- [4] *Smart Grid Resource Center (SGRC)*. Electric Power Research Institute. 2001. Web. 21 Jan. 2013. <smartgrid.epri.com>.
- [5] *SmartGrid.gov*. U.S. Department of Energy. n.d. Web. 21 Jan. 2013.

Distribution Locational Marginal Pricing for Optimal Electric Vehicle Charging Management

Ruoyang Li, Qiuwei Wu and Shmuel Oren

Department of Industrial Engineering and Operations Research, University of California-Berkeley, Berkeley, CA 94720, USA

Email: ruoyang@berkeley.edu

Abstract— This paper presents an integrated distribution locational marginal pricing (DLMP) methodology designed to alleviate congestion resulting from electric vehicles (EVs) load in future power systems. In the proposed approach, the distribution system operator (DSO) determines distribution locational marginal prices (DLMPs) by solving the social welfare optimization of the electric distribution system which considers EV aggregators as price takers in the local DSO market and demand price elasticity. Nonlinear optimization has been used to solve the social welfare optimization in order to obtain the DLMPs. We illustrate the efficacy of the proposed approach using the Roy Billinton Test System (RBTS). The case study results show that the integrated DLMP methodology can successfully manage congestion caused by EVs load. We also show that the socially optimal charging schedule can be implemented through a decentralized mechanism where loads respond autonomously to posted DLMPs by maximizing their individual net surplus.

I. KEY EQUATIONS

$$\max_{r_{i,t}, c_{i,t} \in N_c, i \in T, q_{g,t} \in N_g, i \in T} \sum_{i \in N_c} \sum_{i \in T} \int_0^{c_{i,t}} P_{i,t}(r_{i,t}) dr_{i,t} - \sum_{i \in T} P_i^{LMP} q_{g,t} \quad (1)$$

$$s.t. \quad \sum_{i \in N} r_{i,t} = 0 \quad \forall t \in T \quad (p_t) \quad (2)$$

$$-K_l \leq \sum_{i \in N} D_{i,t} r_{i,t} \leq K_l \quad \forall l \in L, \forall t \in T \quad (\lambda_{l,t}^-, \lambda_{l,t}^+) \quad (3)$$

$$r_{g,t} + q_{g,t} = 0 \quad \forall t \in T \quad (\delta_{g,t}) \quad (4)$$

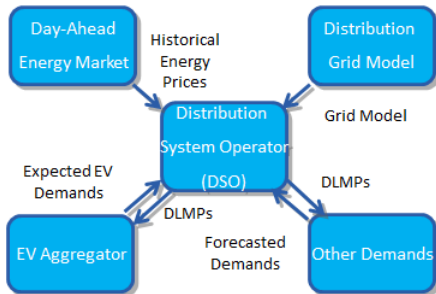
$$r_{i,t} = c_{i,t} + x_{i,t} \quad \forall i \in N_c, \forall t \in T \quad (\rho_{i,t}) \quad (5)$$

$$c_{i,t} \geq 0 \quad \forall i \in N_c, \forall t \in T \quad (\xi_{i,t}) \quad (6)$$

$$0 \leq x_{i,t} \leq E_{i,t} \quad \forall i \in N_c, \forall t \in T \quad (\mu_{i,t}^-, \mu_{i,t}^+) \quad (7)$$

$$S_{i,t}^- \leq S_{i,t} + \sum_{i' \leq t-1} x_{i',t} - \sum_{i' \leq t} d_{i',t} \leq S_{i,t}^+ \quad \forall i \in N_c, \forall t \in T \setminus \{1\} \quad (\kappa_{i,t}^-, \kappa_{i,t}^+) \quad (8)$$

II. MODEL STRUCTURE



III. KEY RESULTS

Theorem1. The efficient allocation of EV charging from DSO's problem is an optimal solution to EV Aggregator's problem under DLMP, if the non-negativity constraint of conventional household demand is not binding.

Proposition1. The efficient allocation from DSO's problem can be achieved in a decentralized system under DLMP, if the non-negativity constraint of conventional household demand is not binding.

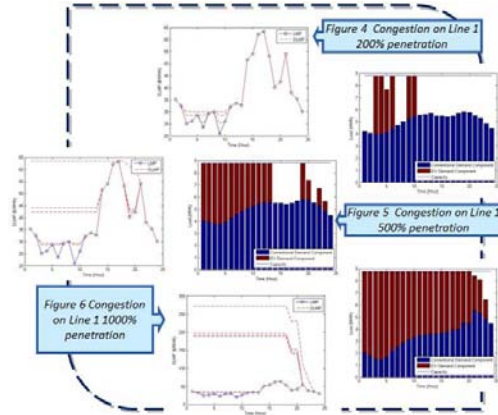


Figure 1 DLMP and Line Loading with 200% 500% 1000% EV Penetration

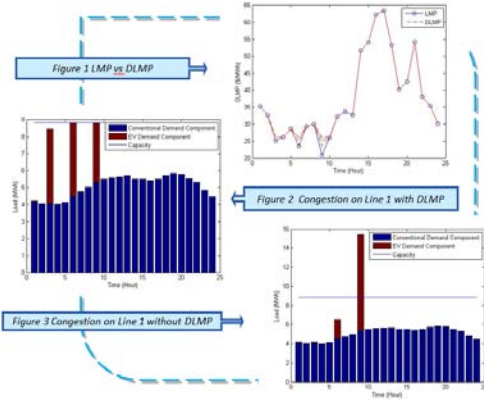


Figure 2 Line Loading with and without DLMPs

A Comparative Analysis of Volt-VAr Control Algorithms for the Distribution System

Griet Devriese, *Student Member*, IEEE, Anurag K Srivastava, *Senior Member*, IEEE

Smart Grid Demonstration and Research Investigation Laboratory, The School of Electrical Engineering and Computer Science,
Washington State University, Pullman, WA 99163, USA,
Email: griet.devriese@email.wsu.edu

Abstract—This study compares the different volt/VAr control techniques to reliably supply power to customers while meeting the operational constraints for one of the distribution system feeders in the Pacific North West. The studied algorithms comply with the ANSI mandated power factor and voltage constraint requirements while meeting the load demand with conservation voltage reduction mechanism.

I. BACKGROUND

Volt-VAr control is critical in operation and control of the electric distribution grid, especially with the rapidly changing smart grid development. With varying customer demand throughout the day, the power and voltage levels must be adjusted. Voltage regulators and capacitors are employed to help maintain voltage levels along distribution feeders; but with today's smart technology, the use of such equipment can be controlled more finely to ensure energy savings [1].

Through the U.S. Department of Energy (DOE) Smart Grid Grant program, the local utility, Avista, is updating 13 distribution feeders in Pullman. The system contains 20 switched and fixed capacitor banks, 45 automated line switches and reclosers, and collects data from over 13,000 smart meters. In collaboration with Avista Utilities, Washington State University is working to quantifying the benefits of smart grid implementation.

II. METHODS

Three possible methods are implemented to achieve Volt-VAr control on the local utilities' distribution feeders. Using 5 minute interval data, the energy savings are studied in each of these possible respective control techniques.

A. Power Factor Control Algorithm

In this study, the utility mandated power factor limits are between 0.95 lagging and 0.98 leading. This technique is implemented in Visual Basic and works with the commercial distribution power flow software, SynerGEE Electric.

B. 60%-40% Rule

The 60%-40% rule determines the desired capacitor state based on its percentage relation to the telemetered reactive power value. The capacitor bank will be turned on if it will not result in more than 40% imbalance, but will provide more than 60% of the reactive power needed. This technique is

implemented in Visual Basic and works with the commercial distribution power flow software, SynerGEE Electric.

C. Capacitor Optimization

In the capacitor optimization method, an algorithm is implemented to iteratively determine the optimal capacitor state to maximize the system's energy savings. The optimization algorithm utilizes a three phase distribution power flow to calculate the system states.

III. RESULTS

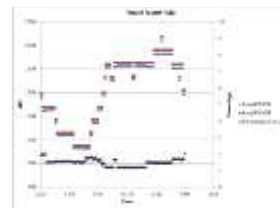


Figure 1. kW Savings for Power Factor Rule

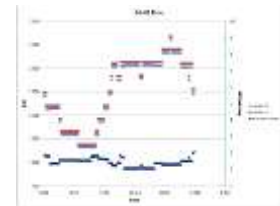


Figure 2. kW Savings for 60%-40% Rule

IV. CONCLUSIONS

The results show similar percentage savings between the power factor and 60%-40% rule for one Pullman feeder. In the 60%-40% rule the capacitors are switched for longer periods of time than with the power factor method. This difference creates the minor variations in percentage savings between the two presented cases.

V. ACKNOWLEDGEMENTS

The authors would like to thank Avista Utilities and the Department of Energy for their financial support.

VI. REFERENCES

- [1] U.S. Department of Energy, "Application of Automated Controls for Voltage and Reactive Power Management – Initial Results", December 2012

Maximizing the Penetration of Plug-In Electric Vehicles in Distribution Network

¹Junhui Zhao, ^{1,2}Yang Wang, ¹Caisheng Wang
¹Wayne State University, Detroit, MI 48202, USA,
²Chongqing University, Chongqing, China,
junhui.zhao@wayne.edu

Abstract- The increasing number of plug-in electric vehicles (PEVs) will post new challenges to the existing power grid, as they as a whole will become a substantially large load to the power grid when they are being charged. In this paper, an algorithm is proposed to maximize the injection of PEVs in distribution networks (DN) without violating power limitations and causing voltage problems. This method is able to optimally calculate the maximum allowed numbers of PEVs in DNs based on the system parameters and load conditions. Voltage stability index, power supply limits, thermal line limits, and power balance equations are taken into account as the constraints of the optimization algorithm. This method is able to provide a clear reference to distribution network operators (DNO) to manage the charging of the PEVs in DNs.

Index Terms - Distribution Network, Plug-In Electric Vehicles, Active Management, Optimization.

I. KEY EQUATIONS

In this paper, the objective is to maximize the total injection of PEVs in a DN

$$f_{min} = \frac{1}{N_1 + N_2 + \dots + N_M} \quad (1)$$

where N_k is the number of PEVs at node k , $k=0, 1, 2 \dots, M$.

Subject to the following constraints:

$$\begin{aligned} \sum P_{load} + \sum P_{PEVs} + \sum P_{loss} &= P_{trans} \\ \sum Q_{load} + \sum Q_{loss} &= Q_{trans} \end{aligned} \quad (2)$$

$$\begin{aligned} P_{trans} &\leq P_{trans}^{max} \\ Q_{trans} &\leq Q_{trans}^{max} \end{aligned} \quad (3)$$

$$ENVCI_k \geq ENVCI_k^{min} \quad (4)$$

$$S_{l,t} < S_l^{max}, \forall l, t \quad (5)$$

Equivalent node voltage collapse index ($ENVCI$) can be represented as:

$$ENVCI = 2(e_{eq,x}v_{k,x} + e_{eq,y}v_{k,y}) - (e_{eq,x}^2 + e_{eq,y}^2) \quad (6)$$

The expression of $ENVCI$ can be re-written in polar coordinates as

$$ENVCI = 2|E_{eq}||V_k| \cos(\theta_{eq} - \theta_k) - |E_{eq}|^2 \quad (7)$$

where θ_{eq} and θ_k is the phasor angles of E_{eq} and V_k , respectively; θ is the angle deference of θ_{eq} and θ_k .

II. KEY FIGURES

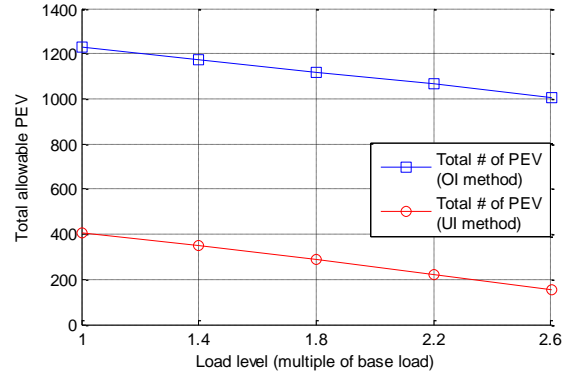


Fig. 1 Total allowable PEVs for two scenarios at five load levels.

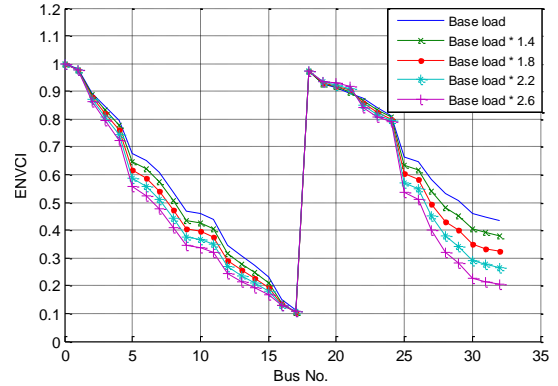


Fig. 2 ENVCI at Bus 1-32 by average injection method under five load levels.

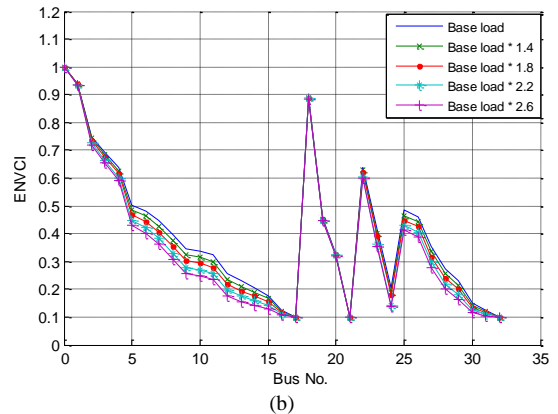


Fig. 3 ENVCI at Bus 1-32 by optimized injection method under five load levels.

An Investigation of the Effectiveness of a Network Reconfiguration Experiment at Drexel University

Nicole Segal, Christian Schegan, & Karen Miu

Center for Electric Power Engineering, Department of Electrical and Computer Engineering
Drexel University, Philadelphia, Pennsylvania, U.S.A.
nus23@drexel.edu, cms68@drexel.edu, karen@coe.drexel.edu

Abstract—This work addresses the effectiveness of a Network Reconfiguration (NR) hardware experiment for the undergraduate and graduate curriculum in power distribution systems. Surveys were issued to students before and after the hardware experiment was performed. The hardware experiment was performed in the Reconfigurable Distribution Automation and Control Laboratory (RDAC) at Drexel University [1].

Several identical rubric questions from both pre- and post-assessment questionnaires were chosen to assess whether the educational objectives outlined in the experiment had been met. The class responses were separated into groups of undergraduate and graduate students. A comparison of the survey responses was performed in order to evaluate the student's comprehension of the experiment's objectives. Undergraduate responses indicated that the hardware experiment assisted in their understanding of the theoretical and practical concepts.

Distribution systems are electrically unbalanced across phases. In this experiment, the concept of multi-phase switching was introduced and employed by students for load balancing. The macro-goal of the hardware exercise was to provide students with practical and theoretical analysis skills for planning and operating distribution networks.

Network Reconfiguration is the process of changing the topological structure of distribution systems by opening and/or closing sectionalizing (normally closed) switches and tie (normally open) switches. Network Reconfiguration is used to improve system operating conditions by load balancing, which reduces the real power losses in the network.

Before the NR laboratory exercise is disseminated to other universities as a remote hardware experiment, it was examined in detail to determine its significance in power distribution systems curriculum.

I. SELECTED NETWORK RECONFIGURATION OBJECTIVES

Below are several objectives from the NR experiment laboratory manual. These key objectives have been addressed in the pre and post experiment surveys performed by Drexel University Power Systems graduate and undergraduate students. The goals are to:

1. Understand the need for network reconfiguration for load balancing and loss reduction in a real-life environment;

2. Experience how to place new switches for network reconfiguration – planning;
3. Study how to schedule network reconfiguration for different loading conditions – planning and operation;
4. Understand how to select and operate existing three-phase or single-phase switches to reconfigure network– operation;

II. SELECTED RUBRIC QUESTIONS

Sample questions for assessing how to perform NR:

1. Maintaining a radial system structure while servicing loads is _____ when reconfiguring the network.
 - a. Preferred
 - b. Impossible
 - c. Not Necessary
 - d. Don't Know
2. Single phase switching of sectionalizing and tie switches may be necessary for multiphase distribution power systems. (agree/disagree)

III. KEY FIGURE

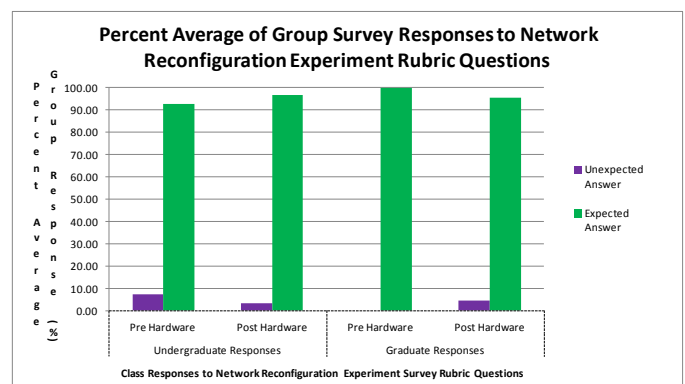


Fig. 1. Graph of Class Survey Responses to Network Reconfiguration Experiment Rubric Questions

REFERENCES

- [1] X. Yang, V. Cecchi, K. Miu, C. Nwankpa, "Reconfigurable Distribution Automation and Control Laboratory: A Network Reconfiguration Experiment for Load Balancing and Loss Reduction in Power Distribution Systems," Proceedings of the ASEE Annual Conference and Exposition 2005, Portland, OR, June 12-15, 2005.

Standardization of Power System Protection Settings Using IEC 61850 for Improved Interoperability

Qiteng Hong, Steven M. Blair, Victoria M. Catterson,
Adam Dyško, Campbell D. Booth
Institute for Energy and Environment
University of Strathclyde
Glasgow, G1 1XW, UK
q.hong@strath.ac.uk

Tahasin Rahman
National Grid
Warwick, CV34 6DA, UK
tahasin.rahman@nationalgrid.com

Abstract— One of the potential benefits of smart grid development is that data becomes more open and available for use by multiple applications. Many existing protection relays use proprietary formats for storing protection settings. This paper proposes to apply the IEC 61850 data model and System Configuration description Language (SCL), which are formally defined, to represent protection settings. Protection setting files in proprietary formats are parsed using rule-based reasoning, mapped to the IEC 61850 data model, and exported as SCL files. An important application of using SCL-based protection setting files is to achieve protection setting interoperability, which could bring multiple compelling benefits, such as significantly streamlining the IED configuration process and releasing utilities from being “locked in” to one particular vendor. For this purpose, this paper proposes a uniform configuration process for future IEDs. The poster will present the process of representing protection settings using IEC 61850 data model, exporting the settings in SCL-based file and using the approach to achieve protection setting interoperability and simplifying IED configuration process.

I. KEY FIGURES

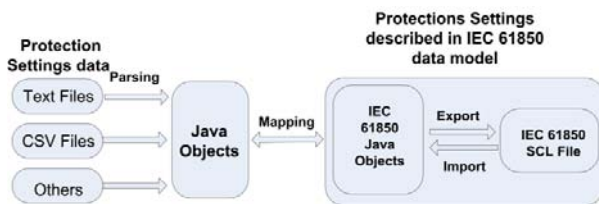


Fig. 1. Overall process of converting protection setting data into IEC 61850 format

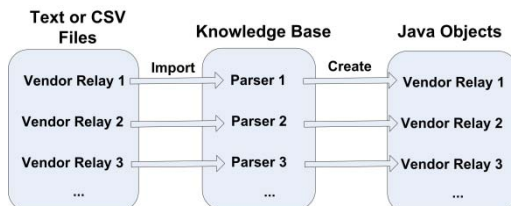


Fig. 2. Parsing protection setting information from text or CSV files

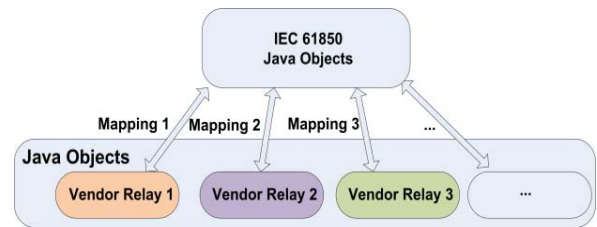


Fig. 3. Mapping proprietary protection settings to IEC 61850 represented Java objects

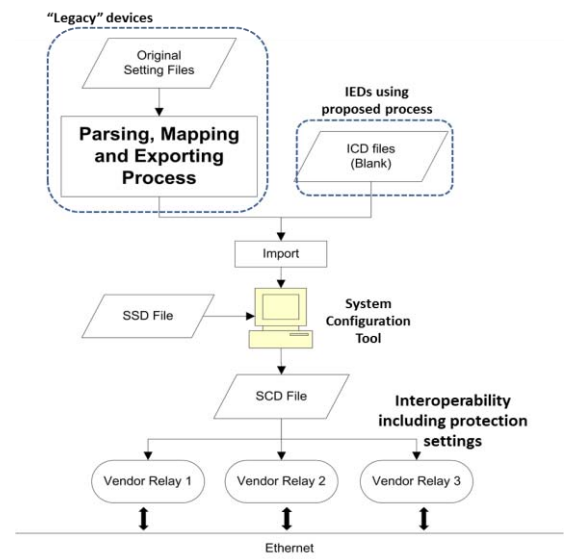


Fig. 4. Proposed simplified IED configuration process

PDC Testing and Characterization of Synchrophasor Based Applications

Jeong Hun Kim, *Student Member, IEEE* and Anurag K Srivastava, *Senior Member, IEEE*
 Smart Grid Demonstration and Research Investigation Laboratory (SGDRIL),
 The School of Electrical Engineering and Computer Science, Washington State University, Pullman,
 E-mail: jeong.kim@email.wsu.edu

Abstract—The performance of synchrophasor devices varies with operating conditions - balanced, unbalanced, off-nominal frequency and with harmonics conditions for steady-state and dynamic conditions. Accuracy of synchrophasor devices depends on their phasor estimation algorithms and is very critical for the system applications such as situational awareness, decision support, wide area monitoring and automatic control. In order to analyze the performance of synchrophasor devices, characterization of Phasor Measurement Units (PMU) and Phasor Data Concentrator (PDC) with various operating conditions and system architectures are needed as discussed in this poster. This work also aims to characterize the impact of PMU error on synchrophasor applications.

I. KEY FIGURES

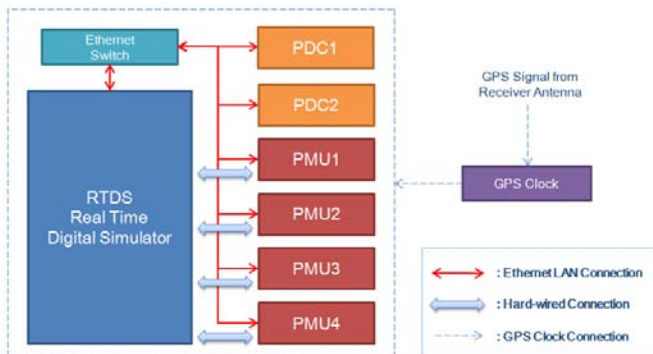


Figure 1. Testbed in SGDRIL

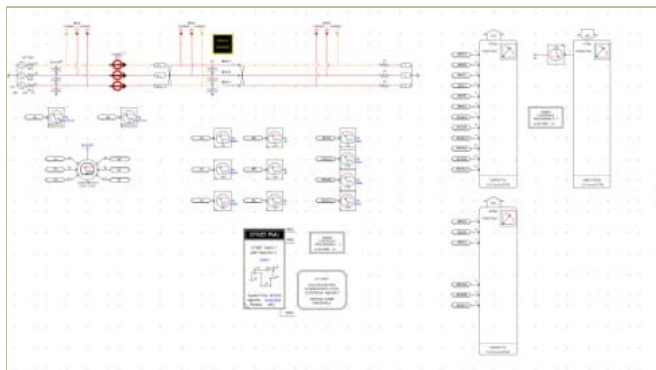


Figure 2. Testing Model on RTDS

II. CASES FOR SYSTEM CONDITIONS

The cases for testing synchrophasor device are developed based on IEEE standards C37.118.1 and C37.244, which are related to PMU and PDC respectively.

	System Conditions
PMU Tests	Balanced system, unbalanced system, system at off-nominal frequency and system with harmonics

Table 1. List of System Conditions for PMU

PDC Tests	Description
Data Validation	Evaluation of the quality of an input synchrophasor data using CRC check.
Data Resampling	PMUs at different substations may send in data at different rates, which the PDC needs to up-sample or down-sample accordingly. This conversion of input data rate in the PDC needs to be tested for errors
Data Alignment	Alignment or ordering of synchrophasor data needs to be done on the basis of the timestamp on the data. This kind of data stream should be checked for correct time sequence (for each data)
Data Retrieval	While there is data transfer between a PMU and a PDC, some data might be lost. The PDC should be able to recognize the missing data and send a request to the concerned PMU/PMUs to resend the missing data. Once the PDC receives this missing data, it should be able to reposition this data in correct time sequence based on its original timestamp.
Data Latency	The time difference between the arrival time of the first complete data message with a given timestamp and its egress time from the PDC.

Table 2. List of PDC Tests

III. KEY RESULT

	Balanced	Unbalanced	Off-nominal Frequency	With Harmonics (3rd,5th,7th,9th)
Average of %TVE for PMU	0.6517 %	0.6526 %	0.7028 %	0.6703 %

Table 3. Result of PMU Testing for Magnitude Change Measurement Test with Steady State

The result above shows that the performance of PMU varies with operating conditions. This work also aims to characterize impact of PMU error on synchrophasor based applications and suggests choosing different phasor estimation algorithms within PMU according to the operating conditions.

Action Research for Power System Engineering Education

Mostafa Farrokhbabadi and Luigi Vanfretti

Electric Power Systems Department
KTH Royal Institute of Technology
Stockholm, Sweden
luigiv@kth.se, mostafaf@kth.se

Abstract— This poster will present results of an educational research project aiming to implement “action research” methodologies for enhancing power systems engineering education. The poster consists of three parts, the first dealing with design and implementation of Constructive Alignment Theory (CAT) in the power system analysis course through a consensus-based process, and the impact of the CAT implementation on student learning. The second part is dedicated to the evaluation of the CAT implementation using the Repertory Grid structured interview technique to gather data from students whose learning approach was pre-classified through a new ranking algorithm for the Revised-Two Factor Study Process Questionnaire. The third part presents a “data mash-up” approach to systematically scrutinize student feedback and determine the most relevant one that can be used for making enhancements in course design and delivery.

Keywords- Power Systems; Constructive-Alignment Theory; Two-Factor Study Process Questionnaire; Repertory Grid

I. THE PROCESS OF THE RESEARCH

Firstly, the CAT implementation in the power system course is elaborated through a consensus-based design process. Fig. 1 shows one example on how to efficiently align the teaching and learning (T&L) activities with the course intended learning outcomes (ILO). To examine the effect of this approach, three different course evaluations were conducted by querying the students during different stages of the course.

Specifically, the Two-Factor Study Process Questionnaire (R-SPQ-2F) [3] was utilized to identify the students that adopted a deep or surface approach. During this process, several limitations that affect the quality of the results from the R-SPQ-2F questionnaire were identified. In view of these limitations, a new ranking algorithm was developed which is verified through statistical correlation of the course final grades and the students’ learning approach (Fig. 2).

It is important to measure how the students perceive the learning environment. To this end, Personal Construct Theory (PCT) can be utilized [2]. A structured interview methodology known as the Repertory Grid [1] technique is used. It is shown that the Repertory Grid technique provides a plethora of valuable and insightful quantitative and qualitative data.

Finally, the poster presents a method that combines different evaluation techniques to identify relevant feedback. The results from all different evaluation techniques are correlated to find out logical patterns. These logical patterns can be used later on to identify students with the deeper approach

toward the course. Fig. 3 provides an outline of the proposed mechanism.

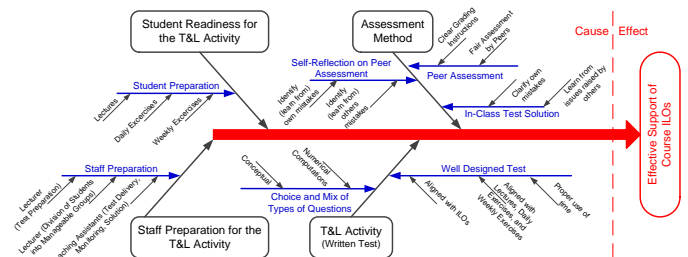


Fig. 1. Fishbone Diagram integrating the rule for implementing CAT - Example for the “Weekly Tests” T&L Activity

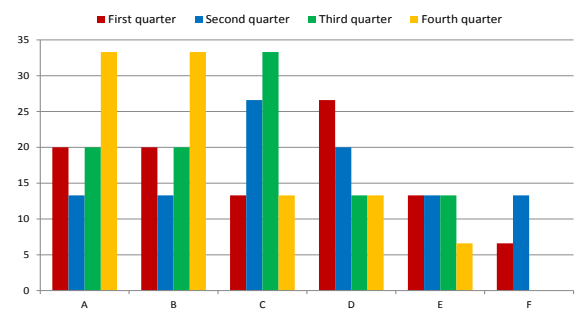


Fig. 2. Final Grades and R-SPQ-2F Correlation

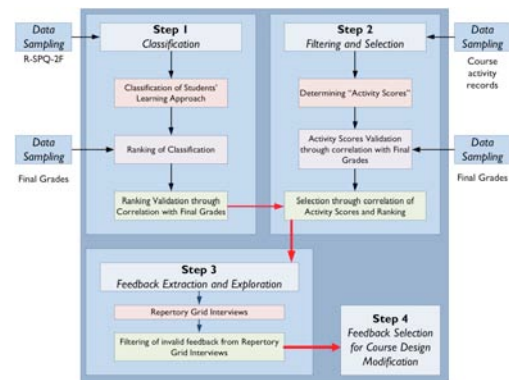


Fig. 5. Flowchart of the proposed method

REFERENCES

- [1] Neenar Thota, “Repertory Grid: Investigating Personal Constructs of Novice Programmers,” 11th Koli Calling International Conference on Computing Education Research. Koli National Park, Finland, 2011.
- [2] G.A. Kelly, The Psychology of Personal Constructs. New York, NY, 1955.
- [3] John Biggs, “The revised two-factor study process questionnaire: R-SPQ-2F,” British Journal of Educational Psychology, 2011.